



# **The Design, Synthesis and Optimisation of Kinase Inhibitors as Potential Anti-Inflammatory agents**

Zoë A. Harrison

A Thesis submitted for a Degree of Doctor of Philosophy

DEPARTMENT OF PURE AND APPLIED CHEMISTRY  
UNIVERSITY OF STRATHCLYDE AND GLAXOSMITHKLINE

May 2014

## **Declaration of Authenticity and Author's Rights**

This thesis is the result of the author's original research. It has been composed by the author and has not been previously submitted for examination which has led to the award of a degree.

The copyright of this thesis belongs to GSK in accordance with the author's contract of engagement with GSK under the terms of the United Kingdom Copyright Acts. Due acknowledgement must always be made of the use of any material contained in, or derived from, this thesis.

Signed:

Date:

# Table of Contents

Please note that each main section of this thesis has a self-contained reference section.

Acknowledgements .....	xvi
Abstract .....	xvii
Abbreviations .....	xix
<b>1. Emerging Mechanisms and Therapies for the Treatment of Inflammatory Airway Diseases .....</b>	<b>1</b>
1.1. Inflammatory Airway Diseases .....	2
1.1.1. Asthma and Chronic Obstructive Pulmonary Disease (COPD) .....	2
1.1.2. Established Therapies for the Treatment of Asthma and COPD .....	6
1.2. Emerging Mechanisms for the Treatment of Inflammatory Airway Diseases ...	13
1.2.1. Kinase Inhibitors .....	14
1.3. References .....	23
<b>2. Properties of Orally Bioavailable Drugs .....</b>	<b>28</b>
2.1. Drug-likeness and the Physicochemical Properties of Oral Drugs .....	29
2.1.1. Solubility .....	30
2.1.2. Permeability .....	34
2.1.3. Human Serum Albumin Binding .....	35
2.1.4. Toxicity .....	36
2.1.5. Rules-of-Thumb .....	41
2.2. Drug Metabolism and Pharmacokinetics (DMPK) .....	45
2.2.1. Metabolism and Clearance .....	45
2.2.2. <i>In vivo</i> Pharmacokinetics .....	49

2.2.3.	Approaches to Predicting Human Pharmacokinetics .....	51
2.3.	References.....	55
<b>3.</b>	<b>The Design, Synthesis and Optimisation of IKK2 Inhibitors as Potential Anti-Inflammatory Agents.....</b>	<b>60</b>
3.1.	Introduction.....	61
3.1.1.	IκB Kinase .....	61
3.1.2.	The Role of IκB Kinases in Disease.....	63
3.1.3.	IKK2 as a Target for Respiratory Disease.....	64
3.1.4.	IKK2 Inhibitors .....	65
3.1.5.	IKK2 Structural Biology .....	68
3.1.6.	Indole Carboxamides as IKK2 Inhibitors.....	74
3.2.	Aims.....	79
3.3.	Results and Discussion .....	81
3.3.1.	3-Substituted Indole Carboxamides .....	81
3.3.1.1.	Hansch Analysis .....	81
3.3.1.2.	Synthesis of 3-Cyano-1 <i>H</i> -indole-7-carboxamides .....	87
3.3.1.3.	Biological Results for 3-Cyano-1 <i>H</i> -indole-7-carboxamides.....	98
3.3.1.4.	Synthesis of Other 3-Substituted 1 <i>H</i> -Indole-7-carboxamides.....	102
3.3.1.5.	Biological Results for 3-Substituted 1 <i>H</i> -Indole-7-carboxamides ....	109
3.3.2.	3-(Oxetan-3-yl)-1 <i>H</i> -indole-7-carboxamides .....	117
3.3.2.1.	Oxetanes in Drug Molecules and Nature.....	117
3.3.2.2.	Structure and Properties of Oxetanes .....	118
3.3.2.3.	Property Changes Arising from the Presence of Oxetanes .....	122
3.3.2.4.	Synthesis and Biological Results of 3-(Oxetan-3-yl)indazole-7-carboxamides.....	126



3.3.2.5. Synthesis and Biological Results for 3-Oxetane Substituted Indole-7-carboxamides .....	133
3.4. Conclusion .....	165
3.5. References.....	167
<b>4. The Design, Synthesis and Optimisation of PI3K<math>\delta</math> Inhibitors as Potential Anti-Inflammatory Agents.....</b>	<b>176</b>
4.1. Introduction.....	177
4.1.1. Phosphoinositide Kinases and Related Proteins.....	177
4.1.1.1. The Phosphoinositide 3-Kinases (PI3Ks).....	177
4.1.1.2. Class I PI3Ks .....	178
4.1.1.3. Class II and III PI3Ks .....	179
4.1.1.4. PI3K-related Kinases.....	182
4.1.2. The Role of Class I PI3Ks in Disease .....	182
4.1.3. PI3K $\delta$ as a Target for Respiratory Disease .....	185
4.1.4. PI3K $\delta$ Inhibitors .....	186
4.1.5. Small Molecule Inhibitors of PI3K $\delta$ .....	187
4.1.6. The Impact of Structural Biology on the Design of Selective Inhibitors .....	193
4.1.7. 4,6-Dihydroisobenzofurans as Oral PI3K $\delta$ Inhibitors.....	201
4.2. Aims.....	207
4.3. Results and Discussion .....	210
4.3.1. Exploration of Dihydroisobenzofuran 4-Position .....	210
4.3.1.1. Synthesis of Truncated Compounds <b>174 - 180</b> .....	210
4.3.1.2. Synthesis of Compounds <b>181 - 184</b> .....	219
4.3.1.3. Conformational Analysis of Compounds in their Free and Protein-bound States.....	229

---

4.3.1.4. Further Exploration of 4-Substituted Dihydroisobenzofurans .....	255
4.3.1.5. Optimisation of the PK Profile of 4-Ether substituted Dihydroisobenzofurans.....	259
4.4. Conclusion .....	295
4.5. References.....	299
<b>5. Thesis Conclusion</b> .....	<b>309</b>
<b>6. Experimental</b> .....	<b>312</b>
6.1. General Details .....	312
6.2. Preparation of 3-Cyanoindole-7-carboxamides .....	325
6.2.1. Methyl 5-bromo-3-formyl-1 <i>H</i> -indole-7-carboxylate, <b>11b</b> .....	325
6.2.2. Ethyl 5-bromo-3-(hydroxyimino)methyl-1 <i>H</i> -indole-7-carboxylate, <b>12</b> .....	325
6.2.3. Ethyl 5-bromo-3-cyano-1 <i>H</i> -indole-7-carboxylate, <b>13a</b> .....	326
6.2.4. Methyl 5-bromo-3-cyano-1 <i>H</i> -indole-7-carboxylate, <b>13b</b> .....	327
6.2.5. 5-Bromo-3-cyano-1 <i>H</i> -indole-7-carboxylic acid, <b>14</b> .....	328
6.2.6. 5-Bromo-3-cyano-1 <i>H</i> -indole-7-carboxamide, <b>15</b> .....	328
6.2.7. 3-Cyano-5-{5-[(dimethylamino)methyl]-3-thienyl}-1 <i>H</i> -indole-7- carboxamide, <b>16a</b> .....	329
6.2.8. 3-Cyano-5-(4-fluorophenyl)-1 <i>H</i> -indole-7-carboxamide, <b>16b</b> .....	330
6.2.9. 3-Cyano-5-(4,4,5,5-tetramethyl-1,3,2-dioxaborolan-2-yl)-1 <i>H</i> -indole- 7-carboxamide, <b>17</b> .....	330
6.2.10. 5-{5-[(1 <i>S</i> )-1-Amino-2,2,2-trifluoroethyl]-3-furanyl}-3-cyano-1 <i>H</i> - indole-7-carboxamide, <b>16c</b> .....	331
6.2.11. 5-[5-(1-Amino-1-methylethyl)-3-thienyl]-3-cyano-1 <i>H</i> -indole-7- carboxamide, <b>16d</b> .....	332
6.2.12. 2-(4-Bromo-2-thienyl)-2-propanamine, <b>19</b> .....	333

6.2.13.	3-(1,1-Dioxidotetrahydro-2 <i>H</i> -thiopyran-4-yl)-5-(4,4,5,5-tetramethyl-1,3,2-dioxaborolan-2-yl)-1 <i>H</i> -indole-7-carboxamide, <b>21</b> .....	334
6.2.14.	5-{5-[(1 <i>S</i> )-1-Amino-2,2,2-trifluoroethyl]-3-furanyl}-3-(1,1-dioxidotetrahydro-2 <i>H</i> -thiopyran-4-yl)-1 <i>H</i> -indole-7-carboxamide, <b>22a</b> .....	335
6.2.15.	5-[5-(1-Amino-1-methylethyl)-3-thienyl]-3-(1,1-dioxidotetrahydro-2 <i>H</i> -thiopyran-4-yl)-1 <i>H</i> -indole-7-carboxamide, <b>22b</b> .....	336
6.3.	Preparation of 3-Chloroindole-7-carboxamides.....	336
6.3.1.	5-Bromo-3-chloro-1 <i>H</i> -indole-7-carboxylic acid, <b>24</b> .....	336
6.3.2.	5-Bromo-3-chloro-1 <i>H</i> -indole-7-carboxamide, <b>25</b> .....	337
6.3.3.	3-Chloro-5-(4-fluorophenyl)-1 <i>H</i> -indole-7-carboxamide, <b>26</b> .....	338
6.4.	Preparation of 3-Methylsulfonyl Indole Carboxamides.....	338
6.4.1.	5-Bromo-3-(methylthio)-1 <i>H</i> -indole-7-carboxamide, <b>33</b> .....	338
6.4.2.	5-Bromo-3-(methylsulfonyl)-1 <i>H</i> -indole-7-carboxamide, <b>34</b> .....	339
6.5.	Preparation of 3-Nitroindole-7-carboxamides .....	340
6.5.1.	Methyl 5-bromo-3-nitro-1 <i>H</i> -indole-7-carboxylate, <b>35</b> .....	340
6.5.2.	5-Bromo-3-nitro-1 <i>H</i> -indole-7-carboxylic acid, <b>36</b> .....	341
6.5.3.	5-Bromo-3-nitro-1 <i>H</i> -indole-7-carboxamide, <b>37</b> .....	341
6.5.4.	5-(4-Fluorophenyl)-3-nitro-1 <i>H</i> -indole-7-carboxamide, <b>38</b> .....	342
6.6.	Preparation of 3-Trifluoromethylindole-7-carboxamides.....	343
6.6.1.	7-Bromo-3-hydroxy-3-(trifluoromethyl)indolin-2-one, <b>40</b> .....	343
6.6.2.	7-Bromo-3-(trifluoromethyl)indolin-3-ol, <b>41</b> .....	343
6.6.3.	5,7-Dibromo-3-(trifluoromethyl)indolin-3-ol, <b>42</b> .....	344
6.6.4.	5,7-Dibromo-3-(trifluoromethyl)-1 <i>H</i> -indole, <b>43</b> .....	344
6.6.5.	<i>tert</i> -Butyl 5,7-dibromo-3-(trifluoromethyl)-1 <i>H</i> -indole-1-carboxylate, <b>44</b> .....	345

---

6.6.6.	5-Bromo-1-( <i>tert</i> -butoxycarbonyl)-3-methyl-1 <i>H</i> -indole-7-carboxylic acid, <b>45</b> .....	345
6.6.7.	<i>tert</i> -Butyl 5-bromo-7-carbamoyl-3-(trifluoromethyl)-1 <i>H</i> -indole-1-carboxylate, <b>46</b> .....	346
6.6.8.	5-Bromo-3-(trifluoromethyl)-1 <i>H</i> -indole-7-carboxamide, <b>47</b> .....	346
6.6.9.	5-Phenyl-3-(trifluoromethyl)-1 <i>H</i> -indole-7-carboxamide, <b>48</b> .....	347
6.7.	Preparation of 3-(Oxetan-3-yl)indazole-7-carboxamides .....	347
6.7.1.	Diethyl 2-nitrobenzylphosphonate, <b>66</b> .....	347
6.7.2.	3-(2-Nitrobenzylidene)oxetane, <b>67</b> .....	348
6.7.3.	2-(Oxetan-3-ylmethyl)aniline, <b>68</b> .....	349
6.7.4.	2,4-Dibromo-6-(oxetan-3-ylmethyl)aniline, <b>69</b> .....	349
6.7.5.	5,7-Dibromo-3-(oxetan-3-yl)-1 <i>H</i> -indazole, <b>70</b> .....	350
6.7.6.	<i>tert</i> -Butyl 5,7-dibromo-3-(oxetan-3-yl)-1 <i>H</i> -indazole-1-carboxylate, <b>71</b> .....	351
6.7.7.	5-Bromo-3-(oxetan-3-yl)-1 <i>H</i> -indazole-7-carboxylic acid, <b>72</b> .....	352
6.7.8.	5-Bromo-3-(oxetan-3-yl)-1 <i>H</i> -indazole-7-carboxamide, <b>73</b> .....	353
6.7.9.	5-(4-Fluorophenyl)-3-(oxetan-3-yl)-1 <i>H</i> -indazole-7-carboxamide, <b>74a</b> .....	353
6.7.10.	5-(6-Methylpyridin-3-yl)-3-(oxetan-3-yl)-1 <i>H</i> -indazole-7-carboxamide, <b>74b</b> .....	354
6.8.	Preparation of 3-(Oxetan-3-yl)indole-7-carboxamides .....	355
6.8.1.	3,3'-(Oxetane-3,3-diyl)bis(5-bromo-1 <i>H</i> -indole-7-carboxamide, <b>89</b> , (2-(5-Bromo-3-(3-(5-bromo-7-carbamoyl-1 <i>H</i> -indol-3-yl)oxetan-3-yl)-1 <i>H</i> -indol-7-yl)oxazol-4-yl)methyl acetate, <b>90</b> , and (2,2'-(3,3'-(Oxetane-3,3-diyl)bis(5-bromo-1 <i>H</i> -indole-7,3-diyl))bis(oxazole-4,2-diyl))bis(methylene) diacetate, <b>91</b> .....	355

6.8.2.	Dimethyl 3,3-(oxetane-3,3-diyl)bis(5-bromo-1 <i>H</i> -indole-7-carboxylate), <b>102</b> and Methyl 5-bromo-3-(5-bromo-7-(methoxycarbonyl)indolin-2-yl)-1 <i>H</i> -indole-7-carboxylate, <b>103</b> .....	357
6.8.3.	Ethyl 2-(oxetan-3-ylidene)acetate, <b>107</b> .....	358
6.8.4.	Ethyl 2-(oxetan-3-yl)acetate, <b>108</b> .....	359
6.8.5.	2-(Oxetan-3-yl)ethanol, <b>109</b> .....	359
6.8.6.	2-(Oxetan-3-yl)acetaldehyde, <b>110</b> .....	360
6.8.7.	2-Amino-5-bromobenzamide, <b>114</b> .....	360
6.8.8.	5-Bromo-1,2-dihydro-3 <i>H</i> -indazol-3-one, <b>115</b> .....	361
6.8.9.	2,4-(Dibromophenyl)hydrazine, <b>117</b> .....	362
6.8.10.	1-(2,4-Dibromophenyl)-2-(2-(oxetan-3-yl)ethylidene)hydrazine, <b>118</b> .....	362
6.8.11.	1-(2,4-Dibromophenyl)-2-(3-methylbutylidene)hydrazine, <b>120</b> .....	363
6.8.12.	5-Bromo-3-(3-hydroxyoxetan-3-yl)-1 <i>H</i> -indole-7-carboxamide, <b>86</b> .....	364
6.8.13.	3-(3-Hydroxyoxetan-3-yl)-5-(thiophen-3-yl)-1 <i>H</i> -indole-7-carboxamide, <b>122a</b> .....	365
6.8.14.	3-(3-Hydroxyoxetan-3-yl)-5-(6-methylpyridin-3-yl)-1 <i>H</i> -indole-7-carboxamide, <b>122b</b> .....	366
6.8.15.	5-(4-Fluorophenyl)-3-(3-hydroxyoxetan-3-yl)-1 <i>H</i> -indole-7-carboxamide, <b>122c</b> .....	367
6.8.16.	Methyl 5-bromo-3-iodo-1 <i>H</i> -indole-7-carboxylate, <b>126</b> .....	368
6.8.17.	Methyl 5-bromo-3-iodo-1-tosyl-1 <i>H</i> -indole-7-carboxylate, <b>127</b> .....	368
6.8.18.	Methyl 5-bromo-3-(3-hydroxyoxetan-3-yl)-1-tosyl-1 <i>H</i> -indole-7-carboxylate, <b>129</b> .....	369
6.8.19.	5-Bromo-3-(3-hydroxyoxetan-3-yl)-1 <i>H</i> -indole-7-carboxylic acid, <b>131</b> .....	370

6.8.20.	Methyl 5-bromo-3-(3-fluorooxetan-3-yl)-1-tosyl-1 <i>H</i> -indole-7-carboxylate, <b>132</b> .....	371
6.8.21.	Conditions Attempted for the Deoxofluorination of 5-Bromo-3-(3-hydroxyoxetan-3-yl)-1 <i>H</i> -indole-7-carboxamide <b>86</b> .....	373
6.8.22.	Conditions Attempted for the Deoxygenation of 5-Bromo-3-(3-hydroxyoxetan-3-yl)-1 <i>H</i> -indole-7-carboxamide <b>86</b> .....	374
6.9.	Preparation of Truncated Dihydroisobenzofuran Compounds <b>175, 176, 178-180</b> .....	375
6.9.1.	<i>N</i> -(2-Methoxy-5-(7-((1,1,1-trifluoropropan-2-yl)amino)-1,3-dihydroisobenzofuran-5-yl)pyridin-3-yl)methanesulfonamide, <b>175</b> .....	375
6.9.2.	<i>N</i> -Allyl- <i>N</i> -(5-(7-iodo-1,3-dihydroisobenzofuran-5-yl)-2-methoxypyridin-3-yl)methanesulfonamide, <b>188a</b> .....	376
6.9.3.	<i>N</i> -(5-(7-Iodo-1,3-dihydroisobenzofuran-5-yl)-2-methoxypyridin-3-yl)- <i>N</i> -(4-methoxybenzyl)methanesulfonamide, <b>188b</b> .....	377
6.9.4.	<i>N</i> -Allyl- <i>N</i> -(2-methoxy-5-(7-(3-methoxyoxetan-3-yl)-1,3-dihydroisobenzofuran-5-yl)pyridin-3-yl)methanesulfonamide, <b>196</b> .....	378
6.9.5.	<i>N</i> -Allyl- <i>N</i> -(2-methoxy-5-(7-(3-methoxyoxetan-3-yl)-1,3-dihydroisobenzofuran-5-yl)pyridin-3-yl)methanesulfonamide, <b>198</b> .....	379
6.9.6.	<i>N</i> -(2-Methoxy-5-(7-(3-methoxyoxetan-3-yl)-1,3-dihydroisobenzofuran-5-yl)pyridin-3-yl)methanesulfonamide, <b>180</b> .....	380
6.9.7.	Methyl 6-(6-methoxy-5-(methylsulfonamido)pyridin-3-yl)-1,3-dihydroisobenzofuran-4-carboxylate, <b>179</b> .....	381
6.9.8.	<i>N</i> -(2-Methoxy-5-(7-propionyl-1,3-dihydroisobenzofuran-5-yl)pyridin-3-yl)methanesulfonamide, <b>178</b> .....	382

6.9.9.	<i>N</i> -(5-(7-Ethoxy-1,3-dihydroisobenzofuran-5-yl)-2-methoxypyridin-3-yl)methanesulfonamide, <b>176</b> .....	383
6.10. Preparation of Fully Elaborated Dihydroisobenzofuran Compounds <b>181-184</b> .384		
6.10.1.	6-(6-Methoxy-5-(methylsulfonamido)pyridin-3-yl)- <i>N</i> -((tetrahydro-2 <i>H</i> -pyran-4-yl)methyl)-1,3-dihydroisobenzofuran-4-carboxamide, <b>182</b> .....	384
6.10.2.	<i>N</i> -(2-Methoxy-5-(7-(((tetrahydro-2 <i>H</i> -pyran-4-yl)methyl)imino)methyl)-1,3-dihydroisobenzofuran-5-yl)pyridin-3-yl)methanesulfonamide, <b>206</b> .....	385
6.10.3.	<i>N</i> -(5-(7-Formyl-1,3-dihydroisobenzofuran-5-yl)-2-methoxypyridin-3-yl)- <i>N</i> -(4-methoxybenzyl)methanesulfonamide, <b>215</b> .....	386
6.10.4.	<i>N</i> -(5-(7-(((tert-Butylsulfinyl)imino)methyl)-1,3-dihydroisobenzofuran-5-yl)-2-methoxypyridin-3-yl)methanesulfonamide, <b>216a</b> .....	387
6.10.5.	<i>N</i> -(5-(7-(((tert-Butylsulfinyl)imino)methyl)-1,3-dihydroisobenzofuran-5-yl)-2-methoxypyridin-3-yl)- <i>N</i> -(4-methoxybenzyl)methanesulfonamide, <b>216b</b> .....	388
6.10.6.	<i>N</i> -(5-(7-(1-(1,1-Dimethylethylsulfonamido)-2,2,2-trifluoroethyl)-1,3-dihydroisobenzofuran-5-yl)-2-methoxypyridin-3-yl)methanesulfonamide, <b>217a</b> .....	389
6.10.7.	<i>N</i> -(5-(7-(1-(1,1-Dimethylethylsulfonamido)-2,2,2-trifluoroethyl)-1,3-dihydroisobenzofuran-5-yl)-2-methoxypyridin-3-yl)- <i>N</i> -(4-methoxybenzyl)methanesulfonamide, <b>217b</b> .....	390
6.10.8.	<i>N</i> -(5-(7-(1-Amino-2,2,2-trifluoroethyl)-1,3-dihydroisobenzofuran-5-yl)-2-methoxypyridin-3-yl)- <i>N</i> -(4-methoxybenzyl)methanesulfonamide, <b>218</b> .....	391

6.10.9.	<i>N</i> -(2-Methoxy-5-(7-(2,2,2-trifluoro-1-(((tetrahydro-2H-pyran-4-yl)methyl)amino)ethyl)-1,3-dihydroisobenzofuran-5-yl)pyridin-3-yl)- <i>N</i> -(4-methoxybenzyl)methanesulfonamide, <b>219</b> .....	392
6.10.10.	<i>N</i> -(5-(7-(1-Amino-2,2,2-trifluoroethyl)-1,3-dihydroisobenzofuran-5-yl)-2-methoxypyridin-3-yl)methanesulfonamide, trifluoroacetic acid salt, <b>220</b> .....	393
6.10.11.	<i>N</i> -(2-Methoxy-5-(7-(2,2,2-trifluoro-1-(((tetrahydro-2H-pyran-4-yl)methyl)amino)ethyl)-1,3-dihydroisobenzofuran-5-yl)pyridin-3-yl)methanesulfonamide, <b>183</b> .....	393
6.10.12.	<i>N</i> -(5-(7-Allyl-1,3-dihydroisobenzofuran-5-yl)-2-methoxypyridin-3-yl)methanesulfonamide, <b>221</b> .....	395
6.10.13.	<i>N</i> -(2-Methoxy-5-(7-(oxiran-2-ylmethyl)-1,3-dihydroisobenzofuran-5-yl)pyridin-3-yl)methanesulfonamide, <b>222</b> .....	396
6.10.14.	<i>N</i> -(5-(7-(2-Hydroxy-3-morpholinopropyl)-1,3-dihydroisobenzofuran-5-yl)-2-methoxypyridin-3-yl)methanesulfonamide, <b>223</b> .....	396
6.10.15.	<i>N</i> -(2-Methoxy-5-(7-(3-morpholino-2-oxopropyl)-1,3-dihydroisobenzofuran-5-yl)pyridin-3-yl)methanesulfonamide, <b>181</b> .....	397
6.11.	Preparation of Intermediate for Dihydroisobenzofuran Array.....	398
6.11.1.	2-Chloro- <i>N</i> -(6-(6-methoxy-5-(methylsulfonamido)pyridin-3-yl)-1,3-dihydroisobenzofuran-4-yl)acetamide, <b>224</b> .....	398
6.12.	Preparation of 4-Ether Substituted Dihydroisobenzofurans .....	399
6.12.1.	<i>N</i> -(5-(7-( <i>cis</i> -2,6-Dimethylmorpholino)ethoxy)-1,3-dihydroisobenzofuran-5-yl)-2-methoxypyridin-3-yl)methanesulfonamide, <b>226</b> .....	399
6.12.2.	<i>tert</i> -Butyl-2-(((6-(6-methoxy-5-(methylsulfonamido)pyridin-3-yl)-1,3-dihydroisobenzofuran-4-yl)oxy)methyl)morpholine-4-carboxylate, <b>232</b> .....	400



---

6.12.3.	<i>N</i> -(5-(7-Hydroxy-1,3-dihydroisobenzofuran-5-yl)-2-methoxypyridin-3-yl)methanesulfonamide, <b>233</b> .....	401
6.12.4.	<i>N</i> -(5-(7-Hydroxy-1,3-dihydroisobenzofuran-5-yl)-2-methoxypyridin-3-yl)- <i>N</i> -(4-methoxybenzyl)methanesulfonamide, <b>235</b> .....	402
6.12.5.	<i>(R)</i> - <i>tert</i> -Butyl-2-(((6-(6-methoxy-5-( <i>N</i> -(4-methoxybenzyl)methylsulfonamido)pyridin-3-yl)-1,3-dihydroisobenzofuran-4-yl)oxy)methyl)morpholine-4-carboxylate, <b>239a</b> .....	403
6.12.6.	<i>(S)</i> - <i>tert</i> -Butyl-2-(((6-(6-methoxy-5-( <i>N</i> -(4-methoxybenzyl)methylsulfonamido)pyridin-3-yl)-1,3-dihydroisobenzofuran-4-yl)oxy)methyl)morpholine-4-carboxylate, <b>239b</b> .....	404
6.12.7.	<i>(R)</i> - <i>N</i> -(2-Methoxy-5-(7-(morpholin-2-ylmethoxy)-1,3-dihydroisobenzofuran-5-yl)pyridin-3-yl)methanesulfonamide, <b>240a</b> .....	405
6.12.8.	<i>(S)</i> - <i>N</i> -(2-Methoxy-5-(7-(morpholin-2-ylmethoxy)-1,3-dihydroisobenzofuran-5-yl)pyridin-3-yl)methanesulfonamide, <b>240b</b> .....	406
6.12.9.	<i>(R)</i> - <i>N</i> -(2-Methoxy-5-(7-((4-methylmorpholin-2-yl)methoxy)-1,3-dihydroisobenzofuran-5-yl)pyridin-3-yl)methanesulfonamide, <b>228a</b> .....	407
6.12.10.	<i>(S)</i> - <i>N</i> -(2-Methoxy-5-(7-((4-methylmorpholin-2-yl)methoxy)-1,3-dihydroisobenzofuran-5-yl)pyridin-3-yl)methanesulfonamide, <b>228b</b> .....	408
6.12.11.	<i>(R)</i> - <i>N</i> -(2-Methoxy-5-(7-(morpholin-2-ylmethoxy)-1,3-dihydroisobenzofuran-5-yl)pyridin-3-yl)- <i>N</i> -(4-methoxybenzyl)methanesulfonamide, <b>250</b> .....	409

6.12.12.	<i>N</i> -(5-(7-((4,4-Difluoropiperidin-3-yl)methoxy)-1,3-dihydroisobenzofuran-5-yl)-2-methoxypyridin-3-yl)- <i>N</i> -(4-methoxybenzyl)methanesulfonamide, <b>251</b> .....	410
6.12.13.	<i>(R)</i> - <i>N</i> -(2-Methoxy-5-(7-((4-(2-methoxyethyl)morpholin-2-yl)methoxy)-1,3-dihydroisobenzofuran-5-yl)pyridin-3-yl)- <i>N</i> -(4-methoxybenzyl)methanesulfonamide, <b>253</b> .....	411
6.12.14.	<i>N</i> -(5-(7-((4,4-Difluoro-1-(2-methoxyethyl)piperidin-3-yl)methoxy)-1,3-dihydroisobenzofuran-5-yl)-2-methoxypyridin-3-yl)- <i>N</i> -(4-methoxybenzyl)methanesulfonamide, <b>254</b> .....	412
6.12.15.	<i>(R)</i> - <i>N</i> -(2-Methoxy-5-(7-((4-(2-methoxyethyl)morpholin-2-yl)methoxy)-1,3-dihydroisobenzofuran-5-yl)pyridin-3-yl)methanesulfonamide, <b>242</b> .....	413
6.12.16.	<i>N</i> -(5-(7-((4,4-Difluoro-1-(2-methoxyethyl)piperidin-3-yl)methoxy)-1,3-dihydroisobenzofuran-5-yl)-2-methoxypyridin-3-yl)methanesulfonamide, <b>243</b> .....	414
6.12.17.	<i>(R)</i> - <i>N</i> -(2-Methoxy-5-(7-((4-(2,2,2-trifluoroethyl)morpholin-2-yl)methoxy)-1,3-dihydroisobenzofuran-5-yl)pyridin-3-yl)- <i>N</i> -(4-methoxybenzyl)methanesulfonamide, <b>252</b> .....	415
6.12.18.	<i>(R)</i> - <i>N</i> -(2-Methoxy-5-(7-((4-(2,2,2-trifluoroethyl)morpholin-2-yl)methoxy)-1,3-dihydroisobenzofuran-5-yl)pyridin-3-yl)methanesulfonamide, <b>241</b> .....	416
6.12.19.	<i>(R)</i> - <i>tert</i> -Butyl-3-(((6-(6-methoxy-5-( <i>N</i> -(4-methoxybenzyl)methylsulfonamido)pyridin-3-yl)-1,3-dihydroisobenzofuran-4-yl)oxy)methyl)piperidine-1-carboxylate, <b>257</b> .....	417
6.12.20.	<i>(R)</i> - <i>N</i> -(2-Methoxy-5-(7-(piperidin-3-ylmethoxy)-1,3-dihydroisobenzofuran-5-yl)pyridin-3-yl)methanesulfonamide, <b>258</b> .....	418

6.12.21.	<i>(R)</i> - <i>N</i> -(2-Methoxy-5-(7-((1-(oxetan-3-yl)piperidin-3-yl)methoxy)-1,3-dihydroisobenzofuran-5-yl)pyridin-3-yl)methanesulfonamide, <b>244</b> .....	419
6.12.22.	<i>(R)</i> - <i>N</i> -(2-Methoxy-5-(7-((4-(oxetan-3-yl)morpholin-2-yl)methoxy)-1,3-dihydroisobenzofuran-5-yl)pyridin-3-yl)methanesulfonamide, <b>245</b> .....	420
6.12.23.	<i>(R)</i> - <i>N</i> -(2-Methoxy-5-(7-((4-((3-methyloxetan-3-yl)methyl)morpholin-2-yl)methoxy)-1,3-dihydroisobenzofuran-5-yl)pyridin-3-yl)methanesulfonamide, <b>247</b> .....	421
6.12.24.	<i>(R)</i> - <i>N</i> -(2-Methoxy-5-(7-((4-(3-((phenylsulfonyl)methyl)oxetan-3-yl)morpholin-2-yl)methoxy)-1,3-dihydroisobenzofuran-5-yl)pyridin-3-yl)- <i>N</i> -(4-methoxybenzyl)methanesulfonamide, <b>261</b> .....	422
6.12.25.	<i>(R)</i> - <i>N</i> -(2-Methoxy-5-(7-((4-(3-methyloxetan-3-yl)morpholin-2-yl)methoxy)-1,3-dihydroisobenzofuran-5-yl)pyridin-3-yl)- <i>N</i> -(4-methoxybenzyl)methanesulfonamide, <b>262</b> .....	423
6.12.26.	<i>(R)</i> - <i>N</i> -(2-Methoxy-5-(7-((4-(3-methyloxetan-3-yl)morpholin-2-yl)methoxy)-1,3-dihydroisobenzofuran-5-yl)pyridin-3-yl)methanesulfonamide, <b>248</b> .....	425
6.13.	References .....	426
<b>7.</b>	<b>Appendix</b> .....	427

## Acknowledgements

Firstly, I would very much like to thank my supervisors Professor Jonathan Percy and Dr Vipulkumar Patel for all their help and guidance throughout my PhD studies; their support has been invaluable.

I would like to thank the IKK2 and PI3K $\delta$  project leaders, Dr Vipulkumar Patel and Dr Nicole Hamblin, and everyone else involved in the projects: Paul Cox, Paul Gore, Santu Mandal, Aoife Maxwell, Charlotte Smith, Ian Smith, Jessica Renaux, Lee Thorp and Emily Wix for their chemistry input on the IKK2 project and Ken Down, Craig Donoghue, Julia Hyslop, Michael James, Stefano Livia, Scott MacDougall, Camille Metier, Martin Peek and Etienne Schmitt for their chemistry input on the PI3K $\delta$  project. I would also like to thank Toni Lewis, Fiona Lucas, James Rowedder, Sarah Smith, Dan Thomas, Gareth Wayne and the many other scientists involved in compound screening and profiling. My thanks go to Chris Edwards, Rosal Khoury and Dave Mallett for their DMPK work; Nick Barton, Paul Bamborough, Gianpaolo Bravi, Xiao Lewell, Paul Rowland, and Alan Hill and Klara Valko for their computational and structural chemistry and physchem expertise. Thanks also go to Andy Craven for chemistry outsourcing and Richard Briers, Eric Hortense, Sean Lynn, Martin Read, Steve Richards and Richard Upton for their analytical expertise.

I would like to thank those involved throughout the preparation of my thesis; thank you to Richard Horan, John Pritchard and Eric Talbot for their advice and Amanda Gladwin, Gavin Fowler and Judith Pritchard from Corporate Intellectual Property for reading over the copies of my thesis.

I would like to give thanks to Dr Harry Kelly and Professor William Kerr for providing me with the opportunity to further my education and I would like to thank Dr Edith Hessel, Dave Allen and Dr Patrick Vallance for their support of my studies.

Throughout my PhD studies I have also had great support from my friends and family so I would also like to thank them all.

## Abstract

Signal transduction pathways involving kinases are implicated in inflammatory airway diseases. The modulation of two kinases, IKK2 and PI3K $\delta$ , was explored for the treatment of airway diseases such as asthma and Chronic Obstructive Pulmonary Disease. Small molecule inhibitors of IKK2 and PI3K $\delta$  were designed using a variety of drug design strategies.

A Hansch analysis was carried out to investigate the quantitative structure-activity relationships of a series of 3,5-substituted indole carboxamide compounds. This led to the design and synthesis of a set of novel IKK2 inhibitors. Ligand efficiency was used to focus on compounds with the optimal combination of physicochemical and pharmacological properties and 3-cyano-substituted indole carboxamides were discovered as ligand efficient inhibitors of IKK2.

Homology modelling and knowledge from the contemporary medicinal chemistry literature aided the design of an alternative 3-position substituent and this led to the challenging syntheses of IKK2 inhibitors incorporating the 3-oxetanyl group. The chemistries explored led to the discovery of a novel oxazole formation from primary amides and 3-oxetanone, which represented a highly competitive method for formation of these heteroarenes.

Structure-based drug design was utilised to design a series of PI3K $\delta$  inhibitors. 4-Substituted dihydroisobenzofurans were synthesised and conformational analyses showed that potent PI3K $\delta$  inhibitors bound to the enzyme in low energy conformations. Crystal structures of the inhibitor-enzyme complexes identified additional interactions required for PI3K $\delta$  potency and selectivity over related PI3Ks. Amides or ethers based on the 4-(dihydroisobenzofuranyl) core were preferred; however the oral PK profile of the compounds required optimisation. Strategies to reduce metabolic clearance were implemented, including reducing lipophilicity and incorporating metabolically stable groups. A set of compounds were synthesised and analysis of the data showed that lipophilicity was not a good predictor of metabolic clearance. However, the *in vitro* microsomal stability assay effectively predicted *in vivo* clearance and will now be used routinely as a screen for future compounds.

From this optimisation work, a PI3K $\delta$  inhibitor with a superior oral drug profile and significantly reduced predicted once-daily human dose was discovered.

## Abbreviations

°	Degree
°C	Degree Celsius
2-MeTHF	2-Methyltetrahydrofuran
6-31G*	Valence double-zeta polarized basis set
6HIS	Hexahistidine
Å	Ångstrom
ABL	V-abl Abelson murine leukemia viral oncogene homolog 1
Ac	Acetyl
ACD	Advanced chemistry development
ACR	American College of Rheumatology
ADMET	Absorption, distribution, metabolism, elimination and toxicity
AHR	Airway hyperresponsiveness
AIBN	Azobisisobutyronitrile
Akt	V-akt murine thymoma viral oncogene homolog 1
Ala	Alanine
AML	Acute myeloid leukemia
AMP	Artificial membrane permeability
AO	Aldehyde oxidase
APC	Allophycocyanin
app	Apparent
aq	Aqueous
#Ar	Number of aromatic rings
Ar	Aryl
Arg	Arginine
Asn	Asparagine

Asp	Aspartic acid
ATM	Ataxia–telangiectasia mutated
ATP	Adenosine triphosphate
ATR	Ataxia–telangiectasia related
ax	Axial
B-cell	Bone marrow lymphocytes
BCR	Breakpoint cluster region gene
BEH	Ethylene bridged hybrid
Boc	<i>tert</i> -Butyloxycarbonyl
Boc <sub>2</sub> O	Di- <i>tert</i> -butyl dicarbonate
br	Broad
BSA	Bovine serum albumin
Bu	<i>n</i> -Butyl
C	Molar concentration
Caco-2	Human epithelial colorectal adenocarcinoma cells
calc.	Calculated
cAMP	Cyclic adenosine monophosphate
cChromlogD <sub>pH7.4</sub>	Calculated log(distribution coefficient) using the Chromatographic LogD model v5
CDK-2	Cyclin-dependent kinase 2
cDNA	Complementary DNA
CHAPS	3-[(3-Cholamidopropyl)dimethylammonio]-1-propanesulfonate
c-Kit	Mast/stem cell growth factor receptor
Cl <sub>b</sub>	Blood clearance
CLL	Chronic lymphocytic leukemia
CLND	Chemiluminescence nitrogen detector
clogP	Calculated log(partition coefficient) using the Biobyte



	(Daylight) calculation method
cm <sup>-1</sup>	Wavenumber
CMBP	Cyanomethylenetriethylphosphorane
CNS	Central nervous system
COPD	Chronic obstructive pulmonary disease
CXCR2	Chemokine (C-X-C motif) receptor 2
CYP	Cytochrome p450
Cys	Cysteine
cysLT	Cysteinyl-leukotriene
d	Doublet
Da	Dalton
DAG	Diacylglycerol
DAST	Diethylaminosulfur trifluoride
dba	Dibenzylideneacetone
DCM	Dichloromethane
DEAD	Diethyl azodicarboxylate
DGK	Diacylglycerol kinase
DIBAL-H	<i>Diisobutylaluminium</i> hydride
DIPEA	<i>Diisopropylethylamine</i>
DMA	Dimethylacetamide
DMAP	4-Dimethylaminopyridine
DMC	Dimethyl carbonate
DMEM	Dulbecco's modified Eagle's medium
DMF	<i>N,N</i> -Dimethylformamide
DMP	Dess-Martin periodinane
DMPK	Drug metabolism and pharmacokinetics
DMSO	Dimethylsulfoxide
DNA	Deoxyribonucleic acid

DNA-PK	DNA-dependent protein kinase
dppf	1,1'- <i>Bis</i> (diphenylphosphino)ferrocene
DTT	Dithiothreitol
EDTA	Ethylenediaminetetraacetic acid
EGFR	Epidermal growth factor receptor
eq.	Equivalents
eq	Equatorial
ESI	Electrospray ionisation
Et	Ethyl
<i>et al.</i>	et alii
Et <sub>2</sub> O	Diethyl ether
EtOAc	Ethyl acetate
EtOH	Ethanol
EU	European Union
F	Bioavailability
F	Field constant
FassiF	Fasted state simulated intestinal fluid
FDA	US Food and Drug Administration
FT-IR	Fourier transform infrared spectroscopy
g	Gram
G	Gibbs free energy
GHz	GigaHertz
Gln	Glutamine
Glu	Glutamic acid
Gly	Glycine
GPCR	G-protein coupled receptor
GRP-1	General receptor for phosphoinositides isoform 1
GST	Glutathione S-transferase

h	Hour
HAC	Heavy atom count
HATU	2-(7-Aza-1 <i>H</i> -benzotriazol-1-yl)-1,1,3,3-tetramethyluronium hexafluorophosphate
HBA	Hydrogen bond acceptor
HBD	Hydrogen bond donor
hCl <sub>int</sub>	Intrinsic clearance in human liver microsomes
HEPES	2-[4-(2-Hydroxyethyl)piperazin-1-yl]ethanesulfonic acid
HER2	Human epidermal growth factor receptor 2
hERG	Human-Ether-à-go-go related gene
HF	Hartree-Fock
His	Histidine
HIV	Human immunodeficiency virus
HLB	Hydrophilic lipid balanced
HLM	Human liver microsomes
HMBC	Heteronuclear multiple bond correlation
HMPA	Hexamethylphosphoramide
HPLC	High performance liquid chromatography
HR	High resolution
HRMS	High resolution mass spectrometry
HRV	Human rhinovirus
HSA	Human serum albumin
hTNF $\alpha$	Human tumor necrosis factor alpha
HTRF	Homogeneous time resolved fluorescence
HWB	Human whole blood
HWE	Horner-Wadsworth-Emmons
Hz	Hertz
IC <sub>50</sub>	Half maximal inhibitory concentration

ICS	Inhaled corticosteroid
IFN $\gamma$	Interferon gamma
IgE	Immunoglobulin E
IKK	I $\kappa$ B kinase
IKK1/IKK $\alpha$	I $\kappa$ B kinase 1/ $\alpha$
IKK2 /IKK $\beta$	I $\kappa$ B kinase 2/ $\beta$
IKK $\gamma$	I $\kappa$ B kinase $\gamma$
IL-1 $\beta$	Interleukin 1 $\beta$
Ile	Isoleucine
IPA	<i>Isopropanol</i>
<i>i</i> -Pr	<i>Isopropyl</i>
IspE	4-Diphosphocytidyl-2-C-methyl-D-erythritol kinase
IVC	<i>In vitro</i> clearance
IVIVE	<i>In vitro-in vivo</i> extrapolation
I $\kappa$ B	Inhibitor of kappa B
I $\kappa$ B $\alpha$	Inhibitor of kappa B $\alpha$
<i>J</i>	Coupling constant Hertz
JAK	Janus kinase
K	Kelvin
KCa	Ca <sup>2+</sup> -dependent K <sup>+</sup>
kcal mol <sup>-1</sup>	Kilocalories per mole
kDa	Kilodalton
K <sub>i</sub>	Inhibitor constant
K <sub>m</sub>	Michaelis constant
L	Litre
LABA	Long acting $\beta_2$ -agonist
LAMA	Long-acting muscarinic antagonist
LBF	Liver Blood Flow

---

LCMS	Liquid chromatography-mass spectrometry
LE	Ligand efficiency
Leu	Leucine
LLE	Lipophilic ligand efficiency
ln	Natural logarithm
log	Logarithm
logD <sub>pH</sub>	log(distribution coefficient)
logP	log(partition coefficient)
LPS	Lipopolysaccharide
LTB4	Leukotriene B4
Lys	Lysine
m	Multiplet
M	Molarity
[M-H] <sup>+</sup>	Positive molecular ion
[M-H] <sup>-</sup>	Negative molecular ion
MAO	Monoamine oxidases
MAP	Mitogen-activated protein
MAP2K	Mitogen-activated protein kinase kinase
MAPK	Mitogen-activated protein kinase
MAPKAPK2	MAP kinase-activated protein kinase 2
MBI	Mechanism-based inhibition
mChromlogD <sub>pH7.4</sub>	log(distribution coefficient) at pH 7.4 measured chromatographically
mChromlogP	log(partition coefficient) measured chromatographically
mCPBA	<i>meta</i> -Chloroperoxybenzoic acid
MDAP	Mass-directed autoperative chromatography
MDCK	Madin-Darby canine kidney
Me	Methyl

MeCN	Acetonitrile
MEK1	Dual specificity mitogen-activated protein kinase kinase 1
MEK2	Dual specificity mitogen-activated protein kinase kinase 2
MeOH	Methanol
Met	Methionine
mg	Milligram
MHz	Megahertz
MIDA	<i>N</i> -Methyliminodiacetic acid
min	Minutes
mL	Millilitre
mM	Millimolar
mmHg	Millimeter of mercury
mmol	Millimole
mol	Mole
MP2	Møller–Plesset perturbation theory to second order
MR (aliphatic)	Molar refractivity (aliphatic)
MR (aromatic)	Molar refractivity (aromatic)
mRNA	Messenger ribonucleic acid
MS	Mass spectrometry
Ms	Mesyl
MSD	Mesoscale Discovery
mTOR	Mammalian target of rapamycin
MW	Molecular weight
N	Number of test occasions
NBS	<i>N</i> -Bromosuccinimide
<i>n</i> -Bu	Butyl
NCS	<i>N</i> -Chlorosuccinimide
NEMO	NF- $\kappa$ B essential modulator

NF- $\kappa$ B	Nuclear factor kappa-B
NIS	<i>N</i> -Iodosuccinimide
NK	Natural killer
nM	Nanomolar
nm/s	Nanometres per second
NMR	Nuclear magnetic resonance
Nu	Nucleophile
OW	Octanol/water
PA	Phosphatidic acid
PBPK	Physiological based pharmacokinetic
PBS	Phosphate buffered saline
PDB	Protein data bank
PDE	Phosphodiesterase
PDE4	Phosphodiesterase type 4
PDK1	Phosphoinositide-dependent kinase-1
PES	Potential energy surface
PFI	Property forecast index
Ph	Phenyl
pH	Decimal logarithm of the reciprocal of the hydrogen ion activity in a solution
PH	Pleckstrin homology
Phe	Phenylalanine
PI3K	Phosphoinositide 3-kinases
PI4K	Phosphoinositide 4-kinases
pIC <sub>50</sub>	$-\log(\text{IC}_{50})$
PIKAP	PI3K $\gamma$ adaptor protein of 87 kDa
PIKK	PI3K-related kinase
pin	Pinacolato

PIP2	Phosphatidylinositol (4,5)-bisphosphate
PIP3	Phosphatidylinositol (3,4,5)-trisphosphate
PK	Pharmacokinetics
$pK_a$	Acid dissociation constant at logarithmic scale
PKB	Protein Kinase B
$pK_{BHX}$	Hydrogen bond complexation constant at logarithmic scale
$pK_i$	$-\log(K_i)$
pM	Picomolar
PMB	<i>para</i> -Methoxybenzyl
ppm	Parts per million
Pro	Proline
PtdIns	Phosphatidylinositol
PtdIns(3)P	Phosphatidylinositol-3-phosphate
PtdIns(3,4)P <sub>2</sub>	Phosphatidylinositol-3,4-bisphosphate
PtdIns(3,4,5)P <sub>3</sub>	Phosphatidylinositol-3,4,5-trisphosphate
PtdIns(4)P	Phosphatidylinositol-4-phosphate
PtdIns(4,5)P <sub>2</sub>	Phosphatidylinositol-4,5-bisphosphate
PTEN	Phosphatase and tensin homolog
<i>p</i> TSA	<i>para</i> -Toluenesulfonic acid monohydrate
py	Pyridine
PyBop	Benzotriazol-1-yl-oxytripyrrolidinophosphonium hexafluorophosphate
QSAR	Quantitative structure-activity relationships
quant	Quantitative
R	Ideal gas constant
R	Resonance constant
R <sup>2</sup>	Coefficient of determination



rpm	Revolutions per minute
RPMI	Roswell Park Memorial Institute medium
rt	Room temperature
R <sub>t</sub>	Retention time
s	Singlet
SABA	Short acting $\beta_2$ -agonist
SAR	Structure-activity relationships
SCX	Strong cation exchanger
SDD	Scaffold/dimerisation domain
Ser	Serine
SGF	Simulated gastric fluid
SH-2	Src Homology 2
SHIP1	SH-2 domain-containing inositol phosphatase 1
SHIP2	SH-2 domain-containing inositol phosphatase 2
SLE	Systemic lupus erythematosus
SMG-1	Suppressor of morphogenesis in genitalia-1
S <sub>N</sub> 2	Bi-molecular nucleophilic substitution
sol	Solubility
SPhos <sup>®</sup>	2-Dicyclohexylphosphino-2',6'-dimethoxybiphenyl
STAB	Sodium triacetoxyborohydride
STAT	Signal transducers and activators of transcription
Strep	Streptomycin
Syk	Spleen tyrosine kinase
T	Temperature
t	Triplet
t <sub>1/2</sub>	Half-life
T3P	2,4,6-Tripropyl-1,3,5,2,4,6-trioxatriphosphorinane- 2,4,6-trioxide

TBAF	Tetrabutylammonium fluoride
TBAT	Tetrabutylammonium triphenyldifluorosilicate
TBK1	Tank-binding kinase 1
TBME	<i>tert</i> -Butyl methyl ether
<i>t</i> -Bu	<i>tert</i> -Butyl
T-cell	Thymus lymphocyte
TDI	Time-dependent inhibition
Tf	Triflyl (trifluoromethyl sulfonyl)
TFA	Trifluoroacetic acid
TFAA	Trifluoroacetic anhydride
T <sub>H</sub> 2-cell	T Helper cell
THF	Tetrahydrofuran
Thr	Threonine
TIMS	Tool for interactive monomer selection
TMS	Trimethylsilyl
TNF $\alpha$	Tumor necrosis factor alpha
TPSA	Polar surface area
TR-FRET	Time-resolved fluorescence energy transfer
Trp	Tryptophan
TRRAP	Transformation/transcription domain associated protein
Ts	Tosyl
TYK	Tyrosine kinase
Tyr	Tyrosine
UB	Ubiquitin
UGT	Uridine glucuronosyl transferases
ULD	Ubiquitin-like domain
UPLC	Ultra performance liquid chromatography
US	United States

---

UV	Ultraviolet
v/v	Volume/volume
Val	Valine
V <sub>dss</sub>	Volume of Distribution
VerloopB1	Steric parameter (width)
VerloopB2	Steric parameter (width)
VerloopB3	Steric parameter (width)
VerloopB4	Steric parameter (width)
VerloopL	Steric parameter (length)
Vps34	Vacuolar protein sorting mutant 34 protein
w/v	Weight/volume
w/w	Weight/weight
WHO	World Health Organisation
wrt	With regard to
Xantphos <sup>®</sup>	4,5-Bis(diphenylphosphino)-9,9-dimethylxanthene
XPhos <sup>®</sup>	2-Dicyclohexylphosphino-2',4',6'-triisopropylbiphenyl
δ	NMR chemical shift in ppm downfield from a standard (tetramethylsilane)
μg	Microgram
μL	Microlitre
μM	Micromolar
μwave	Microwave
π (aliphatic)	Lipophilicity (aliphatic)
π (aromatic)	Lipophilicity (aromatic)
σ*	Polar substituent constant
σ <sub>m</sub>	Hammett <i>meta</i> -substituent constant
σ <sub>p</sub>	Hammett <i>para</i> -substituent constant
τ	Torsion Angle

# **Chapter 1**

## **Emerging Mechanisms and Therapies for the Treatment of Inflammatory Airway Diseases**

## **1.1. Inflammatory Airway Diseases**

### **1.1.1. Asthma and Chronic Obstructive Pulmonary Disease (COPD)**

Asthma and chronic obstructive pulmonary disease (COPD) are diseases characterised by airway obstruction, which is variable and reversible in asthma but progressive and often irreversible in COPD.<sup>1</sup> Both diseases involve chronic inflammation of the respiratory tract mediated by the increased expression of inflammatory proteins. Acute episodes or exacerbations, where the intensity of inflammation is increased, are also experienced in both diseases.<sup>1</sup>

Asthma affects over 300 million people worldwide.<sup>2</sup> Although mortality is rare, asthma patients are extensive users of health care systems throughout the world, for example the annual economic cost for asthma patient care is around \$20 billion in the United States alone.<sup>2</sup>

Asthma is a complex syndrome where allergen exposure leads to chronic inflammation, mucus production, bronchoconstriction and airway hyperresponsiveness (AHR) (Figure 1.1.1). This often induces intermittent attacks of breathlessness, wheezing and coughing.<sup>2</sup>

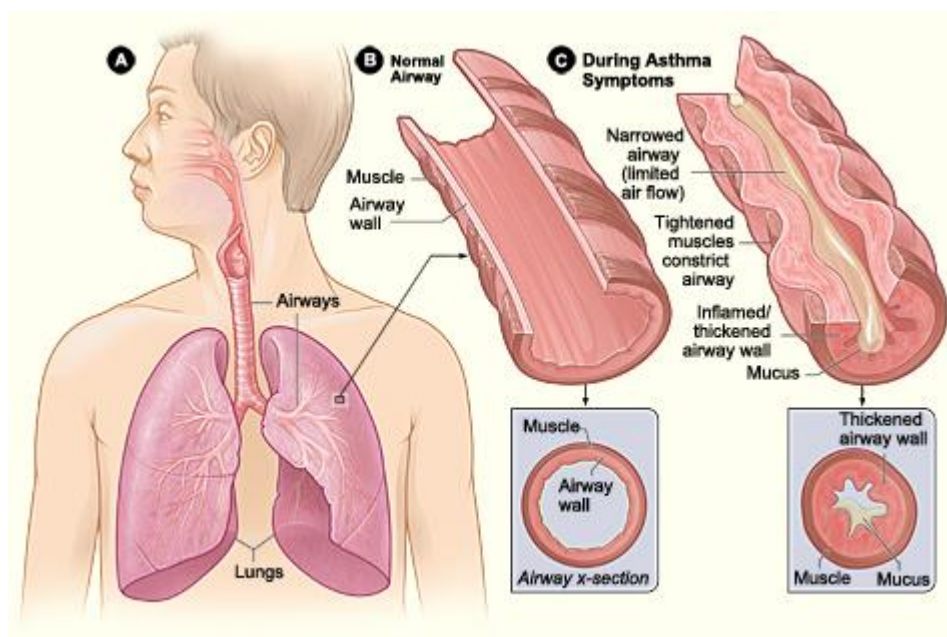


Figure 1.1.1. Changes to the airway anatomy during asthma symptoms.<sup>3</sup>

The mechanism of allergic asthma involves the presentation of allergens that enter the respiratory tract to T helper 2 cells (T<sub>H</sub>2-cells), which drive the generation of IgE antibodies.<sup>4</sup> Most patients with asthma are atopic (genetically predisposed to produce IgE antibodies in serum).<sup>4</sup> Atopic (extrinsic) asthma can be triggered by the inhalation of allergens such as pollen, animal dander and dust mites. A few patients are non-atopic (intrinsic asthma) and their symptoms are triggered by factors not related to allergies, for example anxiety, exercise, smoke or other irritants. Patients with intrinsic asthma often have a more severe form of the disease and clinicians have defined different asthma phenotypes based on severity.<sup>5</sup> Severe asthma is often characterised by specific features such as propensity for exacerbations or lower lung function. Almost all patients with asthma will have at least one moderate-to-severe exacerbation; however some patients are predisposed to very severe, frequent exacerbations.<sup>5</sup> Risk factors for severe exacerbators include an early age of asthma onset, being of African origin and having psychological disorders such as depression.<sup>5</sup> Another subset of severe asthma includes asthma patients who have chronic airflow restriction but who do not necessarily have exacerbation-prone

disease. The main risk factor for progressive loss of lung function is an early age of childhood-onset asthma.<sup>5</sup> Approximately 5-10% of patients have severe asthma and are poorly treated at present. These patients have increased mortality compared to those with mild-moderate asthma and possess some of the characteristics of Chronic Obstructive Pulmonary Disease (COPD).<sup>6</sup>

COPD is a leading cause of increased mortality rates throughout the world, with approximately 65 million people having moderate to severe COPD and the percentage of deaths caused by COPD projected by the World Health Organisation (WHO) to increase by more than 30% over the next 10 years.<sup>7</sup>

COPD is characterised by airflow limitation that is not fully reversible.<sup>8</sup> The chronic airflow characteristic of COPD is caused by a combination of small airway disease (chronic bronchitis) and emphysema (parenchymal destruction).<sup>8</sup> The pathologic changes associated with COPD are a result of these co-existing diseases of the lungs and are found in much of the lung vasculature and airways. The inflammation associated with chronic bronchitis is located in the epithelium of the central airway and causes increased production of mucus, as well as thickening of the bronchial walls (Figure 1.1.2).<sup>9</sup> Alongside this inflammation, emphysematous destruction of the lungs' elastic recoil force means the tissues necessary to support the shape and function of the lungs are destroyed (Figure 1.1.2).<sup>9</sup> These pathologic changes lead to symptoms such as a long-term cough with mucus, shortness of breath and chest tightness.

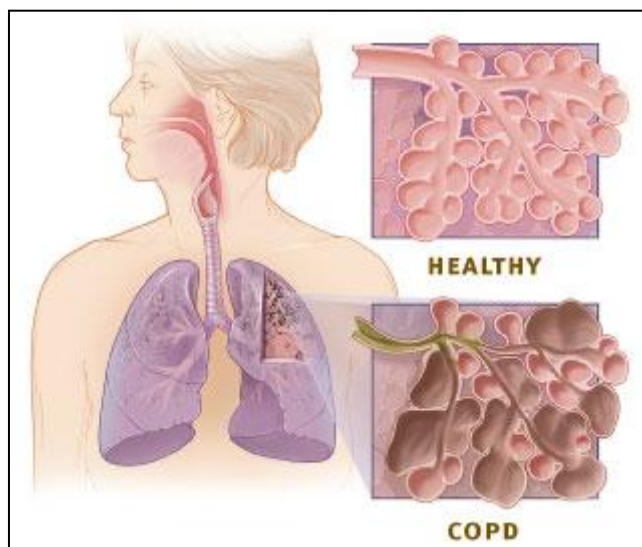


Figure 1.1.2. Differences in the airway anatomy between a healthy lung and one with COPD - airways become thicker than normal and mucus production increases. The floppy airways are obstructed, making it difficult to get air out of the lungs.<sup>10</sup>

The clinical manifestations of COPD are not just restricted to pulmonary inflammation and structural remodelling; there are also extrapulmonary effects. Systemic inflammation leads to additional clinical manifestations such as muscle wasting and weight loss, fatigue, depression and cardiac disease.<sup>11</sup>

Alongside the symptoms associated with pulmonary inflammation and the additional systemic effects, it is also possible for a patient to experience an exacerbation of COPD, where a sudden worsening of the symptoms occurs and lasts for several days. This is the most common cause of hospital admissions for patients with COPD and severe exacerbations are associated with a high risk of death, with a mortality rate of 10-30% during hospital admission and 40-60% in the year following admission.<sup>12</sup>

The inflammation of the respiratory tract in COPD patients is an amplification of the normal inflammatory response to common irritants such as cigarette smoke.<sup>8</sup> Smoking is therefore the major risk factor in the development of COPD, with 10-20% of smokers developing clinically significant COPD.<sup>13</sup> Other



risk factors include air pollution, prolonged exposure to dust and chemicals or genetic factors, principally the deficiency of  $\alpha_1$  antitrypsin, a glycoprotein with antiprotease activity, which leads to accelerated development of COPD.<sup>13</sup>

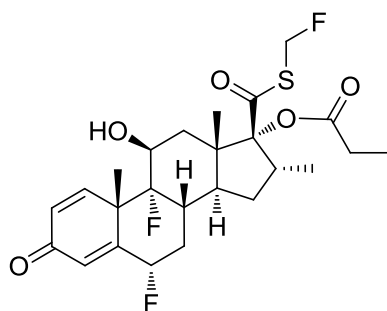
At present, COPD is poorly treated. There is no current cure and no therapies have been shown to slow progression of the disease. Since cigarette smoking is the major cause of COPD, overcoming nicotine addiction and the cessation of smoking is the only therapeutic intervention that has been proven to reduce disease progression.<sup>14</sup>

Although some of the clinical features of asthma and COPD are similar there are differences in the pattern of inflammation that occurs in the respiratory tract; different inflammatory cells, mediators and responses to therapy.<sup>1</sup> In addition, inflammation in asthma predominantly involves the large airways, whereas in COPD the small airways and lung parenchyma are primarily affected. However, patients with severe asthma often have airway inflammation more similar to that seen in patients with COPD and COPD patients can often have similar inflammatory changes in their larger airways to those of individuals with asthma.<sup>1</sup> Asthma and COPD do respond differently to anti-inflammatory drug therapies, however many of the established treatments are the same for both diseases.

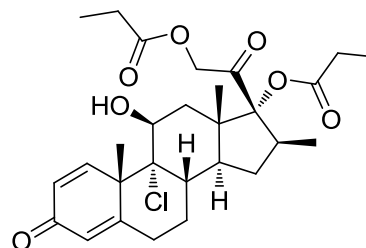
### **1.1.2. Established Therapies for the Treatment of Asthma and COPD.**

Inhaled corticosteroids (ICSs) revolutionised the treatment of asthma, giving control of symptoms and reductions in hospitalisations and mortality.<sup>1</sup> T<sub>H</sub>2-cell mediated inflammation in asthmatic airways is suppressed by corticosteroids through the inhibition of the expression of inflammatory cytokines.<sup>4</sup> Corticosteroids have to be taken by inhalation; they diffuse across the cell membrane in the lung and interact with glucocorticoid receptors in the cytoplasm.<sup>4</sup> These receptors are thereby activated and translocate to the nucleus, where several different mechanisms lead to

the modulation of the transcriptional activity of target genes.<sup>4</sup> Examples of ICSs include fluticasone propionate (Flovent<sup>®</sup>/Flixotide<sup>®</sup>) and beclomethasone dipropionate (Clenil<sup>®</sup>).



Fluticasone propionate

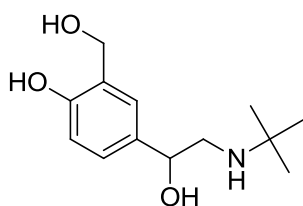


Beclomethasone dipropionate

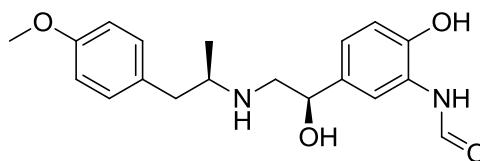
Corticosteroids are the most common control therapy for asthma but are largely ineffective in virus-induced exacerbations, asthmatics who smoke and patients with severe asthma.<sup>4</sup> Other drawbacks to this therapy are the potential for a patient to develop corticosteroid resistance and the fact that ICSs have to be absorbed from the lungs and may have systemic side effects. In addition, oral medications are often preferred by patients and may offer advantages in patient compliance.<sup>15</sup> ICSs are now widely used in high doses to treat COPD patients; however they have been shown to provide little benefit and fail to reduce disease progression or mortality.

Bronchodilators are the main therapy for the treatment of COPD and are also used for the rapid relief of asthma symptoms.<sup>4,16</sup> Inhaled short-acting  $\beta_2$ -agonists (SABAs), for example Salbutamol (Ventolin<sup>®</sup>),<sup>17</sup> are used to give immediate relief to COPD symptoms because they have rapid onset of action and help relax airway smooth muscle and decrease airway resistance. This occurs after binding of the agonist to the  $\beta_2$ -adrenoreceptor, whereupon the production of cyclic adenosine 3'5'-monophosphate (cAMP) is increased.<sup>4</sup> This leads to smooth muscle relaxation by opening  $\text{Ca}^{2+}$ -dependent  $\text{K}^+$  (KCa) channels, which relieves bronchoconstriction.<sup>4</sup>

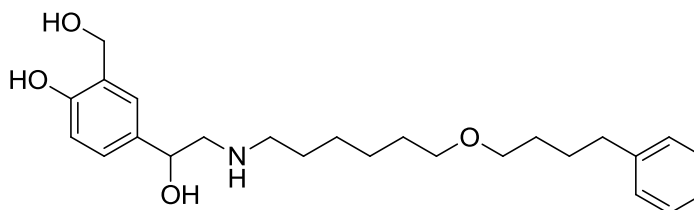
Long-acting  $\beta_2$ -agonists (LABAs) such as Formoterol and Salmeterol are now the preferred treatment as they have a longer duration of action.



Salbutamol

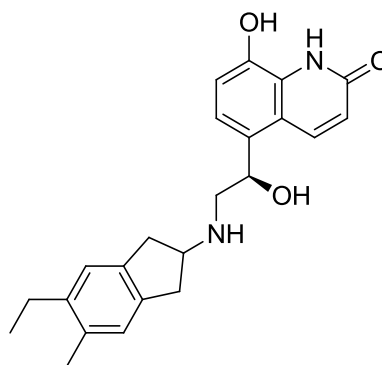


Formoterol



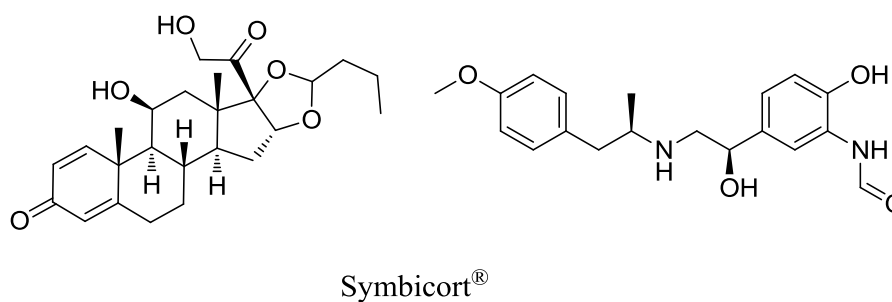
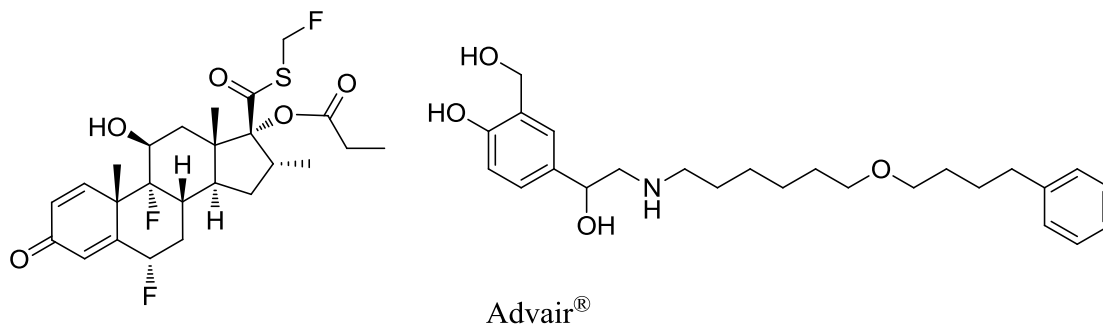
Salmeterol

Once daily LABAs are an emerging class of medicines for the treatment of COPD as they can provide sustained bronchodilation and help to improve compliance. Indacaterol is the first once-daily  $\beta_2$ -agonist for the treatment of COPD as it has shown 24 hour duration of bronchodilation and fast onset of action, with improved lung function being observed compared with placebo and other long-acting bronchodilators.<sup>18</sup>

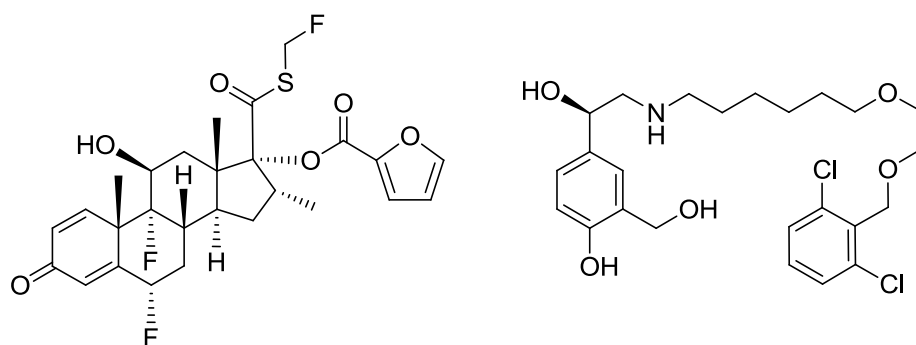


Indacaterol

Combinations of ICSs and LABAs are preferred for the treatment of asthma since monotherapy with a LABA is not recommended as it can mask worsening inflammation in asthma.<sup>4</sup> Examples include Advair<sup>®</sup>/Seretide<sup>®</sup> (fluticasone propionate/salmeterol)<sup>19</sup> and Symbicort<sup>®</sup> (budesonide/formoterol fumarate dehydrate).<sup>20</sup>

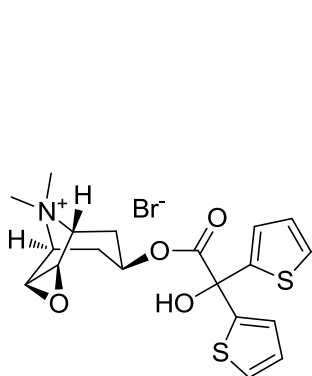


ICS/LABA combinations have also been approved by the FDA for the treatment of COPD, most recently Breo<sup>®</sup>/Relvar<sup>®</sup> in April 2013. This combination of fluticasone furoate and the novel once-daily LABA Vilanterol will also be used to treat COPD patients with a history of exacerbations.<sup>21,22</sup>

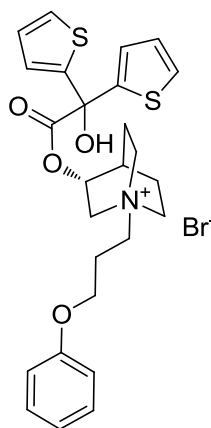


Breo<sup>®</sup>/Relvar<sup>®</sup>

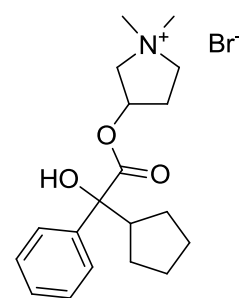
Other bronchodilatory drugs include anticholinergics (also known as long-acting muscarinic antagonists, LAMAs), which block the muscarinic acetylcholine receptors in the bronchial smooth muscle, leading to a reduction in smooth muscle contraction and mucus secretion.<sup>23</sup> The first LAMA discovered, Tiotropium Bromide, was shown to be a once-daily inhaled treatment that led to a significant improvement in a COPD patient's quality of life as well as reducing their susceptibility for exacerbations.<sup>24</sup> Novel LAMAs such as Acclidinium Bromide and Glycopyrrolate have recently been discovered and are currently in advanced clinical development.<sup>23</sup>



Tiotropium Bromide



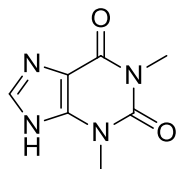
Acclidinium Bromide



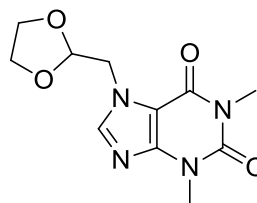
Glycopyrrolate

Since there is an additive effect between LABA and LAMA, LABA-LAMA combinations and single molecules that link a muscarinic antagonist to a  $\beta_2$ -agonist are also in clinical development. It has also been suggested that a triple therapy (ICS/LABA/LAMA) may be useful in patients with severe COPD and asthma, although combining three drugs in one inhaler and ensuring the duration of action for all the components is greater than 24 h remain significant challenges.<sup>25</sup>

Another class of bronchodilator are xanthines, such as theophylline or doxofylline. These are most often used to treat severe COPD as these drugs have a narrow therapeutic index and serious side effects such as nausea, cardiac arrhythmias and convulsions.<sup>26</sup>

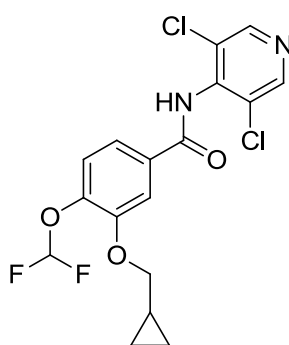


Theophylline

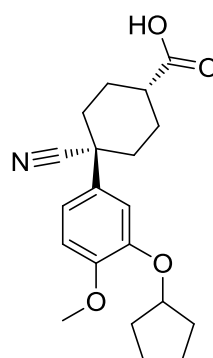


Doxofylline

These xanthines are weak, non-selective phosphodiesterase (PDE) inhibitors that prevent the degradation of cAMP. It has been suggested that theophylline also has a weak anti-inflammatory effect; however selective inhibitors of PDE4, the predominant family of PDEs in inflammatory cells, have been shown to be much more effective at suppressing a wide range of inflammatory effects.<sup>27</sup> Roflumilast (Daliresp<sup>®</sup>/Daxas<sup>®</sup>) and Cilomilast are examples of inhibitors of PDE4.



Roflumilast



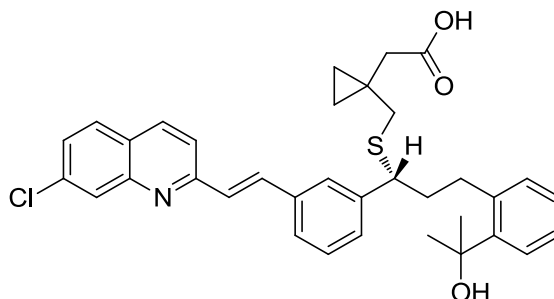
Cilomilast

Roflumilast is marketed for selected COPD patients with severe disease and frequent exacerbations; it improved lung function and reduced exacerbations in COPD patients in a 12 month clinical trial.<sup>28</sup> Cilomilast is currently in advanced clinical development for the treatment of COPD; an improvement in lung function and a reduction in symptoms were observed in a 6-week study of patients with moderate to severe COPD.<sup>29</sup>

PDE4 inhibitors may have anti-inflammatory effects also relevant to asthma. Studies with Roflumilast have shown that it may have some efficacy in reducing responses to allergen and improving lung function in asthmatic patients after long-term dosing.<sup>30</sup> Roflumilast and Cilomilast are dosed orally so this could be considered an advantage for the treatment of asthma; however a shortcoming of PDE4 inhibitors is that their therapeutic advantages may be outweighed by potential adverse effects such as nausea, gastrointestinal upset and headaches, which are also mediated by PDE4 inhibition.<sup>16</sup>

Another oral drug that is marketed for the treatment of asthma is Montelukast (Singulair<sup>®</sup>), a cysteinyl-leukotriene (cysLT) receptor-1 antagonist.<sup>31</sup> The production of cysLTs is increased in asthmatics and anti-leukotrienes, such as Montelukast, inhibit several bronchoconstrictor challenges, for example allergen, exercise and irritants.<sup>32</sup> They represent a different class of anti-asthmatics; however they are less effective than ICSs and do not represent a suitable alternative therapy for the treatment of mild, persistent asthma.<sup>32</sup> They are also unsuitable as add-on therapies

to ICSs and hence are not predicted to have a major impact in asthma therapy. In addition, there is no evidence that cysLTs are implicated in COPD.<sup>32</sup>



Montelukast

It is becoming increasingly important to discover drugs that suppress inflammation in different ways to those exploited by established therapies, which often have significant shortcomings. Accordingly, targeting the complex signal transduction pathways involved in chronic inflammation is being investigated as a novel approach for the treatment of inflammatory airway diseases such as asthma and COPD.<sup>33</sup>

## 1.2. Emerging Mechanisms for the Treatment of Inflammatory Airway Diseases

The same signal transduction pathways are often involved in the regulation of several inflammatory processes and are relevant in many cell types; therefore drugs that modulate these pathways are of interest.<sup>33</sup> Inflammatory signals activate cell surface receptors, which in turn activate signal transduction pathways that involve cascades of kinases (Figure 1.2.1).<sup>33</sup> These kinases may activate transcription factors that regulate inflammatory genes, hence signal transduction modulators that inhibit these processes may prevent inflammation. When considering this approach, it is important to target pathways in specific cell types that are only activated in the



inflammatory disease in order to avoid adverse side effects due to lack of specificity.<sup>33</sup>

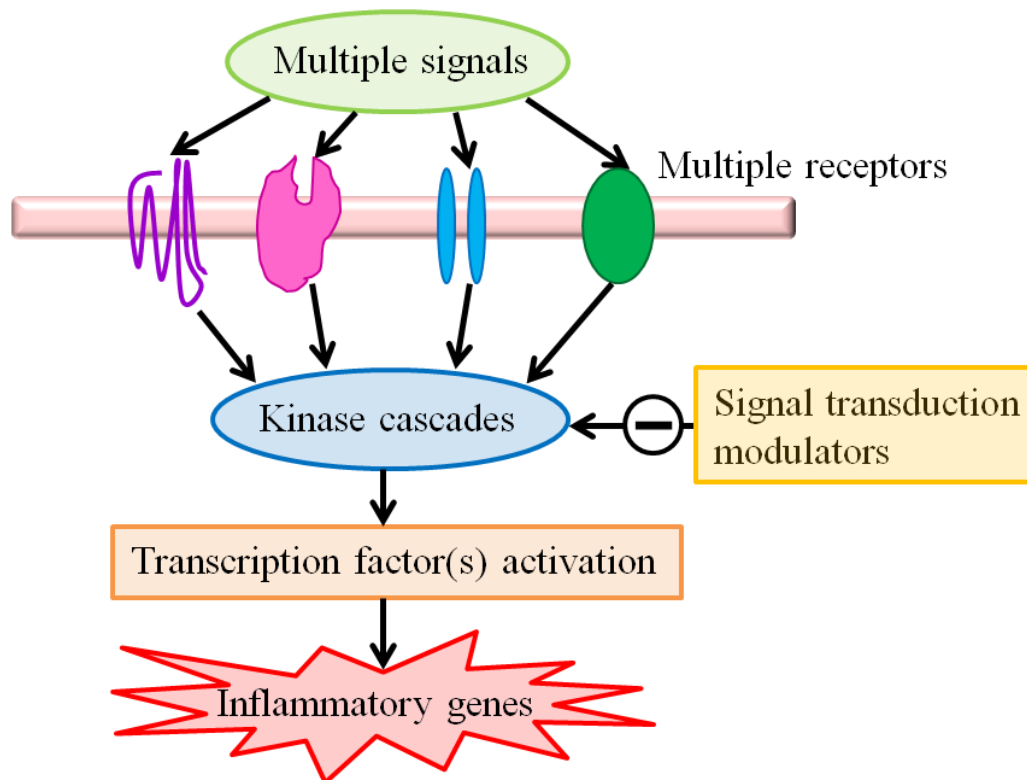


Figure 1.2.1. Signal transduction pathways involved in inflammation.<sup>33</sup>

PDE4 inhibitors are the most advanced treatments in this category; however other approaches such as kinase and transcription factor inhibition have yielded molecules that are currently in clinical development, although there is yet to be such a drug approved for use in the clinic.

### 1.2.1. Kinase Inhibitors

Kinases modify substrates by chemically adding a phosphate group from adenosine triphosphate (ATP) and it is this phosphorylation event that controls many cellular processes.<sup>34</sup> Kinases can be divided into classes based upon their substrate, for example proteins, lipids and carbohydrates. The human kinome contains an

estimated 518 protein kinases, the largest group of kinases that constitutes approximately 2% of all human genes.<sup>35</sup>

Kinase inhibitors that modulate cell signalling pathways are of considerable interest for the development of novel drugs. As there are many kinase targets for the treatment of inflammatory disorders, strategies to develop low molecular weight inhibitors of kinases are needed. Often structure-based drug design can be used as the three-dimensional structure of the protein target can be obtained through X-ray crystallography or NMR spectroscopy. At present there are approximately 2600 protein kinase crystal structures deposited in the Protein Data Bank (PDB) that can be used for structure-based drug design,<sup>36</sup> although it is likely that pharmaceutical companies have many more structures available internally.

The first protein kinase crystal structure was solved for cyclic adenosine monophosphate-dependent protein kinase in 1991.<sup>37</sup> This structure provided a template for all other protein kinases, which share a conserved ATP-binding site where the fold of the kinase core and the positioning of key residues at the active site are maintained across the protein family. The core typically consists of two lobes, the *N*-terminal small lobe and the *C*-terminal large lobe, which provide a cleft that forms the active site or hinge-binding region (Figure 1.2.2).<sup>38</sup>

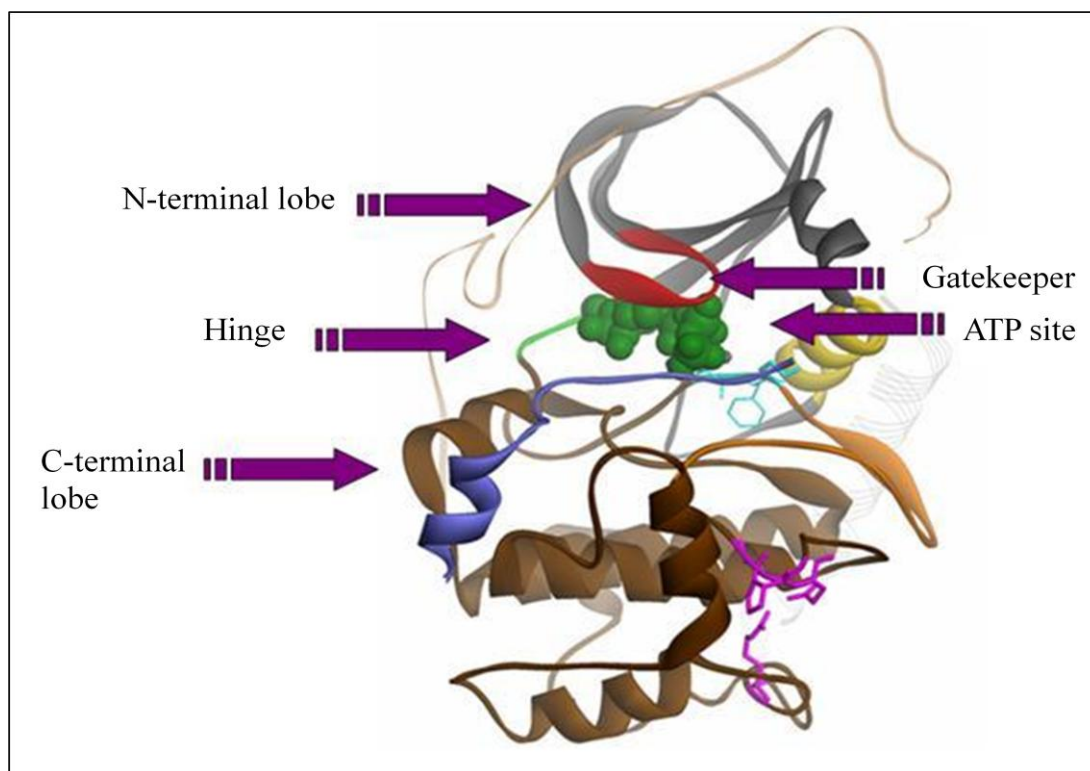


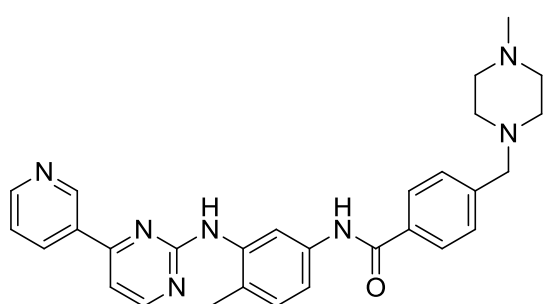
Figure 1.2.2. General architecture of the protein kinase catalytic core with a bound inhibitor (green).<sup>38</sup>

It is this region that accommodates ATP and where nearly all kinase inhibitors bind. The gatekeeper is the first residue of the hinge connecting the C- and N-terminal lobes and the nature of the side chain residue controls the size and shape of the back cavity, which is mostly hydrophobic and is not accessed by ATP.<sup>39</sup> Similarities in the ATP-binding sites of kinases and the millimolar ATP concentrations present in cells make it difficult to develop potent and selective kinase inhibitors.<sup>40</sup>

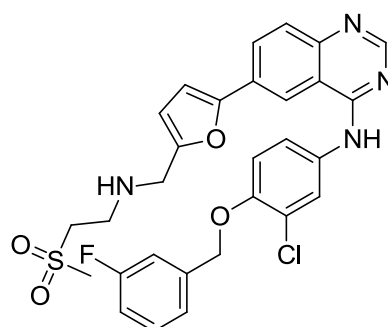
Many kinase targets have been associated with inflammatory disease; however there is only one kinase inhibitor currently in the clinic (Tofacitinib for the treatment of rheumatoid arthritis). There are currently no approved kinase inhibitors for the treatment of inflammatory airway disease. The challenge in developing kinase

inhibitors for the treatment of inflammatory diseases comes from the requirement for highly selective inhibitors to ensure the risk of undesired side effects is minimal.

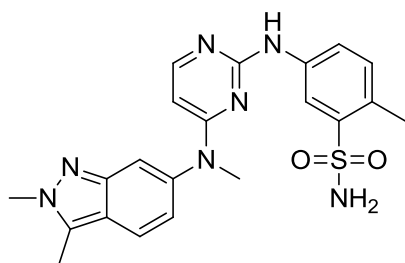
Most early kinase inhibitors exhibited poor selectivity between kinases. The first marketed inhibitor, Imatinib (Glivec<sup>®</sup>) had activity against several tyrosine kinases, for example proto-oncogenes c-Kit and BCR-ABL, and was launched in 2001 for the treatment of chronic myelogenous leukemia.<sup>41</sup> Most current marketed kinase inhibitors have applications in oncology since multikinase activity delivers efficacy for treating complex diseases such as cancer. For example, Lapatinib (Tykerb<sup>®</sup>) is a dual targeted tyrosine kinase inhibitor that prevents the activity of two oncogenes, EGFR and HER2, and has been approved for the treatment of breast cancer.<sup>42</sup> Pazopanib (Votrient<sup>®</sup>) is also a multi-targeted tyrosine kinase inhibitor for the treatment of renal cell carcinoma and, most recently, Trametinib (Mekinist<sup>®</sup>), which inhibits the mitogen-activated protein kinase kinase (MAP2K) enzymes MEK1 and MEK2, has been approved for the treatment of melanoma.<sup>43,44</sup>



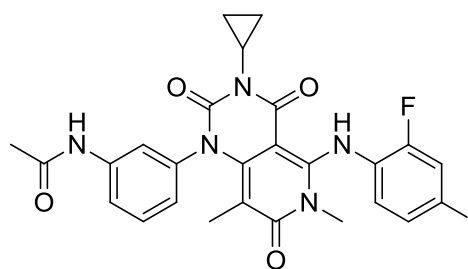
Imatinib



Lapatinib

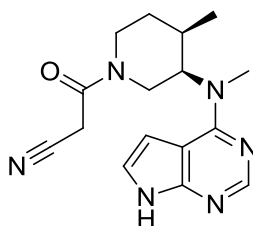


Pazopanib



Trametinib

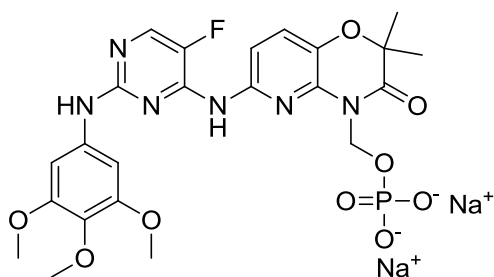
The only kinase target where inhibitors have been approved for the treatment of inflammatory disorders is the JAK family of non-receptor tyrosine kinases. This is made up of four members (JAK1, JAK2, JAK3 and TYK2), which are key mediators of cytokine signalling events. Cytokine receptors have no catalytic kinase activity and rely on the JAKs to activate downstream proteins, therefore, when a cytokine binds to its receptor, the resulting conformational change leads to activation of members of the JAK family through phosphorylation of specific tyrosine residues.<sup>45</sup> These sites can then recruit signal transducers and activators of transcription (STATs) which also become phosphorylated on a single tyrosine residue. The activated STATs then dissociate, dimerise and translocate to the nucleus where they modulate the expression of selected genes.<sup>45</sup> Inhibiting this pathway has been shown to prevent the production of pro-inflammatory cytokines and display immunosuppressant activity.<sup>46,47</sup> The JAK3 inhibitor Tofacitinib (Xeljanz<sup>®</sup>) was approved for the treatment of rheumatoid arthritis in November 2012 and is also progressing in clinical development for the treatment of psoriasis and inflammatory bowel disease.<sup>48</sup> Interestingly, this JAK3 inhibitor has recently been shown to inhibit eosinophilia in a mouse model of allergic pulmonary inflammation, therefore indicating its potential as a therapy for the treatment of conditions associated with airway eosinophilia, such as asthma or rhinitis.<sup>49</sup>



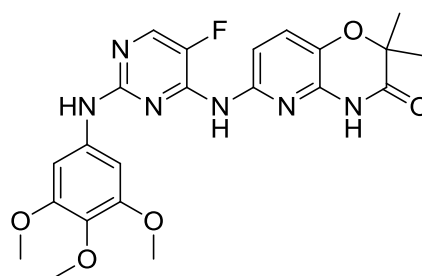
Tofacitinib

Another non-receptor tyrosine kinase that has been implicated in inflammatory disorders is Syk. Syk plays a key role in intracellular signalling in the inflammatory response, mainly in the transmission of signals within B-cells. B-cells are antigen-presenting cells that provide the signals necessary for T-cell activation,

and it is T-cells that produce pro-inflammatory cytokines.<sup>50</sup> B-cells have emerged to be critical in the pathogenesis of rheumatoid arthritis and the most advanced Syk inhibitor Fostamatinib, which is a pro-drug of Tamatinib, is currently in Phase II clinical trials for the treatment of rheumatoid arthritis.<sup>51</sup>



Fostamatinib

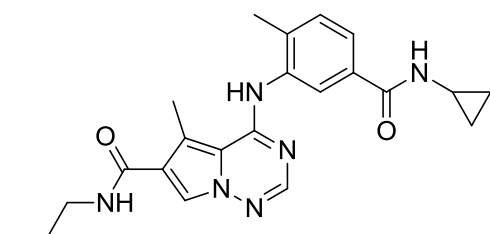


Tamatinib

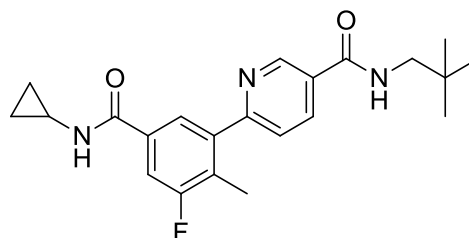
Syk is also an attractive target for the treatment of inflammatory lung disorders as it has recently been described in non-immune cells such as the airway epithelium.<sup>52</sup> Studies have shown Syk to mediate human rhinovirus (HRV) entry in epithelial cells and, since HRV incites exacerbations in asthma and COPD, targeting Syk could provide effective treatment for these diseases.<sup>52</sup>

The MAP kinases are activated downstream of Syk, hence they have also been targeted by small molecule kinase inhibitors for the treatment of inflammatory disorders. MAPK is activated by pro-inflammatory stimuli, such as cytokines or LPS, and the resulting signalling cascades lead to strong immune responses.<sup>53</sup> p38 MAP kinases are a class within this family whose inhibition with small molecules resulted in the downregulation of pro-inflammatory cytokines and prompted interest in them as anti-inflammatory targets.<sup>54</sup> Although a number of p38 $\alpha/\beta$  inhibitors have progressed into clinical development, many of the earlier examples showed liver and CNS toxicity at therapeutic doses.<sup>55</sup> This may be due to the fact that many other cellular functions are regulated by signalling through p38 $\alpha$ ; however there is no evidence of the observed toxicities being linked specifically to p38 inhibition. There has therefore been substantial effort in developing very selective p38 inhibitors but the desired efficacy is yet to be achieved. The most promising results have been seen

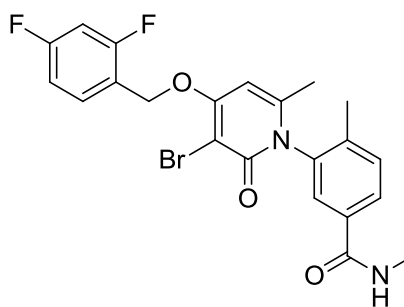
with BMS-582949, which is in Phase II clinical trials for the treatment of rheumatoid arthritis and has shown an ACR20 response significantly greater than placebo,<sup>56</sup> that is a 20% reduction in the number of swollen or tender joints and a 20% reduction in at least three of five other core measures set by the American College of Rheumatology.<sup>57</sup> p38 inhibitors that are in development for the treatment of COPD include Losmapimod and PH-797804.<sup>58,59</sup> A recent study with Losmapimod in COPD patients showed that it was well tolerated over a 12 week period with no undesired side effects.<sup>60</sup> There were no significant effects on lung function but a reduction in plasma fibrinogen, which is often present in elevated amounts in COPD, was observed.<sup>60</sup>



BMS-582949



Losmapimod



PH-797804

Other kinases that are implicated in inflammatory disease are the I $\kappa$ B kinases (IKKs) and the phosphoinositide-3-kinases (PI3Ks).

The IKKs are specific kinases that are important for the activation of NF- $\kappa$ B by inflammatory stimuli. NF- $\kappa$ B was first classified as a DNA-binding protein that targets a sequence in the immunoglobulin  $\kappa$  light chain enhancer and is restricted to

occurrence in B cells.<sup>61</sup> Since this early work, NF- $\kappa$ B proteins have been identified in the cytoplasm of many other cell types and their dysregulation is associated with many disease states, in particular those relating to inflammation.<sup>62</sup> Inhibition of one isoenzyme of the IKKs, IKK2 or IKK $\beta$ , has been exploited as an approach to inhibiting this transcription factor. Other approaches include inhibiting NF- $\kappa$ B-inducing kinase (NIK) and I $\kappa$ B ubiquitin ligase, which both regulate the activity of NF- $\kappa$ B.<sup>33</sup>

The PI3Ks are a family of enzymes that lead to the generation of lipid second messengers that regulate a number of cellular events through activation of the serine/threonine protein kinases Akt (also known as protein kinase B) and mTOR.<sup>63</sup> The phosphorylation of these serine/threonine kinases promotes cell growth, survival and proliferation. The PI3K/Akt/mTOR pathway is an intracellular signalling pathway that is activated in cancers and is also implicated in inflammatory disease.<sup>64,65</sup>

The development of small-molecule inhibitors of IKK2 and PI3K $\delta$ , a single isoenzyme of the PI3K family, represent potential approaches for the treatment of inflammatory airway disease and will be discussed further in Chapters 3 and 4.

In summary, it is recognised that several kinases involved in the activation of pro-inflammatory transcription factors and increased expression of inflammatory genes represent emerging mechanisms for the treatment of airway diseases such as asthma and COPD (Figure 1.2.3).



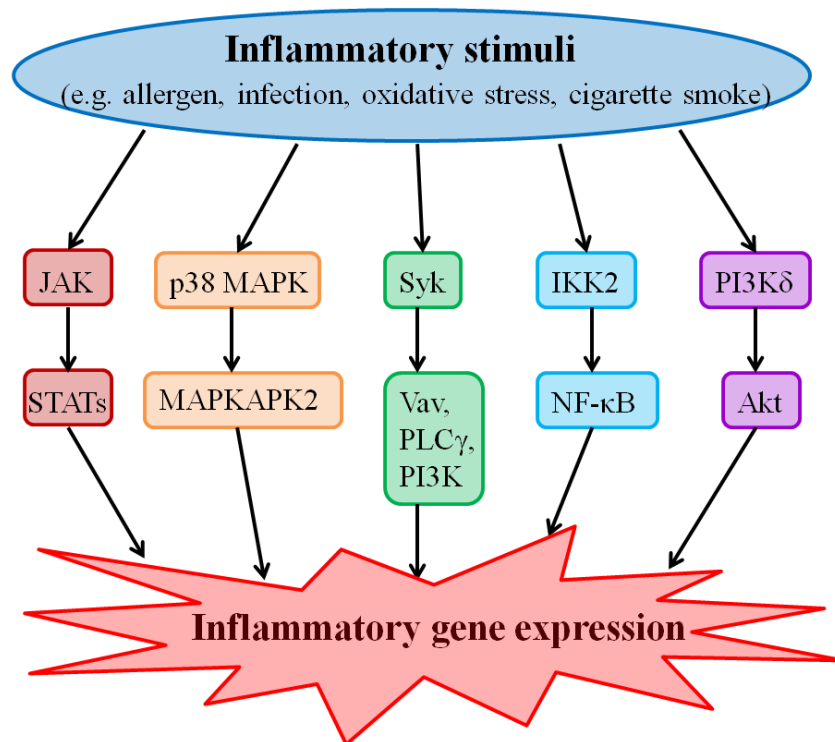


Figure 1.2.3. Kinases involved in inflammation.

## 1.3. References

- (1) Barnes, P. J. *Nat. Rev. Immunol.* **2008**, *8*, 183-192.
- (2) Locksley, R. M. *Cell* **2010**, *140*, 777-783.
- (3) <http://www.nhlbi.nih.gov/health/health-topics/topics/asthma/>, accessed on 16th August 2013.
- (4) Holgate, S. T.; Polosa, R. *Nat. Rev. Immunol.* **2008**, *8*, 218-230.
- (5) Wenzel, S. E. *Lancet* **2006**, *368*, 804-813.
- (6) Holgate, S. T.; Polosa, R. *Lancet* **2006**, *368*, 780-793.
- (7) <http://www.who.int/mediacentre/factsheets/fs315/en/index.html>, accessed on 16th August 2013.
- (8) Rabe, K. F.; Hurd, S.; Anzueto, A.; Barnes, P. J.; Buist, S. A.; Calverley, P.; Fukuchi, Y.; Jenkins, C.; Rodriguez-Roisin, R.; van Weel, C.; Zielinski, J. *Am. J. Respir. Crit. Care Med.* **2007**, *176*, 532-555.
- (9) Hogg, J. C. *Lancet* **2004**, *364*, 709-721.
- (10) <http://www.nhlbi.nih.gov/health/public/lung/copd/campaign-materials/html/copd-patient.htm>, accessed on 16th August 2013.
- (11) Decramer, M.; De Benedetto, F.; Del Ponte, A.; Marinari, S. *Respir. Med.* **2005**, *99 Suppl. 2*, S3-10.
- (12) Anto, J. M.; Vermeire, P.; Vestbo, J.; Sunyer, J. *Eur. Respir. J.* **2001**, *17*, 982-994.
- (13) Devereux, G. *BMJ* **2006**, *332*, 1142-1144.
- (14) Barnes, P.; Hansel, T. *Lancet* **2004**, *364*, 985-996.
- (15) Barnes, P. J. *Semin. Respir. Crit. Care Med.* **2012**, *33*, 685-694.
- (16) Barnes, P. J. *Curr. Med. Chem.* **2013**, *20*, 1531-1540.
- (17) <http://www.ventolin.com>, accessed on 16th August 2013.
- (18) Dahl, R.; Chung Kian, F.; Buhl, R.; Magnussen, H.; Nonikov, V.; Jack, D.; Bleasdale, P.; Owen, R.; Higgins, M.; Kramer, B. *Thorax* **2010**, *65*, 473-479.
- (19) <http://www.advair.com>, accessed on 16th August 2013.
- (20) <http://copd.symbicort.com/>, accessed on 16th August 2013.

- (21) Procopiou, P. A.; Barrett, V. J.; Bevan, N. J.; Biggadike, K.; Box, P. C.; Butchers, P. R.; Coe, D. M.; Conroy, R.; Emmons, A.; Ford, A. J.; Holmes, D. S.; Horsley, H.; Kerr, F.; Li-Kwai-Cheung, A.-M.; Looker, B. E.; Mann, I. S.; McLay, I. M.; Morrison, V. S.; Mutch, P. J.; Smith, C. E.; Tomlin, P. J. *Med. Chem.* **2010**, *53*, 4522-4530.
- (22) <http://www.reuters.com/article/2013/04/17/us-glaxosmithkline-theravance-idUSBRE93G0YQ20130417?type=companyNews>, accessed on 16th August 2013.
- (23) Joos, G. F. *Expert Opin. Invest. Drugs* **2010**, *19*, 257-264.
- (24) Tashkin, D. P.; Celli, B.; Senn, S.; Burkhart, D.; Kesten, S.; Menjoge, S.; Decramer, M. N. *Engl. J. Med.* **2008**, *359*, 1543-1554.
- (25) Barnes, P. J. *Expert Rev. Respir. Med.* **2011**, *5*, 297-300.
- (26) Shukla, D.; Chakraborty, S.; Singh, S.; Mishra, B. *Expert Opin. Pharmacother.* **2009**, *10*, 2343-2356.
- (27) Boswell-Smith, V.; Cazzola, M.; Page, C. P. *J. Allergy Clin. Immunol.* **2006**, *117*, 1237-1243.
- (28) Calverley, P. M. A.; Rabe, K. F.; Goehring, U.-M.; Kristiansen, S.; Fabbri, L. M.; Martinez, F. J. *Lancet* **2009**, *374*, 685-694.
- (29) Compton, C. H.; Gubb, J.; Nieman, R.; Edelson, J.; Amit, O.; Bakst, A.; Ayres, J. G.; Creemers, J. P. H. M.; Schultze-Werninghaus, G.; Brambilla, C.; Barnes, N. C. *Lancet* **2001**, *358*, 265-270.
- (30) Lipworth, B. J. *Lancet* **2005**, *365*, 167-175.
- (31) Jarvis, B.; Markham, A. *Drugs* **2000**, *59*, 891-928.
- (32) Barnes, P. J. *Curr. Opin. Pharmacol.* **2003**, *3*, 257-263.
- (33) Barnes, P. J. *Pharmacol. Ther.* **2006**, *109*, 238-245.
- (34) Manning, G.; Plowman, G. D.; Hunter, T.; Sudarsanam, S. *Trends Biochem. Sci.* **2002**, *27*, 514-520.
- (35) Manning, G.; Whyte, D. B.; Martinez, R.; Hunter, T.; Sudarsanam, S. *Science* **2002**, *298*, 1912-1916 and 1933-1934.
- (36) <http://www.pdb.org>, accessed on 16th August 2013.

- (37) Knighton, D. R.; Zheng, J.; Ten Eyck, L. F.; Ashford, V. A.; Nguyen Huu, X.; Taylor, S. S.; Sowadski, J. M. *Science* **1991**, *253*, 407-414.
- (38) Bamborough, P.; GlaxoSmithKline: 2009, unpublished results.
- (39) Zuccotto, F.; Ardini, E.; Casale, E.; Angiolini, M. *J. Med. Chem.* **2010**, *53*, 2681-2694.
- (40) Cohen, P.; Alessi, D. R. *ACS Chem. Biol.* **2013**, *8*, 96-104.
- (41) Deininger, M. W. N.; Druker, B. J. *Pharmacol. Rev.* **2003**, *55*, 401-423.
- (42) Nelson, M. H.; Dolder, C. R. *Ann. Pharmacother.* **2006**, *40*, 261-269.
- (43) Bukowski, R. M.; Yasothan, U.; Kirkpatrick, P. *Nat. Rev. Drug Discovery* **2010**, *9*, 17-18.
- (44) <http://www.reuters.com/article/2013/05/30/us-glaxosmithkline-approvals-idUSBRE94S1A020130530>, accessed on 16th August 2013.
- (45) Kisseleva, T.; Bhattacharya, S.; Braunstein, J.; Schindler, C. W. *Gene* **2002**, *285*, 1-24.
- (46) Ghoreschi, K.; Jesson, M. I.; Li, X.; Lee, J. L.; Ghosh, S.; Alsup, J. W.; Warner, J. D.; Tanaka, M.; Steward-Tharp, S. M.; Gadina, M.; Thomas, C. J.; Minnerly, J. C.; Storer, C. E.; LaBranche, T. P.; Radi, Z. A.; Dowty, M. E.; Head, R. D.; Meyer, D. M.; Kishore, N.; O'Shea, J. J. *J. Immunol.* **2011**, *186*, 4234-4243.
- (47) Changelian, P. S.; Flanagan, M. E.; Ball, D. J.; Kent, C. R.; Magnuson, K. S.; Martin, W. H.; Rizzuti, B. J.; Sawyer, P. S.; Perry, B. D.; Brissette, W. H.; McCurdy, S. P.; Kudlacz, E. M.; Conklyn, M. J.; Elliott, E. A.; Koslov, E. R.; Fisher, M. B.; Strelevitz, T. J.; Yoon, K.; Whipple, D. A.; Sun, J.; Munchhof, M. J.; Doty, J. L.; Casavant, J. M.; Blumenkopf, T. A.; Hines, M.; Brown, M. F.; Lillie, B. M.; Subramanyam, C.; Chang, S.-P.; Milici, A. J.; Beckius, G. E.; Moyer, J. D.; Su, C.; Woodworth, T. G.; Gaweco, A. S.; Beals, C. R.; Littman, B. H.; Fisher, D. A.; Smith, J. F.; Zagouras, P.; Magna, H. A.; Saltarelli, M. J.; Johnson, K. S.; Nelms, L. F.; Des Etages, S. G.; Hayes, L. S.; Kawabata, T. T.; Finco-Kent, D.; Baker, D. L.; Larson, M.; Si, M.-S.;

- Paniagua, R.; Higgins, J.; Holm, B.; Reitz, B.; Zhou, Y.-J.; Morris, R. E.; O'Shea, J. J.; Borie, D. C. *Science* **2003**, *302*, 875-878.
- (48) Garber, K. *Nat. Biotechnol.* **2013**, *31*, 3-4.
- (49) Kudlacz, E.; Conklyn, M.; Andresen, C.; Whitney-Pickett, C.; Changelian, P. *Eur. J. Pharmacol.* **2008**, *582*, 154-161.
- (50) Currie, K. S. *Annu. Rep. Med. Chem.* **2010**, *45*, 175-190.
- (51) Genovese, M. C.; Kavanaugh, A.; Weinblatt, M. E.; Peterfy, C.; DiCarlo, J.; White, M. L.; O'Brien, M.; Grossbard, E. B.; Magilavy, D. B. *Arthritis Rheum.* **2011**, *63*, 337-345.
- (52) Sanderson, M. P.; Lau, C. W.; Schnapp, A.; Chow, C.-W. *Inflammation Allergy: Drug Targets* **2009**, *8*, 87-95.
- (53) Chang, L.; Karin, M. *Nature* **2001**, *410*, 37-40.
- (54) Lee, J. C.; Laydon, J. T.; McDonnell, P. C.; Gallagher, T. F.; Kumar, S.; Green, D.; McNulty, D.; Blumenthal, M. J.; Heyes, J. R. *Nature* **1994**, *372*, 739-746.
- (55) Zhang, J.; Shen, B.; Lin, A. *Trends Pharmacol. Sci.* **2007**, *28*, 286-295.
- (56) Genovese, M. C.; Gao, L.; Yin, J.; Smith, S.; Weinblatt, M. E.; Smolen, J. S.; Wang, X. In *Arthritis Rheum.* 2010; Vol. 62 Suppl. 10, p 1119.
- (57) Felson, D. T.; Anderson, J. J.; Boers, M.; Bombardier, C.; Furst, D.; Goldsmith, C.; Katz, L. M.; Lightfoot, R., Jr.; Paulus, H.; Strand, V. *Arthritis Rheum.* **1995**, *38*, 727-735.
- (58) Aston, N. M.; Bamborough, P.; Buckton, J. B.; Edwards, C. D.; Holmes, D. S.; Jones, K. L.; Patel, V. K.; Smee, P. A.; Somers, D. O.; Vitulli, G.; Walker, A. L. *J. Med. Chem.* **2009**, *52*, 6257-6269.
- (59) Selness, S. R.; Devraj, R. V.; Devadas, B.; Walker, J. K.; Boehm, T. L.; Durley, R. C.; Shieh, H.; Xing, L.; Rucker, P. V.; Jerome, K. D.; Benson, A. G.; Marrufo, L. D.; Madsen, H. M.; Hitchcock, J.; Owen, T. J.; Christie, L.; Promo, M. A.; Hickory, B. S.; Alvira, E.; Naing, W.; Blevis-Bal, R.; Messing, D.; Yang, J.; Mao, M. K.; Yalamanchili, G.; Vonder Embse, R.;

- Hirsch, J.; Saabye, M.; Bonar, S.; Webb, E.; Anderson, G.; Monahan, J. B. *Bioorg. Med. Chem. Lett.* **2011**, *21*, 4066-4071.
- (60) Lomas, D. A.; Lipson, D. A.; Miller, B. E.; Willits, L.; Keene, O.; Barnacle, H.; Barnes, N. C.; Tal-Singer, R. *J. Clin. Pharmacol.* **2012**, *52*, 416-424.
- (61) Sen, R.; Baltimore, D. *Cell* **1986**, *46*, 705-716.
- (62) Kumar, A.; Takada, Y.; Boriek, A. M.; Aggarwal, B. B. *J. Mol. Med.* **2004**, *82*, 434-448.
- (63) Vanhaesebroeck, B.; Stephens, L.; Hawkins, P. *Nat. Rev. Mol. Cell Biol.* **2012**, *13*, 195-203.
- (64) Yap, T. A.; Garrett, M. D.; Walton, M. I.; Raynaud, F.; de Bono, J. S.; Workman, P. *Curr. Opin. Pharmacol.* **2008**, *8*, 393-412.
- (65) Weichhart, T.; Saemann, M. D. *Ann. Rheum. Dis.* **2008**, *67*, iii70-iii74.

## **Chapter 2**

# **Properties of Orally Bioavailable Drugs**

## 2.1. Drug-likeness and the Physicochemical Properties of Oral Drugs

The concept of drug-likeness is fundamental in small molecule drug discovery. The idea that the physicochemical properties of a compound are key to achieving a profile that provides the desired efficacy at an acceptable dose whilst minimising toxicological liabilities has been primarily based on analyses comparing marketed drugs with those compounds that have failed during development.<sup>1</sup> Projects often fail as lead compounds are not developable for their intended indication although there may be other reasons for attrition, for example the biological target may not be relevant to the human disease or there may be commercial or strategic issues. Several studies have linked the likelihood of compounds failing in development to poor ADMET (absorption, distribution, metabolism, elimination and toxicity) properties resulting from increases in fundamental physicochemical properties such as lipophilicity and molecular weight.<sup>2,3</sup>

The importance of lipophilicity on overall compound quality is well-established. Lipophilicity is quantified by octanol/water partition coefficients, measured using octanol/water (OW) shake flask methods.<sup>4</sup> The intrinsic lipophilicity ( $\log P$ ) describes the partition of unionised forms of molecules between octanol and an aqueous buffer and is constant for any given compound.<sup>4</sup> The effective lipophilicity ( $\log D_{\text{pH}}$ ) reflects the distribution of all species present between the phases for a given buffer pH (typically physiological pH, 7.4).<sup>4</sup> A high-throughput chromatographic method is used to measure lipophilicity, where values are derived from the gradient retention time of the compound in reversed phase HPLC and denoted as  $\text{mChromlogP}$  and  $\text{mChromlogD}_{\text{pH}7.4}$ .<sup>5</sup> A positive offset of  $\text{mChromlogD}_{\text{pH}7.4}$  of 2 log units is observed when compared to OW  $\log D_{\text{pH}7.4}$  due to a scaling factor.  $\log P$  and  $\log D$  can also be readily predicted by *in silico* packages, although the available methods will have some degree of error. In this thesis  $\text{clogP}$  is calculated using the Daylight/Biobyte calculation method and  $\text{cChromlogD}_{\text{pH}7.4}$  is



calculated using the Global Chromatographic LogD model v5.<sup>6,7</sup> The majority of literature reports use clogP, which in general correlates well with experimental logP.<sup>8</sup> However, many analyses do not validate the calculated values with measured data and the use of different calculation methods may mean that different data may not be on the same scale. Despite this, the links between surrogate measures of drug-likeness and lipophilicity are well described and are usually comparable across different studies. The importance of lipophilicity on measurable ADMET parameters will be highlighted in subsequent sections, along with other physicochemical properties that affect these ADMET properties.

### **2.1.1. Solubility**

The reduction of logP is desirable for improving solubility and, although ionisation state has a role, high logP compounds with low solubility will still have issues with regards to pH dependent solubility.<sup>2</sup> An analysis of 44,584 compounds at GSK carried out by Gleeson showed the inverse correlation with clogP was strong.<sup>3</sup> While neutral molecules are generally less soluble than those in any other ionisation state, reducing clogP to less than 3 brought the neutral species into the solubility range for ionisable molecules.<sup>3</sup> It has been proposed by Hill and Young that logD should be used preferentially as the descriptor for solubility and that summing  $\text{clogD}_{\text{pH}7.4}$  with the number of aromatic rings (#Ar) provides a readily calculated indicator of the likely solubility category for a molecule.<sup>4</sup> In fact, the effect of the number of aromatic rings on solubility measured by a high-throughput method was much bigger than their contributions to lipophilicity. It was concluded that if  $\text{clogD}_{\text{pH}7.4} + \text{\#Ar}$  is less than 5, the compound has a reasonable chance of having good solubility.<sup>4</sup> Molecular weight is another predictor of solubility that can be readily calculated. As the size of a molecule increases, solubility on average decreases and it has been found that the effects of molecular weight and clogP on solubility are mutually independent.<sup>3</sup>

Using physicochemical properties to predict solubility is valuable for drug design but it is also necessary to have robust methods of measuring a compound's solubility. Aqueous solubility determination using chemiluminescence nitrogen detection (CLND) is used as a high-throughput method for solubility measurements, made by determination of the precipitative solubility from a DMSO solution of the compound that is diluted with buffer at pH 7.4.<sup>9,10</sup> A caveat with this method is that it measures the amount of compound remaining in solution and not the solubility directly from solid. The method also assumes that the standard solution used is made up from exactly 10  $\mu\text{L}$  of a 10 mM DMSO solution of the compound, which may not always be the case. Therefore, this method is most suitable for giving a broad indication of low, moderate or high solubility. The range covered is 1  $\mu\text{M}$  to 500  $\mu\text{M}$  and a compound's solubility is determined as low if below 30  $\mu\text{M}$  and high if greater than 200  $\mu\text{M}$ .

The assessment of solubility in biorelevant dissolution media is often preferred, since the simulation of gastrointestinal conditions is important in predicting the *in vivo* behaviour of drug molecules. Fasted State Small Intestinal Fluid (FaSSIF) is used to simulate fasting conditions in the proximal small intestine.<sup>11</sup> The majority of drug absorption occurs in the duodenum and jejunum where the surface area is largest; there is a large concentration of villi and microvilli that increases the absorptive area.<sup>12</sup> Since this is the area most relevant to drug absorption, solubility is determined in a high-throughput FaSSIF solubility assay, which measures the solubility in this media from solid compound. A caveat with this method is that the solid form of the compound may not have been determined to be crystalline and, since solubility is highly dependent on the crystal form, this method is also most suitable for giving an indication of whether the solubility in FaSSIF is likely to be low or high. Using this method, high FaSSIF solubility is classed as greater than 100  $\mu\text{g/mL}$ .<sup>13</sup> The FaSSIF solubility of 10 known drugs has been determined *via* this method; these drug compounds were commercially available and had literature data in FaSSIF so were being considered as assay standards.<sup>14</sup> An

analysis of the data highlights some of the aforementioned relationships with physicochemical properties, for example lipophilicity and molecular weight.

Figure 2.1.1 shows the relationship between FaSSIF solubility and lipophilicity. It was observed that the most soluble drugs were ionisable compounds but high solubility could also be achieved for neutral species with a clogP less than 3, which is in keeping with the literature observations made by Gleeson.<sup>3</sup>

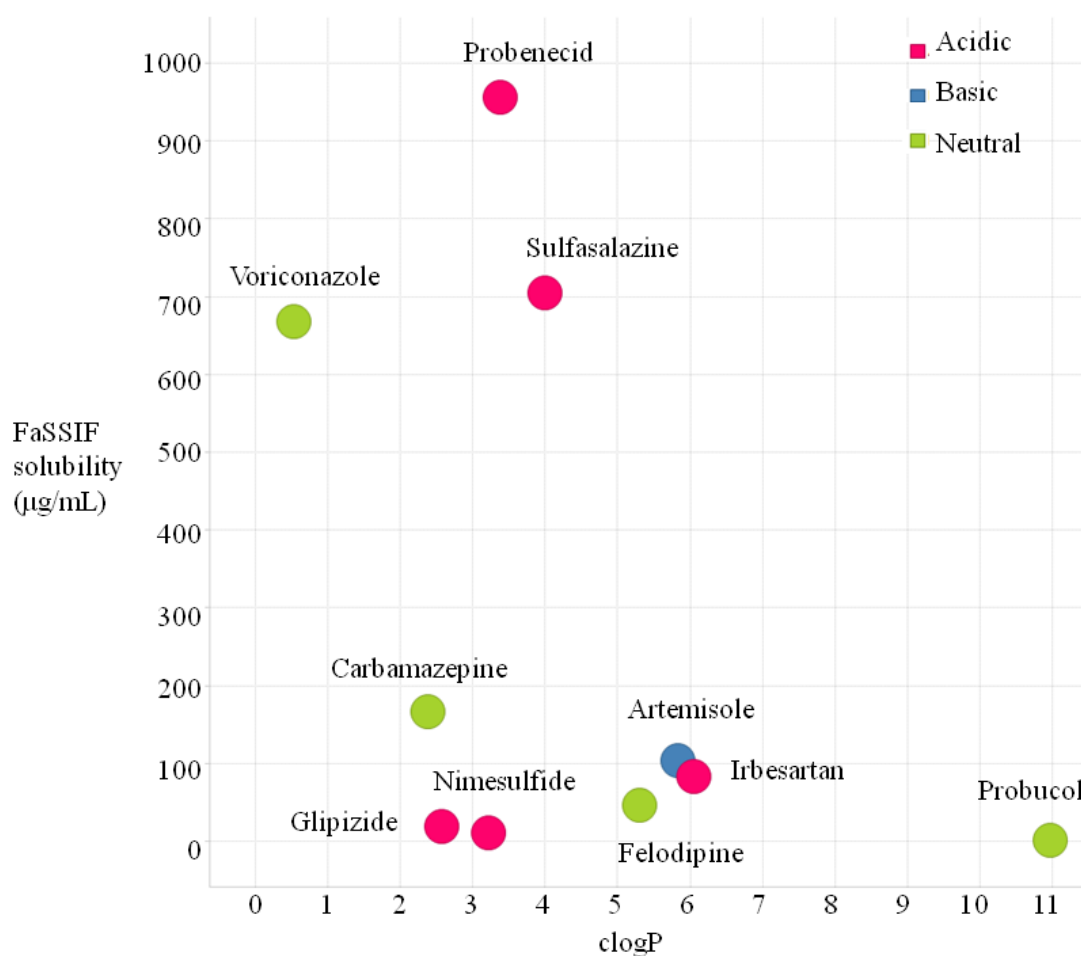


Figure 2.1.1. Measured FaSSIF solubility vs. lipophilicity for 10 known drugs.

The relationship between FaSSIF solubility and molecular weight is shown in Figure 2.1.2 and reflects the trend that solubility is reduced with increased molecular

weights. The most soluble drugs assessed here had molecular weights less than 420 Da.

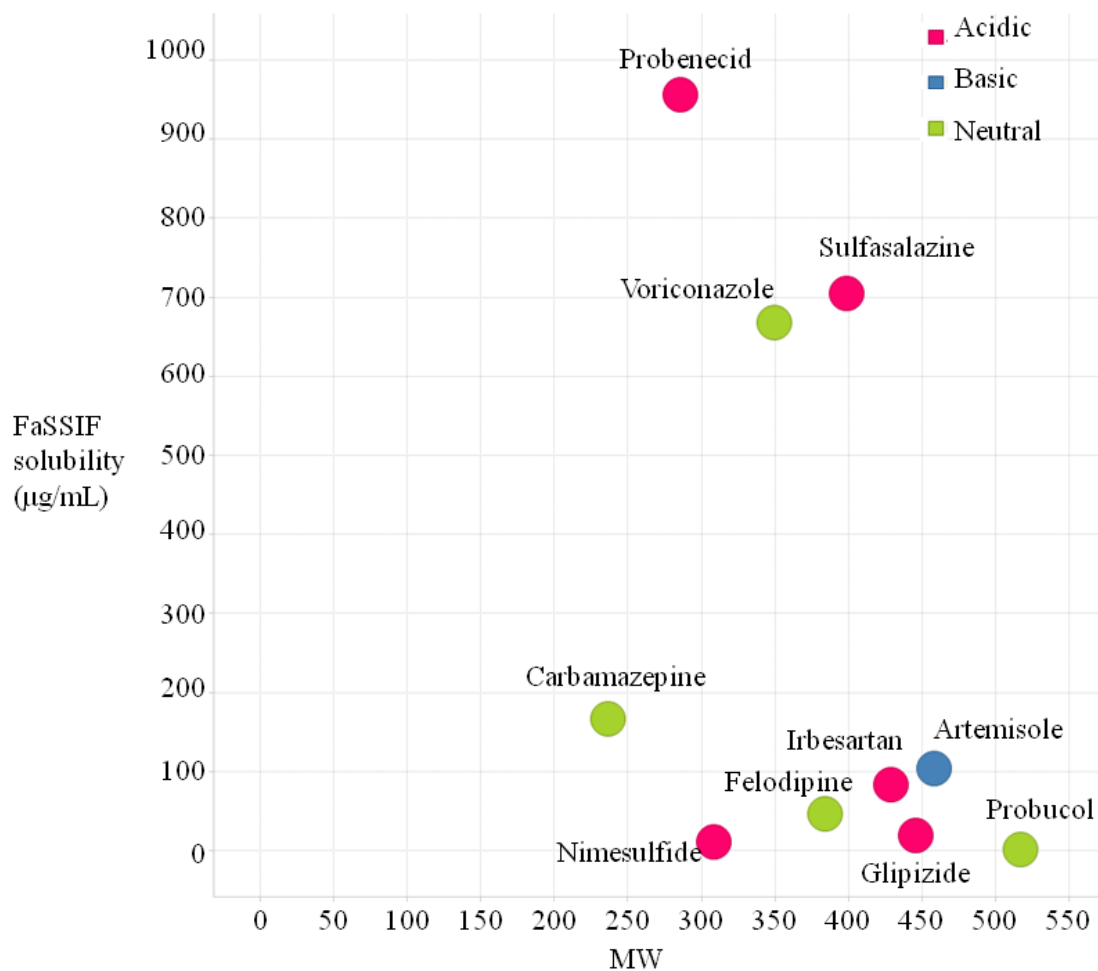


Figure 2.1.2. Measured FaSSIF solubility vs. molecular weight for 10 known drugs.

These key physicochemical properties also influence other ADMET properties such as permeability.

### **2.1.2. Permeability**

Increased lipophilicity often leads to increased cellular permeability. In the majority of cases it is the neutral form of an ionisable compound that contributes most significantly to permeability; polar compounds have reduced affinity for the phospholipid bilayers that form the cell membrane.<sup>2</sup> Analysing permeability data for 50,641 compounds from GSK showed that polar acids and zwitterions were the least permeable, neutral molecules were most permeable and bases lay inbetween.<sup>3</sup> A lower lipophilicity limit to allow for sufficient permeability is often not utilised in drug optimisation since other physicochemical properties can be used to ensure that a compound's polarity is not so high as to impact permeability negatively.<sup>2</sup> For example molecular weight, polar surface area and hydrogen bond donor and acceptor counts are all key descriptors in this regard. The GSK analysis showed that permeability decreased as molecular weight increased.<sup>3</sup> Topological polar surface area (TPSA) also correlates inversely with permeability, since it describes that portion of the surface which belongs to polar atoms.<sup>15,16</sup> Permeability also decreases with hydrogen-bonding capability, which can be described by the total number of hydrogen bond donors and acceptors, although simple counting does not take into account the effects of ionisation or conformational flexibility that may shield or attenuate hydrogen bonding sites or strength, respectively.<sup>17</sup> Despite this, the total number of hydrogen bond donors and acceptors is an easily calculated descriptor to use and the number of rotatable bonds can also be calculated to give an indication of whether permeability is likely to be impacted by increased flexibility.

Permeability is measured in a high-throughput artificial membrane permeation assay, which is based on permeation through planar polycarbonate filter supported lipid bilayers.<sup>18,19</sup> Permeation rates range from 0.1 to 2000 nm/s, with the maximum rate limited by the filter pore size. A compound's permeability is classed as low if less than 50 nm/s, and high if greater than 200 nm/s. Since this method uses an artificial membrane, it is also of interest to measure a compound's permeability in cultured cell lines. A method that uses Madin Darby canine kidney (MDCK) cells is

also available, but it is lower throughput. The method uses MDCK cells to form monolayers of polarised cells; the compound is added on the surface of the cell membrane. Transport across the monolayer is monitored over a 60 min time period.<sup>20</sup> Since MDCK cells originate from the canine kidney, measuring permeability in cells that are of human intestinal origin is often preferred. This is possible using Caco-2 cells isolated from human colon carcinoma, however this method requires 20 days to form a cell monolayer compared with only 4 days for MDCK cells.<sup>21</sup>

### **2.1.3. Human Serum Albumin Binding**

The extent to which compounds bind to plasma proteins may not have a direct impact on attrition but higher plasma protein binding can affect a drug's efficacy and distribution since the free fraction of drug (i.e. unbound) that is able to diffuse across membranes and interact with the intended therapeutic target is lowered.<sup>22</sup> Increased plasma protein binding is often a feature of lipophilic compounds and can therefore relate indirectly to attrition risk. There are several plasma proteins, including alpha-1-acid glycoprotein,  $\alpha$ -,  $\beta$ - and  $\gamma$ - globulins and fibrinogen; however human serum albumin (HSA) binding is the most abundant protein in human plasma (approximately 60%). It has been shown that there is a direct correlation between logP and the extent of binding to human serum albumin from an analysis of 135 diverse drugs and simpler organic compounds.<sup>23</sup> Lipophilicity can therefore be an indicator of HSA binding and it has been shown that it is also affected by molecular weight and ionisation state. 2,939 GSK compounds were analysed and it was found that plasma protein binding increased with increasing molecular weight and that the trend of acids > neutrals > zwitterions > basic molecules was followed.<sup>3</sup>

A high-throughput HSA binding assay, which employs a fast gradient HPLC method with silica-supported human serum albumin, can be used to measure a compound's plasma protein binding.<sup>19,23</sup> The chromatographic retention factor directly relates to the proportion of the number of molecules in the stationary phase

compared to the mobile phase and this proportion is converted to a percentage bound value, with >95% HSA binding representing the high range.<sup>23</sup>

Lower throughput methods are also available for assessment of a compound's plasma protein binding, and *in vitro* methods that use equilibrium dialysis are commonly used to give a value for the fraction of compound not bound to proteins.<sup>24</sup> This method uses a semi-permeable membrane that separates a protein-containing compartment from a protein-free compartment. The test compound is allowed to equilibrate and the amount present in each compartment is quantified by LC-MS/MS.<sup>24</sup> This method uses whole plasma and hence has the full complement of plasma proteins and not just HSA. A low fraction unbound value (i.e. <0.1, where greater than 90% of the compound is bound to plasma proteins) represents a compound that binds extensively.<sup>24</sup>

#### **2.1.4. Toxicity**

Toxicity is a major cause of late-stage drug attrition. Acute toxicity due to adverse drug reactions has been estimated to result in 15% of hospital admissions and up to 100,000 deaths per year in US hospitals.<sup>25</sup> Compounds that engage in multiple interactions with off-targets have been shown to have a detrimental contribution to side effects and toxicology, since the additional targets may have unwanted pharmacology. This higher promiscuity has been linked to discontinued clinical candidates and withdrawn drugs.<sup>26</sup> A review of a large number of literature studies has shown that lipophilicity and basic character are the key physicochemical properties that influence drug promiscuity.<sup>27</sup> Lipophilic compounds are more likely to bind to any target since binding affinity is often increased by gains in entropy through desolvation. This effect has poor specificity and impacts the affinity of a molecule to many targets. An analysis of the activity of 2,133 drugs and reference compounds in 200 assays by Leeson and Springthorpe showed that promiscuity was increased for compounds with  $\log P > 3.0$ .<sup>28</sup> Young also showed a positive correlation of promiscuity with measured ChromlogP for a set of approximately 800 compounds

that had been screened in >490 assays.<sup>29</sup> The intrinsic lipophilicity was more important in governing binding affinity than  $\text{ChromlogD}_{\text{pH}7.4}$ .<sup>29</sup> Undesirable promiscuity can be overcome both through a reduction in lipophilicity or by designing specific protein-ligand interactions that contribute to selectivity.<sup>27</sup>

The Leeson and Springthorpe analysis also showed that a molecular weight from 350 to 500 Da was optimal if neutral and basic compounds were to avoid promiscuity, with a positive correlation observed for acid compounds.<sup>28</sup> A positive correlation between promiscuity and molecular weight was also observed by Gleeson.<sup>30</sup> According to Young, aromatic ring count has also been associated with an increased risk of promiscuity.<sup>29</sup> A statistically significant increase in the number of active hits in >490 assays (>30% inhibition at 10  $\mu\text{M}$ ) was observed for aromatic ring increments between one and four.<sup>29</sup>

The increased promiscuity of basic compounds can be attributed to the nature of the binding sites of promiscuous targets, for example ion channels that coordinate ligands bearing positive charge.<sup>27</sup> One such example is the hERG (human *ether-a-go-go* related gene) potassium ( $\text{K}^+$ ) channel, which is essential for normal electrical activity in the heart; drug-induced blockage of these channels can lead to potentially fatal cardiac arrhythmia.<sup>31</sup> This liability is a key target for identifying cardiovascular risk in drug development.<sup>32</sup> Just as lipophilicity and basicity make a strong contribution to drug promiscuity, positively charged lipophilic compounds are more likely to trigger problematic levels of hERG activity ( $\text{pIC}_{50} > 5.0$ ).<sup>33</sup> A study of 7,685 AstraZeneca compounds quantified hERG inhibition as a function of measured  $\text{logD}_{\text{pH}7.4}$  for separate ionisation classes.<sup>33</sup> For neutral and basic compounds,  $\text{logD}$  values of  $< 3.3$  and  $< 1.4$  respectively were required for a greater than 70% chance of a compound being less active than  $\text{pIC}_{50} = 5.0$ .<sup>33</sup> Since  $\text{logD}$  does not represent the intrinsic lipophilicity of a compound in different ionisation classes, it may be more informative to use  $\text{logP}$ . The measured  $\text{ChromlogP}$  value of 18,600 compounds analysed by Young at GSK showed a stronger trend than measured  $\text{ChromlogD}_{\text{pH}7.4}$ .<sup>29</sup> This analysis also showed increased propensity for hERG activity with increasing numbers of aromatic rings and this was more significant for



positively charged compounds.<sup>29</sup> *In vitro* screening of potential drug molecules is used widely to assess hERG inhibition during lead optimisation and an IonWorks<sup>®</sup> electrophysiology-based system was used to this effect in the programmes of work described here.<sup>34,35</sup>

Cytochromes p450 (CYP) enzyme pharmacology may also result in adverse drug reactions.<sup>36</sup> This family of heme-containing proteins are a major component of metabolism and are particularly concentrated in the liver. Absorption of a drug compound from the gastrointestinal tract into the hepatic portal vein delivered it to the liver, where the CYP enzymes catalyse metabolism. This can lead to either direct deactivation of the molecule, or facilitation of its excretion, thereby affecting the amount of compound that enters circulation in the plasma, and transforming the compound into metabolites that may be harmful.<sup>36</sup> The inhibition or induction of CYP enzymes by drug compounds can also impact the metabolism and clearance of other bioactive molecules, which may be administered in tandem.<sup>37</sup> For example, if one drug is a potent CYP substrate this could lead to a reduction in the metabolism of another co-administered drug, so that its plasma levels increase and toxic effects ensue. Drug-drug interactions of this type are recognised to be a major cause of adverse drug reactions.

Of the 57 human CYP enzymes, five isoforms are accountable for the metabolism of known drugs; these are 1A4, 2C9, 2C19, 2D6 and 3A4.<sup>36</sup> Of these, 3A4, 2D6 and 2C9 are the most active for drug metabolism. CYP 3A4 is the most abundantly expressed and is responsible for the metabolism of approximately 50% of clinically used drugs (Figure 2.1.3).<sup>38</sup> 2D6 is involved in the metabolism of approximately 20% of clinically used drugs (Figure 2.1.3).<sup>38</sup>

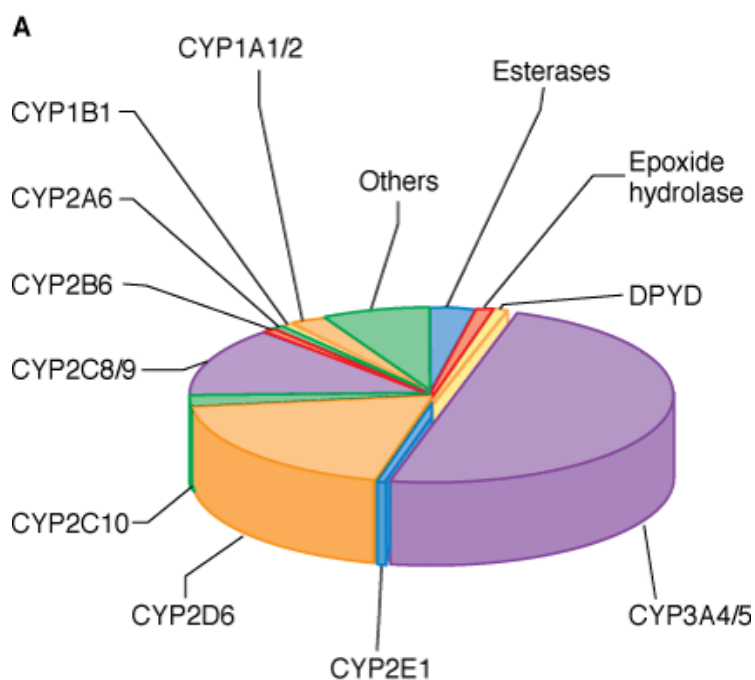


Figure 2.1.3. Fraction of clinically used drugs metabolised by CYP and other key metabolising enzymes.<sup>38</sup>

All CYP substrates, whether inhibitors or inducers, must bind within their active site, so common features of these substrates are observed. These five CYP isoforms have a preference for lipophilic molecules since their binding sites are generally lipophilic in nature and binding affinities are significantly lower for compounds with  $\log P < 3.0$ .<sup>3</sup> Lewis and Dickins identified additional characteristics of substrates that discriminate between the CYP isoforms (Table 2.1.1).<sup>39</sup>

CYP isoform	Average logP	Other characteristics
1A2	2.1	Planar molecules, neutral or basic
2D6	3.0	Medium-sized basic molecules
2C9	3.3	Medium-sized acidic molecules with 1–2 hydrogen bond acceptors
2C19	2.4	Medium-sized molecules, mostly basic with 2–3 hydrogen bond acceptors
3A4	2.8	Relatively large, structurally diverse molecules

Table 2.1.1. Summary of characteristics of human CYP substrates.<sup>39</sup>

The 3A4 isoform has the largest active site cavity.<sup>40</sup> An analysis of 42,987 molecules with measured 3A4 pIC<sub>50</sub>s found that inhibition increased with molecular weight.<sup>3</sup> However the increase in 3A4 activity was found not to be due simply to increases in molecular weight but was also highly dependant on lipophilicity.<sup>3</sup> This study also identified a dependency on ionisation state that was not reflected in the analysis of substrate SAR carried out by Lewis and Dickins. It was found that although neutral molecules had the highest 3A4 activities, the mean potency of bases was larger than acids, and almost equivalent to neutral molecules for a given clogP.<sup>3</sup> This corroborated an earlier investigation based on descriptors in *in silico* QSAR models, which found that 3A4 inhibitors are typically neutral or basic.<sup>41</sup>

The risk of drug-drug interactions projected from CYP inhibition and the effects on compound tolerability is now widely used as a developability measure. A high-throughput *in vitro* bactosome assay for the 3A4 CYP isoform was used in the programmes of work described here in order to assess a compound's propensity to interfere with the enzyme.<sup>42</sup>

In addition to CYP inhibition by a reversible mechanism, it is possible that a compound may be involved in time-dependent inhibition (TDI), where an increase in potency is experienced during a dosing period *in vivo*.<sup>43</sup> A possible cause of this is mechanism-based inhibition (MBI), in which the enzyme is deactivated by

chemically reactive metabolites.<sup>43</sup> MBI often results in irreversible inhibition of the enzyme and the effects can be more profound after multiple-dosing.<sup>43</sup> CYP TDI is of high toxicological concern as irreversible inhibition is viewed as more serious than reversible inhibition; the inhibitory effect will remain even after the parent drug has been eliminated from the body.<sup>44</sup> CYP TDI can also be assessed in an *in vitro* system, for example using pre-incubation of a compound in human liver microsomes, to assess changes in activity.<sup>43</sup>

### **2.1.5. Rules-of-Thumb**

The relationships between developability measures (*e.g.* solubility, permeability, promiscuity) and the fundamental physicochemical properties of potential drug molecules are obviously important for successful drug discovery. Since ADMET properties can be described by the physicochemical properties of compounds, the assessment of drug-likeness often takes the form of rules-of-thumb that are focused on a few of these properties. The first of these to be described was Lipinski's rule-of-five, which concerned the absorption of oral drugs and examined property distributions for compounds taken into Phase II clinical trials.<sup>45</sup> The analysis concluded that poor absorption or permeation was more likely when there were more than 5 hydrogen bond donors, 10 hydrogen bond acceptors, the molecular weight was greater than 500 and the clogP was greater than 5.<sup>45</sup> This work inspired a number of refinements such as Pfizer's 3/75 rule, where analysis of 245 pre-clinical compounds showed that compounds with clogP greater than 3 and TPSA lower than 75 Å were 2.5 times more likely to encounter safety issues in *in vivo* studies.<sup>46</sup> Also, Gleeson's analysis of the molecular properties of ~30,000 diverse GSK molecules and their ADMET-related data led to the 4/400 rule, where compounds with clogP greater than 4 and a molecular weight greater than 400 had a less favourable ADMET profile.<sup>3</sup>

One recent suggested rule of thumb is the GSK Property Forecast Index (PFI), which came from an analysis of the relationships of the sum of

ChromlogD<sub>pH7.4</sub> and the number of aromatic rings with various developability criteria.<sup>29</sup> This was an extension of the work that initially investigated the impact of clogD<sub>pH7.4</sub> on solubility.<sup>4</sup> The measured or calculated ChromlogD<sub>pH7.4</sub> gave better differentiation for developability parameters than measured or calculated OW logD<sub>pH7.4</sub> values and the summation with #Ar showed that risks for developability were exacerbated above a PFI of 7 (Table 2.1.2).<sup>29</sup>

	PFI = mChrom log D <sub>pH7.4</sub> + #Ar								
Assay / target value	<3	3-4	4-5	5-6	6-7	7-8	8-9	9-10	>10
<b>Solubility</b> >200 μM	89	83	72	58	33	13	5	3	2
<b>%HSA</b> <95%	88	80	74	64	50	30	17	8	4
<b>2C9 pIC<sub>50</sub></b> <5	97	90	83	68	48	32	23	22	38
<b>2C19 pIC<sub>50</sub></b> <5	97	95	91	82	67	52	42	42	56
<b>3A4 pIC<sub>50</sub></b> <5	92	83	80	75	67	60	58	61	66
<b>Cl<sub>int</sub></b> <3 ml/min/kg	79	76	68	61	54	42	41	39	52
<b>Papp</b> >200 nm/s	20	30	46	65	74	77	65	50	33
	iPFI = mChrom log P + #Ar								
<b>hERG pIC<sub>50</sub></b> <5 (+1 charge)	86	93	88	70	54	36	29	21	11
<b>Promiscuity</b> <5 hits with pIC <sub>50</sub> >5	85	78	74	65	49	30	20	13	7

Table 2.1.2. Percentages of compounds achieving defined target values in various developability assays categorised by PFI bins.<sup>29</sup>

PFI was used to assess the quality of potential drug molecules synthesised in the programmes of work described here. It is important to note that PFI does not take into account molecular weight and the studies have so far not described how #Ar is correlated with molecular weight. This may be something worthy of further exploration as molecular weight has been shown to be another important factor for drug-likeness.

The guidelines discussed so far have been widely accepted by the pharmaceutical industry and are often used as hard cut-offs, for example when filtering libraries of compounds. However, despite compounds often being compliant

with such rules there has still been a decline in productivity within small molecule drug discovery over the past two decades. Leeson and Springthorpe analysed patent data from several pharmaceutical companies and found that the physical properties of molecules synthesised in leading drug discovery companies from 2001 to 2007 differed significantly from those of oral drugs approved from 1983 to 2007 and those of compounds in clinical development in July 2007.<sup>28</sup> Overall upward trends in median clogP values and molecular weights were identified.<sup>28</sup>

A key parameter pursued in many medicinal chemistry projects is high *in vitro* potency. Most drugs are believed to exert their biological response as a consequence of enzyme inhibition and the interaction of a drug with a receptor gives a drug-receptor complex that elicits that biological response.<sup>47</sup> The amount of drug required to produce an effect of a given intensity gives a measure of the drug's activity (potency). The half maximal inhibitory concentration ( $IC_{50}$ ) is a commonly used measure of antagonist drug potency and quantifies the amount of drug required to inhibit a given biological response by half.<sup>47</sup>  $IC_{50}$  can be converted to the log scale ( $pIC_{50}$ ) so higher values indicate exponentially greater potency. The tendency to enhance potency through increasing lipophilicity has been termed 'molecular obesity' and leads to conflicts with good ADMET properties.<sup>48</sup> It is suggested that the pursuit of high potency has driven the higher lipophilicity of recent drug compounds.<sup>48</sup>

Medicinal chemistry optimisation cannot focus solely on potency and rules-of-thumb that take this into account alongside physicochemical and ADMET-related parameters have recently been described.

Ligand efficiency has emerged as a useful guide to optimize fragment and lead selection in the drug discovery process and gives an estimation of the efficiency of a ligand binding interaction as a function of ligand size. Kuntz first quantified the free energy of ligand binding ( $\Delta G$ ) in relation to the number of non-hydrogen atoms,<sup>49</sup> and Hopkins extended this to define the term 'ligand efficiency' (Equation 1.1), where HAC is the heavy atom count.<sup>50</sup>

$$LE = \frac{\Delta G}{HAC} = \frac{-RT \ln K_i}{HAC} = \frac{1.37(pK_i)}{HAC}$$

Equation 1.1. Ligand Efficiency (LE).<sup>50</sup>

The lowest LE value acceptable for a typical project where a compound with potency of 10 nM and MW of 500 is desired has been established as 0.3.<sup>50</sup> This was determined from analysis of Pfizer corporate screening data, which showed that a compound with a MW of 500 would contain an average of 38 heavy atoms, and if the binding constant were 10 nM, the ligand efficiency equates to 0.29 kcal mol<sup>-1</sup> per heavy atom.<sup>50</sup>

Leeson and Springthorpe recently proposed an alternative parameter, the ligand-lipophilicity efficiency (LLE) (Equation 1.2).<sup>28</sup> This takes into account the increase in lipophilicity per unit of *in vitro* potency and they suggested that maximising the LLE would help to achieve one major goal of lead optimisation, which is to increase potency without increasing lipophilicity.<sup>28</sup>

$$LLE = (pIC_{50} \text{ or } pK_i) - clogP$$

Equation 1.2. Lipophilic ligand Efficiency (LLE).<sup>28</sup>

These two equations have been used by Mortenson and Murray to define an alternative LLE index (LLE<sub>AT</sub>, Equation 1.3), where a modified free energy change, ΔG\*, is used so that the non-specific binding component due to lipophilicity is removed. In addition, a constant term is added in order to make a direct comparison with conventional LE.<sup>51</sup>

$$LLE_{AT} = 0.111 + \left( 1.37 \times \left( \frac{pIC_{50} - clogP}{HAC} \right) \right)$$

Equation 1.3. Alternative definition of LLE.<sup>51</sup>

Typically  $LLE_{AT}$  and LE have been used in hit-to-lead efforts, for example in fragment optimisation, as these parameters give an indication of the impact of each atom. Targeting values greater than 0.3 and ensuring  $LLE_{AT}$  is not less than LE allows for optimisation of potency without increasing lipophilicity. The LLE parameter becomes more important with time during lead optimisation and target values of greater than 5 would imply high *in vitro* potency and sufficiently low lipophilicity. LE and  $LLE_{AT}$  will be used as descriptors of compound quality in the programmes of work described here, as they are on the same scale.

## **2.2. Drug Metabolism and Pharmacokinetics (DMPK)**

### **2.2.1. Metabolism and Clearance**

Drug metabolism refers to the biochemical transformation of a compound to another chemical form. Metabolism is a drug clearance process and the pathways of metabolism of a drug are studied in order to understand the behaviour of a drug after administration. Therefore one of the most important properties of a drug is clearance, which is the hypothetical volume of distribution from which the drug is entirely removed or cleared in unit time.<sup>47</sup> It is a function of both the ability of organs, such as the liver and kidneys, to metabolise and excrete the drug, and of the blood flow rate to these organs. Drug metabolising enzymes are present in most tissues but the liver is the primary site of drug metabolism; however other organs involved in drug metabolism include the gastrointestinal tract, lung, kidneys and skin. Therefore, the overall clearance of a drug is primarily represented by the renal clearance (i.e. excretion of a drug in its unchanged form) and hepatic clearance, both through hepatic metabolism and biliary excretion (Figure 2.2.1).<sup>52</sup>



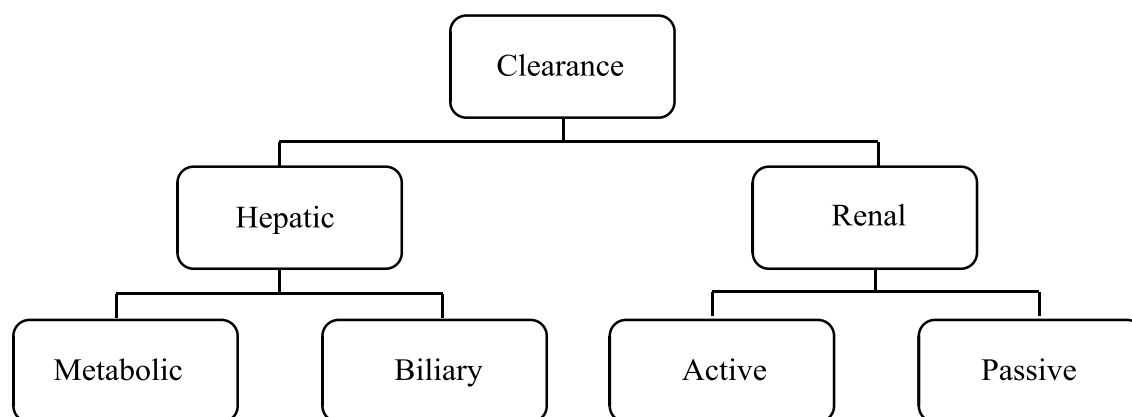


Figure 2.2.1. Components of total clearance.<sup>52</sup>

As described previously, CYP enzymes are key mediators of first pass metabolism, the phenomenon by which drugs are metabolised in the liver after being transported there by the hepatic portal vein following absorption from the gut. The CYP enzymes have been implicated in the metabolism of 60-80% of marketed drugs.<sup>53</sup> This group of enzymes is responsible for the oxidative metabolism of drugs, which represents one of the most common metabolic reactions and is categorised as a phase I biotransformation. Other phase I reactions include hydroxylation, reduction and hydrolysis.<sup>47</sup> In these enzymatic reactions either a new functional group is introduced, an existing functional group is modified or a functional group for a phase II reaction is exposed, making the molecule more polar and therefore more readily excreted in urine.<sup>47</sup> Phase II reactions occur after phase I; these are conjugation reactions whereby a functional group, such as an alcohol or amine, is masked by the addition of a hydrophilic moiety, such as a sulfate or glucuronic acid group.<sup>47</sup> This increases the polarity of the molecule so elimination is facilitated further.

Since the metabolism of drug molecules is primarily mediated by CYP enzymes in human liver microsomes (HLMs), high-throughput assays have been developed to monitor the oxidative stability of drug molecules. Compounds that have low metabolic turnover are likely to have low intrinsic clearance ( $Cl_{int}$ ) values for oxidative metabolism in the liver.<sup>54</sup>

In the programmes of work described here, the *in vitro* clearance (IVC) of the compounds was measured in microsomes obtained *via* differential centrifugation of liver homogenates, which mainly contain fragments of the endoplasmic reticulum, for three species; rat, dog and human. The disappearance of test compound was monitored over a 45 minute time period and the elimination rate constant was determined in order to ascertain the intrinsic clearance.<sup>55</sup> From these data, the compounds can be categorised into low, medium or high clearance bands by taking the liver blood flow (LBF) of each species into account.<sup>56,57</sup>

	Human	Dog	Rat
Liver blood flow (ml/min/kg)	21	30	85
IVC (ml/min/kg) - scales to <1/3 LBF	<0.53	<0.53	<1.0
IVC (ml/min/kg) - scales to 1/3 - 2/3 LBF	0.53 - 1.7	0.53 - 1.7	1.0 - 4.0
IVC (ml/min/kg) - scales to >2/3 LBF	>1.7	>1.7	>4

Table 2.2.1. IVC cut-offs for low, moderate and high turnover in different species.<sup>56,57</sup>

It is possible that the metabolic elimination of a molecule is *via* non-CYP enzymes that are not represented in liver microsomes.<sup>54</sup> Other enzymes that may contribute to drug metabolism include monoamine oxidases (MAO), aldehyde oxidase (AO) and uridine glucuronosyl transferases (UGT).<sup>58</sup> Additionally, microsomal preparations predominantly involve only phase I reactions since they lack the co-factors required for phase II conjugations. *In vitro* screening for non-CYP mediated metabolism is less readily available, for example in liver hepatocytes, which are a more sophisticated model of hepatic metabolism containing the full complement of drug metabolising enzymes (phase I and II) maintained within the intact cell.<sup>59</sup>

These *in vitro* metabolism studies are useful for gaining an understanding of the metabolism of a compound before embarking on an *in vivo* pharmacokinetic study. Metabolism and the subsequent *in vivo* clearance of drugs are considered the

most difficult ADMET parameters to predict. One general principle suggested for reducing compound metabolism is lowering lipophilicity. The study of 11,490 GSK compounds by Gleeson suggested a weak but statistically significant relationship between logP and *in vivo* clearance.<sup>3</sup> For bases and neutral molecules, more lipophilic compounds had increased clearance; however acids and zwitterions showed decreased clearance with increased logP.<sup>3</sup> Overall, acids showed lower clearance than neutral and zwitterionic molecules and bases were generally cleared most rapidly, although these differences were most notable at logP > 5.<sup>3</sup> Another study of 47,018 Pfizer compounds showed a broad trend of decreasing logD and molecular weight leading to a higher proportion of compounds with low *in vitro* intrinsic clearance in HLMS.<sup>60</sup> An interesting observation of the effect of PFI on the *in vitro* intrinsic clearance of a set of 8,700 GSK compounds was that a statistically significant differentiation point occurred, where a PFI value greater than 7 led to more than 50% of compounds having high intrinsic clearance.<sup>29</sup>

Although these predictable parameters can be used to help guide the medicinal chemist to improve the metabolic liabilities of their compounds, the complexity of metabolic pathways means that the implications of changing a molecule's structure must also be considered. For example, the reduction of clearance when reducing lipophilicity could also be due to structural changes that remove or block sites of metabolism. Indeed, alongside replacing potentially metabolically liable groups with a bioisostere, removing or blocking known sites of metabolism represents a key strategy in reducing clearance.<sup>54</sup>

Since high metabolic instability leads to high *in vivo* plasma clearance values, it also impacts other *in vivo* pharmacokinetic parameters that are critical for achieving a suitable oral drug profile.

### **2.2.2. *In vivo* Pharmacokinetics**

Pharmacokinetics describes the time course of a drug's ADME processes that take place following administration of a drug.<sup>47</sup> Clearance is obviously a key

parameter in this regard and high *in vivo* plasma clearance values, which approach hepatic blood flow, can manifest in poor bioavailability (F) and short elimination half-life ( $t_{1/2}$ ).

Bioavailability is a property of the oral dosage form that allows the active drug to be delivered to the bloodstream in an amount and at a rate sufficient to produce the desired therapeutic effect; it is the percentage of the dose that reaches the systemic circulation.<sup>47</sup> Achieving good *in vivo* bioavailability therefore relies on a combination of factors; these are low clearance to minimise first pass elimination, high solubility, and permeability to maximise absorption. It has been suggested that lipophilicity is the key determinant of an optimal balance of these properties. If too low, permeability would be compromised; if too high, solubility and metabolism will be limiting.<sup>2</sup> However studies have failed to find clear relationships between lipophilicity and bioavailability in the rat; for example Gleeson's analysis of 4,431 GSK compounds found no statistically significant correlation between bioavailability and clogP, and an analysis of 553 Abbott compounds also showed no clear direct relationship between logD and rat bioavailability.<sup>3,61</sup> Lipiniski's rules state that good oral bioavailability is more likely for  $\log P < 5$ , but no lower limit, which would be relevant for achieving good permeability was discussed.<sup>45</sup> A retrospective analysis of human data found that compounds in the logD range of -2 to 3 were found to have increased bioavailability.<sup>62</sup> In general, it has been suggested that the optimal range for achieving oral bioavailability is between 0 and 3. For solubility and permeability, it might also be expected that logD is a relevant parameter, with an optimal range is between 1 and 3.<sup>2</sup> Other guidelines for selecting bioavailable compounds have also been proposed; for example low PSA ( $\leq 140 \text{ \AA}$ ), hydrogen bond donor and acceptor count (12 or fewer) and reduced molecular flexibility determined by low numbers of rotatable bonds (10 or fewer).<sup>63</sup> These general guidelines can be followed in a medicinal chemistry programme but it will be most helpful to assess specific compound series to determine relevant relationships between bioavailability and physicochemical parameters to aid compound design.

Another *in vivo* pharmacokinetic parameter of importance in selecting a good oral drug is the elimination half-life. This is the time for the concentration of drug in the blood or plasma to decline to half its original level.<sup>47</sup> The half-life of a drug is related to its clearance and volume of distribution ( $V_{\text{dss}}$ ). The volume of distribution relates the amount (g) and concentration ( $L^{-1}$ ) of drug in the body at a given time.<sup>47</sup> Drugs with small volumes of distribution ( $<1$  g/L) may be highly bound to plasma proteins or very water soluble and drugs with large volumes of distribution ( $>6$  g/L) bind outside the serum or are highly lipid soluble. An increase in volume of distribution or a decrease in clearance will cause an increase in half-life. The half-life of a drug is a major factor in determining dosing frequency; drugs with short half-lives are more likely to require frequent administration whereas those with long half-lives tend to require dosing once daily.<sup>47</sup> The dosing regimen is also related to other pharmacokinetic properties since the magnitude of the required pharmacological response and any undesired toxicities are both functions of drug concentration in the blood (Figure 2.2.2).<sup>47</sup>

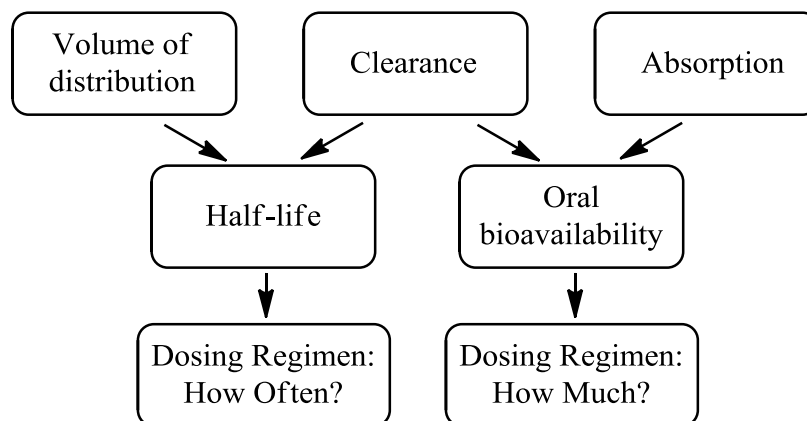


Figure 2.2.2. The relationships between pharmacokinetic parameters and human kinetics.<sup>47</sup>

A summary of the relationships between *in vivo* pharmacokinetic parameters and key relationships with lipophilicity are shown in Figure 2.2.3.

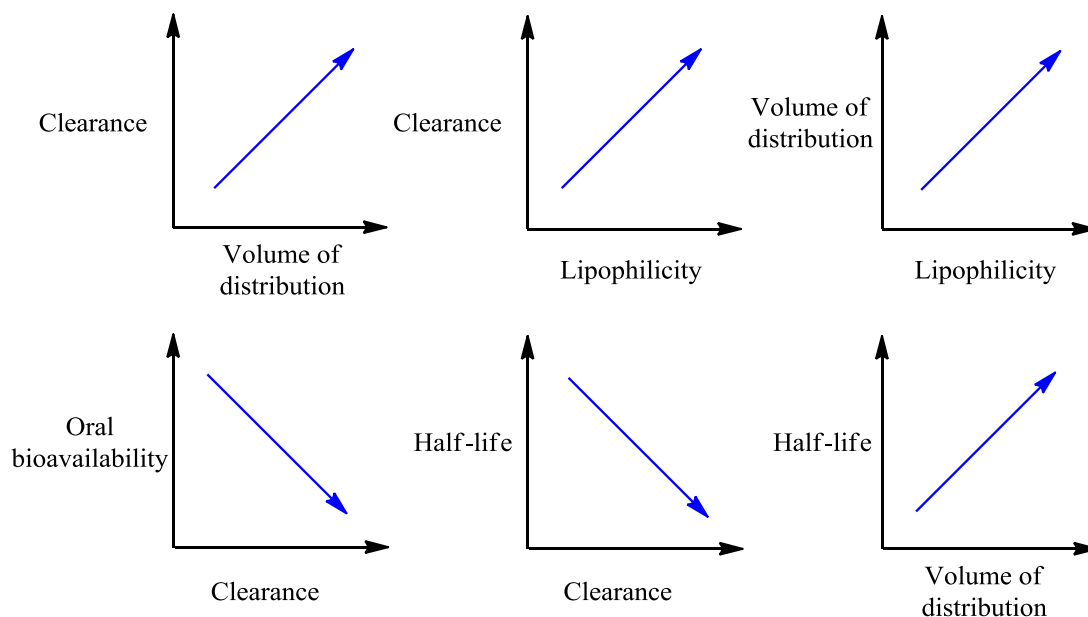


Figure 2.2.3. The general trends between pharmacokinetic parameters, and with lipophilicity.

### 2.2.3. Approaches to Predicting Human Pharmacokinetics

The ultimate model for drug metabolism and pharmacokinetics in man is man. However, in general the DMPK profiles of compounds in animal species usually exhibit some similarity with that of humans. Interspecies differences are difficult to predict but can often be rationalised on the basis of known species differences. Similarities occur in drug-metabolising enzymes across species. For example, at a genetic level there was observed to be approximately an 80% homology of the amino acid sequences for cDNA clones that encode for CYP enzymes between animal species commonly used in metabolism studies (rat, mouse, rabbit and dog) and humans. This study also revealed >90% homology between human and monkey species.<sup>64</sup> In addition to metabolic differences, there are differences in the anatomy, physiology and biochemistry of the gastrointestinal tracts of humans and laboratory animals. These differences are well described and can be

used to aid selection of the most appropriate animal models for the assessment of bioavailability of compounds in humans.<sup>65</sup> Differences in plasma binding proteins are also observed across species, for example there may be differences in the affinity or number of binding sites on the protein molecule.<sup>66</sup> This can lead to differences in the tissue distribution of compounds in different species.

The understanding of species differences has allowed approaches that correlate animal pharmacokinetic parameters with those of humans, in order to predict human drug absorption, clearance and distribution. The most obvious differences between species are their size and shape and most anatomical and physiological parameters can be described as functions of body weight.<sup>56,67</sup>

The two main approaches are physiological based pharmacokinetic (PBPK) modelling and allometric scaling. The physiological model is based on a mechanistic approach, where organs of interest are arranged according to organ size and blood flow to each organ.<sup>68</sup> Biochemical parameters determined *in vitro* and *in vivo*, such as plasma protein binding and clearance, are incorporated into the model.<sup>68</sup> Although this method gives a more rigorous prediction of the kinetic behaviour of drugs in humans, it is mathematically complex, time-consuming and costly. The other, more empirical, approach uses allometric scaling to examine the relationships between body size, time and pharmacokinetic consequences without understanding the underlying mechanisms.<sup>68</sup> This method makes use of the fact that logarithmic plots of pharmacokinetic parameters such as clearance, volume of distribution and half-life against body weight will usually be linear.<sup>69</sup>

Drug metabolism in humans is one of the most difficult processes to predict from animals. Allometric scaling can be used to predict clearance; however it does not take into account species differences in metabolising enzymes and tends to have limited predictive capability for low clearance compounds.<sup>52</sup> *In vitro-in vivo* extrapolation (IVIVE) of metabolic clearance from *in vitro* tissue preparations such as microsomes or hepatocytes has therefore been used for this purpose. Extrapolation from *in vitro* hepatic clearance values, based on scaling from liver blood flow of different species, was also found to be more successful at predicting human clearance

than allometric scaling for a set of 103 non-peptide xenobiotics.<sup>70</sup> Another study investigating prediction of human plasma clearance for 33 marketed oral drugs showed that for >90% of the test compounds, the predicted human clearance using IVIVE (from intrinsic clearance values obtained from human liver hepatocytes), together with a renal clearance estimate, was within two-fold of that observed clinically.<sup>52</sup> Since the IVIVE approach assumes that hepatic metabolic clearance is the predominant route of elimination, underestimation of total clearance may be a limitation, as alternative clearance routes are not taken into account. It is therefore important that the *in vitro* experiment is performed under appropriate conditions.

The prediction of oral absorption can be carried out effectively using allometric scaling. An assessment of marketed drugs showed that the fraction absorbed in human correlated linearly with that estimated from rat PK studies.<sup>71</sup> However, a more recent study showed that the estimation was often lower than that calculated from clinical human PK studies, even when solubility and permeability were not limiting.<sup>52</sup> Typically the dog demonstrates greater oral absorption than human for compounds absorbed *via* the paracellular route (i.e. low molecular, hydrophilic compounds).<sup>52</sup> This has been attributed to the greater size and frequency of gap junctions in dog *vs* human, although there are also other anatomical and physiological differences in their gastrointestinal tracts.<sup>72</sup> For compounds absorbed *via* a transcellular pathway, estimations using bioavailability and *in vivo* clearance have been shown to be effective.<sup>52</sup> Therefore, a suggested approach for predicting human oral absorption is to assess any risks from permeability or solubility and, where possible, utilise absorption estimated in both rat and dog.<sup>52</sup>

Volume of distribution has been successfully predicted for humans using an allometric scaling approach from that estimated in rat and dog, with 73% of the 26 marketed compounds investigated having predicted values within two-fold of those observed clinically.<sup>52</sup> It was important to correct for plasma protein binding differences between the species. Predicted volume can be used alongside predicted human clearance (using IVIVE) to predict the human half-life. The accuracy of these predictions for 22 marketed compounds found that the overall trend was to under-



predict half-life; however this was not attributed to an over-prediction of clearance or under prediction of volume.<sup>52</sup> Although the predictions of half-life were conservative, 68% of the predicted values were within two-fold of those observed clinically.<sup>52</sup>

The implementation of approaches for the prediction of human pharmacokinetics has been significant in reducing attrition due to sub-optimal DMPK properties. The use of appropriate preclinical profiling strategies and medicinal chemistry design principles such as those described in this Chapter will hopefully result in an improvement in drug candidate quality and hence increase productivity and success rates in small molecule drug discovery. In the programmes of work described in this thesis, lipophilicity remained a key property for consideration in compound design and the literature observations that suggest that reducing lipophilicity leads to higher compound quality were reflected in the discovery of potent IKK2 inhibitors and the optimisation of the oral PK profile of PI3K $\delta$  inhibitors. The use of rules-of-thumb such as ligand efficiency and PFI were also important in the work described here and taking these into consideration allowed for the discovery of high quality kinase inhibitors.

## 2.3. References

- (1) Wenlock, M. C.; Austin, R. P.; Barton, P.; Davis, A. M.; Leeson, P. D. *J. Med. Chem.* **2003**, *46*, 1250-1256.
- (2) Waring, M. J. *Expert Opin. Drug Discovery* **2010**, *5*, 235-248.
- (3) Gleeson, M. P. *J. Med. Chem.* **2008**, *51*, 817-834.
- (4) Hill, A. P.; Young, R. J. *Drug Discov. Today* **2010**, *15*, 648-655.
- (5) Valko, K.; Bevan, C.; Reynolds, D. *Anal. Chem.* **1997**, *69*, 2022-2029.
- (6) <http://www.daylight.com/dayhtml/doc/clogp/index.html#PCMsc1.1.2>, accessed on 21st August 2013.
- (7) Luscombe, C.; GlaxoSmithKline: 2013, unpublished results.
- (8) Mannhold, R.; Poda, G. I.; Ostermann, C.; Tetko, I. V. *J. Pharm. Sci.* **2009**, *98*, 861-893.
- (9) Bhattachar, S. N.; Wesley, J. A.; Seadeek, C. J. *J. Pharm. Biomed. Anal.* **2006**, *41*, 152-157.
- (10) Hill, A. P.; McDonough, P.; Blaschke, S. C.; GlaxoSmithKline: 2006, unpublished results.
- (11) Klein, S. *AAPS J.* **2010**, *12*, 397-406.
- (12) Magee, D. F.; Dalley, A. F. *Digestion and the Structure and Function of the Gut*; Karger: Basel, 1986.
- (13) Hill, A. P.; Blowey, P.; GlaxoSmithKline: 2013, unpublished results.
- (14) Soederlind, E.; Karlsson, E.; Carlsson, A.; Kong, R.; Lenz, A.; Lindborg, S.; Sheng, J. J. *Mol. Pharmaceutics* **2010**, *7*, 1498-1507.
- (15) Ertl, P.; Rohde, B.; Selzer, P. *J. Med. Chem.* **2000**, *43*, 3714-3717.
- (16) Palm, K.; Luthman, K.; Ungell, A.-L.; Strandlund, G.; Beigi, F.; Lundahl, P.; Artursson, P. *J. Med. Chem.* **1998**, *41*, 5382-5392.
- (17) van de Waterbeemd, H.; Camenisch, G.; Folkers, G.; Raevsky, O. A. *Quant. Struct.-Act. Relat.* **1996**, *15*, 480-490.
- (18) Kansy, M.; Senner, F.; Gubernator, K. *J. Med. Chem.* **1998**, *41*, 1007-1010.

- (19) Bardoni, S.; Nunhuck, S.; Blaschke, S. C.; GlaxoSmithKline: 2010, unpublished results.
- (20) <http://www.cyprotex.com/admepk/in-vitro-permeability/wild-type-mdck-permeability/>, accessed on 21st August 2013.
- (21) <http://www.cyprotex.com/admepk/in-vitro-permeability/caco-2-permeability/>, accessed on 21st August 2013.
- (22) Smith, D. A.; Di, L.; Kerns, E. H. *Nat. Rev. Drug Discovery* **2010**, *9*, 929-939.
- (23) Valko, K.; Nunhuck, S.; Bevan, C.; Abraham, M. H.; Reynolds, D. P. *J. Pharm. Sci.* **2003**, *92*, 2236-2248.
- (24) [http://www.cyprotex.com/admepk/protein\\_binding/plasma-protein-binding/](http://www.cyprotex.com/admepk/protein_binding/plasma-protein-binding/), accessed on 21st August 2013.
- (25) Nigsch, F.; Lounkine, E.; McCarren, P.; Cornett, B.; Glick, M.; Azzaoui, K.; Urban, L.; Marc, P.; Mueller, A.; Hahne, F.; Heard, D. J.; Jenkins, J. L. *Expert Opin. Drug Metab. Toxicol.* **2011**, *7*, 1497-1511.
- (26) Bowes, J.; Brown, A. J.; Hamon, J.; Jarolimek, W.; Sridhar, A.; Waldron, G.; Whitebread, S. *Nat. Rev. Drug Discovery* **2012**, *11*, 909-922.
- (27) Tarcsay, A.; Keseru, G. M. *J. Med. Chem.* **2012**, *56*, 1789-1795.
- (28) Leeson, P. D.; Springthorpe, B. *Nat. Rev. Drug Discovery* **2007**, *6*, 881-890.
- (29) Young, R. J.; Green, D. V. S.; Luscombe, C. N.; Hill, A. P. *Drug Discov. Today* **2011**, *16*, 822-830.
- (30) Gleeson, M. P.; Hersey, A.; Montanari, D.; Overington, J. *Nat. Rev. Drug Discovery* **2011**, *10*, 197-208.
- (31) Sanguinetti, M. C.; Tristani-Firouzi, M. *Nature* **2006**, *440*, 463-469.
- (32) Redfern, W. S.; Carlsson, L.; Davis, A. S.; Lynch, W. G.; MacKenzie, I.; Palethorpe, S.; Siegl, P. K. S.; Strang, I.; Sullivan, A. T.; Wallis, R.; Camm, A. J.; Hammond, T. G. *Cardiovasc. Res.* **2003**, *58*, 32-45.
- (33) Waring, M. J.; Johnstone, C. *Bioorg. Med. Chem. Lett.* **2007**, *17*, 1759-1764.
- (34) Bridgland-Taylor, M. H.; Hargreaves, A. C.; Easter, A.; Orme, A.; Henthorn, D. C.; Ding, M.; Davis, A. M.; Small, B. G.; Heapy, C. G.; Abi-Gerges, N.;

- Persson, F.; Jacobson, I.; Sullivan, M.; Albertson, N.; Hammond, T. G.; Sullivan, E.; Valentin, J. P.; Pollard, C. E. *J. Pharmacol. Toxicol. Methods* **2006**, *54*, 189-199.
- (35) Patel, M.; Chen, Y. H.; Downie, D.; Standing, D.; Donovan, B.; Vulimiri, P.; Smith, G.; Gillie, D.; Leesnitzer, T.; Powell, A.; Brough, S.; GlaxoSmithKline: 2011, unpublished results.
- (36) Guengerich, F. P. *Chem. Res. Toxicol.* **2008**, *21*, 70-83.
- (37) Bibi, Z. *Nutr. Metab.* **2008**, *5*, 27.
- (38) Gonzalez, F. J.; Coughtrie, M.; Tukey, R. H. in *"Goodman and Gilman's the Pharmacological Basis of Therapeutics"*; McGraw-Hill: New York, 2011.
- (39) Lewis, D. F. V.; Dickins, M. *Drug Discov. Today* **2002**, *7*, 918-925.
- (40) Shimada, T.; Yamazaki, H.; Mimura, M.; Inui, Y.; Guengerich, F. P. *J. Pharmacol. Exp. Ther.* **1994**, *270*, 414-423.
- (41) Gleeson, M. P.; Davis, A. M.; Chohan, K. K.; Paine, S. W.; Boyer, S.; Gavaghan, C. L.; Arnby, C. H.; Kankkonen, C.; Albertson, N. *J. Comput.-Aided Mol. Des.* **2007**, *21*, 559-573.
- (42) Smith, S.; Leveridge, M.; GlaxoSmithKline: 2010, unpublished results.
- (43) Riley, R. J.; Grime, K.; Weaver, R. *Expert Opin. Drug Metab. Toxicol.* **2007**, *3*, 51-66.
- (44) Atkinson, A.; Kenny, J. R.; Grime, K. *Drug Metab. Dispos.* **2005**, *33*, 1637-1647.
- (45) Lipinski, C. A.; Lombardo, F.; Dominy, B. W.; Feeney, P. J. *Adv. Drug Delivery Rev.* **1997**, *23*, 3-25.
- (46) Hughes, J. D.; Blagg, J.; Price, D. A.; Bailey, S.; DeCrescenzo, G. A.; Devraj, R. V.; Ellsworth, E.; Fobian, Y. M.; Gibbs, M. E.; Gilles, R. W.; Greene, N.; Huang, E.; Krieger-Burke, T.; Loesel, J.; Wager, T.; Whiteley, L.; Zhang, Y. *Bioorg. Med. Chem. Lett.* **2008**, *18*, 4872-4875.
- (47) Lemke, T. L.; Williams, D. A.; Rocher, V. F.; Zito, W. S. *Foye's Principles of Medicinal Chemistry*; 7th ed.; Lippincott Williams & Wilkins: Baltimore, 2012.

- (48) Hann, M. M. *MedChemComm* **2011**, 2, 349-355.
- (49) Kuntz, I. D.; Chen, K.; Sharp, K. A.; Kollman, P. A. *PNAS* **1999**, 96, 9997-10002.
- (50) Hopkins, A. L.; Groom, C. R.; Alex, A. *Drug Discov. Today* **2004**, 9, 430-431.
- (51) Mortenson, P. N.; Murray, C. W. *J. Comput.-Aided Mol. Des.* **2011**, 25, 663-667.
- (52) McGinnity, D. F.; Collington, J.; Austin, R. P.; Riley, R. J. *Curr. Drug Metab.* **2007**, 8, 463-479.
- (53) Williams, J. A.; Hyland, R.; Jones, B. C.; Smith, D. A.; Hurst, S.; Goosen, T. C.; Peterkin, V.; Koup, J. R.; Ball, S. E. *Drug Metab. Dispos.* **2004**, 32, 1201-1208.
- (54) Stepan, A. F.; Mascitti, V.; Beaumont, K.; Kalgutkar, A. S. *MedChemComm* **2013**, 4, 631-652.
- (55) <http://www.cypotex.com/admepk/in-vitro-metabolism/microsomal-stability/>, accessed on 21st August 2013.
- (56) Davies, B.; Morris, T. *Pharm. Res.* **1993**, 10, 1093-1095.
- (57) Brown, R. P.; Delp, M. D.; Lindstedt, S. L.; Rhomberg, L. R.; Beliles, R. P. *Toxicol. Ind. Health* **1997**, 13, 407-484.
- (58) Strolin-Benedetti, M.; Whomsley, R.; Baltes, E. *Expert Opin. Drug Metab. Toxicol.* **2006**, 2, 895-921.
- (59) Le Cluyse, E. L.; Alexandre, E. *Methods Mol. Biol.* **2010**, 640, 57-82.
- (60) Johnson, T. W.; Dress, K. R.; Edwards, M. *Bioorg. Med. Chem. Lett.* **2009**, 19, 5560-5564.
- (61) Martin, Y. C. *J. Med. Chem.* **2005**, 48, 3164-3170.
- (62) Yoshida, F.; Topliss, J. G. *J. Med. Chem.* **2000**, 43, 2575-2585.
- (63) Veber, D. F.; Johnson, S. R.; Cheng, H.-Y.; Smith, B. R.; Ward, K. W.; Kopple, K. D. *J. Med. Chem.* **2002**, 45, 2615-2623.
- (64) Sakuma, T.; Kamataki, T. *Drug News Perspect.* **1994**, 7, 82-96.
- (65) Kararli, T. T. *Biopharm. Drug Dispos.* **1995**, 16, 351-380.

- (66) Kosa, T.; Maruyama, T.; Otagiri, M. *Pharm. Res.* **1997**, *14*, 1607-1612.
- (67) Huxley, J. S.; Teisslier, G. *Nature* **1936**, *137*, 780-781.
- (68) Lin, J. H. *Drug Metab. Dispos.* **1995**, *23*, 1008-1021.
- (69) Boxenbaum, H. J. *J. Pharmacokinet. Biopharm.* **1982**, *10*, 201-227.
- (70) Ward, K. W.; Smith, B. R. *Drug Metab. Dispos.* **2004**, *32*, 603-611.
- (71) Chiou, W. L.; Barve, A. *Pharm. Res.* **1998**, *15*, 1792-1795.
- (72) He, Y.-L.; Murby, S.; Warhurst, G.; Gifford, L.; Walker, D.; Ayrton, J.; Eastmond, R.; Rowland, M. *J. Pharm. Sci.* **1998**, *87*, 626-633.

## **Chapter 3**

# **The Design, Synthesis and Optimisation of IKK2 Inhibitors as Potential Anti- Inflammatory Agents**

## **3.1. Introduction**

### **3.1.1. I $\kappa$ B Kinase**

The proinflammatory signalling molecule NF- $\kappa$ B is naturally inhibited by I $\kappa$ B. NF- $\kappa$ B usually exists in the cytoplasm as inactive homo- or heterodimers complexed with I $\kappa$ B inhibitory proteins.<sup>1</sup> Upon cellular activation by stimuli such as cytokines (including TNF- $\alpha$  and IL-1 $\beta$ ), bacterial products (such as LPS), viral products or environmental stress, the I $\kappa$ B protein is phosphorylated at two specific serine residues (serines 32 and 36 on I $\kappa$ B $\alpha$ ) (Figure 3.1.1).<sup>2</sup> This results in ubiquitination and subsequent degradation to liberate NF- $\kappa$ B from the I $\kappa$ B/NF- $\kappa$ B complex. The NF- $\kappa$ B dimers (p50 and p65) are then free to translocate to the nucleus where the transcription of an array of genes responsible for cell survival and growth occurs. This transcription drives the expression of inflammatory mediators such as cytokines, chemokines, inflammatory enzymes, and growth and transcription factors (Figure 3.1.1).<sup>2</sup>



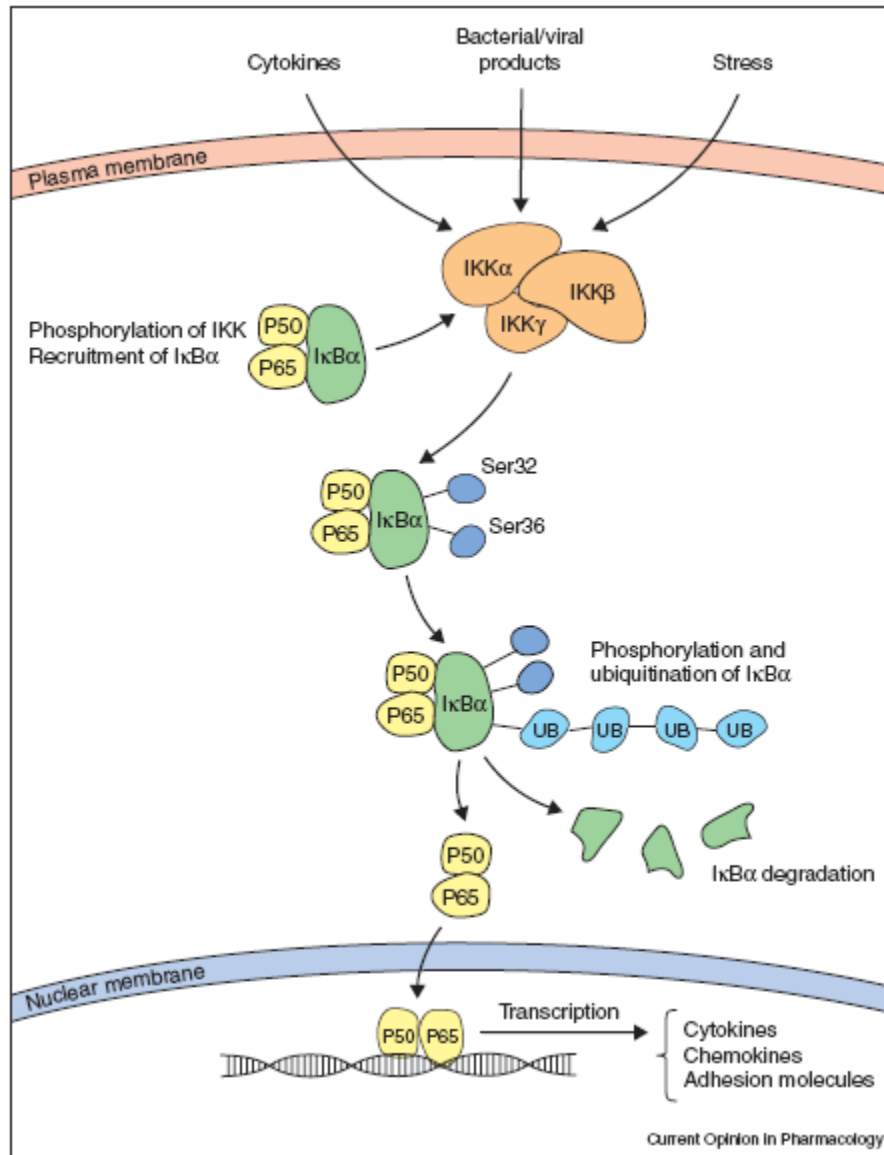


Figure 3.1.1. Activation of NF-κB.<sup>2</sup>

The activation of NF-κB by stimulus-induced phosphorylation of IκBα is initiated by specific kinases, which were identified in 1997.<sup>3</sup> The IκB kinase (IKK) signalosome was discovered to directly phosphorylate IκBα at Ser32 and Ser36. This complex is made up of various subunits, including IKK1 (or IKKα), IKK2 (or IKKβ) and NF-κB essential modulator (NEMO, also known as IKKγ).<sup>4,5</sup>

IKK1 and IKK2 are both serine/threonine protein kinases and are catalytically active. They both phosphorylate I $\kappa$ B proteins, but IKK1 is not required for NF- $\kappa$ B activation.<sup>6</sup> NEMO is the regulatory subunit of the IKK signalosome and has been found to interact preferentially with IKK2 to activate the IKK complex.<sup>5</sup> The IKK2 enzyme therefore plays a key role in the classical pathway of NF- $\kappa$ B activation, as downstream of the inflammatory stimulus the IKK signalosome is recruited to the activating receptor and IKK2 is phosphorylated, and then itself activated. The activated IKK2 enzyme then goes on to phosphorylate I $\kappa$ B $\alpha$ , causing its ubiquitination and degradation.<sup>6</sup>

### **3.1.2. The Role of I $\kappa$ B Kinases in Disease**

The canonical pathway responsible for NF- $\kappa$ B activation involves IKK2, whereas the non-canonical pathway involves IKK1. Although IKK1 does not play a critical role in activating inflammation, it is a key enzyme that is required for lymphoid organ development and B cell maturation.<sup>7</sup> There is some evidence that IKK1 has a role in inflammatory resolution due to its role in controlling the cell cycle by phosphorylating Aurora A.<sup>8,9</sup> Inactivation of IKK1 was shown to enhance inflammation in mice, indicating an opposing but complementary role to that of IKK2 for the control of inflammation.<sup>9</sup> IKK1 also has a key role in epidermal differentiation, which is independent of its kinase activity.<sup>10</sup> Mutations of the enzyme in humans have been linked to lethal fetal malformations that manifest in multiple skeletal defects and abnormally thick, shiny skin.<sup>11</sup> A critical role of IKK1 in the development of human skin cancer has been found, with a marked reduction in IKK1 expression in human squamous cell carcinomas.<sup>12</sup>

The only clinical relevance of NEMO in disease is its implication in immunodeficiency disorders such as incontinentia pigmenti and hypohidrotic ectodermal dysplasia.<sup>13,14</sup>

It is now widely accepted that IKK2 inhibition alone leads to disruption of IKK activation and degradation in response to pro-inflammatory stimuli and since

IKK2 plays such a critical role in NF- $\kappa$ B activation, IKK2 inhibition should provide an effective treatment for a range of diseases where this pathway is implicated.

### **3.1.3. IKK2 as a Target for Respiratory Disease**

The IKK2 enzyme represents a target both for asthma and COPD. The NF- $\kappa$ B pathway has been shown to be activated in asthmatics; one study showed a 44% greater level of NF- $\kappa$ B DNA-binding in bronchial biopsies from asthma patients, and another gave evidence of increasing NF- $\kappa$ B activation with increasing disease severity.<sup>15,16</sup> Targeting NF- $\kappa$ B activation for the treatment of asthma is therefore an attractive strategy and *in vitro* and *in vivo* studies have supported this. The administration of an IKK2 inhibitor blocked cytokine release from human airway smooth muscle cells and led to reduced inflammatory cytokine, gene and protein expression, and airway eosinophilia in a rat model of lung inflammation.<sup>17</sup>

Several studies have also been carried out to validate whether NF- $\kappa$ B activation plays a role in the inflammatory process in COPD. Di Stefano has characterised the expression and localisation of p65, the major sub-unit of NF- $\kappa$ B, and showed that in bronchial biopsies, p65 positive epithelial cells and p65 nuclear localization were increased in COPD patients and correlated with the level of airflow limitation.<sup>18</sup> Additionally, it has been shown that macrophages within sputum and lung parenchyma obtained from COPD patients during an exacerbation contained increased p65 nuclear localization.<sup>19</sup> NF- $\kappa$ B is activated when I $\kappa$ B $\alpha$ , its inhibitor, is phosphorylated and degraded by IKK2 and COPD patients have also shown a greater percentage of airway epithelial cells that were positive for phosphorylated-I $\kappa$ B $\alpha$ .<sup>20</sup> Furthermore, increased NF- $\kappa$ B DNA binding has been observed in the skeletal muscle of COPD patients who have low body weight, which reinforces NF- $\kappa$ B activation as a mechanism that leads to skeletal muscle atrophy in COPD.<sup>21</sup> Ablation of IKK2 has been shown to improve skeletal muscle mass, strength and fibre type.<sup>22</sup> It has been shown that cigarette smoke contains a number of reactive species that promote the activation of NF- $\kappa$ B; preventing this activation could provide an

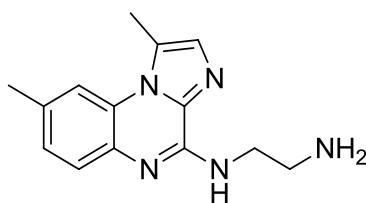
effective therapy for the prolonged inflammation observed in the lungs of patients with COPD.<sup>23</sup>

Analysis of the target validation work shows the potential an IKK2 inhibitor could have in the treatment of asthma and COPD and the current landscape of the development of IKK2 inhibitors will be reviewed here.

### **3.1.4. IKK2 Inhibitors**

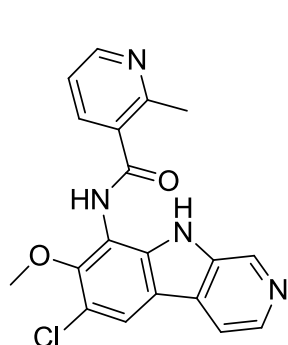
Currently there is only one IKK2 inhibitor in active clinical development and relatively few chemical series have been disclosed in the literature. Many IKK2 inhibitors also inhibit IKK1 and other kinases so the development of selective IKK2 inhibitors remains a key requisite.

One of the first IKK2 inhibitors that had selectivity over IKK1 was reported by researchers from Bristol Myers-Squibb. BMS-345541, a tricyclic imidazo[1,2-*a*]quinoxaline, exhibited approximately 10-fold selectivity for IKK2 ( $pIC_{50} = 6.5$ ) over IKK1 ( $pIC_{50} = 5.4$ ) and was shown to inhibit cytokine release in a mouse model of inflammation.<sup>24</sup> The compound was initially reported to have selectivity over a panel of 15 protein kinases; however the selectivity was assessed more widely and the compound inhibited several other kinases. No further development of the compound has been reported, presumably due to its lower activity of IKK2 inhibition and poorer selectivity profile compared to other inhibitors.

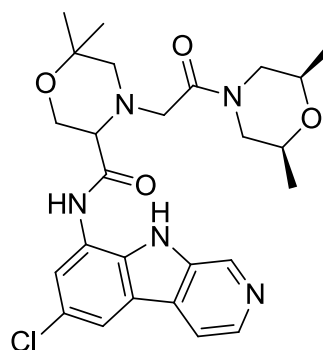


**BMS-345541**

A series of  $\beta$ -carboline compounds have been reported by Millenium Pharmaceuticals to be more potent IKK2 inhibitors with improved selectivity profiles. MLN-120B inhibits IKK2 with a  $pIC_{50}$  of 7.2 and exhibits excellent selectivity over IKK1 and NEMO ( $pIC_{50} < 4$  for both), as well as a panel of tyrosine and serine/threonine kinases.<sup>25</sup> A related compound, MLN-0415, was the first compound to be progressed to Phase I clinical trials for the treatment of inflammatory disorders; however its development was discontinued in 2010 due to a non-specified unfavourable safety profile.<sup>26</sup>

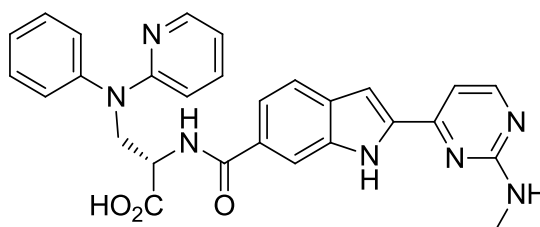


**MLN-120B**



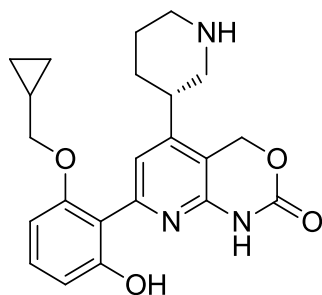
**MLN-0415**

The only IKK2 inhibitor still in clinical development is SAR-113495, which completed a Phase I study for the treatment of osteoarthritis in 2011.<sup>27</sup> SAR-113495 has been described as a sub-nanomolar IKK2 inhibitor and may have the structure shown below, based upon a single compound patent filing.<sup>28</sup>

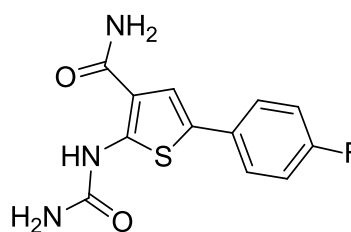


**SAR-113495**

There is no reported clinical development of other IKK2 inhibitors; however there are other chemical series that have been reported as IKK2 inhibitors where compounds have shown effects in *in vivo* models of inflammation. Examples include 2-amino-6-(2-hydroxyphenyl)pyridines, such as BAY-65-1942, and thiophene carboxamides, such as TPCA-1.



**BAY-65-1942**



**TPCA-1**

BAY-65-1942 is a highly potent IKK2 inhibitor ( $pK_i = 8.7$ ) with some selectivity over IKK1 ( $pK_i = 6.9$ ) that showed inhibition of stress-induced NF- $\kappa$ B transactivation and cytokine expression in rodents.<sup>29</sup> TPCA-1 inhibited IKK2 with a  $pIC_{50}$  of 7.8 and IKK1 with a  $pIC_{50}$  of 6.4, and also blocked NF- $\kappa$ B activation and inflammatory mediator release in a steroid-sensitive animal model of airway inflammation.<sup>30,31</sup>

These data provide further evidence that IKK2 inhibitors offer an effective therapeutic approach for inhibiting pulmonary inflammation and efforts are still ongoing for the discovery of IKK2 inhibitors that exhibit the desired kinase selectivity and developability characteristics. The next section will describe the potential for structure-based drug design in this endeavour.

### 3.1.5. IKK2 Structural Biology

The IKK signalosome is an isolated branch of the human kinome, so the enzymes are relatively dissimilar to the other human protein kinases (Figure 3.1.2).<sup>32</sup>

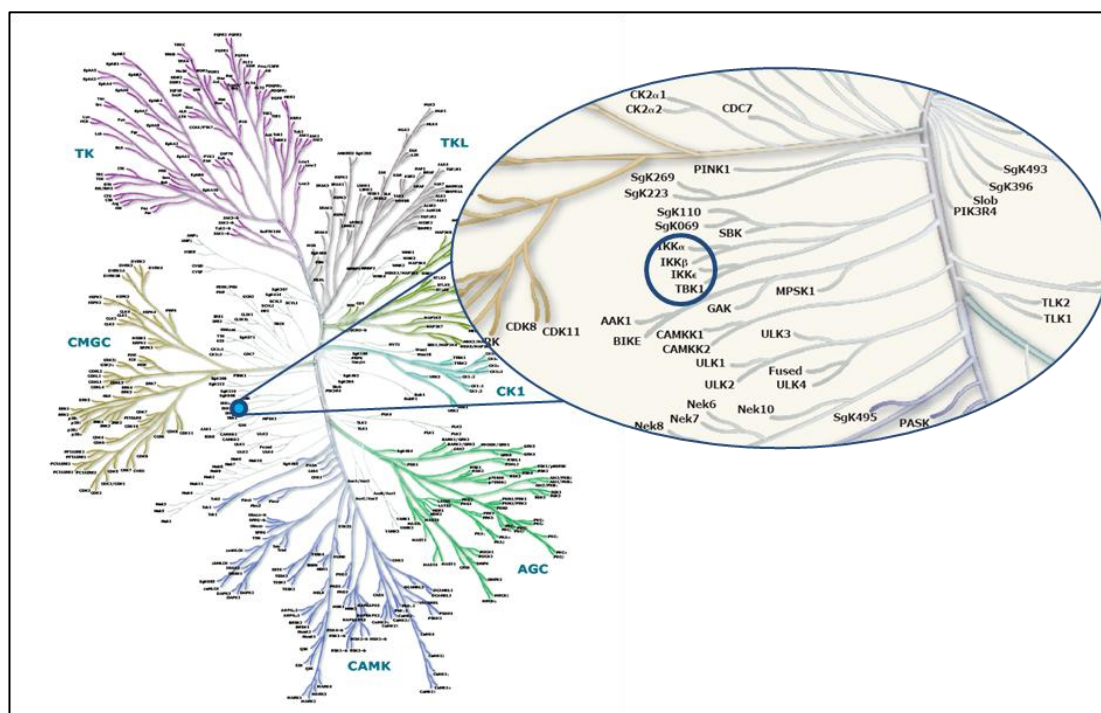


Figure 3.1.2. The positioning of the IKK family within the human kinome.<sup>32</sup>

The IKKs have low sequence homology to the other protein kinases (<25% amino acid identity in the kinase domain).<sup>33</sup> IKK2 is most similar in structure to IKK1, with 66% identity shared in the kinase domain, and although the other members of the IKK family, NEMO and TBK1, are related to one another, they only share 30-32% sequence identity with the kinase domains of IKK1 and IKK2.<sup>33</sup> Obtaining an IKK2 inhibitor that is selective over IKK1 is therefore a key challenge.

A structure-based drug design approach could be advantageous for the discovery of selective IKK2 inhibitors; however obtaining an IKK2 crystal structure has been difficult. The first crystal structure for the enzyme isolated from *Xenopus*

*laevis* was reported in 2011.<sup>34</sup> The crystal structure was not suitable for structure-based drug design as it was of lower resolution (3.6-4 Å) than is usually required (2-3 Å). Evidence for its unsuitability was observed when the authors initially modelled the observed electron density incorrectly to the active site ligand.<sup>35</sup> This compound is made up of 4 ring structures (labelled A, B, C and D) and it can be seen that within ring C, a pyrimidine, the carbon adjacent to both nitrogens is modelled to be  $sp^3$  hybridised (Figure 3.1.3a).<sup>34</sup> The structure has since been refined by the authors so that the ligand is in a better conformation (Figure 3.1.3b).<sup>36</sup> Nevertheless, the poor resolution of the crystal structure led to ambiguity in the modelling and it is possible that the electron density the authors attributed to the ligand may have been that of the side chains of the protein.

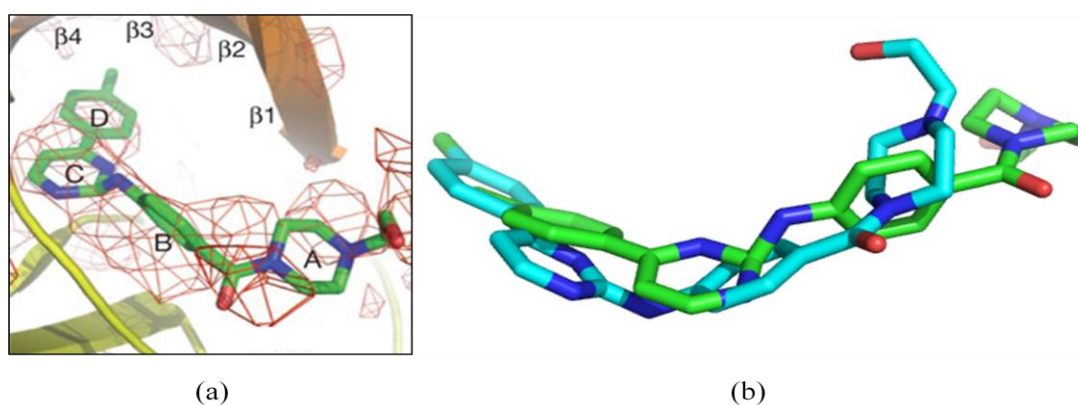


Figure 3.1.3. (a) Electron density map for an inhibitor complexed with IKK2; (b) the ligand conformations.<sup>34</sup>

However, the crystal structure did give confidence that an inhibitor would bind at the hinge loop connecting the N and C lobes, as is common for most kinase inhibitors (Figure 3.1.4).<sup>34</sup>



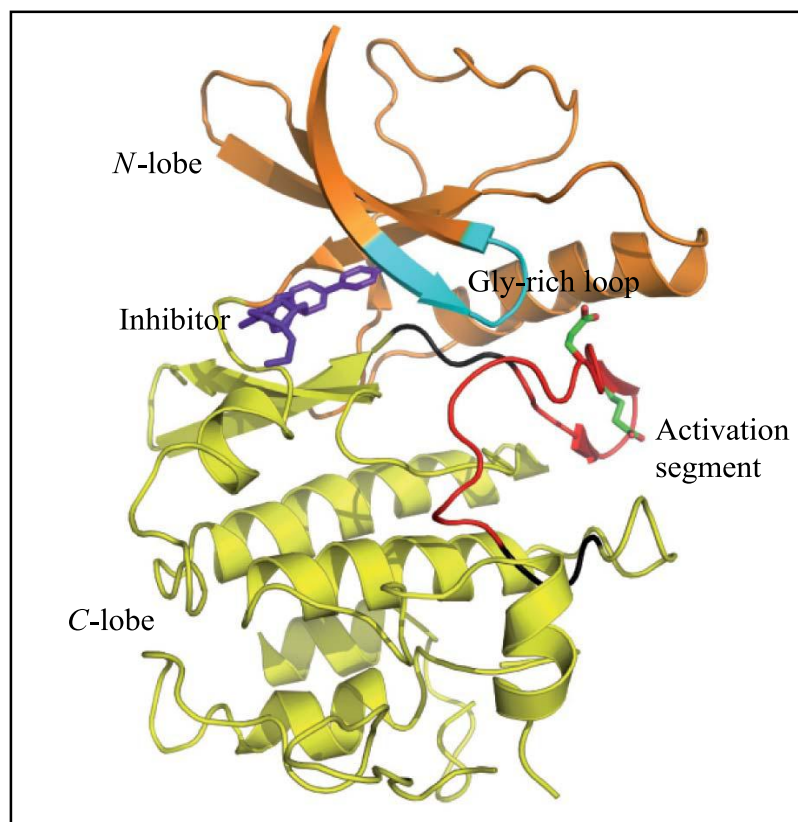


Figure 3.1.4. Structure of the IKK2 kinase domain and binding position of an inhibitor.<sup>34</sup>

The crystal structure also showed that the kinase domain of the protein made up one component of a trimodular architecture that also includes an ubiquitin-like domain (ULD) and an elongated,  $\alpha$ -helical scaffold/dimerisation domain (SDD) (Figure 3.1.5).<sup>34</sup>

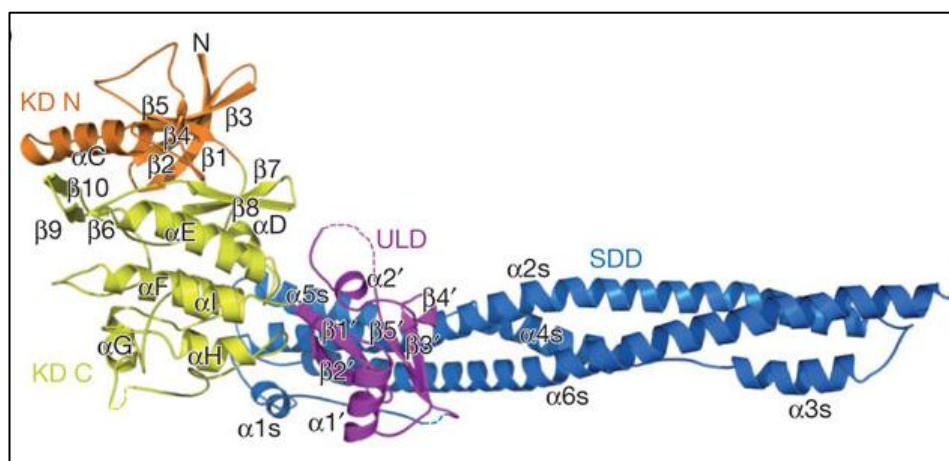


Figure 3.1.5. Ribbon diagram of *Xenopus laevis* IKK2 structure.<sup>34</sup>

It was concluded that this structure is important for IKK2 function as the ULD-SDD region interacts directly with the C-terminal portion of I $\kappa$ B $\alpha$  so that its phosphorylation sites are presented to the kinase domain active site of IKK2, which allows IKK2 to activate the NF- $\kappa$ B pathway specifically and efficiently.<sup>34</sup>

This observation was corroborated in work to obtain a human IKK2 crystal structure, which was reported in August 2013.<sup>37</sup> A near full-length human IKK2 wild type protein phosphorylated at the activation loop was isolated and this was observed to have the same trimodular structure as the structure from *Xenopus laevis*.<sup>37</sup> The crystal structure of human IKK2 showed that it existed as an asymmetric dimer in which one kinase domain was phosphorylated and in its active conformation and the other was not phosphorylated and adopted an inactive conformation. This suggested that the structure of IKK2 from *Xenopus laevis* described the inactive state that precedes the intermediate active, open state represented by the structure of phosphorylated human IKK2.<sup>37</sup>

The structure of human IKK2 was of 2.8 Å resolution and the ATP-pockets of both the kinase domains of the dimer had a staurosporine analogue (K252a) bound.<sup>37</sup> The binding mode of K252a showed key hydrogen bond contacts to Glu97 and Cys99 residues of the hinge region, as well as an additional hydrogen bond from the hydroxyl to the carbonyl of Glu149 (Figure 3.1.6).<sup>37</sup>

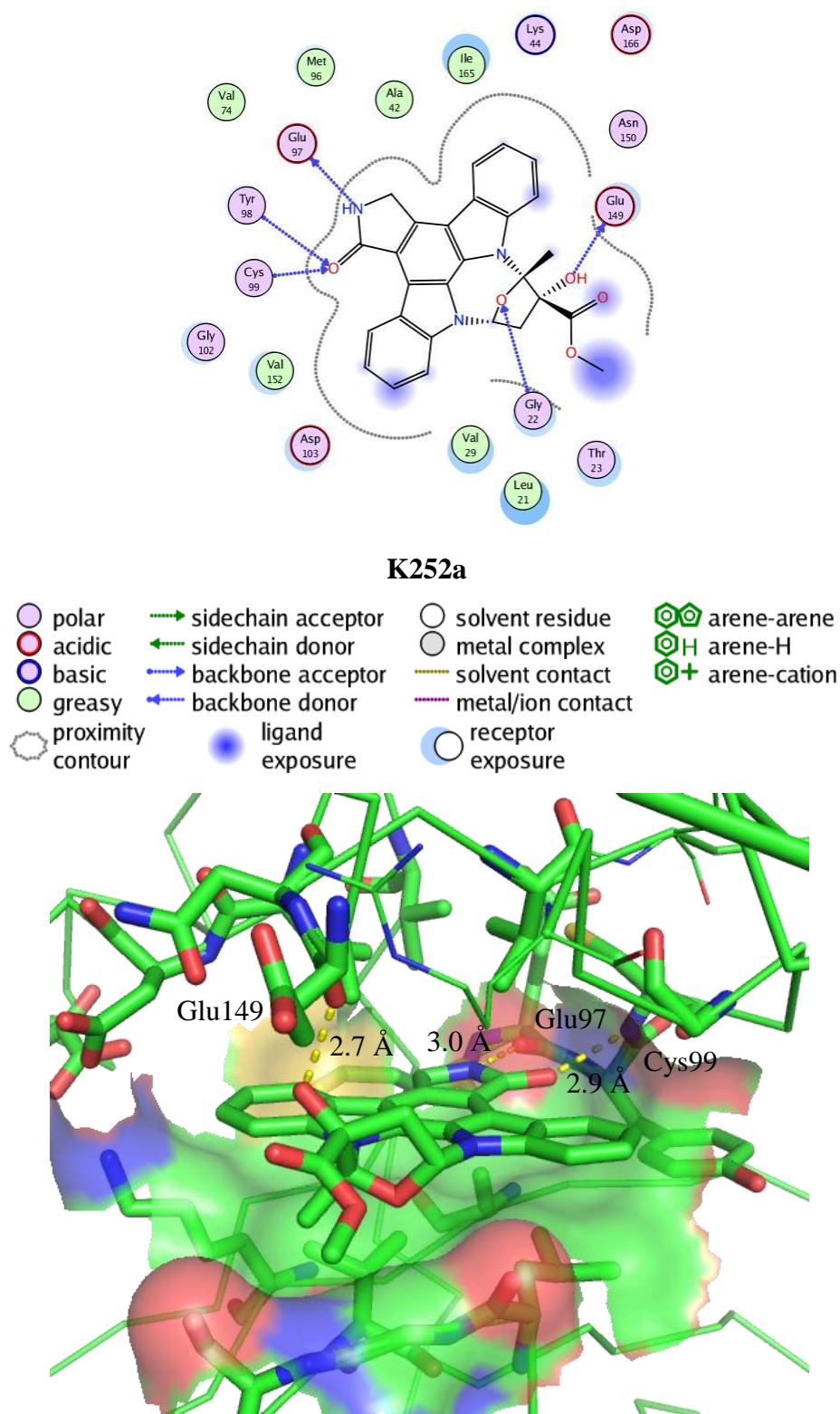


Figure 3.1.6. Hinge interactions of K252a bound in human IKK2 (2.8 Å resolution).<sup>37</sup>

This high resolution structure may now permit structure-based drug design, which will be advantageous for the future development of selective IKK2 inhibitors.

Since disclosure of this crystal structure only occurred very recently, a homology model was initially developed to aid the design of novel inhibitors.<sup>38</sup> The sequence of IKK2 was aligned to a large panel of protein kinase structures and although CDK-2 was only 27% identical to IKK2 in the kinase domain, CDK-2 was chosen as a template on which to build the model. The kinase chain from a complex of CDK-2 cells with cyclin A was extracted to give an active-like ATP site conformation that was used to generate IKK2 co-ordinates.<sup>38</sup> Complexing a close analogue (**1**) of the thiophene carboxamide IKK2 inhibitor TPCA-1 with CDK-2 allowed refinement of the model and helped define the key interactions of an IKK2 inhibitor and the kinase; a pharmacophore was developed based on this protein-ligand complex (Figure 3.1.7).<sup>39</sup>

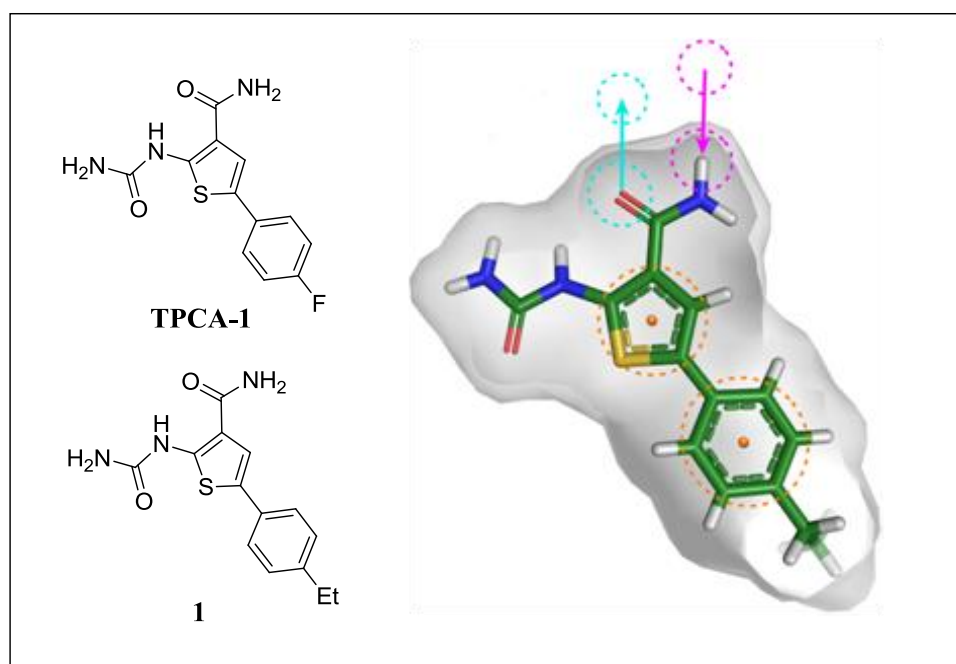
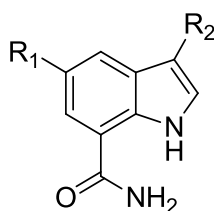


Figure 3.1.7. IKK2 pharmacophore showing aromatic and hydrogen bond vectors.<sup>39</sup>

Three-dimensional pharmacophore searching identified several hundred compounds that were tested for IKK2 inhibition and the most common motif of the weakly active hits contained a primary carboxamide that was held in a constrained conformation by an adjacent hydrogen-bonding functionality.<sup>39</sup> Substructure searching and subsequent SAR exploration led to the discovery of potent inhibitors with a common 1*H*-indole-7-carboxamide core structure.<sup>39</sup>

### 3.1.6. Indole Carboxamides as IKK2 Inhibitors

Based on the background detailed above, 3,5-disubstituted indole-7-carboxamides of general structure **2** have been explored within our laboratories as inhibitors of IKK2 and have shown potential as therapeutic agents for disorders associated with inappropriate IKK2 activity.<sup>40</sup>



**2**

Compounds from the indole carboxamide series have been tested for activity against IKK2 in an enzyme assay and were shown to be selective inhibitors of IKK2 with pIC<sub>50</sub> values of >5.0.<sup>41</sup> Docking of a representative compound (**3**) into the IKK2 homology model shows the main interactions of the indole carboxamides with the protein kinase (Figure 3.1.8).<sup>39</sup>

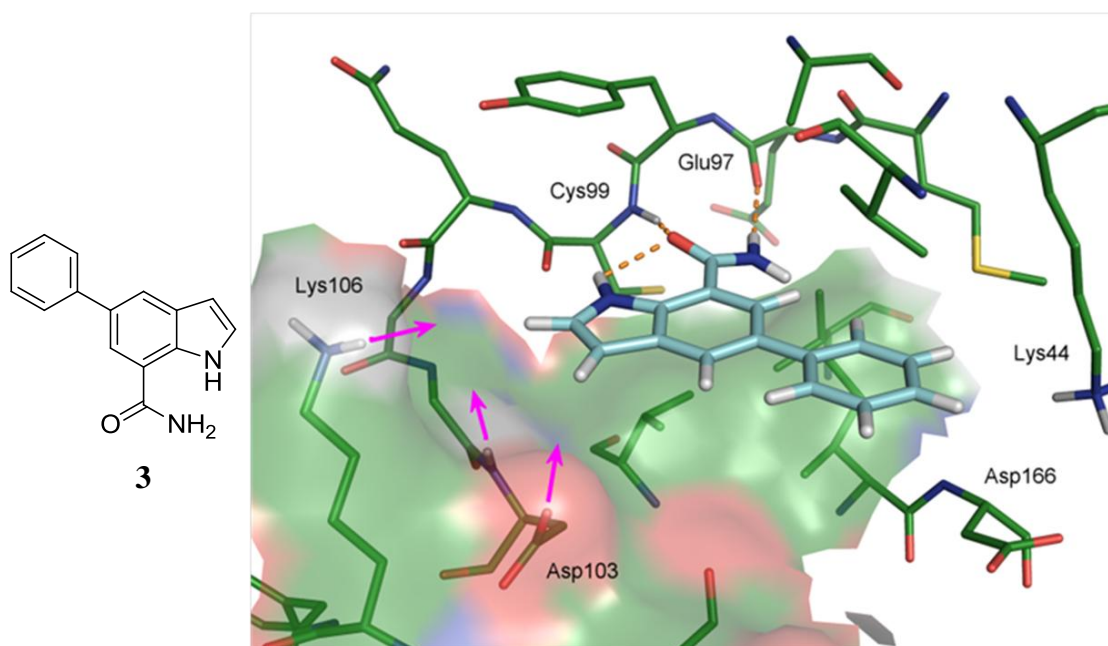


Figure 3.1.8. Compound **3** docked into IKK2 homology model, purple arrows show potential hydrogen-bonding vectors.<sup>39</sup>

In the model the primary carboxamide makes a pair of hydrogen bonds to the Glu97 and Cys99 residues of the hinge region. The indole N-H also makes a hydrogen bond to the carbonyl that ensures the carboxamide remains co-planar with the indole.<sup>39</sup> It is possible that the indole N-H also makes a hydrogen bond to the outer carbonyl of Cys99, as the N-H...O distance is between 2 and 3 Å. The opportunity to vary substituents around the indole ring makes this series highly attractive. Substitution at the indole 2- or 3-positions to target hydrogen-bonding interactions with Lys106 and Asp103 is one strategy for improving potency in this series. Furthermore, since Asp103 is an acidic residue the introduction of a basic group at the 3-position could be beneficial both for potency and physicochemical properties (*e.g.* solubility). The indole 5-position also represents an attractive vector for exploration of hydrogen-bonding interactions with Lys44 and Asp166. Although this region of the kinase looks to be fairly spacious in the homology model, SAR exploration of the 5-position showed that only aromatic substituents that maintain co-



planarity with the indole core were tolerated.<sup>42</sup> Therefore, neither non-aromatic groups nor *ortho*-substituted aromatics could be installed at this position. This highlights one disadvantage of utilising a homology model and reinforces the importance of carrying out effective SAR analysis.

It has since been possible to compare the homology model with a docked pose of compound **3** in the human IKK2 crystal structure that has recently been reported (Figure 3.1.9).<sup>43</sup> The docking pose identifies the same hydrogen bonding interactions with the Glu97 and Cys99 residues of the hinge region. The positioning of the Lys106 and Asp103 residues, which could be potential targets for hydrogen-bonding by substitution from the 2- or 3-positions of the indole, also compares well with that of the homology model.

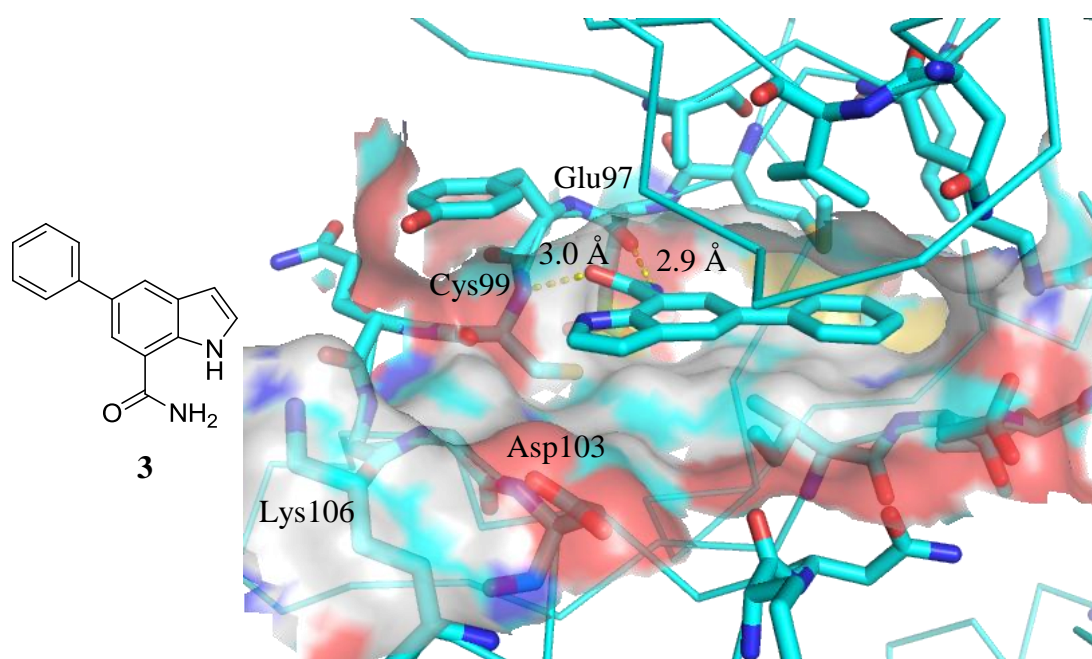


Figure 3.1.9. Compound **3** docked into the human IKK2 crystal structure.<sup>43</sup>

Interestingly, the region around the 5-phenyl substituent of compound **3** does appear to be less spacious than that observed in the homology model, which

corroborates the observation that 5-position substituents that are not co-planar with the core or have  $sp^3$  character are not tolerated (Figure 3.1.10).

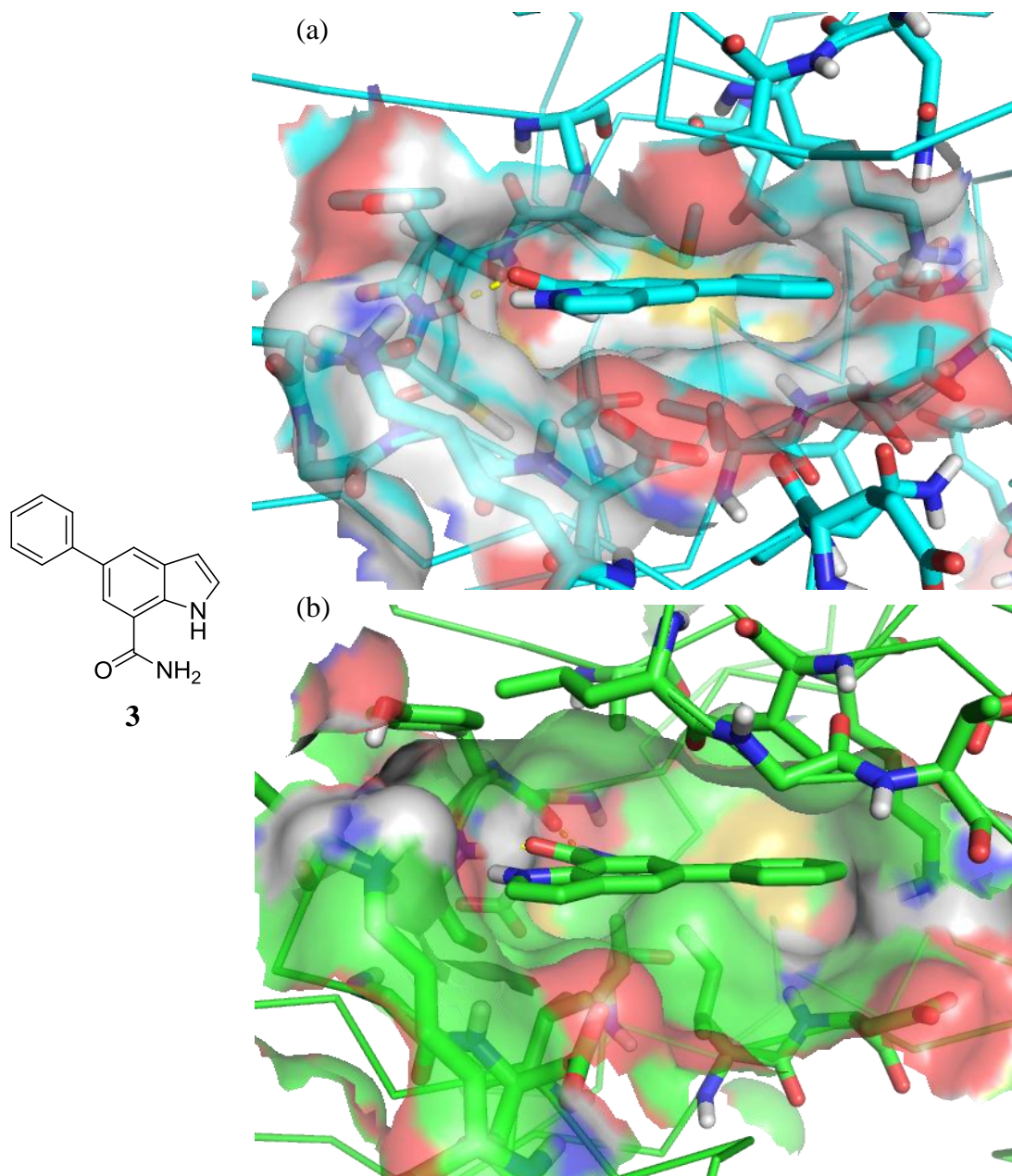
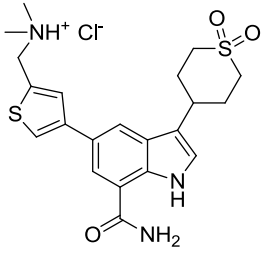
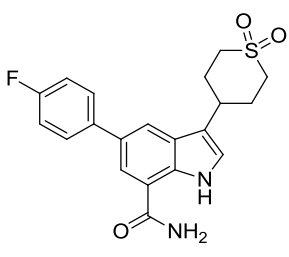


Figure 3.1.10. (a) Compound 3 docked into the human IKK2 crystal structure; (b) compound 3 docked into the IKK2 homology model.<sup>43</sup>



To date, work performed in our laboratories has shown that the leading indole carboxamide compounds (**4a** and **4b**) are potent against IKK2, selective over IKK1 and have good ligand efficiency (>0.3) and PFI values (<7.0).<sup>41</sup>

Structure		
Compound	<b>4a</b>	<b>4b</b>
Mean IKK2 pK <sub>i</sub> (N)	9.5 (12) <sup>a</sup>	8.3 (1)
Mean IKK1 pK <sub>i</sub> (N)	7.5 (10)	6.6 (2)
Mean HWB pIC <sub>50</sub> (N)	7.2 (18)	5.9 (2)
LE/LLE <sub>AT</sub>	0.45/0.51	0.42/0.44
PFI	5.0	6.5
mChromlogD <sub>pH7.4</sub>	1.95	3.51
clogP	1.1	1.7
MW	432	386
TPSA	96	93
AMP (pH 7.05, nm/sec)	20.9	280
CLND solubility (μM)	398	-
FaSSIF solubility (μg/mL)	258	-
hERG pIC <sub>50</sub>	<4.3	-
CYP 3A4 pIC <sub>50</sub>	<4.3	-

<sup>a</sup> Returned value >10.1 on one test occasion.

Table 3.1.1. Lead indole carboxamides.

Compound **4a** has the highest potency in the IKK2 enzyme assay, excellent ligand efficiency and is 100-fold selective over IKK1 (Table 3.1.1). Compound **4a** also has excellent cellular activity in the HWB assay and there are no hERG or CYP liabilities, which is important in order to avoid potential drug safety issues. Despite the encouraging potency and selectivity of compound **4a**, the compound has low

permeability and high *in vivo* clearance ( $Cl_b = 99$  ml/min/kg), so the compound has no oral bioavailability ( $F = 0\%$ ).<sup>42</sup>

## **3.2. Aims**

Based on the preliminary studies from our laboratory to the lead compound types detailed above, the aims of the current research are to deliver a compound with an oral PK profile consistent with low predicted oral clinical dose (~10 mg), whilst maintaining good IKK2 enzyme and cellular potency and 100-fold selectivity over other kinases. The physicochemical properties of the molecule must therefore be within the low attrition guidelines for oral drugs, and the compound must have no potential toxicities (e.g. hERG, CYP).<sup>44,45</sup>

The desired molecular profile for an oral, chronically administered IKK2 inhibitor is shown in Table 3.2.1.

Parameter	Desired value
IKK2 pK <sub>i</sub>	>8.0
IKK1 selectivity	>100-fold
Wider kinase selectivity	>100-fold
HWB pIC <sub>50</sub>	>7.0
PFI	<7.0
LE	>0.3
LLE <sub>AT</sub>	>0.3
hERG pIC <sub>50</sub>	<4.3
CYP 3A4 pIC <sub>50</sub>	<4.3
FaSSIF solubility	>100 µg/mL
Permeability	High
Clearance	Low
Bioavailability	High

Table 3.2.1. Desired molecular profile of an oral IKK2 inhibitor.

Firstly, a Hansch substituent analysis of previously synthesised indole carboxamide compounds, for which the IKK2 enzyme data had been measured, was carried out by Xiao Lewell (Computational and Structural Chemistry, GSK) to determine if any 3- and 5-position substituents were contributing favourably to the IKK2 potency.<sup>46</sup> Compounds with similar substituents were then synthesised and tested for their biological activity. Further exploration of the incorporation of small substituents at the 3-position of the indole carboxamide was then carried out, with a view to installing an oxetan-3-yl group at this position.

## 3.3. Results and Discussion

### 3.3.1. 3-Substituted Indole Carboxamides

#### 3.3.1.1. Hansch Analysis

Hansch analysis involves the investigation of the quantitative relationship between the biological activities of a series of compounds and their calculated physicochemical parameters, such as lipophilicity, polarizability, and other steric and electronic properties.<sup>47</sup> In his seminal work, Hansch established a correlation between the biological activities of substituted phenoxyacetic acids and constants that described the lipophilicity and electronic nature of the substituent.<sup>48</sup> The Hammett substituent constant,  $\sigma$ , was used to describe the electronic nature of a substituent and  $\pi$ , a constant that represented the difference in the logarithms of the partition coefficients of the unsubstituted and substituted compounds, was used to describe the lipophilicity. Linear regression analysis was used to fit the observed biological activities with the substituent constants in order to develop an equation to describe the relationship between structure and activity (Equation 3.3.1), where C is the molar concentration of compound that produces a biological response (e.g. IC<sub>50</sub>).<sup>48</sup>

$$\log\left(\frac{1}{C}\right) = k_1\pi + k_2\sigma + k_3$$

Equation 3.3.1. Relationship between biological activity and substituent constants.<sup>48</sup>

This equation could then be used to predict the biological activity of the different phenoxyacetic acids and the overall agreement between the predicted and observed biological activities was found to be ‘surprisingly good’.<sup>48</sup> This work was the first example of quantitatively relating the structure of a compound to its activity, and this has since become known as a quantitative structure-activity relationship (QSAR).

QSAR are now developed using a variety of parameters as descriptors of the structural properties of molecules. Hammett  $\sigma$  values are often used for electronic parameters, but there are many other substituent constants to describe several other electronic, steric and lipophilic substituent effects.<sup>49</sup>

For this programme of work, a Hansch analysis was carried out by Xiao Lewell (Computational and Structural Chemistry, GSK). The 3- and 5-substituents of indole carboxamides with measured biological activities were analysed separately with a view to developing a QSAR model to determine substituents for each position that would be predicted to have high IKK2 potency.<sup>46</sup> Fourteen parameters that describe various properties of the substituents were used to assess whether there were any correlations with the measured biological data.<sup>46</sup> There are many more parameters to describe the properties of the substituents; however fourteen were readily available for the computational analysis carried out here. Unfortunately, there was no correlation between the properties of the 5-substituents and the biological data; however, three compounds with different 3-substituents were observed to have a good correlation with most of the parameters (represented in Table 3.3.1 by the  $R^2$  value).<sup>46</sup>

Structural Parameter	Definition	R <sup>2</sup>
$\sigma^*$	Polar substituent constant	1
VerloopB3	Steric parameter (width)	0.9998
VerloopB4	Steric parameter (width)	0.9998
$\sigma_p$	Hammett <i>para</i> -substituent constant	0.9995
VerloopL	Steric parameter (length)	0.9994
$\pi$ (aliphatic)	Lipophilicity (aliphatic)	0.9981
$\pi$ (aromatic)	Lipophilicity (aromatic)	0.9974
$\sigma_m$	Hammett <i>meta</i> -substituent constant	0.9956
F	Field constant	0.9943
MR (aliphatic)	Molar refractivity (aliphatic)	0.9860
MR (aromatic)	Molar refractivity (aromatic)	0.9839
R	Resonance constant	0.8832
VerloopB1	Steric parameter (width)	0.6464
VerloopB2	Steric parameter (width)	0.6464

Table 3.3.1. Substituent parameters and their correlation with measured IKK2 activity of 3-substituted indole carboxamides.<sup>46</sup>

The correlations would not usually be of note as they were based on only three data points; however most of the correlations identified here were observed to be very strong. Several correlations had R<sup>2</sup> values close to 1, which represented a near perfect prediction of one term by the other. However, a larger set of small 3-substituted indole carboxamides was desired so that the observed structure-activity relationships could be substantiated.

Linear regression analysis was used to develop equations that related the IKK2 potency to the fourteen substituent parameters in order that the biological activity of compounds containing novel 3-substituents could be predicted.<sup>46</sup> An example is Equation 3.3.2, which relates IKK2 potency to  $\sigma^*$ , the polar substituent constant.

$$IKK2\ pK_i = 4.8637 + 0.7228(\sigma^*)$$

Equation 3.3.2. Regression equation relating IKK2 potency and the  $\sigma^*$  value of the substituent.<sup>46</sup>

A large number of potential 3-substituents were identified from the original Hansch table, giving 163 groups to consider.<sup>49</sup> The equations for each substituent parameter gave a separate predicted potency; hence fourteen predicted IKK2  $pK_i$  values were obtained for each of the compounds containing a novel 3-substituent. The fourteen predicted IKK2 activities were then used to produce a rank score using an AdamantisPro<sup>®</sup> utility ranking.<sup>46</sup> This ranking method takes into account the contributions of each of the fourteen Hansch parameters, meaning that although some substituents have high predicted IKK2 activity, they are not favoured when interrogated by the Adamantis score rank as they have only been predicted to have high activity by less than half of the fourteen parameters. This helped to optimise the predicted IKK2 activity for the 163 substituents from the least to the most active values. Figure 3.3.1 plots the average predicted IKK2 potency against Adamantis rank score for the 163 potential 3-substituents, with compounds in the red region having high predicted IKK2  $pK_i$  but low rank score, therefore indicating that their potency has only been predicted to be high by a few of the 14 Hansch equations. These compounds are therefore of less interest, and Table 3.3.2 identifies the highest ranked substituents with good predicted IKK2  $pK_i$  values to be considered as potential 3-position groups (in the green region *cf.* the plot).<sup>46</sup>

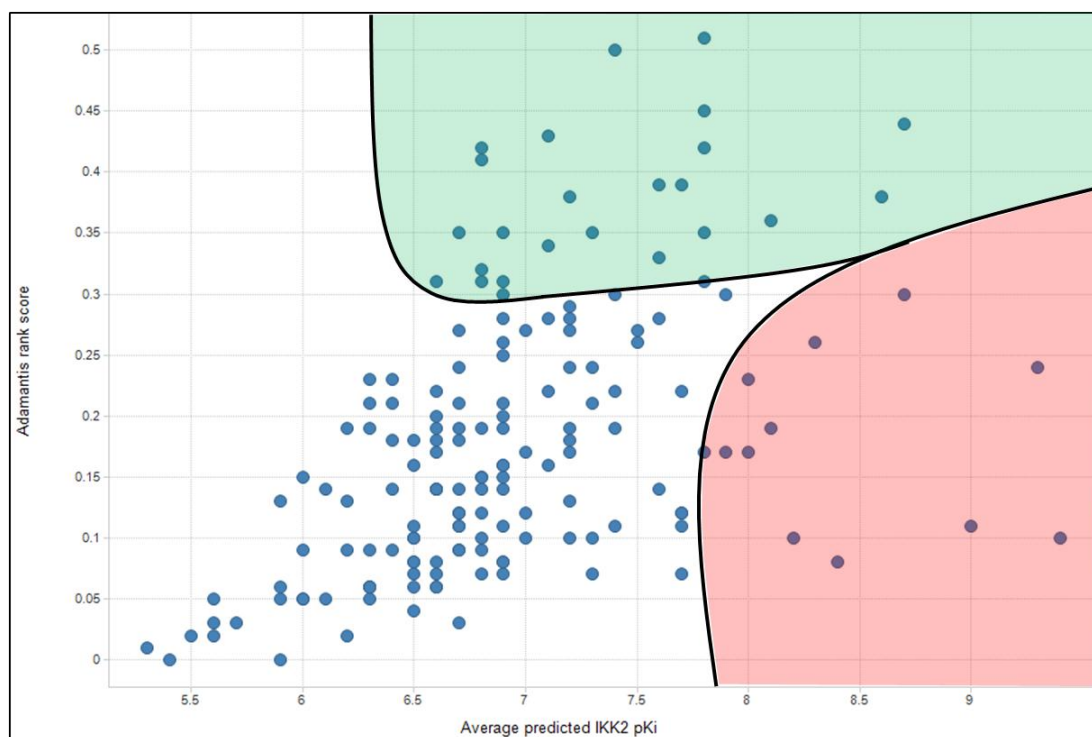


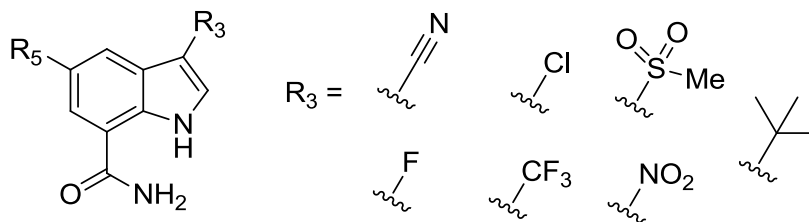
Figure 3.3.1. Predicted potency of compounds with a range of 3-substituents.<sup>46</sup>



3-substituent	Adamantis Pro Rank Score	Predicted IKK2 pKi	3-substituent	Adamantis Pro Rank Score	Predicted IKK2 pKi
*-NMe <sub>3</sub> <sup>+</sup>	0.44	8.7	*-CO <sub>2</sub> H	0.38	7.2
*-NH <sub>2</sub>	0.38	8.6	*-CF <sub>3</sub>	0.43	7.1
*-N=O	0.36	8.1	*-OMe	0.34	7.1
*-≡N	0.51	7.8	*-COMe	0.35	6.9
*-N <sup>+</sup> (O <sup>-</sup> ) <sub>2</sub>	0.42	7.8	*-Me	0.28	6.9
*-OH	0.45	7.8	*-C <sub>2</sub> F <sub>5</sub>	0.31	6.9
*-SO <sub>2</sub> Me	0.31	7.8	*-Cl	0.42	6.8
*-SO <sub>2</sub> CF <sub>3</sub>	0.35	7.8	*-≡-H	0.32	6.8
*-SO <sub>2</sub> F	0.39	7.7	*-CO <sub>2</sub> Me	0.31	6.8
*-S <sup>+</sup> (O) <sub>2</sub>	0.33	7.6	*-Br	0.41	6.8
*-H	0.39	7.6	*-I	0.35	6.7
*-F	0.50	7.4	*-SH	0.31	6.6

Table 3.3.2. 3-position substituent ranking.<sup>46</sup>

From these 24 highly ranked compounds, a subset of six compounds with 3-position substituents were selected for synthesis.<sup>46</sup> The *tert*-butyl analogue was also synthesised within our laboratory in a separate area of work, so was also included in the analysis of the set of 3-substituted compounds.<sup>50</sup>

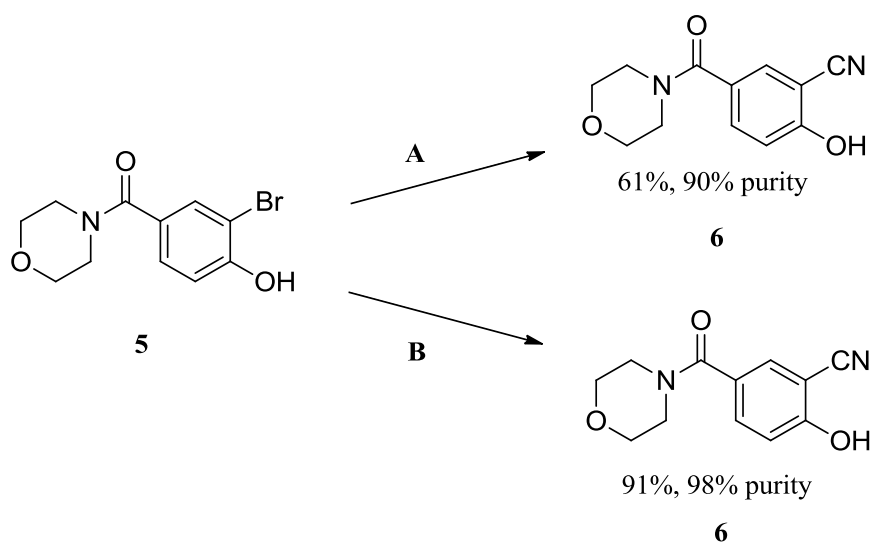


These key substituents were chosen as it was thought they could be accessed synthetically and because they spanned a range of predicted IKK2 potencies and AdamantisPro<sup>®</sup> rank scores, which would allow the effectiveness of the model to be evaluated.

### **3.3.1.2. Synthesis of 3-Cyano-1*H*-indole-7-carboxamides**

An initial investigation into alternative 3-position substituents focused on the incorporation of a 3-cyano group, as this was ranked highly from the Hansch analysis. A variety of aryl units will also be introduced at the 5-position in order to provide compounds as direct comparators to the lead indole carboxamide compounds and build structural diversity within the 3-cyano series.

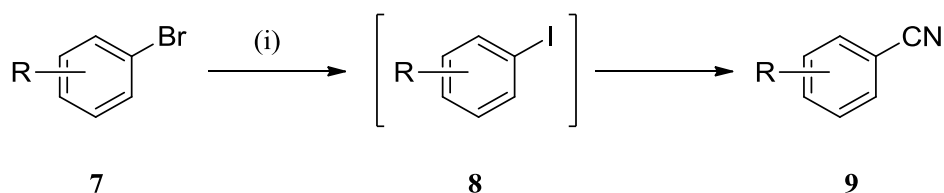
There are various methods of installing an aryl nitrile group; for example, the classic Rosenmund-von Braun synthesis involving the cyanation of aryl halides with an excess of copper(I) cyanide.<sup>51,52</sup> The reaction is carried out in polar, high-boiling solvents and often requires heating at elevated temperatures, which can lead to poor yields due to the potential for decomposition at high temperatures and the difficulty in removing heavy metal by-products. An example of these issues was highlighted in the cyanation of aryl bromide **5**, where heating with CuCN at 165 °C gave a yield of 61% but improved conditions utilising Zn(CN)<sub>2</sub> and Pd/C at lower temperature gave a higher yield of 91% and improved product purity (Scheme 3.3.1).<sup>53</sup>



Reagents and Conditions: **A** (i) CuCN, DMA, 165 °C, 3.5 h; (ii) HCl; (iii) sparging with air at 80 °C; (iv) crystallisation, 61%. **B** (i) Zn(CN)<sub>2</sub>, Pd/C, PPh<sub>3</sub>, Zn, Br<sub>2</sub>, 115 °C, 4 h, 91%.

Scheme 3.3.1. An improved synthesis of aryl nitriles employing heterogeneous (Pd/C) rather than typical Rosemund-von Braun conditions.<sup>53</sup>

Since the Rosemund-von Braun reaction employs such extreme conditions it often has low functional group tolerance. Buchwald has recently shown that improved functional group tolerance can be achieved using milder conditions and catalytic amounts of copper to convert aryl bromides to nitriles *via in situ* halogen exchange to the corresponding iodides (Scheme 3.3.2).<sup>54</sup>



Reagents and Conditions: i) CuI, KI, *N*<sup>1</sup>,*N*<sup>2</sup>-dimethylethane-1,2-diamine, NaCN, toluene, 110 °C, 24 h, 74-98%.

Scheme 3.3.2. Formation of aryl nitriles from aryl bromides by *in situ* formation of the corresponding iodides.<sup>54</sup>

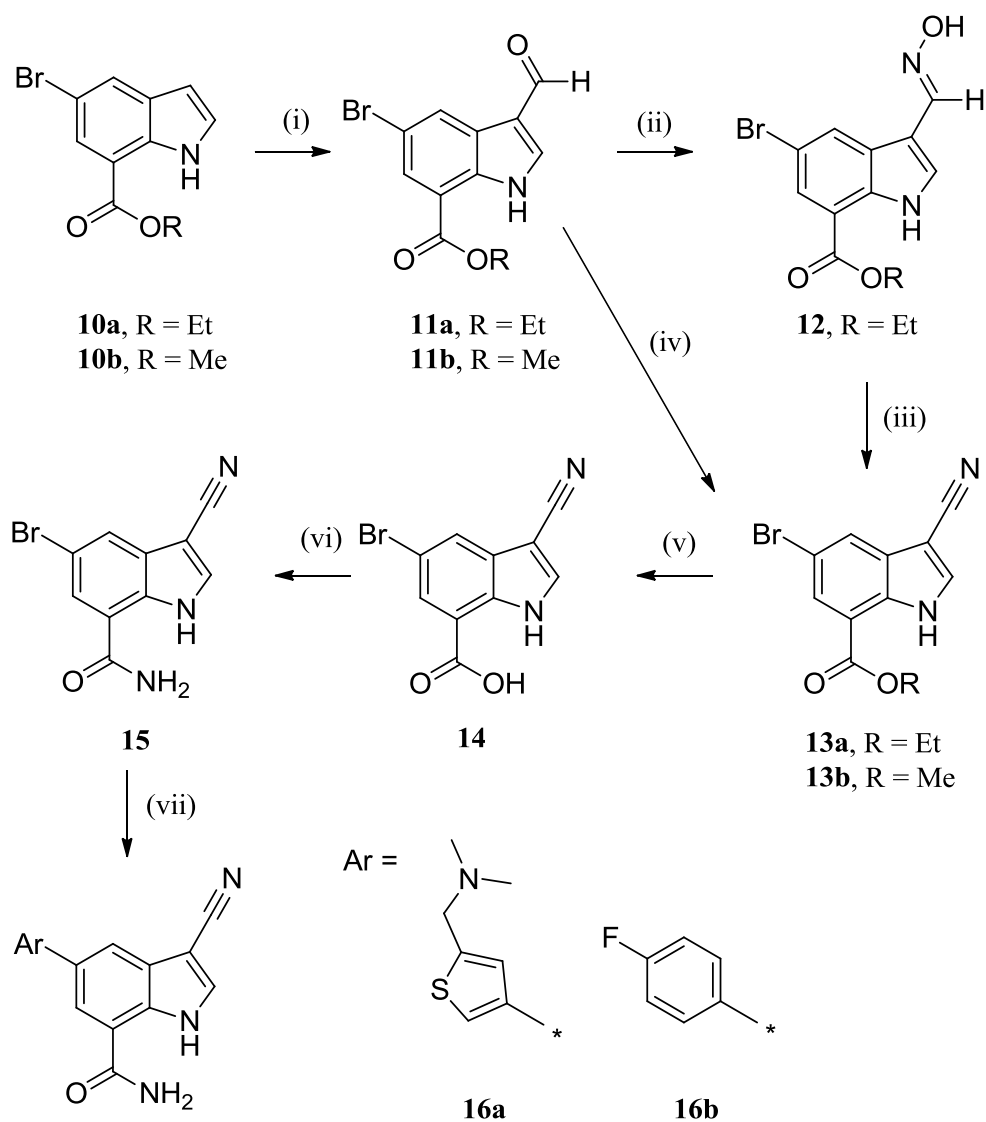
The copper-mediated cyanation could proceed *via* an Ullman-type mechanism, in which oxidative addition of an aryl halide to a catalytically active copper(I)-ligand complex would result in an intermediate copper(III) species (R-[Cu(III)]-X), which is trapped by the cyanide ion of the cyanide source.<sup>55</sup> The product (R-[Cu(III)]-CN) undergoes reductive elimination to form the expected nitrile product (R-CN) and regenerate the active copper(I) species.<sup>55</sup>

Transition-metal mediated cyanation has evolved as an important methodology over the last decade. The use of palladium catalysis has been widely investigated; unfortunately, highly toxic environmentally hazardous cyanide sources are often required, for example Zn(CN)<sub>2</sub> as seen in Scheme 3.3.1. Palladium is often the most expensive metal for these transformations and additional ligands are sometimes required, which also increases the cost of these catalytic systems. Beller has recently described the use of copper catalysis for the cyanation of aryl bromides *via* a less expensive and more environmentally friendly method.<sup>56</sup> A copper-ligand system of CuI and 1-butylimidazole was used to provide efficient catalyst activity and acetone cyanohydrin was used as the cyanide source.<sup>56</sup> Addition of acetone cyanohydrin was controlled in order that the concentration of CN<sup>-</sup> remained low.<sup>56</sup> High concentrations of CN<sup>-</sup> lead to inactivation of the catalyst through binding of cyanide at the active metal centre.<sup>57</sup> Beller's group has previously avoided this problem by utilising a potassium ferrocyanide(II) complex that delivers CN<sup>-</sup>

slowly,<sup>58</sup> but the syringe-pump addition of acetone cyanohydrin as an alternative cyanide source would allow for more precise control of CN<sup>-</sup> concentration for larger scale applications.<sup>56</sup> However, this method is not ideal since acetone cyanohydrin is also a highly toxic reagent as it readily decomposes in water to generate hydrogen cyanide. Other approaches that produce the cyano group *in situ* have also been described, for example using DMF and a stoichiometric amount of a copper species or, more recently, a procedure that is catalytic in copper and uses DMF and ammonium bicarbonate as combined source of cyanide.<sup>59,60</sup>

Although there are many efficient procedures for the cyanation of aryl halides using transition metals, this approach was not favoured for the synthesis of 3-cyano-5-bromo-1*H*-indole-7-carboxamide. The method would involve an additional halogenation step and the presence of the 5-bromo substituent could cause selectivity issues during the cyanation reaction, therefore another approach that avoided this risk was considered.

The general synthetic route that was chosen for the synthesis of the desired 3-cyano-1*H*-indole-7-carboxamides is shown in Scheme 3.3.3. This route made use of the dehydration of an oxime to form the required nitrile and proved to be robust and high-yielding, which was important when larger quantities of the 3-cyano intermediates were required.

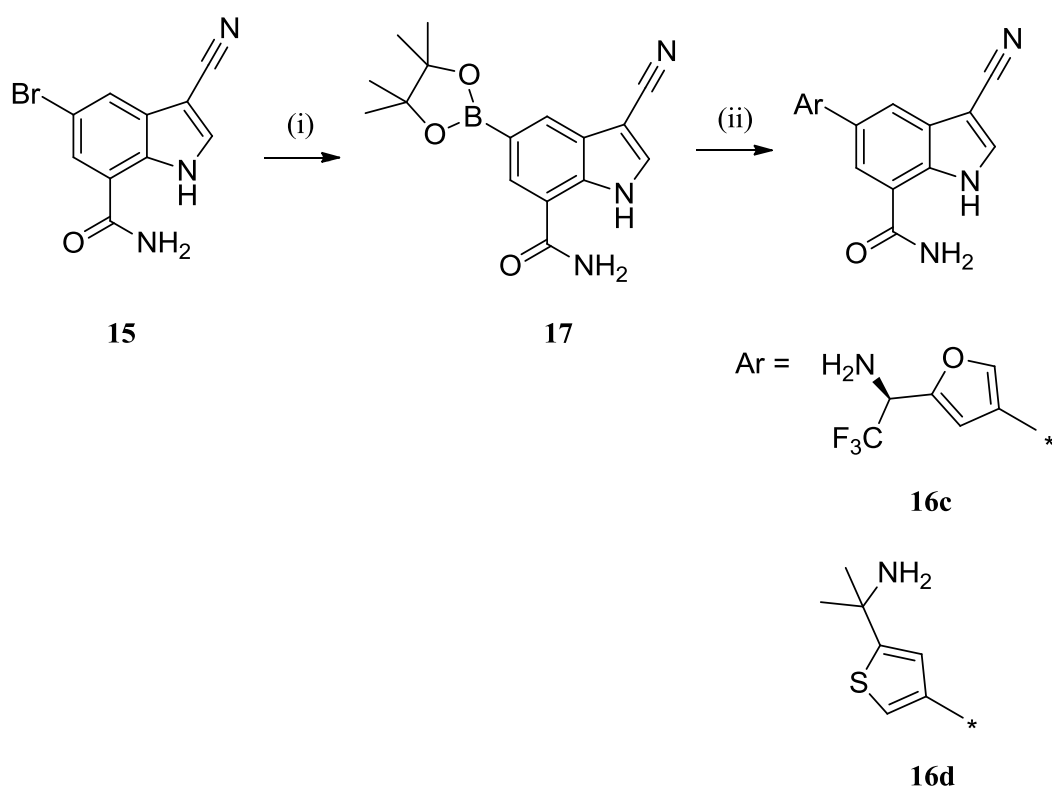


Reagents and Conditions: (i) POCl<sub>3</sub>, DMF, rt, 97% (**11a**, not described in Experimental as synthesised by J. Renaux, GSK),<sup>61</sup> 82% (**11b**); (ii) HO-NH<sub>2</sub>.HCl, py, 120 °C, 93%; (iii) TFAA, NEt<sub>3</sub>, THF, rt, 78%; (iv) HO-NH<sub>2</sub>.HCl, py, 80 °C then SeO<sub>2</sub>, MgSO<sub>4</sub>, 80 °C, 95%; (v) using **13b** only - NaOH, MeOH, rt, 81%; (vi) HATU, DIPEA, NH<sub>3</sub>/MeOH, DMF, rt, 82%; (vii) ArB(OH)<sub>2</sub>, PdCl<sub>2</sub>(dppf), K<sub>2</sub>CO<sub>3</sub> (**16a**) or Na<sub>2</sub>CO<sub>3</sub> (**16b**), 1,4-dioxane/H<sub>2</sub>O (3:1), 120 °C,  $\mu$ wave, 6% (**16a**), 10% (**16b**).

Scheme 3.3.3. Synthetic route to 3-cyano-1H-indole-7-carboxamides.

The Vilsmeier-Haack reaction<sup>62,63</sup> was used to formylate of the 3-position of indoles **10a** and **10b**. *N*-Formylation was also observed but the formamides hydrolysed in aqueous sodium bicarbonate during the work-up to give **11a**<sup>61</sup> and **11b**. Oxime formation and subsequent dehydration installed the desired 3-cyano substituent (**13a** and **13b**). This could be achieved either in two separate steps or *via* a one-pot reaction, in which selenium dioxide-mediated elimination of the intermediate oxime generates the desired nitrile.<sup>64</sup> The synthesis of **11b** and **13b** was outsourced to Manchester Organics, where the practical chemistry was carried out. Another one-pot procedure for the conversion of aldehydes to nitriles has recently been described; this uses T3P<sup>®</sup>,<sup>65</sup> a reagent commonly used as a coupling agent and water scavenger in peptide synthesis.<sup>66</sup> T3P<sup>®</sup> acts to dehydrate the intermediate oxime in the one-pot transformation of aromatic, heteroaromatic or aliphatic aldehydes to nitriles, giving almost quantitative yields and showing excellent functional group tolerance.<sup>65</sup> Therefore, if the synthesis of the 3-cyano-1*H*-indole-7-carboxamides were to be repeated, this methodology could be applied in order to reduce the number of transformations and potentially improve yields.

Once the 3-cyano group was installed, hydrolysis of the ester, and amide coupling gave carboxamide **15**. The final step was a Suzuki cross-coupling reaction to install various 5-aryl groups.<sup>67</sup> If the desired aryl boronic acids were unavailable, the route shown in Scheme 3.3.4 was employed as an alternative, using a boronate ester bearing the indole core (**17**) as a coupling partner for a range of aryl bromides.



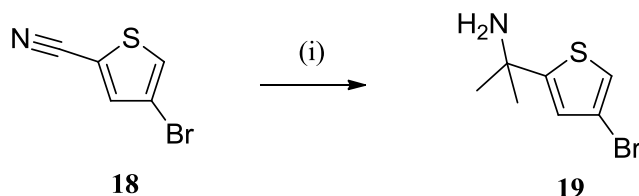
Reagents and Conditions: (i)  $B_2pin_2$ ,  $Pd_2(dba)_3$ , XPhos<sup>®</sup>, KOAc, dioxane, 110 °C,  $\mu$ wave, 41%; (ii) ArBr,  $PdCl_2(dppf)$ ,  $K_2CO_3$ , dioxane/ $H_2O$  (1:1), 100 °C,  $\mu$ wave, 2% (**16c**), 11% (**16d**).

Scheme 3.3.4. Alternative route to 5-substituted-1*H*-indole-7-carboxamides.

Compounds **16c** and **16d** were designed in order to reduce the likelihood of the compounds having a hERG liability associated with the presence of a primary amine. It has been found that a key feature of potent hERG blockers is a basic amine,<sup>68</sup> therefore a trifluoromethyl group was introduced adjacent to the primary amine of compound **16c** in order to reduce its basicity. Also, the addition of the  $\alpha$ -trifluoromethyl group helps block the position adjacent to the amine, which could be susceptible to metabolism by oxidative deamination.<sup>69</sup> If a high level of first pass metabolism were to occur, the compound could be highly cleared from the body, and oxidative deamination is often prevented by disubstitution of the  $\alpha$ -carbon.<sup>69</sup> The 5-substituent of compound **16d** was also designed with this in mind, as the *gem*-



dimethyl group blocks the potentially metabolically labile position adjacent to the amine. Synthesis of the bromide monomer **19** was required for the synthesis of **16d** and was obtained from the nitrile starting material, **18** (Scheme 3.3.5).<sup>70</sup>



Reagents and Conditions: (i)  $\text{CeCl}_3$ , MeLi, THF,  $-78\text{ }^\circ\text{C}$ , then  $\text{NH}_3/\text{H}_2\text{O}$ , 28%.

Scheme 3.3.5. Monomer synthesis.

Table 3.3.3 shows the yields of the final stage Suzuki cross-couplings to obtain compounds **16a-d**.

Compound	Ar	Yield (%)	Compound	Ar	Yield (%)
<b>16a</b>		6	<b>16c</b>		2
<b>16b</b>		10	<b>16d</b>		11

Table 3.3.3. Suzuki cross-coupling yields with different aryl bromides.

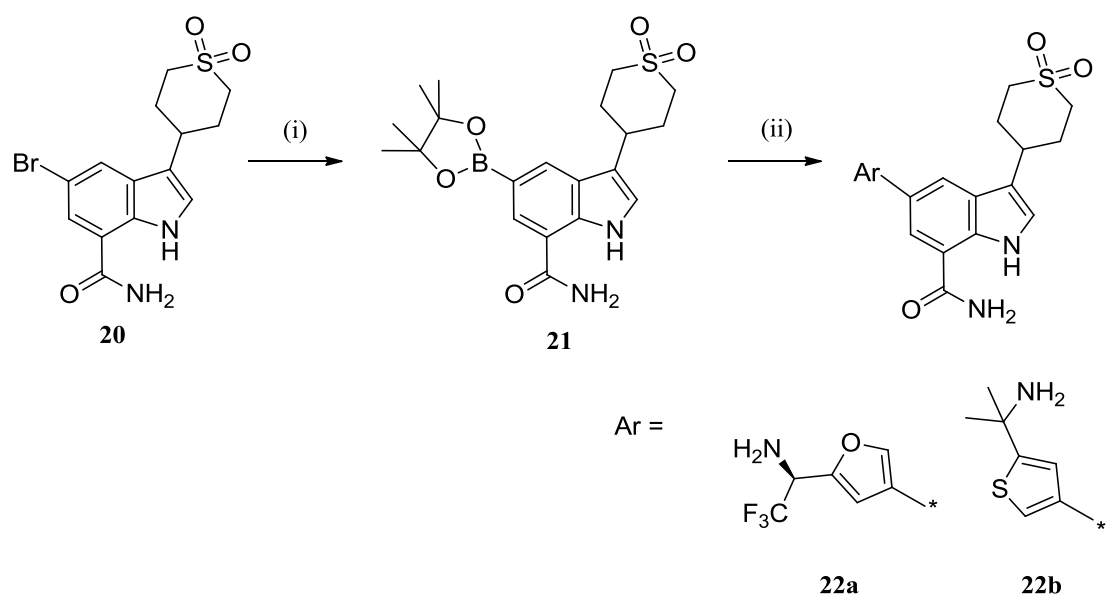
The poor yields of the Suzuki cross-coupling reactions used to incorporate the desired 5-substituents (Table 3.3.3) are similar to those carried out previously on this indole-7-carboxamide template.<sup>41</sup> There is evidence<sup>71</sup> of more successful Suzuki

cross-coupling reactions of indole-5-pinacolboronates analogous to compound **17** so the poor yields observed here indicate a problem with this type of substrate, which could be due to the poor solubility of the indole-7-carboxamide compounds. The 3,5-disubstituted indole-7-carboxamides are thought to be very flat due to both the ability of the primary carboxamide to form a hydrogen bond to the indole N-H, and to the  $sp^2$  nature of the 5-position substituents. This planarity would enable tighter crystal packing and hence lead to poor solubility. This causes problems both in attaining full conversion during the Suzuki reaction and also in the purification and isolation of these compounds, which is typically carried out by generic high-throughput techniques and not bespoke methods optimised for each compound.

An analysis of the performance of arylboronic acids and arylpinacolboronate esters in Suzuki couplings with indoles has shown that the coupling of indolylpinacolboronates with aryl halides generally led to lower yields of the desired biaryls than the couplings with the indolylboronic acids.<sup>72</sup> Therefore, the yields of the cross-couplings shown here could be improved by using an indole-5-boronic acid intermediate. Alternatively a more stable boron species could be used, for example a MIDA boronate<sup>73</sup> or trifluoroborate salt,<sup>74</sup> to help avoid the possible decomposition that could be rendering the boronate esters inefficient in the cross-coupling reactions.

It was also found that protecting the indole nitrogen was essential for conversion to the biaryl products when indolylpinacolboronates were used as substrates.<sup>72</sup> Therefore, a protecting group strategy could be implemented here in order to improve yields of the final Suzuki cross-coupling; however this would involve two additional steps and may not lead to an overall increase in yield.

In order to evaluate the effect of the 3-cyano group, the analogous 3-tetrahydrothiopyran-dioxide compounds were also synthesised (Scheme 3.3.6).



Reagents and Conditions: (i)  $B_2pin_2$ ,  $Pd_2(dba)_3$ , XPhos<sup>®</sup>, KOAc, dioxane, 100 °C,  $\mu$ wave, 74%; (ii) ArBr,  $PdCl_2(dppf)$ ,  $K_2CO_3$ , dioxane/ $H_2O$  (1:1), 80 °C,  $\mu$ wave, 23% (**22a**), 25% (**22b**).

Scheme 3.3.6. Synthesis of 5-aryl-3-(1,1-dioxidotetrahydro-2H-thiopyran-4-yl)-1H-indole-7-carboxamides.

$^1H$  NMR analysis of the 3-(1,1-dioxidotetrahydro-2H-thiopyran-4-yl)-1H-indole-7-carboxamides was not straightforward and so assignment of the saturated ring system at the 3-position was looked at in more detail (Figure 3.3.2).

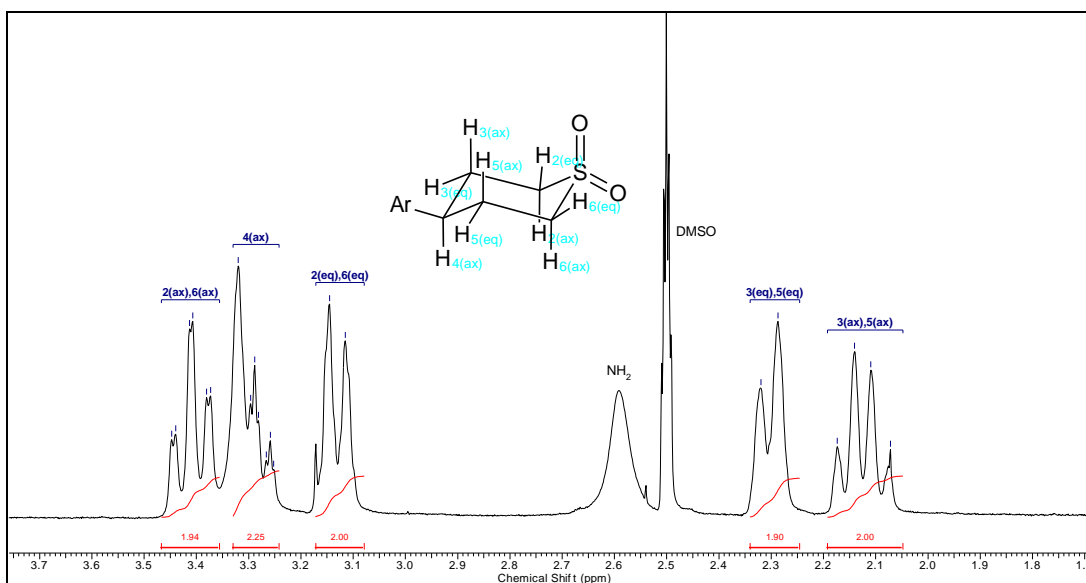


Figure 3.3.2. Aliphatic region of the  $^1\text{H}$  NMR spectrum of a 3-(1,1-dioxidotetrahydro-2*H*-thiopyran-4-yl)-1*H*-indole-7-carboxamide compound (**22a**).

Table 3.3.4 shows the coupling constants between protons on the ring system, which explains the peak splitting observed in Figure 3.3.2.

Splitting	q	br. d	br. d	tt	td	
Proton signal	$\text{H}_{3(\text{ax})}, \text{H}_{5(\text{ax})}$	$\text{H}_{3(\text{eq})}, \text{H}_{5(\text{eq})}$	$\text{H}_{2(\text{eq})}, \text{H}_{6(\text{eq})}$	$\text{H}_{4(\text{ax})}$	$\text{H}_{2(\text{ax})}, \text{H}_{6(\text{ax})}$	
Coupling constant $J$ (Hz)		12.1	not measurable	12.1	12.1	$\text{H}_{3(\text{ax})}, \text{H}_{5(\text{ax})}$
	12.6		not measurable	3.0	3.0	$\text{H}_{3(\text{eq})}, \text{H}_{5(\text{eq})}$
	not measurable	not measurable		-	12.1	$\text{H}_{2(\text{eq})}, \text{H}_{6(\text{eq})}$
	12.6	not measurable	-		-	$\text{H}_{4(\text{ax})}$
	12.6	not measurable	12.1	-		$\text{H}_{2(\text{ax})}, \text{H}_{6(\text{ax})}$

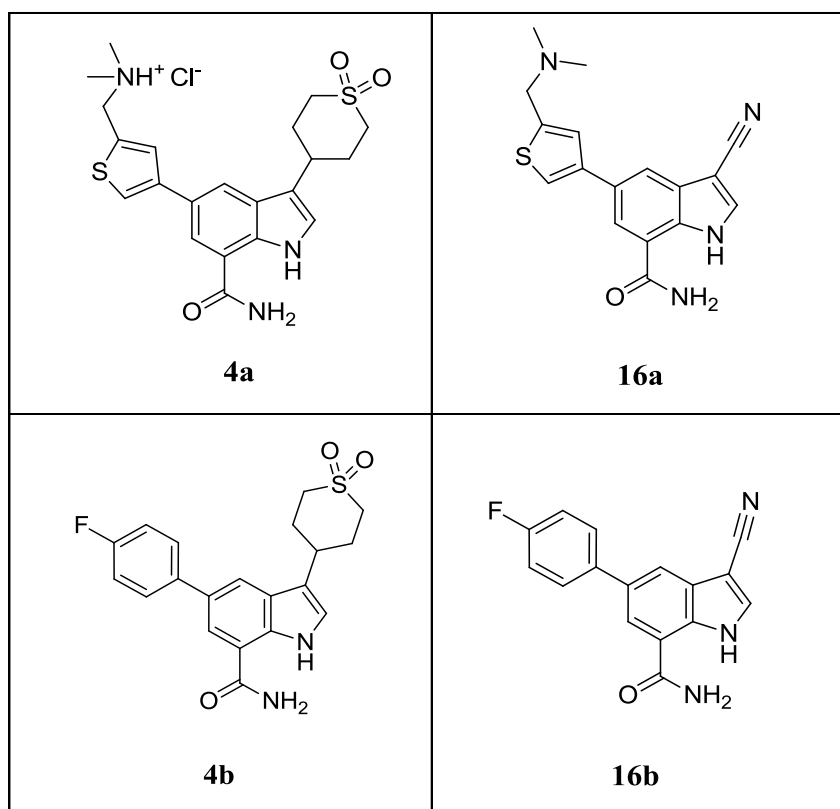
Table 3.3.4. Couplings between protons on the saturated ring system of compound **22a**.

Equivalent protons H<sub>2(ax)</sub> and H<sub>6(ax)</sub> have one large geminal coupling and one large axial coupling with the same coupling constant, as well as one small equatorial coupling and therefore split into the observed triplet of doublets. The equatorial protons on the same carbon, H<sub>2(eq)</sub> and H<sub>6(eq)</sub>, also have one geminal coupling but the expected equatorial coupling is too small to be defined in the peak shape, and this is also the case for the signal attributed to H<sub>3(eq)</sub> and H<sub>5(eq)</sub>. Equivalent protons H<sub>3(ax)</sub> and H<sub>5(ax)</sub> have three large couplings such that the peak is observed to be a quartet. Finally H<sub>4(ax)</sub> is seen to be a triplet of triplets due to one large axial coupling and one small equatorial coupling. The peaks observed in the aliphatic region of compound **22a** (Figure 3.3.2) are typical of those seen for all indole carboxamide compounds bearing a saturated 6-membered ring at the indole 3-position.

### 3.3.1.3. Biological Results for 3-Cyano-1*H*-indole-7-carboxamides

The biological results for compounds **4a**, **16a**, **4b** and **16b** are shown in Table 3.3.5. Replacement of the 3-position tetrahydrothiopyrandioxides by a cyano group led to a significant decrease in molecular weight and reduced the number of hydrogen bond acceptors whilst maintaining IKK2 potency and selectivity over IKK1, resulting in an increase in ligand efficiency. However, in a more general sense, the potency in the whole blood assay is lower than that of the tetrahydrothiopyran-dioxide compounds, in particular for **16b** where there appears to be no whole blood activity.

The *in vitro* clearance (IVC) of the compounds has been determined from a study in rat and human microsomes and is reported in Table 3.3.5. This IVC data and all that subsequently reported in this Chapter were determined within Cyprotex.<sup>43</sup> It can be seen that compound **16a** has moderate *in vitro* clearance and high permeability, which indicates that oral absorption may be achievable with compounds containing the 3-cyano group; however the compound was not progressed to an *in vivo* rat PK study due to its poor human whole blood potency.



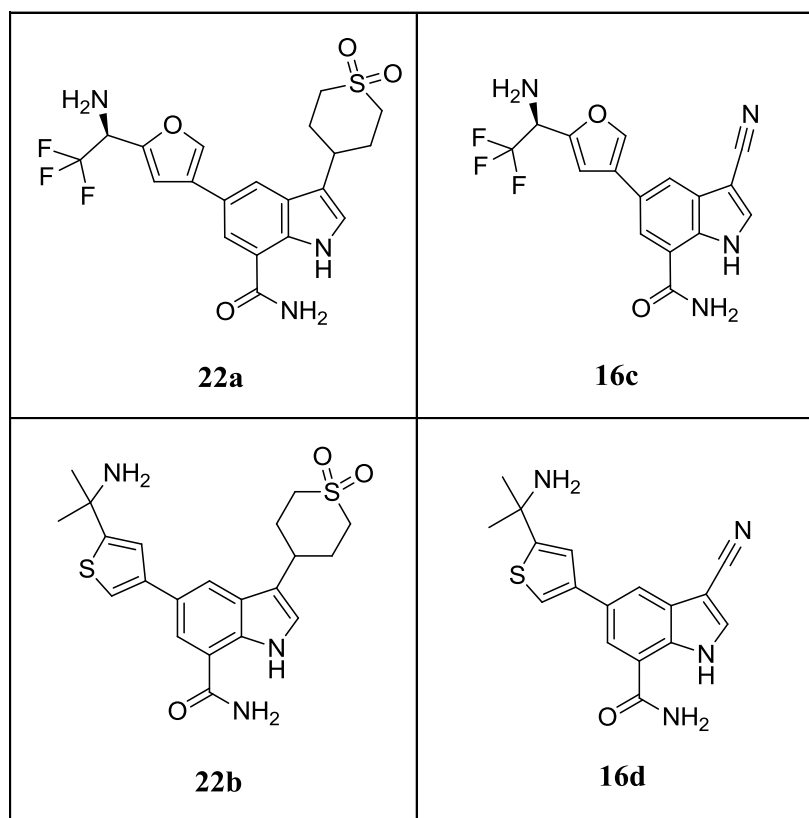
Compound Number	4a	16a	4b	16b
Mean IKK2 pK <sub>i</sub> (N)	9.5 (12) <sup>a</sup>	8.9 (2)	8.3 (1)	7.6 (4)
Mean IKK1 pK <sub>i</sub> (N)	7.5 (10)	6.8 (2)	6.6 (2)	6.1 (3)
Mean HWB pIC <sub>50</sub> (N)	7.2 (18)	6.0 (3) <sup>b</sup>	5.9 (2)	<5.0 (2)
LE/LLE <sub>AT</sub>	0.45/0.51	0.53/0.51	0.42/0.44	0.50/0.42
PFI	5.0	5.3	6.5	7.1
mChromlogD <sub>pH7.4</sub>	1.95	2.25	3.51	4.09
clogP	1.1	2.1	1.7	2.8
MW	432	324	386	279
TPSA	96	86	93	83
AMP (pH 7.05, nm/sec)	10.2	330	280	150
CLND solubility (μM)	398	200	-	1
FaSSIF solubility (μg/mL)	258	-	-	-
hERG pIC <sub>50</sub>	<4.3	4.7	-	4.9
CYP 3A4 pIC <sub>50</sub>	<4.3	<4.3	-	<4.3
IVC (mL/min/kg)	0.97 (rat), <0.53 (human)	9.70 (rat), 1.92 (human)	-	<0.53 (rat), 2.97 (human)

<sup>a</sup> Returned value >10.1 on one test occasion. <sup>b</sup> Returned values <5.0 on two test occasions.

Table 3.3.5. Results for compounds **4a**, **16a**, **4b** and **16b**.

Table 3.3.6 shows the biological results for compounds **22a**, **22b**, **16c** and **16d**, where heterocyclic amines have been incorporated at the 5-position of the indole. Compounds **22a** and **22b** have high IKK2 potencies and both achieve greater than 100-fold selectivity over IKK2. Compounds **16c** and **16d** show a significant reduction in IKK2 enzyme potency compared to the analogous tetrahydrothiopyran-dioxide compounds and therefore show a negligible increase in ligand efficiency.

It was hoped that reducing the basicity of the primary amine or blocking the potentially metabolically labile site would lead to lower clearance and hence improve oral absorption. The pK<sub>a</sub> of compound **4a** was calculated to be 8.3 by the ACD pK<sub>a</sub> software package and measured spectroscopically as 9.1, whereas that of compound **22a** was calculated by ACD to be 4.4. It can be seen that compound **22a** has similar *in vitro* clearance values to those of compound **4a** in rat and human microsomes and that compound **22b** has low *in vitro* clearance in both species. A potential advantage of compound **22a** over compound **4a** is that it may have better oral absorption due to its increased permeability; however, due to their poor human whole blood potency, the compounds could not be progressed.



Compound	22a	16c	22b	16d
Mean IKK2 pK <sub>i</sub> (N)	9.0 (5)	7.5 (1)	9.2 (2)	7.9 (1)
Mean IKK1 pK <sub>i</sub> (N)	6.9 (5)	5.6 (1)	7.1 (2)	6.2 (1)
Mean HWB pIC <sub>50</sub> (N)	6.5 (4) <sup>a</sup>	-	5.8 (5)	5.3 (2)
LE/LLE <sub>AT</sub>	0.40/0.49	0.41/0.44	0.44/0.50	0.47/0.46
PFI	5.7	6.1	4.5	4.9
mChromlogD <sub>pH7.4</sub>	2.74	3.14	1.51	1.93
clogP	0.5	1.5	0.9	2.0
MW	455	348	432	324
TPSA	132	122	132	109
AMP (pH 7.05, nm/sec)	94	-	3	170
CLND solubility (μM)	163	196	245	238
hERG pIC <sub>50</sub>	5.1 <sup>b</sup>	<4.0	<4.3	4.5
CYP 3A4 pIC <sub>50</sub>	5.6 <sup>b</sup>	<4.3	4.4	<4.3
IVC (mL/min/kg)	1.24 (rat), <0.53 (human)	-	<0.53 (rat), 0.56 (human)	-

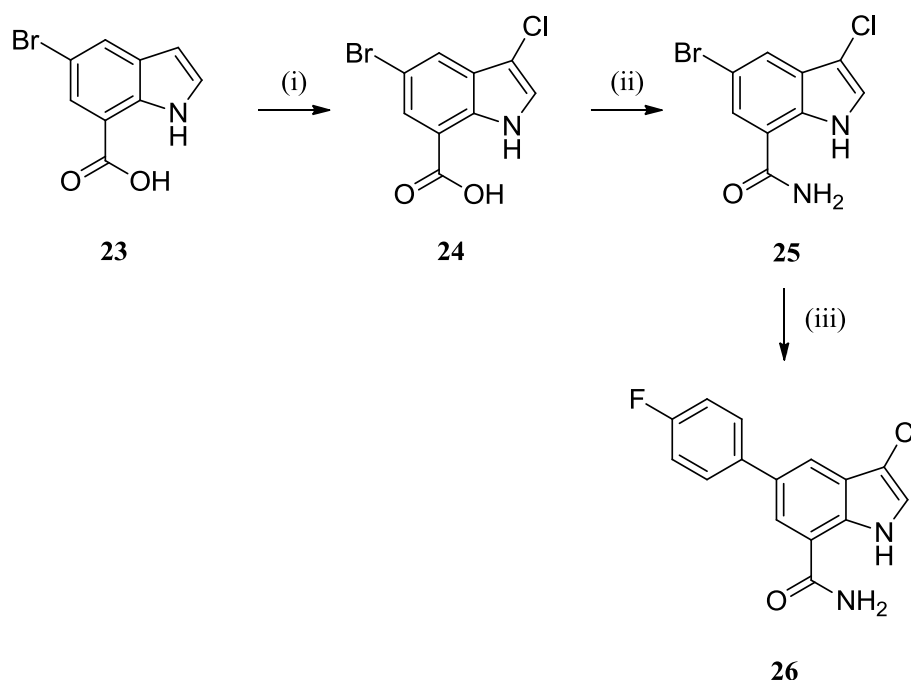
<sup>a</sup> Returned values <5.0 on two test occasions. <sup>b</sup> Returned values <4.3 on two test occasions.

Table 3.3.6. Results for compounds **22a**, **16c**, **22b** and **16d**.



### 3.3.1.4. Synthesis of Other 3-Substituted 1*H*-Indole-7-carboxamides

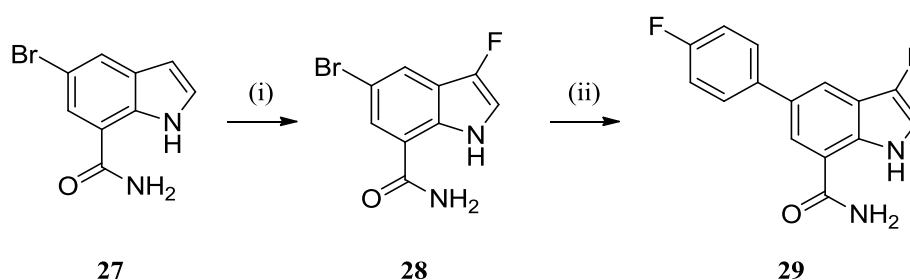
Since replacement of the bulky 3-position tetrahydrothiopyran-dioxide by a cyano group was successful in increasing ligand efficiency, especially for compound **16a** relative to compound **4a**, further investigation into other potentially ligand efficient 3-substituents was carried out. 3-Chloro, 3-fluoro, 3-nitro, 3-methylsulfonyl substituents were also highly ranked in the Hansch analysis and had high predicted IKK2 pIC<sub>50</sub> values. Scheme 3.3.7 shows the synthetic route to the 3-chloro-1*H*-indole-7-carboxamides from carboxylic acid **23**.



Reagents and Conditions: (i) NCS, MeOH, rt, 44%; (ii) HATU, DIPEA, NH<sub>3</sub>, DMF, rt, 22%; (iii) 4-(fluorophenyl)boronic acid, PdCl<sub>2</sub>(dppf)-CH<sub>2</sub>Cl<sub>2</sub> adduct, Na<sub>2</sub>CO<sub>3</sub>, 1,4-dioxane/H<sub>2</sub>O (2.5:1), 130 °C,  $\mu$ wave, 28%.

Scheme 3.3.7. Synthetic route to 3-chloro-1*H*-indole-7-carboxamides.

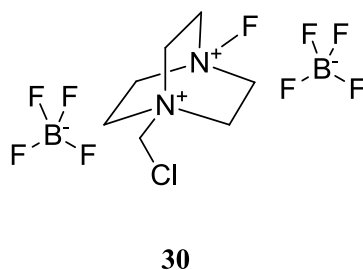
The chlorination step proceeded effectively with the 7-carboxylic acid substituent in place and subsequent amide formation gave compound **25**. A Suzuki cross-coupling of 4-(fluorophenyl)boronic acid with compound **25** afforded compound **26**. This 5-position substituent was also incorporated in compounds with different 3-substituents and the route in Scheme 3.3.8 shows the synthesis of the desired 3-fluoro-1*H*-indole-7-carboxamides from primary carboxamide **27**.<sup>75</sup>



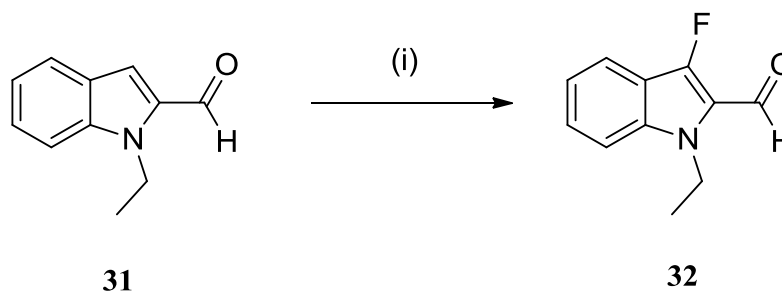
Reagents and Conditions: (i) Selectfluor<sup>®</sup>, MeCN/DMSO (1:1), 0 °C, 18%; (ii) 4-fluorophenylboronic acid, PdCl<sub>2</sub>(dppf), K<sub>2</sub>CO<sub>3</sub>, 1,4-dioxane/H<sub>2</sub>O (5:1), 130 °C,  $\mu$ wave, 40%.

Scheme 3.3.8. Synthetic route to 3-fluoro-1*H*-indole-7-carboxamides (not described in Experimental as synthesised by I. Smith, GSK).<sup>75</sup>

Functionalisation of the 3-position of 5-bromo-1*H*-indole-7-carboxamide with the fluorinating agent Selectfluor<sup>™</sup> (**30**) gave indole carboxamide **28** directly, although the yield was low.<sup>75</sup>



The low yield was unsurprising as similar transformations reported in the literature for the 3-fluorination of indoles with Selectfluor<sup>™</sup> also report fairly poor yields. For example, substrate **31** delivered product **32** in only 33% yield and 90% purity, with the main impurity being unreacted starting material (Scheme 3.3.9).<sup>76</sup>

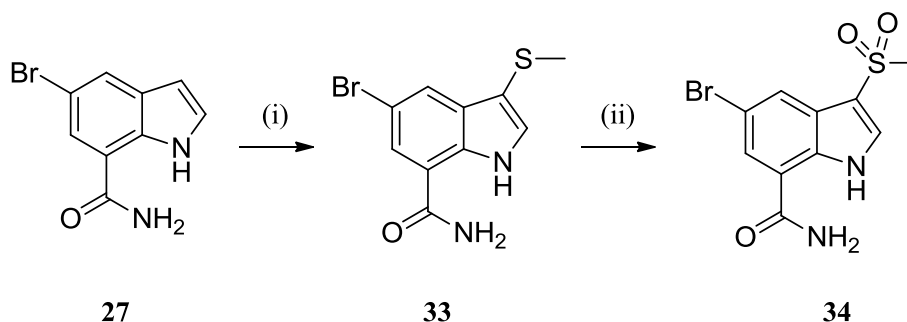


Reagents and Conditions: (i) Selectfluor<sup>®</sup>, MeCN, rt, 33%.

Scheme 3.3.9. Precedent for the fluorination of indoles.

Another reason for the poor yield could be due to the fluorination of **27** requiring DMSO to aid solubility. DMSO reacts rapidly and exothermically with Selectfluor<sup>™</sup> hence the use of an alternative co-solvent such as methanol may have avoided side reactions and led to an improved yield.<sup>77</sup>

In addition to halogenation at the 3-position, sulfenylation and subsequent oxidation afforded the desired 3-methylsulfonyl substituent (Scheme 3.3.10).



Reagents and Conditions: (i) MeSSMe, SO<sub>2</sub>Cl<sub>2</sub>, DCM/DMF (1:1), rt, 11%; (ii) *m*CPBA, CHCl<sub>3</sub>, rt, 38%.

Scheme 3.3.10. Synthetic route to 3-methylsulfonyl-1*H*-indole-7-carboxamides.

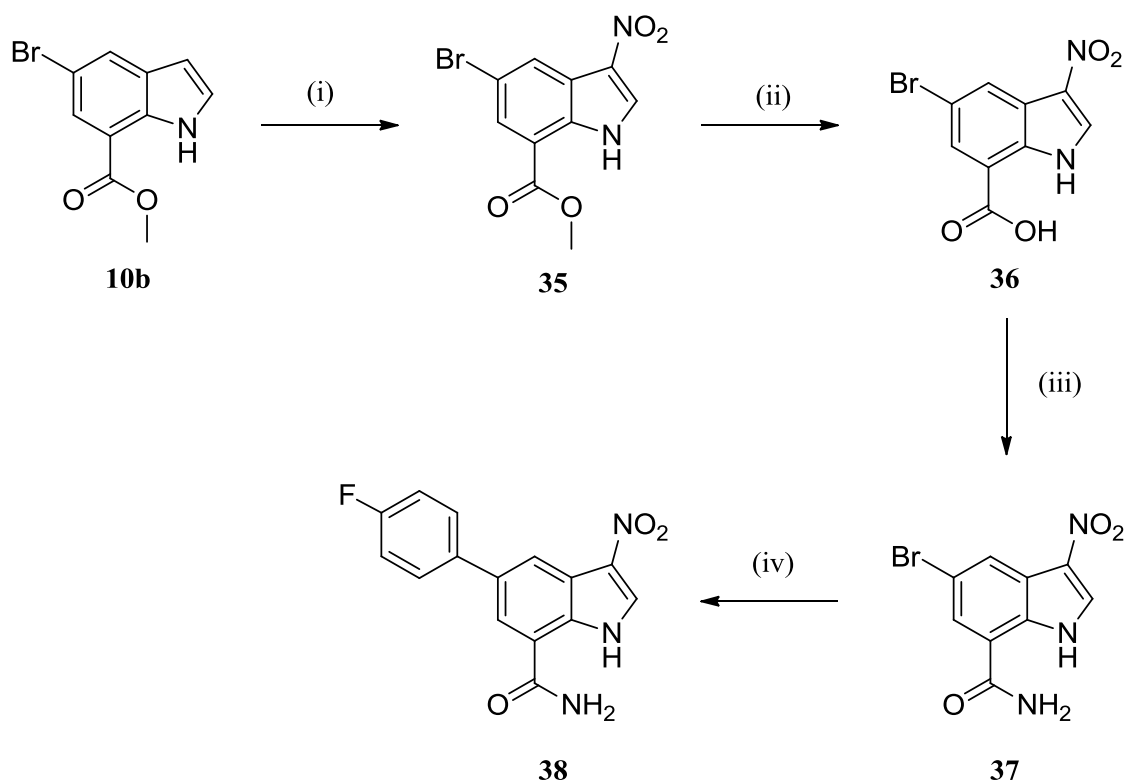
Compound **33** was obtained from the reaction of indole **27** with methanesulfonyl chloride, which was formed *in situ* from dimethyl disulfide and sulfuryl chloride.<sup>78</sup> The chlorination of dimethyl disulfide is carried out in a chlorinated solvent, typically DCM, but here a co-solvent was also required to aid solubility. The combination of dimethyl disulfide/sulfuryl chloride/DMSO has been shown to successfully sulfenylate alkenes but this reagent combination did not yield the desired product in this instance.<sup>79</sup> An alternative donor solvent (DMF) was then used and some desired product was observed. However, these reactions are not ideal as both DMSO and DMF may react with sulfuryl chloride, so if the reaction were to be repeated, it would be better to pre-form methanesulfonyl chloride using dimethyl disulfide and sulfuryl chloride in DCM then add this to a solution of indole **27** in DMF.

The poor yield of the reaction could also be attributed to the formation of by-products where sulfenylation could occur at the indole nitrogen.<sup>80</sup> An improvement in yield could therefore possibly have been achieved by protecting the indole nitrogen to avoid the formation of any *N*-sulfenylation by-products. Investigating alternative chlorinating agents, such as NCS, or using different electrophilic sulfenylating agents could also have helped improve the reaction. Methyl thiophthalimides could have been used as more stable sulfenylating agents that

would have avoided the need for harsh chlorination conditions and helped preclude any decomposition that can often occur with sulfenyl chlorides due to their low stability.<sup>81</sup>

Next, *m*CPBA was used to oxidise **33** to give sulfone **34** (Scheme 3.3.10). However, the low yield of this reaction gave insufficient material to be taken forward for a Suzuki cross-coupling to install the 4-fluorophenyl substituent at the indole carboxamide 5-position. Compound **34** was screened for its activity against IKK2 and since its potency was disappointing, the synthesis was not scaled up or investigated further.

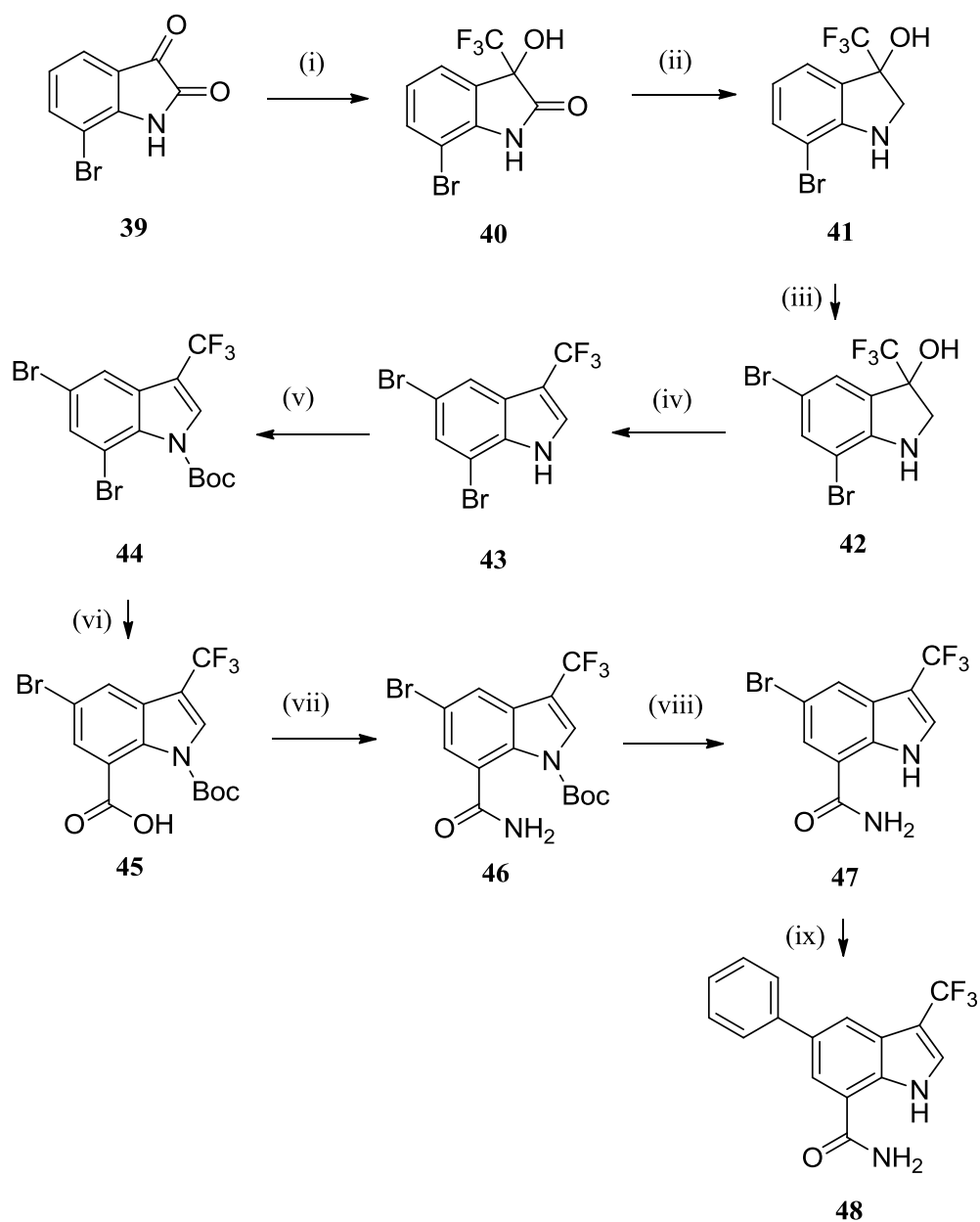
Installation of the 3-nitro group was then investigated. Neither typical conditions using nitric acid and sulfuric acid nor the *in situ* formation of acetyl nitrate as the nitrating agent led to successful nitration at the 3-position of primary carboxamide **27**. However, the reaction of acetyl nitrate, generated *in situ* using copper nitrate and acetic anhydride, with the analogous ester (**10b**) did afford the desired product (Scheme 3.3.11). The nitration was carried out successfully on an 8 mmol scale to give intermediate **35**. Scheme 3.3.11 shows how intermediate **35** was then converted to the desired 3-nitro compounds, **37** and **38**, for biological evaluation.



Reagents and Conditions: (i)  $\text{Cu}(\text{NO}_3)_2$ ,  $\text{Ac}_2\text{O}$ , 0 °C to rt, 44%; (ii)  $\text{NaOH}$ ,  $\text{MeOH}$ , rt, 75%; (iii) HATU, DIPEA,  $\text{NH}_3/\text{MeOH}$ ,  $\text{DMF}$ , rt, 32%; (iv) 4-fluorophenylboronic acid,  $\text{PdCl}_2(\text{dppf})$ ,  $\text{K}_2\text{CO}_3$ , 1,4-dioxane/ $\text{H}_2\text{O}$  (2:1), 150 °C,  $\mu\text{wave}$ , 4%.

Scheme 3.3.11. Synthetic route to 3-nitro-1H-indole-7-carboxamides.

The final target compounds contained a trifluoromethyl group at the indole carboxamide 3-position. The synthetic route was designed using literature and in-house precedent then outsourced to Manchester Organics, where the practical chemistry was carried out. The synthetic route is shown in Scheme 3.3.12 starting from commercially available 7-bromoindoline-2,3-dione (**39**).



Reagents and Conditions: (i)  $\text{TMSCF}_3$ ,  $\text{KF}$ ,  $\text{KO}t\text{-Bu}$ ,  $0\text{ }^\circ\text{C}$  to  $\text{rt}$ , 64%; (ii)  $\text{BH}_3\text{-THF}$ ,  $\text{THF}$ ,  $66\text{ }^\circ\text{C}$ , 80%; (iii)  $\text{NBS}$ ,  $\text{DCM}$ ,  $\text{rt}$ , used crude; (iv)  $\text{TsOH}$ ,  $\text{toluene}$ ,  $\text{Dean-Stark}$ ,  $110\text{ }^\circ\text{C}$ , 82% over two steps; (v)  $\text{Boc}_2\text{O}$ ,  $\text{NEt}_3$ ,  $\text{DMAP}$ ,  $\text{DCM}$ ,  $\text{rt}$ , 74%; (vi)  $n\text{-BuLi}$ ,  $\text{CO}_2$ ,  $\text{THF}$ ,  $-70\text{ }^\circ\text{C}$ , 66%; (vii)  $\text{HATU}$ ,  $\text{NEt}_3$ ,  $\text{DMF}$ ,  $\text{NH}_3$  (14% in  $\text{MeOH}$ ),  $\text{rt}$ , 58%; (viii)  $4\text{M HCl}$  in  $1,4\text{-dioxane}$ ,  $40\text{ }^\circ\text{C}$ , 83%; (ix) Tetraphenyltin,  $\text{Pd}(\text{PPh}_3)_4$ ,  $\text{DMF}$ ,  $150\text{ }^\circ\text{C}$ ,  $\mu\text{wave}$ , 15%.

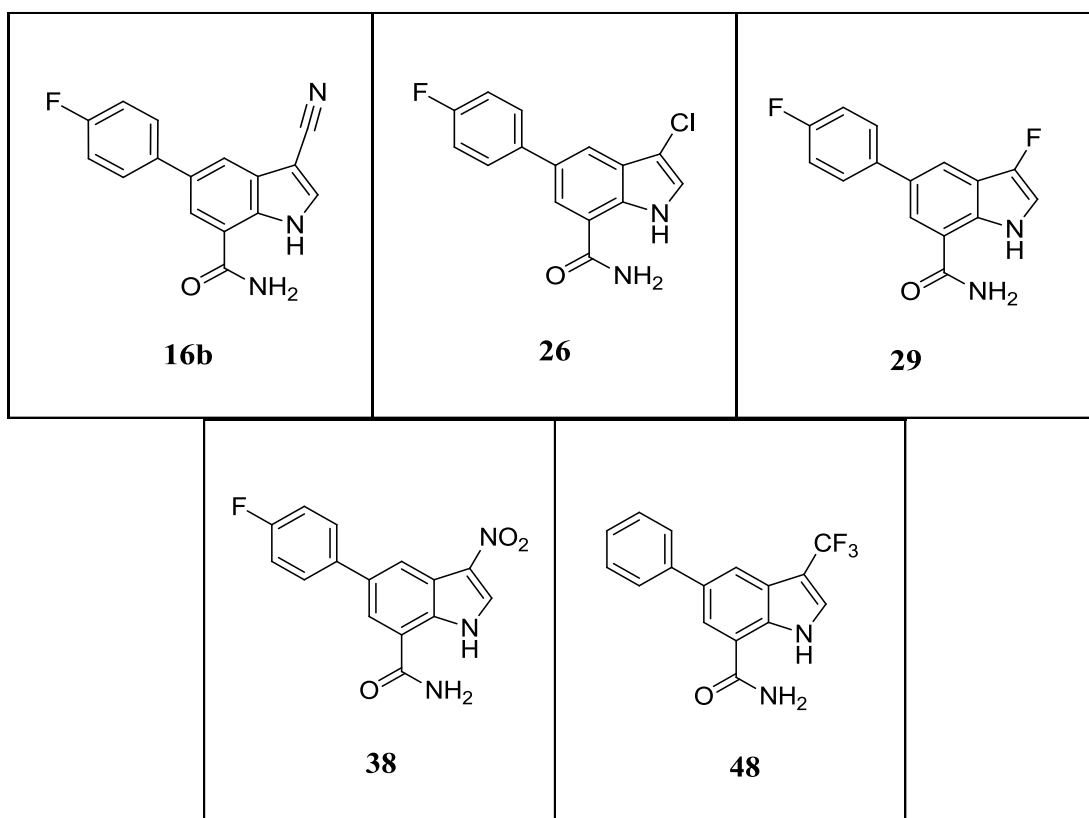
Scheme 3.3.12. Synthetic route to 3-trifluoromethyl-1H-indole-7-carboxamides.

7-Bromoindoline-2,3-dione (**39**) underwent nucleophilic trifluoromethylation with (trifluoromethyl)trimethylsilane and potassium fluoride to give intermediate **40** (see Chapter 4 for further details on this nucleophilic trifluoromethylation reaction). Intermediate **40** was subsequently reduced using literature conditions that had proven to be successful on a similar 7-bromoindoline-2,3-dione system.<sup>82</sup> Next, bromination led to formation of 5,7-dibromo intermediate **42**, which was then dehydrated under Dean-Stark conditions to afford the desired 3-trifluoromethyl indole (**43**). After the 3-substituted indole had been formed, *N*-protection gave intermediate **44**, which then underwent directed metal-halogen exchange to lithiate the 7-position. Quenching with carbon dioxide afforded the desired 7-carboxylic acid **45**. This was converted to primary carboxamide **46** *via* an amide coupling and subsequent removal of the Boc protecting group afforded compound **47**. A Suzuki cross-coupling reaction with compound **47**, which would have installed the desired 4-fluorophenyl substituent at the 5-position, was unsuccessful due to facile hydrolysis of the trifluoromethyl group under basic conditions, so a Stille cross-coupling with tetraphenyltin was carried out in order to obtain compound **48** for biological evaluation (Scheme 3.3.12).

#### 3.3.1.5. Biological Results for 3-Substituted 1*H*-Indole-7-carboxamides

The biological data for the novel 3-substituted 1*H*-indole-7-carboxamides is shown in Table 3.3.7.





Compound	16b	26	29	38	48
Mean IKK2 pK <sub>i</sub> (N)	7.6 (4)	7.3 (1)	6.9 (2)	7.1 (2)	6.8 (2)
Mean IKK1 pK <sub>i</sub> (N)	6.1 (3)	6.1 (1)	6.0 (2)	<4.8 (3)	5.6 (2)
Mean HWB pIC <sub>50</sub> (N)	<5.0 (2)	<5.0 (4)	<5.0 (1)	<5.0 (1)	-
LE/LLE <sub>AT</sub>	0.50/0.42	0.50/0.35	0.47/0.37	0.44/0.36	0.42/0.29
PFI	7.1	8.5	8.0	7.5	8.8
mChromlogD <sub>pH7.4</sub>	4.09	5.50	4.99	4.49	5.84
clogP	2.8	3.7	3.2	3.1	3.9
MW	279	288	272	299	304
TPSA	83	59	59	104	59
AMP (pH 7.05, nm/sec)	150	150	220	-	110
CLND solubility (μM)	1	1	8	3	182
hERG pIC <sub>50</sub>	-	<4.3	<4.0	<4.0	<4.0
CYP 3A4 pIC <sub>50</sub>	<4.3	<4.3	<4.8	<4.3	<4.8
IVC (mL/min/kg)	<0.53 (rat), 2.97 (human)	0.59 (rat), 2.30 (human)	5.6 (rat), 8.1 (human)	-	-

Table 3.3.7. Results for compounds **16b**, **26**, **29**, **38** and **48**.

The data shows that the 3-cyano substituent remains the most ligand efficient 3-position group, although the other small 3-substituents also have moderate IKK2 potency and show some selectivity over IKK1. Disappointingly, none of the compounds showed any activity in the HWB assay and those tested in the IVC study showed high clearance so these compounds were not progressed further. However, as a result of the high ligand efficiency observed for the compound containing the 3-cyano substituent, further compounds were prepared to investigate the effect of varying the 5-substituent whilst maintaining the cyano-group at the 3-position, although this work will not be discussed here.

The measured biological data was also used to test the predictive QSAR model. Figure 3.3.3 shows the predicted vs measured IKK2  $pK_i$  values.

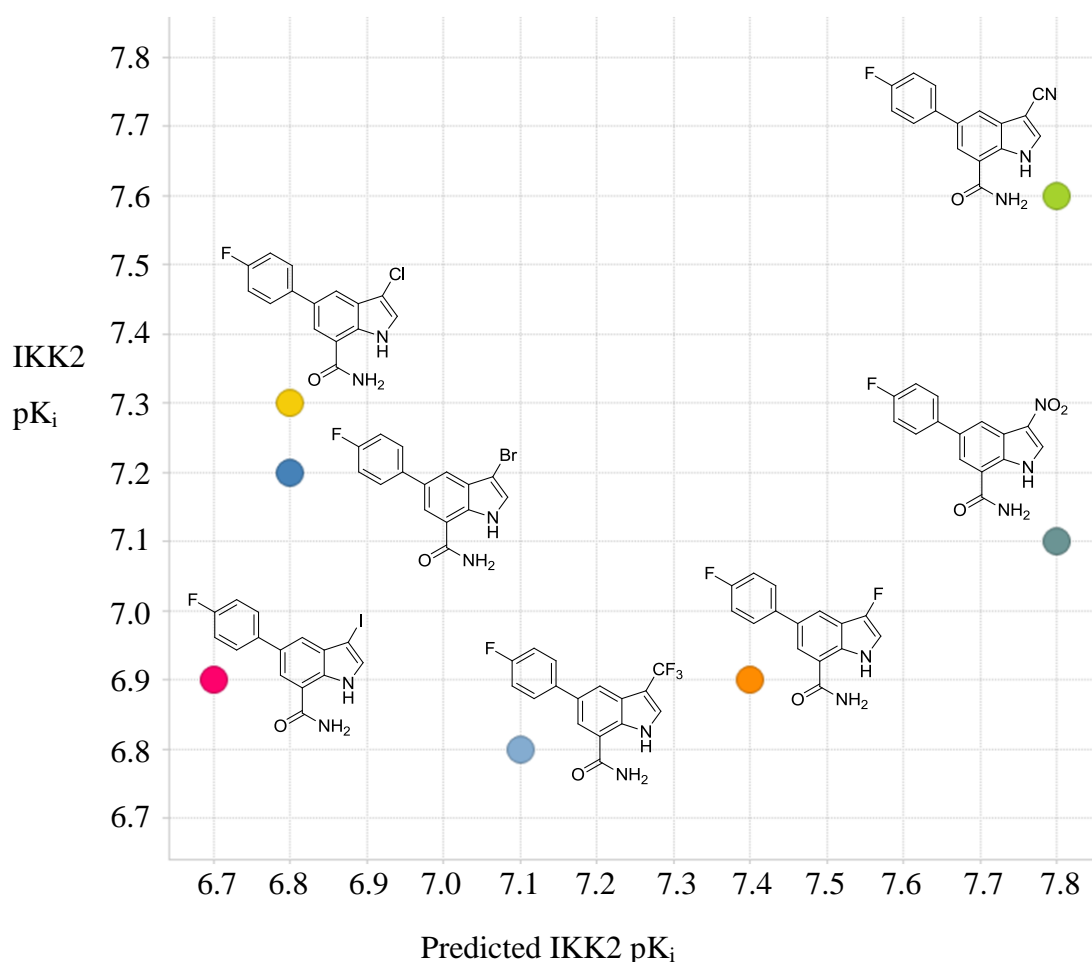
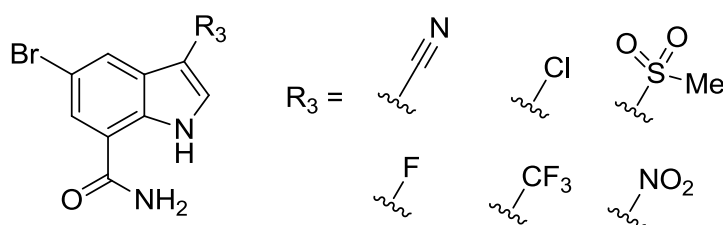
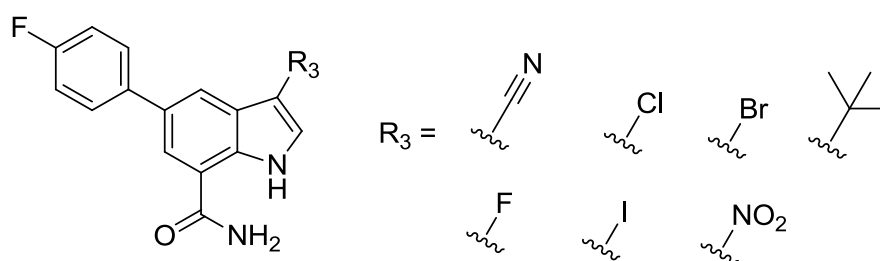


Figure 3.3.3. Measured vs predicted IKK2 potency.

Unfortunately, the correlation between the measured and predicted data was poor. This means that the regression equations developed to predict IKK2 potency from the various substituent parameters were not suitable, most probably because they were based on observed data from only three compounds. Since the set of 3-substituted indole carboxamides with measured IKK2 potencies has now been expanded, the Hansch analysis was carried out again to re-evaluate the correlations between IKK2 potency and the fourteen substituent parameters.

Two compound sets were evaluated separately; set A had the same 5-*para*-fluorophenyl substituent and set B had the same 5-bromo substituent.



Disappointingly, Hansch analysis of set B did not result in any obvious structure-activity relationships. However, analysis of set A identified trends between IKK2 potency and three substituent parameters;  $\sigma^*$  (the polar substituent constant),  $\pi$  (lipophilicity) and F (the field constant), where the  $R^2$  values were potentially significant (0.85, 0.72 and 0.67, respectively). The inclusion of a *tert*-butyl group at the 3-position<sup>50</sup> gave evidence that non-polar substituents were disfavoured, leading

to reduced IKK2 potency. Indeed, there was a positive relationship between IKK2 potency and  $\sigma^*$  (Figure 3.3.4), and a negative relationship between potency and  $\pi$  (Figure 3.3.5).

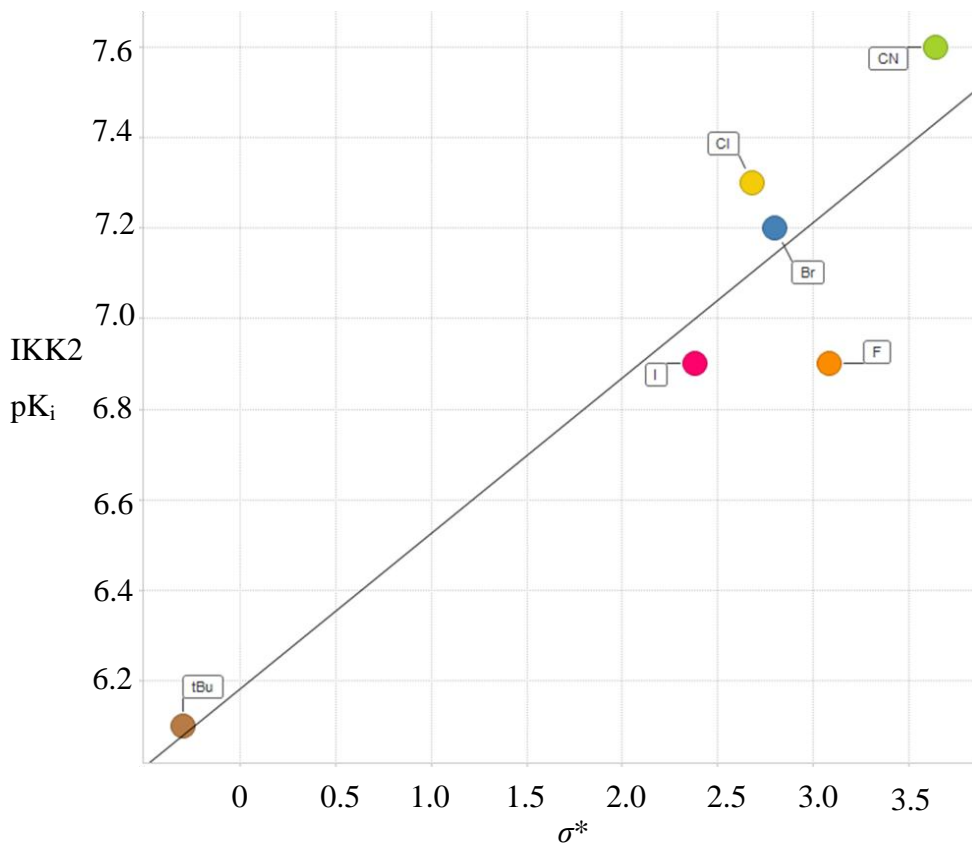


Figure 3.3.4. Relationship of the IKK2 pK<sub>i</sub> with  $\sigma^*$ , the polar substituent parameter.

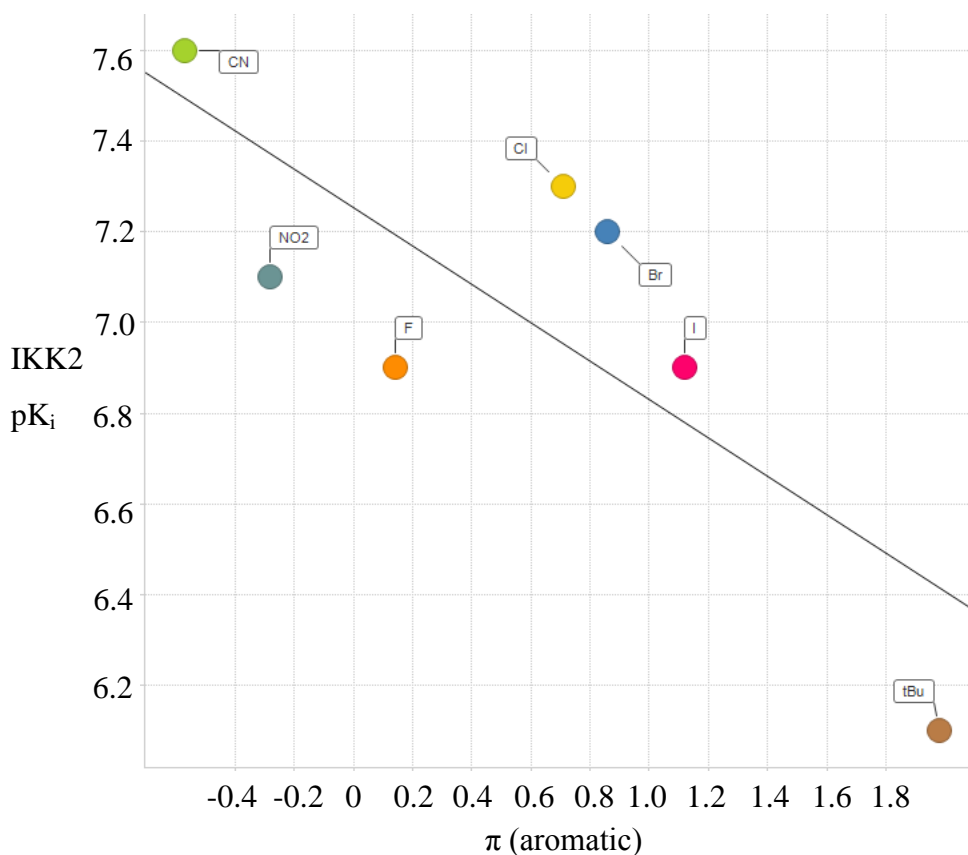


Figure 3.3.5. Relationship of the IKK2 pK<sub>i</sub> with π, a measure of lipophilicity.

These relationships indicate that more polar groups at the 3-position may enhance the biological activity of the compounds. The increased potency could be attributed to favourable polar interactions with residues predicted to be in the vicinity of this position of the indole carboxamides (*vide supra* for the IKK2 crystal structure).

Figure 3.3.6 shows the positive trend in IKK2 potency with the field constant, F.

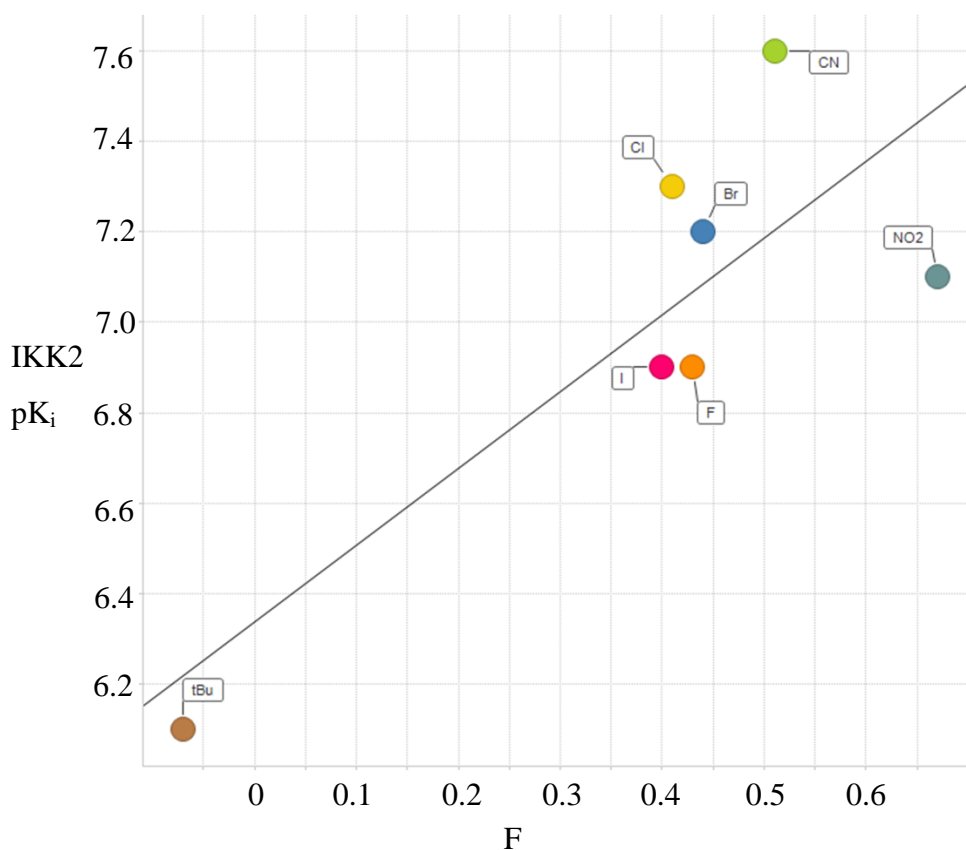


Figure 3.3.6. Relationship of the IKK2 pK<sub>i</sub> with F, the field constant.

The field constant represents the electronic nature of the substituent and takes into account the direct electrostatic influence of a substituent as well as its inductive effects, with higher values indicating higher electron-withdrawing capability.<sup>83</sup> The positive trend could be attributed to the increasing electron-withdrawing strength at the 3-position, which may strengthen the hydrogen bond from the indole N-H to the outer carbonyl of Cys99 in the hinge region of the kinase (Figure 3.3.7).

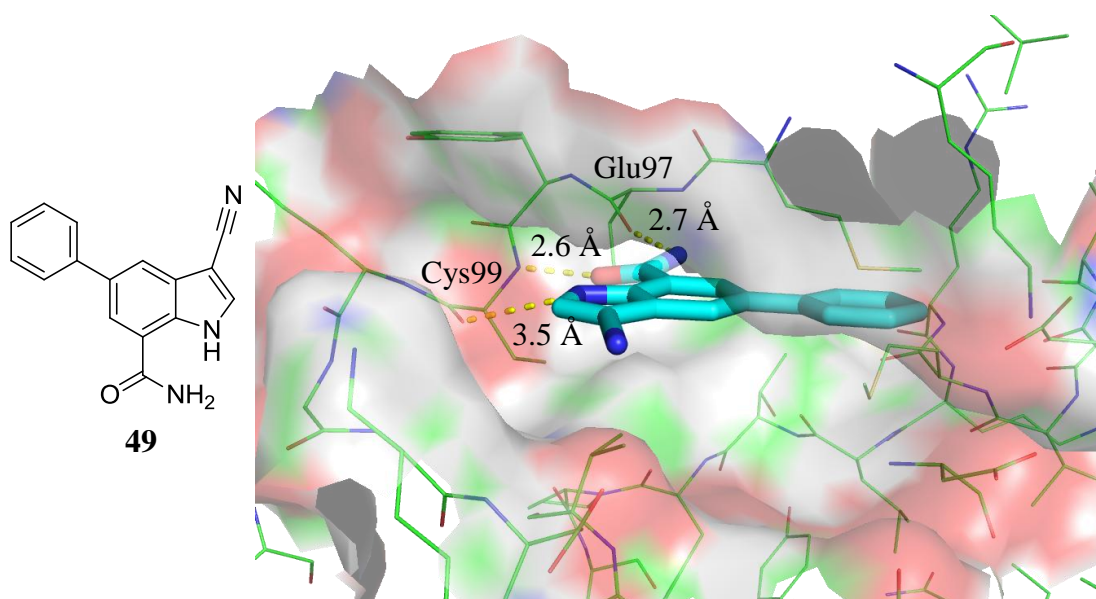


Figure 3.3.7. Hinge interaction from indole N-H of compound **49** to Cys99 as shown in a docking using the homology model (the IKK2 crystal structure was unavailable at the time of this analysis).

Even though some structure-activity trends have been observed, there were eight or fewer compounds within each set, and set A did not contain a very diverse range of 3-substituents. Therefore, it would be advantageous to synthesise further 3-substituted compounds in order to corroborate the observed trends between IKK2 activity and the substituent parameters and develop regression equations that better relate the structure and activity of 3-substituted indole carboxamides. A more recent review of Hansch analysis contains a wider table of substituents so it would be of interest to assess this broader range of groups for incorporation at the 3-position.<sup>49</sup> At this stage, rather than synthesising a broad range of 3-substituted indole carboxamides whose biological activity could not be predicted, the focus of the work shifted to designing compounds containing novel 3-substituents that would function as direct replacements for the 3-tetrahydrothiopyran-dioxide group.

### 3.3.2. 3-(Oxetan-3-yl)-1*H*-indole-7-carboxamides

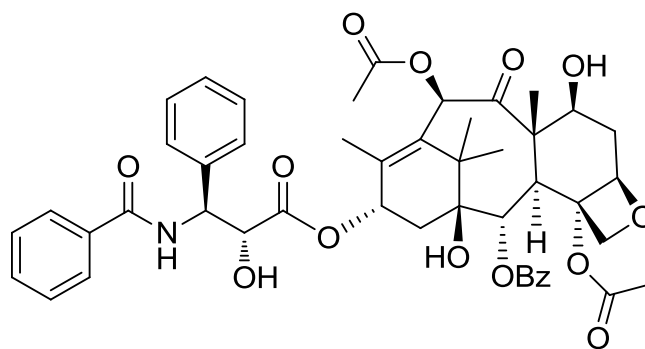
Having analysed small substituents at the 3-position of the indole carboxamide and concluded that replacement of the tetrahydrothiopyran-dioxide group by a cyano group maintained IKK2 potency and selectivity, work to install an oxetan-3-yl group at the indole carboxamide 3-position was initiated. The 3-tetrahydro-2*H*-pyran-4-yl group was also investigated within our laboratories but the ligand efficiencies of the compounds were not comparable to the tetrahydrothiopyran-dioxide equivalents,<sup>42</sup> so the smaller oxetan-3-yl group was of more interest.

In recent years, oxetanes have begun to receive considerable interest from the medicinal chemistry community as small structural units with the potential to modify physicochemical and metabolic properties of the compounds in which they reside.<sup>84</sup> 3-Substituted oxetanes are of most interest as they are achiral and do not add much complexity to molecules in which they are incorporated. Historically, oxetanes have been neglected in medicinal chemistry due to concerns over their chemical and metabolic stability, and ease of synthesis. A recent review has shown progress in addressing these concerns and has described recent advances in the synthesis and utility of these units.<sup>85</sup>

#### 3.3.2.1. Oxetanes in Drug Molecules and Nature

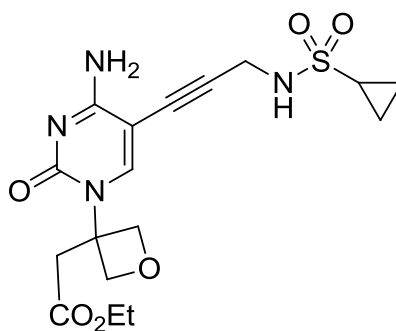
Currently there are only a few marketed drugs containing an oxetane unit; one example is Taxol<sup>®</sup>, which is used in cancer chemotherapy.<sup>86</sup>



Taxol<sup>®</sup>

Taxol is a member of a family of oxetane-containing natural products, the *Taxus* genus, and was first isolated from the stem bark of the western yew, *Taxus brevifolia*.<sup>86</sup>

Small drug molecules that contain oxetanes have also been identified, including the cytosine-containing inhibitor of IspE (**50**).<sup>87</sup> This compound was the only inhibitor from a series of analogous compounds that was fully water-soluble.<sup>87</sup>

**50**

### 3.3.2.2. Structure and Properties of Oxetanes

Müller and Carreira have identified the oxetane as a small, stable unit with low lipophilicity and reduced metabolic degradation.<sup>84</sup> The initial work concentrated on the analogy of a 3-substituted oxetane with a *gem*-dimethyl group and the

advantages this may bring to drug-like molecules.<sup>88</sup> Geminal dimethyl units are often introduced into molecules in order to add steric bulk or block metabolically labile sites. This leads to an undesired increase in lipophilicity and the presence of two methyl groups that could themselves present a metabolic risk. The oxetanyl group represents a more polar and more metabolically stable alternative to the *gem*-dimethyl unit (Figure 3.3.8).

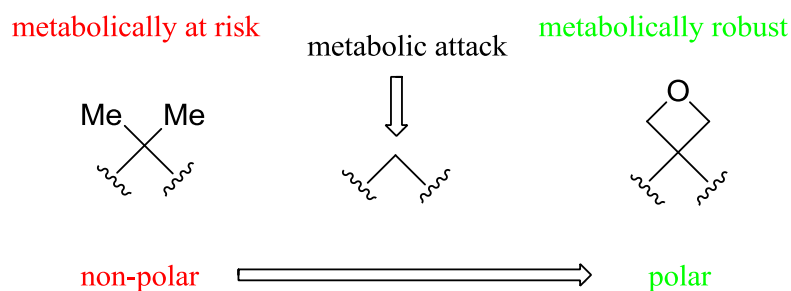


Figure 3.3.8. Structural analogy of oxetane with *gem*-dimethyl groups.<sup>88</sup>

A 3-substituted oxetane also resembles a carbonyl group in its ability to act as an acceptor of hydrogen bonds. This would allow the same hydrogen-bonding interaction between Lys106 and the tetrahydrothiopyran-dioxide substituent to be engaged, which is shown in Figure 3.3.9, where a 3-tetrahydrothiopyran-dioxide compound (**51**) and a 3-oxetan-3-yl compound (**52**) are overlaid in the IKK2 homology model.

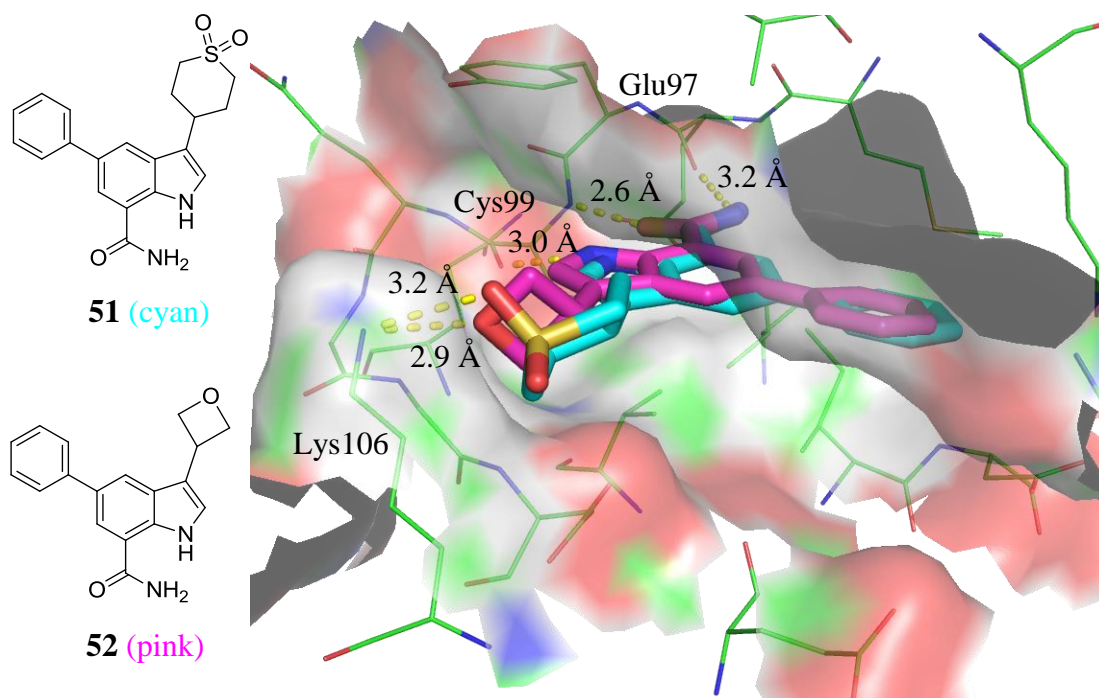


Figure 3.3.9. IKK2 homology model showing the predicted binding modes of compounds **51** and **52**.

The analogy of oxetane with a carbonyl group is based on its resemblance to the van't Hoff picture of a C=O double bond (Figure 3.3.10).<sup>84</sup> The spatial arrangement of the oxygen lone pairs is comparable and the two functionalities are polarised similarly. However, the non-bonding distance from the oxetane oxygen to the disubstituted carbon is approximately 0.9 Å longer than a C=O double bond (Figure 3.3.10).<sup>84</sup>

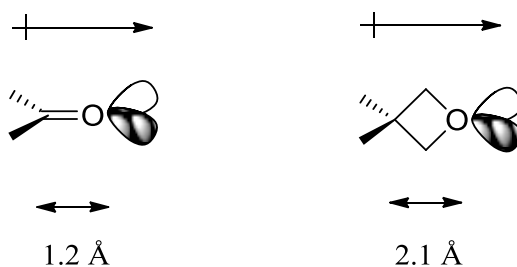


Figure 3.3.10. Structural analogy between oxetane and a carbonyl unit.<sup>84</sup>

The hydrogen-bond acceptor ability of the oxetane exceeds that of aliphatic ketones, aldehydes and esters and is at its best when compared to other cyclic ethers.<sup>89</sup> Müller suggested oxetanes are the best hydrogen-bond acceptors among the cyclic ethers; though an increase in s character of the lone pair nonbonding orbitals in smaller ring systems makes them less available to hydrogen bond donors, the small endocyclic C-O-C angle allows better steric exposure of the oxygen atom to hydrogen bond donors.<sup>84</sup> The hydrogen-bonding ability of the oxetanyl group has been observed in a crystal structure of compound **53**, in which the oxetane oxygen accepts a hydrogen bond from the hydroxyl of another molecule (Figure 3.3.10).<sup>90</sup>

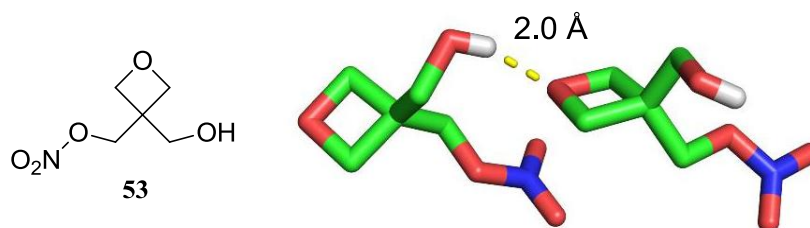


Figure 3.3.11. Compound **53** engaging in hydrogen-bonding.<sup>90</sup>

Additional properties of the oxetane group are its ability to act as a Lewis base through donation of electron density from the oxygen atom, whilst itself being electron-withdrawing. These properties, as well as those already described, mean that

oxetanes are able to influence the physicochemical properties of the molecules in which they reside.

### 3.3.2.3. Property Changes Arising from the Presence of Oxetanes

The placement of an oxetane within chemical structures has been shown to have significant effects on several physicochemical properties including aqueous solubility, lipophilicity and metabolic stability.

Evidence from studies carried out by Müller has shown that molecules containing an oxetane rather than a *gem*-dimethyl group are less lipophilic, and that the corresponding carbonyl-containing compounds are more hydrophilic (Figure 3.3.12).<sup>85</sup> These changes in lipophilicity are mirrored in the observed differences in aqueous solubility, with carbonyl compounds typically having higher aqueous solubility than their oxetane or *gem*-dimethyl counterparts (Figure 3.3.12).<sup>85</sup>

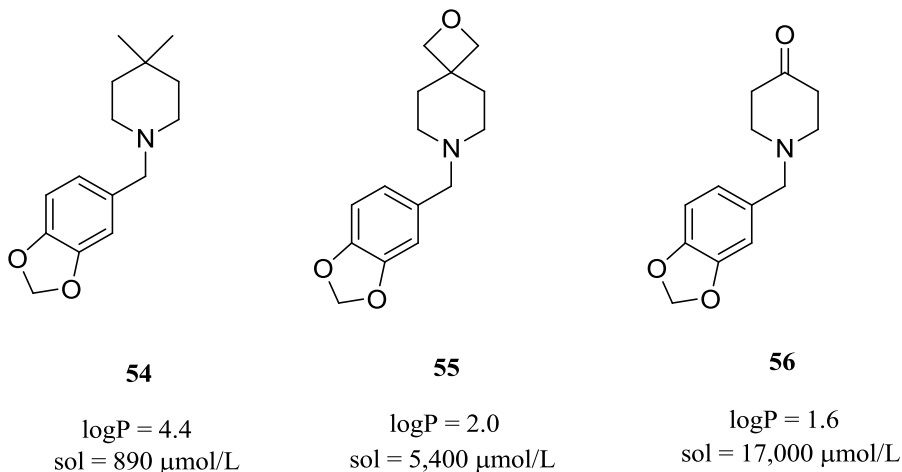
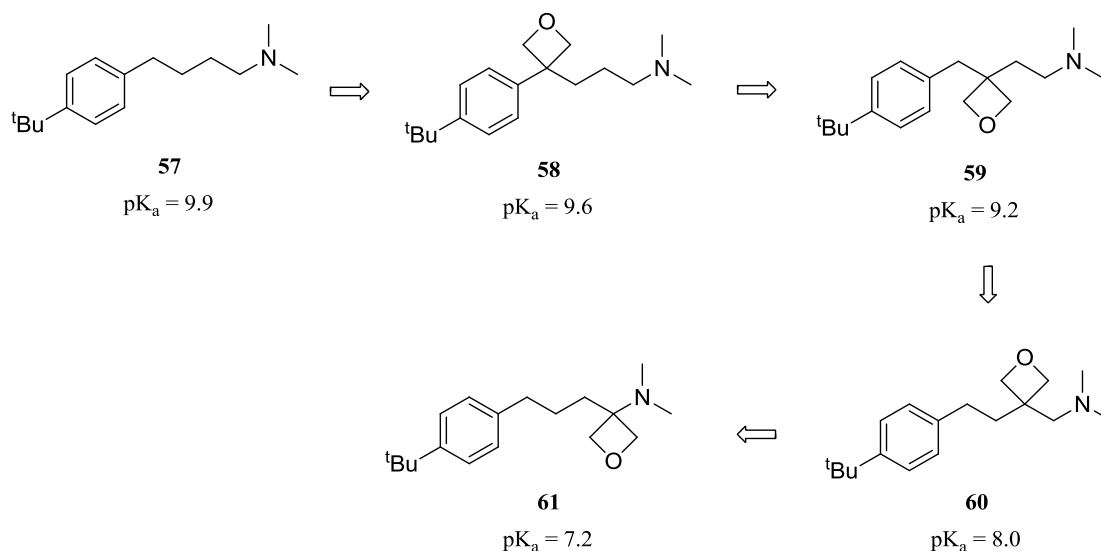


Figure 3.3.12. Differences in lipophilicity and aqueous solubility.

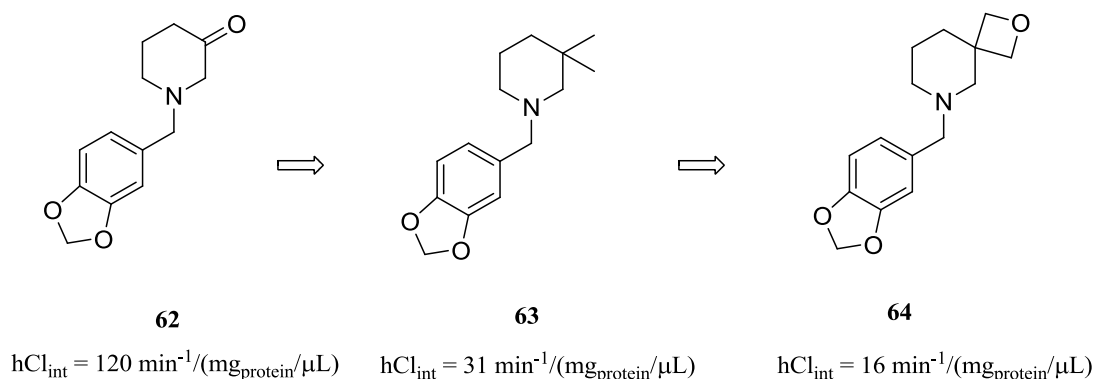
Changes in aqueous solubility on introducing an oxetanyl group to a molecule were most marked when the scaffold was highly lipophilic, with the increase upon replacement of a *gem*-dimethyl group with an oxetane being as large as 4000-fold.<sup>84</sup>

It was observed that the placement of an oxetane in the proximity of an amine moderated its basicity due to the electron-withdrawing nature of the oxetanyl group (Scheme 3.3.13).<sup>85</sup>



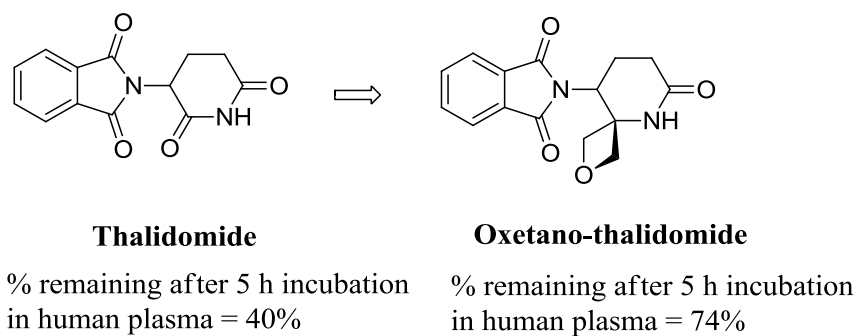
Scheme 3.3.13. Altering basicity through the introduction of oxetanes.

In addition to the effects of oxetanes on lipophilicity, solubility and basicity, marked changes in metabolic susceptibility have also been observed. Measurement of the intrinsic clearance rates in *in vitro* human and mouse microsomal assays for several oxetane-containing compounds showed a reduction in oxidative degradation compared to analogous *gem*-dimethyl or carbonyl compounds (Scheme 3.3.14).



Scheme 3.3.14. Intrinsic clearance rate of oxetane-containing compounds in human liver microsomes.

Another interesting example was provided by the replacement of one of the carbonyl functionalities of thalidomide, an antiemetic and sedative that has serious side effects that are potentially due to *in vivo* instability/metabolism. Initial studies showed that the introduction of the oxetanyl group as a carbonyl surrogate led to an increase in human plasma stability (Scheme 3.3.15).<sup>91</sup>



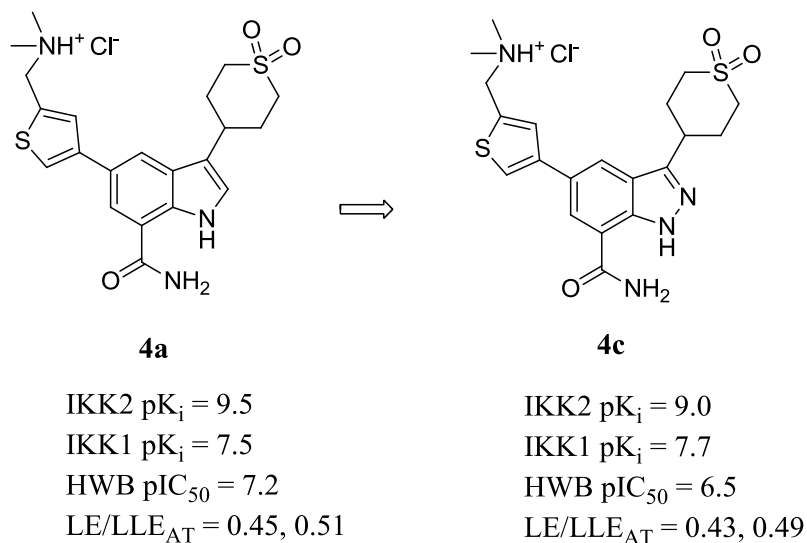
Scheme 3.3.15. Human plasma stability of thalidomide and its oxetanyl-substituted analogue.<sup>91</sup>

As well as metabolic stability, investigations into the chemical stability of 3,3-disubstituted oxetanes showed all compounds to be stable in aqueous solutions of

pH 1 to 10 when heated at 37 °C for 2 h.<sup>84</sup> Some decomposition of monosubstituted oxetanes was observed but only in strongly acidic conditions.<sup>84</sup>

The improvements observed in the physicochemical properties of molecules containing an oxetanyl group supported the decision to include such a functional unit at the 3-position of the indole-7-carboxamide scaffold. Replacement of the 3-tetrahydrothiopyran-dioxide substituent by an oxetan-3-yl group would help reduce molecular weight and lipophilicity, and the ability of the oxetane to form hydrogen bonds should maintain IKK2 potency and thereby increase ligand efficiency. The intrinsic polarity of the oxetanyl group along with a concomitant reduction in lipophilicity should also help to increase solubility of the indole scaffold.

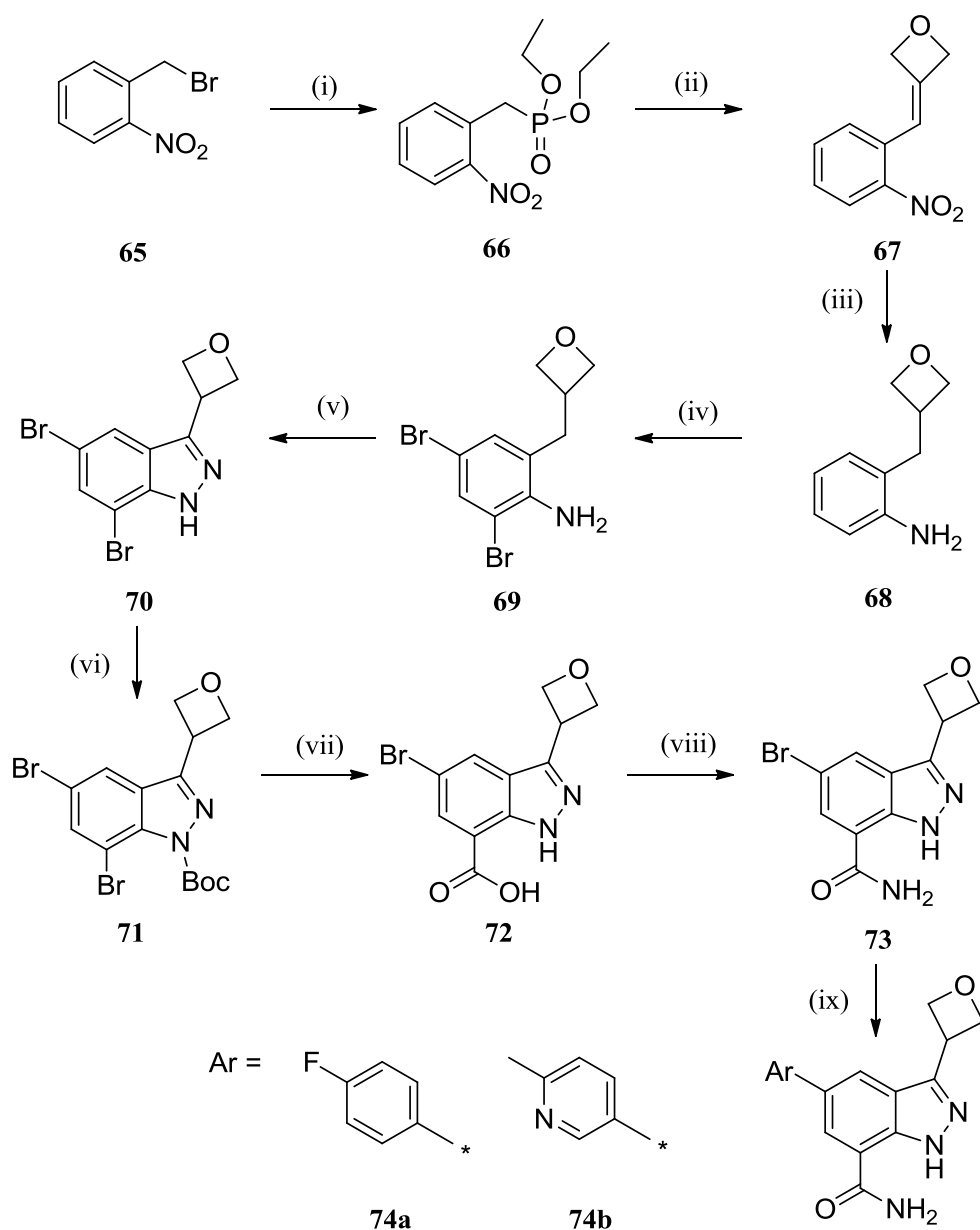
Although the indole core was of most interest for the programme, chemistry was carried out in parallel to install an oxetanyl group at the 3-position of both indole-7-carboxamides and indazole-7-carboxamides since it was thought the synthesis of 3-(oxetan-3-yl)indazole-7-carboxamides was more tractable. Typically, indazole carboxamides have similar ligand efficiency to the analogous indole carboxamides and are active in the whole blood assay; however they can have poorer selectivity against IKK1. For example, indazole carboxamide **4c** has 20-fold selectivity over IKK1 compared with indole carboxamide **4a**, which has 100-fold selectivity.





#### **3.3.2.4. Synthesis and Biological Results of 3-(Oxetan-3-yl)indazole-7-carboxamides**

Since the synthetic route for the formation of indazole-7-carboxamides from commercially available 2-nitrobenzyl bromide was precededented, the synthesis of 3-(oxetan-3-yl)indazole carboxamide compounds was investigated (Scheme 3.3.16).<sup>92</sup>



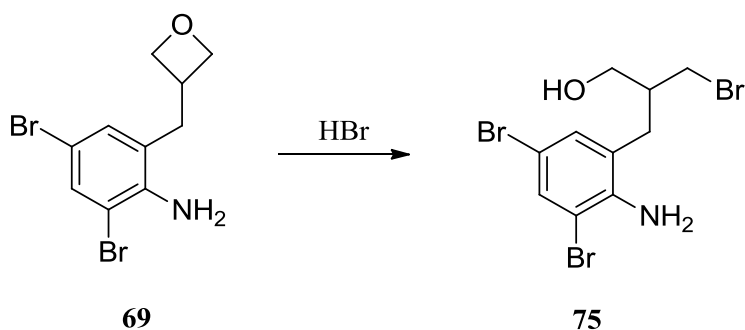
Reagents and Conditions: (i)  $\text{P}(\text{OEt})_3$ , toluene,  $110\text{ }^\circ\text{C}$ , 77%; (ii) 3-oxetanone, NaH, DMF,  $0\text{ }^\circ\text{C}$  to rt, 70%; (iii) Pd/C,  $\text{H}_2$  (8 bar), MeOH,  $45\text{ }^\circ\text{C}$ , 97%; (iv) NBS, DCM,  $0\text{ }^\circ\text{C}$ , 64%; (v)  $\text{Ac}_2\text{O}$ , KOAc, 18-crown-6,  $\text{CHCl}_3$ , rt then  $\text{Ac}_2\text{O}$ , AcOH, *t*-butylnitrite,  $\text{CHCl}_3$ ,  $61\text{ }^\circ\text{C}$ , 65%; (vi)  $\text{Boc}_2\text{O}$ , DMAP,  $\text{NEt}_3$ , DCM, rt to  $35\text{ }^\circ\text{C}$ , 90%; (vii) *t*-BuLi,  $\text{CO}_2$ , THF,  $-78\text{ }^\circ\text{C}$  to rt, 76%; (viii) HATU, DIPEA,  $\text{NH}_3/\text{MeOH}$ , DMF, rt, 45%; (ix)  $\text{ArB}(\text{OH})_2$ ,  $\text{Pd}(\text{PPh}_3)_4$ ,  $\text{K}_2\text{CO}_3$ , IPA/ $\text{H}_2\text{O}$  (3:1),  $120\text{ }^\circ\text{C}$ ,  $\mu\text{wave}$ , 25% (**74a**), 19% (**74b**).

Scheme 3.3.16. Synthetic route to 3-(oxetan-3-yl)-1H-indazole-7-carboxamide.

Firstly, reaction of 2-nitrobenzyl bromide (**65**) with triethylphosphite gave alkyl phosphonate **66** via the Michaelis-Arbuzov reaction.<sup>93,94</sup> The phosphonate then underwent a Horner-Wadsworth-Emmons (HWE) olefination with 3-oxetanone to form alkene **67**.<sup>95,96</sup>

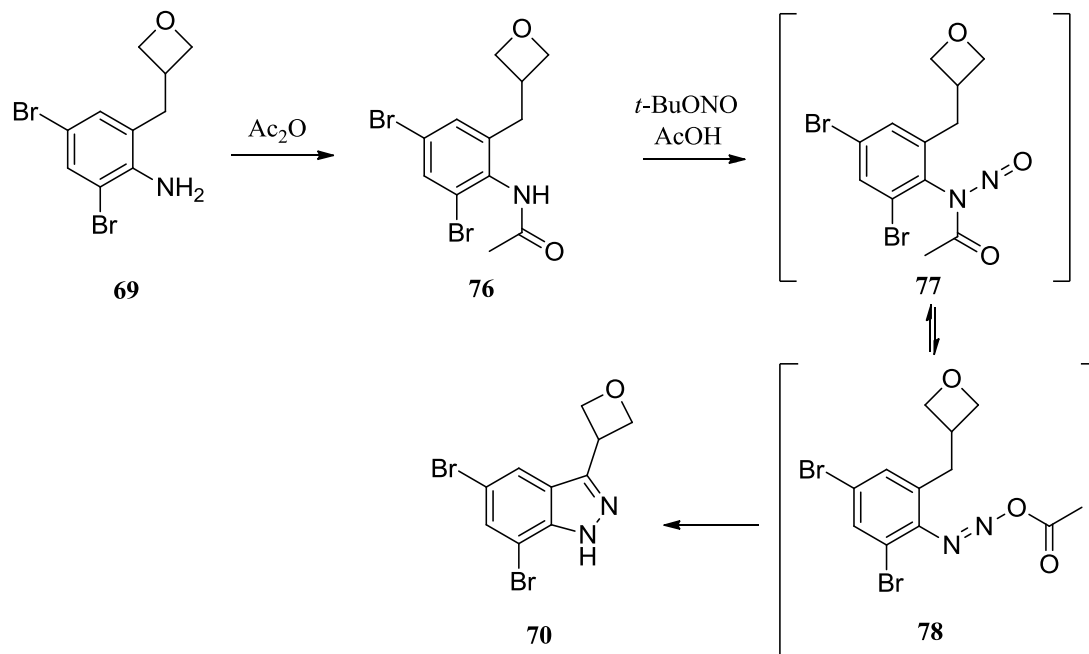
The next step involved reduction of both the alkenyl and nitro groups, which was carried out using an H-cube<sup>®</sup> continuous-flow hydrogenation reactor to isolate aniline **68**.<sup>97</sup> The substrate solution was passed through a 10% Pd/C catalyst cartridge (CatCart<sup>®</sup>) and combined with hydrogen generated *in situ* from the electrolysis of water. Using the H-cube<sup>®</sup>, the reaction was performed at elevated temperature (45 °C) and pressure (8 bar) to ensure full reduction. In contrast, it was found that the nitro group could not be reduced fully at room temperature and atmospheric pressure, using either 10% Pd/C or 10% Pt/C catalysts. The reaction also led to an increase in by-products over time.

As expected, bromination led to disubstitution in the aniline *ortho*- and *para*-positions. A major by-product from this reaction was the ring-opened compound **75**, which was observed in the crude NMR spectrum. Formation of this was brought about by the presence of HBr that was not quenched sufficiently during the work-up (Scheme 3.3.17). It was found to be important to keep the reaction mixture cold, and to quench with saturated sodium bicarbonate solution to minimise formation of the by-product.



Scheme 3.3.17. Formation of bromination by-product **75**.

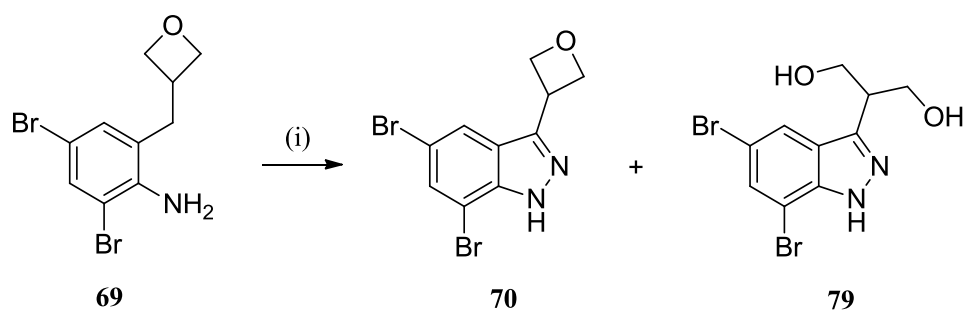
The indazole system was built up *via* diazotisation and cyclisation using *tert*-butylnitrite (Scheme 3.3.18).<sup>98,99</sup>



Reagents and conditions: (i)  $\text{Ac}_2\text{O}$ , KOAc, 18-crown-6,  $\text{CHCl}_3$ , rt then  $\text{Ac}_2\text{O}$ , AcOH, *t*-butylnitrite,  $\text{CHCl}_3$ , 61 °C, 65%.

Scheme 3.3.18. Indazole formation.

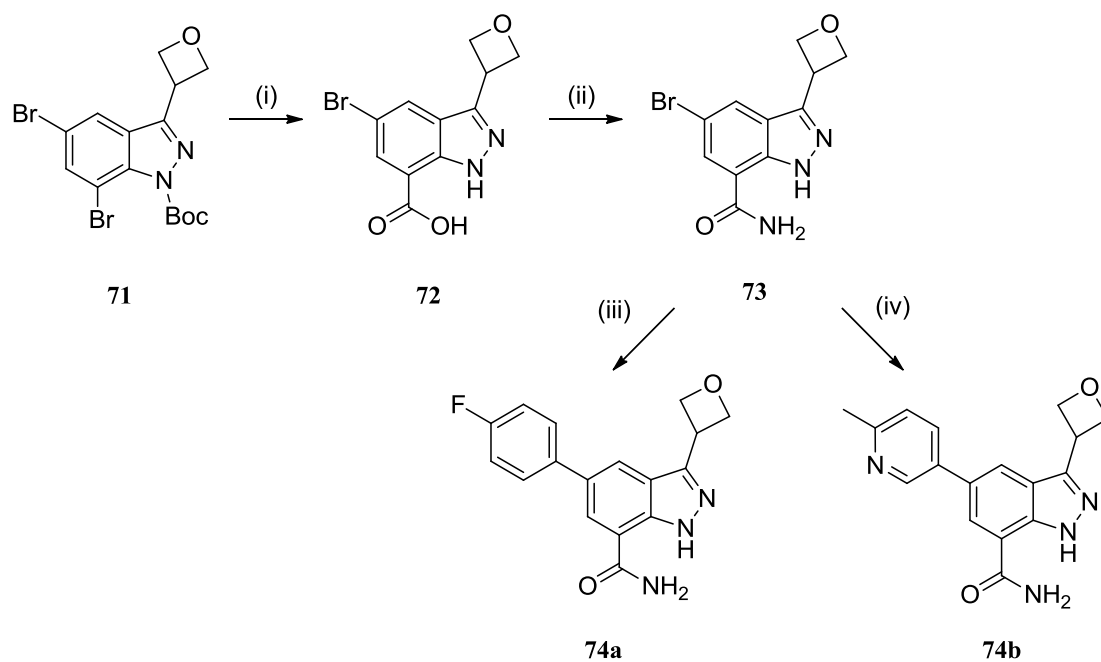
The use of potassium acetate and 18-crown-6 ensured that the solution was buffered in order to avoid acidic conditions under which oxetane ring-opening could occur. 18-Crown-6 ensures the base is soluble in chloroform, hence producing the  $\text{AcO}^-/\text{AcOH}$  buffer. Oxetane has been shown to undergo hydrolysis catalysed by sulfuric or perchloric acid,<sup>100</sup> and it was also observed here that the removal of 18-crown-6 from the reaction led to the generation of significant amounts of the ring-opened by-product **79** (1:2 ratio of product to by-product), which was observed in the crude NMR spectrum (Scheme 3.3.19).



Reagents and conditions: (i) Ac<sub>2</sub>O, KOAc, AcOH, *t*-butylnitrite, CHCl<sub>3</sub>, 61 °C.

Scheme 3.3.19. Formation of ring-opened by-product.

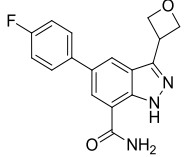
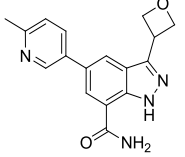
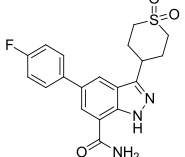
After the heterocycle had been formed, protection of the indazole nitrogen gave intermediate **71**, which then underwent directed metal-halogen exchange to lithiate the 7-position. Quenching with carbon dioxide afforded the desired 7-carboxylic acid **72** (Scheme 3.3.20) with concomitant Boc-deprotection aided by the intermediate 7-carboxylate anion. The acid was converted to the primary carboxamide **73** (*via* an amide coupling) and final Suzuki cross-coupling reactions with the required boronic acids successfully gave compounds **74a** and **74b** (Scheme 3.3.20).



Reagents and conditions: (i) *t*-BuLi, CO<sub>2</sub>, THF, -78°C to rt, 76%; (ii) HATU, DIPEA, NH<sub>3</sub>/MeOH, DMF, rt, 45%; (iii) 4-FC<sub>6</sub>H<sub>4</sub>B(OH)<sub>2</sub>, Pd(PPh<sub>3</sub>)<sub>4</sub>, K<sub>2</sub>CO<sub>3</sub>, IPA/H<sub>2</sub>O (3:1), 120 °C, μwave, 25%; (iv) (6-Me-pyridin-3-yl)B(OH)<sub>2</sub>, Pd(PPh<sub>3</sub>)<sub>4</sub>, K<sub>2</sub>CO<sub>3</sub>, IPA/H<sub>2</sub>O (3:1), 120 °C, μwave, 19%.

Scheme 3.3.20. Synthesis of target 3-oxetane indazole compound.

The biological data for compounds **74a**, **74b** and the tetrahydrothiopyran-dioxide-substituted analogue **80** are shown in Table 3.3.8.

Structure			
Compound Number	<b>74a</b>	<b>74b</b>	<b>80</b>
Mean IKK2 pK <sub>i</sub> (N)	7.2 (4)	6.5 (2)	8.1 (3) <sup>a</sup>
Mean IKK1 pK <sub>i</sub> (N)	6.8 (4)	5.9 (2)	7.2 (10) <sup>b</sup>
Mean HWB pIC <sub>50</sub> (N)	5.9 (4)	-	-
LE/LLE <sub>AT</sub>	0.43/0.43	0.39/0.46	0.41/0.45
PFI	6.2	4.5	6.0
mChromlogD <sub>pH7.4</sub>	3.17	1.53	2.99
clogP	1.8	0.7	1.4
MW	311	308	387
TPSA	81	94	106
AMP (pH 7.05, nm/sec)	325	130	140
CLND solubility (μM)	1	361	1
hERG pIC <sub>50</sub>	4.3 <sup>c</sup>	<4.0	-
CYP 3A4 pIC <sub>50</sub>	<4.3	<4.3	-
IVC (mL/min/kg)	0.74 (rat), 1.45 (human)	-	-

<sup>a</sup> Returned value < 4.1 on one test occasion. <sup>b</sup> Returned value < 4.9 on one test occasion. <sup>c</sup> Returned values <4.0 on two test occasions.

Table 3.3.8. Results for compounds **74a** and **74b**.

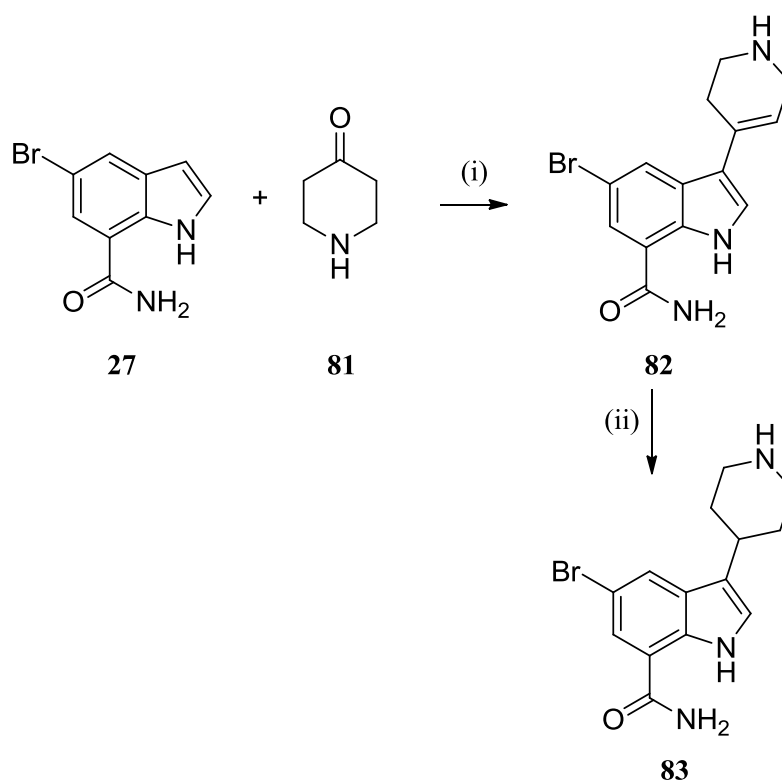
The indazole-7-carboxamides containing the oxetan-3-yl substituent at the 3-position can be seen to have moderate activity against IKK2, but poor selectivity over IKK1, which is a general trend observed with compounds containing the indazole core rather than the indole (*vide supra* for compounds **4a** and **4c**). The compounds show good permeability and **74a** was shown to have moderate turnover in an IVC study. The stability of compound **74a** was investigated to confirm that the turnover was not due to chemical instability and incubation in SGF at a concentration of 50 μg/mL and a temperature of 40 °C showed decomposition of the compound only after 66 h. This is most probably due to the instability of the oxetane ring in acidic conditions; however, the observed decomposition was slow and since residence time in the gut is typically less than 4 h, this level of instability in acid is

not of major concern. It was concluded that indazole compounds **74a** and **74b** are not suitable for progression due to poor IKK1 selectivity. However, the incorporation of a 3-oxetanyl group on an indole scaffold should maintain IKK2 activity and confer improved selectivity over the indazole compounds.

### 3.3.2.5. Synthesis and Biological Results for 3-Oxetane Substituted Indole-7-carboxamides

Initial investigation into the installation of an oxetanyl group at the 3-position of the indole carboxamide focused on alkylation with 3-oxetanone. In general, alkylation on the 3-position of indoles can be achieved using either alkyl halides, which can lead to issues with regioselectivity (C3 versus N1), or aldehydes/ketones as alkylating agents. In this case, the intermediate alkenes (formed by alcohol dehydration) are usually isolated and reduction is required as an additional step. This strategy had been implemented previously within our laboratories to install a piperidine substituent at the 3-position of 5-bromo-1*H*-indole-7-carboxamide (**27**) *via* acid-mediated alkylation with ketone **81**, followed by reduction of alkene **82** (Scheme 3.3.21).<sup>101</sup>

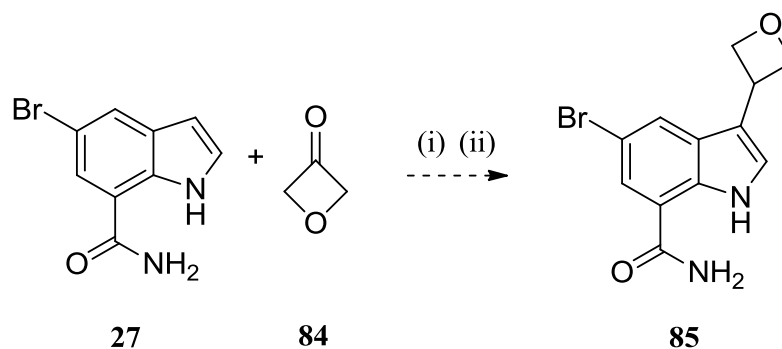




Reagents and Conditions: (i) H<sub>3</sub>NSO<sub>3</sub>, AcOH, 80 °C, 92%;<sup>101</sup> (ii) NaBH<sub>4</sub>, AcOH, THF, rt, 85%.

Scheme 3.3.21. Synthesis of *tert*-butyl 4-(5-bromo-7-carbamoyl-1*H*-indol-3-yl)piperidine-1-carboxylate (not described in Experimental as synthesised by S. Sollis, GSK).<sup>101</sup>

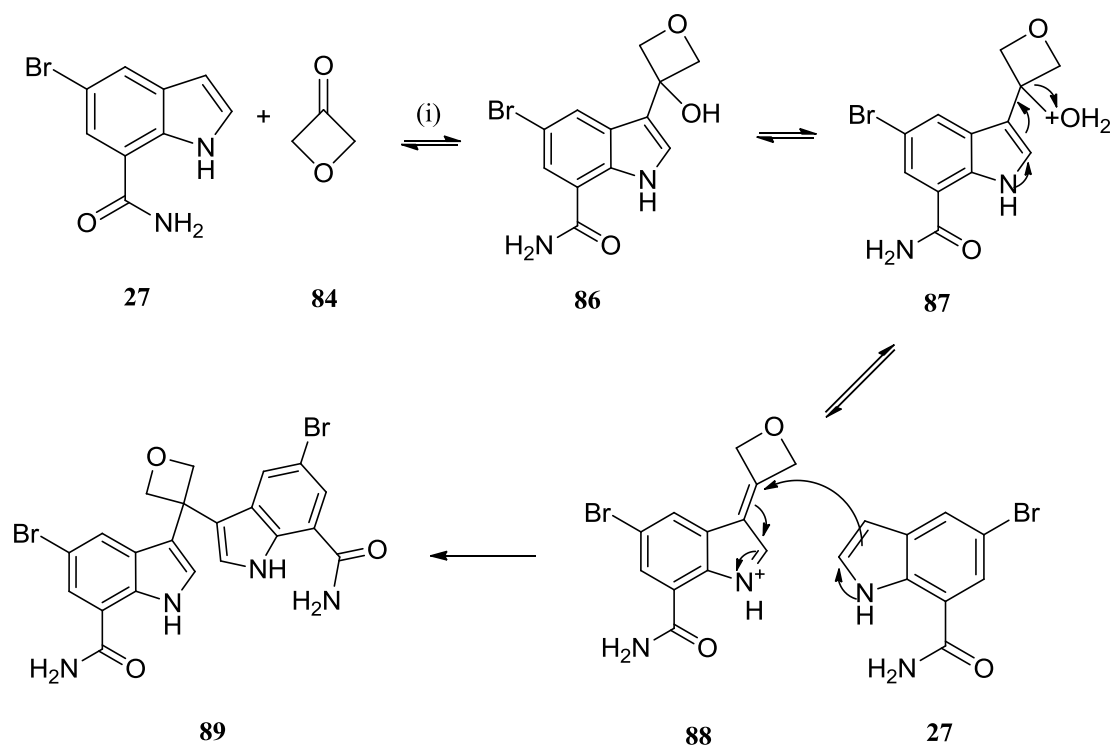
This approach was applied to the synthesis of the desired oxetane product, **85** (Scheme 3.3.22).



Reagents and Conditions: (i)  $\text{H}_3\text{NSO}_3$ , AcOH, 80 °C; (ii)  $\text{H}_2$ , catalyst.

Scheme 3.3.22. Proposed alkylation of 5-bromo-1*H*-indole-7-carboxamide with 3-oxetanone.

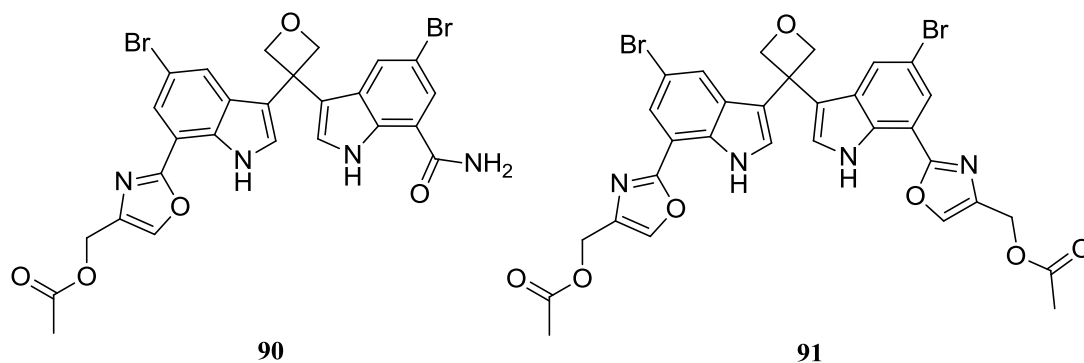
However, the main product was the *bis*-derivative, **89**, which could arise from addition of another indole nucleus to the intermediate indolium species **88** (Scheme 3.3.23). The analogous *bis*-derivative was also observed in the formation of piperidine derivative **83** but prolonged heating promoted fragmentation to give the desired product. However, this fragmentation was not observed even after extensive heating of carboxamide **27** with 3-oxetanone. This indicates that the *bis*-derivative **89** is more stable than the monomer. To obtain the desired monomer, formation of an endocyclic alkene is required, which is unfavourable as it raises angle strain in the 4-membered ring.



Reagents and Conditions: (i)  $\text{H}_3\text{NSO}_3$ , AcOH, 80 °C.

Scheme 3.3.23. Formation of bis-derivative **89**.

In addition to the main dimer product, two further species (**90** and **91**) were produced from the reaction.



NMR analysis led to determination of their structure, with HMBC correlations indicating the formation of a 1,3-oxazole from the 7-position carboxamide (Figure 3.3.13).<sup>102</sup>

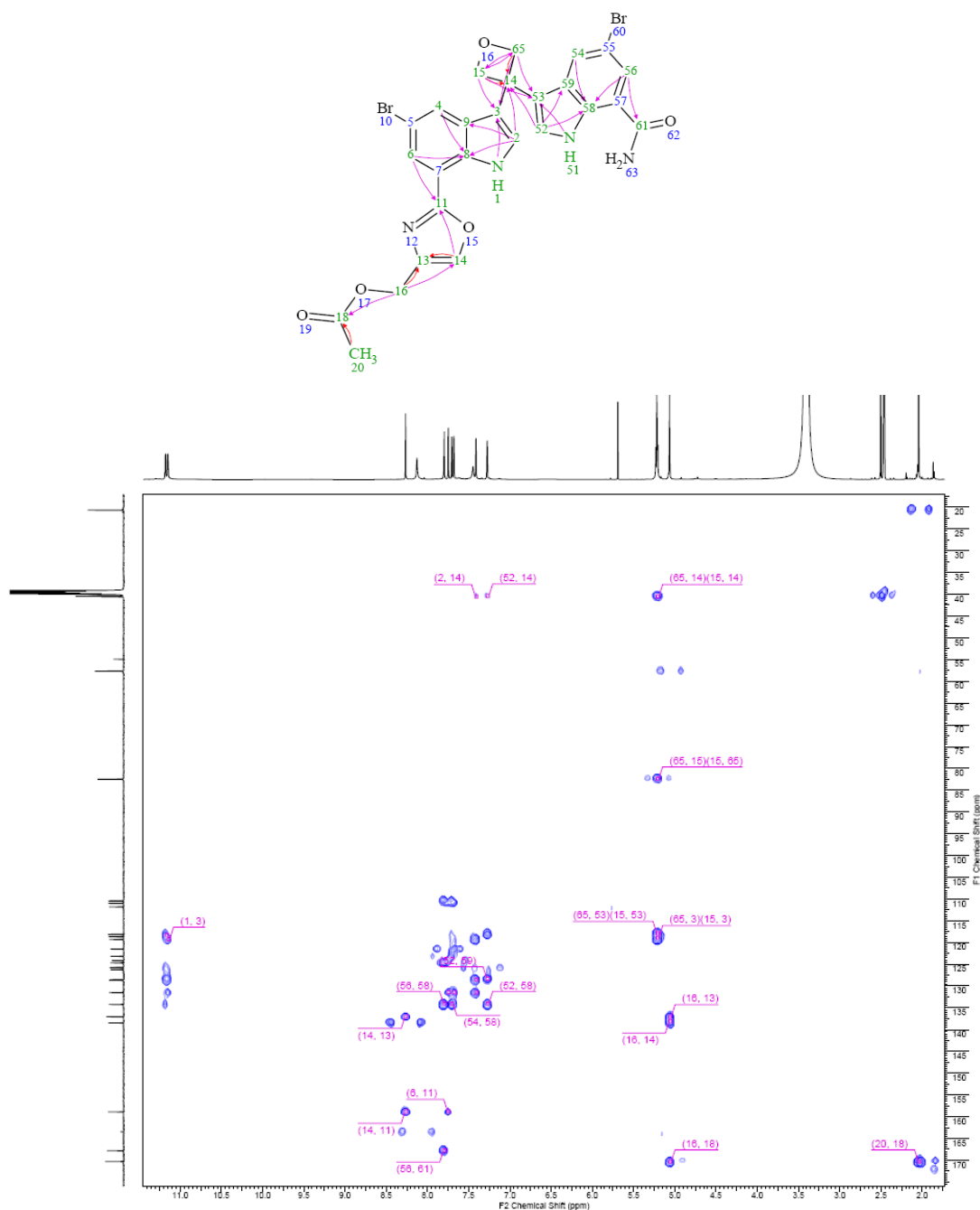
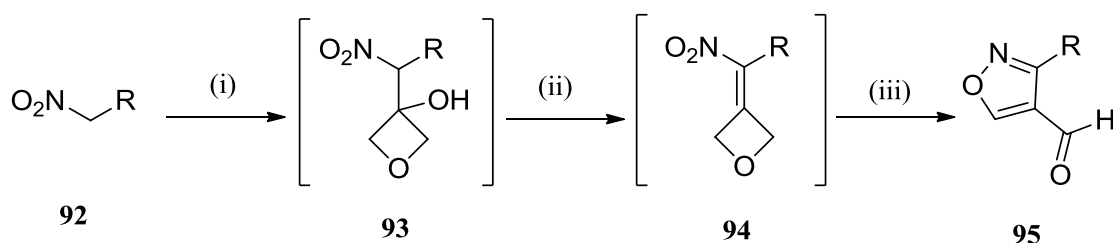


Figure 3.3.13. Key HMBC correlations for the determination of by-product structure (numbers in brackets correspond to the proton(s) or carbon as labelled in the structure).<sup>102</sup>

Key HMBC correlations between H<sub>22,24</sub> and C<sub>22,24</sub> as well as correlations of these protons with C<sub>21</sub>, C<sub>3</sub> and C<sub>53</sub>, confirmed the by-products to be indole dimers. Oxazole formation was identified from key HMBC correlations between H<sub>14</sub>, C<sub>11</sub> and C<sub>13</sub>, as depicted in Figure 3.3.13.<sup>102</sup>

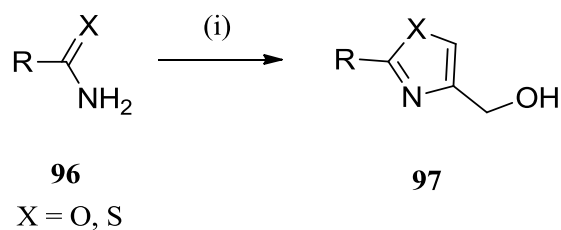
Interestingly, a recent paper has been published on the serendipitous discovery of the one-pot synthesis of isoxazoles from 3-oxetanone and nitroalkanes.<sup>103</sup> This occurs through the Henry addition of a nitroalkane to 3-oxetanone and subsequent elimination to form a 3-(nitromethylene)oxetane (**94**), which then undergoes a rearrangement to give a variety of isoxazoles (Scheme 3.3.24).<sup>103</sup>



Reagents and Conditions: (i) NEt<sub>3</sub>, rt; (ii) MsCl, NEt<sub>3</sub>, rt; (iii) DIPEA, rt.

Scheme 3.3.24. Formation of isoxazole-4-carbaldehydes *via* a cascade reaction.<sup>103</sup>

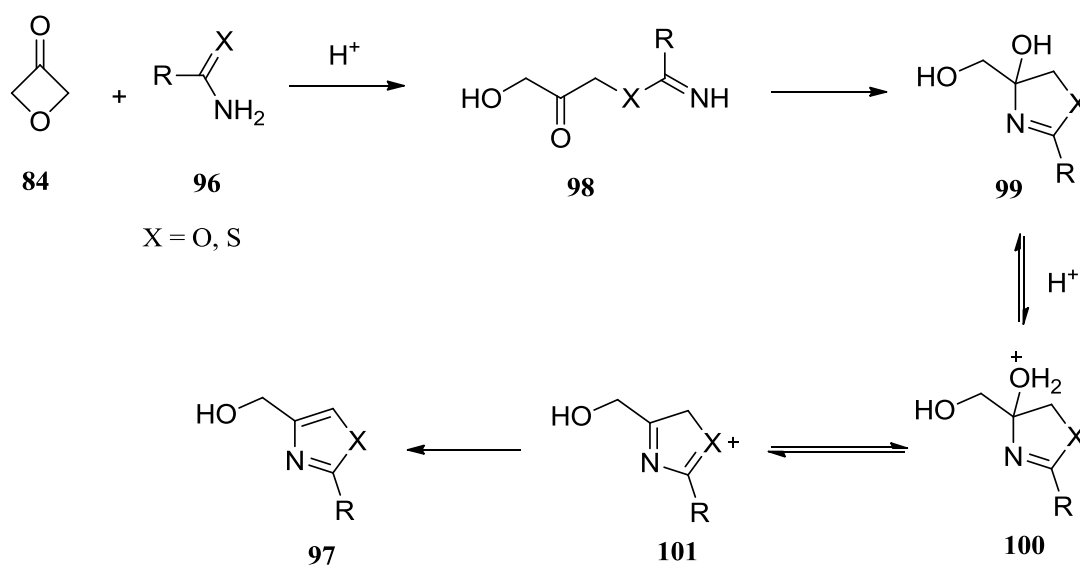
The oxazole formation observed in this programme of work was investigated further to see if a useful synthetic method could be discovered. Optimisation of the reaction conditions and expansion of the substrate scope to include primary thioamides for the synthesis of thiazoles resulted in a useful single-step microwave-mediated synthesis of oxazoles and thiazoles from 3-oxetanone (Scheme 3.3.25).<sup>104</sup>



Reagents and Conditions: (i) 3-oxetanone, MsOH, DMC, 120 °C,  $\mu$ wave, 13-64%.

Scheme 3.3.25. Microwave-mediated oxazole and thiazole syntheses.<sup>104</sup>

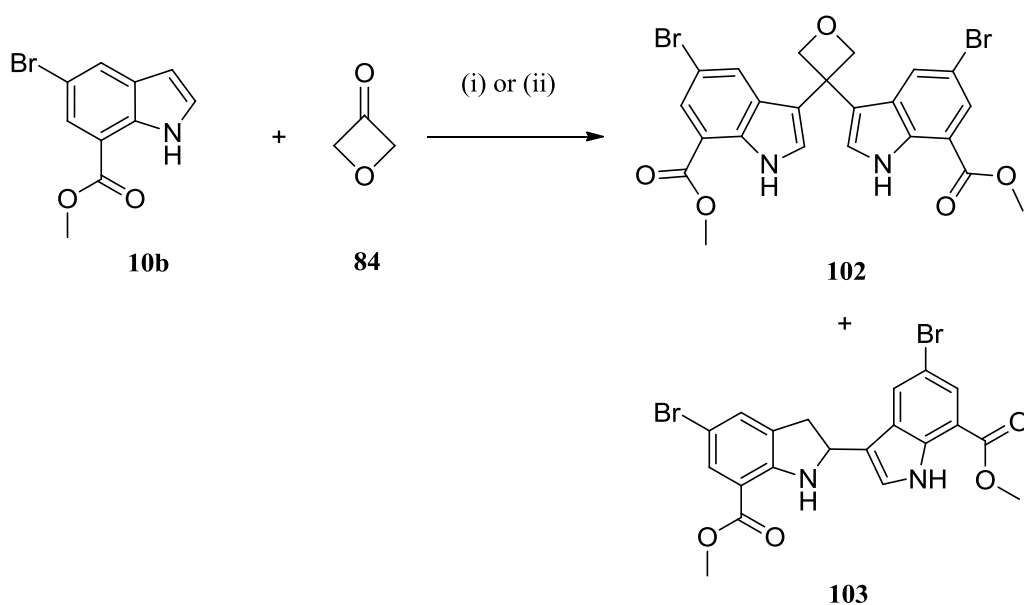
The mechanism of the reaction was explored and is believed to proceed by ring-opening of 3-oxetanone *via* C-O scission and the subsequent sequence of conventional steps leads to the desired products (Scheme 3.3.26).<sup>104</sup>



Scheme 3.3.26. Proposed mechanism for the formation of heteroarene products.<sup>104</sup>

In order to avoid the formation of the *bis*-indolylmethanes, the intermediate indolium ion must undergo reduction before a second indole moiety adds to it. This can be achieved by using an *in situ* reductant, therefore avoiding the need to isolate

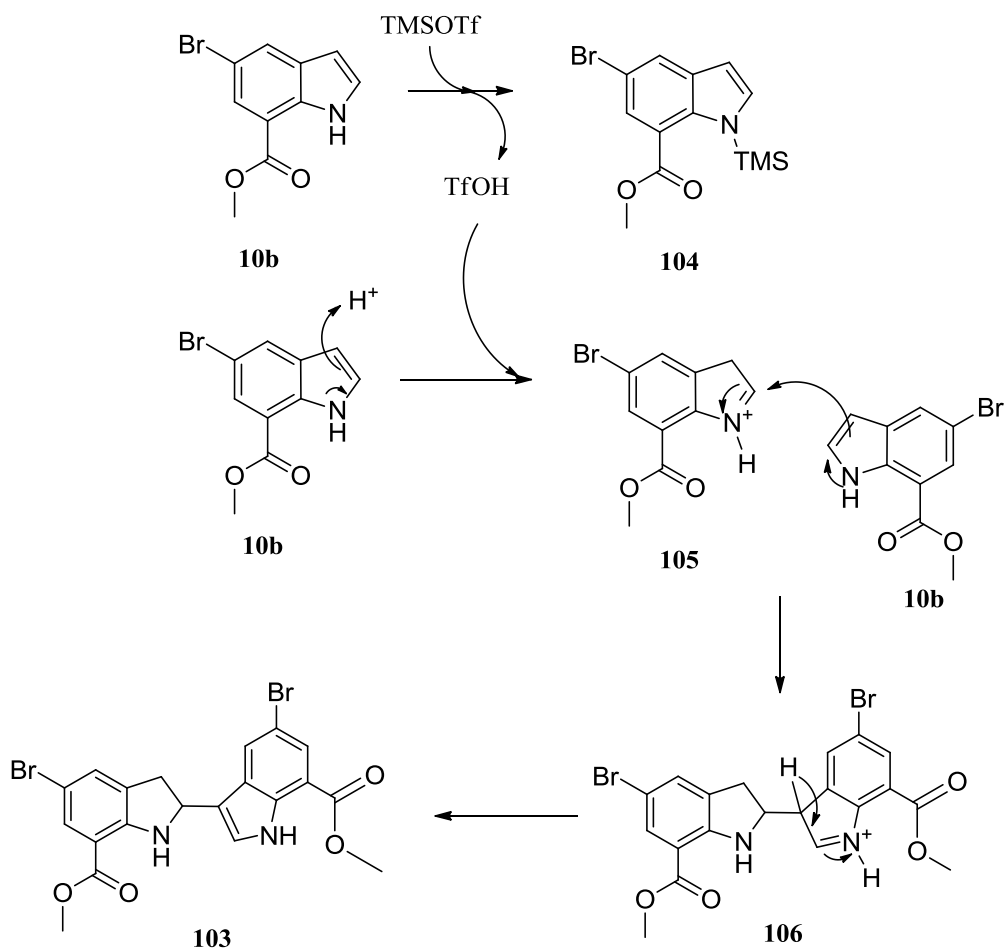
the intermediate alkene, which could be unstable when using a 4-membered cyclic ketone such as 3-oxetanone. Recent literature has shown how common Lewis or Brønsted acids can be used under reductive conditions to afford 3-substituted indoles.<sup>105,106</sup> Acid-mediated reductive alkylation with 3-oxetanone using triethylsilane as the reductant was therefore attempted on methyl 5-bromo-1*H*-indole-7-carboxylate. The risk of forming the oxazole by-product was moderated by carrying out the reductive alkylation on the ester; however this did not afford the desired methyl 5-bromo-3-(oxetan-3-yl)-1*H*-indole-7-carboxylate. The corresponding *bis*-derivative (**102**) was again the major product (~70% by LCMS) and an additional by-product (**103**) was also obtained in varying levels (6-20% by LCMS) (Scheme 3.3.27). Unfortunately, formation of the *bis*-derivative could not be prevented despite the use of a large excess of 3-oxetanone, or by attempting the reductive alkylation with trichloroacetic acid, which has been shown to facilitate the formation of monoalkylated products of 1,2-unsubstituted indoles.<sup>106</sup>



Reagents and Conditions: (i) TMSOTf, Et<sub>3</sub>SiH, DCM, -5 °C; (ii) CCl<sub>3</sub>CO<sub>2</sub>H, Et<sub>3</sub>SiH, toluene, 70 °C, 74% (**102**).

Scheme 3.3.27. Reductive alkylation of methyl 5-bromo-1*H*-indole-7-carboxylate.

The additional by-product was possibly formed by dimerisation facilitated by protonation of the starting material with triflic acid, which could be produced from the reaction of indole **10b** with trimethylsilyl triflate (Scheme 3.3.28). The sequence is catalytic in Brønsted acid.

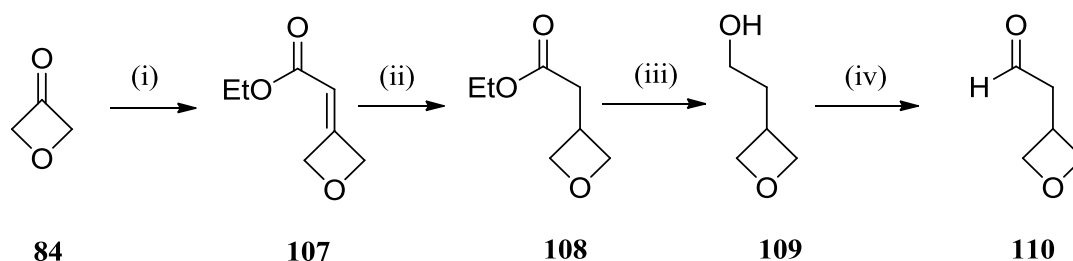


Scheme 3.3.28. Proposed mechanism for the formation of by-product **103**.

Due to the challenges in functionalising the C3 position of an already established indole core, a different approach to install the 3-oxetan-3-yl group was explored using the classical Fischer indole synthesis. It was thought that if the required oxetane-containing aldehyde could be isolated, it could be reacted with a substituted phenylhydrazine to afford the desired 3-oxetan-3-yl indole. Recent



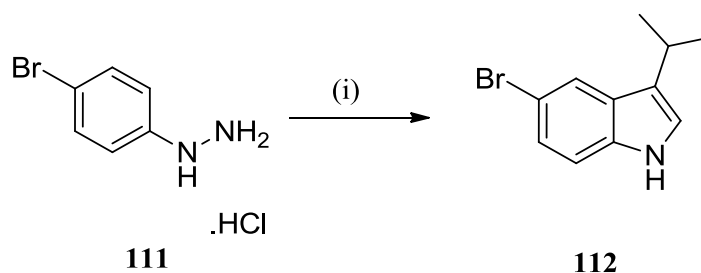
literature has shown how 3-oxetanone easily undergoes Wittig reactions to homologate the carbon skeleton.<sup>84</sup> This methodology was employed to synthesise ester **107**, which was hydrogenated to yield the unsaturated ester **108** (Scheme 3.3.29). These steps were also attempted using the aldehyde-containing phosphorane, rather than ethyl ester, and although the alkene was obtained in moderate yield, the hydrogenation gave no identifiable products. Unfortunately, reduction of **108** to give the desired aldehyde was not achievable using DIBAL-H, so the ester was fully reduced and subsequent oxidation with Dess-Martin periodinane successfully yielded aldehyde **110** (Scheme 3.3.29).



Reagents and Conditions: (i)  $\text{EtO}_2\text{CCHPh}_3$ , DCM, 0 °C, 81%; (ii)  $\text{H}_2$  (8 bar), Pd/C, EtOH, 76%; (iii)  $\text{LiAlH}_4$ , THF, 1 °C to rt, 68%; (iv) DMP, DCM, rt, 16%.

Scheme 3.3.29. Synthesis of 2-(oxetan-3-yl)acetaldehyde.

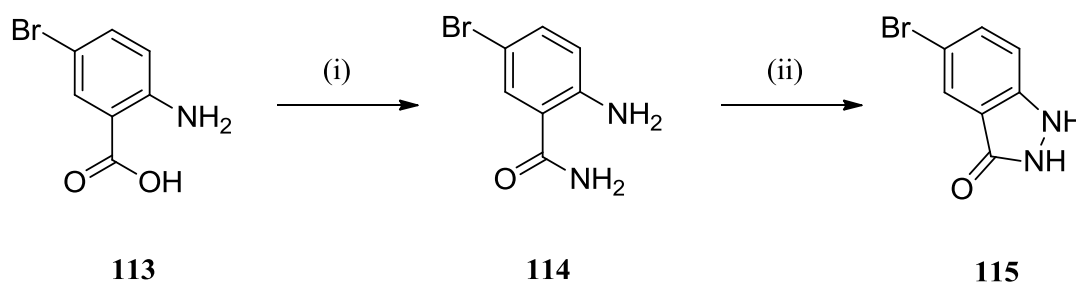
Ideally, the hydrazine partner for the Fischer indole cyclisation would have been furnished with the desired 4-bromo and 2-carboxamide substituents. There was precedent for thermally and acid-promoted Fischer indolisations of 4-bromo-substituted phenylhydrazines, for example the reaction of 4-bromophenylhydrazine hydrochloride with isovaleraldehyde (Scheme 3.3.30).<sup>107,108</sup>



Reagents and Conditions: (i) NaOH, H<sub>2</sub>O, then isovaldehyde, AcOH, rt, 100%.

Scheme 3.3.30. Fischer indole synthesis from 4-bromophenyl hydrazine hydrochloride.<sup>107</sup>

However, the desired hydrazine starting material could not be obtained due to the facile cyclisation of the intermediate diazonium species to give indazol-3(2*H*)-one (Scheme 3.3.31).

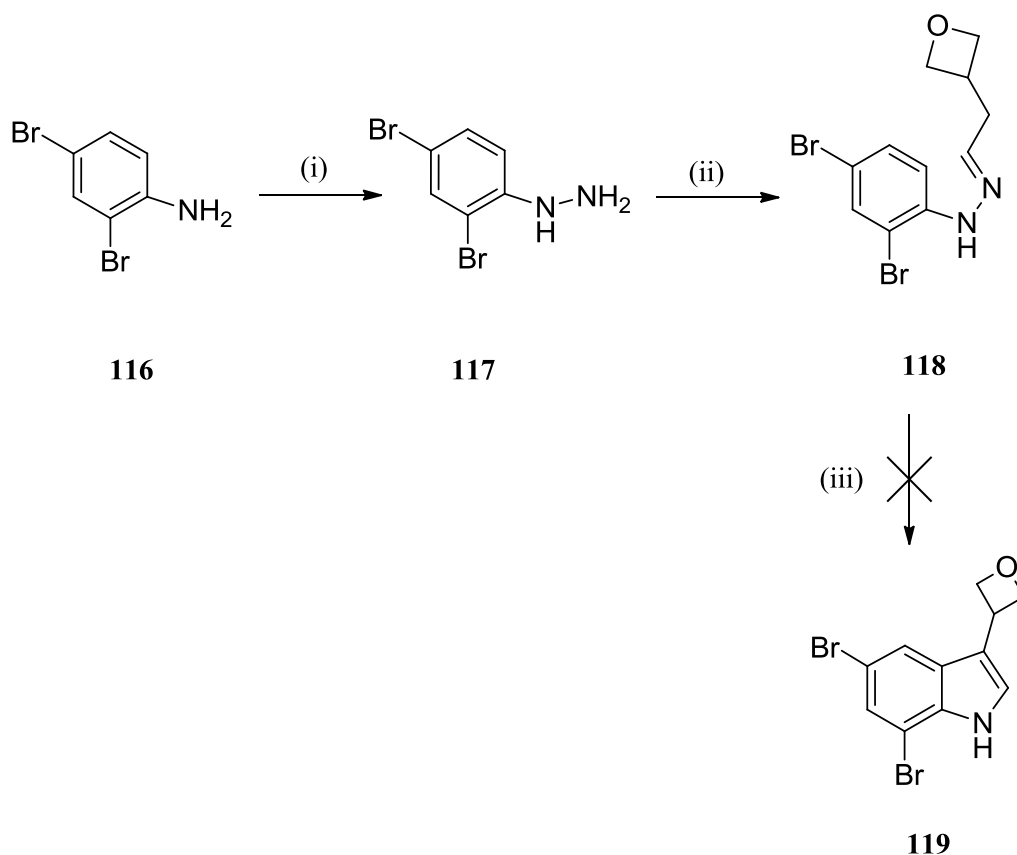


Reagents and Conditions: (i) HATU, DIPEA, NH<sub>3</sub>/MeOH, DMF, rt, 81%; (ii) HCl (37%, aq.), NaNO<sub>2</sub>, H<sub>2</sub>O then Na<sub>2</sub>S<sub>2</sub>O<sub>5</sub>, 9%.

Scheme 3.3.31. Synthesis of indazol-3(2*H*)-one.

Since there were literature examples of successful Fischer indolisations with dihalo-substituted phenylhydrazines,<sup>109</sup> phenylhydrazine **117** was synthesised from 2,4-dibromoaniline (Scheme 3.3.32) so that conversion of the 2-bromo substituent to the carboxamide could be carried out later in the synthesis. Condensation of

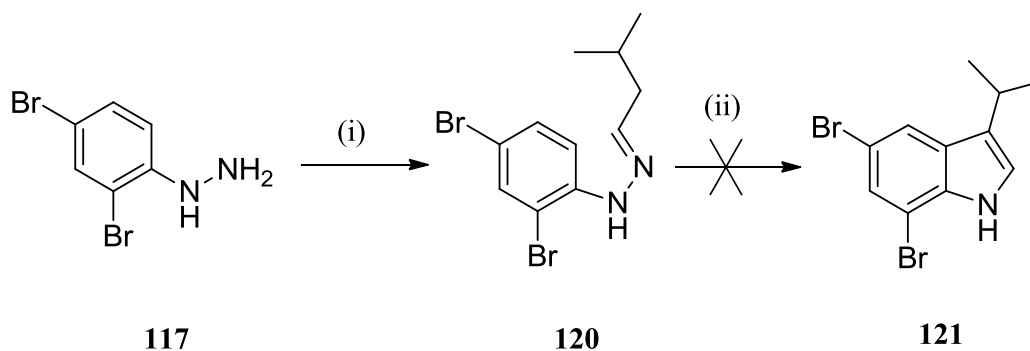
hydrazine **117** with the required aldehyde led to formation of the desired hydrazone species (**118**) but the final cyclisation was unsuccessful under a variety of conditions (Scheme 3.3.32). Extreme heating in various solvents, either thermally or using microwave irradiation, only led to recovery of starting material. Furthermore, the addition of a Lewis acid catalyst ( $\text{ZnCl}_2$ ) led to complex reaction mixtures without any identifiable products. This is probably due to ring-opening of the oxetane, which could occur under acidic conditions with protonation of the oxygen making the oxetane susceptible to attack from nucleophiles.



Reagents and Conditions: (i) HCl (37%, aq.),  $\text{NaNO}_2$ ,  $\text{H}_2\text{O}$  then  $\text{SnCl}_2 \cdot 2(\text{H}_2\text{O})$ , HCl (37% aq.), 63%; (ii) 2-(oxetan-3-yl)acetaldehyde, toluene, rt to 60 °C, 20%; (iii) 1,4-dioxane or toluene, 100-150 °C, or  $\text{ZnCl}_2$ , 1,4-dioxane, 100-150 °C.

Scheme 3.3.32. Attempted Fischer indole synthesis to obtain 3-(oxetan-3-yl)-1H-indole-7-carboxamide **119**.

Further investigations showed that hydrazone formation using isovaleraldehyde was also successful but that cyclisation was not achievable in this case either, with only starting material present after extreme heating in either the absence or presence of a Lewis acid (Scheme 3.3.33).



Reagents and Conditions: (i) isovaleraldehyde, toluene, rt, 66%; (ii) 1,4-dioxane, 150 °C or ZnCl<sub>2</sub>, 1,4-dioxane, 150 °C.

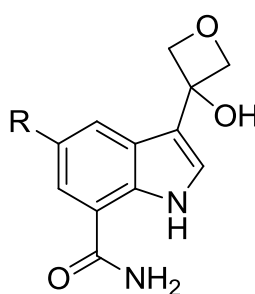
Scheme 3.3.33. Attempted Fischer indole synthesis to obtain 3-isopropyl-1H-indole-7-carboxamide **121**.

Further experimental work on the Fischer indolisations could not be carried out due to time constraints but reasons for the failure of the attempted reactions can be postulated. A recent paper used quantum-mechanical methods to study the mechanism of the Fischer indole synthesis and suggested reasons for reaction failures.<sup>110</sup> The thermal reaction has a higher activation barrier to the [3,3]-sigmatropic rearrangement transition state than the acid-catalysed indolisation, where the activation energy is lowered by 11-13 kcal/mol.<sup>110</sup> The study showed that the substituents on the carbonyl component are critical for the success of the reaction. Strong electron-donating substituents promote *N-N* heterolytic bond cleavage rather than [3,3]-sigmatropic rearrangement and this competing dissociative pathway results in side reactions rather than indolisation. Also, computational studies have shown that disubstituted hydrazone intermediates have lower energy reaction

transition states, when compared to monosubstituted hydrazone intermediates, so the [3,3]-sigmatropic rearrangement is more favoured.<sup>110</sup> Here both the oxetane and dimethylsubstituted hydrazone intermediates failed to cyclise. The second result was surprising since isoveraldehyde reacted successfully in a Fischer indolisation with 4-bromophenylhydrazine.<sup>107</sup>

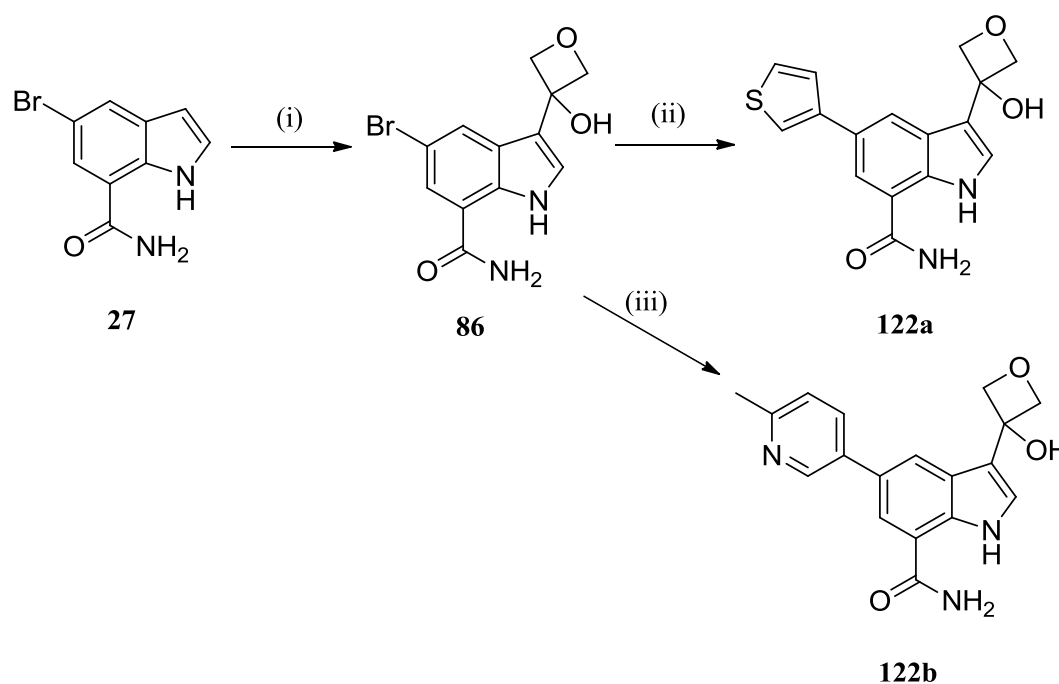
Since the failed indolisation cannot solely be attributed to the presence of the oxetane moiety, it was thought that the hydrazine component could be causing the reaction to be unsuccessful. Electron-withdrawing substituents on the aromatic ring of the hydrazine are generally detrimental to the reaction and *ortho*-substituted hydrazines often react slowly.<sup>111</sup> Further investigation into the choice of acid catalyst could lead to indolisation, as this is often an important factor in the success or failure of the reaction; however, with the oxetane present it was thought that ring-opening of the oxetane would persist and cause side reactions. It has recently been shown that T3P<sup>®</sup> can be used successfully in a microwave-assisted Fischer indole synthesis,<sup>112</sup> so this could be an alternative reagent to try out in the indolisation described here.

An alternative approach was sought and the observation that 3-substituted oxetan-3-ols can be successfully deoxygenated to give the analogous 3-substituted oxetanes led to investigation into the synthesis of 5-substituted-3-(3-hydroxyoxetan-3-yl)-1*H*-indole-7-carboxamides (**122**).<sup>88</sup>

**122**

R = aryl, heteroaryl

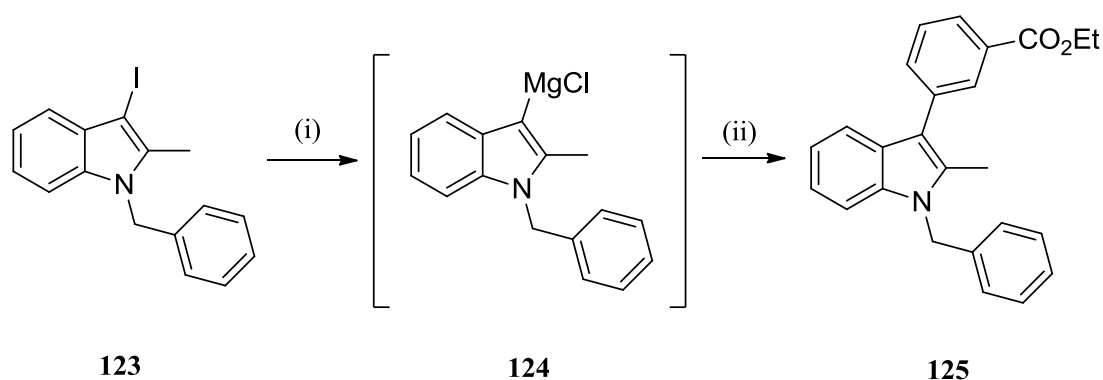
5-Bromo-3-(3-hydroxyoxetan-3-yl)-1*H*-indole-7-carboxamide (**86**) was a key intermediate that could be formed by the reaction of 3-oxetanone and an anion formed at the 3-position of the indole (Scheme 3.3.34). Methods for Grignard reagent formation at the indole 3-position from 3*H*-indoles, followed by *in situ* addition to electrophiles, have been published in the literature.<sup>113,114</sup> Various conditions for Grignard reagent formation at the 3-position of carboxamide **27** were investigated, including MeMgI in the absence and presence of zinc(II) chloride, but the best conversion to 5-bromo-3-(3-hydroxyoxetan-3-yl)-1*H*-indole-7-carboxamide (**86**) was achieved using MeMgBr, although only 40% conversion could be achieved and the isolated yield was poor (Scheme 3.3.34). Two target compounds (**122a,b**) were then synthesised *via* Suzuki cross-coupling with the required boronic acid or ester coupling partner (Scheme 3.3.34).



Reagents and Conditions: (i) MeMgBr, DCM, 0 °C then 3-oxetanone, rt, 3%; (ii) 4,4,5,5-tetramethyl-2-(thiophen-3-yl)-1,3,2-dioxaborolane, Pd(PPh<sub>3</sub>)<sub>4</sub>, K<sub>2</sub>CO<sub>3</sub>, IPA/H<sub>2</sub>O (10:1), 100 °C, 30%; (iii) 6-methylpyridin-3-yl boronic acid, Pd(PPh<sub>3</sub>)<sub>4</sub>, K<sub>2</sub>CO<sub>3</sub>, IPA/H<sub>2</sub>O (10:1), 100 °C, 17%.

Scheme 3.3.34. Synthesis of 5-substituted-3-(3-hydroxyoxetan-3-yl)-1H-indole-7-carboxamides.

A method for improving the synthesis of intermediate **86** was investigated. Since Grignard reagent formation from the 3H-indole was inadequate, an alternative strategy was to synthesise the desired Grignard reagent through I/Mg exchange. This had been shown to be effective in the synthesis of an indole magnesium reagent (**124**) generated using the “Turbo Grignard” reagent *i*-PrMgCl.LiCl developed by Knochel, which was then taken forward for an *in situ* Kumada coupling (Scheme 3.3.35).<sup>115</sup>

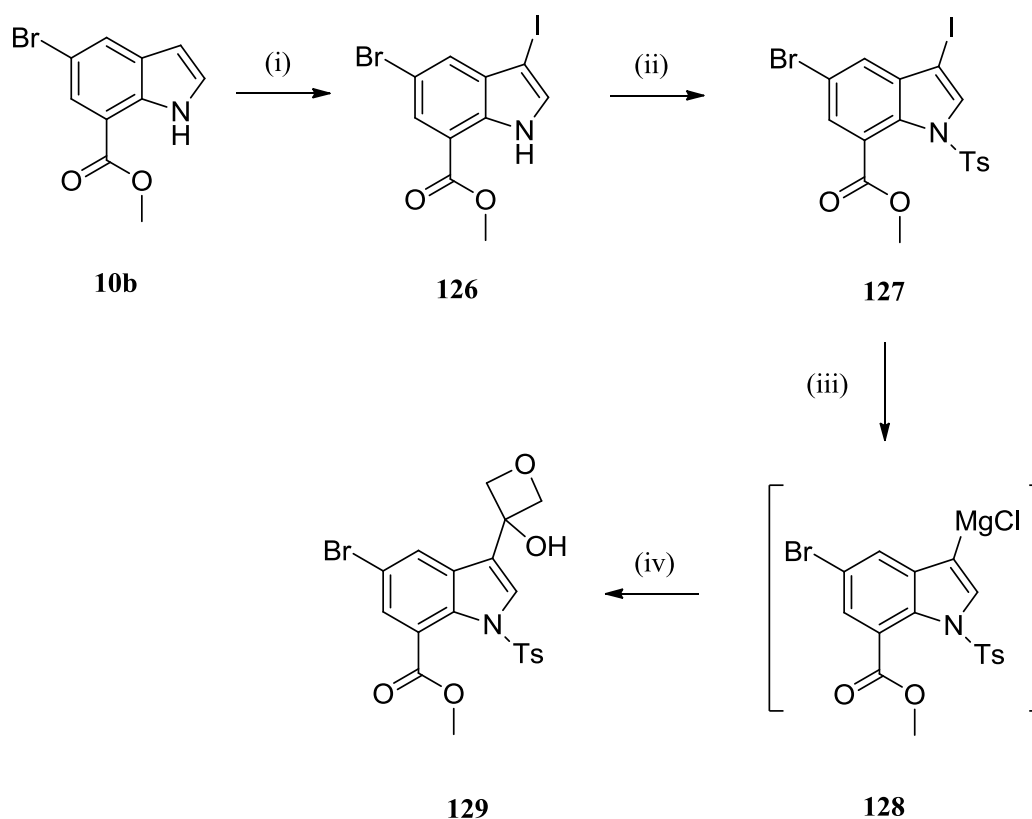


Reagents and Conditions: (i) *i*-PrMgCl.LiCl, THF, -20 °C; (ii) ethyl 3-bromobenzoate, Pd(OAc)<sub>2</sub>, SPhos<sup>®</sup>, THF, 25 °C, 79%.

Scheme 3.3.35. I/Mg exchange and subsequent Kumada coupling of indole magnesium reagent **124**.<sup>115</sup>

Grignard reagent formation at the indole 3-position was carried out using the approach shown in Scheme 3.3.36. The methyl ester at the 7-position was converted to the desired primary carboxamide later in the synthesis and the indole nitrogen was protected as the tosylate, thereby allowing deprotection and ester hydrolysis to be carried out in one step.

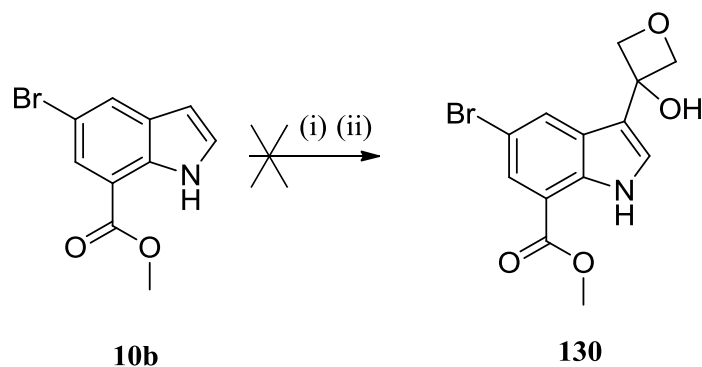




Reagents and Conditions: (i) NIS, DCM, rt, 76%; (ii) NaH, TsCl, DMF, 0 °C to rt, 69%; (iii) *i*-PrMgCl.LiCl, THF, -15 °C; (iv) 3-oxetanone, THF, -15 °C to 0 °C, 97%.

Scheme 3.3.36. Functionalisation of the indole 3-position.

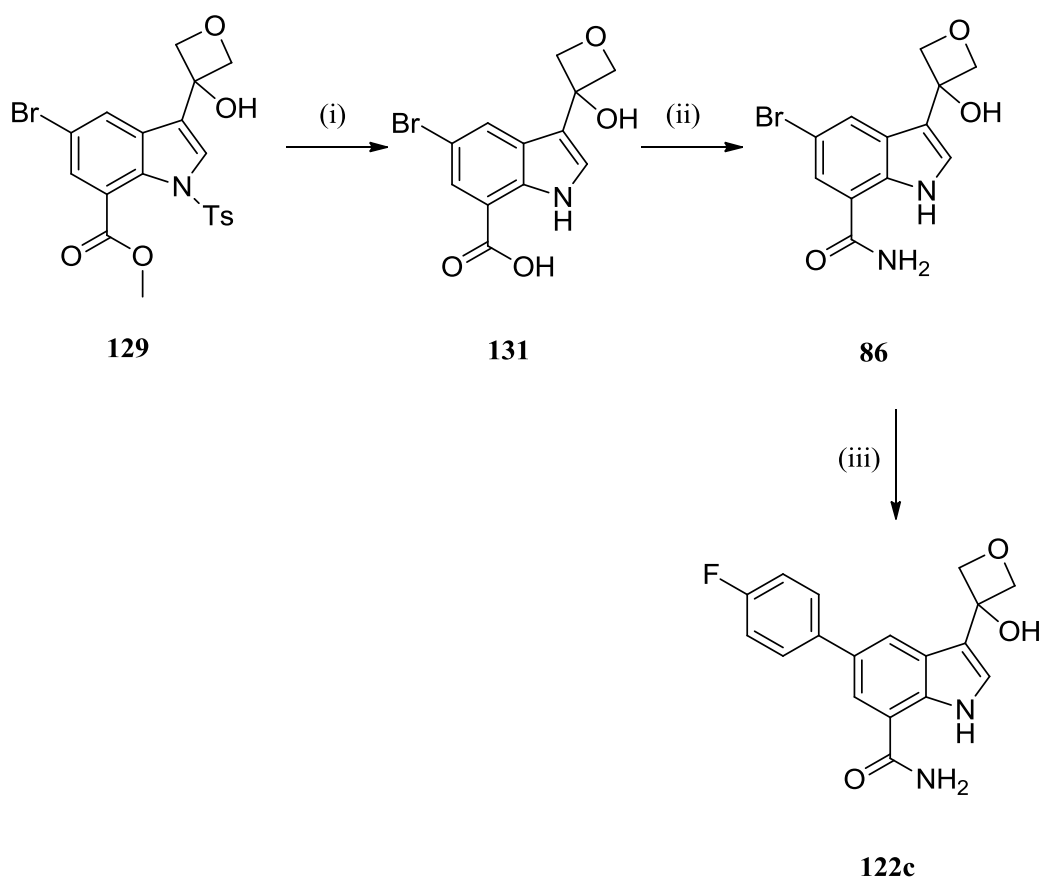
I/Mg exchange and subsequent addition of the organomagnesium species to 3-oxetanone occurred in high yield and was carried out successfully on 9 mmol scale. The same conditions were attempted with the analogous 3*H*-indole (Scheme 3.3.37) but only starting material was recovered, so I/Mg exchange represents a significantly improved method for installation of the 3-(3-hydroxyoxetan-3-yl) group.



Reagents and Conditions: (i) *i*-PrMgCl.LiCl, THF, -15 °C; (ii) 3-oxetanone, THF, -15 °C to 0 °C.

Scheme 3.3.37. Attempted Grignard reagent formation of 3*H*-indole **10b** and subsequent addition to 3-oxetanone.

Intermediate **129** was taken forward for deprotection and concomitant ester hydrolysis then amide formation (Scheme 3.3.38). This gave primary carboxamide **86** in 14% overall yield in 5 steps from the starting material (**10b**). Another target compound (**122c**) was then synthesised *via* Suzuki cross-coupling with the required boronic acid (Scheme 3.3.38).



Reagents and Conditions: (i) NaOH, 1,4-dioxane, rt, 84%; (ii) HATU, DIPEA, NH<sub>3</sub>, DMF, rt, 34%; (iii) 4-fluorophenylboronic acid, Pd(PPh<sub>3</sub>)<sub>4</sub>, K<sub>2</sub>CO<sub>3</sub>, IPA/H<sub>2</sub>O (10:1), 100 °C,  $\mu$ wave, 9%.

Scheme 3.3.38. Synthesis of **122c**.

Compounds **122a**, **122b** and **122c** were submitted for testing versus IKK2 and IKK1 to assess their potency and selectivity. Figure 3.3.14 shows a plot of IKK2 pK<sub>i</sub> vs IKK1 pK<sub>i</sub> for the 3-hydroxyoxetan-3-yl compounds **122a**, **122b** (NB. IKK1 pK<sub>i</sub> = 5.7 but tested <4.8 on one test occasion) and **122c** and some direct comparators. The shape of the markers indicates the 5-position substituent and the markers are coloured according to the 3-position substituent. The plotted lines represent the level of selectivity for IKK2 over IKK1, with compounds around the light green (y=x+2) line achieving 100-fold selectivity.

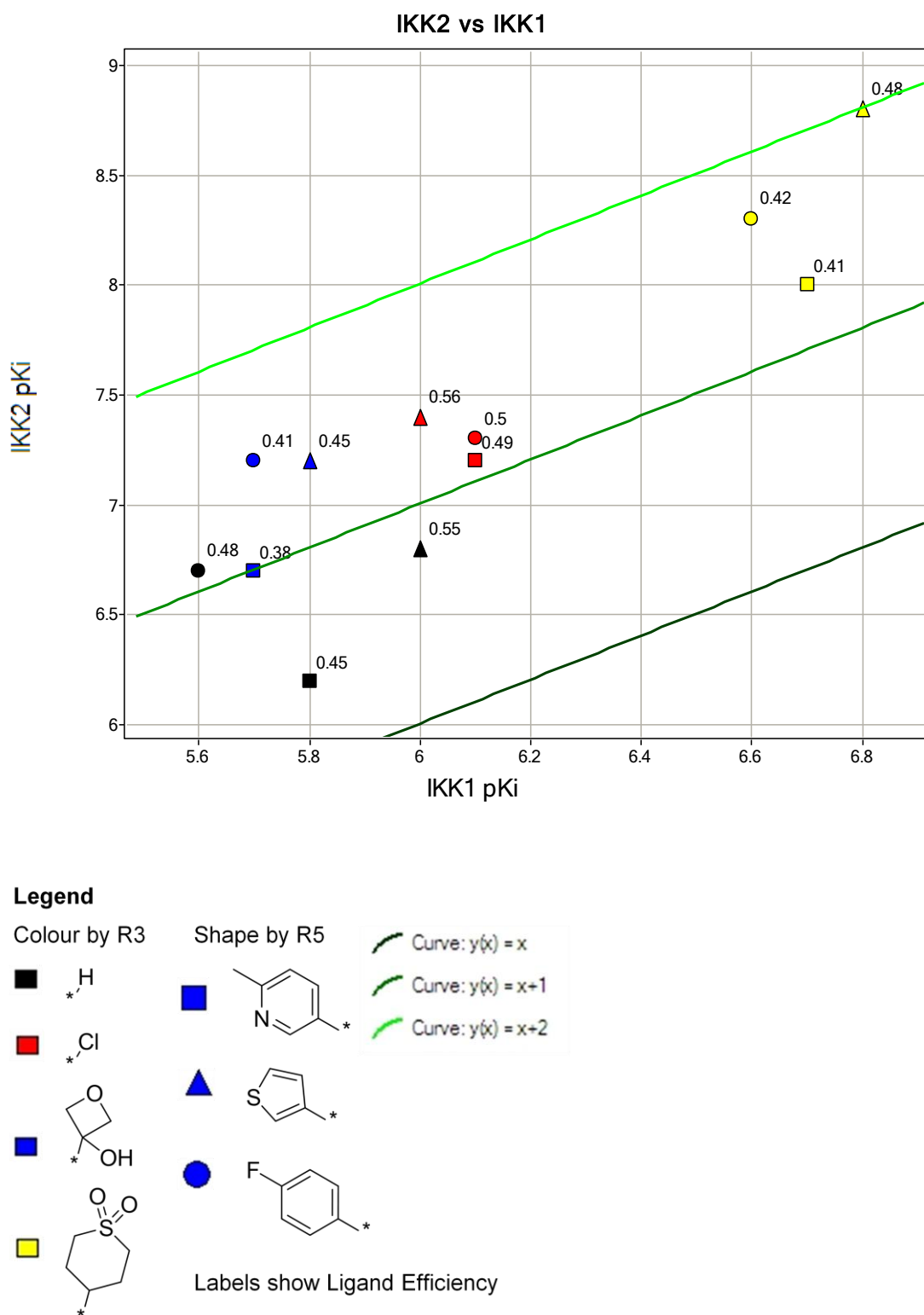


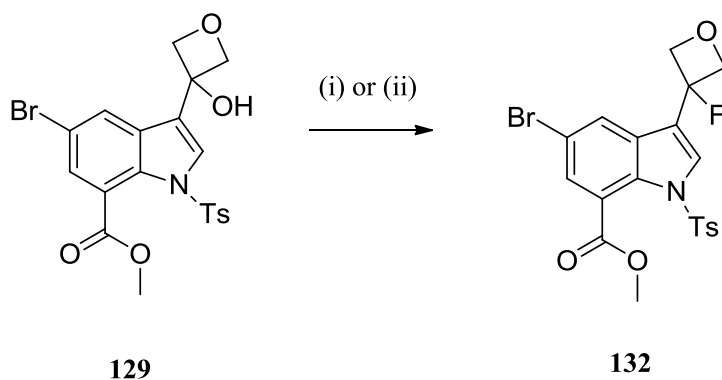
Figure 3.3.14. Potency and selectivity of indole-7-carboxamide compounds.

Figure 3.3.14 shows the general trend that 5-thiophenyl and 5-(4-fluorophenyl) compounds are more active against IKK2 than the analogous 5-pyridyl compounds. The 3-hydroxyoxetan-3-yl containing compounds have increased potency and selectivity over the 3-unsubstituted compounds but decreased ligand efficiencies, similar to those of the 3-tetrahydrothiopyran-dioxide containing compounds, and were much less efficient than the 3-chloro substituted compounds. The desired selectivity over IKK1 (100-fold) is only achieved by the 3-tetrahydrothiopyran-dioxide compound with the highest IKK2 activity but, encouragingly, 30-fold selectivity is attained by both the 3-hydroxyoxetan-3-yl and 3-chloro containing compounds. From these results, it can be concluded that the 3-hydroxyoxetan-3-yl substituted compounds are active against IKK2 and selective over IKK1, but that compounds containing this group do not achieve the desired ligand efficiencies. This may be due to the hydroxyl group sitting out of plane with the indole core as the presence of electronegative groups at this position typically has a detrimental effect on IKK2 potency *cf.* tetrahydropyran-dioxide analogues. An exception to this is fluorine, which does not have this same unfavourable effect on IKK2 potency as evidenced by the tolerance of a trifluoromethyl group at the indole 3-position. From these observations, removal of the hydroxyl group or its replacement by a fluorine was desired.

Literature precedent for the deoxofluorination of a 3-hydroxyoxetan-3-yl group by treatment with diethylaminosulfur trifluoride (DAST) suggested that this methodology could be successful here.<sup>88</sup> DAST has been widely used as a reagent of choice in deoxofluorination reactions alongside Deoxo-fluor™ (bis(2-methoxyethyl)aminosulfur trifluoride).<sup>116,117</sup> These dialkylaminosulfur trifluorides have been shown to be successful nucleophilic fluorinating reagents for reactions with alcohols, aldehydes and ketones but there are significant safety issues associated with their use.<sup>118</sup> They are liquids that fume in air, which makes them difficult to handle. DAST has been shown to have low thermal stability due to the ease with which it disproportionates to give sulfur tetrafluoride and bis(diethylamino)sulfur difluoride.<sup>119</sup> The difluoride is much less stable and undergoes a catastrophic

decomposition upon heating, leading to explosion with gas evolution.<sup>119</sup> Although Deoxo-fluor™ is thermally less sensitive than DAST, it still decomposes with a significant exotherm and so neither of these reagents are amenable to high temperature reactions or large-scale use.<sup>117</sup> A recent advance has been the development of a continuous process for the use of DAST or Deoxo-fluor™ in the deoxofluorination of a steroid allowing the reagents be used on a large scale.<sup>120</sup> However, this type of processing may not be generally applicable for deoxofluorination reactions using DAST or Deoxo-fluor™ and significant optimisation may be required for individual reactions if they were to be scaled up. As there are many disadvantages in the use of these common deoxofluorinating agents, the development of more stable, easy-to-handle reagents is desired.

A recent paper has detailed the discovery of 4-*tert*-butyl-2,6-dimethylphenylsulfur trifluoride (Fluolead™), a deoxofluorinating agent with high thermal and hydrolytic stability.<sup>121</sup> In addition, it is a white crystalline solid that is significantly easier to handle than DAST or Deoxo-fluor™ and it also has higher fluorinating capability. Unlike other fluorinating reagents, it can convert carboxyl groups to trifluoromethyl groups and can also fluorinate thioketones or thioesters. The use of this reagent was therefore of interest for the deoxofluorination of compound **129** (Scheme 3.3.39).

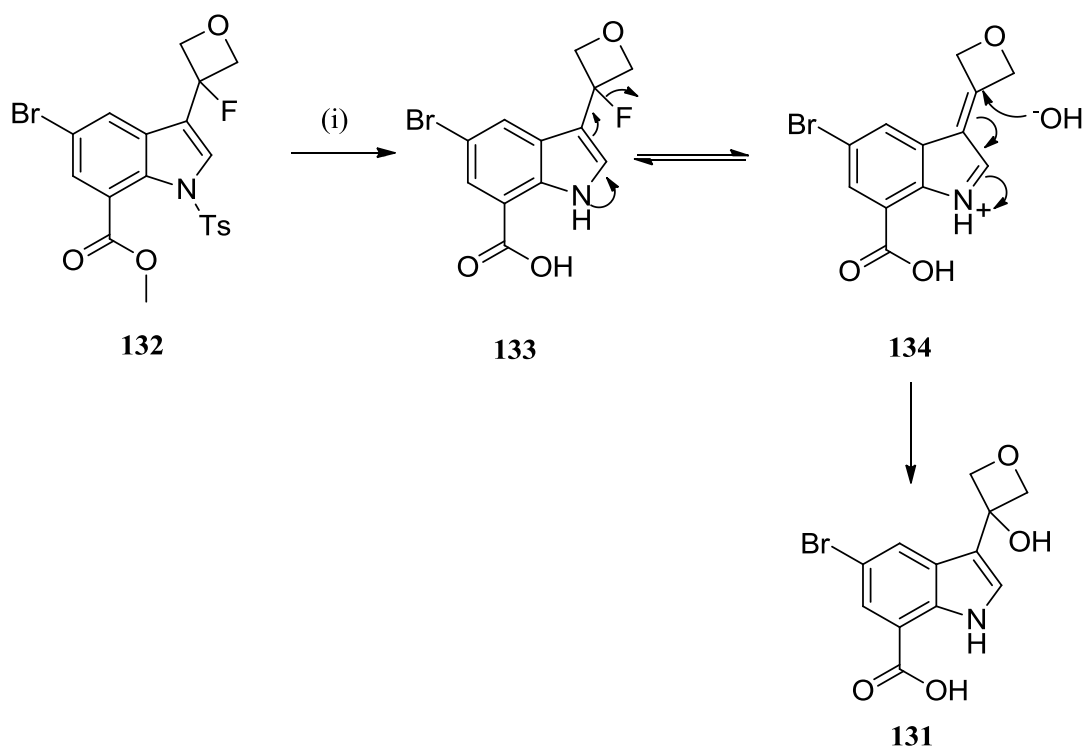


Reagents and Conditions: (i) DAST, DCM, -78 °C, 28%; (ii) Fluolead™, DCM, 0 °C, 73%.

Scheme 3.3.39. Deoxofluorination of compound **129**.

It was found that the use of Fluolead™ resulted in a significant increase in yield for the deoxofluorination of compound **129** when compared with DAST. Furthermore, no cryogenic cooling or drying of glassware was required; additional controls were not needed when handling the reagent and the sulfinyl fluoride by-product was easily removed *via* a basic wash. All these features gave considerable practical advantages for the use of Fluolead™ over DAST.

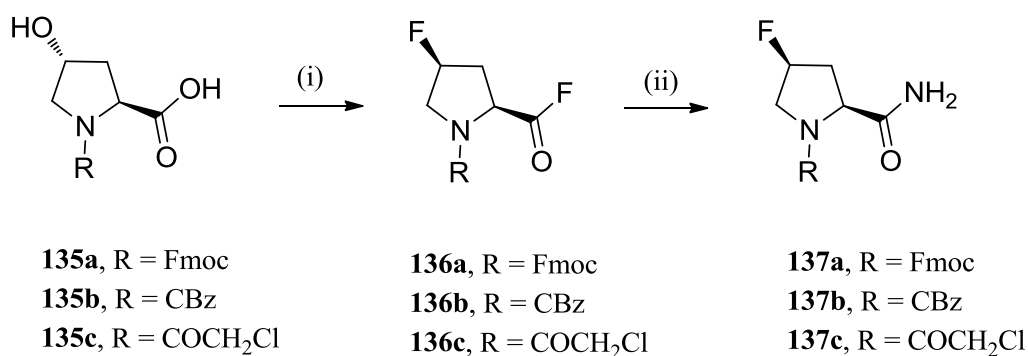
With the 3-fluoro-3-oxetanyl group in hand, functionalisation of the indole 7-position to give the primary carboxamide was required. The first step in the synthetic sequence was ester hydrolysis and concomitant deprotection; however the basic aqueous conditions led to displacement of the previously installed fluorine substituent (Scheme 3.3.40). After deprotection the fluorine was positioned such that it was extremely labile, generating the reactive intermediate **134** (Scheme 3.3.40).



Reagents and Conditions: (i) NaOH (xs), 1,4-dioxane, rt, 28%.

Scheme 3.3.40. Hydrolysis of compound **132**.

An alternative approach to install the C-F structural feature and obtain the desired primary carboxamide was investigated. After Umemoto had developed Fluolead™ as a novel deoxofluorinating agent they utilised the reagent for the synthesis of 4-fluoropyrrolidine-2-carbonyl fluorides (**136a-c**, Scheme 3.3.41).<sup>122</sup> It was observed that the carbonyl fluorides could be converted into useful intermediates such as Weinreb amides, carboxylate methyl esters or carbonitriles through reaction with various nucleophiles.<sup>122</sup> However, of most relevance to this work was the reaction of these carbonyl fluorides with ammonia to generate the corresponding primary carboxamides (**137a-c**, Scheme 3.3.41).<sup>122</sup>

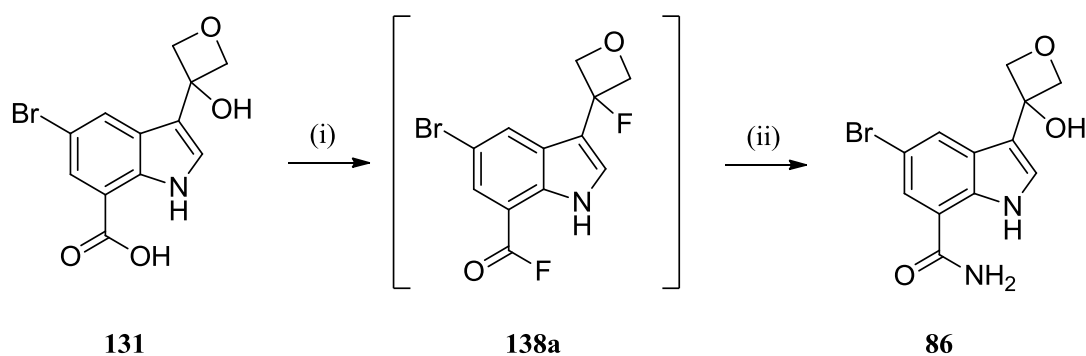


Reagents and Conditions: (i) Fluolead™, DCM, 0°C → rt, 75-78%; (ii) NH<sub>3</sub>, DCM, rt, 74-95%.

Scheme 3.3.41. Synthesis of 4-fluoropyrrolidine-2-carbonyl fluorides and their conversion to primary carboxamides.<sup>122</sup>

This methodology was used in the attempted formation of carboxamide **86** from carboxylic acid **131** (Scheme 3.3.42).

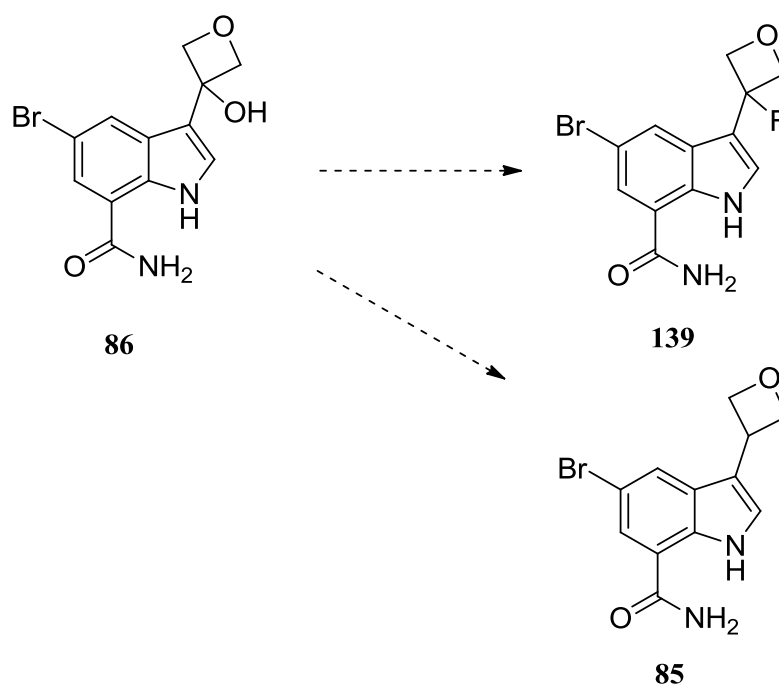




Reagents and Conditions: (i) Fluolead™, DCM, 0 °C then (ii) NH<sub>3</sub>, 0 °C, not isolated.

Scheme 3.3.42. Formation of carbonyl fluoride **138** and *in situ* conversion to carboxamide **86**.

It was hoped that deoxofluorination of the 3-hydroxyoxetan-3-yl group would also occur during the reaction with Fluolead™; however this was not observed. The deoxofluorination was therefore attempted as a separate synthetic step on indole carboxamide intermediate **86**, and deoxygenation of this intermediate to give the monosubstituted 3-oxetanyl intermediate (**85**) was also attempted (Scheme 3.3.43).



Scheme 3.3.43. Proposed deoxofluorination and deoxygenation of compound **86**.

A range of conditions were tried for the deoxofluorination and deoxygenation reactions of compound **86** (Table 3.3.9); however none of the desired products were obtained.

Reaction	Conditions
Deoxofluorination	Fluolead™, DCM, 0 °C to rt
	DAST, DCM, -78 °C to 0 °C
	DAST, THF -78 °C to rt
Deoxygenation	NaBH <sub>4</sub> , THF, 0 °C to rt
	LiAlH <sub>4</sub> , THF, 0 °C to rt
	(i) NaH, THF, 0 °C; (ii) TsCl, 0 °C; (iii) LiAlH <sub>4</sub> , -78 °C; (iv) NaOH, H <sub>2</sub> O

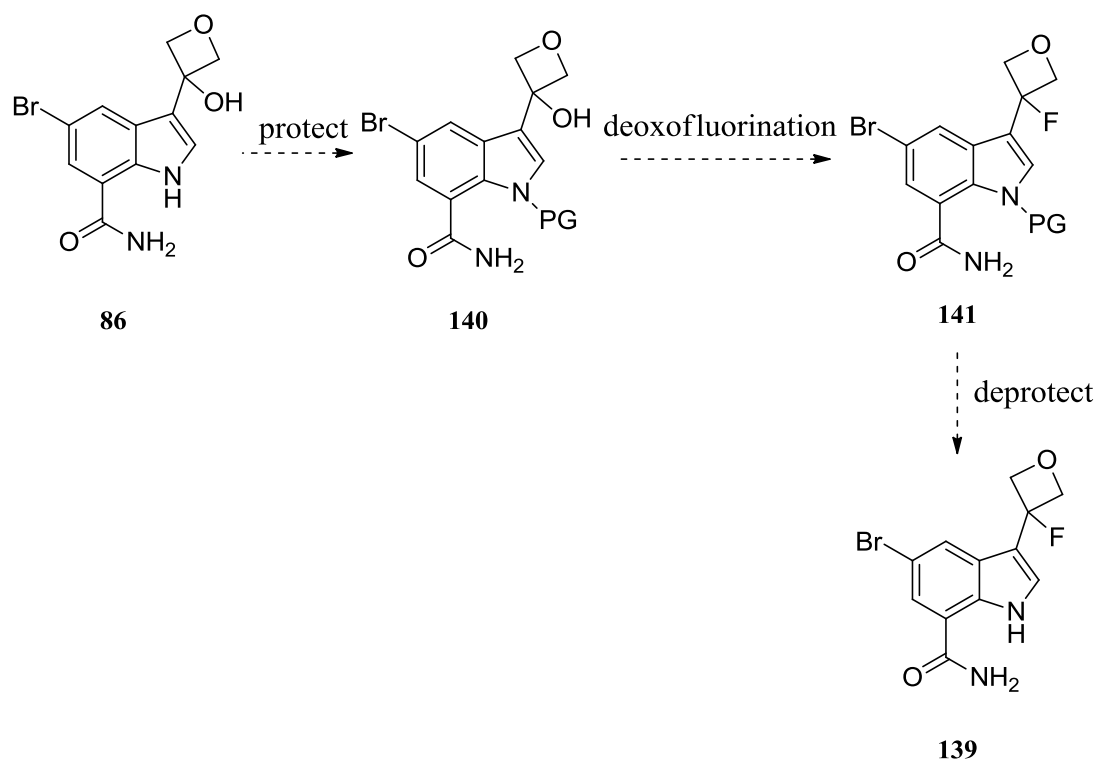
Table 3.3.9. Attempted deoxofluorination and deoxygenation reactions.

No reaction was observed in the deoxofluorination reactions with Fluolead™ or DAST, with the major component of the reaction mixtures being unreacted starting material. It was initially thought that the poor solubility of compound **86** in DCM could have caused the failure of these reactions; hence the reaction with DAST was also carried out in THF. The starting material was soluble in this solvent but still no desired reaction was observed.

The failure of the deoxofluorination reactions of compounds **86** and **131** could be because the indole nitrogen was not protected, since the *N*-tosyl indole intermediate **129** reacted successfully. It may be that the deoxofluorination occurs successfully but facile loss of the fluoride substituent from the unprotected indole intermediates leads to *in situ* hydrolysis to return the starting material.

Further work to achieve successful deoxofluorination of the indole carboxamide intermediates would therefore need to investigate an alternative protecting group strategy so that the indole nitrogen is protected with the carboxamide in place (**140**, Scheme 3.3.44). From previous observations,

deoxofluorination of the *N*-protected indole carboxamide would be more likely to succeed and subsequent deprotection would give the desired product (Scheme 3.3.44).

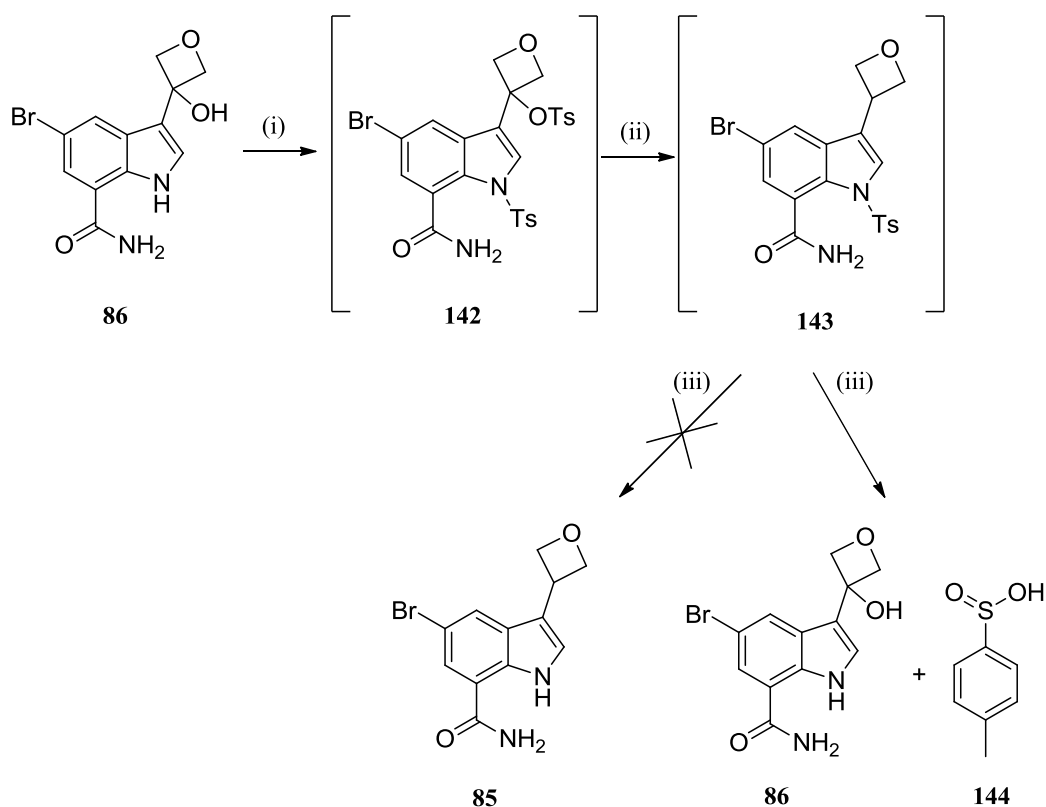


Scheme 3.3.44. Future deoxofluorination work.

The choice of the protecting group would have to be carefully considered since the installed fluoride substituent is sensitive. If the tosyl group were used, alternative deprotection conditions could be used to ensure that no fluoride displacement occurs, for example *n*-Bu<sub>4</sub>NF in refluxing THF<sup>123</sup> or KF on alumina under microwave conditions.<sup>124</sup>

Unfortunately, none of the deoxygenation reactions attempted were successful either. It was hoped that displacement of the hydroxyl group may have been facilitated by the nucleophilic indole nitrogen in a similar way to the fluoride displacement previously observed. However, reaction with a hydride source did not

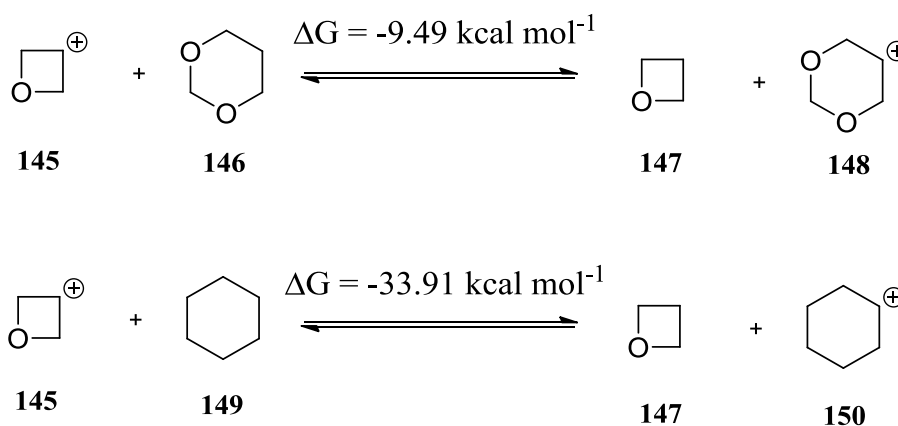
lead to the desired deoxygenated product. The use of  $\text{NaBH}_4$  resulted solely in unreacted starting material, whereas  $\text{LiAlH}_4$  led to a complex mixture of unidentifiable products. Next, the formation of the tosylate as a better leaving group was attempted and deprotonation with sodium hydride (2 equivalents) and subsequent reaction with tosyl chloride (2 equivalents) looked to have formed the desired di-tosylated material (Scheme 3.3.45), although the main component was poorly ionised by LCMS. It was envisaged that the addition of  $\text{LiAlH}_4$  and a basic work-up, which would remove the *N*-tosyl group, would result in the formation of compound **85** (Scheme 3.3.45). However, this only led to recovery of the starting material alongside an unwanted by-product, sulfinic acid **144**.



Reagents and Conditions: (i)  $\text{NaH}$ , THF,  $0\text{ }^\circ\text{C}$  then  $\text{TsCl}$ ,  $0\text{ }^\circ\text{C}$ ; (ii)  $\text{LiAlH}_4$ ,  $-78\text{ }^\circ\text{C}$ ; (iii)  $\text{NaOH}$ ,  $\text{H}_2\text{O}$ , rt.

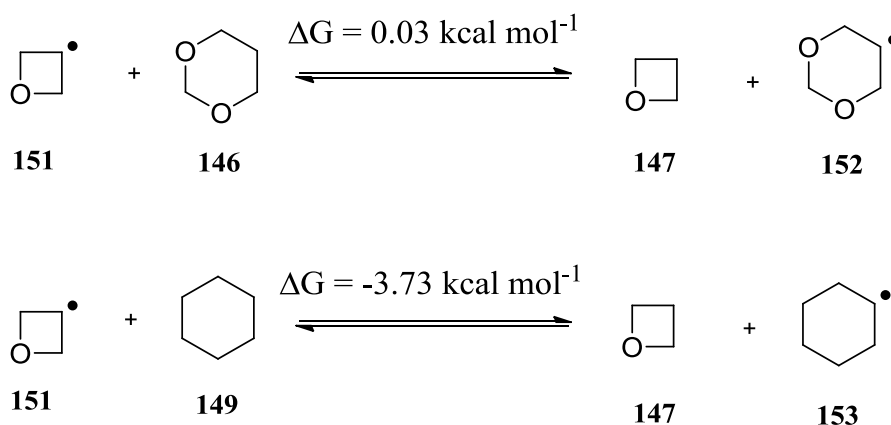
Scheme 3.3.45. Unsuccessful deoxygenation of compound **86**.

It may be that the desired tosylated intermediates did not form, but another explanation could be that heterolysis of the oxetanyl C-O bond is too difficult since the intermediate oxetanyl cation required to achieve deoxygenation is highly destabilised. Molecular modelling of the systems shown in Scheme 3.3.46, using a Spartan'08 software (MP2/6-31G\*, gas phase), indicate that these isodesmic reactions are strongly favourable.<sup>125</sup>



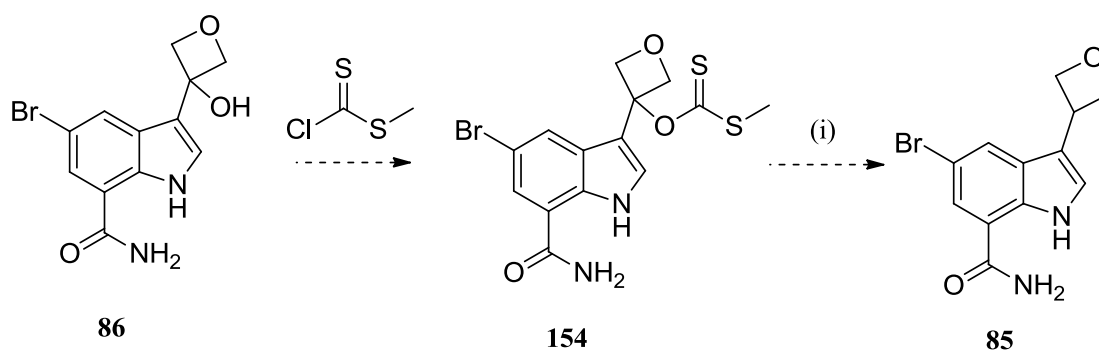
Scheme 3.3.46. Stability of oxetanyl cations w.r.t. model cyclic systems.<sup>125</sup>

In contrast to these observations, molecular modelling (MP2/6-31G\*, gas phase) predicts the stability of an oxetanyl radical (**151**) to be similar to that of the model dioxolanyl radical (**152**), though less stable than the cyclohexyl system (**153**), so homolysis of the exocyclic oxetanyl C-O bond should be less difficult than the corresponding heterolysis (Scheme 3.3.47).<sup>125</sup>



Scheme 3.3.47. Stability of oxetanyl radicals wrt model cyclic systems.<sup>125</sup>

From these observations it would be advantageous to attempt a radical deoxygenation, for example a Barton-McCombie deoxygenation (Scheme 3.3.48), as part of future work into the synthesis of intermediate **85**.<sup>126</sup>

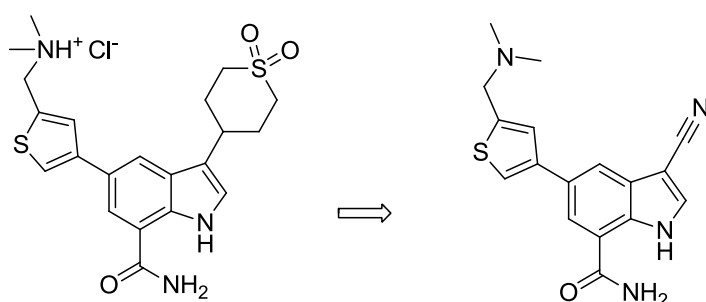


Reagents and Conditions: (i)  $\text{Bu}_3\text{SnH}$ , AIBN.

Scheme 3.3.48. Barton-McCombie deoxygenation of intermediate **86**.

### 3.4. Conclusion

As a result of this programme of work, highly ligand efficient IKK2 inhibitors have been identified. A Hansch analysis of previously synthesised compounds facilitated the design of 3-substituted indole carboxamides and the 3-cyano-substituted indole carboxamides were discovered to have significantly improved ligand efficiency when compared with the lead compound.

**4a**

IKK2  $pK_i$  = 9.5  
 IKK1  $pK_i$  = 7.5  
 LE/LLE<sub>AT</sub> = 0.45, 0.51  
 MW = 432  
 AMP (nm/sec) = 10  
 CLND solubility ( $\mu\text{g/ml}$ ) = 187

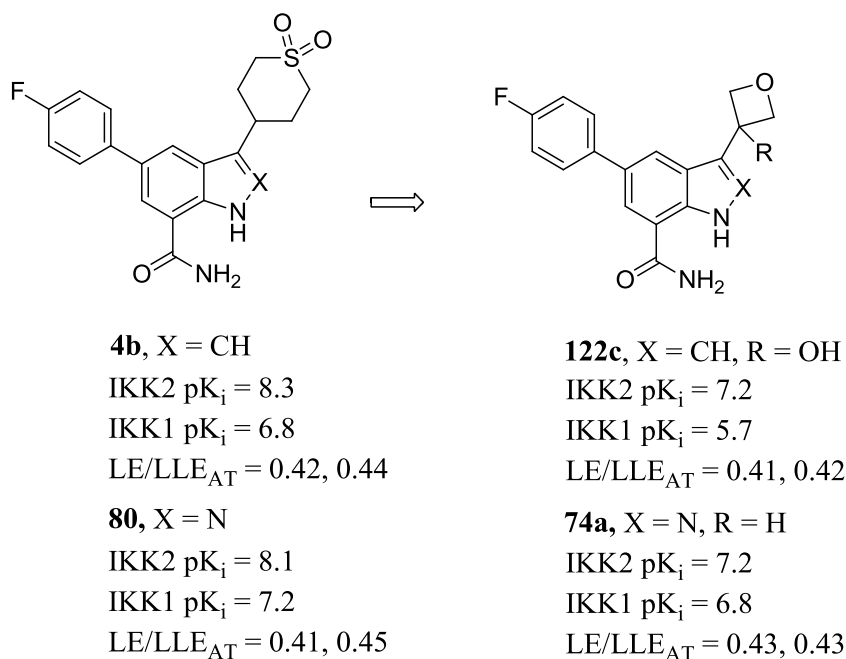
**16a**

IKK2  $pK_i$  = 8.9  
 IKK1  $pK_i$  = 6.8  
 LE/LLE<sub>AT</sub> = 0.53, 0.51  
 MW = 324  
 AMP (nm/sec) = 330  
 CLND solubility ( $\mu\text{g/ml}$ ) = 65

The cyano-containing compounds had much decreased molecular weight and maintained excellent IKK2 potency as well as selectivity over IKK1 (>100-fold). This level of activity and selectivity is comparable to compounds that have been reported to be effective as anti-inflammatory agents in pre-clinical *in vivo* models. In addition, the more ligand efficient compounds had improved permeability and moderate solubility, indicating the potential for obtaining oral absorption in the indole carboxamide series. The results from this programme of work prompted the exploration of further 5-substituents to incorporate on the 3-cyano indole carboxamide core in order to optimise the oral PK profile.



The work carried out here also exemplified how knowledge from contemporary medicinal chemistry literature was applied to an ongoing research programme. Installation of the oxetanyl group in the indole carboxamide series gave compounds with ligand efficiencies comparable to those of the lead compounds, since a smaller substituent with the potential to act as a hydrogen-bond acceptor was incorporated.



The synthesis of 3-oxetan-3-yl indole carboxamide compounds in this programme of work also led to the discovery of a novel, synthetically useful methodology for the synthesis of oxazoles and thiazoles. Further investigations into the synthesis of these compounds also involved deoxofluorination and deoxygenation reactions of a 3-hydroxyoxetan-3-yl group. Preliminary observations from this work warrant further research into the deoxofluorination of 3-hydroxyoxetanes and the stability of resulting 3-fluorooxetanes, as well as the application of a radical deoxygenation on this template.

### 3.5. References

- (1) Whiteside, S. T.; Israel, A. *Semin. Cancer Biol.* **1997**, *8*, 75.
- (2) Roshak, A. K.; Callahan, J. F.; Blake, S. M. *Curr. Opin. Pharmacol.* **2002**, *2*, 316.
- (3) DiDonato, J. A.; Hayakawa, M.; Rothwarf, D. M.; Zandi, E.; Karin, M. *Nature* **1997**, *388*, 548.
- (4) Zandi, E.; Rothwarf, D. M.; Delhase, M.; Hayakawa, M.; Karin, M. *Cell* **1997**, *91*, 243.
- (5) Rothwarf, D. M.; Zandi, E.; Natoli, G.; Karin, M. *Nature* **1998**, *395*, 297.
- (6) Delhase, M.; Hayakawa, M.; Chen, Y.; Karin, M. *Science* **1999**, *284*, 309.
- (7) Senftleben, U.; Cao, Y.; Xiao, G.; Greten, F. R.; Kraehn, G.; Bonizzi, G.; Chen, Y.; Hu, Y.; Fong, A.; Sun, S.-C.; Karin, M. *Science* **2001**, *293*, 1495.
- (8) Prajapati, S.; Tu, Z.; Yamamoto, Y.; Gaynor, R. B. *Cell Cycle* **2006**, *5*, 2371.
- (9) Lawrence, T.; Bebien, M.; Liu, G. Y.; Nizet, V.; Karin, M. *Nature* **2005**, *434*, 1138.
- (10) Descargues, P.; Sil, A. K.; Karin, M. *Embo J.* **2008**, *27*, 2639.
- (11) Lahtela, J.; Nousiainen, H. O.; Stefanovic, V.; Tallila, J.; Viskari, H.; Karikoski, R.; Gentile, M.; Saloranta, C.; Varilo, T.; Salonen, R.; Kestila, M. *N. Engl. J. Med.* **2010**, *363*, 1631.
- (12) Liu, B.; Park, E.; Zhu, F.; Bustos, T.; Liu, J.; Shen, J.; Fischer, S. M.; Hu, Y. *PNAS* **2006**, *103*, 17202.
- (13) Nelson, D. L. *Curr. Opin. Genet. Dev.* **2006**, *16*, 282.
- (14) Zonana, J.; Elder, M. E.; Schneider, L. C.; Orlow, S. J.; Moss, C.; Golabi, M.; Shapira, S. K.; Farndon, P. A.; Wara, D. W.; Emmal, S. A.; Ferguson, B. M. *Am. J. Hum. Genet.* **2000**, *67*, 1555.
- (15) Hart, L. A.; Krishnan, V. L.; Adcock, I. M.; Barnes, P. J.; Chung, K. F. *Am. J. Respir. Crit. Care Med.* **1998**, *158*, 1585.

- (16) Gagliardo, R.; Chanez, P.; Mathieu, M.; Bruno, A.; Costanzo, G.; Gougat, C.; Vachier, I.; Bousquet, J.; Bonsignore, G.; Vignola Antonio, M. *Am. J. Respir. Crit. Care Med.* **2003**, *168*, 1190.
- (17) Birrell, M. A.; Hardaker, E.; Wong, S.; McCluskie, K.; Catley, M.; De Alba, J.; Newton, R.; Haj-Yahia, S.; Pun, K. T.; Watts, C. J.; Shaw, R. J.; Savage, T. J.; Belvisi, M. G. *Am. J. Respir. Crit. Care Med.* **2005**, *172*, 962.
- (18) Di Stefano, A.; Caramori, G.; Oates, T.; Capelli, A.; Lusuardi, M.; Gnemmi, I.; Ioli, F.; Chung, K. F.; Donner, C. F.; Barnes, P. J.; Adcock, I. M. *Eur. Respir. J.* **2002**, *20*, 556.
- (19) Caramori, G.; Romagnoli, M.; Casolari, P.; Bellettato, C.; Casoni, G.; Boschetto, P.; Chung, K. F.; Barnes, P. J.; Adcock, I. M.; Ciaccia, A.; Fabbri, L. M.; Papi, A. *Thorax* **2003**, *58*, 348.
- (20) Yagi, O.; Aoshiba, K.; Nagai, A. *Respiration* **2006**, *73*, 610.
- (21) Agusti, A.; Morla, M.; Sauleda, J.; Saus, C.; Busquets, X. *Thorax* **2004**, *59*, 483.
- (22) Mourkioti, F.; Kratsios, P.; Luedde, T.; Song, Y.-H.; Delafontaine, P.; Adami, R.; Parente, V.; Bottinelli, R.; Pasparakis, M.; Rosenthal, N. *J. Clin. Invest.* **2006**, *116*, 2945.
- (23) Rajendrasozhan, S.; Yang, S.-R.; Edirisinghe, I.; Yao, H.; Adenuga, D.; Rahman, I. *Antioxid. Redox Signaling* **2008**, *10*, 799.
- (24) Burke, J. R.; Pattoli, M. A.; Gregor, K. R.; Brassil, P. J.; MacMaster, J. F.; McIntyre, K. W.; Yang, X.; Iotzova, V. S.; Clarke, W.; Strnad, J.; Qiu, Y.; Zusi, F. C. *J. Biol. Chem.* **2003**, *278*, 1450.
- (25) Wen, D.; Nong, Y.; Morgan, J. G.; Gangurde, P.; Bielecki, A.; DaSilva, J.; Keaveney, M.; Cheng, H.; Fraser, C.; Schopf, L.; Hepperle, M.; Harriman, G.; Jaffee, B. D.; Ocain, T. D.; Xu, Y. *J. Pharmacol. Exp. Ther.* **2006**, *317*, 989.
- (26) Hicks, F. A.; Cooper, M. I.; Langston, M.; St. Clair Brown, A., "Mesylate salt of an IKK inhibitor", WO 2009054970, 2009.

- (27) "Safety, Tolerability and Pharmacokinetics of SAR113945 Following Intra-articular Administration in Patients With Knee Osteoarthritis", Available from: <http://clinicaltrials.gov/show/NCT01113333> NLM Identifier: NCT01113333.
- (28) Langevin, B. C.; Sherer, D.; Buttrum, M. E.; Rose, S., "Monopotassium salt of an IKK-beta kinase inhibitor", WO 2006076318, 2006.
- (29) Ziegelbauer, K.; Gantner, F.; Lukacs, N. W.; Berlin, A.; Fuchikami, K.; Niki, T.; Sakai, K.; Inbe, H.; Takeshita, K.; Ishimori, M.; Komura, H.; Murata, T.; Lowinger, T.; Bacon, K. B. *Br. J. Pharmacol.* **2005**, *145*, 178.
- (30) Podolin, P. L.; Callahan, J. F.; Bolognese, B. J.; Li, Y. H.; Carlson, K.; Davis, T. G.; Mellor, G. W.; Evans, C.; Roshak, A. K. *J. Pharmacol. Exp. Ther.* **2005**, *312*, 373.
- (31) Birrell, M. A.; Wong, S.; Hardaker, E. L.; Catley, M. C.; McCluskie, K.; Collins, M.; Haj-Yahia, S.; Belvisi, M. G. *Mol. Pharmacol.* **2006**, *69*, 1791.
- (32) Manning, G.; Whyte, D. B.; Martinez, R.; Hunter, T.; Sudarsanam, S. *Science* **2002**, *298*, 1912.
- (33) Bamborough, P.; Callahan, J. F.; Christopher, J. A.; Kerns, J. K.; Liddle, J.; Miller, D. D.; Morse, M. A.; Rumsey, W. L.; Williamson, R. *Curr. Top. Med. Chem.* **2009**, *9*, 623.
- (34) Xu, G.; Lo, Y.-C.; Li, Q.; Napolitano, G.; Wu, X.; Jiang, X.; Dreano, M.; Karin, M.; Wu, H. *Nature* **2011**, *472*, 325.
- (35) <http://www.pdb.org/pdb/explore/obsolete.do?obsoleteId=3QAD>,
- (36) <http://www.pdb.org/pdb/explore/explore.do?structureId=3RZF>,
- (37) Liu, S.; Misquitta, Y. R.; Olland, A.; Johnson, M. A.; Kelleher, K. S.; Kriz, R.; Lin, L. L.; Stahl, M.; Mosyak, L. *J. Biol. Chem.* **2013**, *288*, 22758.
- (38) Christopher, J. A.; Avitabile, B. G.; Bamborough, P.; Champigny, A. C.; Cutler, G. J.; Dyos, S. L.; Grace, K. G.; Kerns, J. K.; Kitson, J. D.; Mellor, G. W.; Morey, J. V.; Morse, M. A.; O'Malley, C. F.; Patel, C. B.; Probst, N.; Rumsey, W.; Smith, C. A.; Wilson, M. J. *Bioorg. Med. Chem. Lett.* **2007**, *17*, 3972.

- (39) Miller, D. D.; Bamborough, P.; Christopher, J. A.; Baldwin, I. R.; Champigny, A. C.; Cutler, G. J.; Kerns, J. K.; Longstaff, T.; Mellor, G. W.; Morey, J. V.; Morse, M. A.; Nie, H.; Rumsey, W. L.; Taggart, J. J. *Bioorg. Med. Chem. Lett.* **2011**, *21*, 2255.
- (40) Baldwin, I. R.; Bamborough, P.; Christopher, J. A.; Kerns, J. K.; Longstaff, T.; Miller, D. D., "Preparation of 7-indolecarboxamides as IKK2 kinase inhibitors for the treatment of such as inflammatory and tissue repair disorders", WO 2005067923, 2005.
- (41) Boehm, J. C.; Busch-Petersen, J.; Fu, W.; Jin, Q.; Kerns, J. K.; Li, H.; Lin, G.; Lin, X.; Neipp, C. E., "Preparation of indolecarboxamide derivatives for use as IKK2 inhibitors", WO 2008118724, 2008.
- (42) Bullion, A., GlaxoSmithKline: 2007, unpublished results.
- (43) Pre-clinical ADME, toxicology and PK, Cyprotex: 2011, unpublished results.
- (44) Lipinski, C. A.; Lombardo, F.; Dominy, B. W.; Feeney, P. J. *Adv. Drug Delivery Rev.* **1997**, *23*, 3.
- (45) Veber, D. F.; Johnson, S. R.; Cheng, H.-Y.; Smith, B. R.; Ward, K. W.; Kopple, K. D. *J. Med. Chem.* **2002**, *45*, 2615.
- (46) Lewell, X., GlaxoSmithKline: 2010, personal communication.
- (47) Verma, J.; Khedkar, V. M.; Coutinho, E. C. *Curr. Top. Med. Chem.* **2010**, *10*, 95.
- (48) Hansch, C.; Muir, R. M.; Fujita, T.; Maloney, P. P.; Geiger, F.; Streich, M. *J. Am. Chem. Soc.* **1963**, *85*, 2817.
- (49) Hansch, C.; Leo, A.; Taft, R. W. *Chem. Rev.* **1991**, *91*, 165.
- (50) Maxwell, A. M., GlaxoSmithKline: 2011, personal communication.
- (51) Rosenmund, K. W.; Struck, E. *Ber. Dtsch. Chem. Ges. B* **1919**, *52B*, 1749.
- (52) Ellis, G. P.; Romney-Alexander, T. M. *Chem. Rev.* **1987**, *87*, 779.
- (53) Hatsuda, M.; Seki, M. *Tetrahedron* **2005**, *61*, 9908.
- (54) Zanon, J.; Klapars, A.; Buchwald, S. L. *J. Am. Chem. Soc.* **2003**, *125*, 2890.
- (55) Cristau, H.-J.; Ouali, A.; Spindler, J.-F.; Taillefer, M. *Chem.--Eur. J.* **2005**, *11*, 2483.

- (56) Schareina, T.; Zapf, A.; Cotte, A.; Gotta, M.; Beller, M. *Adv. Synth. Catal.* **2011**, *353*, 777.
- (57) Sundermeier, M.; Zapf, A.; Mutyala, S.; Baumann, W.; Sans, J.; Weiss, S.; Beller, M. *Chem.--Eur. J.* **2003**, *9*, 1828.
- (58) Schareina, T.; Zapf, A.; Beller, M. *Tetrahedron Lett.* **2005**, *46*, 2585.
- (59) Ding, S.-T.; Jiao, N. *J. Am. Chem. Soc.* **2011**, *133*, 12374.
- (60) Pawar, A. B.; Chang, S. *Chem. Commun.* **2014**, *50*, 448.
- (61) Renaux, J., GlaxoSmithKline: 2009, personal communication.
- (62) Vilsmeier, A.; Haack, A. *Ber. Dtsch. Chem. Ges. B* **1927**, *60B*, 119.
- (63) Meth-Cohn, O.; Stanforth, S. P. *Comprehensive Organic Synthesis - Selectivity, Strategy and Efficiency in Modern Organic Chemistry*; Elsevier: Oxford, 1991; Vol. 2.
- (64) Sosnovsky, G.; Krogh, J. A.; Umhoefer, S. G. *Synthesis* **1979**, 722.
- (65) Augustine, J. K.; Atta, R. N.; Ramappa, B. K.; Boodappa, C. *Synlett* **2009**, 3378.
- (66) Klose, J.; Bienert, M.; Mollenkopf, C.; Wehle, D.; Zhang, C.-w.; Carpino, L. A.; Henklein, P. *Chem. Commun.* **1999**, 1847.
- (67) Miyaura, N.; Yamada, K.; Suzuki, A. *Tetrahedron Lett.* **1979**, *20*, 3437.
- (68) Zolotoy, A. B.; Plouvier, B. P.; Beatch, G. B.; Hayes, E. S.; Wall, R. A.; Walker, M. J. A. *Curr. Med. Chem.: Cardiovasc. Hematol. Agents* **2003**, *1*, 225.
- (69) Lemke, T. L.; Williams, D. A. *Foye's Principles of Medicinal Chemistry*; Sixth Edition ed.; Lippincott Williams & Wilkins: Philadelphia, 2007.
- (70) Taveras, A. G.; Zheng, J.; Biju, P. J.; Yu, Y.; Chao, J.; Fine, J.; Lundell, D.; Priestley, T.; Reggiani, A.; Merritt, J. R.; Baldwin, J. J.; Lai, G.; Wu, M., "Preparation of isothiazole dioxides as CXC- and CC-chemokine receptor ligands", WO 2005068460, 2005.
- (71) Olofsson, K.; Suna, E.; Pelcman, B.; Ozola, V.; Katkevics, M.; Kalvins, I.; Schaal, W., "Preparation of indolecarboxylates as inhibitors of microsomal

- prostaglandin E synthase-1 (mPGE-1) useful in the treatment of inflammation", WO 2005123674, 2005.
- (72) Prieto, M.; Zurita, E.; Rosa, E.; Munoz, L.; Lloyd-Williams, P.; Giralt, E. *J. Org. Chem.* **2004**, *69*, 6812.
- (73) Knapp, D. M.; Gillis, E. P.; Burke, M. D. *J. Am. Chem. Soc.* **2009**, *131*, 6961.
- (74) Molander, G. A.; Ellis, N. *Acc. Chem. Res.* **2007**, *40*, 275.
- (75) Smith, I., GlaxoSmithKline: 2010, personal communication.
- (76) Grewal, G.; Oza, V., "Preparation of heterocyclic sulfonamide compounds as Edg-1 antagonists for treatment of cancer", WO 2008059238, 2008.
- (77) Banks, R. E.; Murtagh, V.; An, I.; Maleczka, R. E. In *e-EROS Encyclopedia of Reagents for Organic Synthesis*; John Wiley & Sons, Inc.: Hoboken, 2007.
- (78) Tupper, D. E.; Pullar, I. A.; Clemens, J. A.; Fairhurst, J.; Risius, F. C.; Timms, G. H.; Wedley, S. *J. Med. Chem.* **1993**, *36*, 912.
- (79) Bellesia, F.; Boni, M.; Ghelfi, F.; Pagnoni, U. M.; Pinetti, A. *Synth. Commun.* **1992**, *22*, 1101.
- (80) Hamel, P.; Preville, P. *J. Org. Chem.* **1996**, *61*, 1573.
- (81) Tudge, M.; Tamiya, M.; Savarin, C.; Humphrey, G. R. *Org. Lett.* **2006**, *8*, 565.
- (82) Bastos, M. M.; Mayer, L. M. U.; Figueira, E. C. S.; Soares, M.; Kover, W. B.; Boechat, N. *J. Heterocycl. Chem.* **2008**, *45*, 969.
- (83) Swain, C. G.; Lupton, E. C., Jr. *J. Am. Chem. Soc.* **1968**, *90*, 4328.
- (84) Wuitschik, G.; Carreira, E. M.; Wagner, B.; Fischer, H.; Parrilla, I.; Schuler, F.; Rogers-Evans, M.; Muller, K. *J. Med. Chem.* **2010**, *53*, 3227.
- (85) Burkhard, J. A.; Wuitschik, G.; Rogers-Evans, M.; Mueller, K.; Carreira, E. *M. Angew. Chem., Int. Ed.* **2010**, *49*, 9052.
- (86) Wani, M. C.; Taylor, H. L.; Wall, M. E.; Coggon, P.; McPhail, A. T. *J. Am. Chem. Soc.* **1971**, *93*, 2325.
- (87) Hirsch, A. K. H.; Alphey, M. S.; Lauw, S.; Seet, M.; Barandun, L.; Eisenreich, W.; Rohdich, F.; Hunter, W. N.; Bacher, A.; Diederich, F. *Org. Biomol. Chem.* **2008**, *6*, 2719.

- (88) Wuitschik, G.; Rogers-Evans, M.; Mueller, K.; Fischer, H.; Wagner, B.; Schuler, F.; Polonnchuk, L.; Carreira, E. M. *Angew. Chem., Int. Ed.* **2006**, *45*, 7736.
- (89) Laurence, C.; Brameld, K. A.; Graton, J.; Le Questel, J.-Y.; Renault, E. *J. Med. Chem.* **2009**, *52*, 4073.
- (90) Korolev, A. M.; Eremenko, L. T.; Meshikhina, L. V.; Eremenko, I. L.; Aleksandrov, G. G.; Konovalova, N. P.; Lodygina, V. P. *Russ. Chem. Bull.* **2003**, *52*, 1859.
- (91) Burkhard, J. A.; Wuitschik, G.; Plancher, J.-M.; Rogers-Evans, M.; Carreira, E. M. *Org. Lett.* **2013**, *15*, 4312.
- (92) Lin, X.; Busch-Petersen, J.; Deng, J.; Edwards, C.; Zhang, Z.; Kerns, J. K. *Synlett* **2008**, 3216.
- (93) Michaelis, C. A. A.; Kaehne, R. *Ber. Dtsch. Chem. Ges.* **1898**, *31*, 1048.
- (94) Arbuzov, B. A. *Pure Appl. Chem.* **1964**, *9*, 307.
- (95) Horner, L.; Hoffmann, H.; Wippel, H. G. *Chem. Ber.* **1958**, *91*, 61.
- (96) Wadsworth, W. S., Jr.; Emmons, W. D. *J. Am. Chem. Soc.* **1961**, *83*, 1733.
- (97) <http://thalesnano.com>, accessed on 14th December 2013.
- (98) Ruechardt, C.; Hassmann, V. *Synthesis* **1972**, 375.
- (99) Sun, J.-H.; Teleha, C. A.; Yan, J.-S.; Rodgers, J. D.; Nugiel, D. A. *J. Org. Chem.* **1997**, *62*, 5627.
- (100) Pritchard, J. G.; Long, F. A. *J. Am. Chem. Soc.* **1958**, *80*, 4162.
- (101) Sollis, S., GlaxoSmithKline: 2009, personal communication.
- (102) Lynn, S., GlaxoSmithKline: 2010, personal communication.
- (103) Burkhard, J. A.; Tchitchanov, B. H.; Carreira, E. M. *Angew. Chem., Int. Ed.* **2011**, *50*, 5379.
- (104) Orr, D.; Tolfrey, A.; Percy, J. M.; Frieman, J.; Harrison, Z. A.; Campbell-Crawford, M.; Patel, V. K. *Chem. - Eur. J.* **2013**, *19*, 9655.
- (105) Mahadevan, A.; Sard, H.; Gonzalez, M.; McKew, J. C. *Tetrahedron Lett.* **2003**, *44*, 4589.
- (106) Rizzo, J. R.; Alt, C. A.; Zhang, T. Y. *Tetrahedron Lett.* **2008**, *49*, 6749.



- (107) Erion, M. D.; Jiang, H.; Boyer, S. H., "Preparation of phosphinic and phosphonic acid-containing liver-selective thymomimetics effective against metabolic diseases", WO 2006128056, 2006.
- (108) Gundersen, E. G., "Preparation of substituted phenyl indoles as plasminogen activator inhibitor-1 inhibitors", US 20050070592, 2005.
- (109) Campos, K. R.; Woo, J. C. S.; Lee, S.; Tillyer, R. D. *Org. Lett.* **2004**, *6*, 79.
- (110) Celebi-Olcum, N.; Boal, B. W.; Hutters, A. D.; Garg, N. K.; Houk, K. N. *J. Am. Chem. Soc.* **2011**, *133*, 5752.
- (111) Kürti, L.; Czakó, B. *Strategic Applications of Named Reactions in Organic Synthesis* Elsevier: London, 2005.
- (112) Desroses, M.; Wieckowski, K.; Stevens, M.; Odell, L. R. *Tetrahedron Lett.* **2011**, *52*, 4417.
- (113) Bernardo, P. H.; Chai, C. L. L.; Heath, G. A.; Mahon, P. J.; Smith, G. D.; Waring, P.; Wilkes, B. A. *J. Med. Chem.* **2004**, *47*, 4958.
- (114) Amir-Heidari, B.; Micklefield, J. *J. Org. Chem.* **2007**, *72*, 8950.
- (115) Manolikakes, G.; Knochel, P. *Angew. Chem., Int. Ed.* **2009**, *48*, 205.
- (116) Middleton, W. J. *J. Org. Chem.* **1975**, *40*, 574.
- (117) Lal, G. S.; Pez, G. P.; Pesaresi, R. J.; Prozonic, F. M.; Cheng, H. *J. Org. Chem.* **1999**, *64*, 7048.
- (118) Singh, R. P.; Shreeve, J. n. M. *Synthesis* **2002**, 2561.
- (119) Messina, P. A.; Mange, K. C.; Middleton, W. J. *J. Fluorine Chem.* **1989**, *42*, 137.
- (120) Negi, D. S.; Koeplling, L.; Lovis, K.; Abdallah, R.; Geisler, J.; Budde, U. *Org. Process Res. Dev.* **2008**, *12*, 345.
- (121) Umemoto, T.; Singh, R. P.; Xu, Y.; Saito, N. *J. Am. Chem. Soc.* **2010**, *132*, 18199.
- (122) Singh, R. P.; Umemoto, T. *J. Org. Chem.* **2011**, *76*, 3113.
- (123) Witulski, B.; Alayrac, C. *Angew. Chem., Int. Ed.* **2002**, *41*, 3281.
- (124) Sabitha, G.; Abraham, S.; Reddy, B. V. S.; Yadav, J. S. *Synlett* **1999**, 1745.
- (125) Percy, J. M., University of Strathclyde: 2011, personal communication.

- (126) Barton, D. H. R.; McCombie, S. W. *J. Chem. Soc., Perkin Trans. 1* **1975**, 1574.

## **Chapter 4**

# **The Design, Synthesis and Optimisation of PI3K $\delta$ Inhibitors as Potential Anti-Inflammatory Agents**

## 4.1. Introduction

### 4.1.1. Phosphoinositide Kinases and Related Proteins

#### 4.1.1.1. The Phosphoinositide 3-Kinases (PI3Ks)

The PI3Ks are a family of enzymes that are central to signalling involving intracellular lipids. They were identified in the mid 1980s as lipid kinases that phosphorylate the 3-hydroxyl group of inositol-containing membrane lipids.<sup>1</sup>

Phosphatidylinositol (PtdIns) is the basic building block for intracellular inositol lipids (Figure 4.1.1.) and up to three of its five free hydroxyl groups have been found to be phosphorylated in cells (the 2- and 6-positions are not known to become esterified as phosphates).<sup>2</sup>

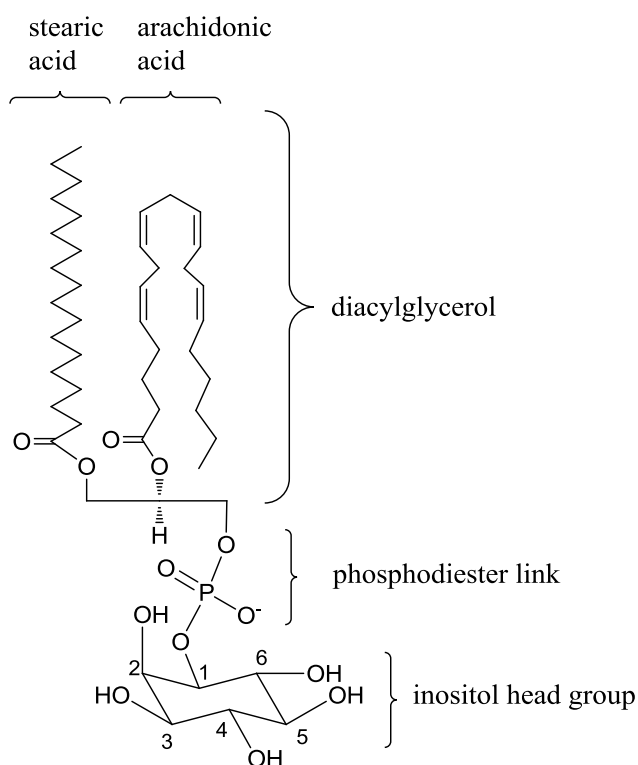


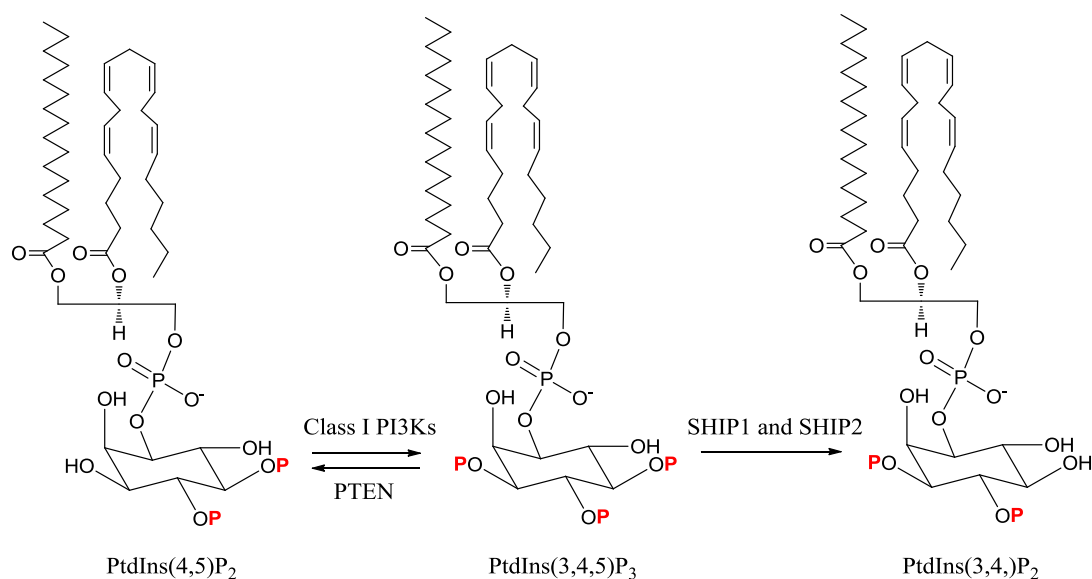
Figure 4.1.1. Chemical structure of phosphatidylinositol (PtdIns).<sup>2</sup>

Four species of 3-phosphoinositides have been identified; these are PtdIns3P, PtdIns(3,4)P, PtdIns(3,5)P and PtdIns(3,4,5)P<sub>2</sub>.<sup>2</sup> These phospholipids have roles as secondary messengers; they interact with the lipid binding domains of a variety of cellular proteins, influencing a diverse array of cellular pathways.<sup>2</sup> They are generated *via* phosphorylation of the 3-hydroxyl group in three substrates: PtdIns, PtdIns4P and PtdIns(4,5)P<sub>2</sub>. PI3Ks are the enzymes that generate these intracellular lipids and several distinct classes of PI3Ks have been identified based upon their structural features and substrate specificity.<sup>3</sup>

#### **4.1.1.2. Class I PI3Ks**

The class I PI3Ks are heterodimeric enzymes that consist of one of four closely related 100-kDa catalytic subunits (p110 $\alpha$ ,  $\beta$ ,  $\gamma$ ,  $\delta$ ) and an associated regulatory subunit.<sup>2</sup> The class IA catalytic subunits (p110 $\alpha$ ,  $\beta$ , and  $\delta$ ) are bound to a p85 regulatory subunit and are activated by tyrosine kinase signalling pathways.<sup>4</sup> The class IB catalytic subunit (p110 $\gamma$ ) does not bind to a p85 regulatory subunit, instead it binds p101, p84 or p87<sup>PIKAP</sup> (PI3K $\gamma$  adaptor protein of 87 kDa).<sup>5,6,7</sup> These regulatory subunits facilitate activation of the p110 $\gamma$  isoform by G $\beta\gamma$  subunits that are released downstream of G-protein coupled receptor activation.<sup>8</sup> Recently, the p110 $\beta$  isoform has also been shown to be activated by GPCRs.<sup>9</sup> The class I PI3Ks are all known to convert phosphatidylinositol-4,5-bisphosphate (PtdIns(4,5)P<sub>2</sub>) to phosphatidylinositol-3,4,5-trisphosphate (PtdIns(3,4,5)P<sub>3</sub>) *in vivo*, which leads to downstream signalling cascades that control cell growth, cell cycle entry and cell survival.<sup>10</sup>

The PtdIns(3,4,5)P<sub>3</sub> generated by class I PI3Ks can be negatively regulated by either dephosphorylation to give PtdIns(4,5)P<sub>2</sub>, which is mediated by phosphatase and tensin homolog (PTEN, Figure 4.1.2), or by conversion to phosphatidylinositol-3,4-bisphosphate (PtdIns(3,4)P<sub>2</sub>) by SH-2 domain-containing inositol phosphatases (SHIP1 and SHIP2, Figure 4.1.2).<sup>10</sup>

Figure 4.1.2. Dephosphorylation of PtdIns(3,4,5)P<sub>3</sub>.

#### 4.1.1.3. Class II and III PI3Ks

The physiological roles of other isoforms of the PI3K families are less well understood. The class II PI3K family is made up of PI3K-C2 $\alpha$ , PI3K-C2 $\beta$  and PI3K-C2 $\gamma$ . While PI3K-C2 $\alpha$  has been shown to be expressed ubiquitously, PI3K-C2 $\beta$  is mostly expressed in the placenta and thymus, and PI3K-C2 $\gamma$  is restricted in its expression to liver, prostate, breast and salivary glands.<sup>11</sup> These isoforms are thought to phosphorylate phosphatidylinositol (PtdIns) to phosphatidylinositol-3-phosphate (PtdIns3P), as this is the main product observed from *in vitro* studies, although the phosphorylation of phosphatidylinositol-4-phosphate (PtdIns4P) by the class II PI3Ks has also been observed.<sup>11</sup> The functional *in vivo* substrates of class II PI3Ks have not been identified, though several studies have provided evidence that PtdIns3P is the main product of PI3K-C2 $\alpha$  and PI3K-C2 $\beta$  activation.<sup>11</sup> The class II PI3Ks could therefore be of interest for pharmacological intervention since PtdIns3P has been shown to be generated after cellular stimulation and acts as an intracellular secondary messenger. Indeed, all three isoforms have been shown to be activated in

response to stimuli such as cytokines (e.g. TNF $\alpha$ ), so they must have roles in intracellular signalling and function. Roles for PI3K-C2 $\alpha$  in insulin signalling<sup>12</sup> and vascular smooth muscle contraction<sup>13</sup> have been identified, and activation of PI3K-C2 $\beta$  has been implicated in the migration of cancer cells.<sup>14</sup> However more research into their intracellular roles is required and it is hoped that the identification of their *in vivo* lipid products will help to define these roles further.

The only member of the class III PI3Ks is Vps34 (vacuolar protein sorting mutant 34 protein), which phosphorylates PtdIns exclusively to generate PtdIns3P *in vivo*.<sup>15</sup> Vps34 has a catalytic subunit with high sequence homology to that of the class I PI3Ks, but its substrate specificity means it has different biological functions. It is thought that Vps34 forms a complex with a serine kinase Vps15 and this binding is required for the activation of Vps34 *in vivo*.<sup>16</sup> Downstream signalling events result from membrane recruitment of proteins that bind to PtdIns3P produced from Vps34 activation, so Vps34 is implicated in cellular processes involved in human disease.<sup>16</sup> For example Vps34 is a key regulator of autophagy and its up-regulation has the potential to lead to enhanced autophagy, which has been shown to clear protein aggregates in neurodegenerative disease and have roles in tumour suppression.<sup>16</sup>

It is clear that the phosphorylation reactions catalysed by the PI3Ks in cells are critical for many biological functions. Figure 4.1.3 shows the main metabolic pathways that interconvert inositol phospholipids, and highlights reactions catalysed by the different classes of PI3Ks.<sup>17</sup>

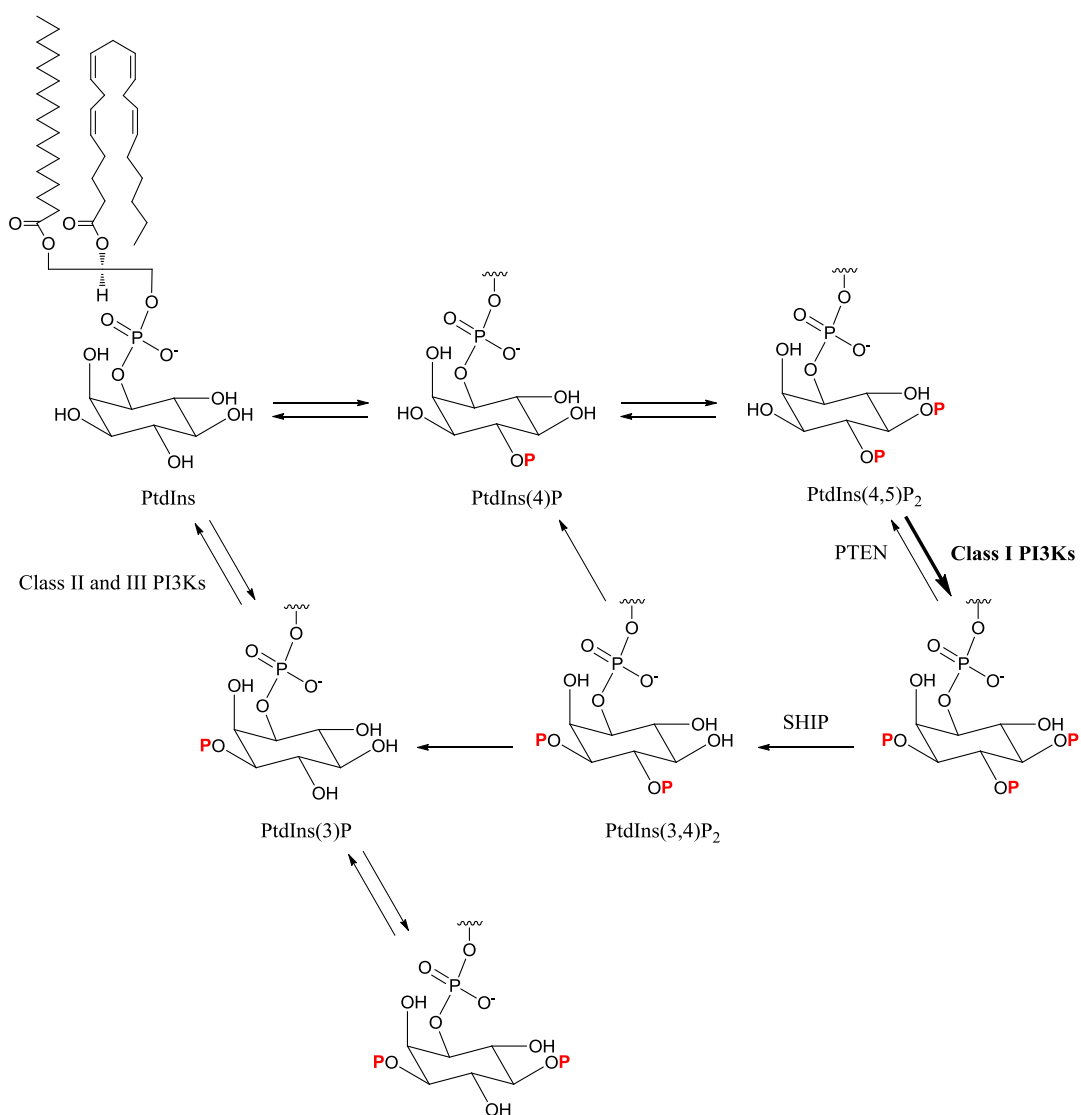


Figure 4.1.3. Reactions catalysed by PI3Ks in cells.<sup>17</sup>

A class of proteins, often called the class IV PI3Ks or PI3K-related kinases, exists alongside the PI3Ks. These proteins have similar sequence homology to the PI3Ks and will be described in the next section.



#### **4.1.1.4. PI3K-related Kinases**

The PI3K-related kinases (PIKKs) are a family of high molecular weight enzymes that have catalytic sites similar to the PI3Ks. Five members of this family are serine-threonine kinases responsible for the phosphorylation of specific proteins and the sixth member, transformation/transcription domain associated protein (TRRAP), has no known phosphotransferase activity.<sup>18</sup> The five protein kinases include ataxia–telangiectasia mutated (ATM) and ataxia–telangiectasia related (ATR) kinases, which control signalling pathways that lead to DNA repair and cellular survival in response to DNA damage, and the DNA-dependent protein kinase (DNA-PK), which is responsible for repairing DNA double-strand breaks.<sup>19</sup> Another member of the PIKK family that responds to DNA damage is a suppressor of morphogenesis in genitalia-1 (SMG-1), which also has a role in mRNA surveillance mechanisms.<sup>20</sup> The only protein kinase of the PIKK family not involved in DNA repair is mammalian target of rapamycin (mTOR), which is activated by various extracellular and intracellular signals and regulates many cellular processes.<sup>21</sup> The activation of mTOR is thought to be mediated by the activation of class I PI3Ks and this represents one of the signalling pathways activated downstream of the PI3Ks. The following section will discuss how class I PI3K signalling is implicated in health and disease.

#### **4.1.2. The Role of Class I PI3Ks in Disease**

PI3K $\alpha$ , PI3K $\beta$  and PI3K $\delta$  are mainly activated by receptor and non-receptor tyrosine kinases while PI3K $\gamma$  is activated downstream of G-protein coupled receptors. The activation of class I PI3Ks leads to the production of PtdIns(3,4,5)P<sub>3</sub>, which acts as a docking site at the plasma membrane where it recruits and activates proteins that contain phospholipid-binding domains.<sup>22</sup> Downstream effectors of PI3Ks include Akt (also known as protein kinase B) and mTOR.<sup>17</sup> The

phosphorylation of these serine-threonine kinases promotes cell growth, survival and proliferation. These downstream pathways may be important in disease pathology and a great deal of research has gone into determining if the functional profiles of class I PI3Ks are relevant in human disease. The expression profiles of the isoforms are also important in determining whether the enzymes are expressed in disease relevant cells. Indeed, the function and expression of the class I PI3Ks has shown them to be suitable drug targets.

PI3K $\alpha$  is expressed ubiquitously and knocking out the gene that encodes the p110 $\alpha$  protein, PIK3CA, leads to lethality in mice.<sup>23</sup> The activation of this isoform has been observed in cancers, where mutations in the PIK3CA gene lead to amplification and over-expression of PI3K $\alpha$  in tumours, so this is a target of interest for cancer therapy.<sup>24</sup>

PI3K $\beta$  is also expressed ubiquitously and its deletion in mice is also lethal.<sup>25</sup> It has been reported that PI3K $\beta$  is a key mediator of tumourigenesis making it a promising target for cancer therapy;<sup>26</sup> however it may also be of interest as an antithrombotic drug target since the isoform has a role in platelet aggregation.<sup>27</sup>

PI3K $\gamma$  expression is more restricted, with this isoform being highly enriched in leukocytes and present at lower levels in the endothelium and heart.<sup>28</sup> PI3K $\gamma$ -deficient mice have been shown to be viable and fertile, and a key role for PI3K $\gamma$  in the cell motility of macrophages and neutrophils has been defined.<sup>29</sup> Since allergic inflammation involves the activation of mast cells and macrophages, and the subsequent influx of leukocytes, such as monocytes and neutrophils, to the area of inflammation, PI3K $\gamma$  has been targeted for the treatment of inflammatory and autoimmune disease.<sup>30</sup> PI3K $\gamma$ -null mice also exhibit significant defects in T-cell signalling and differentiation, so PI3K $\gamma$  is essential for T-cell development and function.<sup>31</sup> In autoimmune disorders such as rheumatoid arthritis (RA) and systemic lupus erythematosus (SLE), T-cell infiltration leads to the production of inflammatory cytokines and the onset of chronic inflammation. It has been shown that in mouse models of these diseases, PI3K $\gamma$ -null mice have milder symptoms and slower disease progression.<sup>30</sup>

There is evidence that PI3K $\delta$  also has a role in T-cell receptor signalling, as well as being essential for B-cell development and function, so this isoform is also of interest for the treatment of autoimmune disorders such as RA.<sup>30</sup> PI3K $\gamma$  has not been reported to have a role in B-cell function, so specific targeting of PI3K $\delta$  might suppress both B-cell and T-cell mediated functions in these diseases. PI3K $\delta$  has also emerged as a potential target for the treatment of cancers, including acute myeloid leukaemia (AML);<sup>32</sup> however there is also potential for PI3K $\delta$  as a target for the treatment of inflammatory lung disorders, since PI3K $\delta$  expression is restricted to leukocytes, and PI3K $\delta$ -deficient mice have been shown to be viable and fertile.<sup>33,34</sup>

Figure 4.1.4 brings together the roles and potential disease targets of the class I PI3Ks.<sup>22</sup>

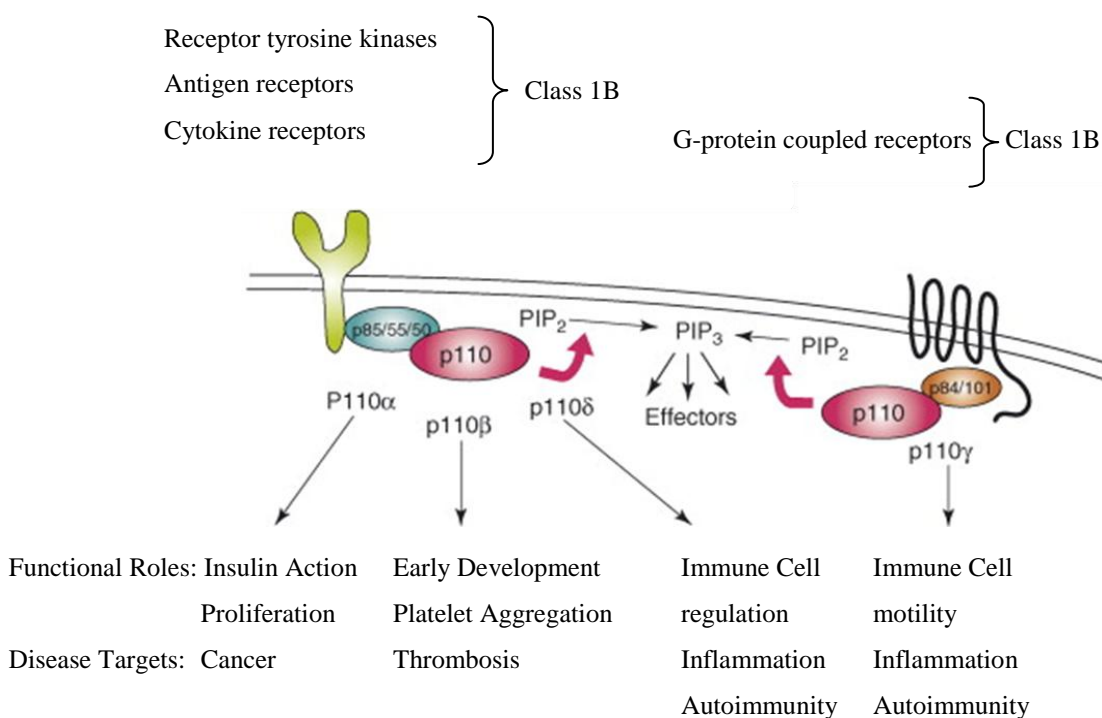


Figure 4.1.4. Functional roles and potential disease targets of class I PI3Ks.<sup>22</sup>

Subsequent sections will focus on PI3K $\delta$  as a promising target for respiratory diseases, and the development of selective inhibitors of this isoform as potential drug molecules.

### **4.1.3. PI3K $\delta$ as a Target for Respiratory Disease**

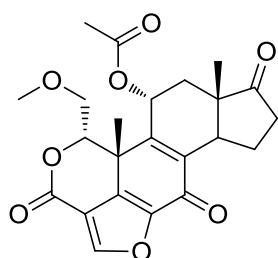
There has been significant research into developing PI3K inhibitors for the treatment of respiratory diseases and most attention has focused on the PI3K $\gamma$  and PI3K $\delta$  isoforms because of their roles in inflammatory lung diseases.<sup>35</sup> The PI3K $\delta$  isoform represents a target for both allergic asthma and COPD. Initial observations that PI3K $\delta$  has a role in T- and B-cell antigen receptor signalling, and that inactivation of PI3K $\delta$  leads to impaired allergen-IgE-induced mast cell degranulation and cytokine release, stimulated interest in targeting this isoform to moderate allergic airway inflammation and AHR.<sup>34,36</sup> Several studies using mouse models of the disease have shown that targeting PI3K $\delta$  is indeed an effective strategy. Administration of a selective PI3K $\delta$  inhibitor led to attenuation of the influx of inflammatory cells and a reduction in IgE serum levels in a murine asthma model, and genetic deletion of PI3K $\delta$  led to a decrease in cytokine levels and a reduction in airway inflammation, as well as mucus production.<sup>37,38</sup>

To date, few studies have reported the effects of inhibiting PI3K $\delta$  in animal models of COPD, but it is known that PI3K $\delta$  affects cell types implicated in the disease such as T-cells, neutrophils and macrophages. For example, there are reports detailing roles for PI3K $\delta$  in neutrophil activation and migration, which are key mechanisms in the pathology of COPD.<sup>39,40</sup> It has been shown that a PI3K $\delta$  inhibitor reduced neutrophil directional movement in response to chemotactic agents and, in a mouse model of pulmonary inflammation, neutrophil influx was reduced by administration of a selective PI3K $\delta$  inhibitor *via* a mechanism thought to modulate the cytokine TNF- $\alpha$ , a key mediator of the inflammatory process in COPD.<sup>41,42</sup> Another study has shown that a potent and dual selective inhibitor of PI3K $\gamma$  and PI3K $\delta$  (pIC<sub>50</sub> = 7.1 and 6.6, respectively) significantly reduced neutrophil

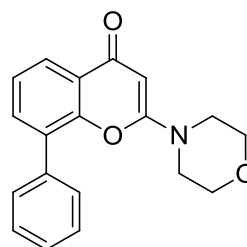
accumulation and production of TNF- $\alpha$  in both an LPS-induced model of COPD, and a smoke model of steroid-resistant COPD.<sup>43</sup> The effects observed in the steroid-resistant model have been attributed to the inhibition of PI3K $\delta$ , rather than PI3K $\gamma$ , as this alone restores glucocorticoid function in smoking-induced airway inflammation in mice.<sup>44</sup> A recent report has also shown that PI3K $\delta$  plays a critical role in airway smooth muscle cell hypertrophy and inhibition of this isoform could prevent the airway remodelling associated with COPD.<sup>45</sup>

#### 4.1.4. PI3K $\delta$ Inhibitors

The discovery of Wortmannin and LY294002, which are both inhibitors of the class I PI3Ks, enabled the initial elucidation of the function of PI3Ks.<sup>46,47</sup>



Wortmannin



LY294002

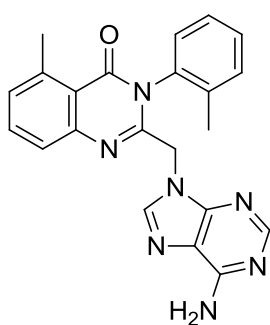
Progress has since been made in the development of inhibitors that have selectivity for the separate isoforms, and these more specific inhibitors have helped to reveal the physiological roles of the different isoforms. This research supports the development of selective inhibitors for the treatment of different human diseases as a viable therapeutic strategy. Selectivity over the other class I PI3Ks is obviously required but wider selectivity, in particular over the class II PI3Ks, Vps34 and the PIKKs is also desired. In addition, there are other lipid kinases that selective inhibitors of the class I PI3Ks will need to avoid. These include the four mammalian PI4Ks, which generate PtdIns4P through phosphorylation of the 4-hydroxyl position

of the inositol ring of PtdIns and whose function is still the subject of investigation,<sup>48</sup> and the diacylglycerol kinases (DGKs), which phosphorylate diacylglycerol (DAG) to produce phosphatidic acid (PA).<sup>49</sup> The reduction in levels of DAG in cell membranes and the production of PA regulates many cellular responses and may be of therapeutic potential in various diseases, but should be avoided when targeting the class I PI3Ks.<sup>49</sup>

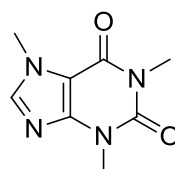
The current landscape of the development of selective PI3K $\delta$  inhibitors will be reviewed here.

#### 4.1.5. Small Molecule Inhibitors of PI3K $\delta$

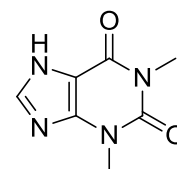
The first synthetic PI3K $\delta$  selective inhibitor was discovered by researchers at Icos (now part of Eli Lilly), who reported that compound IC87114 exhibited selectivity for PI3K $\delta$  ( $pIC_{50} = 6.3$ ) over the other class I isoforms (PI3K $\alpha$   $pIC_{50} < 4.0$ , PI3K $\beta$   $pIC_{50} = 4.1$  and PI3K $\gamma$   $pIC_{50} = 4.5$ ) and did not inhibit the related lipid kinases and PIKKs.<sup>41</sup> This compound is distantly related to the xanthine alkaloid caffeine, which demonstrates weak activity at the class I PI3Ks and some selectivity for PI3K $\delta$  (PI3K $\delta$   $pIC_{50} = 4.1$ , PI3K $\alpha$  and PI3K $\beta$   $pIC_{50} = 3.4$ , PI3K $\gamma$   $pIC_{50} = 3.0$ ) and theophylline, which has similar effects (PI3K $\delta$   $pIC_{50} = 4.1$ , PI3K $\alpha$   $pIC_{50} = 3.5$ , PI3K $\beta$  and PI3K $\gamma$   $pIC_{50} = 3.1$ ).<sup>50</sup>



IC87114

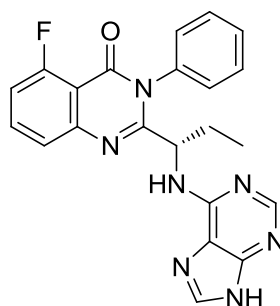


Caffeine



Theophylline

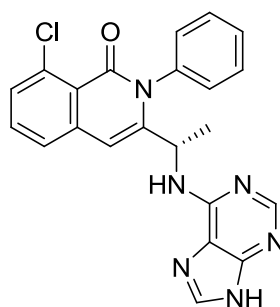
IC87114 was used extensively in determining the role of PI3K $\delta$  in leukocytes and has also been used to inhibit the proliferation and survival of malignant cells in acute myeloid leukaemia.<sup>32</sup> Further compounds from this series of quinazolinones were explored as selective PI3K $\delta$  inhibitors and idelalisib (GS-1101) was discovered to have selectivity against PI3K $\delta$  ( $pIC_{50}$  = 8.6) over the other class I isoforms (PI3K $\alpha$   $pIC_{50}$  = 6.1, PI3K $\beta$   $pIC_{50}$  = 6.2 and PI3K $\gamma$   $pIC_{50}$  = 7.1).<sup>51</sup>



Idelalisib

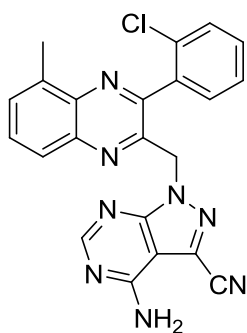
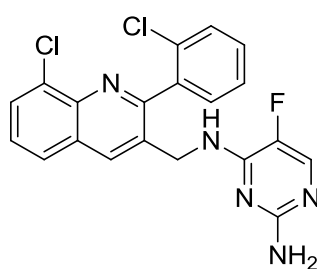
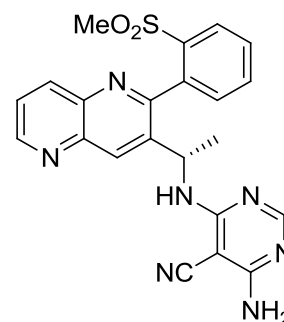
Idelalisib has since been developed as a first-in-class targeted therapy for chronic lymphocytic leukaemia (CLL), as it was shown in preclinical studies to promote apoptosis in CLL cells and not in normal T-cells or natural killer (NK) cells.<sup>52</sup> It also showed preclinical activity in non-Hodgkin lymphoma and is currently in Phase III clinical trials for the treatment of these diseases.<sup>53,54</sup>

A related compound is Duvelisib (IPI-145), which is also in clinical trials for the treatment of non-Hodgkin lymphoma (Phase II).<sup>55</sup> Duvleisib is a dual PI3K $\delta$  and PI3K $\gamma$  inhibitor with significant PI3K $\beta$  activity (PI3K $\delta$   $pIC_{50}$  = 9.4, PI3K $\gamma$   $pIC_{50}$  = 8.1, PI3K $\beta$   $pIC_{50}$  = 7.2 and PI3K $\alpha$   $pIC_{50}$  = 5.6) and is currently the only PI3K inhibitor in Phase II clinical trials for the treatment of inflammatory disease, including asthma and rheumatoid arthritis.<sup>55,56</sup>



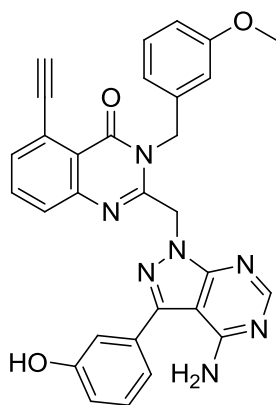
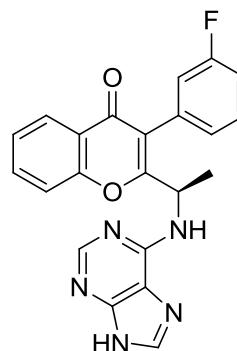
Duvelisib

Another selective PI3K $\delta$  inhibitor currently in clinical development is AM-319, a compound developed by Amgen; it is currently undergoing Phase I trials for the treatment of lymphoid malignancies.<sup>57</sup> Although the structure has not been disclosed, it is believed that it is closely related to that of IC-87114, with the core being either a quinoxaline (**155**) or quinoline (**156**).<sup>58</sup> Compounds from this series have been claimed as treatments for inflammatory disorders as well as for cancers.<sup>59</sup> A recent patent filing from Amgen discloses novel 1,5-naphthyridines as selective PI3K $\delta$  inhibitors (**157**).<sup>60</sup>

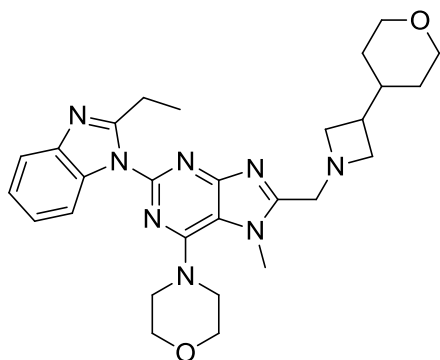
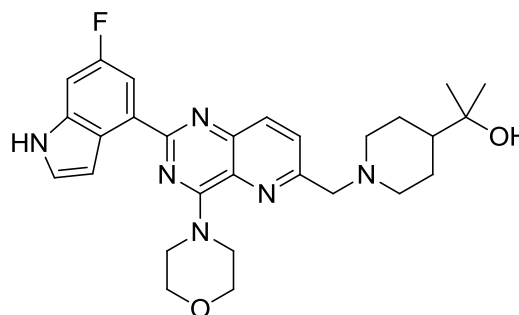
**155****156****157**

Respivert's quinazolinones (**158**) and Rhizen's chromone compounds (**159**) are selective PI3K $\delta$  inhibitors with pharmacophores similar to those of the Gilead and Amgen compounds.<sup>58</sup> Both these companies have claimed compounds for the treatment of inflammatory disorders, with **158** (Respivert) for the treatment of COPD and **159** (Rhizen) showing pre-clinical efficacy in asthma.<sup>58</sup>



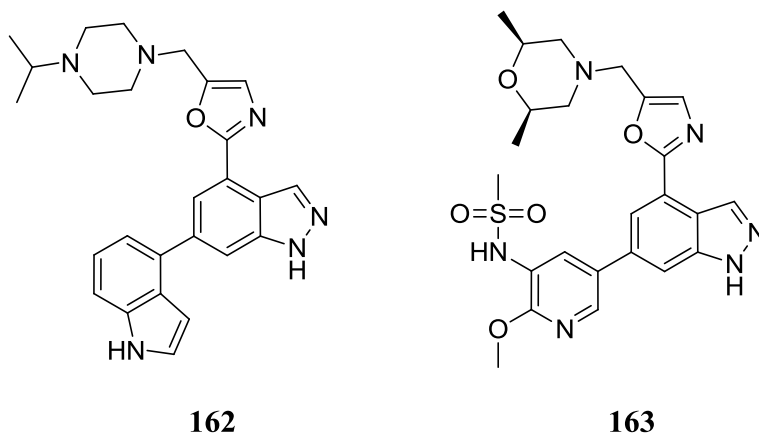
**158****159**

PI3K $\delta$  inhibitors with structures different to the compounds discussed so far have also been claimed by Piramed/Roche for the treatment of inflammatory diseases. The majority of these compounds contain a 4-morpholinylpyrimidine fragment fused to a second ring system, as in 7-methyl-7*H*-purine **160**.<sup>61,62</sup> Pyrido[3,2-*d*]pyrimidine **161** has recently been described as the most selective inhibitor from this series with  $\geq 200$ -fold selectivity over the other class I isoforms.<sup>63</sup>

**160****161**

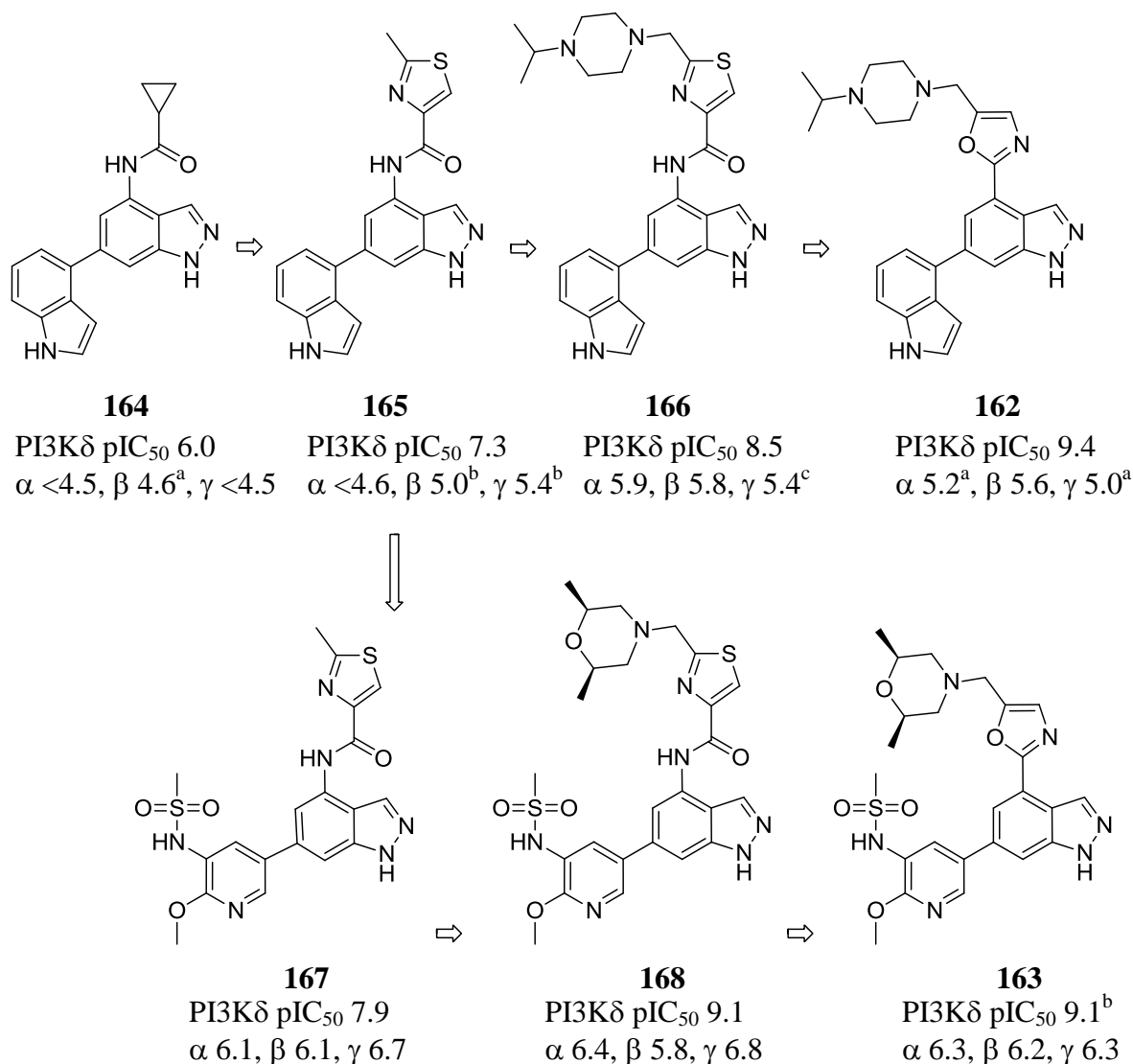
A different pharmacophore was explored by our medicinal chemistry team while they were developing PI3K $\delta$  inhibitors as inhaled drugs for the treatment of respiratory diseases. 4,6-Disubstituted indazoles were found to be potent and selective inhibitors of PI3K $\delta$ .<sup>64</sup> This series originated from a focused set screen for

the protein kinase PIM-1. The original hit series had issues with selectivity over GSK3 $\beta$  and the team modified the structure of the initial hit compound, which led to a change in the kinase profile to give a selective lead series for PI3K $\delta$ . Compound **162** has recently completed Phase I clinical trials to assess safety and tolerability.<sup>65</sup> Compound **162** has a pIC<sub>50</sub> of 9.0 and >1000-fold selectivity against the other PI3K isoforms as well as other lipid and protein kinases. A second, related compound was also identified from this programme of work. Compound **163** has similar potency and selectivity (>1000-fold) but has a different developability profile to that of compound **162**.<sup>66</sup>



The discovery of these compounds followed early work which looked to improve the PI3K $\delta$  potency of compound **164**; this compound contained a cyclopropyl amide substituent at the indazole 4-position and was the first compound with moderate potency for PI3K $\delta$  and selectivity over the other isoforms to be discovered (Scheme 4.1.1).<sup>64</sup> Thiazolyl amide **165** was found to increase PI3K $\delta$  activity and it was postulated that the presence of an *ortho*-heteroatom was critical as it ensured co-planarity of the amide and indazole core, elevating potency (Scheme 4.1.1).<sup>67</sup> The 6-position substituent was explored extensively, with biaryl replacements indicating that the indole was an important contributor to potency and selectivity. Monoheterocyclic arenes were also investigated and the pyridyl sulfonamide of compound **167** was discovered to have excellent potency (Scheme

4.1.1).<sup>67</sup> The addition of pendant lipophilic amine groups improved potency and isoform selectivity and a final iteration in which the amide was replaced with a substituted oxazole led to the candidate compounds (Scheme 4.1.1).<sup>67</sup>



<sup>a</sup> Returned values <4.6 on two test occasions. <sup>b</sup> Returned value <4.6 on one test occasion. <sup>c</sup> Returned no value on one test occasion.

Scheme 4.1.1. Inhibitor evolution and the discovery of compounds **162** and **163**.

The development of these compounds was aided significantly by the availability of a crystal structure of the kinase, which allowed for structure-based design of isoform selective inhibitors.

#### **4.1.6. The Impact of Structural Biology on the Design of Selective Inhibitors**

The class I PI3K isoforms have a high degree of sequence homology within their ATP-binding sites, and the primary sequence and three-dimensional structure is conserved across the human kinome, so developing selective inhibitors of PI3K $\delta$  is challenging. The elucidation of co-crystal structures of the class I PI3Ks has led to a greater understanding of the binding modes of small molecules, allowing significant progress in the development of isoform selective inhibitors.

The resolution of the p110 $\delta$  catalytic core was achieved in 2010 and co-crystal structures with selective PI3K $\delta$  inhibitors were reported.<sup>68</sup> This allowed the regions that are important for inhibitor binding to be defined.

The hinge-binding region contains residues 825-828, which link the *N*- and *C*-terminal lobes of the catalytic domain. Val828 is a key active site residue since its backbone amide forms a hydrogen bond with small molecule inhibitors.<sup>68</sup> The co-crystal structure of the PI3K $\delta$  selective inhibitor IC87114 shows this characteristic hydrogen bond to the adenine N1 (Figure 4.1.5). The backbone carbonyl of Glu826 also makes an additional interaction with the 6-amino substituent of the adenine group (Figure 4.1.5).

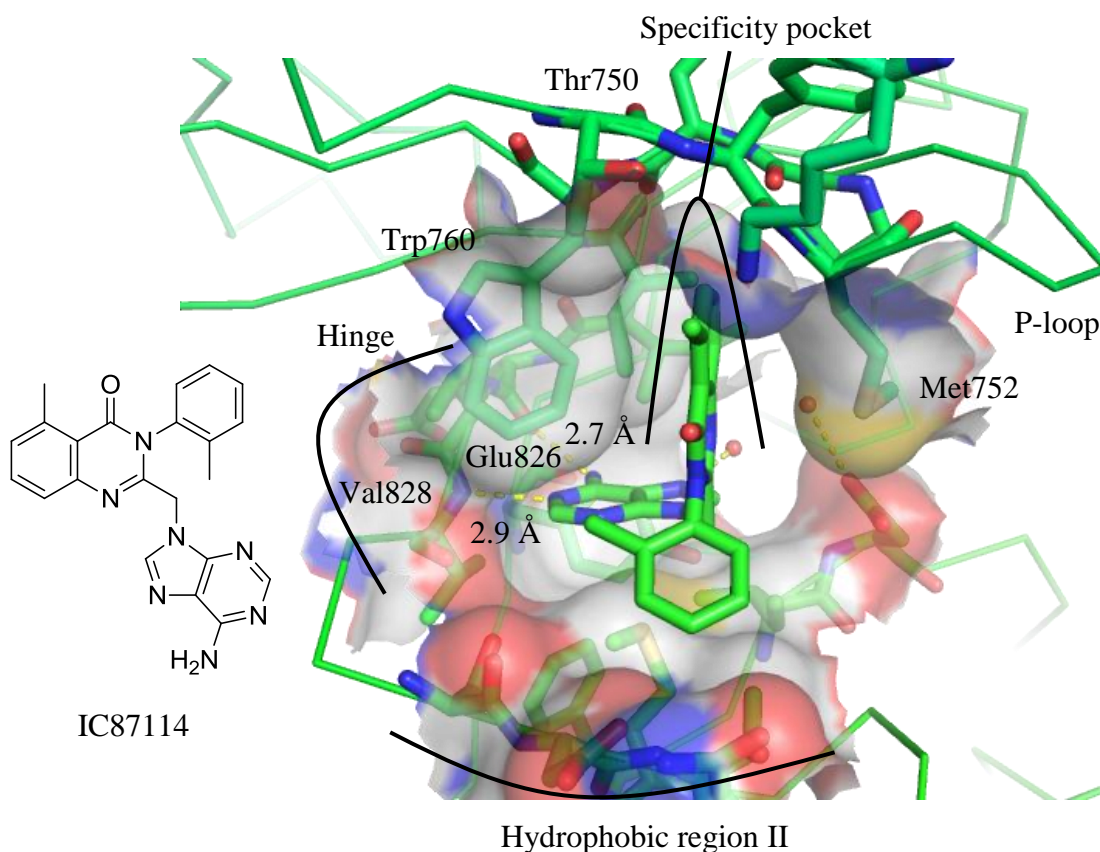


Figure 4.1.5. Active site of p110 $\delta$  in complex with IC87114.<sup>68</sup>

IC87114 adopts a propeller shape within the active site; the ligand then induces a conformational change in the p110 $\delta$  protein, in which a hydrophobic specificity pocket, absent from the apo-structure, is opened between Trp760 and Met752 (Figure 4.1.5).<sup>68</sup> The quinazoline substituent of IC87114 occupies this pocket and the *ortho*-tolyl substituent is projected out towards another hydrophobic region located at the mouth of the active site, referred to as hydrophobic region II (Figure 4.1.5).<sup>68</sup>

The conformational change that occurs when a substituent opens the specificity pocket can lead to selectivity for binding to p110 $\delta$ , since it is more flexible than the other isoforms, and can accommodate opening of the specificity pocket by a local change in the conformation of the P-loop, which comprises residues 752-758 (Figure 4.1.5).<sup>68</sup> This does not occur when the equivalent pocket is

opened in other isoforms; for example in p110 $\gamma$ , the conformational change has been seen to cause movement of the *N*-terminal lobe.<sup>68</sup>

Idelalisib can also adopt the propeller shape that induces the specificity pocket; however other PI3K $\delta$  inhibitors achieve selectivity without bringing about this conformational change. For example, the class of inhibitors described by Piramed/Roche exploit a different area of the protein where sequence differences are apparent between the four PI3K isoforms. These residue differences lie around the solvent exposed area at the entrance to the active site. There are only three positions that differ; these are Thr750 (Lys802 in PI3K $\gamma$ ), Asp832 (Thr886 in PI3K $\gamma$ ) and Asn836 (Lys890 in PI3K $\gamma$ ). A co-crystal structure of the 4-morpholinylpyrimidine compound **169** reported by Piramed/Roche bound to PI3K $\gamma$  showed that the morpholine binds to the hinge and the 4-substituted piperidine occupies the region in front of the conserved tryptophan residue (Figure 4.1.6.).<sup>63</sup>

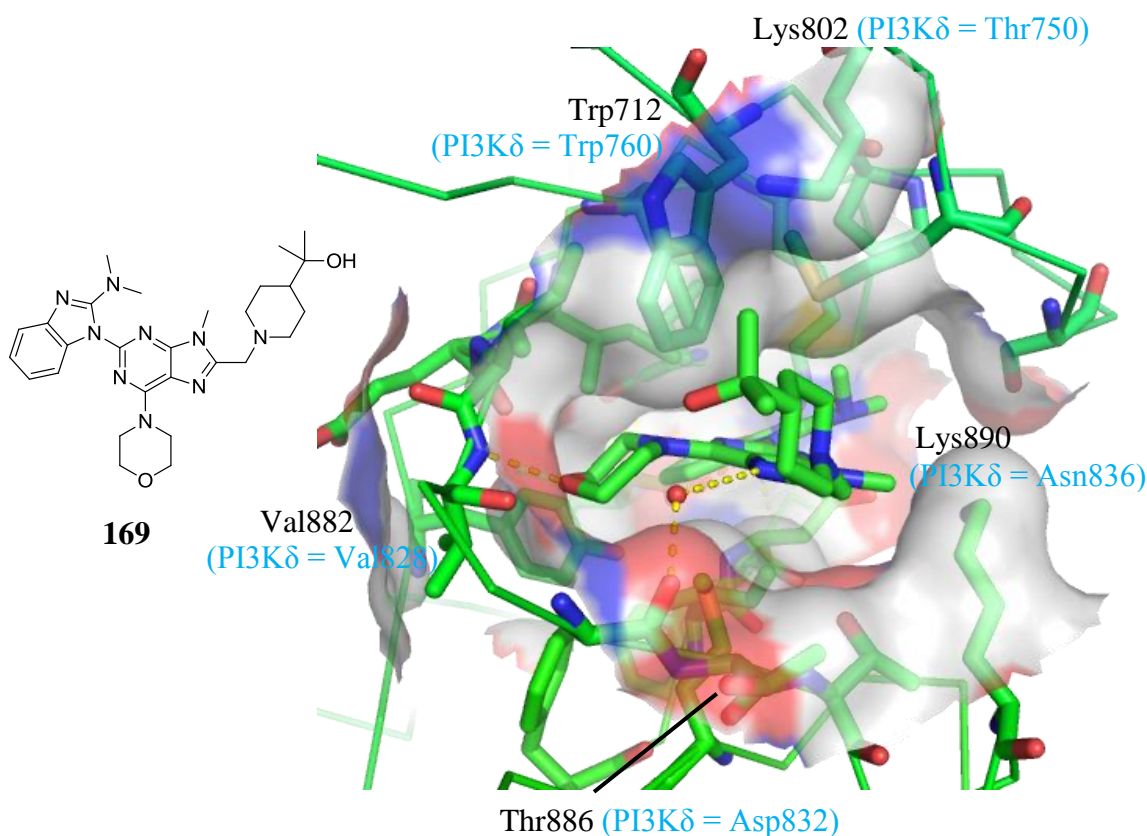


Figure 4.1.6. Co-crystal structure of **169** bound to PI3K $\gamma$  (PI3K $\delta$  residues shown in blue).<sup>63</sup>

In PI3K $\delta$  there is a small threonine residue (Thr750) above Trp760 that creates a ‘tryptophan shelf’, but this residue is a much larger and basic arginine in PI3K $\alpha$ , and lysine in PI3K $\beta$  and PI3K $\gamma$  (Figure 4.1.7).<sup>63</sup> Since the tryptophan shelf is not present in the other isoforms, substituents that occupy this region can confer selectivity for PI3K $\delta$ .



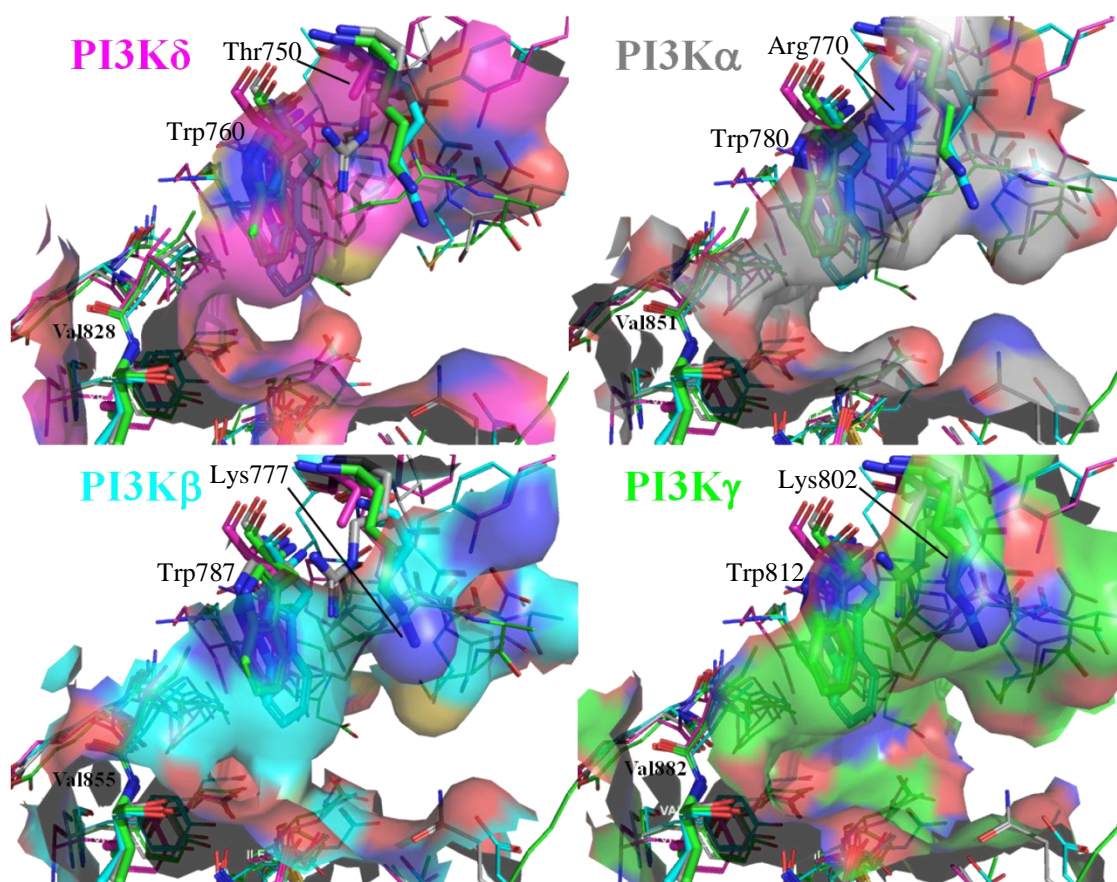


Figure 4.1.7. Residue differences between the PI3K isoforms.

Co-crystal structures of our indazole series of selective PI3K $\delta$  inhibitors showed that these compounds also occupied the tryptophan shelf and hence did not achieve selectivity by opening the specificity pocket.<sup>67</sup> This co-crystal structure and all those subsequently reported in this Chapter were determined within GSK.<sup>69</sup>

The co-crystal structure of compound **162** bound to PI3K $\delta$  shows that the indazole nitrogens engage in hydrogen bonds with Val828 and Glu826 in the hinge-binding region (Figure 4.1.8). The pendant amine group can be accommodated on the tryptophan shelf because of the small threonine residue of PI3K $\delta$ , whereas there would be steric and electronic clashes with the lysine and arginine residues of the other isoforms (Figure 4.1.8).



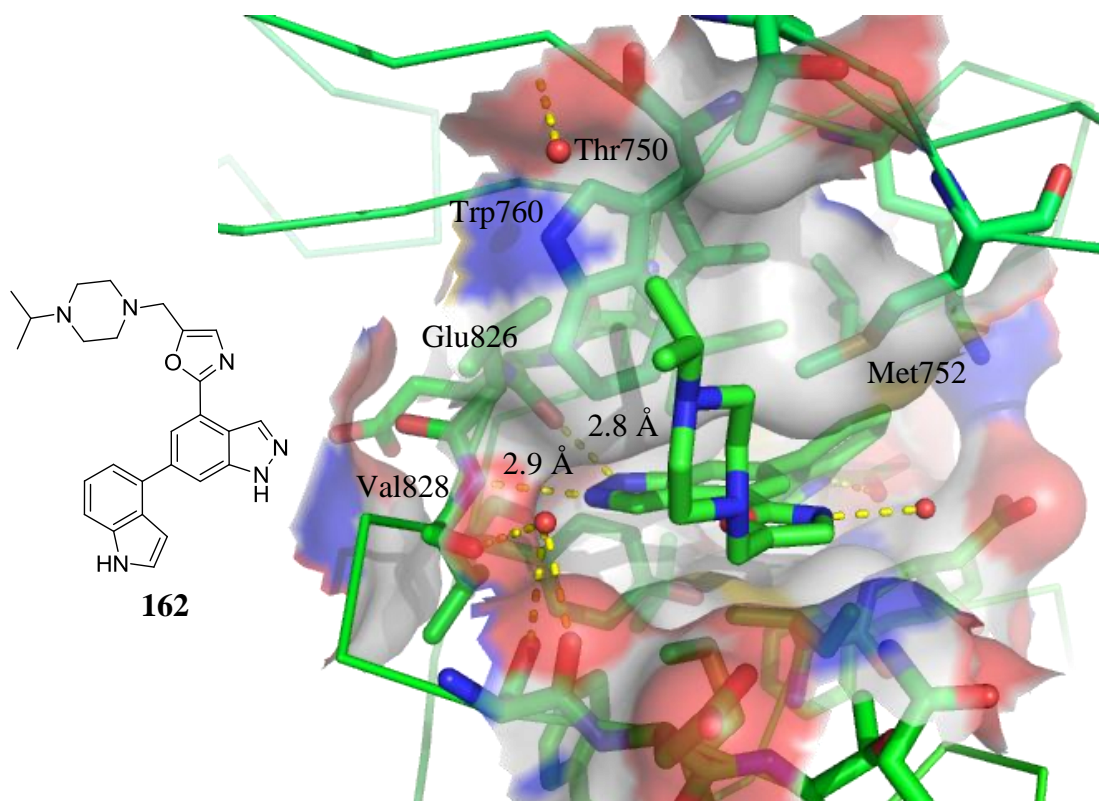


Figure 4.1.8. Co-crystal structure of compound **162** bound to PI3K $\delta$ .

The indole substituent occupies a region of the ATP-binding site denoted as the affinity pocket, in which the triphosphate group of ATP binds. This pocket is defined by the residue Lys779 on the top and Asp787 on the bottom (Figure 4.1.9). This region presents an opportunity for hydrogen-bonding interactions to these side chains, as well as to others such as Asp911 and Tyr813, which can lead to substantial increases in PI3K $\delta$  potency.<sup>68</sup> The indole moiety forms a hydrogen bond with Asp787 that makes a significant contribution to the binding affinity (Figure 4.1.9). A decrease in PI3K $\delta$  pIC<sub>50</sub> of 2 log units was observed on methylating the indole nitrogen.

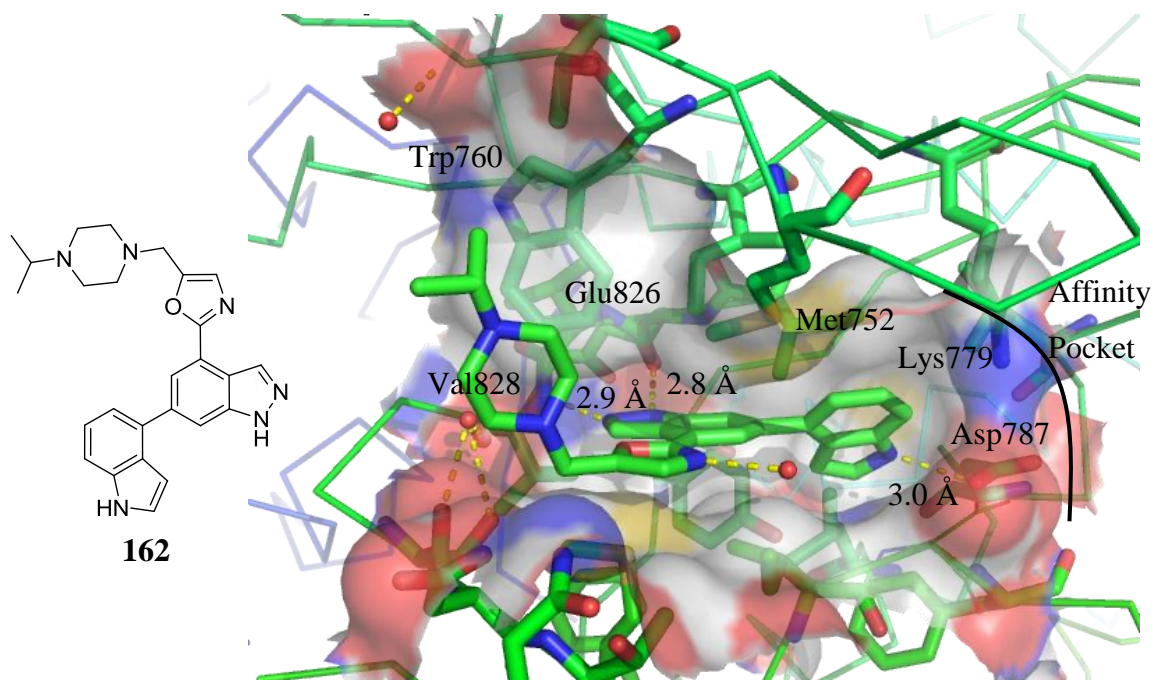


Figure 4.1.9. Compound **162** bound in the affinity pocket of PI3Kδ.

The selectivity arising from binding the indole in the affinity pocket could be attributed to this substituent enabling optimal positioning of the hydrogen bond network between the backbone residues Tyr813 and His909 (Figure 4.1.10).

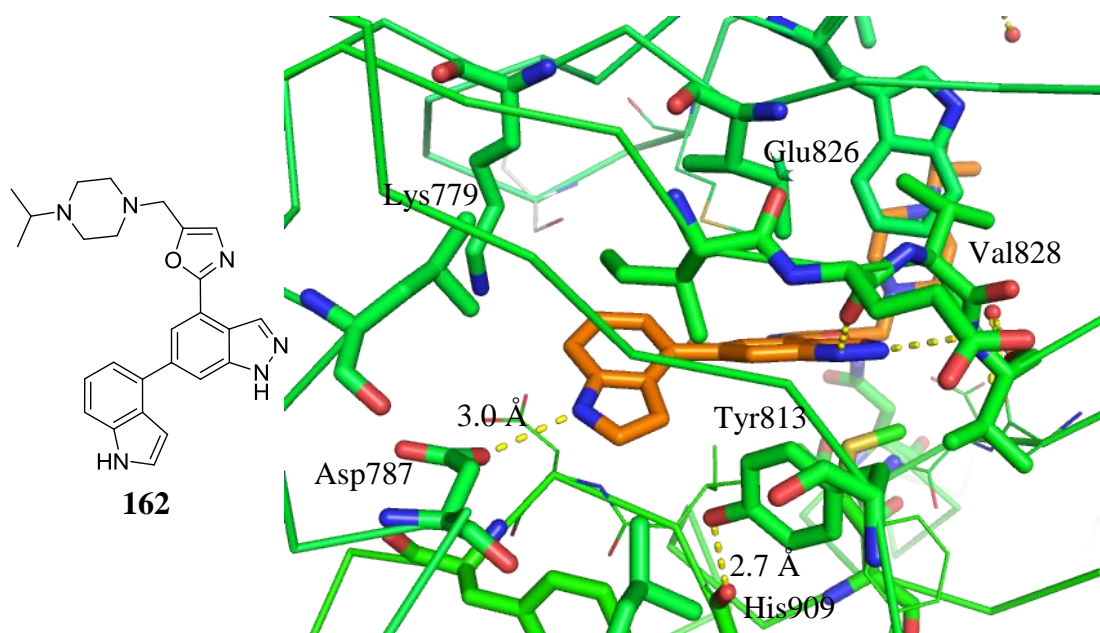


Figure 4.1.10. Hydrogen bond network in the affinity pocket when compound **162** is bound.

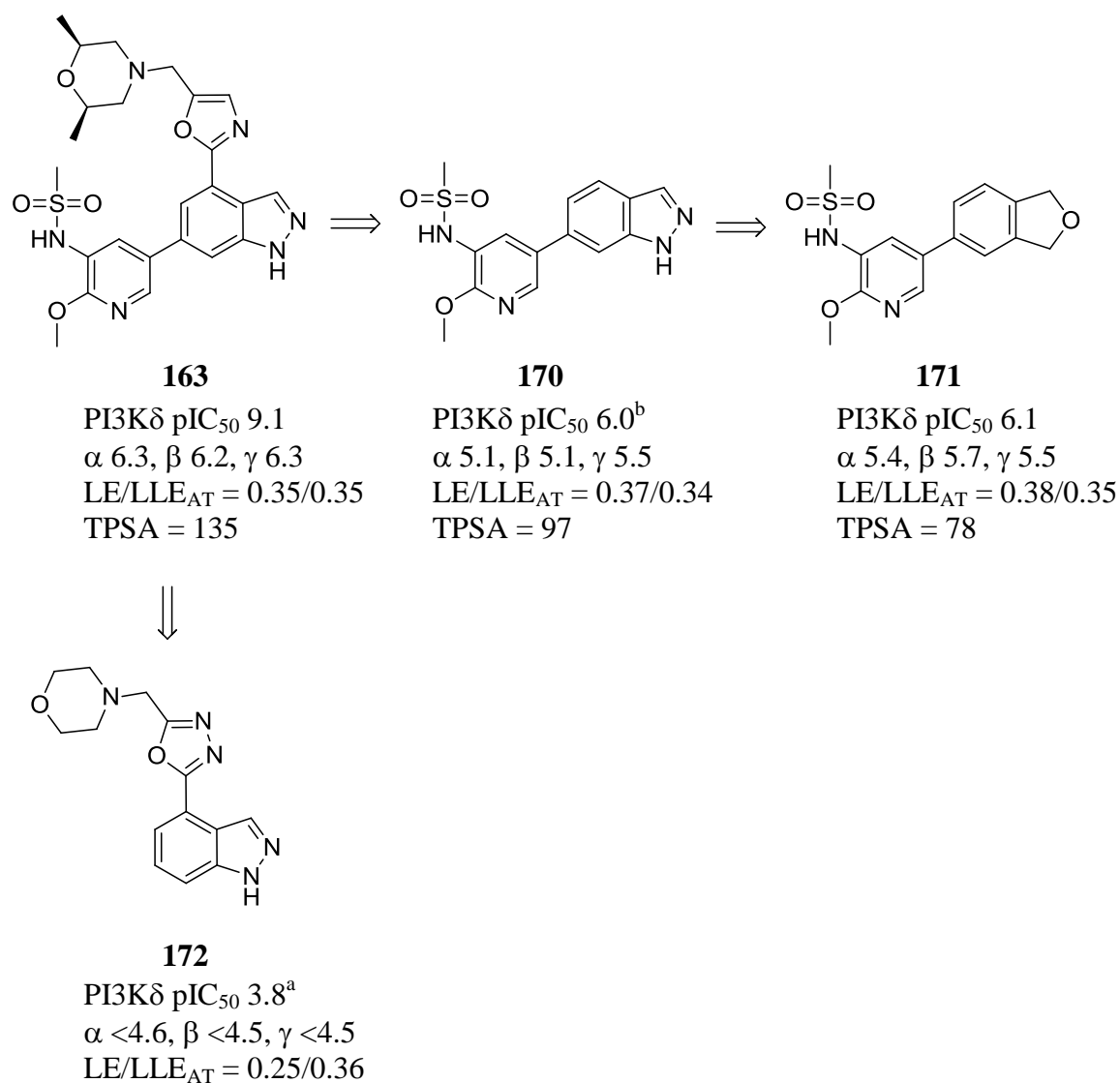
It was observed that replacement of the indole with an indazole led to a decrease in potency for PI3K $\delta$  of approximately 10-fold. A significant decrease in selectivity for PI3K $\delta$  over the other three PI3K isoforms was also observed (approximately a 300-fold difference). The formation of a hydrogen bond with Tyr813 caused a reorganisation of the hydrogen bonding network in this area of the protein and despite the additional interaction, this was detrimental to potency and selectivity. Since the affinity pocket is conserved across the PI3K isoforms, binding of the indole moiety must trigger conformational changes that extend past this region and result in the specificity observed for PI3K $\delta$ . Other groups have also reported that the selectivity for PI3K $\delta$  is eroded when this hydrogen bond network is altered and the distance between the tyrosine and histidine oxygens is increased.<sup>63</sup>

The indazole compounds were highly potent and selective inhibitors of PI3K $\delta$ , and they had a PK profile suitable for inhaled delivery, with low oral bioavailability in rat and dog. This ensured that the systemic exposure was low, since ~80% of the dose is swallowed during inhalation. However, since the majority of the

competitor compounds are being developed as oral drugs, a programme of work to identify a novel oral PI3K $\delta$  inhibitor was initiated to address the risk that the inhaled assets could be displaced by a successful oral PI3K $\delta$  inhibitor from a competitor. The strategy for this work was to take forward the successful indazole series and build in consistent oral exposure.

#### **4.1.7. 4,6-Dihydroisobenzofurans as Oral PI3K $\delta$ Inhibitors**

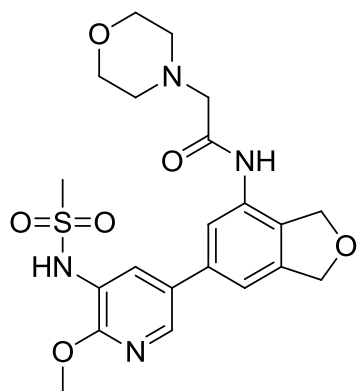
The physicochemical properties of the molecules discovered to date in our laboratories were modified in order to achieve oral exposure with the indazole series of compounds.<sup>70</sup> Compound **163** was truncated to assess the binding efficiency of the fragments and it was observed that occupancy of the affinity pocket by the pyridyl sulfonamide substituent was crucial for high ligand efficiency (compare **163** and **172**, Scheme 4.1.2). Modifying the indazole core to a dihydroisobenzofuran maintained PI3K $\delta$  potency and ligand efficiency (compare **170** and **171**, Scheme 4.1.2), while the isoform selectivity was similar and both the polar surface area and the number of aromatic rings were decreased (Scheme 4.1.2).



<sup>a</sup> Returned value <4.6 on one test occasion. <sup>b</sup> Returned value <4.5 on one test occasion.

Scheme 4.1.2. Discovery of dihydroisobenzofuran core.

The introduction of an amide substituent at the 4-position led to the discovery of compound **173**, which was the initial lead dihydroisobenzofuran compound to show potential as an oral PI3K $\delta$  inhibitor (Figure 4.1.11).<sup>70</sup>

**173**PI3K pIC<sub>50</sub> δ = 6.8, γ = 5.0, β = 5.0, α = 5.3HWB pIC<sub>50</sub> = 6.5<sup>a</sup>LE = 0.29; LLE<sub>AT</sub> = 0.33

clogP = 1.6

mChromlogD<sub>pH7.4</sub> = 2.59

PFI = 4.6

MW = 463

PSA = 119

hERG pIC<sub>50</sub> < 4.3CYP 3A4 pIC<sub>50</sub> < 4.3

AMP (pH 7.4) = 135 nm/sec

FaSSIF solubility = 20 µg/mL

Rat Cl<sub>b</sub> = 14 ml/min/kg

Rat F = 54%

Key: Good, acceptable, poor

<sup>a</sup> Returned no value on two test occasions.

Figure 4.1.11. Lead dihydroisobenzofuran compound.

Compound **173** has moderate PI3Kδ enzyme potency and lower ligand efficiency than the 4-unsubstituted analogue; however the compound shows increased selectivity over the other PI3K isoforms. The compound has moderate whole blood activity and good permeability but poor FaSSIF solubility. The compound was orally absorbed; it had low blood clearance and an oral bioavailability of 54%, obtained from a rat *in vivo* pharmacokinetic study.<sup>71</sup> This *in vivo* PK data and all that subsequently reported in this Chapter were determined within the DMPK group at GSK. Although the compound has high molecular weight, it has an acceptable lipophilicity and hence a PFI of 4.6. In addition, the compound has no hERG or CYP liabilities.

Compound **173** has been co-crystallised with PI3Kδ and the dihydroisobenzofuran oxygen forms the key hydrogen bond with the backbone amide of Val828 (Figure 4.1.12). This hinge-binding interaction leads to acceptable binding efficiency despite the potentially weaker hydrogen bond expected with the

ether oxygen and the absence of the additional interaction with Glu826, which was observed for the indazole compounds. A comparison of pairs of compounds where the only change was the hinge binder showed that the dihydroisobenzofuran compound was approximately 0.5 log units less potent than the indazole analogue. The substituent at the 4-position of the dihydroisobenzofuran projects towards Trp760 (Figure 4.1.12).



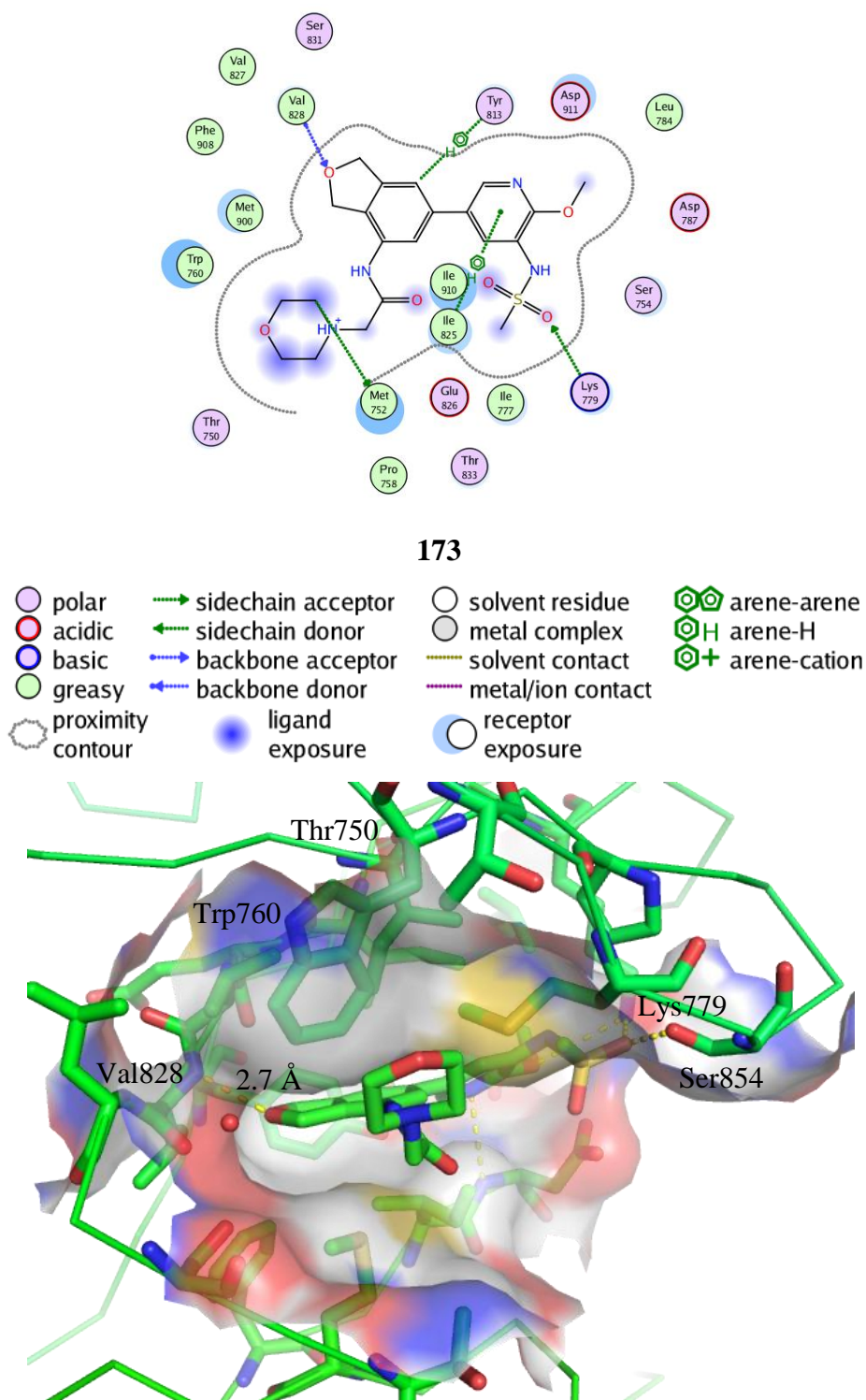


Figure 4.1.12. PI3K $\delta$  in complex with compound **173**.



The substituent at the 6-position occupies the affinity pocket and the sulfonamido oxygen forms hydrogen bonds with both Lys779 and Ser754 (Figure 4.1.13). In addition, it is thought there is an interaction between the protonated Lys779 residue and the sulfonamide nitrogen, which is acidic ( $pK_a \sim 8$ ) and significantly ionised at physiological pH (pH 7.4). Hydrogen bonds involving charged donors or acceptors have been observed to be shorter than those between neutral motifs, indicating stronger interactions.<sup>72</sup> In this case, the interaction between the sulfonamide anion and Lys779 contributes significantly to the binding affinity, with a drop in PI3K $\delta$   $pIC_{50}$  by 1000-fold observed when replacing the sulfonamide with the analogous sulfone.

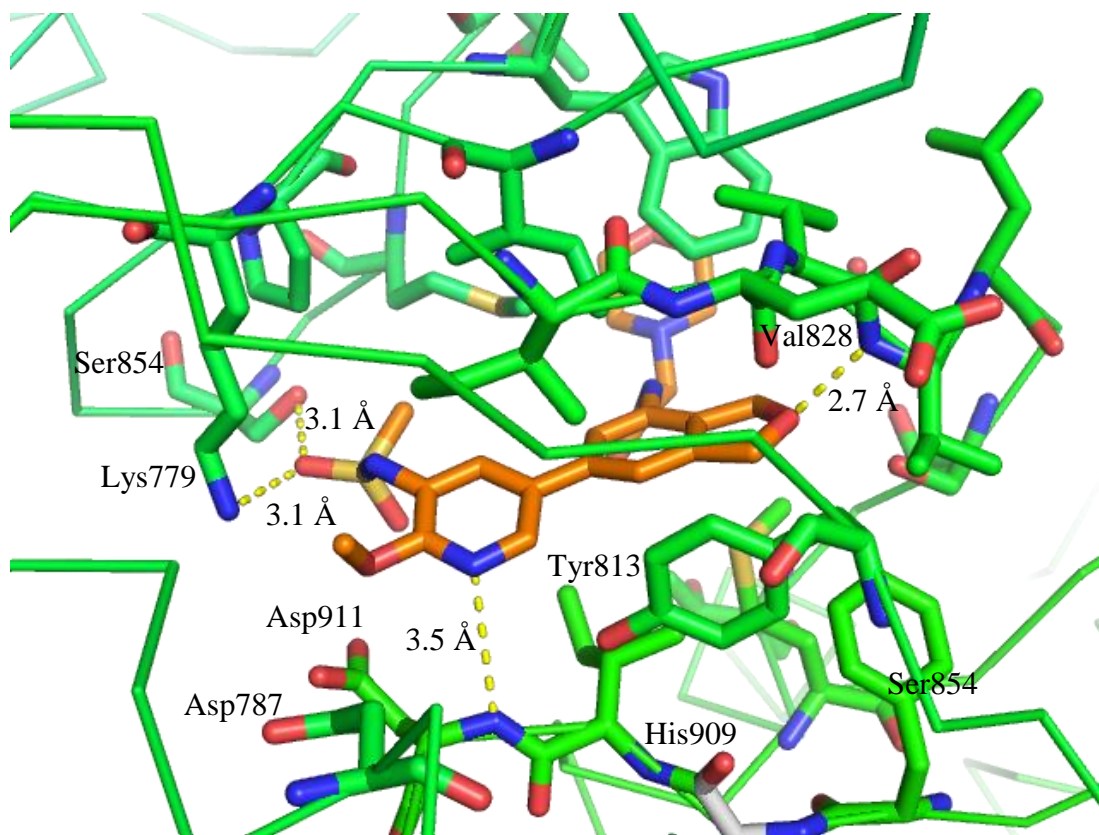


Figure 4.1.13. Pyridyl sulfonamide **173** bound in the affinity pocket of PI3K $\delta$ .

## 4.2. Aims

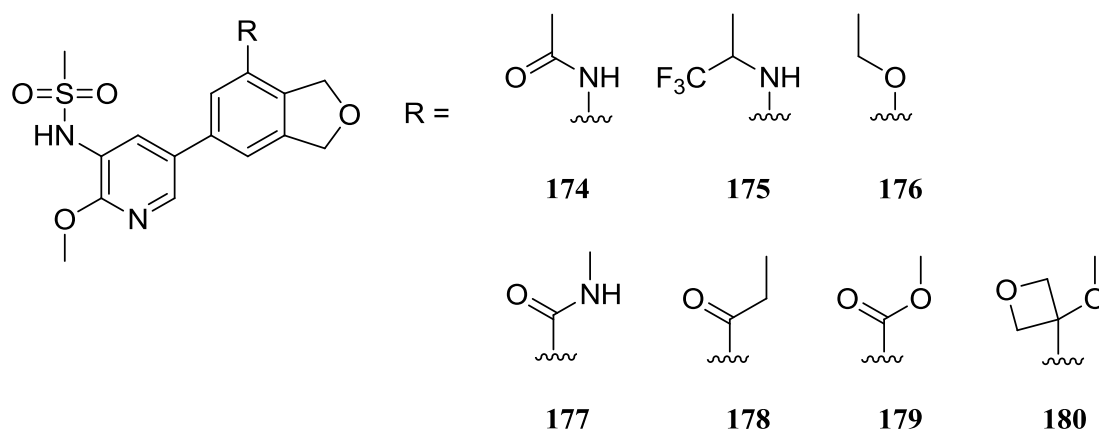
Building from knowledge acquired in our laboratory to date and directly from the results obtained for compound **173**, the aims of the current research are to deliver a compound which has a suitable oral PK profile, good PI3K $\delta$  whole blood potency and 100-fold selectivity over the other PI3K isoforms and a wider set of kinases. The compound must have no potential toxicities (e.g. hERG, CYP) and must achieve high oral bioavailability; the physicochemical properties of the molecule must therefore be within low attrition guidelines for oral drugs.<sup>73,74</sup> This includes a PFI less than 7.0 and good FaSSIF solubility. With the desired pharmacokinetic profile and whole blood potency, it is expected that the predicted human dose will be low as required.

The desired molecular profile for an oral PI3K $\delta$  inhibitor is shown in Table 4.2.1.

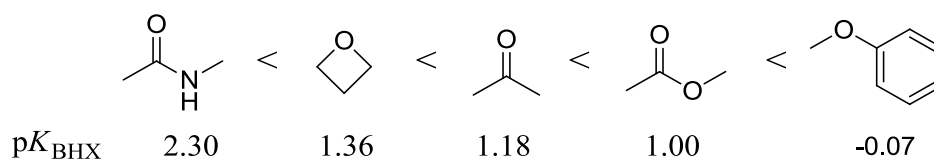
Parameter	Desired value
PI3K $\delta$ pIC <sub>50</sub>	>8.0
PI3K isoform selectivity	>100-fold
Wider kinase selectivity	>100-fold
HWB pIC <sub>50</sub>	>7.0
PFI	<7.0
LE	>0.3
LLE <sub>AT</sub>	>0.3
hERG pIC <sub>50</sub>	<4.3
CYP 3A4 pIC <sub>50</sub>	<4.3 (all)
FaSSIF solubility	>100 $\mu$ g/mL
Permeability	High
Clearance	Low
Bioavailability	High

Table 4.2.1. Desired molecular profile of an oral PI3K $\delta$  inhibitor.

Firstly, compounds which could be used to explore the effect of different functionalities at the dihydroisobenzofuran 4-position on PI3K $\delta$  potency and selectivity over the other PI3K isoforms were designed. An initial set looked to investigate the effect of hydrogen bond donors and acceptors at this position and reveal the impact that different linker conformations have on activity and selectivity.<sup>75</sup>

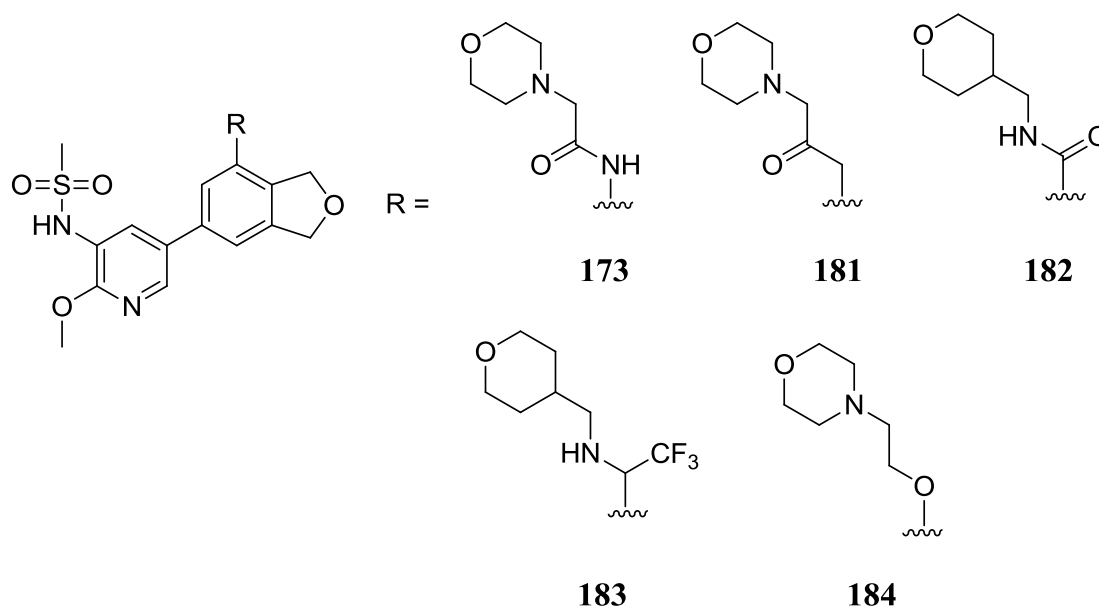


Amides **174** and **177** provided a useful pairwise comparison and ketone **178** and ester **179** allowed assessment of the effect of removing a hydrogen bond donor from the linker. The ether **176** helped to assess both the optimal positioning of the hydrogen bond acceptor and any conformational effects on potency and selectivity. As was observed in Chapter 3, the oxetanyl group can resemble a carbonyl and can act as a hydrogen bond acceptor. The set has a range of functionalities with different hydrogen bonding capabilities. The basicity of hydrogen bond acceptors has been described by the  $pK_{\text{BHx}}$  scale, where X is the reference hydrogen bond donor 4-fluorophenol and B represents different Lewis bases that may act as hydrogen bond acceptors.<sup>76</sup> Large positive values of  $pK_{\text{BHx}}$  represent strong hydrogen bond acceptors, since the formation of the hydrogen bonded complex  $4\text{-FC}_6\text{H}_4\text{OH}\cdots\text{B}$  is favoured and hence a low dissociation constant ( $K_{\text{BHx}}$ ) is measured. On this scale, the strongest hydrogen bond acceptor is the amide carbonyl and the weakest is the acyclic ether.  $pK_{\text{BHx}}$  values for the functional groups can be seen in Figure 4.2.1.<sup>76</sup>

Figure 4.2.1. Hydrogen bond basicities.<sup>76</sup>

In addition to assessing the positioning and potential of hydrogen bonding interactions with the linkers, the size and shape of the groups was investigated *via* this set of truncated compounds. The oxetanyl and trifluoropropylamine groups provided information on how bulkier groups affect potency and selectivity.

A further set of compounds was also synthesised. These compounds were not truncated as the inclusion of pendant groups was synthetically tractable and would allow for better comparisons with compound **173**. The keto- and benzamido-analogues of compound **173** were synthesised (**181** and **182**, respectively), as well as a compound in which the benzamido group was replaced with a trifluoroethylamino-unit (**183**). A fully elaborated ether compound (**184**) was also synthesised.



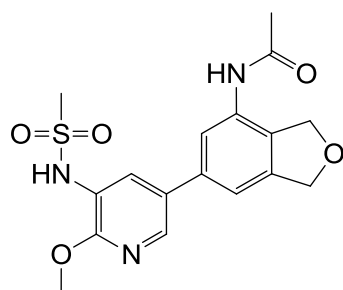
Information from the biological data obtained for these compounds was taken into consideration for the next iteration of compound design. The optimal linker atoms were utilised and investigations around the pendant groups followed in order to improve PI3K $\delta$  potency and selectivity. Compounds that had the desired pharmacodynamic profile were progressed to pharmacokinetic studies. The findings from these studies were then used to optimise the PK profile further.

## 4.3. Results and Discussion

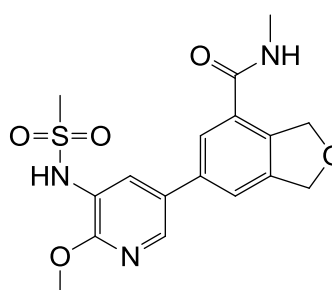
### 4.3.1. Exploration of Dihydroisobenzofuran 4-Position

#### 4.3.1.1. Synthesis of Truncated Compounds 174-180

Compounds **174** and **177** had been synthesised elsewhere in our laboratory.<sup>77</sup>



**174**

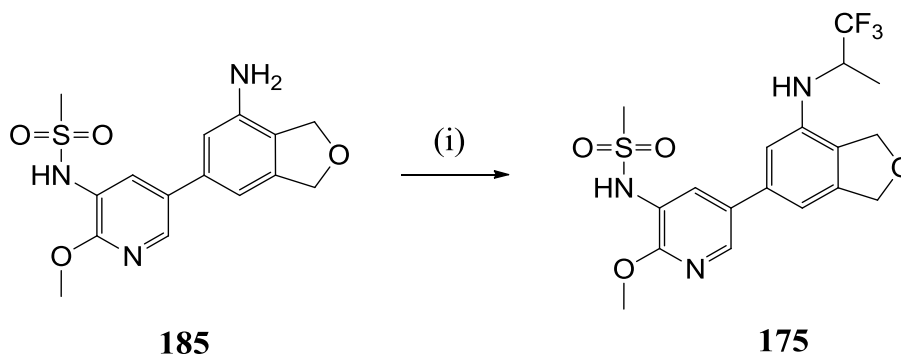


**177**

Synthesis of the trifluoromethyl-containing analogue of anilide **174** was investigated. Amine intermediate **185** (Scheme 4.3.1) had been previously synthesised within our laboratory so a direct reductive amination reaction with trifluoroacetone using sodium triacetoxyborohydride (STAB) and acetic acid was attempted. STAB is widely used for reductive amination reactions since it generally does not reduce the carbonyl group prior to imine formation and is preferred to

sodium cyanoborohydride as it is less toxic.<sup>78</sup> Unfortunately, the conditions were ineffective; no desired product was observed and only unreacted starting material was isolated. The poor nucleophilicity of the aromatic amine may have hindered imine formation and so the condensation reaction did not occur, despite the addition of a stoichiometric amount of acetic acid to aid the reaction. Indirect reductive amination involving isolation of the imine prior to the reduction was therefore attempted. However, using either titanium tetrachloride and triethylamine in DCM, or *para*-toluenesulfonic acid in refluxing toluene with molecular sieves, proved unsuccessful and led only to the isolation of unreacted starting material, corroborating the observation that the initial condensation of the amine and ketone was difficult.

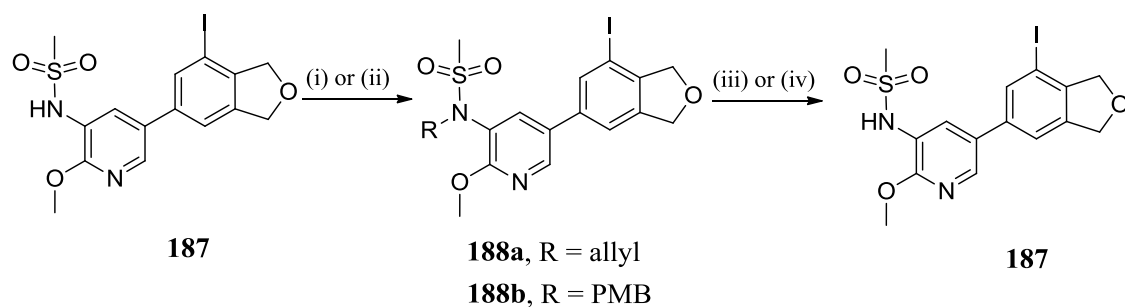
Sodium cyanoborohydride was introduced by Borch in 1971 and is the best known reducing agent for reductive aminations (although it has toxicity issues so is less preferred).<sup>79</sup> This reagent is stable in strongly acidic solutions and the addition of a stronger acid could promote the condensation reaction required here. A direct reductive amination with trifluoroacetone using sodium cyanoborohydride in TFA was successful, yielding the desired product (Scheme 4.3.1).



Reagents and Conditions: (i) Trifluoroacetone, NaBH<sub>3</sub>CN, TFA, 0 °C to rt, 23%.

Scheme 4.3.1. Synthesis of compound **175**.



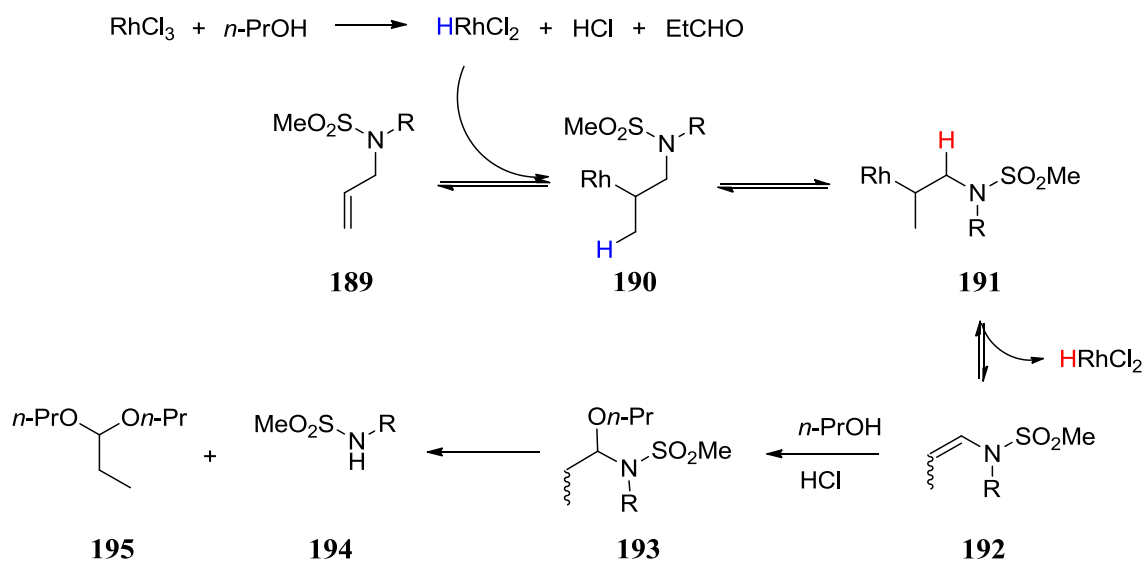


Reagents and Conditions: (i) allyl bromide, KF on alumina, MeCN, 60 °C, 100%; (ii) NaH, PMBCl, DMF, 0 °C to rt, 85%; (iii) R = allyl: RhCl<sub>3</sub>, 1-propanol, 98 °C; (iv) R = PMB: TFA, DCM, 80 °C.

Scheme 4.3.3. Investigation of protecting group strategy.

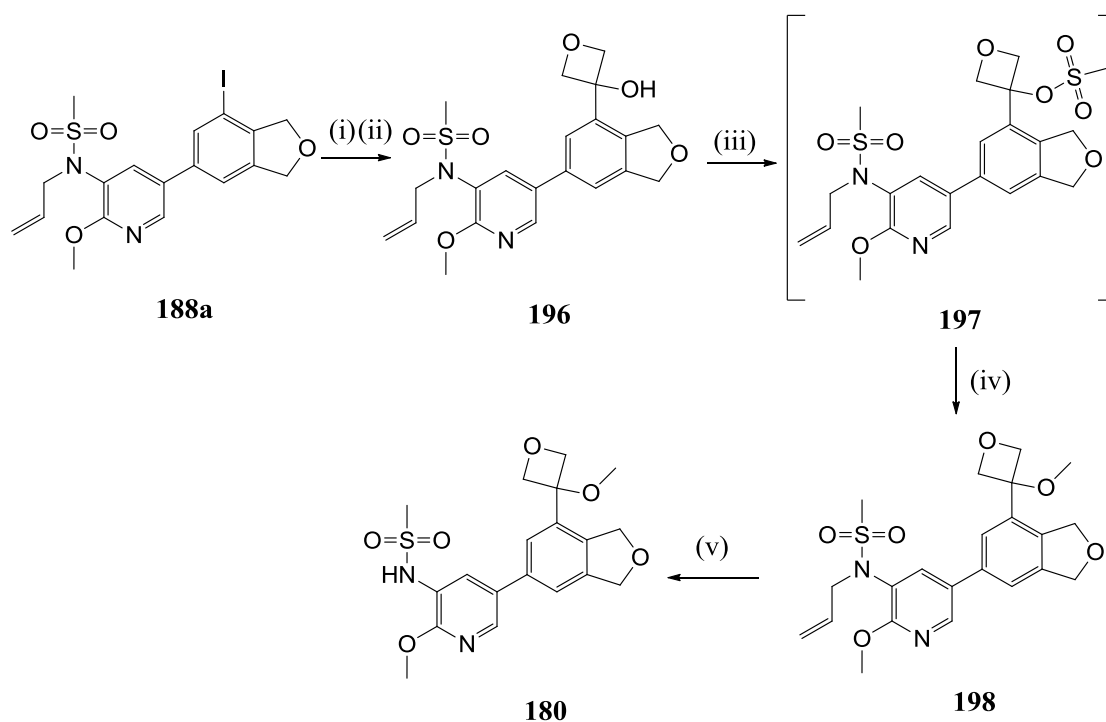
A one-step rhodium(III) chloride catalysed deprotection of acyclic *N*-allyl amides reported in the literature was applied to the deallylation of the secondary sulfonamide substrate synthesised here.<sup>80</sup> The deprotection occurs *via* olefin isomerisation that is facilitated by a rhodium hydride species formed from the reaction of rhodium(III) chloride and the alcoholic solvent at elevated temperature (Scheme 4.3.4).<sup>81</sup> Hydrochloric acid generated from this reaction catalyses conversion of the resulting enamine to the secondary sulfonamide and propionaldehyde dipropyl acetal (Scheme 4.3.4).<sup>80</sup>





Scheme 4.3.4. Deallylation of a secondary sulfonamide.

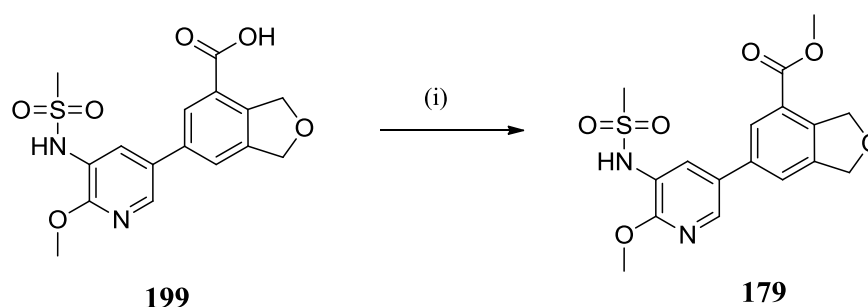
The *para*-methoxybenzyl group was stable to hydrogenation using 10% Pd/C at room temperature and pressure but it could be removed by hydrogenation at elevated temperature (50-70 °C), although the reaction was sluggish and required specialist equipment. It could also be cleaved successfully under acidic conditions; however the successful synthesis of compound **180** was carried out on the allyl protected intermediate in order to avoid the use of acidic deprotection conditions for removal of the *para*-methoxybenzyl group, which may have led to degradation of the oxetanyl moiety (Scheme 4.3.5). A Grignard reagent was synthesised *via* I/Mg exchange using the “Turbo Grignard” reagent that had been applied successfully in a similar reaction described in Chapter 3 (Scheme 4.3.5). Formation of the mesylate facilitated the introduction of the methoxy group and subsequent deallylation led to isolation of the desired oxetanyl-containing compound **180** (Scheme 4.3.5).



Reagents and Conditions: (i) *i*-PrMgCl·LiCl, THF, -72 °C; (ii) 3-oxetanone, -72 °C, 51% over two steps; (iii) MsCl, KO<sup>t</sup>-Bu, THF; (iv) MeOH, 95% over two steps, taken on crude; (v) RhCl<sub>3</sub>, 1-propanol, 98 °C, 13%.

#### Scheme 4.3.5. Synthesis of oxetanyl-containing compound **180**.

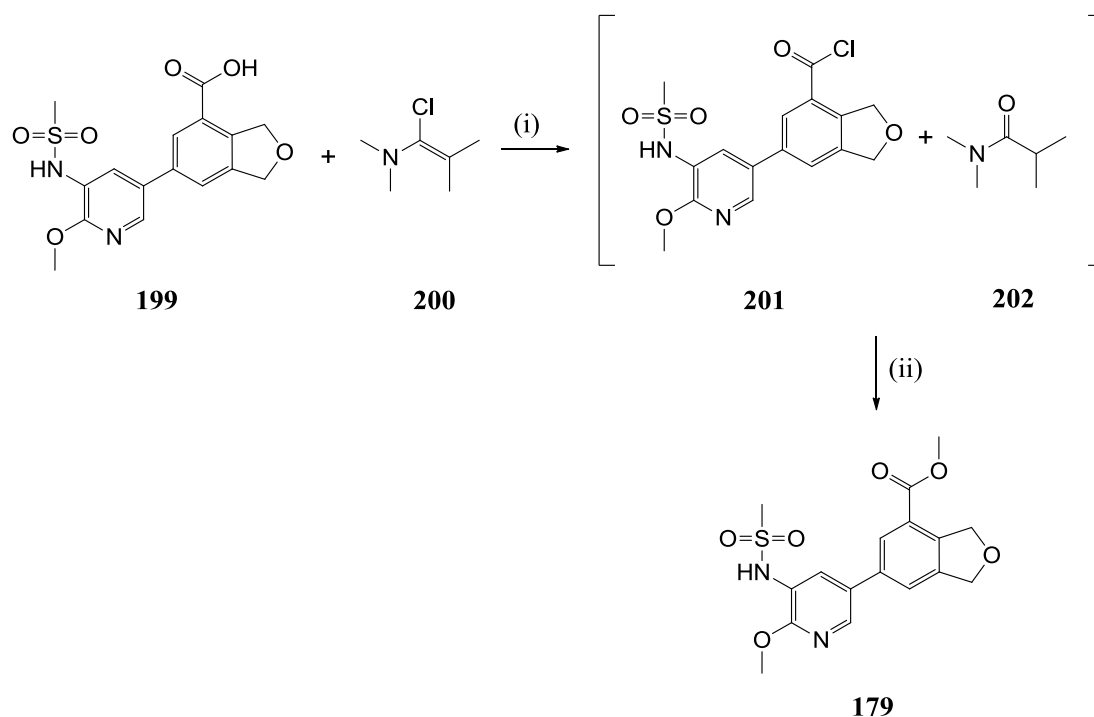
Synthesis of the equivalent ester **179** via a classic Fischer esterification was attempted. Carboxylic acid **199** had been synthesised previously within our laboratories<sup>82</sup> so this intermediate was refluxed in methanol in the presence of hydrochloric or sulfuric acid; however the reaction was sluggish and resulted in only 40% conversion to the ester after 24 h (Scheme 4.3.6).



Reagents and Conditions: (i) MeOH, conc. HCl or H<sub>2</sub>SO<sub>4</sub>, 65 °C, not isolated.

#### Scheme 4.3.6. Attempted esterification of acid intermediate **199**.

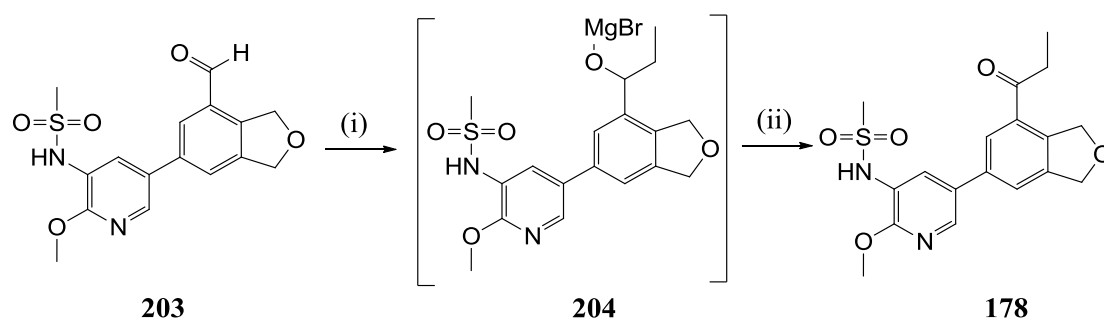
Synthesis of the acid chloride and subsequent ester formation was therefore investigated. The Ghosez reagent, 1-chloro-*N,N*-2-trimethyl-1-propenylamine (**200**, Scheme 4.3.5), was used as it has been shown in the literature to facilitate acyl chloride formation under mild, neutral conditions<sup>83</sup> and the use of thionyl chloride had previously led to demethylation of the methoxyl group of the pyridyl sulfonamide substituent. The Ghosez methodology has primarily been applied in peptide synthesis; because the equivalent 1-bromo-*N,N*-2-trimethyl-1-propenylamine can also be used to prepare acyl bromides, it has represented an efficient method for difficult peptide formations involving sterically hindered amide couplings (these are facilitated by the formation of amino acid bromides).<sup>84</sup> Since the only by-product is amide **224**, the acid chloride was taken forward *in situ* to obtain the desired ester (Scheme 4.3.7).



Reagents and Conditions: (i) THF, rt; (ii) MeOH, rt, 40% over two steps.

Scheme 4.3.7. Use of Ghosez's chlorination reagent for synthesis of ester **179**.

Next, ketone **178** was synthesised from aldehyde intermediate **203**, which had been previously synthesised within our laboratories (Scheme 4.3.8).<sup>82</sup> *N*-*tert*-Butylphenylsulfonimoyl chloride has been used as an *in situ* oxidant to allow the synthesis of ketones directly from aldehydes and this methodology was applied here (Scheme 4.3.8).<sup>85</sup>

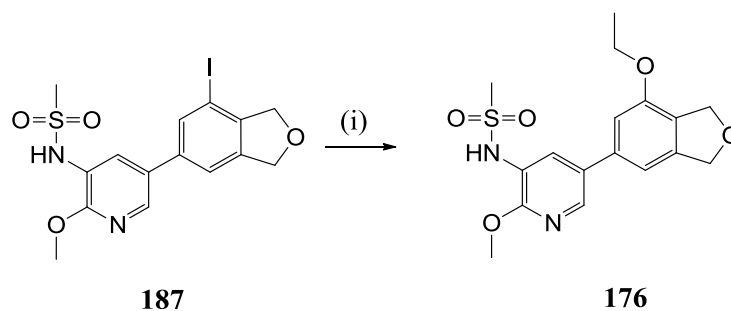


Reagents and Conditions: (i) EtMgBr, THF, -78 °C; (ii) *N*-*tert*-butylphenylsulfinimoyl chloride, THF; rt, 10% over two steps.

Scheme 4.3.8. Synthesis of ketone **178**.

Though the yield of this reaction was poor, it does represent a direct method for the preparation of a ketone from an aldehyde, which usually requires two steps (an alkylation followed by an oxidation). The poor yield could be attributed to incomplete Grignard reagent addition since the intermediate alcohol co-eluted with the starting material in various chromatographic methods, so it was difficult to measure the extent of conversion.

Finally, ether **176** was synthesised *via* a modified Ullman reaction in ethanol (Scheme 4.3.9).



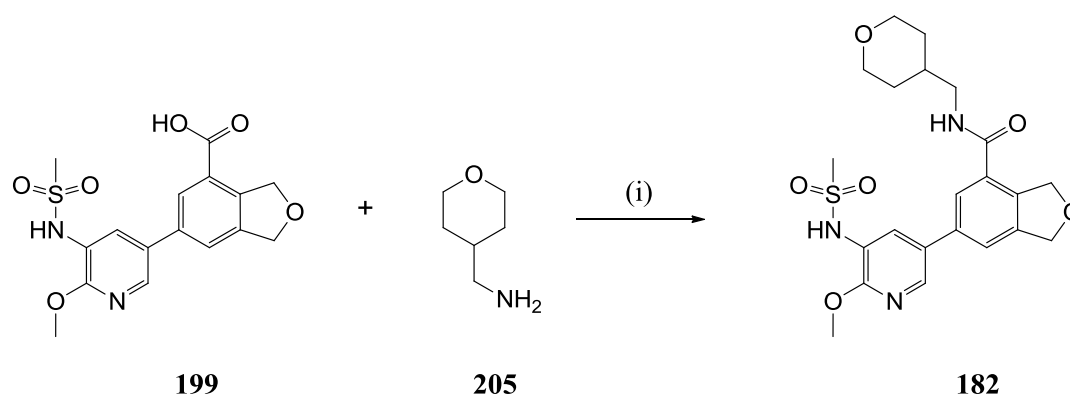
Reagents and Conditions: (i) CuI, 1,10-phenanthroline, KO*t*-Bu (1 M in THF), EtOH, 150 °C,  $\mu$ wave, 50%.

Scheme 4.3.9. Synthesis of compound **176**.

At this point, five novel compounds with various substituents at the 4-positions had been synthesised in order to probe the effects of these groups on PI3K $\delta$  potency and selectivity. The next section will describe the synthesis of fully elaborated compounds followed by the rationalisation of their biological results.

#### 4.3.1.2. Synthesis of Compounds 181-184

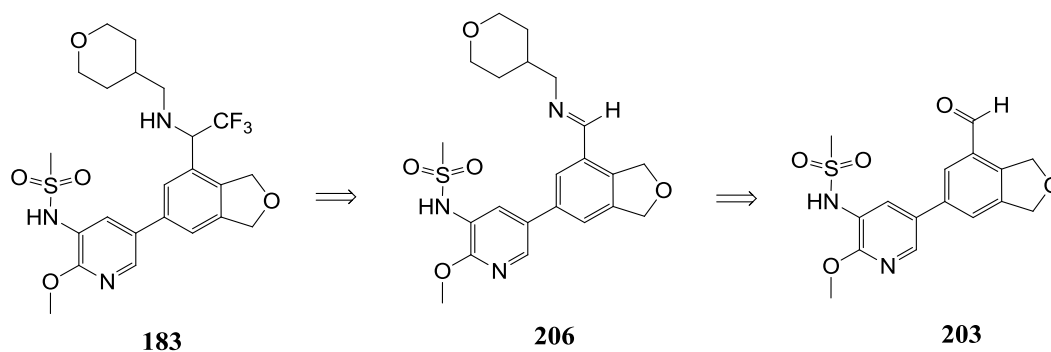
Compound **182**, the ‘reversed’ amide analogue of compound **173**, was synthesised *via* an amide formation reaction with carboxylic acid intermediate **199** (Scheme 4.3.11).



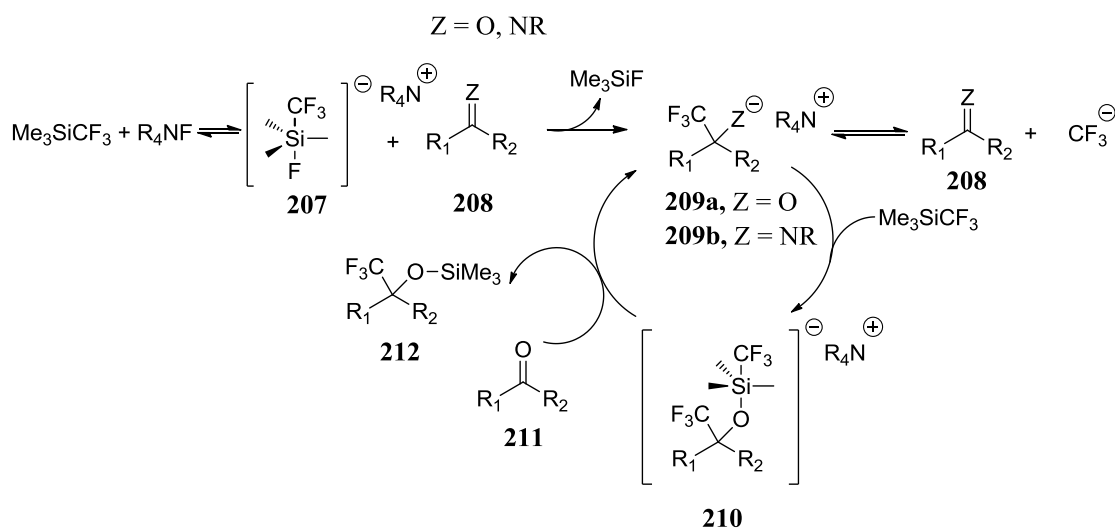
Reagents and Conditions: (i) PyBop<sup>®</sup>, DIPEA, DMF, rt, 20%.

Scheme 4.3.11. Synthesis of compound **182**.

Synthesis of the trifluoroethylamine analogue of compound **182** proved more problematic. Synthesis of **183** was attempted by trifluoromethylation of imine **206** (Scheme 4.3.12).

Scheme 4.3.12. Retrosynthesis of compound **183**.

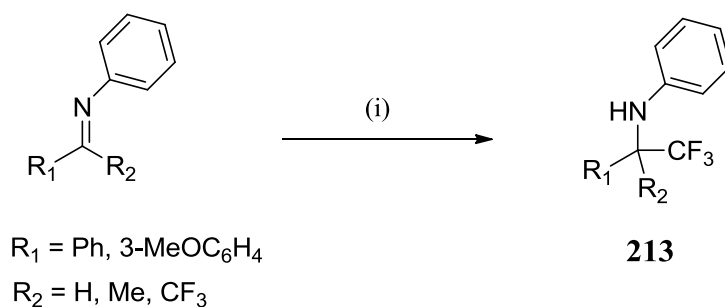
The Ruppert-Prakash reagent, (trifluoromethyl)-trimethylsilane (TMSCF<sub>3</sub>), has been widely reported as an effective reagent for the nucleophilic trifluoromethylation of carbonyl compounds; however, there are few examples of reactions of imines and TMSCF<sub>3</sub>.<sup>86</sup> The nucleophilic reactivity of TMSCF<sub>3</sub> is realised upon addition of a hard Lewis base such as a fluoride source, most commonly tetrabutylammonium fluoride (TBAF). This generates a five-coordinate silicate species which acts as a trifluoromethyl anion equivalent (Scheme 4.3.13). The low reactivity of imines can be attributed to the lower electrophilicity of the C=N double bond compared to the C=O double bond, as well as the differences in the stability of intermediates **209a** and **209b** (Scheme 4.3.13).



Scheme 4.3.13. General mechanism of nucleophilic trifluoromethylation with TMSCF<sub>3</sub>.

The instability of intermediate **209b** means that reversion to the starting material and highly reactive trifluoromethide (Scheme 4.3.13), which can abstract an acidic proton to form trifluoromethane or decompose to form difluorocarbene, is quite favourable. One of the first successful strategies to enable the trifluoromethylation of imines was to trap the required intermediate with an appropriate electrophile. Blazejewski reported that the addition of *N*-(trimethylsilyl)imidazole allowed the formation of trifluoromethylated amines (**213**) in moderate yields.<sup>87</sup>

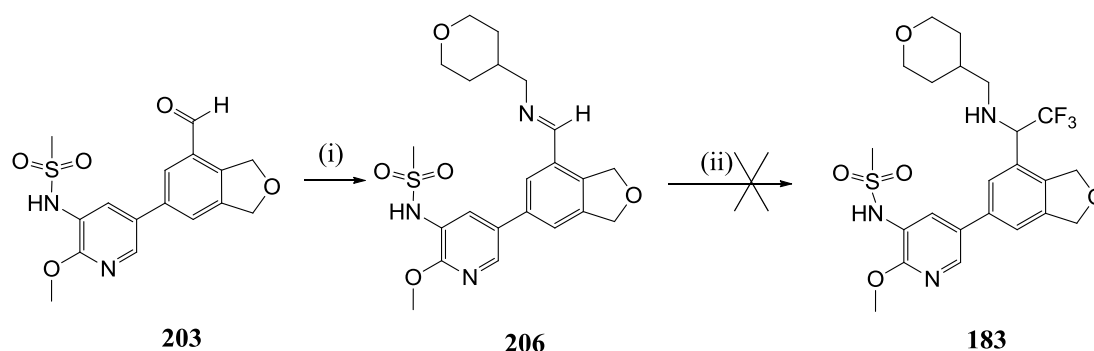




Reagents and Conditions: (i)  $\text{TMSCF}_3$ , TMS-imidazole, CsF, THF, 40-50%.

Scheme 4.3.14. Trifluoromethylation of imines using *N*-(trimethylsilyl)imidazole.<sup>87</sup>

This methodology allowed for the synthesis of monotrifluoromethylated amines in moderate yields and employed a stoichiometric amount of cesium fluoride as the initiator. When the substrate is a carbonyl derivative, only a catalytic amount of Lewis base is required since the oxophilic silicon atom enables formation of intermediate **210** (Scheme 4.3.13), which can transfer a  $\text{CF}_3$  group to the carbonyl substrate and re-enter the catalytic cycle until all the starting material has been consumed.<sup>86</sup> Since the Si-N bond is weaker than the Si-O bond, the formation of an analogous intermediate is much less favoured, so stoichiometric amounts of the initiator are usually required. The Ruppert-Prakash reagent can be used with sub-stoichiometric amounts of initiator for highly reactive substrates such as nitrones or aziridines.<sup>88,89</sup> However, in 2006 Prakash reported a method for the trifluoromethylation of *N*-unactivated aryl imines using a sub-stoichiometric amount of tetrabutylammonium triphenyldifluorosilicate (TBAT).<sup>90</sup> Although the use of this methodology is unprecedented with *N*-alkylamines, the conditions were easy to try for the nucleophilic trifluoromethylation of imine intermediate **206**. Unfortunately, no conversion to the desired product was observed and the starting material was recovered (Scheme 4.3.15).

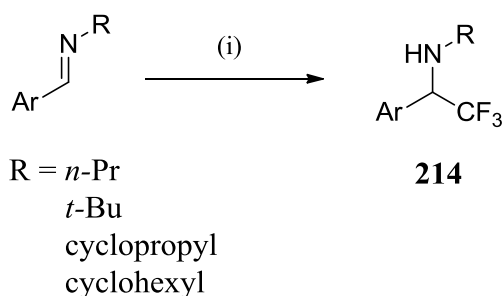


Reagents and Conditions: (i) Tetrahydro-2H-pyran-4-yl methanamine,  $\text{NEt}_3$ ,  $\text{MgSO}_4$ , DCM, rt, 85%;  
(ii)  $\text{TMSCF}_3$ , TBAT, THF, 0 °C to rt.

Scheme 4.3.15. Attempted synthesis of compound **183**.

Failure of the reaction could be attributed to the *N*-alkylamine substrate, since the negative charge on the nitrogen of the required intermediate is not stabilised. Another reason could be that the formation of trifluoromethane, which drives reversion of the desired intermediate to the starting material and prevents effective trifluoromethylation, is facilitated by the acidic sulfonamide present in the substrate. Typically the use of TBAT prohibits the side reaction as it is non-hygroscopic and therefore helps to prevent the formation of trifluoromethane that arises when the basic  $\text{TMSCF}_3$ /Lewis base system readily abstracts acidic protons in the reaction media. However, in this case the acidic proton present in the substrate means this side reaction cannot be prevented despite ensuring that the reaction media is anhydrous. The side reaction could be avoided by protecting the sulfonamide; however this was not followed up as conditions reported to be successful in the trifluoromethylation of *N*-alkyl imines were attempted instead.

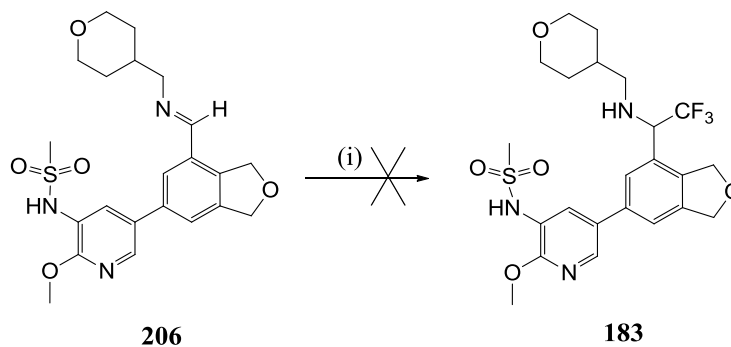
Levin reported that under acidic conditions, where the process is believed to be mediated by hydrofluoric acid produced *in situ* from  $\text{KHF}_2$  and TFA, *N*-alkylimines react successfully to give trifluoromethylated amine products (**238**, Scheme 4.3.16).<sup>91</sup>



Reagents and Conditions: (i) TMSCF<sub>3</sub>, KHF<sub>2</sub>, TFA, MeCN/DMF, rt, 80-90%.

Scheme 4.3.16. Trifluoromethylation of *N*-alkyl imines.<sup>91</sup>

Unfortunately, these conditions did not prove successful for the trifluoromethylation of imine intermediate **206** (Scheme 4.3.17), with imine hydrolysis being the predominant reaction.

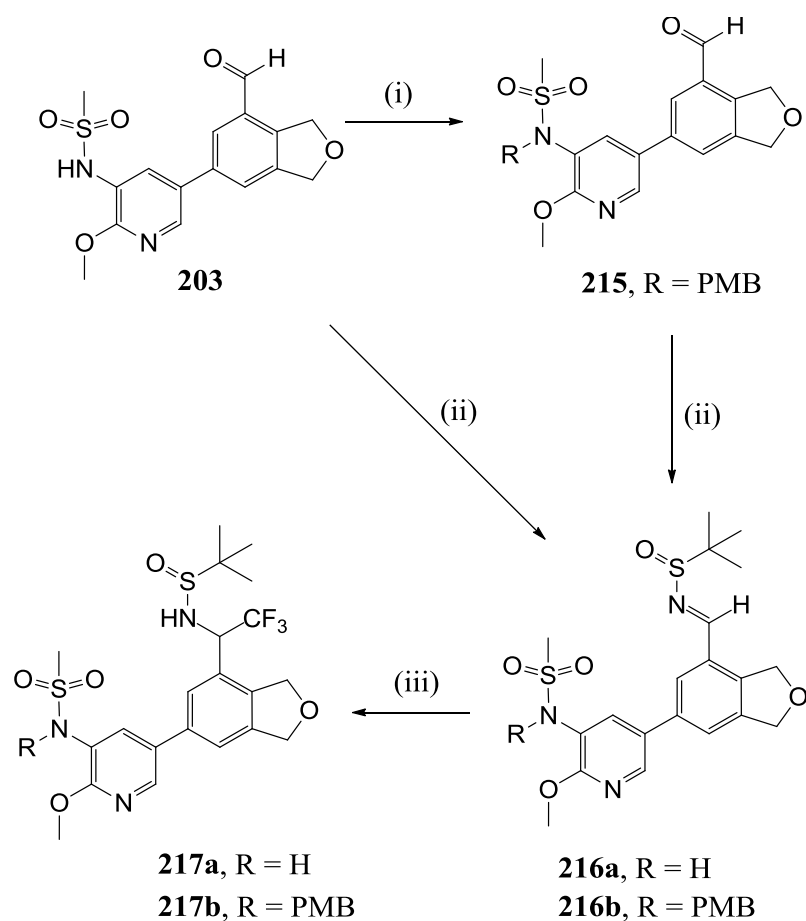


Reagents and Conditions: (i) TMSCF<sub>3</sub>, KHF<sub>2</sub>, TFA, MeCN/DMF (40:1), rt.

Scheme 4.3.17. Attempted trifluoromethylation of imine **206** under acidic conditions.

It was obvious that an alternative strategy was required. In the literature it has been shown that strongly electrophilic imines, for example *N*-tosyl aldimines and *N*-(*tert*-butylsulfinyl)imines, can be elaborated in good yields with TMSCF<sub>3</sub>.<sup>92,93</sup> Sulfinimes **216a** and **216b** were therefore synthesised and the trifluoromethylation

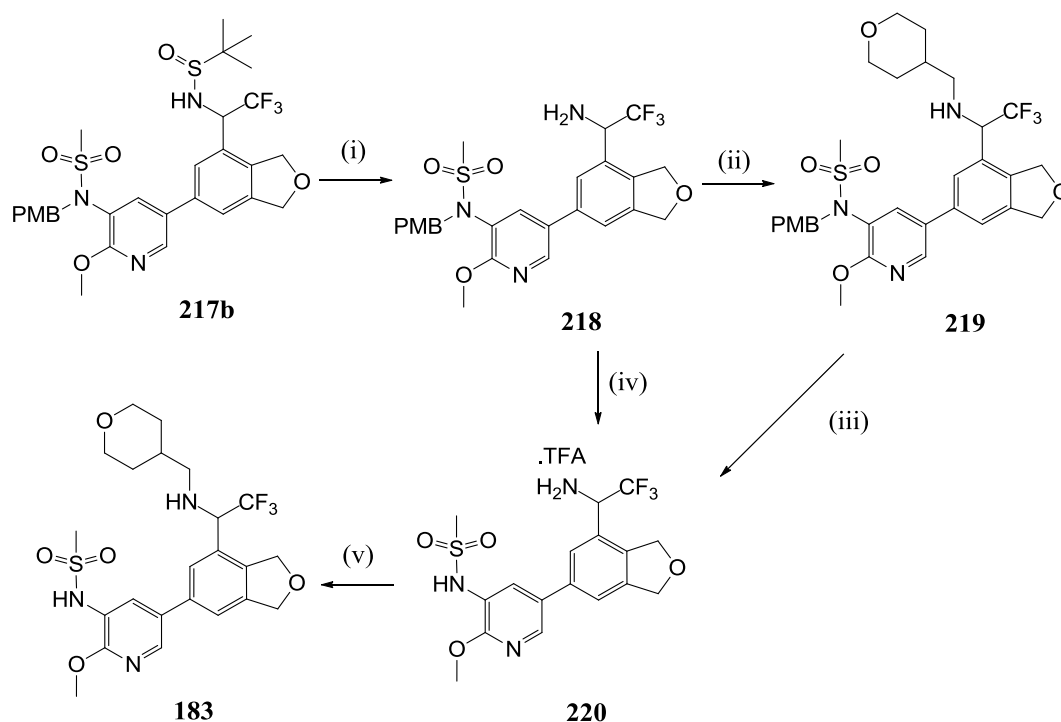
conditions were applied (Scheme 4.3.18). In the absence of a sulfonamide protecting group the isolated yield was only 16%, which may be due to quenching of the silicate active species by abstraction of acidic protons from the substrate, generating trifluoromethane. Removal of this potential side-reaction by protecting the sulfonamide with a *para*-methoxybenzyl group gave a 57% isolated yield of the desired product (Scheme 4.3.18).



Reagents and Conditions: (i) PMBCl, K<sub>2</sub>CO<sub>3</sub>, DMF, rt, 32%; (ii) 2-methyl-2-propanesulfinamide, Ti(OEt)<sub>4</sub>, THF, rt, 16% (**216a**), 86% (**216b**); (iii) TMSCF<sub>3</sub>, TBAT, THF, 0 °C to rt, 16% (**217a**), 57% (**217b**).

Scheme 4.3.18. Successful trifluoromethylation methodology.

Deprotection of the *N*-(*tert*-butylsulfinyl)imine intermediate **217b** was carried out successfully in the presence of the *para*-methoxybenzyl group (Scheme 4.3.19, step (i)). The desired tetrahydropyran substituent was introduced *via* a reductive amination to give intermediate **219**, which was taken forward for the deprotection step without purification (Scheme 4.3.19, step (ii)). Unfortunately, the conditions used to remove the *para*-methoxybenzyl group led to unexpected cleavage of the alkyl group (Scheme 4.3.19, step (iii)). Intermediate **220** was not isolated from this reaction but instead was obtained after removal of the *para*-methoxybenzyl group from intermediate **218** (Scheme 4.3.19, step (iv)). Intermediate **220** was taken forward for the final reductive amination step without further purification to afford the target compound **183** (Scheme 4.3.19, step (v)).

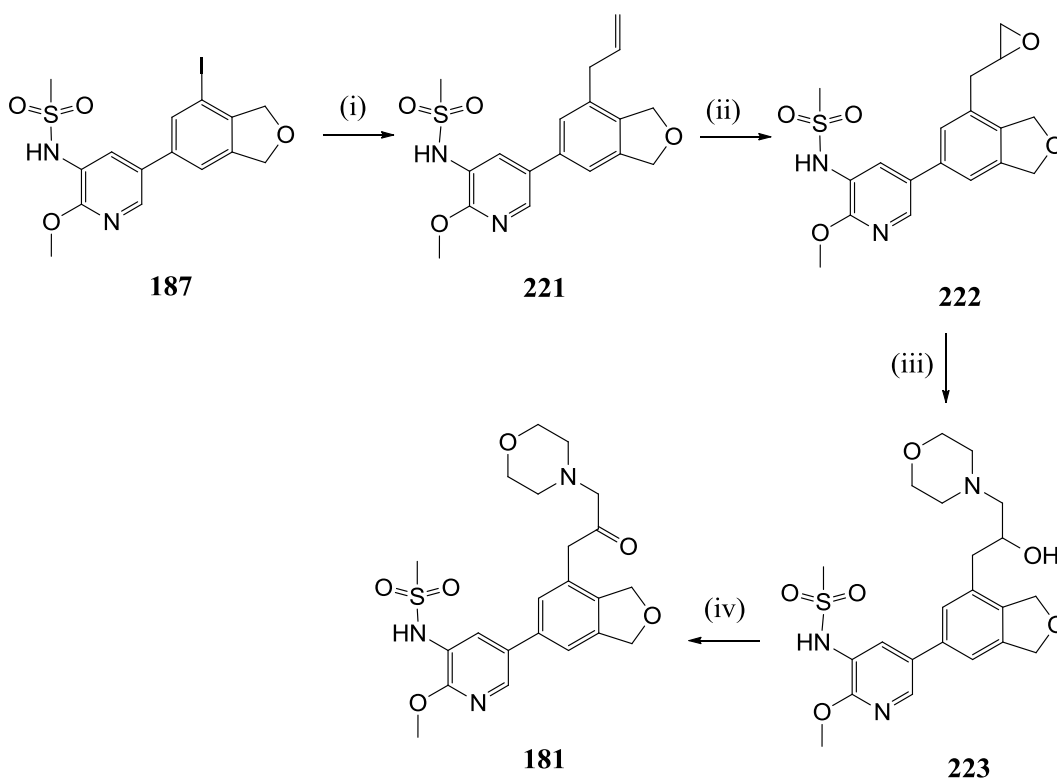


Reagents and Conditions: (i) 4M HCl in 1,4-dioxane, MeOH, rt, 99%; (ii) tetrahydro-2H-pyran-4-carbaldehyde, NaBH(OAc)<sub>3</sub>, NEt<sub>3</sub>, MeCN, rt, 90%; (iii) TFA, DCM, 80 °C, not isolated; (iv) TFA, DCM, 80 °C, taken on crude; (v) tetrahydro-2H-pyran-4-carbaldehyde, NaBH(OAc)<sub>3</sub>, NEt<sub>3</sub>, MeCN, rt, 19%.

Scheme 4.3.19. Synthesis of compound **183** from sulfimine intermediate **217b**.

The use of sulfimine intermediates could allow for an asymmetric synthesis to be developed, as enantiopure 2-methyl-2-propanesulfinamide is commonly employed as a chiral auxiliary.<sup>94</sup> Another asymmetric approach could be to utilise a trifluoromethylketone on the dihydroisobenzofuran core so that chiral products could be accessed *via* an asymmetric reductive amination.

Compound **181** was synthesised by the route shown in Scheme 4.3.20.

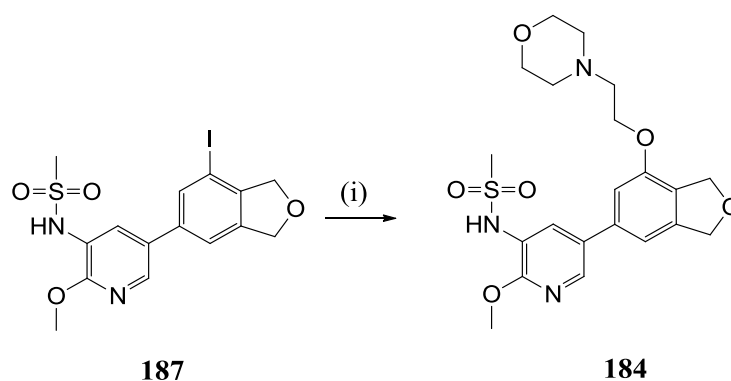


Reagents and Conditions: (i) 2-allyl-4,4,5,5-tetramethyl-1,3,2-dioxaborolane, Pd(PPh<sub>3</sub>)<sub>4</sub>, K<sub>2</sub>CO<sub>3</sub>, 1,4-dioxane/H<sub>2</sub>O (3:1), 100 °C,  $\mu$ wave, 90%; (ii) *m*CPBA, CHCl<sub>3</sub>, rt, 52%, taken on crude; (iii) morpholine, MeOH, 100 °C,  $\mu$ wave, 49%, taken on crude; (iv) SO<sub>3</sub>.py, NEt<sub>3</sub>, DMSO, rt, 18%.

Scheme 4.3.20. Synthesis of compound **181**.

Suzuki cross-coupling afforded allyl intermediate **221**, which underwent epoxidation to afford the epoxide product **222**. This could not be purified so was taken forward in a subsequent ring-opening reaction with morpholine to afford alcohol **223**. A Parikh-Doering oxidation was used to give the desired ketone; however the starting material and product co-eluted using standard reverse and normal phase systems and the reaction did not reach completion, hence bespoke purification using a high pH preparative LCMS method was required and the isolated yield was low.

Ether **184** was synthesised *via* a modified Ullman reaction as described previously. In this case the alcohol was not used as solvent and despite the addition of a large excess, the conversion to product was poor and hence the isolated yield was low (Scheme 4.3.21).<sup>95</sup>



Reagents and Conditions: (i) *N*-2-(hydroxyethyl)morpholine (10 eq.), CuI, 1,10-phenanthroline, KO<sup>t</sup>-Bu (1 M in THF), MeOH, 150 °C,  $\mu$ wave, 17%.

Scheme 4.3.21. Synthesis of compound **184** (not described in Experimental as synthesised by E. Wix, GSK).<sup>95</sup>

#### 4.3.1.3. Conformational Analysis of Compounds in their Free and Protein-bound States

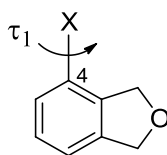
The biological results for compounds **174** - **184** will be discussed with respect to the conformations of the different linkers when bound in the PI3K $\delta$  active site. The binding of a ligand (e.g. a small molecule) to a receptor (e.g. a protein) is best described by ‘induced fit’ theory, where both the ligand and receptor reorganise themselves to find the most compatible conformation for binding.<sup>96</sup> A good ligand must bind in a relatively low energy conformation, although several studies comparing the conformations of a ligand in its free state and protein-bound have shown that many do not adopt their global minimum conformation.<sup>97,98</sup> However, a



more recent study of 100 crystal structures of protein-bound ligands did show that all the ligands adopted local minimum conformations when bound to proteins.<sup>99</sup>

Assessing the torsional preferences of the substituents at the 4-position of the dihydroisobenzofuran and comparing the results with the conformations present in the ligand-protein complexes may help establish how much ligand strain energy can be tolerated and which substituents are able to compensate for the cost in reorganisation energy upon binding. In turn, this could enable a pharmacophore to be defined for the linker atoms at the 4-position of the core dihydroisobenzofuran.

The effect of rotation around the C4-X bond on the potential energy was examined for the different 4-substituents without any other substitution of the dihydroisobenzofuran core by means of computer-assisted relaxed torsional scans using the program Jaguar with Hartree-Fock methodology and a 6-31G\* basis set. The dihedral angle,  $\tau_1$ , was stepped and the structure minimised subject only to the dihedral constraint.



The torsional scans for the 4-position amides show that the preferred conformation of the anilide has the amide carbonyl pointing towards the dihydrofuran of the dihydroisobenzofuran core (Figure 4.3.1.). This was also the case for the benzamide as the amide substituent was positioned away from the adjacent methylene of the furan ring (Figure 4.3.1.).

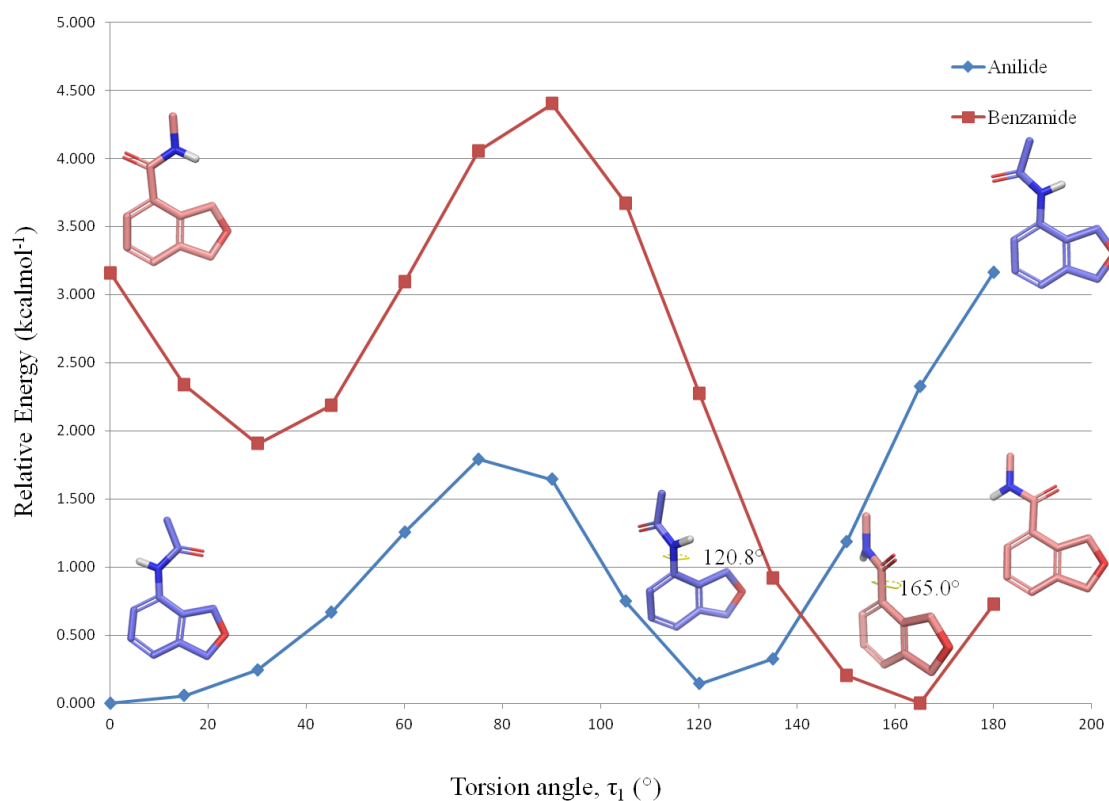
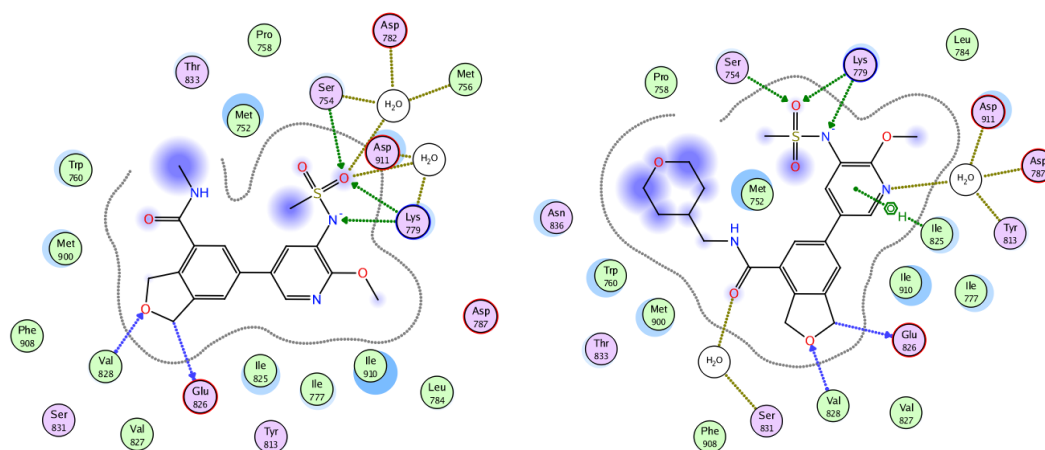


Figure 4.3.1. Torsional scans of the 4-position anilide and benzamide.

If the compounds are able to adopt these conformations when bound to the PI3K $\delta$  enzyme, their binding affinities should not be impacted by ligand strain energy and hence their potencies should be high. Crystal structures obtained for benzamides **177** (purple) and **182** (green) bound to PI3K $\delta$  did show ligand conformations very close to the global minimum, with torsion angles of 154.2° and 177.5°, respectively.



177

182

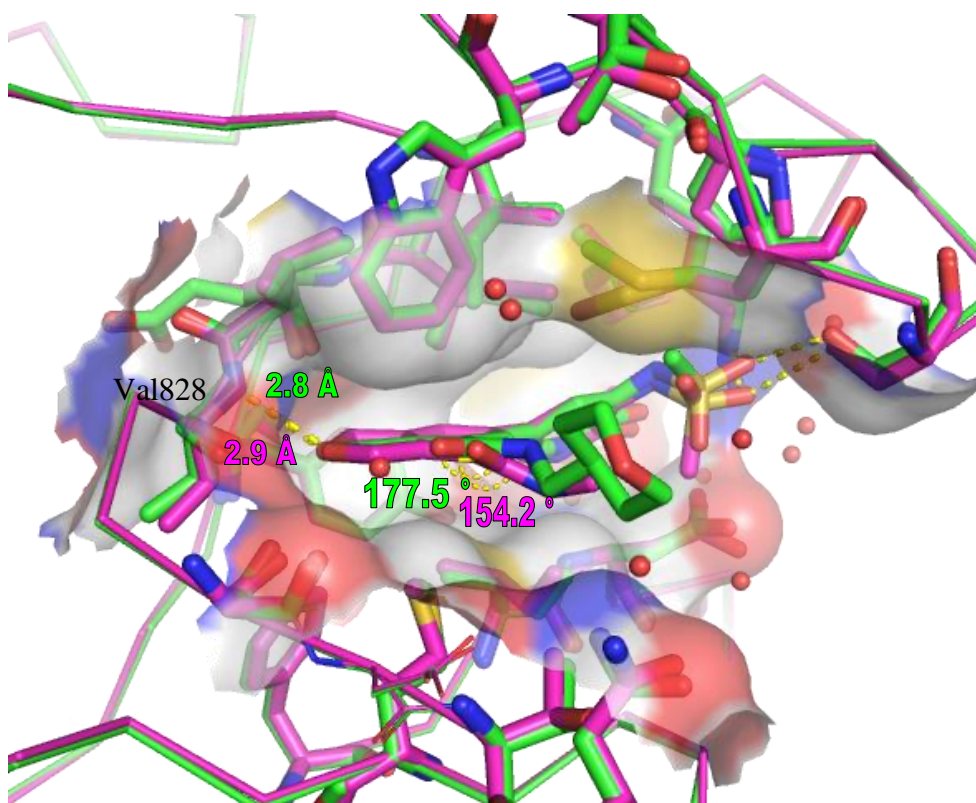
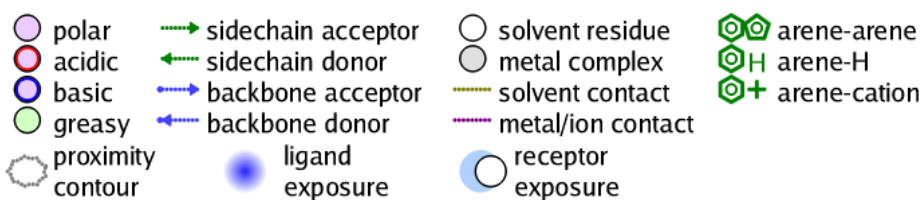


Figure 4.3.2. Co-crystal structures of compounds **177** (purple structure, 2.80 Å resolution) and **182** (green structure, 2.49 Å resolution) bound to PI3Kδ.

The crystal structures of anilides **174** (purple) and **173** (green) both show a twist in the amide, with torsion angles of  $146^\circ$  and  $116^\circ$ , respectively.

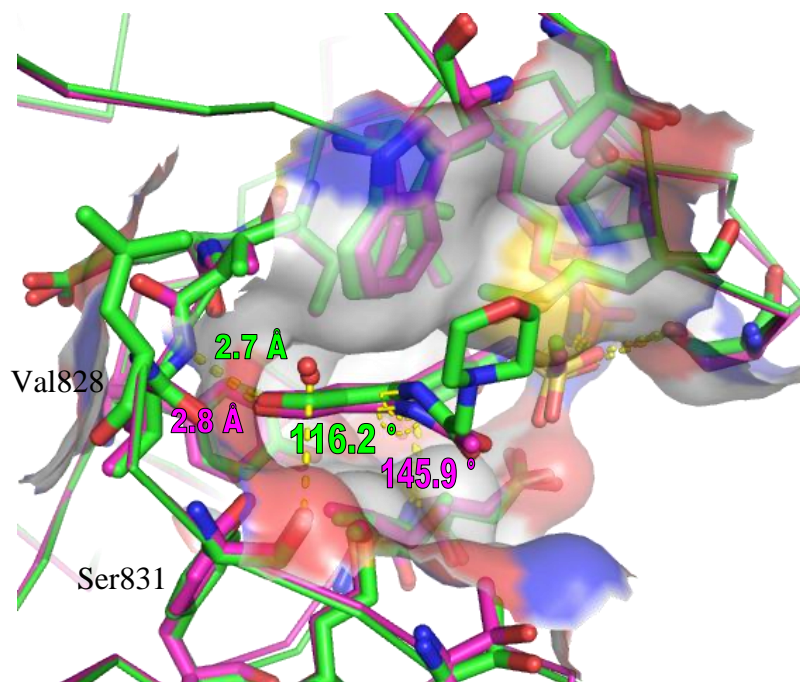
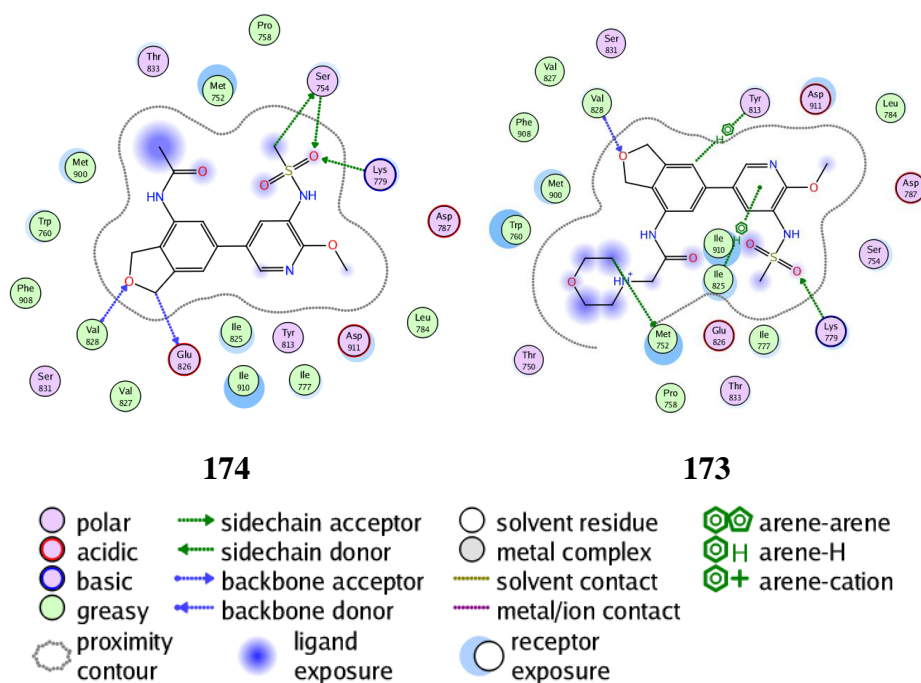
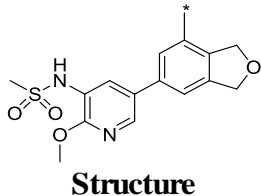
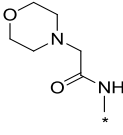
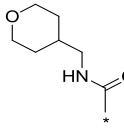
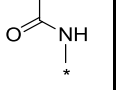


Figure 4.3.3. Co-crystal structures of compounds **174** (purple structure, 3.01 Å resolution) and **173** (green structure, 3.22 Å resolution) bound to PI3Kδ.

These torsion angles do not equate to the global energy minimum of the amide, which is when the carbonyl points towards the furan and  $\tau_1$  equals  $0^\circ$ . This may impact the binding affinity, however the twisted conformation adopted in the active site does correspond to another energy minimum ( $\tau_1 = 120\text{-}130^\circ$ , Figure 4.3.1.), which is energetically indistinguishable from the global minimum; the activity would therefore not be expected to be adversely affected by this conformational change.

The biological data for benzamides **177** and **182** shows that the compounds have high binding affinity and excellent ligand efficiency (Table 4.3.1). The anilides **174** and **173** are 5- to 10-fold less active at PI3K $\delta$  than the benzamides, but show improved selectivity over the other PI3K isoforms (Table 4.3.1). It is interesting to note that the ligand efficiency of compounds **173** and **182** (LE = 0.29 and 0.32, respectively) is much reduced when compared to that of the truncated compounds **174** and **177** (LE = 0.34 and 0.39 respectively), therefore the key atoms required for binding are those of the linker and the addition of the pendant tetrahydropyran group does not contribute as efficiently to binding.

Structure				
Compound Number	<b>173</b>	<b>182</b>	<b>174</b>	<b>177</b>
Mean PI3K $\delta$ pIC <sub>50</sub> (N)	6.8 (3)	7.5 (3)	6.4 (2)	7.4 (7)
Mean PI3K $\alpha$ pIC <sub>50</sub> (N)	5.3 (3)	6.5 (3)	5.8 (2)	6.7 (8)
Mean PI3K $\beta$ pIC <sub>50</sub> (N)	5.0 (3)	6.6 (3)	5.3 (2)	6.5 (7)
Mean PI3K $\gamma$ pIC <sub>50</sub> (N)	5.0 (3)	6.6 (3)	5.3 (2)	7.0 (7)
Mean HWB pIC <sub>50</sub> (N)	6.5 (9) <sup>a</sup>	6.6 (5)	5.6 (2) <sup>b</sup>	6.6 (9) <sup>b</sup>
LE/LLE <sub>AT</sub>	0.29/0.33	0.32/0.37	0.34/0.37	0.39/0.44
PFI	4.6	4.7	4.0	4.1
mChromlogD <sub>pH7.4</sub>	2.59	2.74	1.97	2.08
clogP	1.6	1.4	1.5	1.1
MW	463	462	377	377
TPSA	119	116	107	107
AMP (pH 7.4, nm/s)	135	91	-	73
CLND Solubility ( $\mu$ M)	401	448	426	455
FaSSIF Solubility after 4 h ( $\mu$ g/ml)	20	-	-	228
hERG pIC <sub>50</sub>	<4.3 (3)	4.4 (1) <sup>c</sup>	<4.2 (3)	5.8 (1)
CYP 3A4 pIC <sub>50</sub>	<4.3 (1)	<4.3 (1)	<4.3 (1)	<4.3 (1)

<sup>a</sup> Returned no value on two test occasions. <sup>b</sup> Returned no value on one occasion. <sup>c</sup> Returned value <4.3 on one test occasion.

Table 4.3.1. Biological data for compounds **173**, **182**, **174** and **177**.

Figure 4.3.4 shows a potential through-water interaction between the carbonyl group of the benzamide linker and Ser831, which may be the key interaction responsible for tighter binding in this region of the protein.

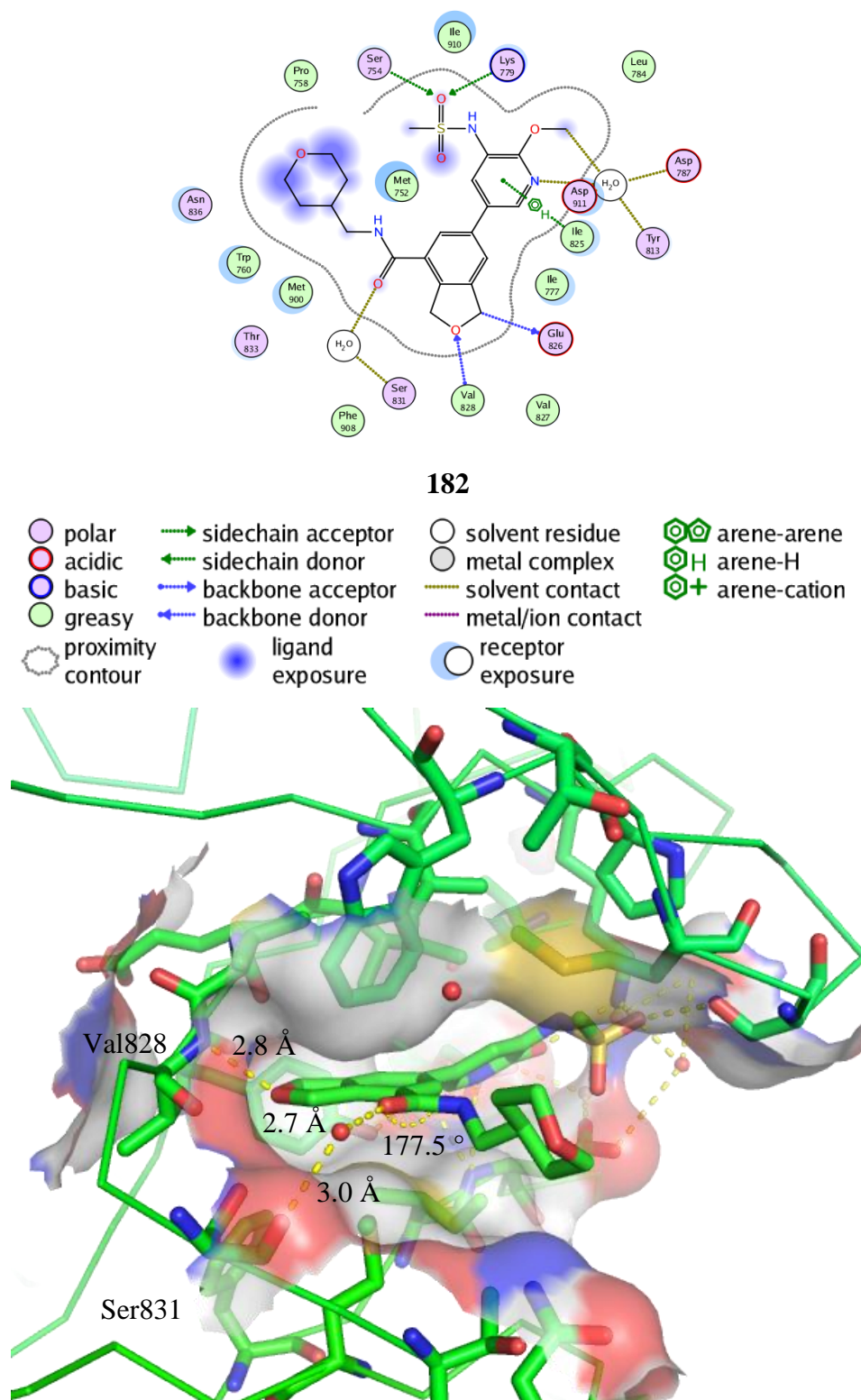


Figure 4.3.4. Co-crystal structures of compound **182** bound to PI3K $\delta$  (2.49 Å resolution).



Unfortunately, the selectivity of the benzamide for PI3K $\delta$  over the other PI3K isoforms is poor at only 5- to 12-fold. Ser831 is conserved in PI3K $\alpha$  and PI3K $\beta$  and the residue in this position is Ala885 in PI3K $\gamma$ , hence the through-water interaction with the carbonyls of these residues could be realised across all the PI3K isoforms. Therefore, despite moderate activity in the human whole blood assay, the benzamide compounds could not be progressed due to their diminished selectivity.

The through-water interaction with Ser831 that was observed for the benzamide compounds was not detected in crystal structures of the anilides, which may account for the decreased affinity of the anilides compared to the benzamides. However the anilide compound **173** has the advantage of achieving better selectivity over the other PI3K isoforms, due to the favourable positioning of the pendant morpholino substituent on the tryptophan shelf. This is not achieved by the pendant substituent of benzamide compound **182** (Figure 4.3.5). This may be due to the ability of the pendant amine to engage in a cation- $\pi$  interaction with the tryptophan, which cannot be achieved by the tetrahydropyran substituent of the benzamide. The cation- $\pi$  interaction is energetically significant in biological systems, often enhancing binding energies by 2-5 kcal/mol, and is mostly electrostatic in nature.<sup>100</sup> The region of negative electrostatic potential on the face of an aromatic system facilitates the attraction of cations to the surface, in this case the ammonium ion of the morpholino substituent, which is approximately 3 Å from the tryptophan.



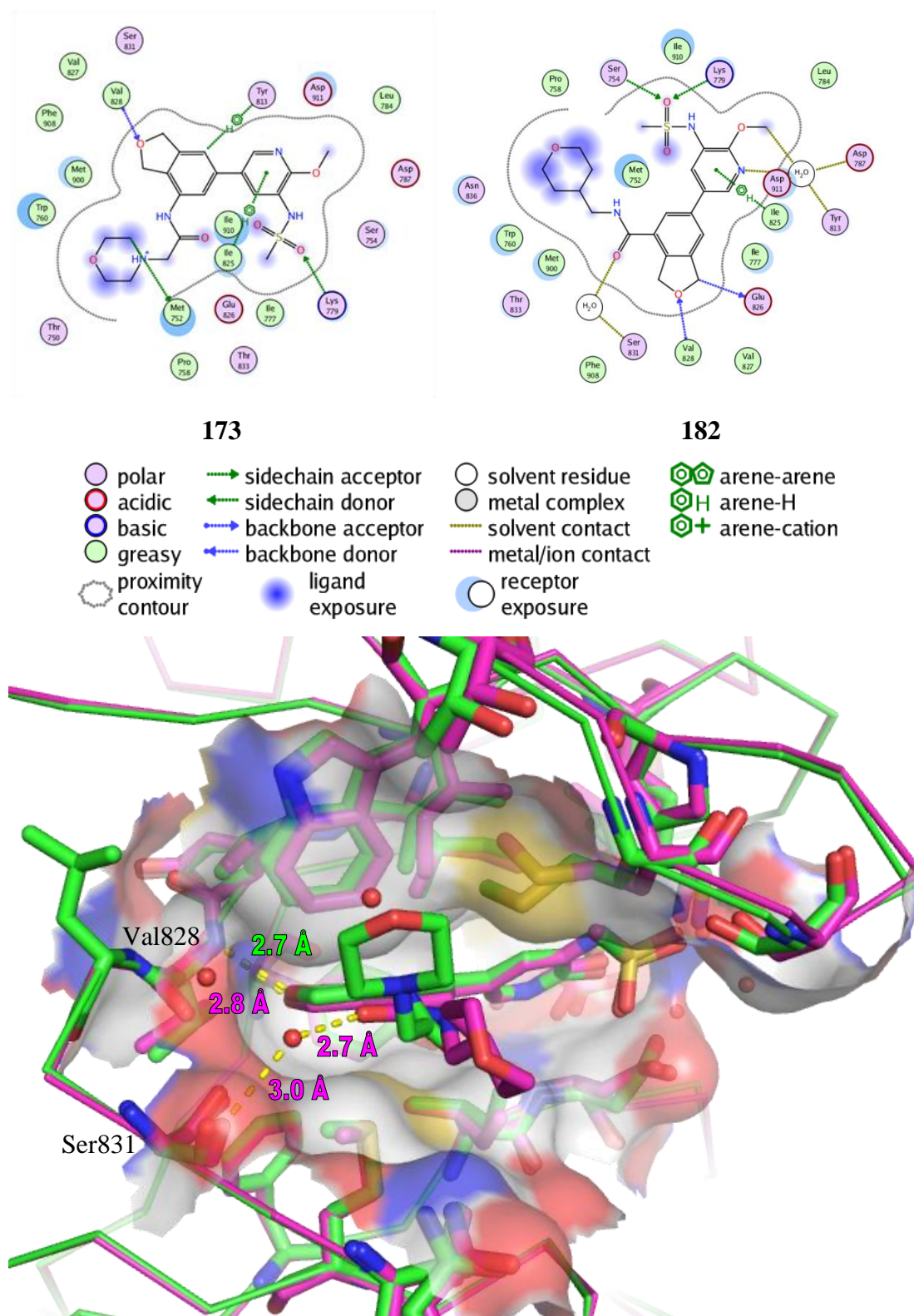


Figure 4.3.5. Overlay of co-crystal structures of anilide **173** (green structure, 3.22 Å resolution) and benzamide **182** (purple structure, 2.49 Å resolution) bound to PI3Kδ.

Since the benzamide has been observed to engage in an additional interaction with Ser831 from the carbonyl through the conserved water, other 4-substituents that maintain the positioning of this carbonyl group may also be able to pick up this interaction to deliver improved activity for PI3K $\delta$  compared to that obtained with the anilides. Torsional scans for dihydroisobenzofurans with keto- and ester groups at the 4-position showed that the global energy minima for these substituents were similar to that of the analogous benzamide, hence their carbonyl groups should occupy a similar position in the active site (Figure 4.3.6). Torsional scans for the oxetan-3-yl containing molecule showed that the preferred conformation was different, with the oxetanyl group pointing away from the furan of the core, which is presumably due to steric effects (Figure 4.3.6).

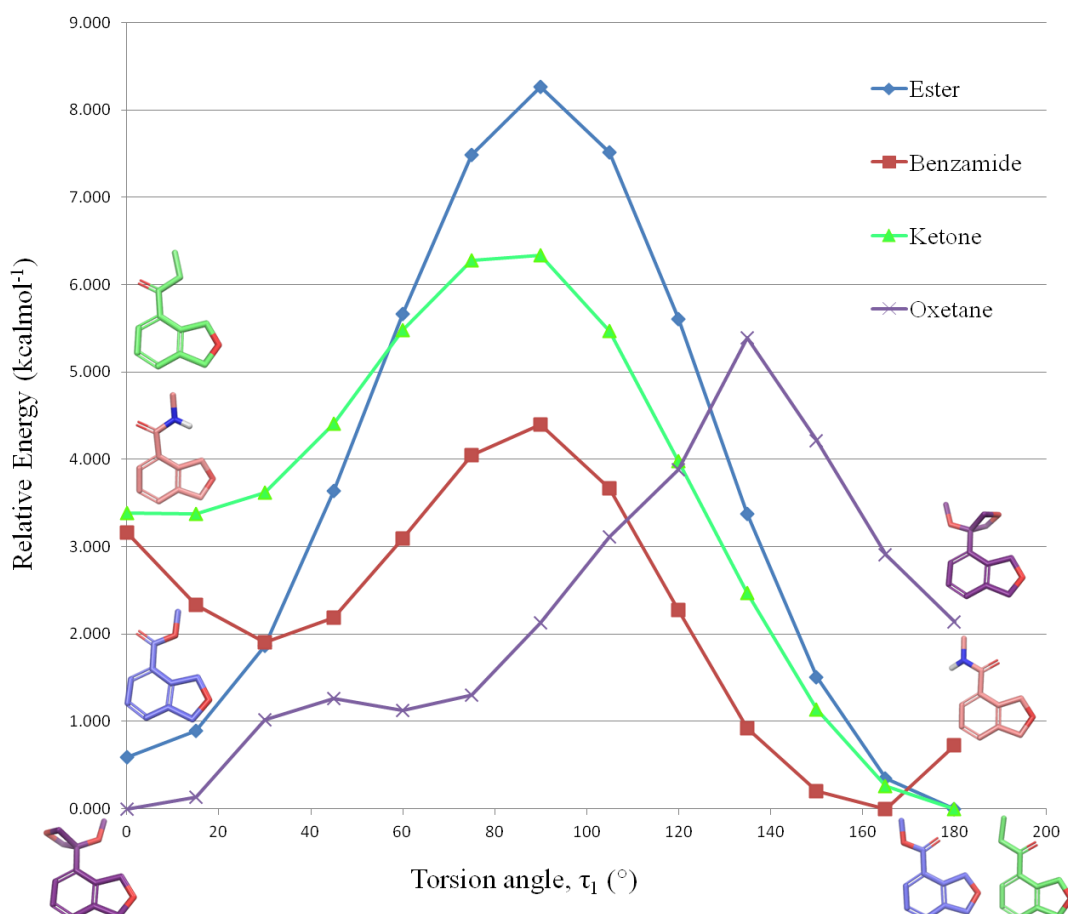
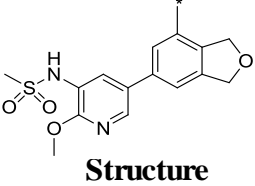
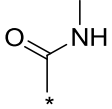
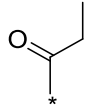
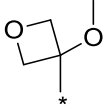


Figure 4.3.6. Torsional scans of 4-position substituents.

The biological data for compounds **178-180** showed that both ketone **178** and ester **179** have higher PI3K $\delta$  potency than benzamide **177**, whereas the oxetanyl compound **180** has significantly lower potency (Table 4.3.2).

 Structure				
Compound Number	<b>177</b>	<b>178</b>	<b>179</b>	<b>180</b>
Mean PI3K $\delta$ pIC <sub>50</sub> (N)	7.4 (7)	8.0 (3)	7.9 (2)	6.0 (2)
Mean PI3K $\alpha$ pIC <sub>50</sub> (N)	6.7 (8)	7.0 (3)	6.8 (2)	5.8 (1) <sup>c</sup>
Mean PI3K $\beta$ pIC <sub>50</sub> (N)	6.5 (7)	7.1 (3)	6.4 (2)	5.4 (3)
Mean PI3K $\gamma$ pIC <sub>50</sub> (N)	7.0 (7)	7.1 (3)	6.9 (2)	5.3 (2)
Mean HWB pIC <sub>50</sub> (N)	6.6 (9) <sup>a</sup>	6.0 (3)	5.8 (5) <sup>b</sup>	4.8 (3) <sup>d</sup>
LE/LLE <sub>AT</sub>	0.39/0.44	0.41/0.40	0.42/0.41	0.29/0.31
PFI	4.1	6.2	5.9	5.1
mChromlogD <sub>pH7.4</sub>	2.08	4.24	3.92	3.07
clogP	1.1	2.3	2.3	2.0
MW	377	376	378	406
TPSA	107	95	104	96
AMP (pH 7.4, nm/s)	73	690	590	340
CLND Solubility ( $\mu$ M)	455	80	429	434
FaSSIF Solubility after 4 h ( $\mu$ g/ml)	228	-	-	-
hERG pIC <sub>50</sub>	5.8 (1)	4.7 (3)	5.4 (2)	<4.2 (3)
CYP 3A4 pIC <sub>50</sub>	<4.3 (1)	4.5 (1)	<4.3 (1)	<4.3 (1)

<sup>a</sup> Returned no value on one test occasion. <sup>b</sup> Returned no value on six test occasions. <sup>c</sup> Returned value <4.6 on one test occasion. <sup>d</sup> Returned value <4.4 on one test occasion.

Table 4.3.2. Biological data for compounds **177**, **178**, **179** and **180**.

The high binding affinities of ketone **178** and ester **179** imply that the carbonyl groups may be engaging in the same water-mediated hydrogen bonding interactions to the protein backbone; however the binding affinity does not appear to correlate with hydrogen bond acceptor strength. In addition to a ligand's electrostatic and van der Waals interactions within the receptor, a crucial contribution to the

binding affinity also arises from desolvation of the ligand. Desolvation of a hydrogen bond donor and acceptor must occur for a hydrogen bond to form and a stronger hydrogen bond also implies higher desolvation costs, so the net free energy gain from a stronger hydrogen bond might be minimal.<sup>72</sup> This may be a reason why, despite the potential for the formation of a stronger hydrogen bond with the amide, the binding affinity is lower than that of the ester and ketone. Unfortunately the ester and ketone compounds still do not exhibit good selectivity over the other PI3K isoforms and, although their increased PI3K $\delta$  potencies suggested further elaborated compounds would be interesting, this was not pursued at this stage as alternative linker atoms at the 4-position, such as an ether oxygen, were thought to have more promise.

Oxetanyl compound **180** does not achieve the same levels of PI3K $\delta$  activity as the carbonyl-containing compounds. The crystal structure of **180** shows that the compound does adopt its lowest energy conformation when bound to PI3K $\delta$  and the oxetanyl group is placed on the opposite side to the carbonyl groups of the other compounds, so a through-water interaction with the hydrogen-bond acceptor of the oxetane is not possible (Figure 4.3.7).

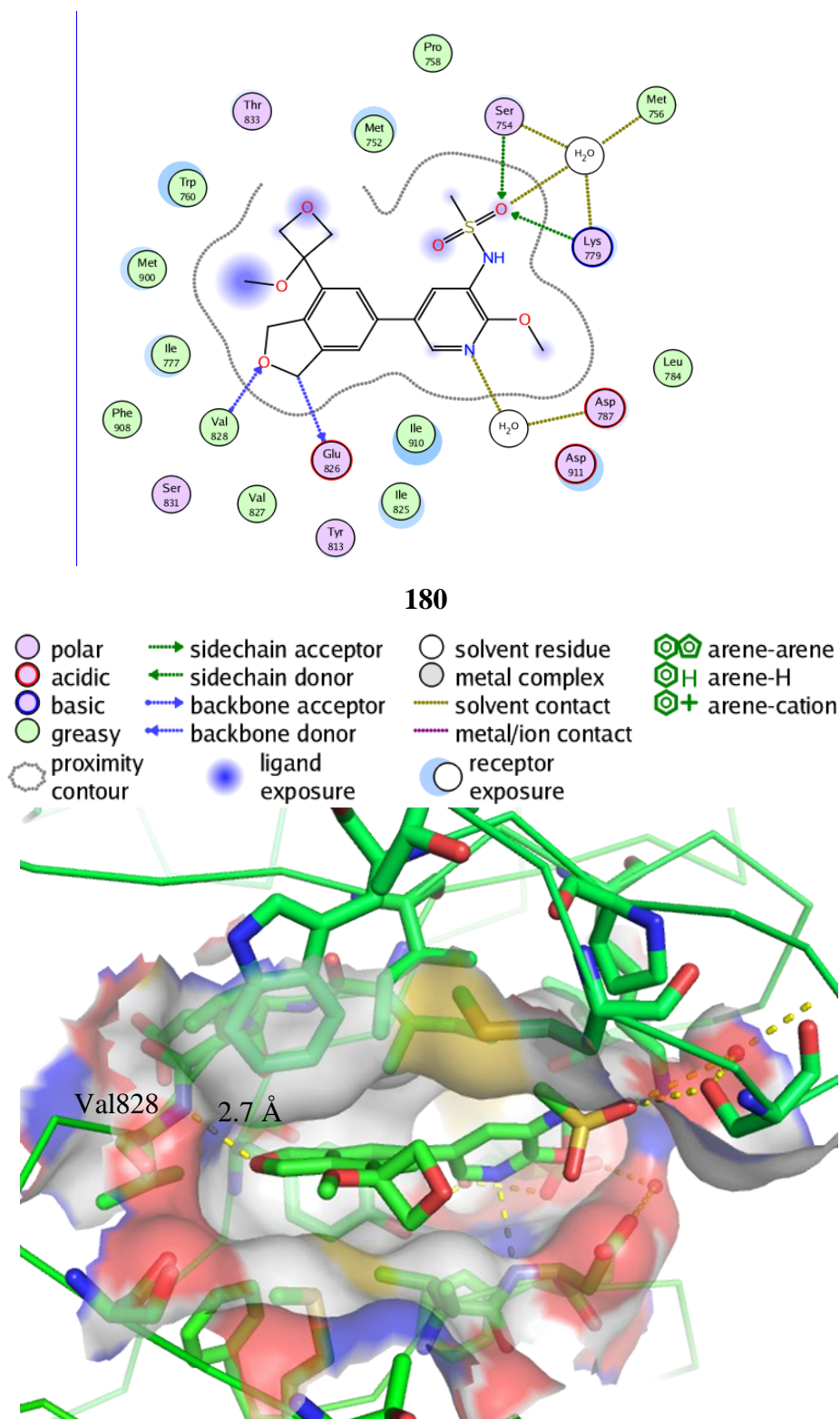


Figure 4.3.7. Co-crystal structure of compound **180** bound to PI3K $\delta$  (2.96 Å resolution).

It is possible that the oxygen of the methoxy substituent could still act as a hydrogen-bond acceptor; however the strength and angular preference of a hydrogen bond to an ether are different to that of a carbonyl. It has been shown that the preferred orientation of a hydrogen bond from a donor to a carbonyl is in plane with the oxygen lone pairs, pointing towards one of the lone pairs such that the angular geometry is trigonal at the carbonyl oxygen.<sup>101</sup> However, the preferred geometry of a hydrogen bond from a donor to an ether oxygen is pyramidal at the oxygen, hence the hydrogen bond is not in plane with the substituents on the ether.<sup>101</sup>

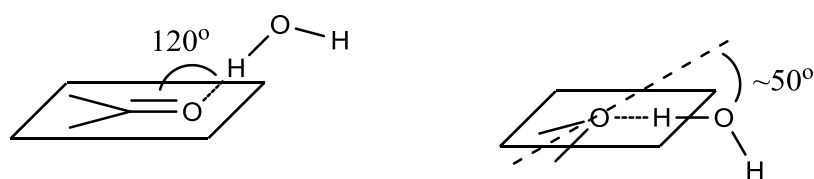


Figure 4.3.8. Preferred hydrogen bond orientations.<sup>101</sup>

The crystal structures show the oxygen of the methoxyl group to directly overlay with that of the carbonyl group of compound **182** (Figure 4.3.9).



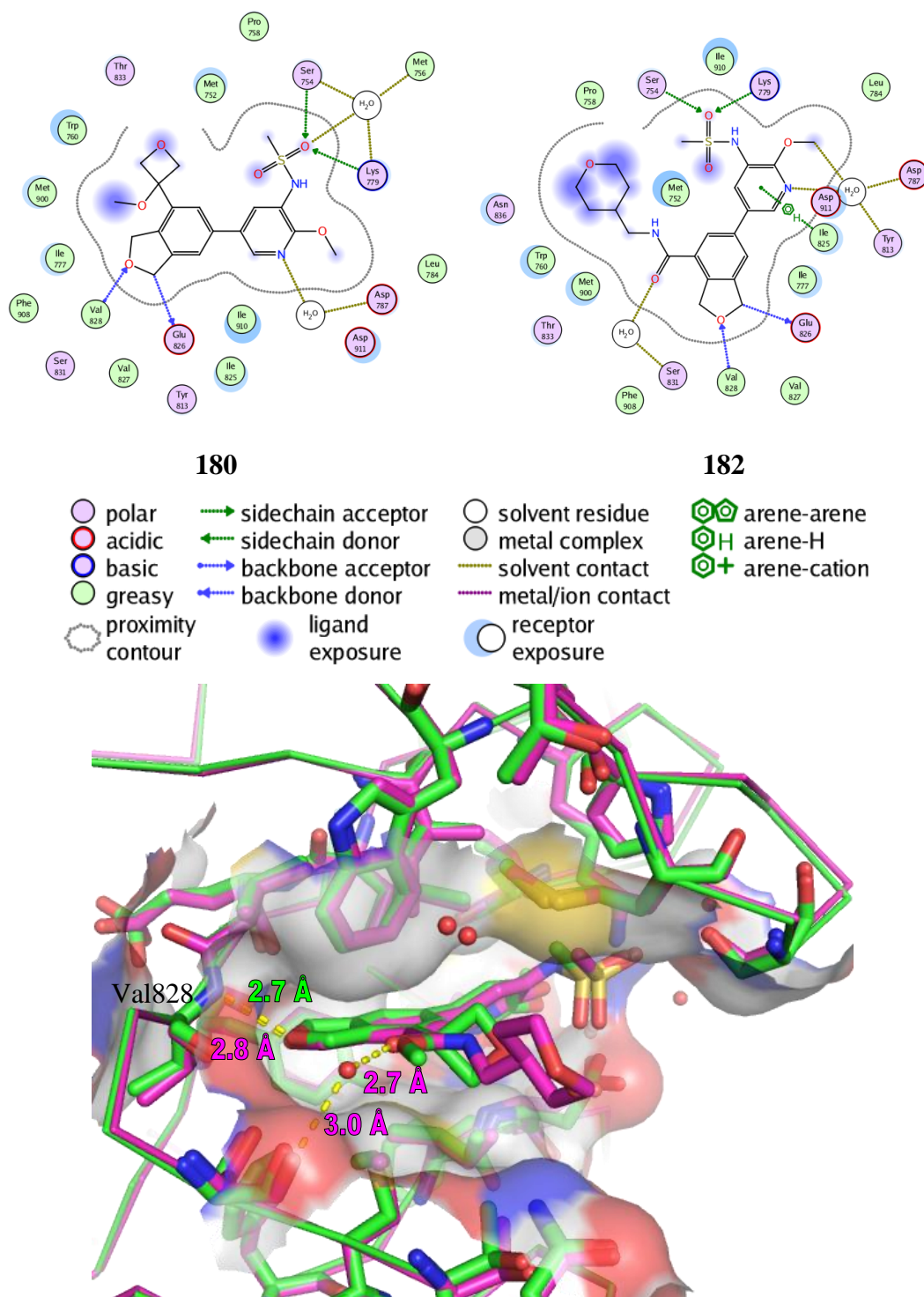
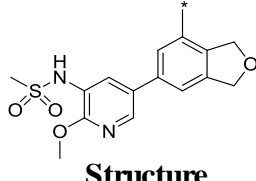
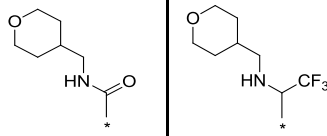


Figure 4.3.9. Overlay of co-crystal structures of benzamide **182** (purple structure, 2.49 Å resolution) and oxetane **180** (green structure, 2.96 Å resolution) bound to PI3Kδ.

Since the hydrogen bond being formed is with a water molecule that could move in order to adopt the most preferred orientation, it is difficult to say whether the differences in angular preference are impacting the formation of this hydrogen bond. It is more likely that the decreased binding affinity of compound **180** arises from the strength of a hydrogen bond with the methoxyl group being much weaker than with a carbonyl, since an ether is a much weaker hydrogen bond acceptor,<sup>76</sup> and also that the increased bulk of the oxetane may not be tolerated in this region of the protein.

Indeed, despite the crystal structure showing there is space available it seems that larger linker groups at the 4-position may not be tolerated. The bulkier trifluoroethylamine group leads to a significant decrease in PI3K $\delta$  potency when compared with its benzamide analogue (Table 4.3.3).



Structure		
<b>Compound Number</b>	<b>182</b>	<b>183</b>
<b>Mean PI3K<math>\delta</math> pIC<sub>50</sub> (N)</b>	7.5 (3)	4.8 (2)
<b>Mean PI3K<math>\alpha</math> pIC<sub>50</sub> (N)</b>	6.5 (3)	4.6 (2) <sup>a</sup>
<b>Mean PI3K<math>\beta</math> pIC<sub>50</sub> (N)</b>	6.6 (3)	<4.5 (3)
<b>Mean PI3K<math>\gamma</math> pIC<sub>50</sub> (N)</b>	6.6 (3)	4.6 (1) <sup>b</sup>
<b>Mean HWB pIC<sub>50</sub> (N)</b>	6.6 (5)	-
<b>LE/LLE<sub>AT</sub></b>	0.32/0.37	0.19/0.19
<b>PFI</b>	4.7	6.80
<b>mChromlogD<sub>pH7.4</sub></b>	2.74	4.77
<b>clogP</b>	1.4	2.7
<b>MW</b>	462	516
<b>TPSA</b>	116	99
<b>AMP (pH 7.4, nm/s)</b>	91	470
<b>CLND Solubility (<math>\mu</math>M)</b>	448	-
<b>FaSSIF Solubility after 4 h (<math>\mu</math>g/ml)</b>	-	-
<b>hERG pIC<sub>50</sub></b>	4.4 (1) <sup>c</sup>	4.6 (2) <sup>d</sup>
<b>CYP 3A4 pIC<sub>50</sub></b>	<4.3 (1)	<4.3 (1)

<sup>a</sup> Returned value <4.5 on one test occasion. <sup>b</sup> Returned value <4.6 on two test occasions.  
<sup>c</sup> Returned value <4.3 on one test occasion. <sup>d</sup> Returned no value on one occasion.

Table 4.3.3. Biological data for compound **183** and benzamide comparator **182**.

The preferred conformation of the trifluoroethylamine compound is with a torsion angle of 45° such that the 4-position substituent is not in plane with the dihydroisobenzofuran core (Figure 4.3.10).

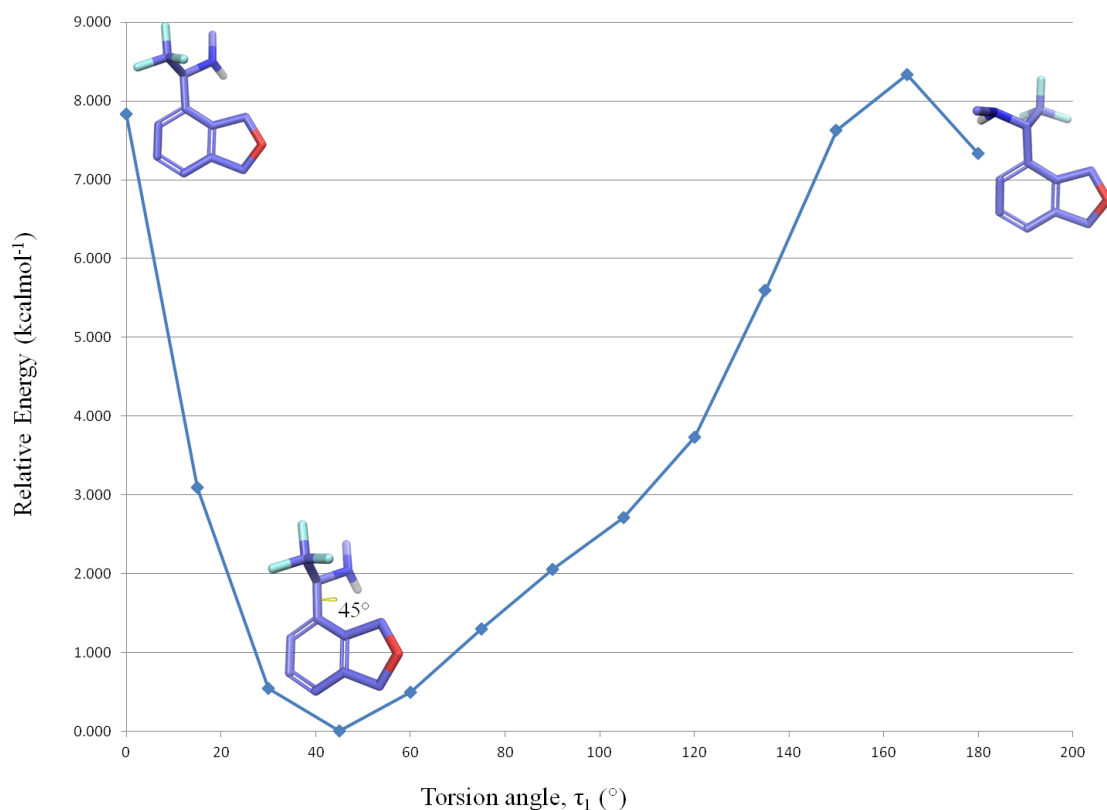
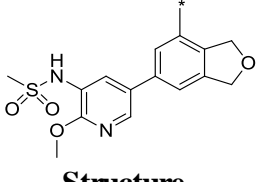
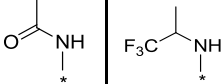
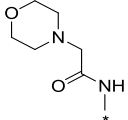
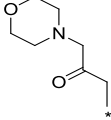


Figure 4.3.10. Torsional scan of trifluoroethyl-substituted dihydroisobenzofuran and the lowest energy conformer.

If the compound does bind in this orientation it could be detrimental to potency as bulk above and below the plane of the dihydroisobenzofuran ring does not seem to be tolerated, although a crystal structure could not be obtained in order to assess whether it was this conformation that was adopted when the compound bound in the active site. In addition the trifluoroethyl group cannot engage in the same interactions as the benzamide, which may also be impacting the binding affinity.

In contrast, the observation that the trifluoroethyl analogue of the anilide was tolerated was interesting. The biological data showed higher PI3K $\delta$  potency and better selectivity over the other PI3K isoforms than the analogous anilide (compare **174** and **175**, Table 4.3.4). It is also obvious that the inclusion of a hydrogen bond

donor is beneficial for binding affinity as removing this led to decreased PI3K $\delta$  potency (compare **173** and **181**, Table 4.3.4).

Structure				
Compound Number	<b>174</b>	<b>175</b>	<b>173</b>	<b>181</b>
Mean PI3K $\delta$ pIC <sub>50</sub> (N)	6.4 (2)	7.0 (2)	6.8 (3)	6.1 (2)
Mean PI3K $\alpha$ pIC <sub>50</sub> (N)	5.8 (2)	6.4 (2)	5.3 (3)	5.2 (2)
Mean PI3K $\beta$ pIC <sub>50</sub> (N)	5.3 (2)	5.6 (2)	5.0 (3)	5.0 (2) <sup>c</sup>
Mean PI3K $\gamma$ pIC <sub>50</sub> (N)	5.3 (2)	5.6 (2)	5.0 (3)	4.8 (2)
Mean HWB pIC <sub>50</sub> (N)	5.6 (2) <sup>a</sup>	5.4 (2) <sup>a</sup>	6.5 (9) <sup>b</sup>	4.7 (1) <sup>d</sup>
LE/LLE <sub>AT</sub>	0.34/0.37	0.33/0.30	0.29/0.33	0.26/0.30
PFI	4.0	6.7	4.6	4.7
mChromlogD <sub>pH7.4</sub>	1.97	4.69	2.59	2.73
clogP	1.5	3.1	1.6	1.8
MW	377	431	463	462
TPSA	107	90	119	107
AMP (pH 7.4, nm/s)	-	660	135	160
CLND Solubility ( $\mu$ M)	426	301	401	365
FaSSIF Solubility after 4 h ( $\mu$ g/ml)	-	-	20	-
hERG pIC <sub>50</sub>	<4.2 (3)	4.6 (3)	<4.3 (3)	<4.2 (3)
CYP 3A4 pIC <sub>50</sub>	<4.3 (1)	4.4 (1)	<4.3 (1)	<4.3 (1)

<sup>a</sup> Returned no value on one test occasion. <sup>b</sup> Returned no value on two test occasions. <sup>c</sup> Returned value <4.5 on one test occasion. <sup>d</sup> Returned value <4.4 on one test occasion and returned no value on one test occasion.

Table 4.3.4. Biological data for compounds **175** and **181** and their comparators.

The preferred conformation of the amine substituent of compound **175** has the trifluoroethyl group pointing away from the dihydrofuran of the dihydroisobenzofuran core (Figure 4.3.11). The bulky trifluoroethyl group would occupy a different position in the active site compared to the trifluoroethyl group of compound **183** as it sits further from the core, which may be why it is tolerated. This

conformation also means the N-H would be in a similar position to that of the anilide. It is unclear whether the N-H is engaging in any electrostatic interactions in the active site; the diminished potency of the ketone, in which this hydrogen bond donor is removed, could just be due to conformational differences. Indeed, the ketone prefers to adopt a conformation in which there is a twist of  $75^\circ$  at the 4-position, which is somewhat different to the conformation adopted by the anilides (Figure 4.3.11).

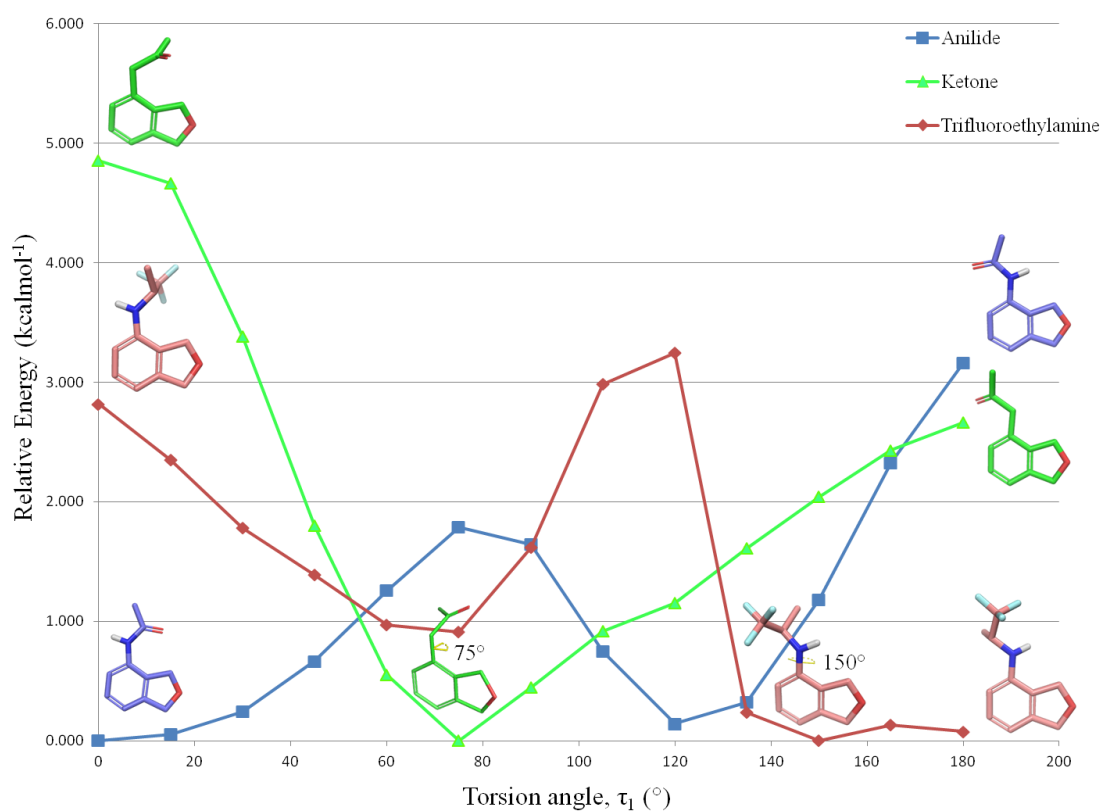
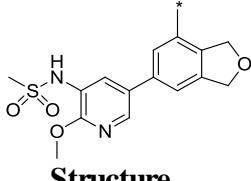
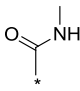
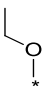
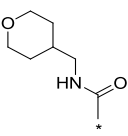
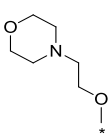


Figure 4.3.11. Torsional scans and low energy conformations of 4-position substituents.

If the N-H were able to engage in hydrogen bonding with the protein backbone *via* an interaction with the conserved water, the increased potency of the trifluoroethyl compound compared with the anilide can be rationalised. The more

electron-withdrawing trifluoroethyl substituent would increase the partial positive charge on the electron-deficient hydrogen of the donor, strengthening the hydrogen bond. However, no co-crystal structures of the 4-substituted anilides (up to now) have confirmed electrostatic interactions with the protein backbone. Indeed, no electrostatic interactions with 4-position linkers other than the benzamides have been identified and one intriguing result was the similar PI3K $\delta$  potency and ligand efficiency of the 4-substituted ethers when compared with the benzamides (Figure 4.3.12).

 Structure				
Compound Number	<b>177</b>	<b>176</b>	<b>182</b>	<b>184</b>
Mean PI3K $\delta$ pIC <sub>50</sub> (N)	7.4 (7)	7.4 (2)	7.5 (3)	7.2 (6) <sup>a</sup>
Mean PI3K $\alpha$ pIC <sub>50</sub> (N)	6.7 (8)	6.8 (2)	6.5 (3)	5.9 (7)
Mean PI3K $\beta$ pIC <sub>50</sub> (N)	6.5 (7)	6.8 (2)	6.6 (3)	6.0 (7)
Mean PI3K $\gamma$ pIC <sub>50</sub> (N)	7.0 (7)	6.6 (2)	6.6 (3)	6.0 (7)
Mean HWB pIC <sub>50</sub> (N)	6.6 (9) <sup>a</sup>	5.7 (3)	6.6 (5)	6.2 (7) <sup>b</sup>
LE/LLE <sub>AT</sub>	0.39/0.44	0.41/0.36	0.32/0.37	0.32/0.32
PFI	4.1	6.8	4.7	5.2
mChromlogD <sub>pH7.4</sub>	2.08	4.78	2.74	3.22
clogP	1.1	2.8	1.4	2.4
MW	377	364	462	449
TPSA	107	87	116	99
AMP (pH 7.4, nm/s)	73	790	91	445
CLND Solubility ( $\mu$ M)	455	220	448	391
FaSSIF Solubility after 4 h ( $\mu$ g/ml)	228	-	-	-
hERG pIC <sub>50</sub>	5.8 (1)	4.7 (5) <sup>a</sup>	4.4 (1) <sup>c</sup>	4.5 (2)
CYP 3A4 pIC <sub>50</sub>	<4.3 (1)	<4.3 (1)	<4.3 (1)	<4.3 (1)

<sup>a</sup> Returned no value on one test occasion. <sup>b</sup> Returned no value on three test occasions. <sup>c</sup> Returned value <4.3 on one test occasion.

Table 4.3.5. Biological data for 4-substituted ethers **176** and **184** and their benzamide comparators.

Torsional scans for the 4-ether substituent showed that the preferred ligand conformation in the free state oriented the ether lone pair towards the furan so that the alkyl substituent points away, which is analogous to the global minimum for the benzamide (Figure 4.3.12).

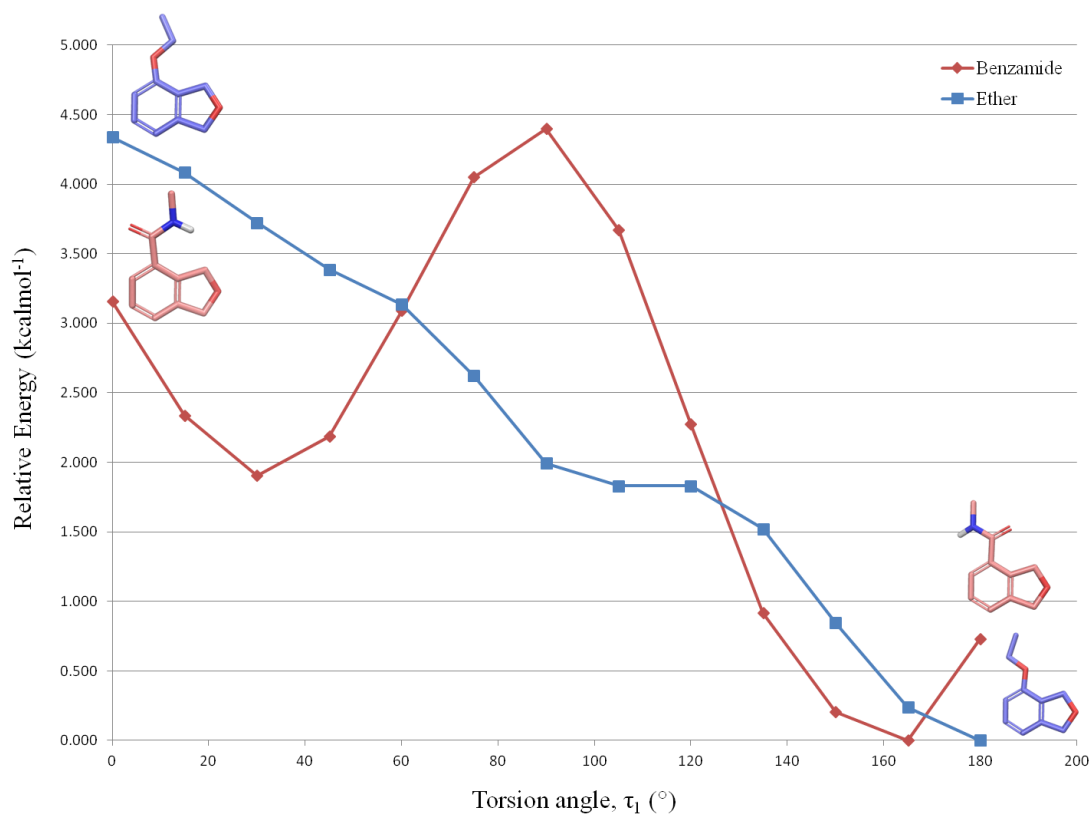


Figure 4.3.12. Torsional scans and low energy conformations of 4-substituent ethers.

The conformational analysis showed an increased energetic preference for the ether to be co-planar with the core dihydroisobenzofuran, which is not consistent with the co-crystal structure (Figure 4.3.13).

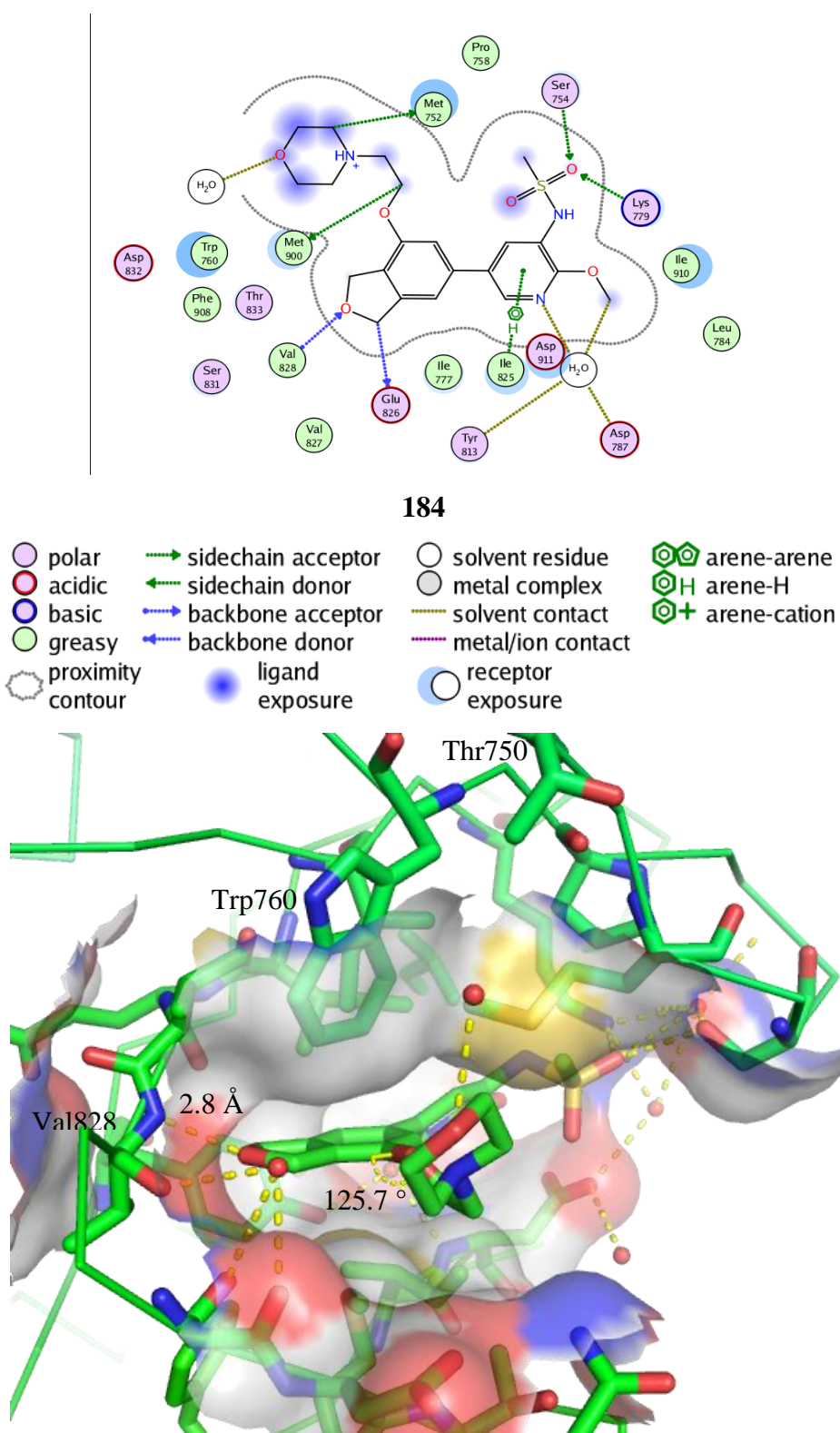


Figure 4.3.13. Co-crystal structure of compound **184** bound to PI3K $\delta$  (2.94 Å resolution).

Although the alkyl substituent is oriented away from the dihydrofuran of the core, the torsion angle in the bound state was observed to be 125.7° (Figure 4.3.13). The torsional scan suggests that this 40° angular displacement from the global minimum would result in an energy penalty of approximately 2 kcal mol<sup>-1</sup>; however, this is not reflected in the binding affinity, as the PI3K $\delta$  activity remains high. The hydrogen bond between the dihydroisobenzofuran oxygen of the fully elaborated ether compound and the valine residue of the hinge region was observed to be slightly shorter (2.6 Å, Figure 4.3.13) than that observed for other compounds previously, so it may be that the potentially stronger hydrogen bond is contributing to the PI3K $\delta$  activity. There are no obvious electrostatic interactions with the protein backbone in which the ether oxygen is participating, unlike the water-mediated interaction confirmed in the co-crystal structure of the benzamide. In the case of the ether, the oxygen is too far away from the conserved water molecule (4.7 Å) for any involvement. The co-crystal structure of the fully elaborated compound also shows a previously unobserved water molecule engaging in an interaction with the morpholino oxygen (Figure 4.3.13). However, it seems this is not contributing to PI3K $\delta$  activity as the ligand efficiency of the fully elaborated compound (**184**, LE = 0.32) is much less than that of the truncated compound (**176**, LE = 0.41); the pendant amine substituent is therefore not contributing to PI3K $\delta$  activity but is solely advantageous in terms of selectivity over the other PI3K isoforms. The amine orients towards the tryptophan residue in order to engage in a cation- $\pi$  interaction, which may also rationalise why the ether does not conform to being co-planar (green structure, Figure 4.3.14). This interaction also ensures that the morpholine occupies the tryptophan shelf; the PI3K isoform selectivity is therefore much improved over the benzamide, in which the tetrahydropyan substituent is unable to engage the tryptophan (cyan structure, Figure 4.3.14). Indeed, the pendant morpholine substituent occupies a similar position to that of the anilide (purple structure, Figure 4.3.14).



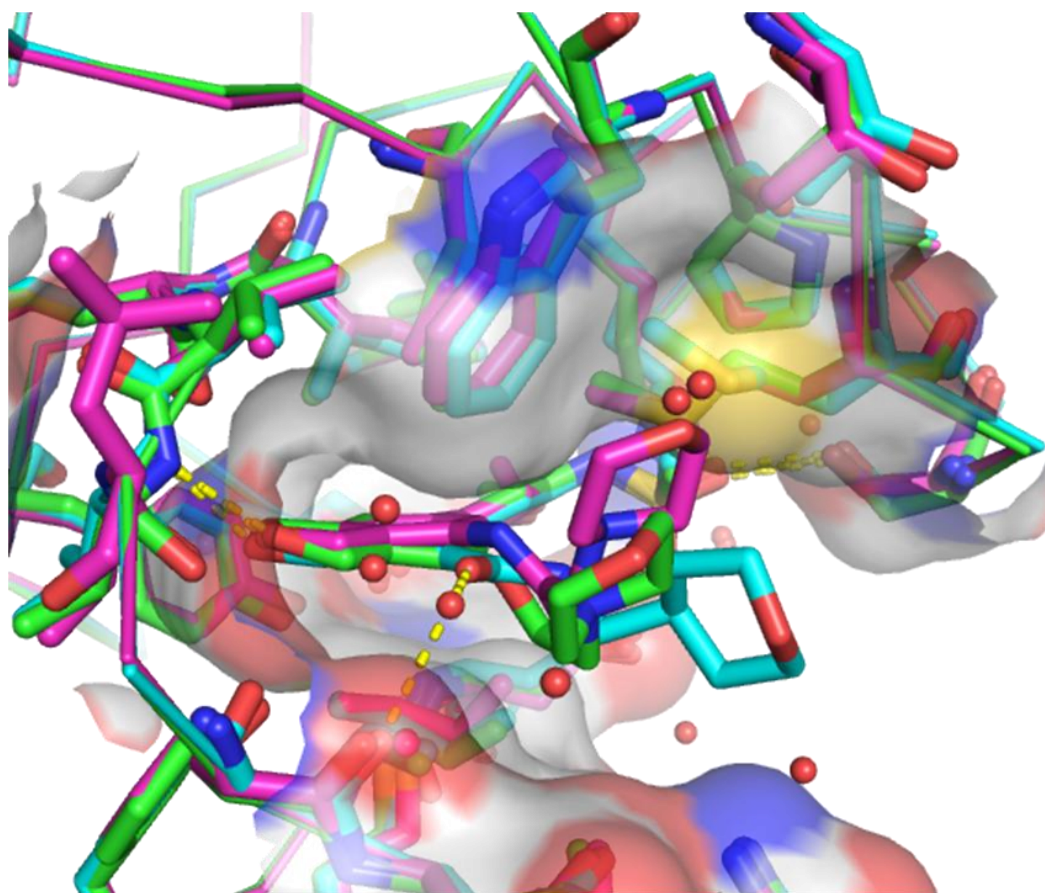


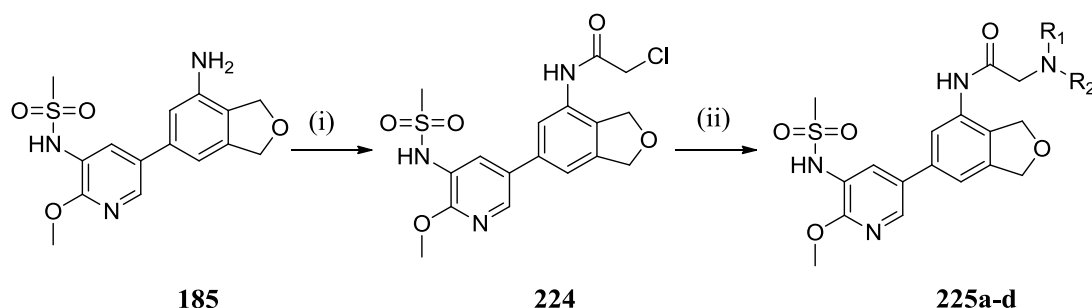
Figure 4.3.14. Overlay of co-crystal structures of anilide **173** (purple structure, 3.22 Å resolution), benzamide **182** (cyan structure, 2.49 Å resolution) and ether **184** (green structure, 2.94 Å resolution).

From this analysis it can be observed that the 4-position linker does have an effect on PI3K $\delta$  potency, however the selectivity is primarily influenced by the nature of the pendant substituent. Additional water-mediated interactions of the 4-position linkers with the protein backbone can be achieved, for example with the carbonyl of the benzamide linker, which leads to increased PI3K $\delta$  activity. Selectivity over the other isoforms has so far only been achieved when the presence of a basic amine ensures the tryptophan shelf is occupied. Therefore as long as the 4-position linker is small and flexible, and a pendant amine substituent is incorporated, good PI3K $\delta$  potency and selectivity are achievable.

#### 4.3.1.4. Further Exploration of 4-Substituted Dihydroisobenzofurans

From the initial investigation into preferred linkers and 4-position substituents, it was observed that anilide and ether linkers with pendant solubilising groups conferred good PI3K $\delta$  potency and selectivity.

An array around compound **173** was designed in order to further explore the anilide substituent at the 4-position. The array used intermediate **224** and various amine monomers to give final compounds with a similar framework to compound **173** (Scheme 4.3.22).<sup>102</sup>



Reagents and Conditions: (i) chloroacetyl chloride, NEt<sub>3</sub>, 2-MeTHF, 0 °C to rt, 73%; (ii) HNR<sub>1</sub>R<sub>2</sub>, DIPEA, MeCN, 70 °C, 8-70%.

Scheme 4.3.22. Amination array (not described in Experimental as array was carried out by E. Maduli, GSK).<sup>102</sup>

The monomers were chosen using a web tool, TIMS (Tool for Interactive Monomer Selection)<sup>103</sup> that gives a set of building blocks which are similar to a structure of interest in order to further explore the chemical space, a selection of which are shown in Table 4.3.6.

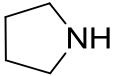
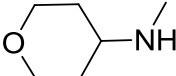
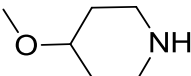
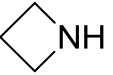
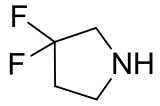
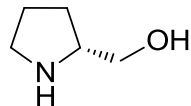
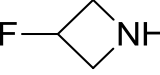
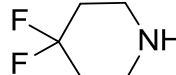
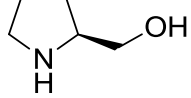
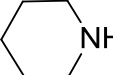
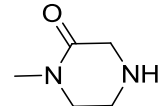
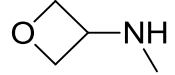
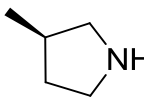
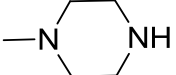
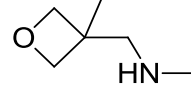
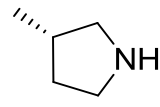
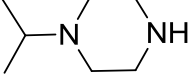
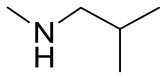
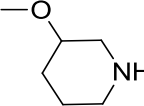
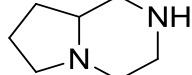
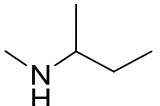
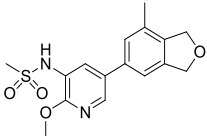
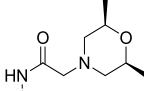
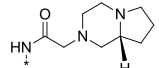
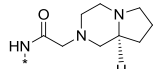
		
		
		
		
		
		
		

Table 4.3.6. Amine monomers.

The compounds were tested for their activity against the PI3K enzymes and four compounds were found to have good PI3K $\delta$  potency and isoform selectivity (Table 4.3.7).

Structure				
Compound Number	225a	225b	225c	225d
Mean PI3K $\delta$ pIC <sub>50</sub> (N)	7.3 (5)	7.4 (2)	7.1 (2)	7.6 (2)
Mean PI3K $\alpha$ pIC <sub>50</sub> (N)	5.1 (6)	5.2 (3)	5.5 (5)	5.7 (5)
Mean PI3K $\beta$ pIC <sub>50</sub> (N)	4.9 (5)	5.3 (2)	5.6 (2)	5.6 (2)
Mean PI3K $\gamma$ pIC <sub>50</sub> (N)	4.8 (4) <sup>a</sup>	<4.5 (3)	5.0 (1) <sup>a</sup>	<4.8 (2)
Mean HWB pIC <sub>50</sub> (N)	6.3 (10) <sup>b</sup>	6.5 (5)	7.0 (6)	7.2 (6)
LE/LLE <sub>AT</sub>	0.29/0.30	0.29/0.34	0.28/0.30	0.30/0.31
PFI	5.7	3.8	4.0	4.1
mChromlogD <sub>pH7.4</sub>	3.71	1.77	2.03	2.05
clogP	2.6	1.5	2.4	2.4
MW	490	503	501	501
TPSA	119	113	113	113
AMP (pH 7.4, nm/s)	327	96	104	98
CLND Solubility ( $\mu$ M)	359	432	342	358
FaSSIF Solubility after 4 h ( $\mu$ g/ml)	15	>900	815	672 <sup>c</sup>
hERG pIC <sub>50</sub>	4.9 (2)	4.4 (2) <sup>d</sup>	<4.6 (2)	<4.6 (2)
CYP 3A4 pIC <sub>50</sub>	<4.3 (2)	4.5 (1)	5.4 (2)	4.9 (2)

<sup>a</sup> Returned value <4.5 on one test occasion. <sup>b</sup> Returned no value on one test occasion. <sup>c</sup> FaSSIF solubility measured at 24 h timepoint. <sup>d</sup> Returned value <4.3 on two test occasions.

Table 4.3.7. Biological data for 4-substituted anilides.

Increasing the bulk of the pendant saturated group, either through alkyl substitution or a fused ring, is thought to be tolerated in PI3K $\delta$  as the tryptophan shelf has space to accommodate this additional bulk. An increase in PI3K $\delta$  potency is observed but there is no concomitant increase in potency for the other PI3K isoforms. This could be because the tryptophan shelf is unavailable and the increased bulk is not tolerated.

The compounds were screened in *in vitro* microsomal stability assays for three species (rat, dog and human) in order to assess the *in vitro* clearance of the compounds. This IVC data and all that subsequently reported in this Chapter were determined within Cyprotex.<sup>104</sup> The data is reported in Table 4.3.8, alongside

that of the lead dihydroisobenzofuran compound (**173**). Two compounds with good whole blood potency (**225b** and **225c**), low *in vitro* clearance in rat microsomes and high FaSSIF solubility were progressed to *in vivo* pharmacokinetic studies in the rat and this data is also reported in Table 4.3.8.<sup>105</sup>

Structure					
Compound Number	<b>173</b>	<b>225a</b>	<b>225b</b>	<b>225c</b>	<b>225d</b>
Mean PI3Kδ pIC <sub>50</sub> (N)	6.8 (3)	7.3 (5)	7.4 (2)	7.1 (2)	7.6 (2)
Mean HWB pIC <sub>50</sub> (N)	6.5 (9) <sup>a</sup>	6.3 (10) <sup>b</sup>	6.5 (5)	7.0 (6)	7.2 (6)
FaSSIF Solubility at 4 h (µg/ml)	20	15	>900	815	672 <sup>c</sup>
Human microsomal IVC (ml/min/kg)	<0.53	<0.53	<0.53	<0.53	<0.53
Rat microsomal IVC (ml/min/kg)	<0.53	<0.53	<0.53	<0.53	<0.53
Dog microsomal IVC (ml/min/kg)	<0.53	<0.53	<0.53	<0.53	<0.53
Rat Cl <sub>b</sub> (ml/min/kg)	14	-	77	121	-
Vd <sub>ss</sub> (L/kg)	1.1	-	3.9	3.8	-
t <sub>1/2</sub> (h)	1.25	-	0.9	0.5	-
Rat F%	54	-	<5	8	-

<sup>a</sup> Returned no value on two test occasions. <sup>b</sup> Returned no value on one test occasion. <sup>c</sup> FaSSIF solubility measured at 24 h timepoint.

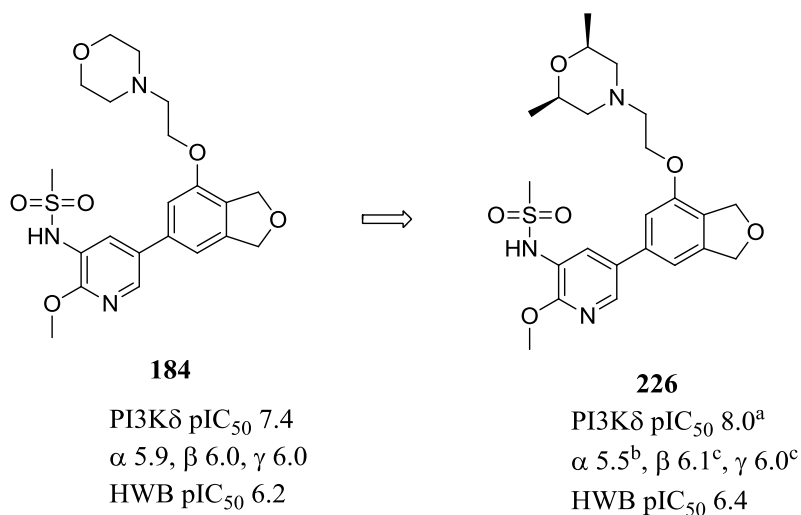
Table 4.3.8. Pharmacokinetic data for 4-anilide compounds.

Unfortunately, the clearance was high for both compounds (> 90% rat liver blood flow) and resulted in short half-lives, despite good volume of distribution. The high clearance of these compounds when compared to that of compound **173** could be due to different mechanisms of metabolism of the pendant basic groups. The high clearance is not predicted by the *in vitro* microsomal stability, which could be attributed to alternative mechanisms of metabolism that are not represented by the *in vitro* rat liver microsomal stability assay, for example phase II reactions mediated by CYP enzymes or metabolism *via* non-CYP enzymes. Therefore the more potent

anilide compounds **225b** and **225c** were found to have no oral bioavailability and since they did not show an improved pharmacokinetic profile compared to compound **173**, the 4-substituted ether compounds, rather than the 4-substituted anilides, were investigated further as part of this programme of work.

#### 4.3.1.5. Optimisation of the PK Profile of 4-Ether Substituted Dihydroisobenzofurans

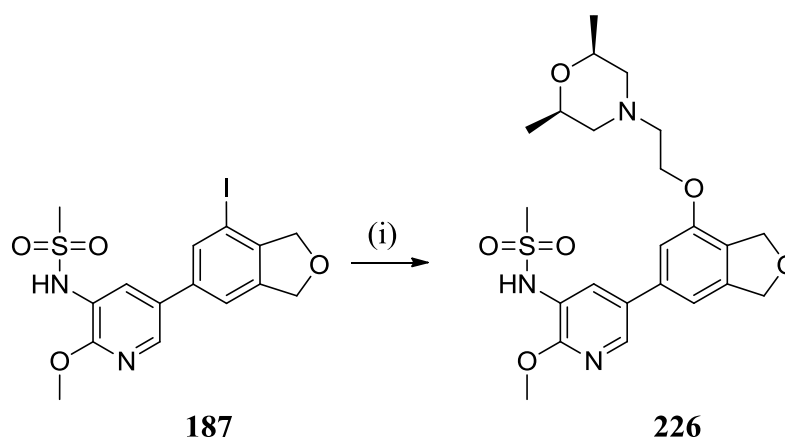
Compound **184** had shown encouraging PI3K $\delta$  activity both at the enzyme and in HWB but had insufficient selectivity over the other PI3K isoforms, therefore compound **226** was synthesised to investigate whether selectivity could be improved by increasing steric demand around the pendant amine as had been observed previously. Compound **226** had increased PI3K $\delta$  enzyme activity and achieved the desired 100-fold selectivity over the other PI3K isoforms; however there was no increase in PI3K $\delta$  HWB activity and it remains unclear as to the reason for this (Scheme 4.3.23).



<sup>a</sup> Returned no value on one test occasion and one value >10.5 on one test occasion. <sup>b</sup> Returned value <4.5 on two test occasions and no value on one test occasion. <sup>c</sup> Returned value <4.5 on one test occasion.

Scheme 4.3.23. Elaboration of compound **184** to improve selectivity.

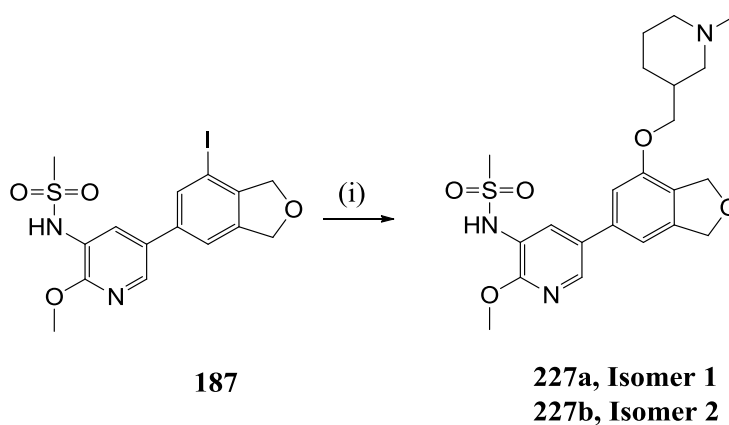
The synthesis of compound **226** took place *via* a ligand-free Ullman reaction (Scheme 4.3.24).<sup>106</sup> In this case, the use of DMSO as the reaction solvent resulted in an increased yield (29%) compared with the aforementioned analogous reaction that used methanol (17%). This may be due to increased solubility of iodide intermediate **187** in DMSO.



Reagents and Conditions: (i) 2-((2*S*,6*R*)-2,6-dimethylmorpholino)ethanol (15 eq.), CuI, Li*O**t*-Bu, DMSO, 150 °C,  $\mu$ wave, 29%.

Scheme 4.3.24. Synthesis of compound **226**.

Further exploration of SAR for the 4-ether substituted dihydroisobenzofurans included the synthesis of compound **227** using a commercially available racemic alcohol (Scheme 4.3.25). The enantiomers were then separated by chiral chromatography.<sup>107</sup>

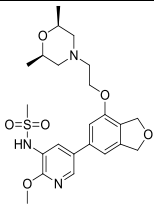
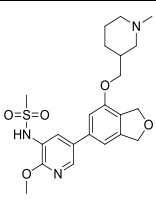
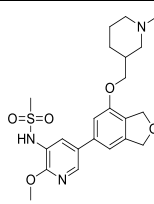


Reagents and Conditions: (i) (1-methylpiperidin-3-yl)methanol (10 eq.), CuI, LiO*t*-Bu, DMSO, 160 °C,  $\mu$ wave, 20% (**227a**), 19% (**227b**).

Scheme 4.3.25. Synthesis of compounds **227a** and **227b** (not described in Experimental as synthesised by E. Schmitt and S. Jackson, GSK).<sup>107</sup>

Pleasingly, a high level of PI3K $\delta$  HWB activity was achieved for compound **227b** and the clearance of compounds **226** and **227b** was assessed *in vitro* in rat and human liver microsomes and through rat *in vivo* pharmacokinetic studies (Table 4.3.9).<sup>108</sup>



Structure			
Compound Number	<b>226</b>	<b>227a</b>	<b>227b</b>
Mean PI3K $\delta$ pIC <sub>50</sub> (N)	8.0 (6) <sup>a</sup>	7.8 (2)	8.3 (2)
Mean PI3K $\alpha$ pIC <sub>50</sub> (N)	5.5 (6) <sup>b</sup>	6.1 (2)	7.0 (2)
Mean PI3K $\beta$ pIC <sub>50</sub> (N)	6.1 (7) <sup>c</sup>	6.2 (2)	6.8 (2)
Mean PI3K $\gamma$ pIC <sub>50</sub> (N)	6.0 (6) <sup>c</sup>	5.3 (2)	5.7 (2)
Mean HWB pIC <sub>50</sub> (N)	6.4 (14)	6.7 (5)	7.1 (5)
LE/LLE <sub>AT</sub>	0.33/0.30	0.34/0.33	0.37/0.35
PFI	6.5	4.3	4.2
mChromlogD <sub>pH7.4</sub>	4.53	2.30	2.17
clogP	3.5	2.8	2.8
MW	478	447	447
TPSA	99	90	90
AMP (pH 7.4, nm/s)	665	340	400
CLND Solubility ( $\mu$ M)	357	388	599
FaSSiF Solubility after 4 h ( $\mu$ g/ml)	107	>1500	>1500
hERG pIC <sub>50</sub>	4.4 (2)	4.3 (2)	4.4 (1) <sup>d</sup>
CYP 3A4 pIC <sub>50</sub>	<4.7 (2)	4.4 (2)	4.6 (2)
IVC (ml/min/g)	3.49 (rat), 1.17 (human)	5.39 (rat), 0.95 (human)	11.80 (rat), <0.53 (human)
Rat Cl <sub>b</sub> (ml/min/kg)	55	-	153
Vd <sub>ss</sub> (L/kg)	3.1	-	3.9
t <sub>1/2</sub> (h)	1.1	-	0.3
F%	44	-	0

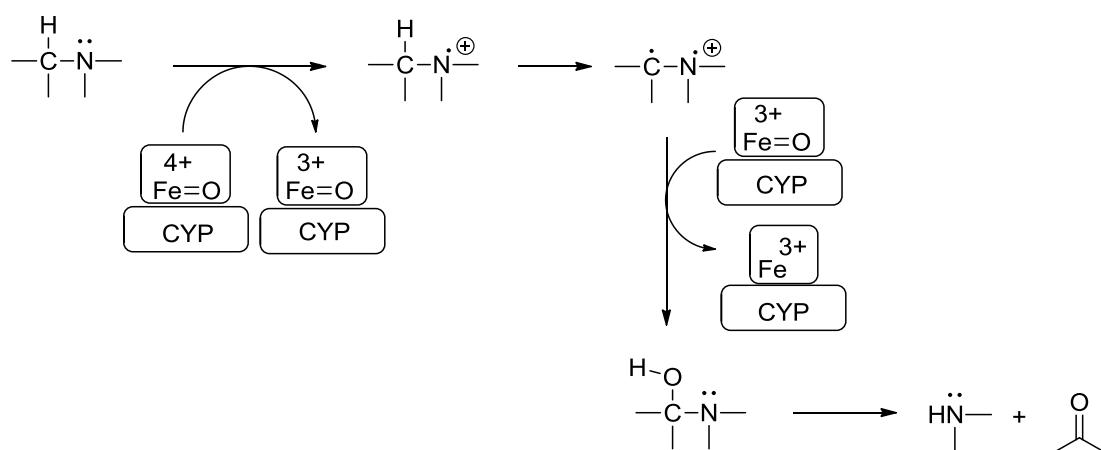
<sup>a</sup> Returned no value on one test occasion and value >10.5 on one test occasion. <sup>b</sup> Returned value <4.5 on two test occasions and no value on one test occasion. <sup>c</sup> Returned no value on one test occasion. <sup>d</sup> Returned value <4.2 on one test occasion.

Table 4.3.9. Data for compounds **226**, **227a** and **227b**.

The rat pharmacokinetic data for compound **226** was encouraging because an oral bioavailability of 44% was achieved; however the half-life was only 1.1 h, which is most likely due to the moderate-to-high clearance of this compound. As the volume of distribution was high, the compound would be distributed extensively throughout in body tissue. A half-life of this brevity would lead to a too frequent dosing regimen. Unfortunately, compound **227b** also showed a very short half-life since the clearance was greater than rat LBF, hence no oral bioavailability was

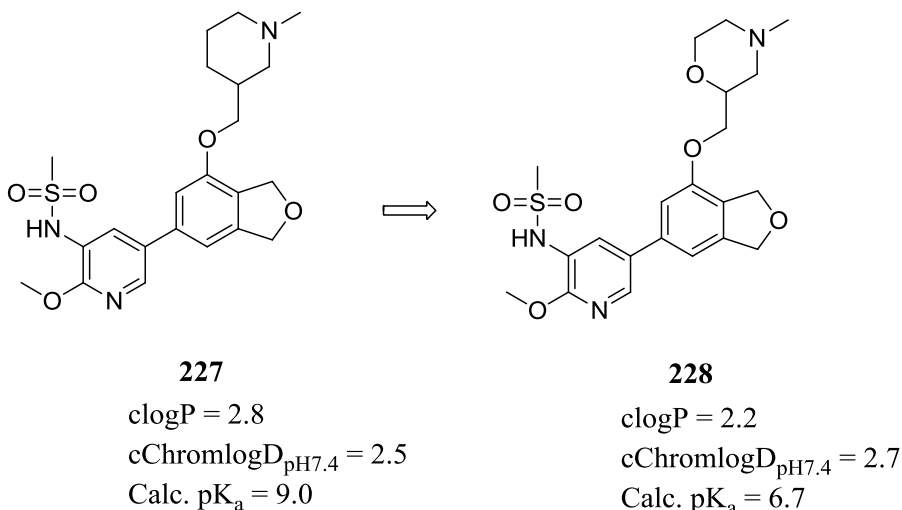
observed for this compound. It can be seen that the *in vivo* clearance values were in accordance with the *in vitro* clearance in rat liver microsomes, so the *in vitro* data could provide a useful indication of the *in vivo* clearance of the 4-ether dihydroisobenzofuran compounds. Interestingly, there was a discrepancy between the *in vitro* clearance of compound **227b** in rat and human microsomes, with the human data showing low clearance. Screening more compounds and also investigating the *in vitro* clearance in other species (*e.g.* dog) may help to examine these differences further.

In order to address the clearance and half-life issues, additional modifications of the 4-alkoxy substituent were investigated with the aim of enhancing metabolic stability whilst maintaining potency and selectivity. One strategy was to modify the potentially metabolically labile *N*-methyl group of compound **227b**. Dealkylation of primary and secondary amines *via* an oxidative mechanism is a common reaction in drug metabolism and is thought to occur *via* a single electron transfer from the heteroatom, generating a radical cation (Scheme 4.3.26).<sup>109</sup> Loss of the  $\alpha$ -proton produces a carbon radical that recombines with a ferric-bound hydroxyl radical to give an unstable hemiaminal that decomposes to the free amine and a carbonyl compound (Scheme 4.3.26).<sup>109</sup>

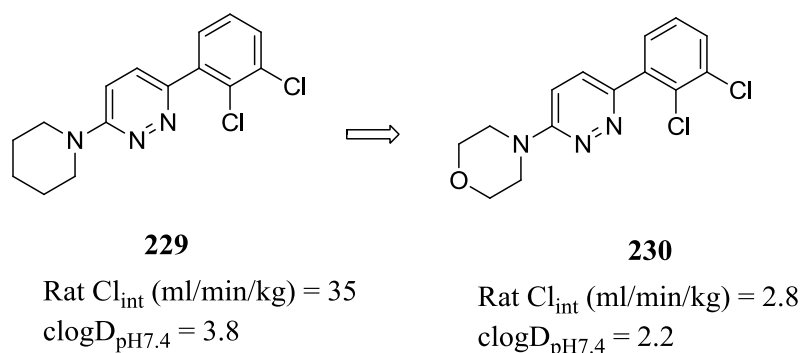


Scheme 4.3.26. Proposed mechanism for *N*-dealkylation.<sup>109</sup>

Modifications to the physicochemical characteristics of the compounds, specifically reducing lipophilicity and nitrogen basicity, were made in order to decrease the potential of the compounds as inhibitors or substrates of CYP enzymes. The first change was to introduce a morpholino-substituent in place of the piperidine in order to achieve lower lipophilicity and basicity.

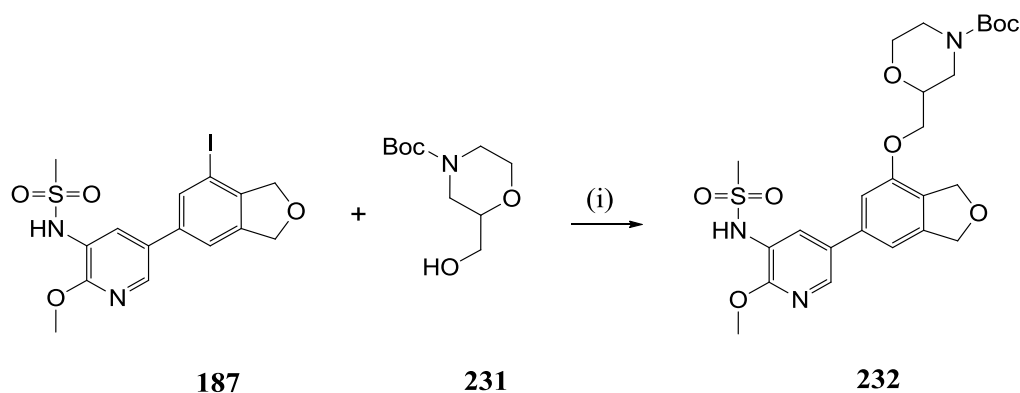


This strategy has been used in drug discovery to improve metabolic stability, for example in the optimisation of cannabinoid receptor 2 agonists where a 10-fold increase in stability in rat liver microsomes was observed.<sup>110</sup>



The 4-substituted ethers had previously been synthesised *via* an Ullman coupling reaction and this methodology was also used for the preparation of

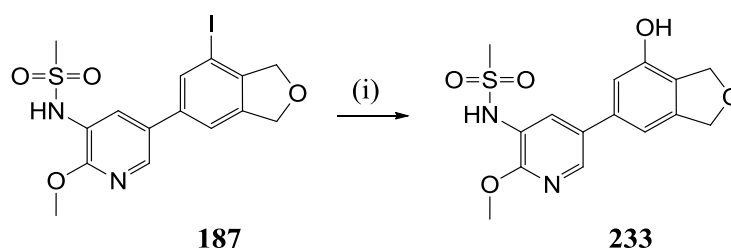
compound **232**, using Boc-protected (hydroxymethyl)morpholine **231** (Scheme 4.3.27).



Reagents and Conditions: (i) CuI, LiOt-Bu, DMSO, 160 °C,  $\mu$ wave, 21%.

Scheme 4.3.27. Synthesis of intermediate **232**.

Again, the Ullman reaction was low yielding and so an alternative route was sought. It was envisaged that the phenol could be accessed from the available iodide intermediate and then derivatised to the desired product *via* a Mitsunobu reaction. The iodide intermediate was converted to the analogous alcohol in good yield *via* a copper-catalysed hydroxylation reaction.<sup>111</sup>

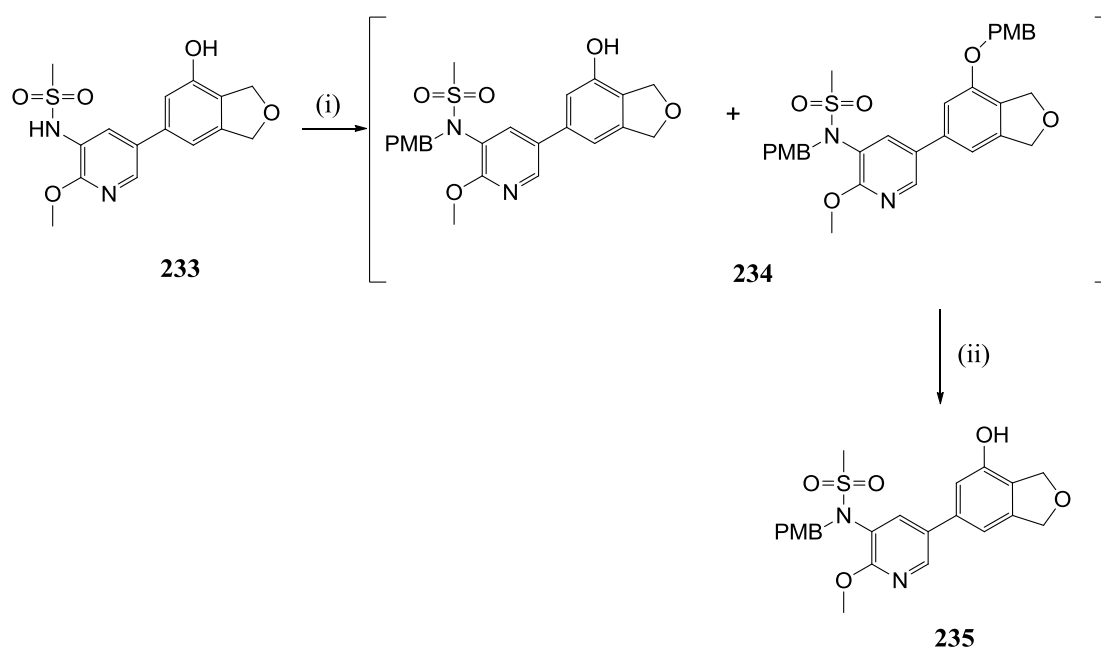


Reagents and Conditions: (i) CuI, *n*-Bu<sub>4</sub>NOH (40% aq. solution), 2-methylquinolin-8-ol, DMSO, 150 °C,  $\mu$ wave, 61%.

Scheme 4.3.28. Synthesis of intermediate **233**.

Microwave heating was used to effect the synthesis of phenol **233** from iodide **187**, which represents a significant advantage over the conditions initially used in hydroxylation reactions of this type. Elevated temperatures and lengthy reaction times were usually required, for example some substrates have needed heating at 150 °C in a steel bomb for 1.5 days.<sup>112</sup> Copper catalysis in high-temperature water (200 °C)<sup>113</sup> under microwave irradiation was reported to be effective for the transformation but alternatives such as DMSO/water and PEG-400/water mixtures have since been shown to have greater utility in this reaction.<sup>114,115</sup> Copper(I) iodide is the most active catalyst for the transformation and a variety of bidentate ligands can be used, for example 1,10-phenanthroline and *N,N'*-dimethylethylenediamine, as well as different bases such as potassium hydroxide and potassium phosphate.<sup>114,116</sup> These bidentate ligands have been found to be efficient in copper-catalysed reactions since they help to prevent the formation of less reactive, multiply ligated cuprate structures.<sup>117</sup> When tetrabutylammonium hydroxide was used as the base, 2-methylquinolin-8-ol was the most effective ligand and this proved effective in the reaction of **187**, giving a respectable 61% isolated yield of phenol **233**.<sup>111</sup>

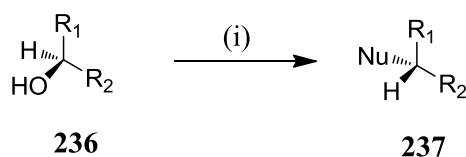
The resulting phenol intermediate then readily underwent sulfonamide protection with *para*-methoxybenzyl chloride in order to generate intermediate **235**, which could be used for subsequent Mitsunobu reactions (Scheme 4.3.29). Formation of the *para*-methoxybenzyl ether at the dihydroisobenzofuran 4-position was also observed to occur (Scheme 4.3.29). The *para*-methoxybenzyl ether could be cleaved with TFA at ambient temperature, while the sulfonamide protecting group was retained under these conditions (Scheme 4.3.29).



Reagents and Conditions: (i) 1-(chloromethyl)-4-methoxybenzene,  $K_2CO_3$ , DMF, rt, taken on crude; (ii) TFA, DCM, rt, 62% over two steps.

#### Scheme 4.3.29. Synthesis of intermediate **235**.

With intermediate **235** in hand, a Mitsunobu reaction with the required alcohol was investigated. The pioneering work of Mitsunobu in the 1960s led to the development of a reaction to convert a primary or secondary alcohol to a variety of products using triphenylphosphine and diethyl azodicarboxylate (DEAD).<sup>118</sup> These conditions were initially used to affect the reaction of an alcohol with acidic nucleophiles such as carboxylic acids and imides.<sup>119</sup> The Mitsunobu protocol has since been applied to many more substrates and represents a powerful synthetic tool, especially as a robust reaction in asymmetric syntheses due to the fact that chiral secondary alcohols undergo complete inversion of stereochemistry (Scheme 4.3.30).<sup>120</sup>

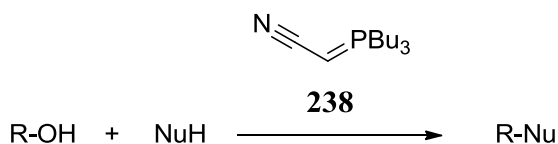


Reagents and Conditions: (i) NuH, PPh<sub>3</sub>, DEAD.

Scheme 4.3.30. Mitsunobu reaction.

The original reagent combination of triphenylphosphine and DEAD led to the generation of triphenylphosphine oxide and a hydrazine by-product, and the need for separation of the product and low atom economy were significant drawbacks. In addition, DEAD must be protonated throughout the reaction hence the nucleophile employed must be acidic; a pK<sub>a</sub> of less than 11 is preferred.

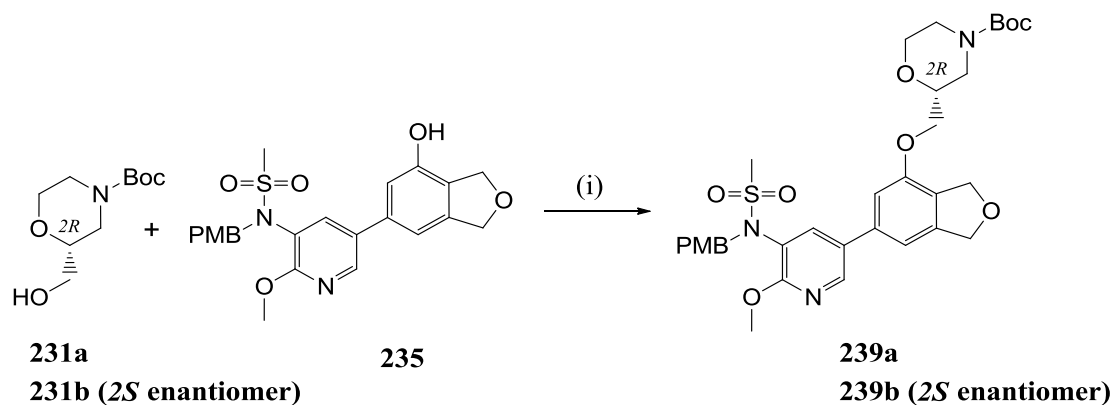
Many modifications have been made to the reaction, including the use of polymer-supported phosphines and reagents such as di-4-chlorobenzyl azodicarboxylate, which can be precipitated from the reaction mixture to aid purification.<sup>120,121</sup> An attractive modification was developed by Tsunoda, who observed that cyanomethylenetriethylphosphorane (CMBP, **238**) was effective in the condensation of secondary alcohols with *O*- and *N*-nucleophiles (Scheme 4.3.31).<sup>122</sup> This represented a more atom efficient protocol, the by-products are acetonitrile and a trialkylphosphine oxide, and the reaction was effective with less acidic nucleophiles.<sup>120,122</sup>



Reagents and Conditions: (i) Toluene, 100 °C, 79-100%.

Scheme 4.3.31. CMBP as a Mitsunobu reagent.<sup>122</sup>

This protocol was used to effect the Mitsunobu reaction required here, using both enantiomers of the Boc-protected (hydroxymethyl)morpholine, with the phosphorane ylid acting as the base (Scheme 4.3.32).

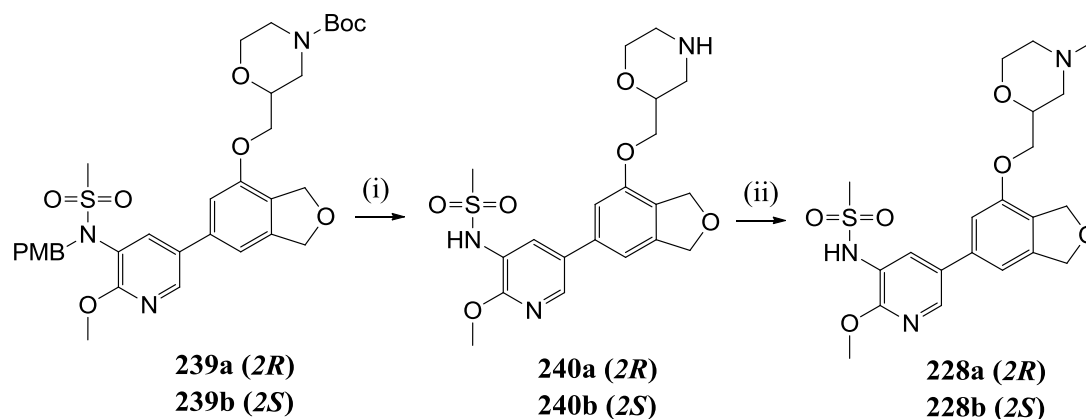


Reagents and Conditions: (i) CMBP, toluene,  $\mu$ wave, 120 °C, 74% (**239a**), 100% (**239b**, taken on crude).

Scheme 4.3.32. Mitsunobu reaction to synthesise **239a** and **239b**.

Intermediates **239a** and **239b** were taken forward for the synthesis of *N*-methyl compounds **228a** and **228b** (Scheme 4.3.33). The amine and sulfonamide protecting groups were cleaved in one step and an Eschweiler-Clarke methylation secured the desired tertiary amines (Scheme 4.3.33).<sup>123,124</sup> Chiral HPLC analysis of **228a** and **228b** gave evidence that the compounds remained single enantiomers.



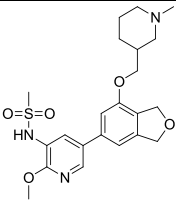
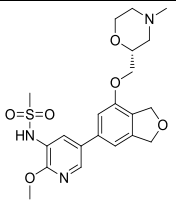
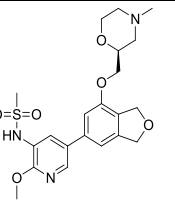


Reagents and Conditions: (i) TFA, DCM,  $\mu$ wave, 70 °C, 93% (**240a**), 83% (**240b**, taken on crude); (ii) HCOOH, CH<sub>2</sub>O, 80 °C, 32% (**228a**), 14% (**228b**);

Scheme 4.3.33. Synthesis of compounds **228a** and **228b**.

The yields of the Eschweiler-Clarke reaction were poor despite almost full conversion to product, with material proving difficult to recover from the aqueous phase after work-up and small scale reverse phase purification being mainly responsible for the poor yields. Despite the low yields, the advantage of using the reductive amination conditions rather than an alkylation is that formation of a quaternary ammonium salt is avoided. Formic acid acts as a hydride donor and reduces the intermediate iminium ion, generating a tertiary amine that cannot undergo further iminium ion formation. In addition, the reductive amination can be carried out in the presence of the secondary sulfonamide.

The data obtained for compounds **228a** and **228b** were compared to the analogous piperidine compound **227b** (Table 4.3.10).

Structure			
Compound Number	<b>227b</b>	<b>228a</b>	<b>228b</b>
Mean PI3K $\delta$ pIC <sub>50</sub> (N)	8.3 (2)	8.0 (6)	7.5 (4)
Mean PI3K $\alpha$ pIC <sub>50</sub> (N)	7.0 (2)	6.3 (6)	6.2 (4)
Mean PI3K $\beta$ pIC <sub>50</sub> (N)	6.8 (2)	6.1 (7)	6.0 (5)
Mean PI3K $\gamma$ pIC <sub>50</sub> (N)	5.7 (2)	6.2 (6)	5.9 (4)
Mean HWB pIC <sub>50</sub> (N)	7.1 (5)	6.6 (5)	6.3 (5)
LE/LLE <sub>AT</sub>	0.37/0.35	0.35/0.37	0.33/0.35
PFI	4.2	5.1	5.1
mChromlogD <sub>pH7.4</sub>	2.17	3.09	3.13
clogP	2.8	2.2	2.2
MW	447	449	449
TPSA	90	99	99
AMP (pH 7.4, nm/s)	400	495	500
CLND Solubility ( $\mu$ M)	599	472	450
FaSSIF Solubility after 4 h ( $\mu$ g/ml)	>1500	650	-
hERG pIC <sub>50</sub>	4.4 (1)	4.8 (2) <sup>a</sup>	<4.2 (3)
3A4 p450 pIC <sub>50</sub> ( $\mu$ M)	4.7 (2)	<4.3 (2)	<4.3 (2)
IVC (ml/min/g)	11.80 (rat), <0.53 (human)	2.45 (rat), 0.91 (human)	2.52 (rat), 0.89 (human)
Rat Cl <sub>b</sub> (ml/min/kg)	153	30	38
Vd <sub>ss</sub> (L/kg)	3.9	1.9	1.7
t <sub>1/2</sub> (h)	0.3	1.3	0.8
F%	0	20	45

<sup>a</sup> Returned value <4.2 on one test occasion.

Table 4.3.10. Data for compounds **228a** and **228b**.

Both compounds **228a** and **228b** were active against PI3K $\delta$  and selective over the other PI3K isoforms, with the *R*-enantiomer showing increased potency and being comparable to that of piperidine compound **227b**. Both compounds **228a** and **228b** displayed reduced *in vitro* and *in vivo* clearance, which in turn led to improved oral bioavailability and a slight increase in half-life.<sup>108</sup> However the predicted dose required for once daily dosing would still be high with a half-life of 1-2 h, so a further reduction in clearance was required in order to achieve a longer half-life. An increase in volume of distribution may also help to increase the half-life but, since

the clearance and volume tend to correlate as they are both driven by lipophilicity, achieving low clearance and high volume was a key challenge. Figure 4.3.15 shows the clearance and volume data for the 4-substituted dihydroisobenzofuran compounds tested in *in vivo* pharmacokinetic studies thus far.

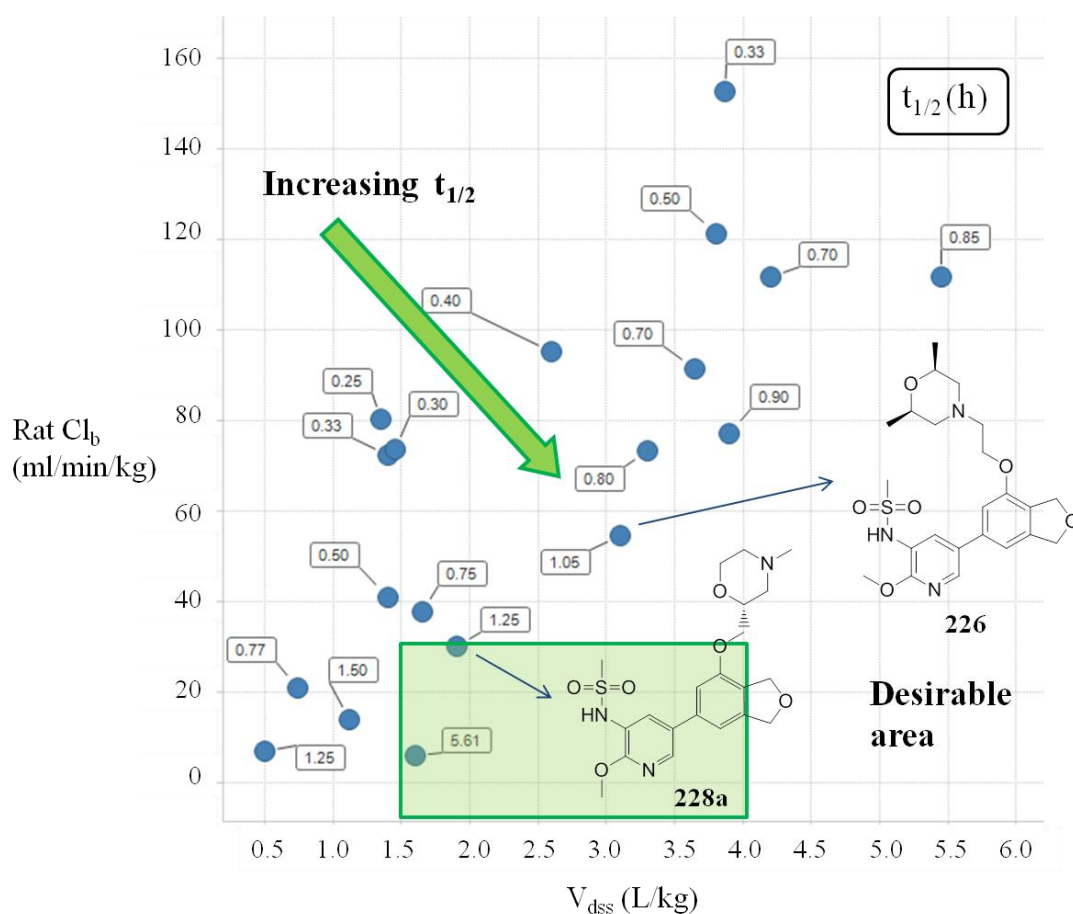


Figure 4.3.15. Relationship between clearance and volume for the 4-substituted dihydroisobenzofurans.

It was thought that reducing the metabolic clearance further would be the most feasible strategy for improving the half-life, since varying the substituent on the morpholine nitrogen was practicable and *N*-dealkylation represented a potential metabolic liability. In addition, it was observed that compounds achieving low clearance ( $< 30$  ml/min/kg) had  $clogP$  values less than or equal to 3 (Figure 4.3.16).

Disappointingly there was no apparent value of measured  $\text{ChromlogD}_{\text{pH}7.4}$  below which compounds were expected to have low clearance (Figure 4.3.16).

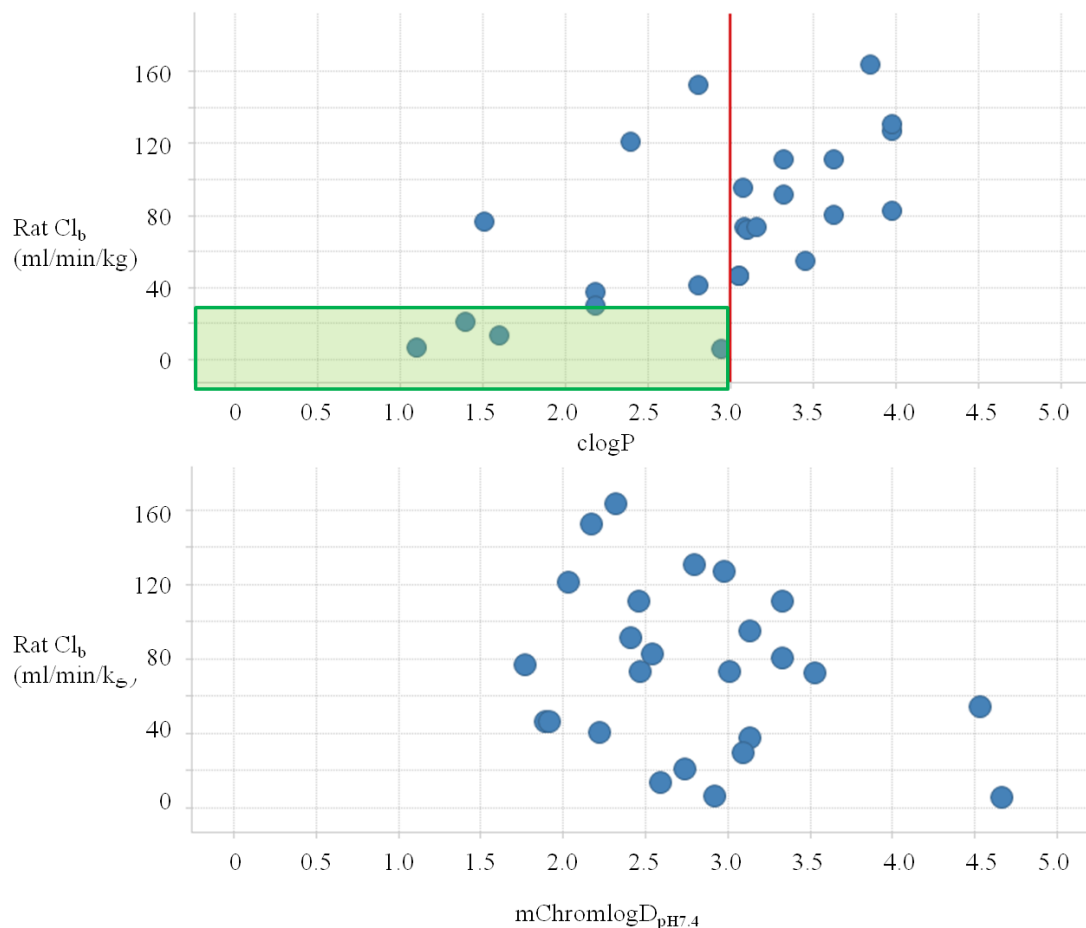
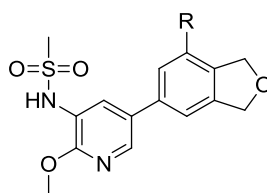


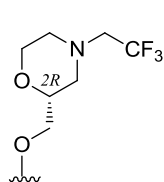
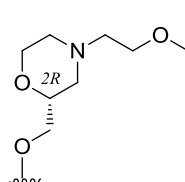
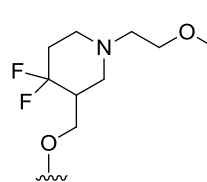
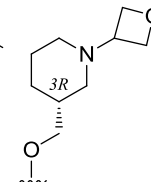
Figure 4.3.16. Relationship between clearance and lipophilicity.

Therefore, this criterion ( $\text{clogP} \leq 3$ ) was used in the next iteration of design, with polar substituents hypothesised to be metabolically stable being incorporated on the amine functionality. These include the oxetanyl group, which was shown to be a polar, metabolically robust group in Chapter 3, and the methoxyethyl group. The latter has been shown to be a metabolically stable amine substituent that does not give large increases in lipophilicity when compared with other more stable alkyl substituents such as cyclopropyl or *tert*-butyl groups.<sup>125</sup> The amine substituents

chosen also gave a range of nitrogen basicities in order to assess the affect of  $pK_a$  on clearance and oral absorption, since the ionisation state of the compounds may affect their CYP specificity, solubility and permeability. Reduction of  $pK_a$  may also decrease the likelihood of the compounds inhibiting hERG. The incorporation of fluorines, as well as the addition at nitrogen of polar groups (i.e. oxetane), was investigated in order to reduce the nitrogen basicity. The strategy of introducing fluorines to modulate  $pK_a$  was explored by Diederich in a series of thrombin inhibitors and was found to be effective at reducing basicity of the nitrogen centre of a pyrrolidine ring.<sup>126</sup> Here the  $pK_a$  values were calculated using the  $pK_a$  calculator from Chemaxon (v5.4.1.1).<sup>127</sup> Synthesis of the *R*-enantiomer was prioritised where possible as this enantiomer had displayed higher PI3K $\delta$  potency previously.



R =

**241****242****243****244**

clogP = 3.0

2.5

2.5

2.5

cChromlogD<sub>pH7.4</sub>(mChromlogD<sub>pH7.4</sub>) = 4.0 (5.40)

2.8 (3.46)

2.9 (5.12)

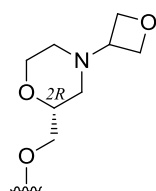
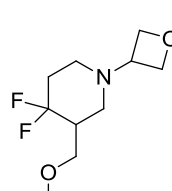
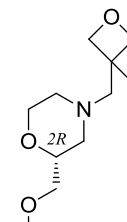
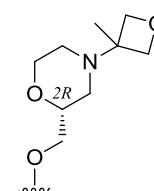
2.9 (4.14)

Calc. pK<sub>a</sub> (measured pK<sub>a</sub>) = 2.5 (2.0)

6.6 (6.3)

8.1 (nt)

7.1 (6.5)

**245****246****247****248**

clogP = 1.8

1.9

1.8

2.4

cChromlogD<sub>pH7.4</sub>(mChromlogD<sub>pH7.4</sub>) = 2.6 (2.90)

3.1 (4.47)

2.5 (4.04)

2.9 (3.65)

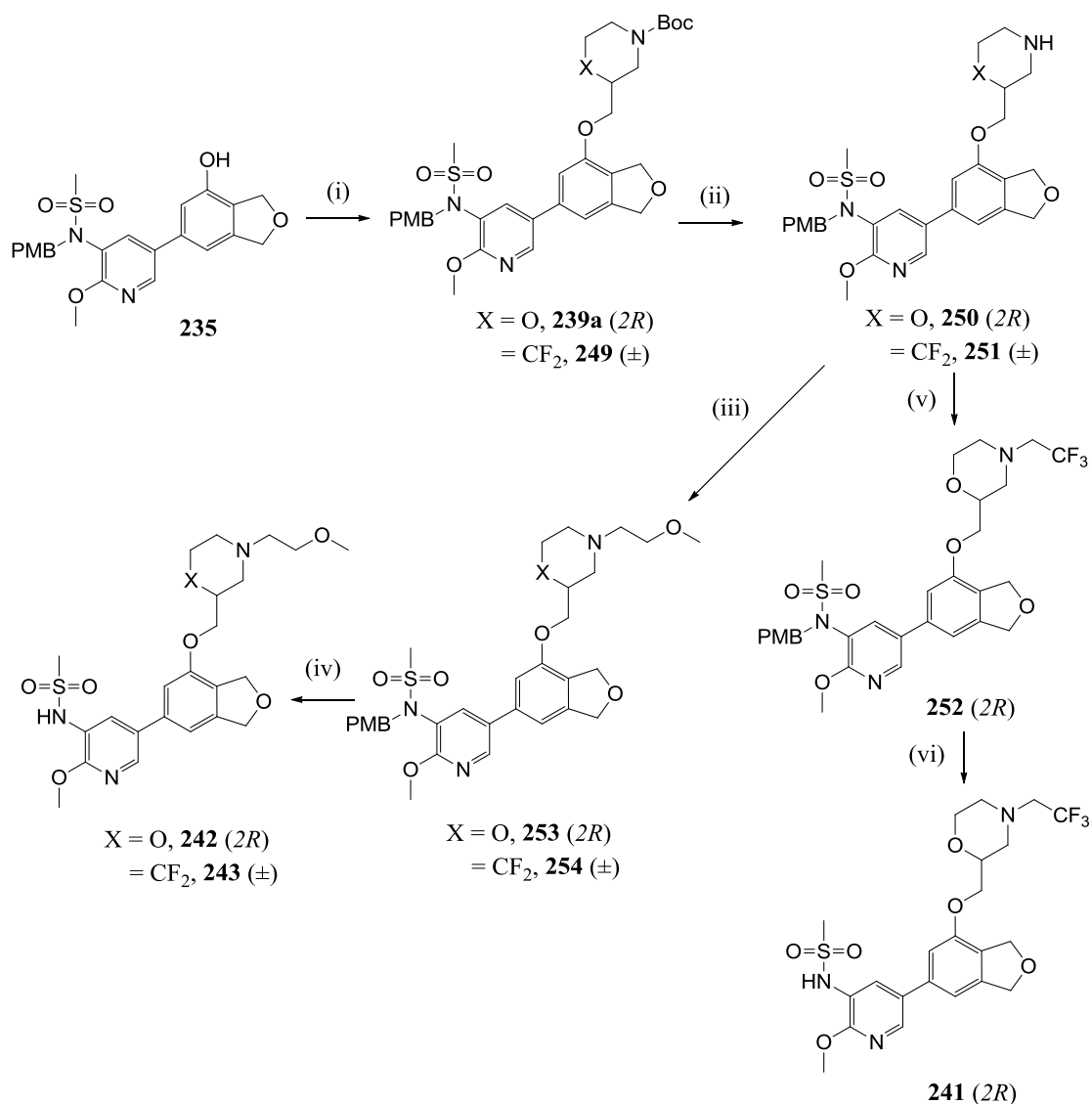
Calc. pK<sub>a</sub> (measured pK<sub>a</sub>) = 5.1 (4.3)

6.2 (4.0)

7.0 (5.5)

5.3 (nt)

Compounds **241**, **242** and **243** were synthesised *via* the route shown in Scheme 4.3.34. Mitsunobu coupling afforded the protected intermediates **239a** and **249** and a selective Boc-deprotection under acidic conditions at room temperature allowed alkylations to be carried out prior to cleavage of the *para*-methoxybenzyl group (Scheme 4.3.34).

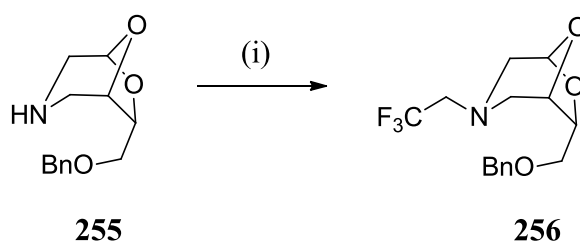


Reagents and Conditions: (i) (*R*)-*tert*-butyl 2-(hydroxymethyl)morpholine-4-carboxylate or *tert*-butyl 4,4-difluoro-3-(hydroxymethyl)piperidine-1-carboxylate, CMBP, toluene,  $\mu$ wave, 120 °C, 74% (**239a**), 93% (**249**, not described in Experimental as synthesised by M. James, GSK)<sup>128</sup>; (ii) TFA, DCM, rt, 52% (**250**), 76% (**251**); (iii) 1-bromo-2-methoxyethane, K<sub>2</sub>CO<sub>3</sub>, NaI, MeCN,  $\mu$ wave, 80 °C, 77% (**253**), 69% (**254**); (iv) TFA, DCM,  $\mu$ wave, 70 °C, 52% (**242**), 40% (**243**); (v) 2,2,2-trifluoroethyl trifluoromethylsulfonate, Na<sub>2</sub>CO<sub>3</sub>, EtOH, 78 °C, 65%; (vi) TFA, DCM,  $\mu$ wave, 70 °C, 56%.

Scheme 4.3.34. Synthesis of *N*-substituted compounds **241**, **242** and **243**.

To install the methoxyethyl group, amines **250** and **251** were reacted with 1-bromo-2-methoxyethane under conventional conditions with an alkali metal carbonate in a polar aprotic solvent.<sup>129</sup> Steric hindrance at the tertiary amine nitrogen prevented overalkylation to the quaternary ammonium salt. The addition of a catalytic amount of sodium iodide facilitated halide exchange with the alkyl bromide, a variant of the Finkelstein reaction. The iodide rapidly displaces the bromide and the small amount of more reactive iodide that is present reacts with the nucleophile, increasing the rate of reaction. Also, the soluble sodium iodide reacts to generate sodium bromide, which is a less soluble salt and this also drives the equilibrium in favour of the products.

Different conditions were used to install the trifluoroethyl group since 2,2,2-trifluoroethyl trifluoromethylsulfonate was readily available commercially and had been used to form a similar *N*-fluoroalkylated product (**256**, Scheme 4.3.35).<sup>130</sup>



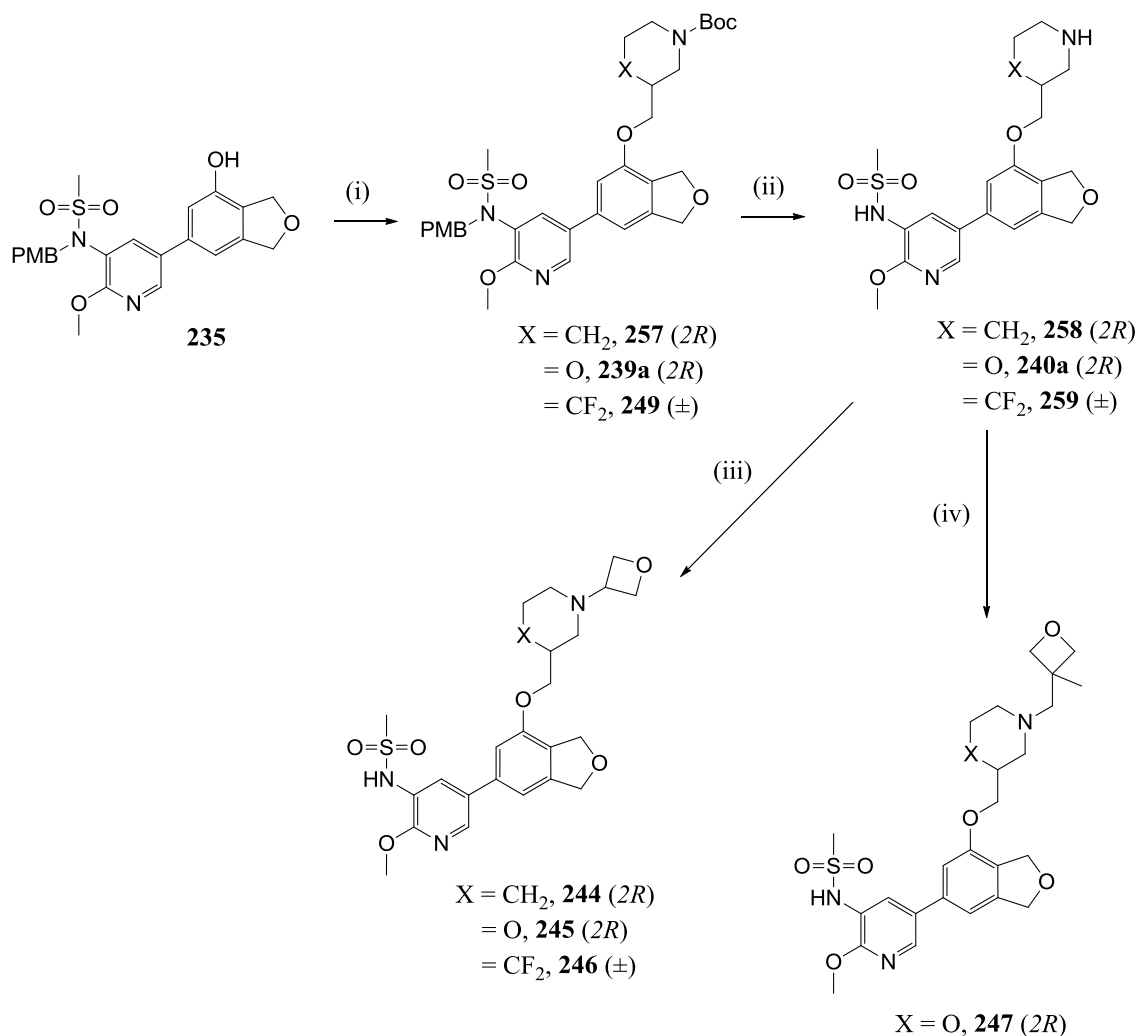
Reagents and Conditions: (i) 2,2,2-trifluoroethyl trifluoromethylsulfonate, Na<sub>2</sub>CO<sub>3</sub>, EtOH, 78 °C, 65%.

Scheme 4.3.35. Synthesis of *N*-fluoroalkyl derivative **256**.<sup>130</sup>

The oxetanyl-containing compounds **244** - **247** were synthesised from intermediates **239a**, **249** and **257**, which could be fully deprotected under acidic conditions in the microwave (Scheme 4.3.36). The direct reductive amination of amines **240a**, **258** and **259** with the required ketone or aldehyde using STAB resulted in the formation of the desired products, although the yields remained poor despite



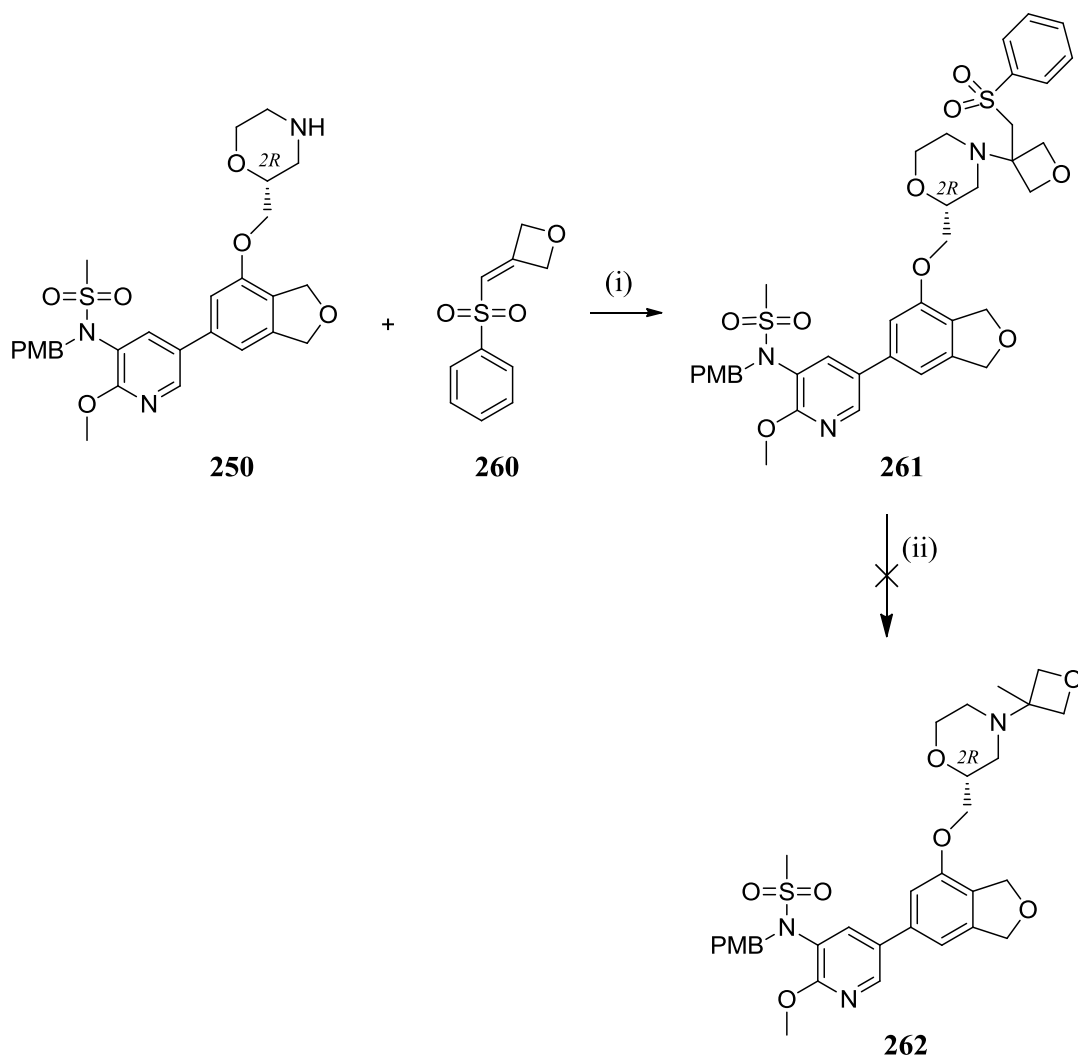
good conversions being observed (>70%), possibly due to poor recovery during small scale purifications (Scheme 4.3.36).



Reagents and Conditions: (i) (*R*)-*tert*-butyl 3-(hydroxymethyl)piperidine-1-carboxylate or (*R*)-*tert*-butyl 2-(hydroxymethyl)morpholine-4-carboxylate or *tert*-butyl 4,4-difluoro-3-(hydroxymethyl)piperidine-1-carboxylate, CMBP, toluene,  $\mu$ wave, 120 °C, 89% (**257**) 74% (**239a**), 93% (**249**, not described in Experimental as synthesised by M. James, GSK)<sup>128</sup>; (ii) TFA, DCM,  $\mu$ wave, 70 °C, 79% (**258**), 93% (**240a**), 83% (**259**, not described in Experimental as synthesised by S. MacDougall, GSK);<sup>131</sup> (iii) 3-oxetanone, NaBH(OAc)<sub>3</sub>, THF, 15% (**244**), 28% (**245**), 25% (**246**);<sup>131</sup> (iv) 3-methyloxetane-3-carbaldehyde, NaBH(OAc)<sub>3</sub>, THF, rt, 39%.

Scheme 4.3.36. Synthesis of *N*-substituted compounds **244** – **247**.

An alternative route was explored for the formation of compound **248**, with conditions from the literature initially investigated (Scheme 4.3.37. ).<sup>132</sup> Compound **261** was synthesised using conditions reported by Wuitschik.<sup>132,133</sup>



Reagents and Conditions: (i) THF, 65 °C, 43%; (ii) Mg, MeOH, ultrasound then I<sub>2</sub>, rt to 50 °C or SmI<sub>2</sub>, NiCl<sub>2</sub>, THF, 65 °C, not isolated.

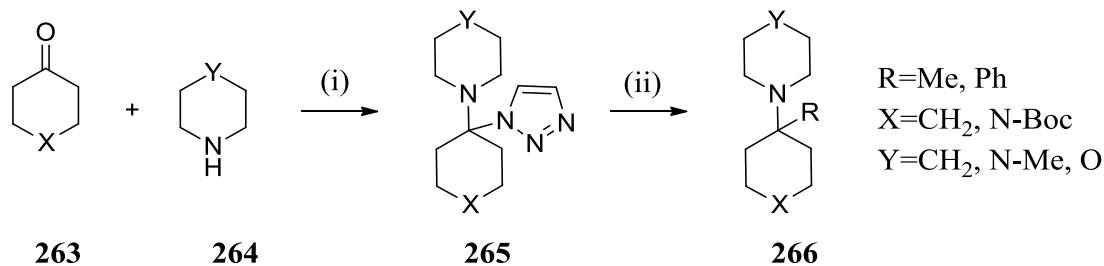
Scheme 4.3.37. Attempted literature conditions for the formation of compound **262**.

Addition of morpholine intermediate **250** to vinylsulfone **260** proceeded in moderate yield; however desulfonylation was unsuccessful using the conditions suggested for this type of motif.<sup>132</sup> Reductive cleavage of C-SO<sub>2</sub>Ar, N-SO<sub>2</sub>Ar and O-SO<sub>2</sub>Ar can be carried out using Mg/MeOH and these conditions are mild and efficient, and less toxic conditions than other frequently employed reagents, for example sodium amalgam.<sup>134</sup> These reactions proceed *via* a single electron transfer from the metal to the sulfone to give a radical anion, which dissociates to the alkyl radical and a sulfinate anion. Reduction of the radical and subsequent protonation affords the desulfonylated product. Unfortunately, the cleavage reaction did not proceed in this case, with unreacted starting material being recovered even when an excess of powdered magnesium was added. Additional modifications to aid the reaction included adding iodine as an activator, utilising highly reactive Rieke<sup>®</sup> magnesium and heating the reaction mixture, but none of these resulted in conversion to product. Optimised conditions reported in the literature often include the addition of a catalytic amount of HgCl<sub>2</sub>;<sup>135</sup> however due to the high toxicity of the metal this modification was not attempted. For the same reason, the use of sodium amalgam was not pursued.

An equivalent metal reagent often used for reductive cleavage reactions of this type is SmI<sub>2</sub>, so this was also attempted here.<sup>136</sup> Common methods for increasing the rate of reactions that use SmI<sub>2</sub> as a single electron donor include the addition of HMPA as a co-solvent, which produces a more powerful reductant, and the addition of a catalytic amount of a metal catalyst.<sup>137,138</sup> NiI<sub>2</sub> has been reported to be superior to other transition metal salts and was used as a catalyst in the SmI<sub>2</sub>-mediated desulfonylation attempted here.<sup>139</sup> Unfortunately the desired reaction did not occur, with starting material remaining unreacted, so alternative synthetic routes to the desired target compound were investigated.

Tertiary amines containing tertiary alkyl groups can be synthesised in two steps *via* a Strecker reaction of a ketone and amine with potassium cyanide followed by a Bruylants reaction of the resulting aminonitrile with a Grignard reagent.<sup>140,141</sup> 1,2,3-Triazole has been reported as a safer and practical alternative to cyanide in the

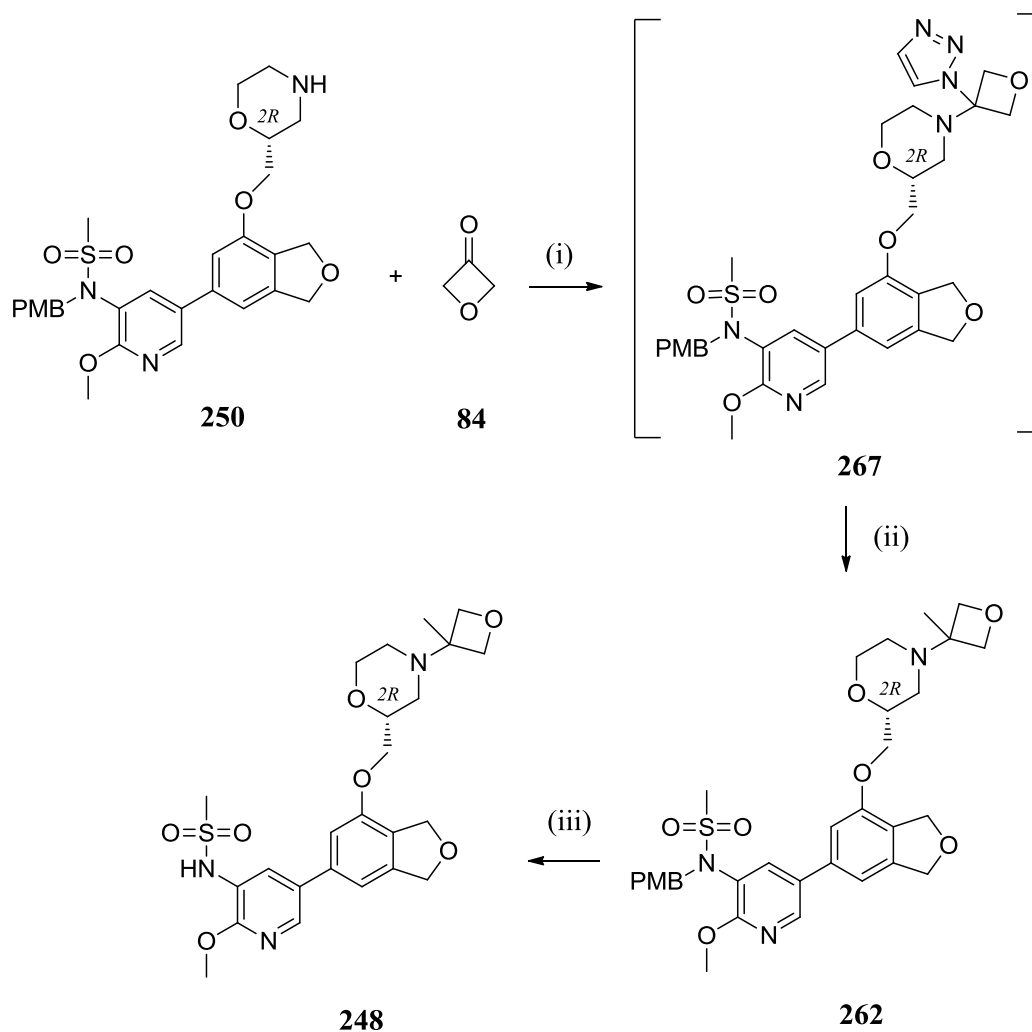
Bruylants reaction and has been used for the synthesis of a variety of substituted amines (Scheme 4.3.38).<sup>142</sup>



Reagents and Conditions: (i) 1,2,3-Triazole, toluene, 110 °C, Dean-Stark, 6-8 h, not isolated; (ii) RMgCl or RMgBr, rt, 1 h, 38-90%.

Scheme 4.3.38. Literature synthesis of tertiary amines containing tertiary alkyl or aryl groups.<sup>142</sup>

These conditions were attempted for the synthesis of compound **262**, which could then undergo deprotection to afford compound **248** (Scheme 4.3.39).

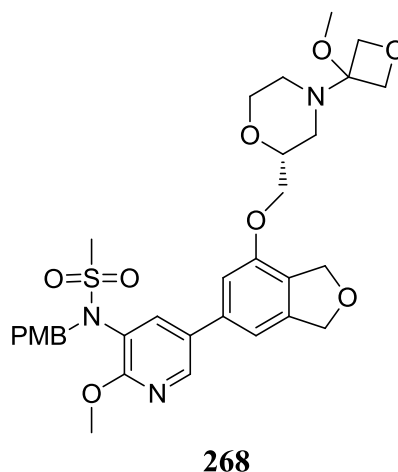


Reagents and Conditions: (i) 1,2,3-Triazole, toluene, 110 °C, Dean-Stark, 8 h, or 1,2,3-triazole, THF, sealed tube,  $\mu$ wave, 120 °C, not isolated; (ii) MeMgBr, rt, 1 h, 2-22% over two steps; (iii) TFA, DCM,  $\mu$ wave, 70 °C, 24%.

Scheme 4.3.39. Bruylants conditions for the synthesis of compound **248**.

The initial attempt to synthesise compound **248** using Dean-Stark conditions to form triazole intermediate **267** and quenching with the Grignard reagent, as reported in the literature, gave poor conversion to the desired product (2% isolated yield). It was thought that poor solubility of the starting material in toluene may have been an issue so the reaction was repeated using THF as the solvent, heating in a

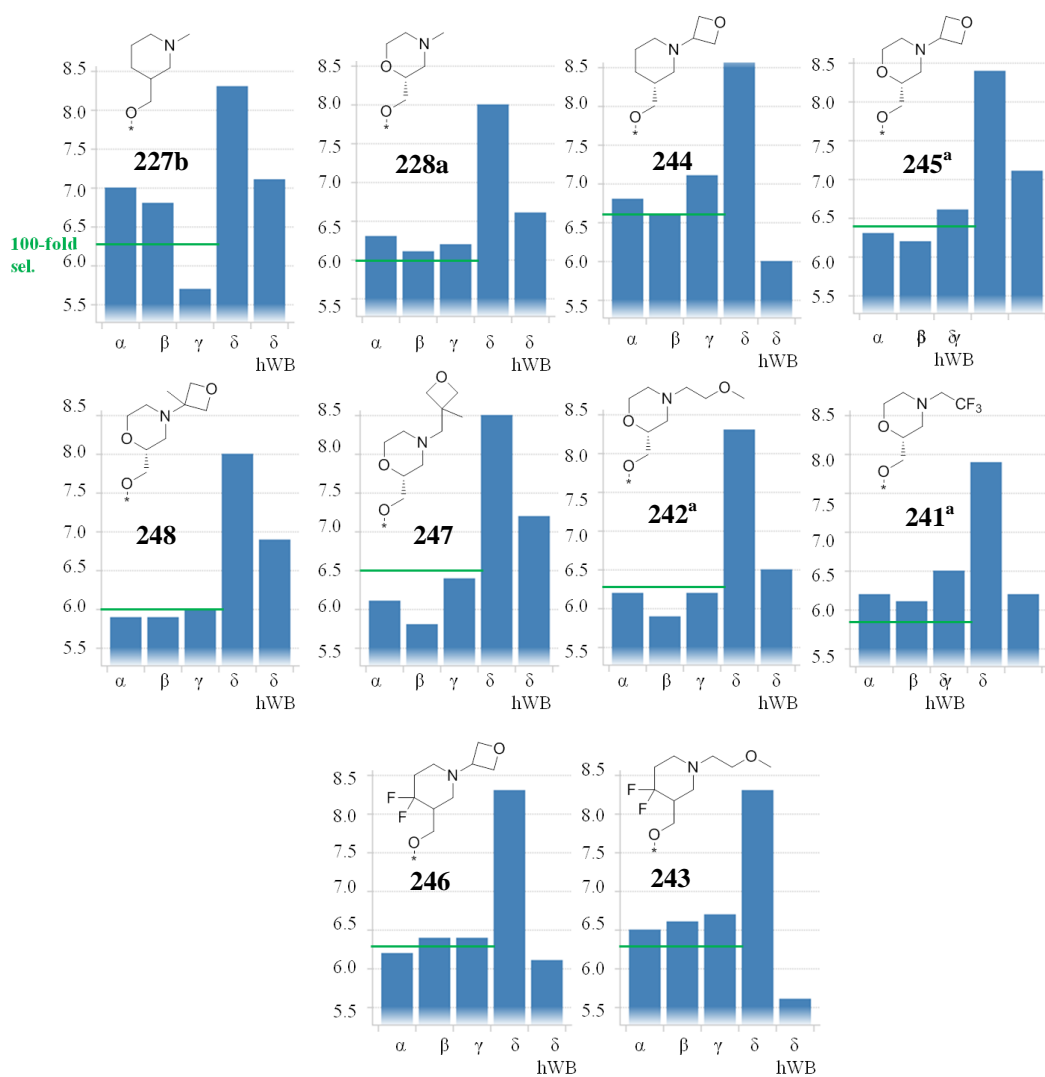
sealed tube in the microwave to drive the condensation. The starting material was readily soluble in THF and easier reaction monitoring was also an advantage. Quenching the reaction with MeOH prior to Grignard reagent addition showed 70% conversion to the 3-methoxyoxetan-3-yl intermediate **268**.



Addition of the Grignard reagent at this stage led to the formation of the desired product, with triazole intermediate still present after 1 h but fully consumed after the addition of further portions of the Grignard reagent. The product was only isolated in 22% yield, reflecting poor conversion of the triazole intermediate to desired product on addition of the Grignard reagent, which gave a complex reaction profile containing several unknown by-products and many baseline impurities. Despite only a small amount of intermediate **262** being isolated, the *para*-methoxybenzyl deprotection was carried out successfully in order that an acceptable amount of compound **248** was obtained for biological testing.

With the required compounds in hand, screening against the PI3Ks and in the *in vitro* clearance assays was carried out to determine whether any of the structural changes had impacted activity, selectivity and pharmacokinetics.

Figure 4.3.17 shows the PI3K selectivity profiles and whole blood potency for the ether-containing dihydroisobenzofuran compounds screened.



<sup>a</sup> hWB data returned no value on one test occasion.

Figure 4.3.17. Potency and selectivity data for ether-containing dihydroisobenzofurans.

It was observed that all the compounds achieved PI3K $\delta$  enzyme potencies of  $\geq 7.8$  (Figure 4.3.17). Compound **244** achieved the highest PI3K $\delta$  activity; however its whole blood potency was considerably less, at a pIC<sub>50</sub> of 6.0. This activity is much lower than the *N*-methyl analogue, which had an HWB pIC<sub>50</sub> of 7.1 (**227b**, Figure 4.3.17). Both compounds have good permeability ( $> 200$  nm/sec) so the difference in whole blood activity could be attributed to the lower plasma protein

binding observed for compound **227b** (73.0%) when compared to that of compound **244** (87.1%). Neither of these piperidine-containing compounds achieved the desired selectivity against all the other PI3K isoforms. Although all the compounds achieved >30-fold selectivity for PI3K $\delta$ , the addition of bulkier *N*-substituents led to >100-fold selectivity, for example compounds **242**, **247** and **248**. Compound **247** also showed high whole blood potency ( $\text{pIC}_{50} = 7.2$ ), so it can be considered that bulkier substituents at this position contribute favourably to both binding affinity and PI3K $\delta$  selectivity, which is in keeping with previous observations. In fact all the oxetanyl-containing compounds **245**, **247** and **248** had higher whole blood potencies than the *N*-methyl analogue **228a**, which only achieved an HWB  $\text{pIC}_{50}$  of 6.6.

Unfortunately, the fluoro-containing compounds did not achieve sufficient activity in HWB ( $\text{pIC}_{50} < 6.5$ ). The low whole blood activities for compounds **241**, **246** and **243** can also be attributed to their higher plasma protein binding of 93.5%, 92.6% and 90.6% respectively. The increased plasma protein binding can be rationalised by the higher lipophilicity of these compounds. For this set of compounds a broad trend of increasing HSA binding with increasing lipophilicity was observed (Figure 4.3.18).



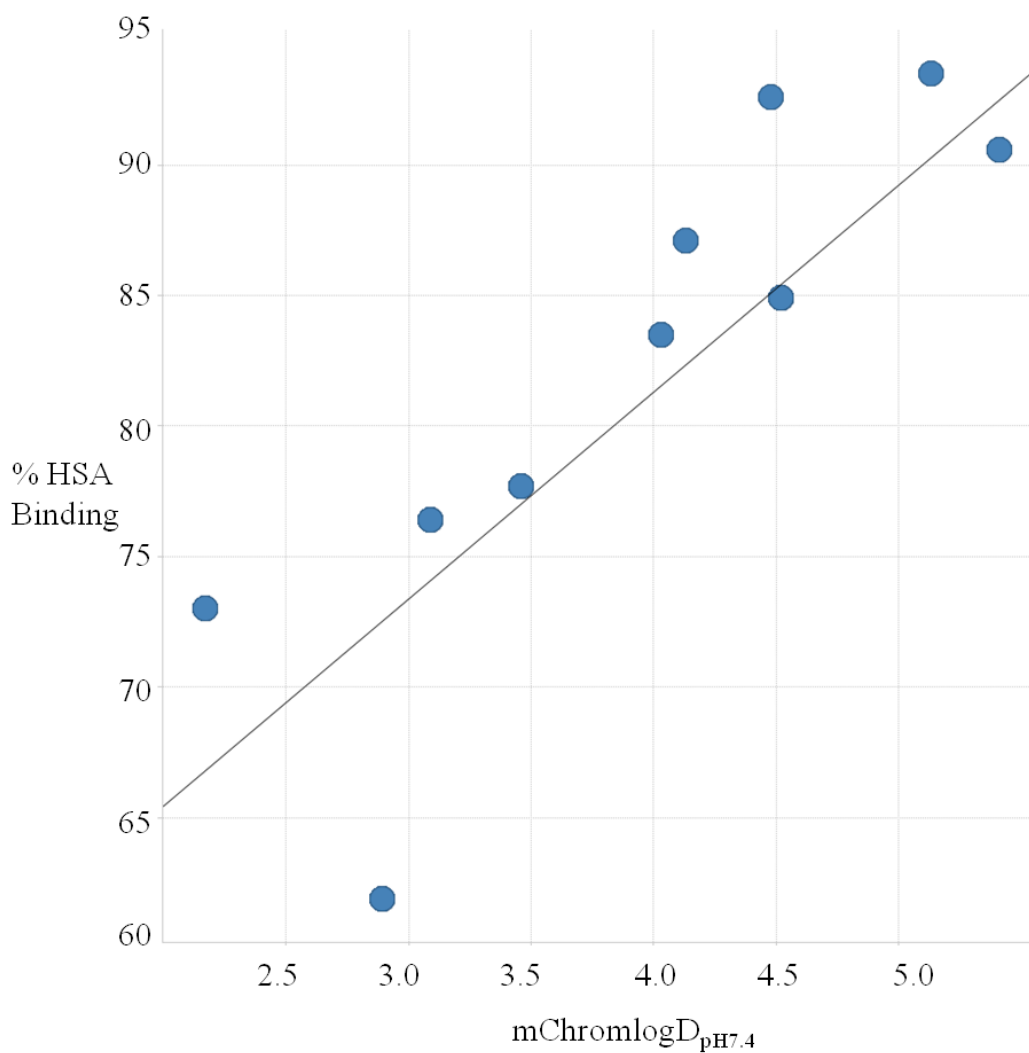


Figure 4.3.18. % HSA binding vs. mChromlogD<sub>pH7.4</sub>.

The compounds were screened in *in vitro* microsomal stability assays; unfortunately, many of the compounds had high clearance despite their clogP being less than 3.0 (Figure 4.3.19).

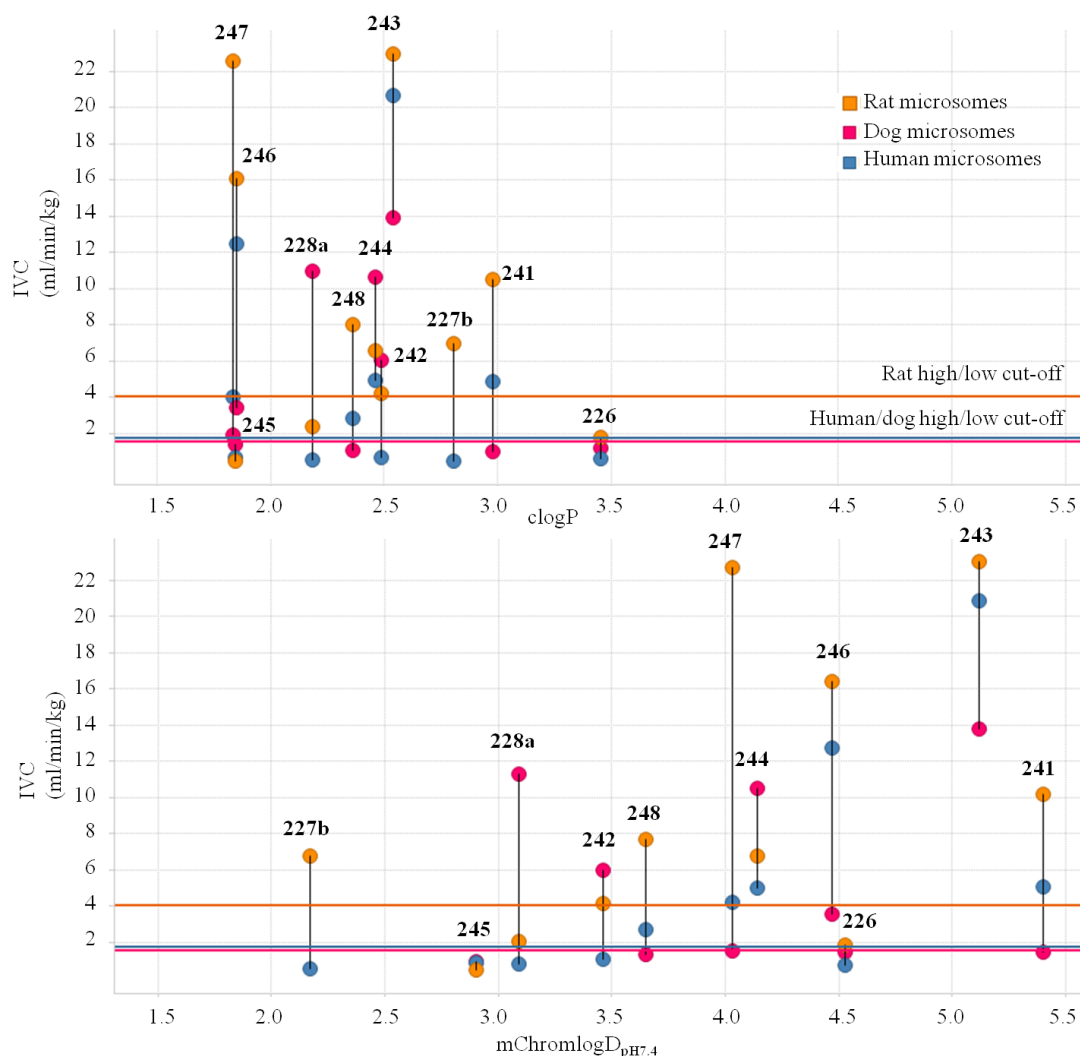


Figure 4.3.19. *In vitro* clearance data for the ether-containing dihydroisobenzofurans.

It can be seen in Figure 4.3.19 that there is a poor correlation between  $\text{clogP}$  and *in vitro* clearance for all the species, however the correlation between measured  $\text{mChromlogD}_{\text{pH}7.4}$  is better for this set of compounds. It appears that  $\text{mChromlogD}_{\text{pH}7.4} < 3.5$  is required to achieve low human *in vitro* clearance, however the clearance can vary across species and some compounds with higher  $\text{mChromlogD}_{\text{pH}7.4}$  values can still achieve low clearance, for example compound **226** (Figure 4.3.19). Pleasingly, compound **245** was observed to have low clearance across the species and was chosen for progression to an *in vivo* rat PK study

alongside compound **242**, which had high *in vitro* clearance in rat and dog microsomes but low *in vitro* clearance in human microsomes (Figure 4.3.19).<sup>143</sup> The compound with highest HWB potency (**247**) was also progressed to an *in vivo* rat PK study as well as one of the fluorine-containing compounds (**241**) that had high *in vitro* rat clearance, so as to assess the *in vitro/in vivo* clearance correlation (Figure 4.3.20).<sup>143</sup>

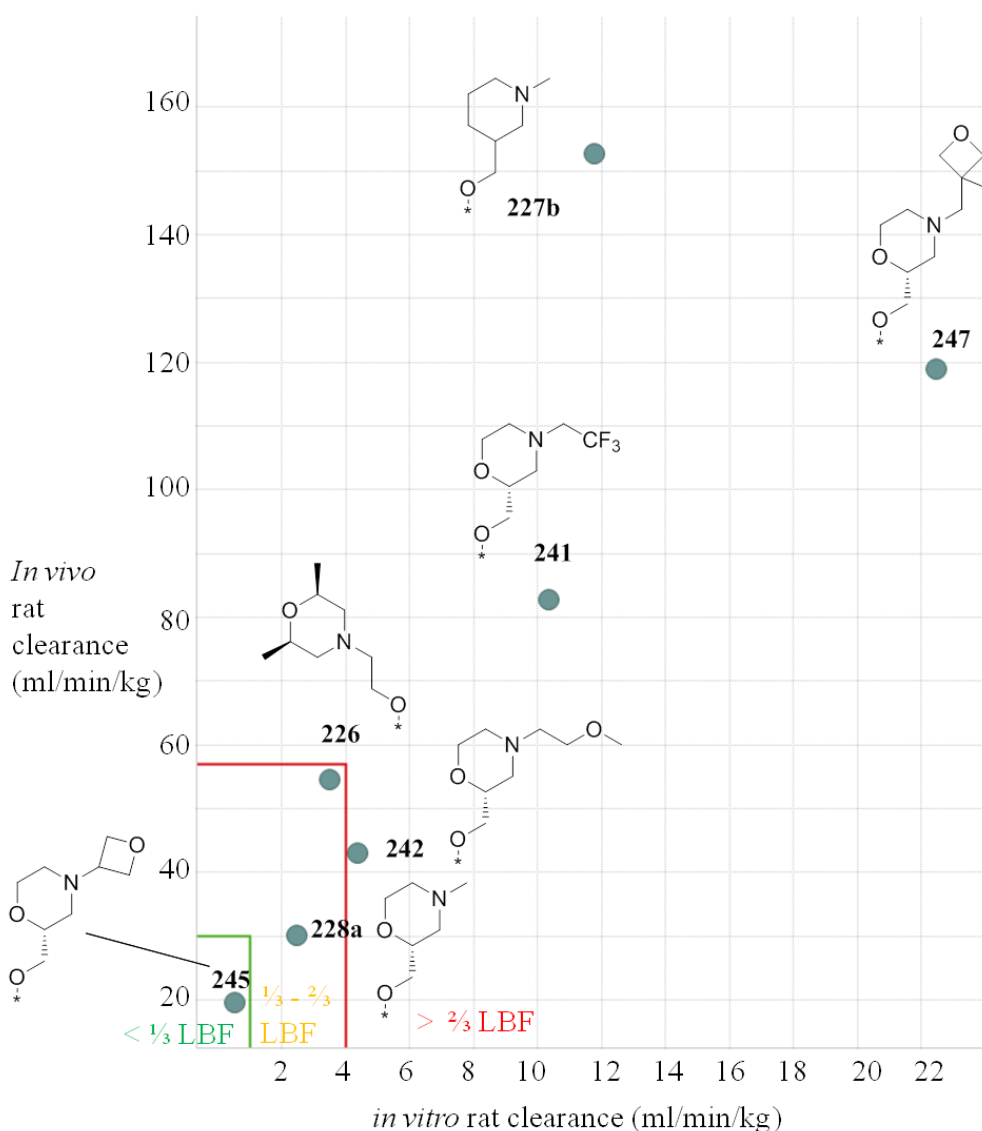


Figure 4.3.20. *In vivo* vs. *in vitro* clearance for 4-ether substituted dihydroisobenzofurans.

It can be seen that the *in vitro/in vivo* clearance correlation is good for this set of compounds; compounds within the low, moderate and high clearance bands also fall within the analogous bands for the clearance measured *in vivo*.

Compound **227b** has a very high *in vivo* clearance and although its microsomal clearance was measured to be greater than two thirds of rat liver blood flow, the *in vivo* clearance is much greater than expected. This could again be attributed to alternative mechanisms of metabolism that are not represented by the *in vitro* rat liver microsomal stability assay.

The only compound to achieve the desired *in vivo* clearance of <30ml/min/kg was compound **245**. The lower clearance of this compound may be due to both its lower lipophilicity as well as the prevention of metabolism at the morpholino-nitrogen *via N*-dealkylation.

The *in vivo* data for this compound can be taken alongside that of the other dihydroisobenzofurans screened to date to seek out trends that could be helpful in the next iteration of design. Previously, it was observed that a clogP less than 3.0 lead to compounds with low *in vivo* clearance; however recent data has shown that this correlation has broken down (Figure 4.3.21). Again, there seems to be no correlation with mChromlogDpH<sub>7.4</sub> (Figure 4.3.21).

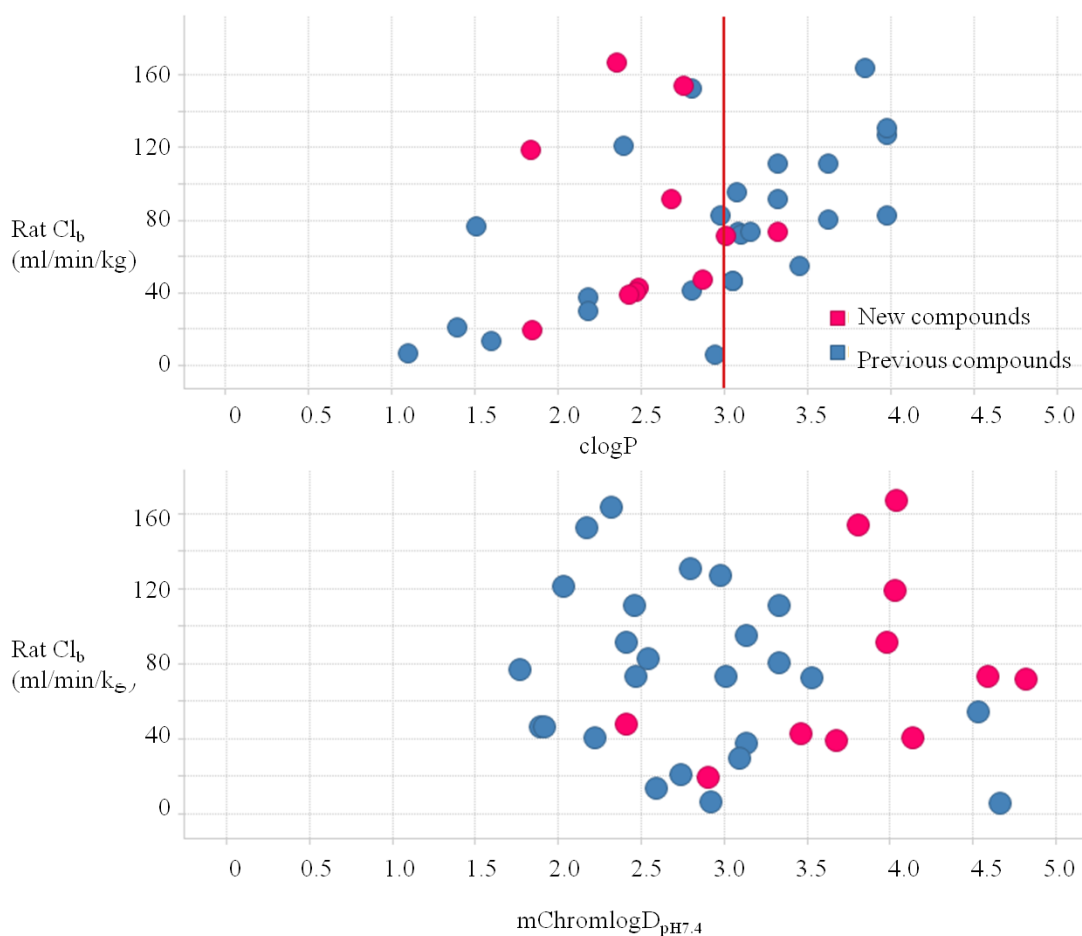


Figure 4.3.21. Relationship between clearance and lipophilicity.

It now appears that lipophilicity cannot be used to predict clearance for this series of compounds; however if the lipophilicity is maintained within the general optimal range reported for achieving oral bioavailability (ChromlogD<sub>pH7.4</sub> between 1 and 3), it is more likely that compounds with *in vivo* clearance values of less than 30 ml/min/kg will be found. In addition, the *in vitro* clearance data can be used as a filter for progression to *in vivo* pharmacokinetic studies since the *in vitro/in vivo* correlation for rat clearance is sufficient for this. A wider analysis of 4-ether substituted dihydroisobenzofurans has shown that *in vivo* clearance values of <40 ml/min/kg are only observed when the *in vitro* clearance in rat microsomes is <3 ml/min/kg (Figure 4.3.22).

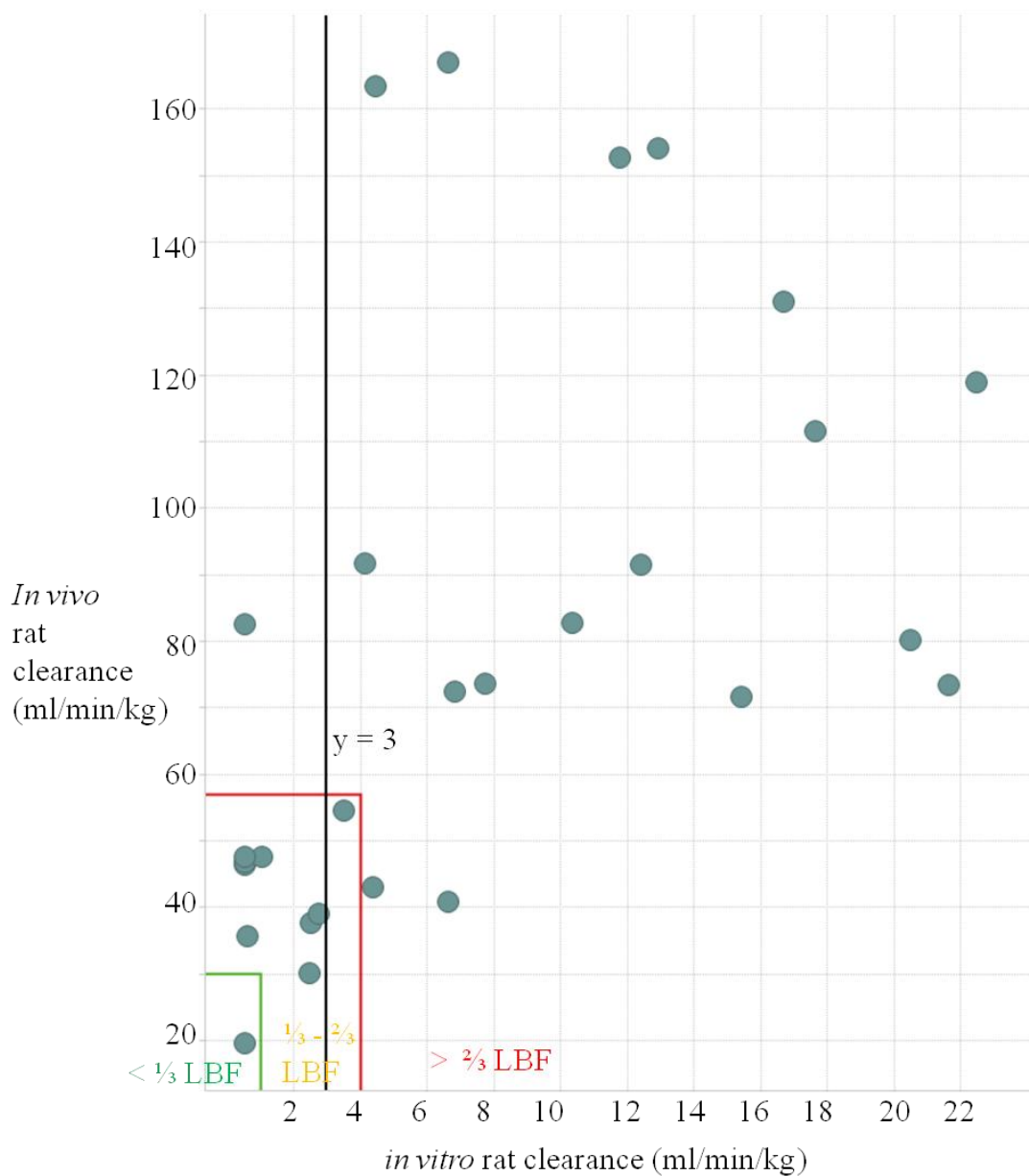
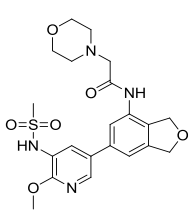
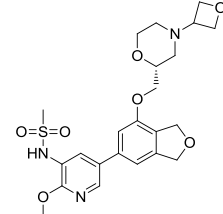


Figure 4.3.22. *In vivo/in vitro* clearance correlation for 4-ether substituted dihydroisobenzofurans.

Though some compounds with *in vitro* clearance values of <3 ml/min/kg do not achieve the desired *in vivo* clearance (<30 ml/min/kg), using the *in vitro* data as a

filter for progression will offer the best chance of discovering compounds that do have low *in vivo* clearance.

A comparison of the lead compound (**173**) and compound **245**, which has superior PI3K $\delta$  potency and isoform selectivity and was the only compound to date to achieve low *in vivo* clearance, was carried out (Table 4.3.11).

Structure		
Compound Number	<b>173</b>	<b>245</b>
Mean PI3K $\delta$ pIC <sub>50</sub> (N)	6.8 (3)	8.4 (6)
Mean PI3K $\alpha$ pIC <sub>50</sub> (N)	5.3 (3)	6.3 (6)
Mean PI3K $\beta$ pIC <sub>50</sub> (N)	5.0 (3)	6.2 (6)
Mean PI3K $\gamma$ pIC <sub>50</sub> (N)	5.0 (3)	6.6 (6)
Mean HWB pIC <sub>50</sub> (N)	6.5 (9) <sup>a</sup>	7.1 (3)
LE/LLE <sub>AT</sub>	0.29/0.33	0.34/0.38
PFI	4.6	4.9
IVC (ml/min/g)	<0.53 (rat), <0.53 (human)	<0.53 (rat), <0.53 (human)
Rat <i>in vivo</i> Cl <sub>b</sub> (ml/min/kg)	14	20
Rat Cl <sub>b</sub> scaled from IVC (ml/min/kg)	<17 (19% LBF)	<17 (19% LBF)
Human Cl <sub>b</sub> scaled from IVC (ml/min/kg)	<8 (38% LBF)	<8 (38% LBF)

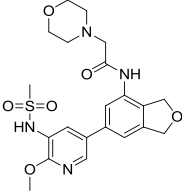
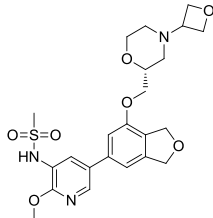
<sup>a</sup> Returned no value on two test occasions

Table 4.3.11. Potency and IVC data for compounds **173** and **245**.

Both compounds had low clearance in the *in vitro* microsomal clearance assays and extrapolation of the rat *in vitro* clearance gave a value of rat *in vivo* clearance that was in agreement with the measured data (Table 4.3.11). Therefore, extrapolation of the human *in vitro* clearance data was used to give an indication of the human *in vivo* clearance (Table 4.3.11).<sup>144</sup> However, since the *in vitro* clearance

could not be measured accurately below 0.53 ml/min/kg, the predicted human clearance using the IVIVE approach could only be confirmed as less than 8 ml/min/kg (38% LBF).

A potentially more accurate value of predicted human *in vivo* clearance was determined by allometric scaling from the rat *in vivo* clearance data using rat and human liver blood flow differences (Table 4.3.12).<sup>144</sup>

Structure		
<b>Compound Number</b>	<b>173</b>	<b>245</b>
<b>Mean PI3K<math>\delta</math> pIC<sub>50</sub> (N)</b>	6.8 (3)	8.4 (6)
<b>Mean PI3K<math>\alpha</math> pIC<sub>50</sub> (N)</b>	5.3 (3)	6.3 (6)
<b>Mean PI3K<math>\beta</math> pIC<sub>50</sub> (N)</b>	5.0 (3)	6.2 (6)
<b>Mean PI3K<math>\gamma</math> pIC<sub>50</sub> (N)</b>	5.0 (3)	6.6 (6)
<b>Mean HWB pIC<sub>50</sub> (N)</b>	6.5 (9) <sup>a</sup>	7.1 (3)
<b>LE/LLE<sub>AT</sub></b>	0.29/0.33	0.34/0.38
<b>PFI</b>	4.6	4.9
<b>Rat <i>in vivo</i> Cl<sub>b</sub> (ml/min/kg)</b>	14	20
<b>Human Cl<sub>b</sub> scaled from rat by LBF (ml/min/kg)</b>	3.5 (16% LBF)	4.9 (24% LBF)
<b>Vd<sub>ss</sub> (L/kg)</b>	1.1	2.0
<b>t<sub>1/2</sub> (h)</b>	1.5	1.1
<b>Rat F%</b>	54	46
<b>Predicted once-daily human dose (mg)</b>	1826	372

<sup>a</sup> Returned no value on two test occasions

Table 4.3.12. *In vivo* PK data and predicted once-daily human dose for compounds **173** and **245**.



Encouragingly, the predicted human *in vivo* clearance was low for both compounds (<30% LBF) and both compounds also achieved good rat oral bioavailabilities (>30%) and moderate volumes of distribution. A predicted once-daily human dose was calculated and this showed a significant decrease in dose amount for compound **245** when compared to compound **173** (Table 4.3.12).<sup>144</sup> The dose calculation takes into account the predicted human *in vivo* clearance, the oral bioavailability and the volume of distribution, and the human whole blood potency. The increased human whole blood potency of compound **245** could be driving the decrease in dose; however the predicted dose is still greater than desired (<100 mg). Therefore, the focus for the programme moving forward was to further increase human whole blood potency and maintain an oral PK profile to achieve a low predicted once-daily human dose.

## 4.4. Conclusion

As a result of this programme of work, ethers based on the 4-(dihydroisobenzofuranyl) core have been identified as potent and selective PI3K $\delta$  inhibitors.

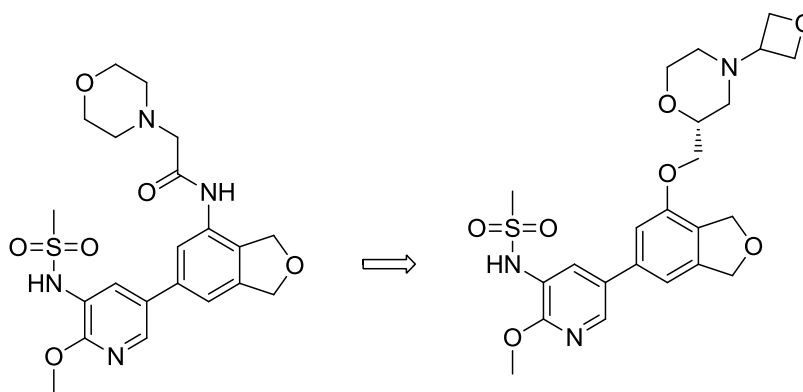
Exploration of substitution at the 4-position of the dihydroisobenzofuran core and a conformational analysis of different substituents showed that most potent compounds adopted a low energy conformation when bound to the PI3K $\delta$  enzyme. Where potent compounds did not bind in a conformation close to the global minimum, potency was achieved through other interactions within the protein backbone, for example, a stronger hinge interaction or additional H-bonding interactions. Therefore, assessing the preferred conformation of small molecule inhibitors and how this may change on binding to the enzyme, including the other interactions that could be targeted, which could be explored by molecular modelling, is essential for the design of future compounds.

Incorporation of pendant substituents on the desired linker atoms at the 4-position was required to achieve the desired selectivity for PI3K $\delta$  over the other PI3K isoforms. The preferred 4-position linkers were the anilide and ether groups; these linkers conferred good PI3K $\delta$  potency and selectivity when further substituted.

Substitution of the anilides led to compounds with desired potencies, including excellent activity in HWB; however the compounds had high clearance and poor oral bioavailability when assessed in a rat *in vivo* PK study, as the substituents required to achieve the desired PI3K $\delta$  potency were not stable to metabolism.

Ethers based on the 4-(dihydroisobenzofuranyl) core had increased enzyme potency and some compounds had high HWB potency; however they also did not achieve the desired oral PK profile since they had moderate clearance and short half-lives. Strategies to reduce the metabolic clearance were employed in order to improve the half-life and ensure good oral absorption; compounds with low lipophilicity and functional groups thought to be metabolically stable were

synthesised. Compound **245** has a superior potency and selectivity profile and much reduced predicted once-daily human dose when compared with the lead compound **173**.



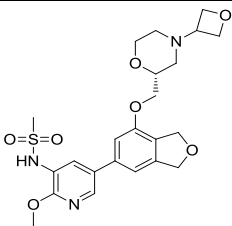
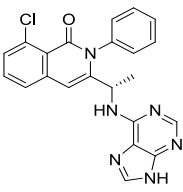
**173**

PI3K $\delta$  pIC<sub>50</sub> 6.8  
 $\alpha$  5.3,  $\beta$  5.0,  $\gamma$  5.0  
 HWB pIC<sub>50</sub> 6.5  
 Rat *in vivo* Cl<sub>b</sub> = 14 ml/min/kg  
 F = 54%  
 Predicted human dose = 1826 mg

**245**

PI3K $\delta$  pIC<sub>50</sub> 8.4  
 $\alpha$  6.3,  $\beta$  6.2,  $\gamma$  6.6  
 HWB pIC<sub>50</sub> 7.1  
 Rat *in vivo* Cl<sub>b</sub> = 20 ml/min/kg  
 F = 46%  
 Predicted human dose = 372 mg

Additionally, compound **245** has a similar potency in human whole blood when compared with clinical candidate Duvelisib, which is currently in Phase II clinical trials for the treatment of inflammatory diseases (Table 4.4.1). Compound **245** has similar permeability and solubility to that of Duvelisib, but has a lower PFI and lower lipophilicity, indicating that the compound is an improved physicochemical space with respect to developability (Table 4.4.1). It is likely that compound **245** will be well absorbed, as indicated by the *in vivo* rat PK profile, hence it will also be efficacious as an oral anti-inflammatory agent.

Structure		
Compound	<b>245</b>	<b>Duvelisib</b>
Mean PI3K $\delta$ pIC <sub>50</sub> (N)	8.4 (6)	9.4 (5)
Mean PI3K $\alpha$ pIC <sub>50</sub> (N)	6.3 (6)	5.6 (4)
Mean PI3K $\beta$ pIC <sub>50</sub> (N)	6.2 (6)	7.2 (4)
Mean PI3K $\gamma$ pIC <sub>50</sub> (N)	6.6 (7)	8.1 (6)
Mean HWB pIC <sub>50</sub> (N)	7.1 (3) <sup>a</sup>	7.2 (6)
LE/LLE <sub>AT</sub>	0.34/0.38	0.43/0.34
PFI	4.9	8.2
mChromlogD <sub>pH7.4</sub>	2.90	3.18
clogP	1.8	4.4
MW	491	416
AMP (pH 7.4, nm/s)	215	320
CLND Solubility ( $\mu$ M)	294	346

<sup>a</sup> Returned no value on one test occasion.

Table 4.4.1. Comparison of compound **245** with clinical candidate Duvelisib.

Further optimisation of the PK profile of compounds of this type will be pursued in order to discover a candidate drug molecule with a predicted once-daily human dose of less than 100 mg.

Throughout the optimisation of the PK profile of the ethers based on the 4-(dihydroisobenzofuranyl) core it was important to analyse whether any calculable properties, for example lipophilicity, could be used to predict compounds that would have the desired ADMET properties. This analysis should not be conducted only at the beginning of a programme of work but periodically to reconfirm whether the initially observed trends hold true. This was not the case in this programme of work and learnings from this can now be utilised in the next iteration of compound design. Predicting a compound's clearance from calculated properties (i.e. lipophilicity) in

this case was not possible; however an *in vitro* measurement of clearance was highlighted as a good predictor of *in vivo* clearance.

In future work, the *in vitro* clearance assay will be run as part of the initial screening of potential PI3K $\delta$  inhibitors alongside the potency and selectivity screens, so as to discover molecules that are more likely to achieve low *in vivo* clearance. It is hoped that this will lead to the discovery of a candidate compound with the desired oral PK profile more rapidly.

## 4.5. References

- (1) Whitman, M.; Kaplan, D. R.; Schaffhausen, B.; Cantley, L.; Roberts, T. M. *Nature* **1985**, *315*, 239.
- (2) Vanhaesebroeck, B.; Leever, S. J.; Ahmadi, K.; Timms, J.; Katso, R.; Driscoll, P. C.; Woscholski, R.; Parker, P. J.; Waterfield, M. D. *Annu. Rev. Biochem.* **2001**, *70*, 535.
- (3) Vanhaesebroeck, B.; Leever, S. J.; Panayotou, G.; Waterfield, M. D. *Trends Biochem. Sci.* **1997**, *22*, 267.
- (4) Jimenez, C.; Hernandez, C.; Pimentel, B.; Carrera, A. C. *J. Biol. Chem.* **2002**, *277*, 41556.
- (5) Stephens, L. R.; Eguinoa, A.; Erdjument-Bromage, H.; Lui, M.; Cooke, F.; Coadwell, J.; Smrcka, A. S.; Thelen, M.; Cadwallader, K.; Tempst, P.; Hawkins, P. T. *Cell* **1997**, *89*, 105.
- (6) Suire, S.; Coadwell, J.; Ferguson, G. J.; Davidson, K.; Hawkins, P.; Stephens, L. *Curr. Biol.* **2005**, *15*, 566.
- (7) Voigt, P.; Dorner, M. B.; Schaefer, M. *J. Biol. Chem.* **2006**, *281*, 9977.
- (8) Brock, C.; Schaefer, M.; Reusch, H. P.; Czupalla, C.; Michalke, M.; Spicher, K.; Schultz, G.; Nurnberg, B. *J. Cell Biol.* **2003**, *160*, 89.
- (9) Guillermet-Guibert, J.; Bjorklof, K.; Salpekar, A.; Gonella, C.; Ramadani, F.; Bilancio, A.; Meek, S.; Smith, A. J. H.; Okkenhaug, K.; Vanhaesebroeck, B. *PNAS* **2008**, *105*, 8292.
- (10) Cantley, L. C. *Science* **2002**, *296*, 1655.
- (11) Falasca, M.; Maffucci, T. *Biochem. J.* **2012**, *443*, 587.
- (12) Falasca, M.; Hughes, W. E.; Dominguez, V.; Sala, G.; Fostira, F.; Fang, M. Q.; Cazzolli, R.; Shepherd, P. R.; James, D. E.; Maffucci, T. *J. Biol. Chem.* **2007**, *282*, 28226.
- (13) Yoshioka, K.; Sugimoto, N.; Takuwa, N.; Takuwa, Y. *Mol. Pharmacol.* **2007**, *71*, 912.

- (14) Maffucci, T.; Cooke, F. T.; Foster, F. M.; Traer, C. J.; Fry, M. J.; Falasca, M. *J. Cell Biol.* **2005**, *169*, 789.
- (15) Schu, P. V.; Takegawa, K.; Fry, M. J.; Stack, J. H.; Waterfield, M. D.; Emr, S. D. *Science* **1993**, *260*, 88.
- (16) Backer, J. M. *Biochem. J.* **2008**, *410*, 1.
- (17) Vanhaesebroeck, B.; Stephens, L.; Hawkins, P. *Nat. Rev. Mol. Cell Biol.* **2012**, *13*, 195.
- (18) Lovejoy, C. A.; Cortez, D. *DNA Repair* **2009**, *8*, 1004.
- (19) Durocher, D.; Jackson, S. P. *Curr. Opin. Cell Biol.* **2001**, *13*, 225.
- (20) Yamashita, A.; Kashima, I.; Ohno, S. *Biochim. Biophys. Acta, Proteins Proteomics* **2005**, *1754*, 305.
- (21) Tsang, C. K.; Qi, H.; Liu, L. F.; Zheng, X. F. S. *Drug Discov. Today* **2007**, *12*, 112.
- (22) Crabbe, T.; Welham, M. J.; Ward, S. G. *Trends Biochem. Sci.* **2007**, *32*, 450.
- (23) Bi, L.; Okabe, I.; Bernard, D. J.; Wynshaw-Boris, A.; Nussbaum, R. L. *J. Biol. Chem.* **1999**, *274*, 10963.
- (24) Samuels, Y.; Wang, Z.; Bardelli, A.; Silliman, N.; Ptak, J.; Szabo, S.; Yan, H.; Gazdar, A.; Powell Steven, M.; Riggins Gregory, J.; Willson James, K. V.; Markowitz, S.; Kinzler Kenneth, W.; Vogelstein, B.; Velculescu Victor, E. *Science* **2004**, *304*, 554.
- (25) Bi, L.; Okabe, I.; Bernard, D. J.; Nussbaum, R. L. *Mamm. Genome* **2002**, *13*, 169.
- (26) Jia, S.; Liu, Z.; Zhang, S.; Liu, P.; Zhang, L.; Lee, S. H.; Zhang, J.; Signoretti, S.; Loda, M.; Roberts, T. M.; Zhao, J. J. *Nature* **2008**, *454*, 776.
- (27) Jackson, S. P.; Schoenwaelder, S. M.; Goncalves, I.; Nesbitt, W. S.; Yap, C. L.; Wright, C. E.; Kenche, V.; Anderson, K. E.; Dopheide, S. M.; Yuan, Y.; Sturgeon, S. A.; Prabakaran, H.; Thompson, P. E.; Smith, G. D.; Shepherd, P. R.; Daniele, N.; Kulkarni, S.; Abbott, B.; Saylik, D.; Jones, C.; Lu, L.; Giuliano, S.; Hughan, S. C.; Angus, J. A.; Robertson, A. D.; Salem, H. H. *Nat. Med.* **2005**, *11*, 507.

- (28) Wymann, M. P.; Marone, R. *Curr. Opin. Cell Biol.* **2005**, *17*, 141.
- (29) Hirsch, E.; Katanaev, V. L.; Garlanda, C.; Azzolino, O.; Pirola, L.; Silengo, L.; Sozzani, S.; Mantovani, A.; Altruda, F.; Wymann, M. P. *Science* **2000**, *287*, 1049.
- (30) Marone, R.; Cmiljanovic, V.; Giese, B.; Wymann, M. P. *Biochim. Biophys. Acta, Proteins Proteomics* **2008**, *1784*, 159.
- (31) Rodriguez-Borlado, L.; Barber, D. F.; Hernandez, C.; Rodriguez-Marcos, M. A.; Sanchez, A.; Hirsch, E.; Wymann, M.; Martinez-A, C.; Carrera, A. C. *J. Immunol.* **2003**, *170*, 4475.
- (32) Billottet, C.; Grandage, V. L.; Gale, R. E.; Quattropiani, A.; Rommel, C.; Vanhaesebroeck, B.; Khwaja, A. *Oncogene* **2006**, *25*, 6648.
- (33) Chantry, D.; Vojtek, A.; Kashishian, A.; Holtzman, D. A.; Wood, C.; Gray, P. W.; Cooper, J. A.; Hoekstra, M. F. *J. Biol. Chem.* **1997**, *272*, 19236.
- (34) Okkenhaug, K.; Bilancio, A.; Farjot, G.; Priddle, H.; Sancho, S.; Peskett, E.; Pearce, W.; Meek, S. E.; Salpekar, A.; Waterfield, M. D.; Smith, A. J. H.; Vanhaesebroeck, B. *Science* **2002**, *297*, 1031.
- (35) Thomas, M.; Owen, C. *Curr. Opin. Pharmacol.* **2008**, *8*, 267.
- (36) Ali, K.; Bilancio, A.; Thomas, M.; Pearce, W.; Gilfillan, A. M.; Tkaczyk, C.; Kuehn, N.; Gray, A.; Giddings, J.; Peskett, E.; Fox, R.; Bruce, I.; Walker, C.; Sawyer, C.; Okkenhaug, K.; Finan, P.; Vanhaesebroeck, B. *Nature* **2004**, *431*, 1007.
- (37) Lee, K. S.; Lee, H. K.; Hayflick, J. S.; Lee, Y. C.; Puri, K. D. *FASEB-J* **2006**, *20*, 455.
- (38) Nashed, B. F.; Zhang, T.; Al-Alwan, M.; Srinivasan, G.; Halayko, A. J.; Okkenhaug, K.; Vanhaesebroeck, B.; HayGlass, K. T.; Marshall, A. J. *Eur. J. Immunol.* **2007**, *37*, 416.
- (39) Barnes, P. J. *Nat. Rev. Immunol.* **2008**, *8*, 183.
- (40) Sapey, E.; Stockley, J. A.; Greenwood, H.; Ahmad, A.; Bayley, D.; Lord, J. M.; Insall, R. H.; Stockley, R. A. *Am. J. Respir. Crit. Care Med.* **2011**, *183*, 1176.



- (41) Sadhu, C.; Masinovsky, B.; Dick, K.; Sowell, C. G.; Staunton, D. E. *J. Immunol.* **2003**, *170*, 2647.
- (42) Puri, K. D.; Doggett, T. A.; Douangpanya, J.; Hou, Y.; Tino, W. T.; Wilson, T.; Graf, T.; Clayton, E.; Turner, M.; Hayflick, J. S.; Diacovo, T. G. *Blood* **2004**, *103*, 3448.
- (43) Doukas, J.; Eide, L.; Stebbins, K.; Racanelli-Layton, A.; Dellamary, L.; Martin, M.; Dneprovskaja, E.; Noronha, G.; Soll, R.; Wrasidlo, W.; Acevedo, L. M.; Cheresh, D. A. *J. Pharmacol. Exp. Ther.* **2009**, *328*, 758.
- (44) Marwick, J. A.; Caramori, G.; Stevenson, C. S.; Casolari, P.; Jazrawi, E.; Barnes, P. J.; Ito, K.; Adcock, I. M.; Kirkham, P. A.; Papi, A. *Am. J. Respir. Crit. Care Med.* **2009**, *179*, 542.
- (45) Ge, Q.; Moir, L. M.; Trian, T.; Niimi, K.; Poniris, M.; Shepherd, P. R.; Black, J. L.; Oliver, B. G.; Burgess, J. K. *J. Cell. Physiol.* **2012**, *227*, 3044.
- (46) Arcaro, A.; Wymann, M. P. *Biochem. J.* **1993**, *296*, 297.
- (47) Vlahos, C. J.; Matter, W. F.; Hui, K. Y.; Brown, R. F. *J. Biol. Chem.* **1994**, *269*, 5241.
- (48) Balla, A.; Balla, T. *Trends Cell Biol.* **2006**, *16*, 351.
- (49) Merida, I.; Avila-Flores, A.; Merino, E. *Biochem. J.* **2008**, *409*, 1.
- (50) Foukas, L. C.; Daniele, N.; Ktori, C.; Anderson, K. E.; Jensen, J.; Shepherd, P. R. *J. Biol. Chem.* **2002**, *277*, 37124.
- (51) Lannutti, B. J.; Meadows, S. A.; Herman, S. E. M.; Kashishian, A.; Steiner, B.; Johnson, A. J.; Byrd, J. C.; Tyner, J. W.; Loriaux, M. M.; Deininger, M.; Druker, B. J.; Puri, K. D.; Ulrich, R. G.; Giese, N. A. *Blood* **2011**, *117*, 591.
- (52) Herman, S. E. M.; Gordon, A. L.; Wagner, A. J.; Heerema, N. A.; Zhao, W.; Flynn, J. M.; Jones, J.; Andritsos, L.; Puri, K. D.; Lannutti, B. J.; Giese, N. A.; Zhang, X.; Wei, L.; Byrd, J. C.; Johnson, A. J. *Blood* **2010**, *116*, 2078.
- (53) "A Randomized, Controlled Study Evaluating the Efficacy and Safety of GS-1101 (CAL-101) in Combination With Ofatumumab for Previously Treated Chronic Lymphocytic Leukemia", Available from: <http://clinicaltrials.gov/show/NCT01659021> NLM Identifier: NCT01659021.

- (54) "A Study Evaluating the Efficacy and Safety of Idelalisib (GS-1101) in Combination With Rituximab for Previously Treated Indolent Non-Hodgkin Lymphomas", Available from: <http://clinicaltrials.gov/show/NCT01732913> NLM Identifier: NCT01732913.
- (55) "A Phase 2 Study of IPI-145 in Subjects With Refractory Indolent Non-Hodgkin Lymphoma", Available from: <http://clinicaltrials.gov/show/NCT01882803> NLM Identifier: NCT01882803.
- (56) "A Phase 2a, Efficacy and Safety Study of IPI-145 in Mild Asthmatic Subjects", Available from: <http://clinicaltrials.gov/show/NCT01653756> NLM Identifier: NCT01653756.
- (57) "AMG 319 Lymphoid Malignancy FIH", Available from: <http://clinicaltrials.gov/show/NCT01300026> NLM Identifier: NCT01300026.
- (58) Norman, P. *Expert Opin. Ther. Pat.* **2011**, *21*, 1773.
- (59) Chen, Y.; Cushing, T. D.; Hao, X.; He, X.; Reichelt, A.; Rzasa, R. M.; Seganish, J.; Shin, Y.; Zhang, D., "3-Substituted quinoline or quinoxaline derivatives and their use as phosphatidylinositol 3-kinase (PI3K) inhibitors and their preparation", WO 2008118455, 2008.
- (60) Cushing, T. D.; Gonzalez Lopez de Turiso, F.; Hao, X.; Shin, Y., "Heterocyclic compounds as PI3K inhibitors and their preparation and use in the treatment of diseases", WO 2011075628, 2011.
- (61) Safina, B. S.; Baker, S.; Baumgardner, M.; Blaney, P. M.; Chan, B. K.; Chen, Y.-H.; Cartwright, M. W.; Castanedo, G.; Chabot, C.; Cheguillaume, A. J.; Goldsmith, P.; Goldstein, D. M.; Goyal, B.; Hancox, T.; Handa, R. K.; Iyer, P. S.; Kaur, J.; Kondru, R.; Kenny, J. R.; Krintel, S. L.; Li, J.; Lesnick, J.; Lucas, M. C.; Lewis, C.; Mukadam, S.; Murray, J.; Nadin, A. J.; Nonomiya, J.; Padilla, F.; Palmer, W. S.; Pang, J.; Pegg, N.; Price, S.; Reif, K.; Salphati, L.; Savy, P. A.; Seward, E. M.; Shuttleworth, S.; Sohal, S.; Sweeney, Z. K.; Tay, S.; Tivitmahaisoon, P.; Waszkowycz, B.; Wei, B.; Yue, Q.; Zhang, C.; Sutherlin, D. P. *J. Med. Chem.* **2012**, *55*, 5887.

- (62) Murray, J. M.; Sweeney, Z. K.; Chan, B. K.; Balazs, M.; Bradley, E.; Castanedo, G.; Chabot, C.; Chantry, D.; Flagella, M.; Goldstein, D. M.; Kondru, R.; Lesnick, J.; Li, J.; Lucas, M. C.; Nonomiya, J.; Pang, J.; Price, S.; Salphati, L.; Safina, B.; Savy, P. P. A.; Seward, E. M.; Ultsch, M.; Sutherlin, D. P. *J. Med. Chem.* **2012**, *55*, 7686.
- (63) Sutherlin, D. P.; Baker, S.; Bisconte, A.; Blaney, P. M.; Brown, A.; Chan, B. K.; Chantry, D.; Castanedo, G.; DePledge, P.; Goldsmith, P.; Goldstein, D. M.; Hancox, T.; Kaur, J.; Knowles, D.; Kondru, R.; Lesnick, J.; Lucas, M. C.; Lewis, C.; Murray, J.; Nadin, A. J.; Nonomiya, J.; Pang, J.; Pegg, N.; Price, S.; Reif, K.; Safina, B. S.; Salphati, L.; Staben, S.; Seward, E. M.; Shuttleworth, S.; Sohal, S.; Sweeney, Z. K.; Ultsch, M.; Waszkowycz, B.; Wei, B. *Bioorg. Med. Chem. Lett.* **2012**, *22*, 4296.
- (64) Harrison, Z. A.; Identification of a selective lead series for a PI3K-delta programme by kinase cross screening. Presented at *244th ACS National Meeting* Philadelphia, PA, US, 19<sup>th</sup> August 2012.
- (65) "Study to Investigate Safety, Tolerability, Pharmacokinetics & Pharmacodynamics of Single & Repeat Doses of GSK2269557", Available from: <http://clinicaltrials.gov/show/NCT01462617> NLM Identifier: NCT01462617.
- (66) Hamblin, N., GlaxoSmithKline: 2013, personal communication.
- (67) Hamblin, N.; Discovery of potent and selective PI3K delta inhibitors for the treatment of respiratory indications. Presented at *245th ACS National Meeting* New Orleans, LA, US, 7<sup>th</sup> April 2013.
- (68) Berndt, A.; Miller, S.; Williams, O.; Le, D. D.; Houseman, B. T.; Pacold, J. I.; Gorrec, F.; Hon, W.-C.; Liu, Y.; Rommel, C.; Gaillard, P.; Rueckle, T.; Schwarz, M. K.; Shokat, K. M.; Shaw, J. P.; Williams, R. L. *Nat. Chem. Biol.* **2010**, *6*, 117.
- (69) Rowland, P., GlaxoSmithKline: 2013, personal communication.
- (70) Peace, S., GlaxoSmithKline: 2011, personal communication.

- (71) Morrell, J.; Smith, C.; Eddershaw, P.; Hachspil, M.; Vitulli, G., GlaxoSmithKline: 2011, unpublished results.
- (72) Bissantz, C.; Kuhn, B.; Stahl, M. *J. Med. Chem.* **2010**, *53*, 5061.
- (73) Lipinski, C. A.; Lombardo, F.; Dominy, B. W.; Feeney, P. J. *Adv. Drug Delivery Rev.* **1997**, *23*, 3.
- (74) Veber, D. F.; Johnson, S. R.; Cheng, H.-Y.; Smith, B. R.; Ward, K. W.; Kopple, K. D. *J. Med. Chem.* **2002**, *45*, 2615.
- (75) Barton, N.; Down, K. D., GlaxoSmithKline: 2011, personal communication.
- (76) Laurence, C.; Brameld, K. A.; Graton, J.; Le Questel, J.-Y.; Renault, E. *J. Med. Chem.* **2009**, *52*, 4073.
- (77) Tame, C. J.; Bouisseau, A., GlaxoSmithKline: 2010, personal communication.
- (78) Abdel-Magid, A. F.; Carson, K. G.; Harris, B. D.; Maryanoff, C. A.; Shah, R. D. *J. Org. Chem.* **1996**, *61*, 3849.
- (79) Borch, R. F.; Bernstein, M. D.; Durst, H. D. *J. Am. Chem. Soc.* **1971**, *93*, 2897.
- (80) Zacuto, M. J.; Xu, F. *J. Org. Chem.* **2007**, *72*, 6298.
- (81) Rebellas, J. C.; Olechowski, J. R.; Jonassen, H. B.; Moore, D. W. *J. Organomet. Chem.* **1967**, *9*, 153.
- (82) Bouisseau, A., GlaxoSmithKline: 2011, personal communication.
- (83) Devos, A.; Remion, J.; Frisque-Hesbain, A. M.; Colens, A.; Ghosez, L. *J. Chem. Soc., Chem. Commun.* **1979**, 1180.
- (84) DalPozzo, A.; Ni, M.; Muzi, L.; Caporale, A.; de Castiglione, R.; Kaptein, B.; Broxterman, Q. B.; Formaggio, F. *J. Org. Chem.* **2002**, *67*, 6372.
- (85) Crawford, J. J.; Henderson, K. W.; Kerr, W. *J. Org. Lett.* **2006**, *8*, 5073.
- (86) Prakash, G. K. S.; Yudin, A. K. *Chem. Rev.* **1997**, *97*, 757.
- (87) Blazejewski, J.-C.; Anselmi, E.; Wilmshurst, M. P. *Tetrahedron Lett.* **1999**, *40*, 5475.
- (88) Nelson, D. W.; Owens, J.; Hiraldo, D. *J. Org. Chem.* **2001**, *66*, 2572.
- (89) Felix, C. P.; Khatimi, N.; Laurent, A. *J. Tetrahedron Lett.* **1994**, *35*, 3303.

- (90) Prakash, G. K. S.; Mogi, R.; Olah, G. A. *Org. Lett.* **2006**, *8*, 3589.
- (91) Levin, V. V.; Dilman, A. D.; Belyakov, P. A.; Struchkova, M. I.; Tartakovsky, V. A. *Eur. J. Org. Chem.* **2008**, 5226.
- (92) Prakash, G. K. S.; Mandal, M.; Olah, G. A. *Synlett* **2001**, 77.
- (93) Prakash, G. K. S.; Mandal, M.; Olah, G. A. *Angew. Chem., Int. Ed.* **2001**, *40*, 589.
- (94) Ellman, J. A.; Owens, T. D.; Tang, T. P. *Acc. Chem. Res.* **2002**, *35*, 984.
- (95) Wix, E., GlaxoSmithKline: 2011, personal communication.
- (96) Koshland, D. E., Jr. *PNAS* **1958**, *44*, 98.
- (97) Nicklaus, M. C.; Wang, S.; Driscoll, J. S.; Milne, G. W. A. *Bioorg. Med. Chem.* **1995**, *3*, 411.
- (98) Perola, E.; Charifson, P. S. *J. Med. Chem.* **2004**, *47*, 2499.
- (99) Wang, Q.; Pang, Y.-P. *PLoS One* **2007**, *2*, e820.
- (100) Dougherty, D. A. *Acc. Chem. Res.* **2013**, DOI: 10.1021/ar300265y.
- (101) Legon, A. C.; Millen, D. J. *Chem. Soc. Rev.* **1987**, *16*, 467.
- (102) Maduli, E., GlaxoSmithKline: 2011, personal communication.
- (103) Chung, J.; Saunders, M., GlaxoSmithKline: 2012, unpublished results.
- (104) Pre-clinical ADME, toxicology and PK, Cyprotex: 2013, unpublished results.
- (105) Edwards, C.; Mallett, D.; Roussett, N.; Sherriff, E.; Young, A., GlaxoSmithKline: 2013, unpublished results.
- (106) Huang, J.; Chen, Y.; Chan, J.; Ronk, M. L.; Larsen, R. D.; Faul, M. M. *Synlett* **2011**, 1419.
- (107) Schmitt, E.; Jackson, S., GlaxoSmithKline: 2012, personal communication.
- (108) Edwards, C.; Mallett, D.; Young, A., GlaxoSmithKline: 2012, unpublished results.
- (109) Lemke, T. L.; Williams, D. A.; Rocher, V. F.; Zito, W. S. *Foye's Principles of Medicinal Chemistry*; 7th ed.; Lippincott Williams & Wilkins: Baltimore, 2012.
- (110) St. Jean, D. J.; Fotsch, C. *J. Med. Chem.* **2012**, *55*, 6002.
- (111) Paul, R.; Ali, M. A.; Punniyamurthy, T. *Synthesis* **2010**, 4268.

- (112) Weller, D. D.; Stirchak, E. P.; Yokoyama, A. *J. Org. Chem.* **1984**, *49*, 2061.
- (113) Kormos, C. M.; Leadbeater, N. E. *Tetrahedron* **2006**, *62*, 4728.
- (114) Zhao, D.; Wu, N.; Zhang, S.; Xi, P.; Su, X.; Lan, J.; You, J. *Angew. Chem., Int. Ed.* **2009**, *48*, 8729.
- (115) Chen, J.; Yuan, T.; Hao, W.; Cai, M. *Catal. Commun.* **2011**, *12*, 1463.
- (116) Mehmood, A.; Leadbeater, N. E. *Catal. Commun.* **2010**, *12*, 64.
- (117) Surry, D. S.; Buchwald, S. L. *Chem. Sci.* **2010**, *1*, 13.
- (118) Mitsunobu, O.; Yamada, M. *Bull. Chem. Soc. Jpn.* **1967**, *40*, 2380.
- (119) Mitsunobu, O. *Synthesis* **1981**, 1.
- (120) Swamy, K. C. K.; Kumar, N. N. B.; Balaraman, E.; Kumar, K. V. P. *Chem. Rev.* **2009**, *109*, 2551.
- (121) Dandapani, S.; Curran, D. P. *Chem.--Eur. J.* **2004**, *10*, 3130.
- (122) Tsunoda, T.; Ozaki, F.; Ito, S. *Tetrahedron Lett.* **1994**, *35*, 5081.
- (123) Eschweiler, W. *Ber. Dtsch. Chem. Ges.* **1905**, *38*, 880.
- (124) Clarke, H. T.; Gillespie, H. B.; Weisshaus, S. Z. *J. Am. Chem. Soc.* **1933**, *55*, 4571.
- (125) Dounay, A. B.; Barta, N. S.; Bikker, J. A.; Borosky, S. A.; Campbell, B. M.; Crawford, T.; Denny, L.; Evans, L. M.; Gray, D. L.; Lee, P.; Lenoir, E. A.; Xu, W. *Bioorg. Med. Chem. Lett.* **2009**, *19*, 1159.
- (126) Schweizer, E.; Hoffmann-Roder, A.; Scharer, K.; Olsen, J. A.; Fah, C.; Seiler, P.; Obst-Sander, U.; Wagner, B.; Kansy, M.; Diederich, F. *ChemMedChem* **2006**, *1*, 611.
- (127) <http://www.chemaxon.com/products/calculator-plugins/property-predictors/>, accessed on 4th December 2013.
- (128) James, M., GlaxoSmithKline: 2013, personal communication.
- (129) Srivastava, S. K.; Chauhan, P. M. S.; Bhaduri, A. P. *Synth. Commun.* **1999**, *29*, 2085.
- (130) Scarpi, D.; Occhiato, E. G.; Guarna, A. *Tetrahedron: Asymmetry* **2009**, *20*, 340.
- (131) MacDougall, S., GlaxoSmithKline: 2013, personal communication.

- (132) Wuitschik, G.; Carreira, E. M.; Wagner, B.; Fischer, H.; Parrilla, I.; Schuler, F.; Rogers-Evans, M.; Muller, K. *J. Med. Chem.* **2010**, *53*, 3227.
- (133) Down, K. D., GlaxoSmithKline: 2013, personal communication.
- (134) Lee, G. H.; Youn, I. K.; Choi, E. B.; Lee, H. K.; Yon, G. H.; Yang, H. C.; Pak, C. S. *Curr. Org. Chem.* **2004**, *8*, 1263.
- (135) Lee, G. H.; Choi, E. B.; Lee, E.; Pak, C. S. *Tetrahedron Lett.* **1993**, *34*, 4541.
- (136) Molander, G. A. *Org. React.* **1994**, *46*, 211.
- (137) Inanaga, J.; Ishikawa, M.; Yamaguchi, M. *Chem. Lett.* **1987**, 1485.
- (138) Girard, P.; Namy, J. L.; Kagan, H. B. *J. Am. Chem. Soc.* **1980**, *102*, 2693.
- (139) Machrouhi, F.; Hamann, B.; Namy, J. L.; Kagan, H. B. *Synlett* **1996**, 633.
- (140) Shibasaki, M.; Kanai, M.; Mita, T. *Org. React.* **2008**, *70*, 1.
- (141) Bruylants, P. *Bull. Soc. Chim. Belg.* **1924**, *33*, 467.
- (142) Prashad, M.; Liu, Y.; Har, D.; Repic, O.; Blacklock, T. J. *Tetrahedron Lett.* **2005**, *46*, 5455.
- (143) Edwards, C.; Mallett, D.; Roussett, N.; Sherriff, E., GlaxoSmithKline: 2012, unpublished results.
- (144) Edwards, C., GlaxoSmithKline: 2013, personal communication.

## **5. Thesis Conclusion**

The programmes of work described in this thesis set out to discover kinase inhibitors as novel anti-inflammatory agents for the treatment of asthma and COPD. There remains a major need to develop new oral drugs for these inflammatory lung diseases as many patients are refractory (their illness is difficult to control despite extensive evaluation and treatment with existing therapies), hence this research is of significant importance.

The main empirical findings were chapter specific and have been summarised within the respective chapters. The broader implications of these findings will be discussed here.

The general literature on the design of orally bioavailable drugs is broad and many rational drug design techniques have been described. Two of the main types of drug design (ligand-based and structure-based) were used in the programmes of work described in this thesis.

There are many examples of the ligand-based drug design technique of Hansch analysis described in the literature and this methodology was implemented here to describe QSARs for a series of IKK2 inhibitors. The application of this method was based on strong structure-activity correlations, albeit with 3 compounds per set; however it was not found to be successful in extrapolating to substituents not included in the original analysis. On reflection, despite the strength of observed correlations, developing a predictive model based on a small number of compounds was not sufficiently robust and one learning from this research is that forecasting biological activity using QSAR equations should only be carried out if a large training set is available. Nevertheless, this work demonstrated that the electronic and steric properties of compounds could be evaluated very efficiently. Therefore, QSAR has a role in the objective design of a series of compounds to give the best chance of discovering an analogue with the combination of properties that gives the desired biological profile; failing that, it can at least ensure that a thorough search of property space is carried out prior to a decision to terminate a series.



In the research carried out here, a small set of compounds was expanded using the additional substituents described by Hansch leading to an advance in the development of IKK2 inhibitors when compounds with increased ligand efficiency were identified within the 3,5-substituted indole carboxamide series. In future, compounds functionalised with the ligand efficient 3-position substituents discovered here could be taken forward to investigate whether the desired candidate profile can be achieved by varying the 5-position substituent. The recent publication of the human IKK2 crystal structure may provide opportunities for the design of such compounds since the accuracy of structure-based drug design will now be improved.

As part of the research into the optimisation of IKK2 inhibitors, a set of compounds was designed using knowledge from the contemporary medicinal chemistry literature. The reported use of oxetanes in drug discovery led to the challenging syntheses of IKK2 inhibitors incorporating the oxetanyl group. The methodical and rigorous approach to the synthesis of the target compounds led to the discovery of novel, synthetically useful methodology for the synthesis of oxazole and thiazoles. Applying this rigour to future work will be important in making innovative contributions to the preparation of potential drug molecules and more generally to the field of synthetic organic chemistry.

Structure-based drug design was the main technique employed in the design of PI3K $\delta$  inhibitors in the programme of work described in this thesis, since a crystal structure of PI3K $\delta$  was available. A strong trend between preferred ligand conformations and those adopted by the ligand upon binding to the target was observed for the series of compounds investigated here. This work has enabled a structure-based design approach based on ligand conformational analysis and molecular modelling to be used for the future design of PI3K $\delta$  inhibitors. This approach could also be used systematically in other programmes; however it will be important to analyse the free and protein-bound ligand states for different series of compounds and biological targets using the method described in this thesis to verify trends.

The development of PI3K $\delta$  inhibitors as oral drugs also included a significant effort to optimise the oral PK profile of the compounds. The discovery of a PI3K $\delta$  inhibitor with a superior oral drug profile and significantly reduced predicted once-daily human dose was an important advance within this programme of work. A common strategy in drug discovery is to focus on improving the potency and selectivity profile of potential drug molecules; however, this can often lead to issues with ADMET properties that are not discovered until later in lead optimisation. Often, the ADMET profile of a compound is not assessed early as low throughput *in vivo* assays are required; however this work substantiated the opinion that high throughput, low cost *in vitro* assays can be used effectively to predict the *in vivo* profile. This work also showed that optimising the oral PK profile of potential drug molecules *a priori* was difficult, so if *in vitro* ADMET assays had a more substantial role in the selection and optimisation of a given lead series, compounds with good oral PK profiles could be chosen as starting points and the PK profile may be more easily maintained during optimisation.

The experiences gained from the work carried out here also showed that achieving good *in vitro* and physicochemical properties does not guarantee the desired *in vivo* PK profile. Progression through *in vivo* PK studies is therefore essential for a full understanding of the molecular properties of drugs and examining the *in vivo* PK profile of suboptimal compounds should not be precluded if it helps to improve this understanding.

The work described in this thesis has led to advances in the identification of novel kinase inhibitors as potential anti-inflammatory agents and several strategies for drug design were applied in practise. The preparation of synthetically difficult molecules also led to the discovery of useful synthetic methodology that could be applied more widely.

## 6. Experimental

### 6.1. General Details

All moisture sensitive reagents were reacted under nitrogen with glassware dried in an oven at >120 °C and cooled under a flow of nitrogen. Reactions were heated by means of DrySyn hotplates unless otherwise stated.

All solvents were reagent grade and supplied by Sigma-Aldrich or Fischer Scientific unless otherwise stated. All reactions were carried out using anhydrous solvents that were supplied under either argon or nitrogen and were transferred in an inert atmosphere.

All starting materials were commercially available unless otherwise stated.

NMR spectra were recorded on Bruker AV-400 (<sup>1</sup>H 400.13 MHz; <sup>13</sup>C 100.61 MHz; <sup>19</sup>F 376.50 MHz) or Bruker AVII-600 (<sup>1</sup>H 600.40 MHz; <sup>13</sup>C 150.97 MHz) spectrometers. <sup>1</sup>H, <sup>13</sup>C and <sup>19</sup>F NMR spectra were recorded using deuterated solvent as the lock and residual solvent as the internal reference. <sup>19</sup>F NMR spectra are decoupled. Chemical shifts ( $\delta_{\text{H}}$ ,  $\delta_{\text{C}}$  or  $\delta_{\text{F}}$ ) are reported in parts per million (ppm) and are referenced to the residual solvent peak. The multiplicities of the spectroscopic data are presented in the following manner: app = apparent, s = singlet, d = doublet, dd = double doublet, dt = doublet of triplets, ddt = doublet of double triplets, t = triplet, td = triple doublet, q = quartet, qd = quartet of doublets, m = multiplet and br. = broad. Homocouplings (H-H) are given in Hertz and specified by *J*; the nuclei involved in heteronuclear couplings are defined with the observed nucleus given first. Unless stated otherwise, all refer to <sup>3</sup>*J* couplings. Spectra recorded on Bruker AVII-600 machine were obtained by Stephen Richards, Sean Lynn or Richard Upton of the NMR Department, GSK, Stevenage.

Microwave reactions were carried out on a Biotage Initiator Microwave System.

Column chromatography was carried out on silica gel (either Biotage Isolute<sup>®</sup> Flash Silica II or Teledyne Isco RediSep<sup>®</sup> Rf Silica) using either a Biotage

FlashMaster II<sup>®</sup> or Teledyne Isco CombiFlash<sup>®</sup> Companion<sup>®</sup> system. Phase separation was accomplished with Isolute<sup>®</sup> SPE Accessories phase separators. Ion exchange chromatography was accomplished with Isolute<sup>®</sup> SCX-2 or NH<sub>2</sub> cartridges. Oasis<sup>®</sup> HLB cartridges were used for sample extraction from aqueous phases where liquid-liquid extraction was not possible.

Melting points were recorded on a Stuart SMP40 melting point apparatus and are uncorrected.

Infra-red spectra were recorded from solid using a Perkin Elmer “Spectrum One” FT-IR Spectrometer. Selected peaks are reported in cm<sup>-1</sup>.

Optical rotations were performed on a Jasco P-1030 Polarimeter using an optical cell (path length 2 mm) at 298 K.

High resolution mass spectra (HRMS) were performed on a Micromass Autospec 500 OAT spectrometer. HRMS was recorded by Bill Leavens, Analytical Chemistry, GSK, Stevenage.

Low resolution mass spectra were carried out by one of two methods:

1. Formic Acid Generic Analytical UPLC Open Access LC/MS 2 Minute Method (Method A).

The UPLC analysis was conducted on an Acquity UPLC BEH C18 column (50 mm x 2.1 mm i.d. 1.7 μm packing diameter) at 40 °C.

The solvents employed were:

A = 0.1% v/v solution of formic acid in water.

B = 0.1% v/v solution of formic acid in acetonitrile.

The gradient employed was:

Time (min)	Flow Rate (mL/min)	% A	% B
0	1	97	3
1.5	1	0	100
1.9	1	0	100
2.0	1	97	3

2. High pH Generic Analytical UPLC Open Access LC/MS 2 Minute Method (Method B).

The UPLC analysis was conducted on an Acquity UPLC BEH C18 column (50 mm x 2.1 mm i.d. 1.7  $\mu$ m packing diameter) at 40 °C.

The solvents employed were:

A = 10 mM ammonium bicarbonate in water adjusted to pH 10 with ammonia solution.

B = Acetonitrile.

The gradient employed was:

<b>Time (min)</b>	<b>Flow Rate (mL/min)</b>	<b>% A</b>	<b>% B</b>
0	1	99	1
1.5	1	3	97
1.9	1	3	97
2.0	1	0	100

Mass Directed Autoprep chromatography was carried out by one of the following methods:

1. Formic acid Open Access Prep LCMS Large Scale Method for up to 90 mg crude material (Method A).

The HPLC analysis was conducted on a Sunfire C18 column (150 mm x 30 mm i.d. 5  $\mu$ m packing diameter).

The solvents employed were:

A = 0.1% v/v solution of formic acid in water.

B = 0.1% v/v solution of formic acid in acetonitrile.

The gradients employed were:

<b>Method</b>	<b>Time (min)</b>	<b>Flow Rate (mL/min)</b>	<b>Gradient</b>
A1	10	40	05-30% B
A2	10	40	10-40% B
A3	10	40	25-55% B
A4	10	40	40-75% B
A5	10	40	60-90% B

2. High pH Open Access Prep LCMS Large Scale Method for up to 90 mg crude material (Method B).

The HPLC analysis was conducted on a Sunfire C18 column (150 mm x 30 mm i.d. 5 µm packing diameter).

The solvents employed were:

A = 10 mM ammonium bicarbonate in water adjusted to pH 10 with ammonia solution.

B = Acetonitrile.

The gradients employed were:

<b>Method</b>	<b>Time (min)</b>	<b>Flow Rate (mL/min)</b>	<b>Gradient</b>
B1	10	40	05-30% B
B2	10	40	10-40% B
B3	10	40	25-55% B
B4	10	40	40-75% B
B5	10	40	60-90% B

3. Trifluoroacetic acid Open Access Prep LCMS Large Scale Method for up to 90 mg crude material (Method C).

The HPLC analysis was conducted on a Sunfire C18 column (150 mm x 30 mm i.d. 5 µm packing diameter).

The solvents employed were:

A = 0.1% v/v solution of trifluoroacetic acid in water.

B = 0.1% v/v solution of trifluoroacetic acid in acetonitrile.

The gradients employed were:

Method	Time (min)	Flow Rate (mL/min)	Gradient
C1	10	40	05-30% B
C2	10	40	10-40% B
C3	10	40	25-55% B
C4	10	40	40-75% B
C5	10	40	60-90% B

4. High pH bespoke Prep LCMS Method (Method D). Method D was carried out by Richard Briers, Analytical Chemistry, GSK, Stevenage.

The HPLC analysis was conducted on an XBridge C18 column (19 mm x 150 mm i.d. 5 µm packing diameter).

The solvents employed were:

A = 0.1% v/v solution of formic acid in water.

B = 0.1% v/v solution of formic acid in acetonitrile.

The gradient employed was:

Time (min)	Flow Rate (mL/min)	% A	% B
0	20	85	15
1	20	85	15
15	20	70	30
15.2	20	1	99
18.2	20	1	99
18.5	20	85	15
20	20	85	15

5. High pH bespoke Prep LCMS Method (Method E). Method E was carried out by Martin Read, Analytical Chemistry, GSK, Stevenage.

The HPLC analysis was conducted on an XBridge BEH Shield column (19 mm x 100 mm i.d. 5 µm packing diameter).

The solvents employed were:

A = 10 mM ammonium bicarbonate in water adjusted to pH 10 with ammonia solution.

B = MeOH.

The gradient employed was:

<b>Time (min)</b>	<b>Flow Rate (mL/min)</b>	<b>% A</b>	<b>% B</b>
0	20	80	20
0.5	20	80	20
15	20	20	80
15.2	20	1	99
18	20	1	99
18.5	20	80	20
20	20	80	20

6. High pH bespoke Prep LCMS Method (Method F). Method F was carried out by Martin Read, Analytical Chemistry, GSK, Stevenage.

The HPLC analysis was conducted on an XBridge BEH Shield column (19 mm x 100 mm i.d. 5 µm packing diameter).

The solvents employed were:

A = 10 mM ammonium bicarbonate in water adjusted to pH 10 with ammonia solution.

B = MeOH.



The gradient employed was:

<b>Time (min)</b>	<b>Flow Rate (mL/min)</b>	<b>% A</b>	<b>% B</b>
0	20	70	30
0.5	20	70	30
15	20	40	60
15.2	20	1	99
18	20	1	99
18.5	20	70	30
20	20	70	30

7. High pH bespoke Prep LCMS Method (Method G). Method G was carried out by Richard Briers, Analytical Chemistry, GSK, Stevenage.

The HPLC analysis was conducted on an XBridge BEH Shield column (19 mm x 100 mm i.d. 5 µm packing diameter).

The solvents employed were:

A = 10 mM ammonium bicarbonate in water adjusted to pH 10 with ammonia solution.

B = MeOH.

The gradient employed was:

<b>Time (min)</b>	<b>Flow Rate (mL/min)</b>	<b>% A</b>	<b>% B</b>
0	20	85	15
0.5	20	85	15
15	20	45	55
15.1	20	1	99
18.1	20	1	99
18.2	20	85	15
20	20	85	15

Chiral analytical chromatography was carried out by Eric Hortense, Analytical Chemistry, GSK, Stevenage. The HPLC analysis was conducted on a Chiralpak IC™ column (250 mm x 4.6 mm i.d. 5 µm packing diameter).

The solvents employed were:

A = 0.1% v/v IPA in heptane.

B = EtOH.

The gradient employed was:

Time (min)	Flow Rate (mL/min)	% A	% B
0	1	50	50
25	1	50	50

Electronic structure calculations were carried out on an IBM IntelliStation Z Pro (Type 9228) (Intel® Xeon 5160 / 3.0 GHz Processor, 2GB RAM) using a Linux-x86 operating system running Maestro V9.2.109. Torsional scans were run using Jaguar V7.9, at the HF/6-31G\* level of theory.

Characterization of Biochemical and Cellular Activities (carried out by colleagues from Screening and Compound Profiling, GSK):

#### IKK2 Time Dependent assay.<sup>1</sup>

Recombinant human IKK2 (residues 5-756) was expressed in baculovirus as a C-terminal GST-tagged fusion protein, and its activity was assessed using a time-resolved fluorescence resonance energy transfer (TR-FRET) assay as follows.

IKK2 (0.5 – 4 nM final concentration) diluted in assay buffer (50 mM HEPES, 10 mM MgCl<sub>2</sub>, 1 mM CHAPS pH 7.4 with 1 mM DTT and 0.01% w/v BSA) was added to wells containing various concentrations of compound or DMSO vehicle (1.7% v/v final). Enzyme and compound were incubated for 1 h at room temperature prior to addition of ATP and IκBα substrate. The reaction was initiated by the addition of GST-IκBα substrate (25 nM final)/ATP (1 µM final), in a total volume of 6 µL. The reaction was incubated for 15 min at room temperature, then

terminated by the addition of 3  $\mu$ L of 50 mM EDTA in buffer (100 mM HEPES, pH 7.4, 150 mM NaCl and 0.01% w/v BSA) containing antiphosphoserine-I $\kappa$ B $\alpha$ -32/36 monoclonal antibody clone 12C2 labelled with W-1024 europium chelate and an APC-labelled anti-GST antibody. The reaction mixture was further incubated for 45 min at room temperature and the degree of phosphorylation of GST-I $\kappa$ B $\alpha$  measured using a Perkin-Elmer Envision as a ratio of specific 665 nm energy transfer signal to reference europium 620 nm signal.

#### IKK1 TR-FRET assay.<sup>1</sup>

Recombinant human IKK1 (residues 5-785) was expressed in baculovirus as a C-terminal 6HIS-tagged fusion protein, and its activity was assessed using a time-resolved fluorescence resonance energy transfer (TR-FRET) assay as follows.

IKK1 (typically 5 – 10 nM final concentration) diluted in assay buffer (50 mM HEPES, 10 mM MgCl<sub>2</sub>, 1 mM CHAPS pH 7.4 with 1 mM DTT and 0.01% w/v BSA) was added to wells containing various concentrations of compound or DMSO vehicle (1.7% v/v final). The reaction was initiated by the addition of GST-I $\kappa$ B $\alpha$  substrate (25 nM final)/ATP (1  $\mu$ M final), in a total volume of 6  $\mu$ L. The reaction was incubated for 15 min at room temperature, then terminated by the addition of 3  $\mu$ L of 50 mM EDTA in buffer (100 mM HEPES, pH 7.4, 150 mM NaCl and 0.01% w/v BSA) containing antiphosphoserine-I $\kappa$ B $\alpha$ -32/36 monoclonal antibody clone 12C2 labelled with W-1024 europium and an APC-labelled anti-GST antibody. The reaction mixture was further incubated for 45 min at room temperature and the degree of phosphorylation of GST-I $\kappa$ B $\alpha$  measured using a Perkin-Elmer Envision as a ratio of specific 665 nm energy transfer signal to reference europium 620 nm signal.

#### IKK2 HWB assay.<sup>1</sup>

Whole Blood Preparation:

Sufficient volumes of blood from any two healthy volunteers were drawn by qualified GSK staff in the Blood Donation Unit, and heparinised with 10  $\mu$ L of 1000

units/mL endotoxin-free heparin per 1 mL of blood (final concentration was 10 units/mL). The blood was transferred into a sterile trough and 100  $\mu$ L was dispensed into microtitre plate wells containing 1.0  $\mu$ L of an appropriately diluted compound solution in DMSO. After 1 h incubation at 37 °C, 5% CO<sub>2</sub>, 25  $\mu$ L LPS solution (*S. typhosa*) in RPMI 1640 (containing 1% L-glutamine and 1% penicillin/streptomycin) was added (50 ng/mL final). The samples were incubated at 37 °C, 5% CO<sub>2</sub> for 20 h, 50  $\mu$ L physiological saline (0.138% NaCl) was added and diluted plasma was collected using a Biomek FX liquid handling robot after centrifugation at 1300 rpm for 10 min.

Detection of TNF $\alpha$  Using Mesoscale Discovery Technology (electrochemiluminescence):

40  $\mu$ L supernatant was transferred using the Biomek FX to a 96-well High-Bind MSD assay plate precoated with anti-hTNF $\alpha$  capture antibody and containing 25  $\mu$ L of MSD human serum cytokine assay diluents. The plates were sealed and shaken at room temperature for 2 h after which they were washed and 40  $\mu$ L of MSD detection antibody was added. The plates were shaken at room temperature for a further 1 h before washing again and adding 150  $\mu$ L of MSD Read Buffer (2X). Plates were then read on the MSD Sector 6000 plate reader. TNF concentrations were derived from a standard curve run on the same plate and pIC<sub>50</sub> values for inhibition of TNF production were derived from the compound dose response curves with non-linear least squares curve fitting using Activity base software.

#### PI3K HTRF assay.<sup>2</sup>

The binding of compounds to PI3K-alpha/beta/delta/gamma is determined by homogeneous time resolved fluorescence (HTRF) assays as follows;

Briefly, solid compound is dissolved in 100% DMSO at a concentration of 2 mM. Dilutions are prepared in 100% DMSO using a 1 in 4 serial step dilution. The dilutions are transferred to black low volume Greiner assay plates ensuring that the DMSO concentration is constant across the plate at 1% (0.1  $\mu$ L/well).

PI3K Reaction Buffer (contains 50 mM HEPES pH 7.0 (NaOH), 150 mM NaCl, 10 mM MgCl<sub>2</sub>, 2.3 mM sodium cholate, 10 μM CHAPS made up in milliQ water). Fresh DTT is added at a final concentration of 1 mM on the day of use. Wortmannin at a concentration sufficient to produce 100% inhibition (8.33e-6 M) is added to column 18 of compound plates.

Enzyme solutions: 1X PI3K assay Buffer containing:

- 550 pM PI3K-Alpha enzyme (275 pM final assay concentration)
- 800 pM PI3K-Beta enzyme (400 pM final assay concentration)
- 3 nM PI3K-Delta enzyme (1.5 nM final assay concentration)
- 10 nM PI3K-Gamma enzyme (5 nM final assay concentration)

These concentrations are optimal to achieve a signal:background of between 1.5-4.5.

The enzyme solution is added to columns 1-24 (3 μL/well) and plates are incubated for 15 min at room temperature.

Substrate solution: 1X PI3K assay buffer containing:

- PI3K-Alpha: 500 μM ATP, 20 μM PIP<sub>2</sub> and 120 nM biotin-PIP<sub>3</sub>. (Final assay concentrations are 250 μM ATP, 10 μM PIP<sub>2</sub> (both at K<sub>m</sub>) and 40 nM biotin-PIP<sub>3</sub>)
- PI3K-Beta: 800 μM ATP, 20 μM PIP<sub>2</sub> and 120 nM biotin-PIP<sub>3</sub>. (Final assay concentrations are 400 μM ATP, 10 μM PIP<sub>2</sub> (both at K<sub>m</sub>) and 40 nM biotin-PIP<sub>3</sub>)
- PI3K-Delta: 160 μM ATP, 20 μM PIP<sub>2</sub> and 120 nM biotin-PIP<sub>3</sub>. (Final assay concentrations are 80 μM ATP, 10 μM PIP<sub>2</sub> (both at K<sub>m</sub>) and 40 nM biotin-PIP<sub>3</sub>)
- PI3K-Gamma: 30 μM ATP, 20 μM PIP<sub>2</sub> and 120 nM biotin-PIP<sub>3</sub>. (Final assay concentrations are 15 μM ATP, 10 μM PIP<sub>2</sub> (both at K<sub>m</sub>) and 40 nM biotin-PIP<sub>3</sub>)

This is added to all wells and plates are incubated for 1 h at room temperature.

Detection solution: PI3K Detection Buffer (contains 50 mM HEPES pH 7.0 (HCl), 150 mM NaCl, 2.3 mM sodium cholate, 10 µM CHAPS, 240 mM KF) containing 2 mM DTT (2X final concentration), 90 nM GRP-1 PH domain, 300 nM Streptavidin-APC and 24 nM Europium-anti-GST (6X final concentrations)

This is mixed and left at room temperature (protected from light).

STOP solution: PI3K STOP Buffer (contains 50 mM HEPES pH 7.0 (HCl), 150 mM NaCl, 2.3 mM sodium cholate, 10 µM CHAPS, 150 mM EDTA).

Detection solution is diluted 1:1 with STOP solution and added to all wells (3 µL/well). Plates are covered and incubated on the bench for 45-60 min.

Plates are read on a PerkinElmer Envision, measuring TR-FRET between the complex formed between the GST-tagged PH domain and biotinylated PIP3 which both recruit fluorophores (Europium-labelled anti-GST & Strep-APC respectively). In the presence of an inhibitor, this complex is disrupted by the competitive action of non-biotinylated PIP3 (formed in the assay by the phosphorylation of PIP2 by the kinase & ATP). From this, the ratio of acceptor/donor was calculated and used for data analysis.

### PI3K HWB assay.<sup>3</sup>

#### Whole Blood Preparation:

The media used for diluting the cytostim (500 mL RPMI low endotoxin RPMI 1640 + 1% Glutamax + 1% penicillin/streptomycin) was pre-warmed in a 37 °C water bath for at least 20 min prior to use. The compound plates were prepared before commencing whole blood preparation – two replicates of each master plate are required to account for donor variability. Solid compounds are dissolved in 100% DMSO at a concentration of 10 mM. The compounds are serially diluted 1:4 in 100% DMSO and 500 nL are dispensed into the assay plates.

Sufficient volumes of blood from any two healthy volunteers were drawn by qualified GSK staff in the Blood Donation Unit, and heparinised with 10 µL of 1000 units/mL endotoxin-free heparin per 1 mL of blood (final concentration was 10 units/mL). The blood was transferred into a sterile trough and 100 µL was added to

each well of a 96-well plate using a multi-channel pipette, with each donor being processed separately. The plates were then incubated at 37°C, 5% CO<sub>2</sub> for 1 h. After 1 h, 25 µL of Cytostim solution (Miltenyi Biotech: 1:300 dilution of stock reagent in low endotoxin RPMI 1640+1% glutamax+1% penicillin/ streptomycin) was added to each well using a Multidrop Combi. The filled plates were then lidded and placed in the humidified primary cell incubator for 18-24 hours at 37°C, 5% CO<sub>2</sub>.

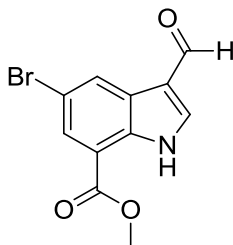
Detection of IFN $\gamma$  Using Mesoscale Discovery Technology (electrochemiluminescence):

Whole blood plates were shaken vigorously on a plate shaker for 5-10 min until all wells were thoroughly mixed. 50 µL of physiological saline (0.85% NaCl) was added to each well in the biosafety cabinet using a Multidrop Combi then the plates were centrifuged at 1300 rpm for 10 min. 50 µL of plasma supernatant was transferred to a 96-well MSD plate, pre-coated with anti-human IFN $\gamma$  capture antibody using the Biomek FX. The plates were then sealed and placed on a shaker at 600 rpm at room temperature for 2 h. The plates were then washed three times with 150 µL of PBS/Tween 20 (0.05% v/v = 250 µL/500 mL). Detection antibody solution was prepared by diluting stock anti-human IFN $\gamma$  antibody (50X, MSD kit) 1:50 in Diluent 100 (MSD) to generate a working solution of 1 µg/mL SULFO-TAG<sup>TM</sup> IFN $\gamma$ , and 40 µL of the working antibody solution was then added to each well of the MSD plates using a Multidrop Combi. The plates were then re-sealed and returned to the shaker for 1 h at 600 rpm at room temperature. The plates were then washed three times with PBS, ensuring there was no liquid remaining in the plate after washing. 150 µL of 2X MSD Read Buffer T (stock 4X MSD Read Buffer T was diluted 50:50 with de-ionised water) was then added to each well using a Multidrop Combi and the plates were then read on the MSD Sector Imager 6000. The resulting data was used for data analysis.

All animal studies (i.e. *in vivo* PK studies) were ethically reviewed and carried out in accordance with Animals (Scientific Procedures) Act 1986 and the GSK Policy on the Care, Welfare and Treatment of Animals.

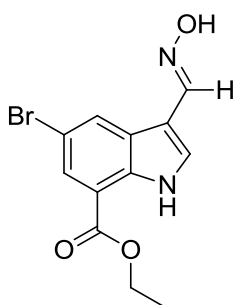
## 6.2. Preparation of 3-Cyanoindole-7-carboxamides

### 6.2.1. Methyl 5-bromo-3-formyl-1*H*-indole-7-carboxylate, **11b**



Phosphorus oxychloride (24.2 g, 157.5 mmol) was added dropwise over 10 min to a solution of methyl 5-bromo-1*H*-indole-7-carboxylate (20.0 g, 78.7 mmol) in DMF (210 mL) at 0 °C. The addition was followed by a line rinse with DMF (10 mL). The reaction was allowed to warm to room temperature and stirring was continued for 1 h. The mixture was poured onto crushed ice (200 g), saturated aqueous NaHCO<sub>3</sub> solution (400 mL) was added and stirring was continued for 30 min. The solid was collected by suction filtration, washed with water (3 x 50 mL) and dried in a vacuum oven (0.01 mmHg) at 40 °C for 18 h to afford **11b** (18.2 g, 82%) as a white solid. <sup>1</sup>H NMR (400 MHz, *d*<sub>6</sub>-DMSO)  $\delta$  3.95 (s, 3 H), 7.85 (d, *J* = 2.0 Hz, 1 H), 8.35 (s, 1 H), 8.40 (d, *J* = 2.0 Hz, 1 H), 9.95 (s, 1 H), 12.15 (br. s, 1 H). Manchester Organics, unpublished results.

### 6.2.2. Ethyl 5-bromo-3-(hydroxyimino)methyl-1*H*-indole-7-carboxylate, **12**

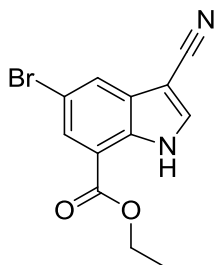


A mixture of ethyl 5-bromo-3-formyl-1*H*-indole-7-carboxylate (1.1 g, 3.7 mmol) and hydroxylamine hydrochloride (0.31 g, 4.5 mmol) in pyridine (40 mL) was stirred at 120 °C for 2 h. The solvent was removed under reduced pressure and the residue was taken up in EtOAc (10 mL) and HCl (as a 2 M aqueous solution, 2 mL)

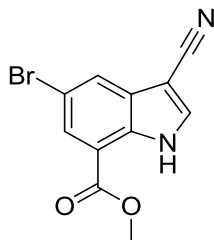


was added. The solid was collected by suction filtration and dried in a vacuum oven (0.01 mmHg) at 40 °C for 18 h to afford **12** (1.1 g, 93%) as a yellow solid. LCMS (Method A, UV, ESI)  $R_t = 1.04$  min,  $[M-H]^+ = 311/313$ , 100% purity;  $^1H$  NMR (400 MHz,  $d_6$ -DMSO)  $\delta$  1.38 (t,  $J = 7.1$  Hz, 3 H), 4.43 (q,  $J = 7.0$  Hz, 2 H), 7.87 (d,  $J = 1.8$  Hz, 1 H), 7.93 (s, 1 H), 8.32 (d,  $J = 3.0$  Hz, 1 H), 8.49 (d,  $J = 1.5$  Hz, 1 H), 11.76 (br. s, 1 H), one proton was not observed, contains ~15%w/w pyridinium hydrochloride. The material was taken forward directly without further purification or characterisation.

### 6.2.3. Ethyl 5-bromo-3-cyano-1H-indole-7-carboxylate, **13a**

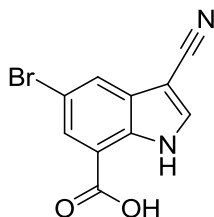


Triethylamine (0.88 mL, 6.30 mmol) and TFAA (0.49 mL, 3.46 mmol) were added to a solution of ethyl 5-bromo-3-(hydroxyimino)methyl-1H-indole-7-carboxylate (0.98 g, 3.15 mmol) in THF (32 mL) at 0 °C under an atmosphere of nitrogen. The mixture was warmed to room temperature and stirring was continued for 5.5 h. The mixture was diluted with DCM (60 mL) and washed with water (60 mL) and brine (60 mL). The organic phase was dried by passing through a hydrophobic frit and concentrated under reduced pressure to give **13a** (0.71 g, 78%) as a yellow solid. LCMS (Method A, UV, ESI)  $R_t = 1.20$  min,  $[M-H]^- = 291/293$ , 86% purity;  $^1H$  NMR (400 MHz,  $d_6$ -DMSO)  $\delta$  1.38 (t,  $J = 7.0$  Hz, 3 H), 4.45 (q,  $J = 7.0$  Hz, 2 H), 7.96 (d,  $J = 1.9$  Hz, 1 H), 8.13 (d,  $J = 1.9$  Hz, 1 H), 8.36 (d,  $J = 3.3$  Hz, 1 H), 12.27 (br. s, 1 H).

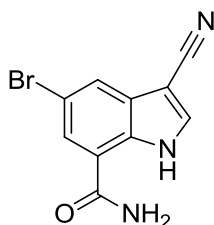
**6.2.4. Methyl 5-bromo-3-cyano-1H-indole-7-carboxylate, 13b**

A mixture of methyl 5-bromo-3-formyl-1H-indole-7-carboxylate (26.6 g, 94.3 mmol), and hydroxylamine hydrochloride (7.0 g, 99.9 mmol) in pyridine (7.8 g, 98.07 mmol) was stirred at 80 °C for 2 h. Selenium dioxide (11.1 g, 99.9 mmol) and magnesium sulfate (8.0 g, 98.1 mmol) were added and heating was continued for a further 2 h. The mixture was allowed to cool to room temperature and stirring was continued for 18 h. The mixture was filtered through Celite<sup>®</sup> and the solid washed with DMF (100 mL). Water (550 mL) was added to the filtrate and the resulting solid was collected by suction filtration. The combined solids were taken up in acetone (725 mL) and heated until the solid dissolved. Charcoal (2.0 g) was added and heating was continued for 30 min. The mixture was cooled to 30 °C then filtered through Celite<sup>®</sup>. The filtrate was concentrated under reduced pressure to afford **13b** (20.0 g, 95%) as a cream solid. LCMS (Method A, UV, ESI)  $R_t = 1.07$  min,  $[M-H]^- = 277/279$ , >95% purity;  $^1H$  NMR (400 MHz,  $d_6$ -DMSO)  $\delta$  3.97 (s, 3 H), 7.94 (d,  $J = 1.9$  Hz, 1 H), 8.11 (d,  $J = 1.9$  Hz, 1 H), 8.36 (s, 1 H), 12.29 (br. s, 1 H);  $^{13}C$  NMR (101 MHz,  $d_6$ -DMSO)  $\delta$  52.5, 85.1, 113.4, 114.8, 116.1, 126.1, 127.7, 130.0, 132.1, 137.5, 164.4; HR-ESIMS ( $m/z$ ) calcd for  $C_{11}H_7BrN_2O_2$   $[M-Na]^+$  300.9589, found 300.9598.

Manchester Organics, unpublished results.

**6.2.5. 5-Bromo-3-cyano-1H-indole-7-carboxylic acid, 14**

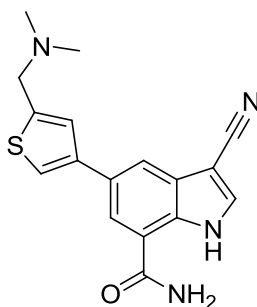
A mixture of methyl 5-bromo-3-cyano-1H-indole-7-carboxylate (5.0 g, 17.9 mmol) and NaOH (as a 2 M aqueous solution, 50 mL) in MeOH (150 mL) was stirred at room temperature for 46 h. The solvent was removed under reduced pressure and the residue was taken up in water (200 mL) and neutralised with HCl (as a 2 M aqueous solution). The solid was collected by suction filtration and washed with MeCN then dried in a vacuum oven (0.01 mmHg) at 40 °C overnight to afford **14** (3.9 g, 81%) as a white solid. LCMS (Method A, UV, ESI)  $R_t = 0.94$  min,  $[M-H]^- = 263/265$ , 100% purity;  $^1H$  NMR (400 MHz,  $d_6$ -DMSO)  $\delta$  7.92 (d,  $J = 1.8$  Hz, 1 H), 8.07 (d,  $J = 1.8$  Hz, 1 H), 8.28 (s, 1 H), 12.23 (br. s, 1 H), one proton signal not observed.

**6.2.6. 5-Bromo-3-cyano-1H-indole-7-carboxamide, 15**

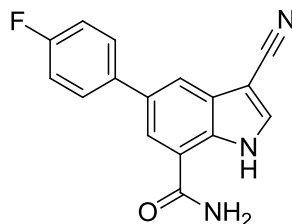
A mixture of 5-bromo-3-cyano-1H-indole-7-carboxylic acid (3.8 g, 14.5 mmol), HATU (5.6 g, 14.8 mmol) and DIPEA (2.6 mL, 14.9 mmol) in DMF (70 mL) was stirred at room temperature. After 30 min, ammonia (8.3 mL of a 7 M solution in methanol, 57.9 mmol) was added. Stirring was continued for 2 h then the mixture was concentrated under reduced pressure. The residue was taken up in water (50 mL) and sonicated before the solid was collected by suction filtration. The filtered solid was dried in air then in a vacuum oven (0.01 mmHg) at 40 °C for 18 h. The solid was taken up in MeCN (30 mL) and heated to 50 °C. Water (30 mL) was added then the mixture was cooled to 0 °C. The solid was collected by suction filtration and dried in

a vacuum oven (0.01 mmHg) at 40 °C for 2 h to afford **15** (3.5 g, 82%) as a cream solid. LCMS (Method A, UV, ESI)  $R_t = 0.85$  min,  $[M-H]^- = 262/264$ , 89% purity;  $^1H$  NMR (400 MHz,  $d_6$ -DMSO)  $\delta$  7.70 (br. s, 1 H), 7.99 (d,  $J = 1.4$  Hz, 1 H), 8.04 (d,  $J = 1.4$  Hz, 1 H), 8.21 (d,  $J = 3.0$  Hz, 1 H), 8.31 (br. s, 1 H), 12.23 (br. s, 1 H).

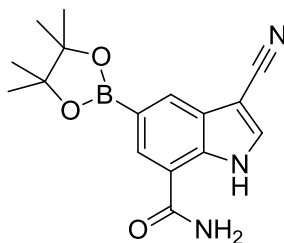
**6.2.7. 3-Cyano-5-{5-[(dimethylamino)methyl]-3-thienyl}-1H-indole-7-carboxamide, 16a**



A mixture of 5-bromo-3-cyano-1H-indole-7-carboxamide (80 mg, 0.30 mmol),  $K_2CO_3$  (132 mg, 0.96 mmol),  $PdCl_2(dppf)$  (25 mg, 0.034 mmol) and 10% {5-[(dimethylamino)methyl]-3-thienyl}boronic acid on alumina (683 mg, 0.37 mmol, synthesised by I. Campbell, GlaxoSmithKline, unpublished results) in 1,4-dioxane (1.5 mL) and water (0.5 mL) was heated in a microwave at 100 °C for 1 h. More 10% {5-[(dimethylamino)methyl]-3-thienyl}boronic acid on alumina (561 mg, 0.30 mmol) and  $PdCl_2(dppf)$  (22 mg, 0.03 mmol) were added and the mixture was heated again in a microwave at 110 °C for 2 h. More  $PdCl_2(dppf)$  (22 mg, 0.03 mmol) and  $K_2CO_3$  (42 mg, 0.30 mmol) were added and the mixture was heated again in a microwave at 120 °C for 2 h. The mixture was diluted with DCM/MeOH (5 mL of a 1:1 mixture) and filtered, washing with more DCM/MeOH (5 mL of a 1:1 mixture). The solvent was removed under a stream of nitrogen and the crude residue was purified by MDAP Method A1. The product-containing fractions were concentrated under reduced pressure to afford **16a** (5.8 mg, 6%) as a cream solid. LCMS (Method A, UV, ESI)  $R_t = 0.51$  min,  $[M-H]^+ = 325$ , 100% purity;  $^1H$  NMR (400 MHz,  $d_4$ -MeOH)  $\delta$  2.79 (s, 6 H), 4.40 (s, 2 H), 7.75 (d,  $J = 1.3$  Hz, 1 H), 7.90 (d,  $J = 1.3$  Hz, 1 H), 8.03 (s, 1 H), 8.11 (d,  $J = 1.5$  Hz, 1 H), 8.17 (d,  $J = 1.5$  Hz, 1 H), three proton signals not observed.

**6.2.8. 3-Cyano-5-(4-fluorophenyl)-1H-indole-7-carboxamide, 16b**

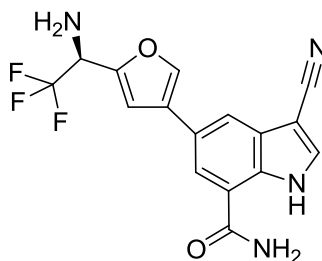
A mixture of 5-bromo-3-cyano-1H-indole-7-carboxamide (83 mg, 0.31 mmol), (4-fluorophenyl)boronic acid (48 mg, 0.35 mmol), PdCl<sub>2</sub>(dppf) (23 mg, 0.031 mmol) and Na<sub>2</sub>CO<sub>3</sub> (67 mg, 0.63 mmol) in 1,4-dioxane (1 mL) and water (1 mL) was heated at 80 °C for 3 h. More (4-fluorophenyl)boronic acid (48 mg, 0.35 mmol) and PdCl<sub>2</sub>(dppf) (23 mg, 0.031 mmol) were added and heating was continued for 18 h. The mixture was then heated in a microwave at 100 °C for 20 min then at 120 °C for 30 min. The mixture was diluted with DCM (5 mL) and MeOH (5 mL) and filtered. The filtered solid was washed with DCM/MeOH (2 mL of a 1:1 mixture) and the filtrate was concentrated under reduced pressure. The crude material was purified by MDAP Method A2 and the product-containing fractions were concentrated under reduced pressure to afford **16b** (9.0 mg, 10%) as a cream solid. LCMS (Method A, UV, ESI) *R*<sub>t</sub> = 0.93 min, [M-H]<sup>-</sup> = 278, 100% purity; <sup>1</sup>H NMR (400 MHz, *d*<sub>6</sub>-DMSO) δ 7.34 (t, *J* = 8.8 Hz, 2 H), 7.63 (br. s, 1 H), 7.87 (dd, *J* = 8.8 Hz, *J*<sub>H-F</sub> = 5.5 Hz, 2 H), 8.02 (d, *J* = 1.4 Hz, 1 H), 8.16 (d, *J* = 1.4 Hz, 1 H), 8.18 (s, 1 H), 8.40 (br. s, 1 H), 12.11 (br. s, 1 H).

**6.2.9. 3-Cyano-5-(4,4,5,5-tetramethyl-1,3,2-dioxaborolan-2-yl)-1H-indole-7-carboxamide, 17**

A mixture of 5-bromo-3-cyano-1H-indole-7-carboxamide (1.1 g, 4.1 mmol), bis(pinacolato)diboron (1.3 g, 4.9 mmol), Pd<sub>2</sub>(dba)<sub>3</sub> (0.39 g, 0.43 mmol), XPhos<sup>®</sup>

(0.39 g, 0.82 mmol) and KOAc (1.24 g, 12.6 mmol) in 1,4-dioxane (10 mL) was heated in a microwave at 110 °C for 1 h. The mixture was partitioned between EtOAc (40 mL) and water (40 mL). The aqueous phase was further extracted with EtOAc (2 x 20 mL). Solids present in the combined organic extracts were removed by suction filtration. The filtrate was dried by passing through a hydrophobic frit and concentrated under reduced pressure. The crude material was purified by chromatography on FlashMaster II silica (2 x 100 g), eluting with 0-100% EtOAc/cyclohexane over 1 h. The product-containing fractions were concentrated under reduced pressure to afford **17** (0.52 g, 41%) as a yellow solid. LCMS (Method A, UV, ESI)  $R_t = 0.93$  min,  $[M-H]^- = 310$ , 91% purity;  $^1H$  NMR (400 MHz,  $d_6$ -DMSO)  $\delta$  1.34 (s, 12 H), 7.49 (br. s, 1 H), 8.09 (s, 1 H), 8.10 (s, 1 H), 8.18 (d,  $J = 3.2$  Hz, 1 H), 8.34 (br. s, 1 H), 12.15 (br. s, 1 H).

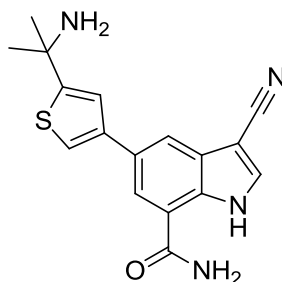
**6.2.10. 5-{5-[(1*S*)-1-Amino-2,2,2-trifluoroethyl]-3-furanyl}-3-cyano-1*H*-indole-7-carboxamide, **16c****



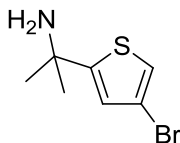
A mixture of 3-cyano-5-(4,4,5,5-tetramethyl-1,3,2-dioxaborolan-2-yl)-1*H*-indole-7-carboxamide (80 mg, 0.26 mmol), [(1*S*)-1-(4-bromo-2-furanyl)-2,2,2-trifluoroethyl]amine hydrochloride (79 mg, 0.28 mmol), PdCl<sub>2</sub>(dppf) (19 mg, 0.026 mmol) and K<sub>2</sub>CO<sub>3</sub> (144 mg, 1.04 mmol) in 1,4-dioxane (1 mL) and water (1 mL) was heated in a microwave at 100 °C for 4 h. Water (5 mL) was added and the aqueous phase was extracted with DCM (2 x 5 mL). The combined organic extracts were concentrated under a stream of nitrogen. The aqueous phase was also concentrated to dryness and the two evaporates were combined. The crude material was purified by MDAP Method D and the product-containing fractions were concentrated under reduced pressure afford **16c** (2.0 mg, 2%) as a cream solid. LCMS (Method A, UV, ESI)  $R_t = 0.68$  min,  $[M-H]^- = 347$ , 97% purity;  $^1H$  NMR

(400 MHz,  $d_4$ -MeOH)  $\delta$  4.67 (q,  $J_{H-F} = 7.5$  Hz, 1 H), 6.61 (d,  $J = 3.5$  Hz, 1 H), 6.89 (d,  $J = 3.5$  Hz, 1 H), 8.02 (s, 1 H), 8.17 (d,  $J = 1.5$  Hz, 1 H), 8.22 (d,  $J = 1.5$  Hz, 1 H), 8.54 (s, 2 H), three proton signals were not observed.

**6.2.11. 5-[5-(1-Amino-1-methylethyl)-3-thienyl]-3-cyano-1H-indole-7-carboxamide, 16d**



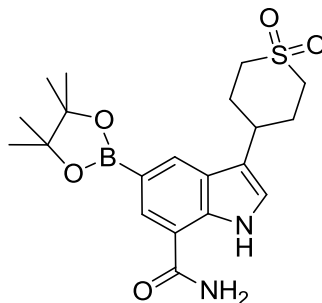
A mixture of 3-cyano-5-(4,4,5,5-tetramethyl-1,3,2-dioxaborolan-2-yl)-1H-indole-7-carboxamide (80 mg, 0.13 mmol), 2-(4-bromo-2-thienyl)-2-propanamine (31 mg, 0.14 mmol), PdCl<sub>2</sub>(dppf) (15 mg, 0.021 mmol) and K<sub>2</sub>CO<sub>3</sub> (79 mg, 0.57 mmol) in 1,4-dioxane (1 mL) and water (1 mL) was heated in microwave at 80 °C for 30 min then at 100 °C for 2 h. The mixture was diluted with DCM/MeOH (5 mL of a 1:1 mixture) and filtered, washing with more DCM/MeOH (5 mL of a 1:1 mixture). The filtrate was concentrated under a stream of nitrogen and the residue was purified by MDAP Method A1. The product-containing fractions were concentrated under reduced pressure to afford **16d** (4.6 mg, 11%) as a cream solid. LCMS (Method A, UV, ESI)  $R_t = 0.58$  min,  $[M-H]^- = 323$ , 97% purity; <sup>1</sup>H NMR (400 MHz,  $d_4$ -MeOH)  $\delta$  1.88 (s, 6 H), 7.75 (d,  $J = 1.5$  Hz, 1 H), 7.80 (d,  $J = 1.5$  Hz, 1 H), 8.03 (s, 1 H), 8.11 (d,  $J = 1.5$  Hz, 1 H), 8.17 (d,  $J = 1.5$  Hz, 1 H), five proton signals were not observed.

**6.2.12. 2-(4-Bromo-2-thienyl)-2-propanamine, 19**

Cerium(III) chloride (983 mg, 3.99 mmol) was added to a flask that had been dried overnight in a vacuum oven (0.01 mmHg) at 40 °C. The solid was heated to 80 °C for 1 h under vacuum (0.01 mmHg). The flask was then filled with nitrogen and THF (4 mL) was added to give a suspension that was stirred for 1 h. The suspension was cooled to -78 °C and methylolithium (1.6 M in THF, 2.49 mL, 3.99 mmol) was added dropwise. After stirring for 30 min at -78 °C, a solution of 4-bromo-2-thiophenecarbonitrile (250 mg, 1.33 mmol) in THF (1 mL) was added. And stirring was continued for 30 min. The mixture was quenched with NH<sub>3</sub> (3 mL of a 28% w/v aqueous solution) and allowed to warm to room temperature. The suspension was diluted with DCM and filtered through Celite<sup>®</sup>, washing with more DCM. The filtrate was washed with water, dried by passing through a hydrophobic frit and concentrated under reduced pressure. The crude material was purified by chromatography on FlashMaster II silica (10 g), eluting with 0-100% EtOAc/cyclohexane over 20 min. The product-containing fractions were concentrated under reduced pressure to afford **19** (81 mg, 28%) as an orange oil. LCMS (Method A, UV, ESI)  $R_t = 0.48$  min,  $[M-H]^- = 203/205$ , 100% purity; <sup>1</sup>H NMR (400 MHz, *d*<sub>6</sub>-DMSO)  $\delta$  1.40 (s, 6 H), 6.93 (d,  $J = 1.6$  Hz, 1 H), 7.38 (d,  $J = 1.6$  Hz, 1 H), two proton signals were not observed.

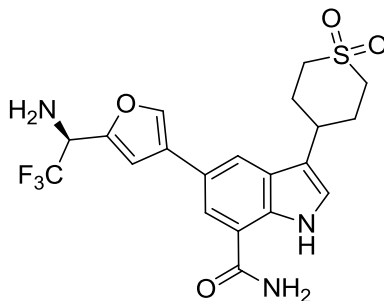


**6.2.13. 3-(1,1-Dioxidotetrahydro-2*H*-thiopyran-4-yl)-5-(4,4,5,5-tetramethyl-1,3,2-dioxaborolan-2-yl)-1*H*-indole-7-carboxamide, **21****

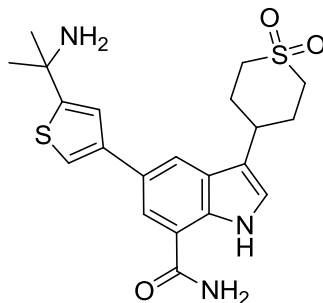


A mixture of 5-bromo-3-(1,1-dioxidotetrahydro-2*H*-thiopyran-4-yl)-1*H*-indole-7-carboxamide (250 mg, 0.67 mmol, synthesised by I. Smith, GlaxoSmithKline, unpublished results), *bis*(pinacolato)diboron (205 mg, 0.81 mmol), XPhos<sup>®</sup> (32 mg, 0.067 mmol), Pd<sub>2</sub>(dba)<sub>3</sub> (31 mg, 0.034 mmol) and KOAc (132 mg, 1.35 mmol) in 1,4-dioxane (3 mL) was heated in a microwave at 100 °C for 30 min. The reaction mixture was partitioned between EtOAc (20 mL) and water (10 mL). The aqueous phase was further extracted with EtOAc (2 x 10 mL). The combined organic extracts were washed with brine (10 mL), passed through a hydrophobic frit and concentrated under reduced pressure. The crude material was purified by chromatography on FlashMaster II silica (20 g), eluting with 0-100% EtOAc/cyclohexane then 0-20% MeOH/EtOAc. The product-containing fractions were concentrated under reduced pressure afford **21** (208 mg, 74%) as a pale yellow solid. LCMS (Method A, UV, ESI) *R*<sub>t</sub> = 0.48 min, [M-H]<sup>-</sup> = 419, 89% purity; <sup>1</sup>H NMR (400 MHz, *d*<sub>6</sub>-DMSO) δ 1.33 (s, 12 H), 2.11 (m, 2 H), 2.26 (m, 2 H), 3.10 (m, 2 H), 3.35-3.45 (m, 3 H), 7.19 (d, *J* = 2.2 Hz, 1 H), 7.23 (br. s., 1 H), 7.93 (s, 1 H), 8.10 (s, 1 H), 8.14 (br. s, 1 H), 11.02 (br. s, 1 H).

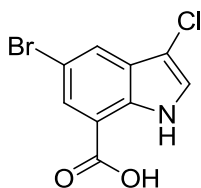
**6.2.14. 5-{5-[(1S)-1-Amino-2,2,2-trifluoroethyl]-3-furanyl}-3-(1,1-dioxidotetrahydro-2H-thiopyran-4-yl)-1H-indole-7-carboxamide, 22a**



A mixture of 3-(1,1-dioxidotetrahydro-2H-thiopyran-4-yl)-5-(4,4,5,5-tetramethyl-1,3,2-dioxaborolan-2-yl)-1H-indole-7-carboxamide (152 mg, 0.36 mmol), [(1S)-1-(4-bromo-2-furanyl)-2,2,2-trifluoroethyl]amine hydrochloride (116 mg, 0.41 mmol), PdCl<sub>2</sub>(dppf) (28 mg, 0.038 mmol) and K<sub>2</sub>CO<sub>3</sub> (234 mg, 1.69 mmol) in 1,4-dioxane (2 mL) and water (2 mL) was heated in a microwave at 80 °C for 30 min. The mixture was partitioned between DCM (10 mL) and water (10 mL). The aqueous phase was neutralised with HCl (as a 2 M aqueous solution) and extracted further with DCM (10 mL). The solid that remained in the aqueous phase was collected by suction filtration. The organic extract and original organic phase were combined and concentrated under reduced pressure and the residue was combined with the filtered solid and purified by MDAP Method A1. The product-containing fractions were concentrated under reduced pressure afford **22a** (39 mg, 23%) as a white solid. Mp 238 °C (decomposed).  $[\alpha]_D^{20} - 50.9$  ( $c = 1$ , DMF). LCMS (Method A, UV, ESI)  $R_t = 0.63$  min,  $[M-H]^+ = 455$ , 100% purity; <sup>1</sup>H NMR (400 MHz, *d*<sub>6</sub>-DMSO)  $\delta$  2.12 (q,  $J = 12.6$  Hz, 2 H), 2.30 (br. d,  $J = 12.1$  Hz, 2 H), 2.50 (br. s, 2 H), 3.13 (br. d,  $J = 12.1$  Hz, 2 H), 3.29 (tt,  $J = 12.1$  Hz, 3.0 Hz, 1 H), 3.41 (td,  $J = 12.1$  Hz, 3.0 Hz, 2 H), 4.67 (m, 1 H), 6.63 (d,  $J = 3.3$  Hz, 1 H), 6.86 (d,  $J = 3.3$  Hz, 1 H), 7.21 (d,  $J = 2.0$  Hz, 1 H), 7.47 (br. s, 1 H), 8.04 (s, 1 H), 8.05 (s, 1 H), 8.17 (br. s, 1 H), 11.00 (br. s, 1 H); <sup>13</sup>C NMR (101 MHz, *d*<sub>6</sub>-DMSO)  $\delta$  31.0 (2C), 31.4, 50.7, 51.6, 51.9, 104.8, 110.5, 116.6, 117.1, 117.5, 118.1, 119.1, 120.8, 123.2, 127.7, 134.2, 148.9, 154.1, 168.7; IR ( $\nu_{max}$ /cm<sup>-1</sup>): 1113, 1266, 1665, 3401 (br.); HR-ESIMS ( $m/z$ ) calcd for C<sub>20</sub>H<sub>20</sub>F<sub>3</sub>N<sub>3</sub>O<sub>4</sub>S [M]<sup>+</sup> 456.1205, found 456.1204.

**6.2.15. 5-[5-(1-Amino-1-methylethyl)-3-thienyl]-3-(1,1-dioxidotetrahydro-2H-thiopyran-4-yl)-1H-indole-7-carboxamide, 22b**

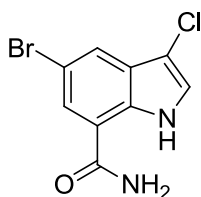
Amide **22b** was prepared as for **22a** from 3-(1,1-dioxidotetrahydro-2H-thiopyran-4-yl)-5-(4,4,5,5-tetramethyl-1,3,2-dioxaborolan-2-yl)-1H-indole-7-carboxamide (54 mg, 0.13 mmol), 2-(4-bromo-2-thienyl)-2-propanamine (31 mg, 0.14 mmol), PdCl<sub>2</sub>(dppf) (9 mg, 0.013 mmol) and K<sub>2</sub>CO<sub>3</sub> (71 mg, 0.52 mmol) using the same procedure, work-up and purification to afford **22b** (14 mg, 25%) as a cream solid. LCMS (Method A, UV, ESI) *R*<sub>t</sub> = 0.54 min, [M-H]<sup>+</sup> = 430, 100% purity; <sup>1</sup>H NMR (400 MHz, *d*<sub>4</sub>-MeOH) δ 1.89 (s, 6 H), 2.34-2.46 (m, 4 H), 3.14 (m, 2 H), 3.26-3.30 (m, 1 H), 3.39 (m, 2 H), 7.25 (s, 1 H), 7.72 (d, *J* = 1.6 Hz, 1 H), 7.75 (d, *J* = 1.6 Hz, 1 H), 7.99 (d, *J* = 1.6 Hz, 1 H), 8.09 (d, *J* = 1.6 Hz, 1 H), 8.32 (br. s, 1 H), five protons not observed.

**6.3. Preparation of 3-Chloroindole-7-carboxamides****6.3.1. 5-Bromo-3-chloro-1H-indole-7-carboxylic acid, 24**

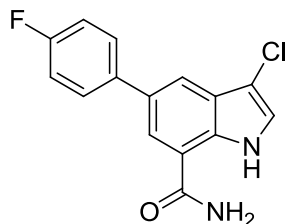
A mixture of 5-bromo-1H-indole-7-carboxylic acid (1.50 g, 6.25 mmol) and NCS (1.08 g, 8.12 mmol) in MeOH (60 mL) was stirred at room temperature under an atmosphere of nitrogen for 72 h. The solvent was removed under reduced pressure to give a red solid (2.51 g). The crude material was purified by chromatography on a

C18 column (360 g), eluting with 40-85% MeCN/water with a formic acid modifier. The product-containing fractions were concentrated under reduced pressure to afford **24** (0.76 g, 44%) as a pink solid. LCMS (Method A, UV, ESI)  $R_t = 1.11$  min,  $[M-H]^- = 273$ , 97% purity;  $^1\text{H NMR}$  (400 MHz,  $d_6$ -DMSO)  $\delta$  7.56 (d,  $J = 4.0$  Hz, 1 H), 7.86 (d,  $J = 2.4$  Hz, 1 H), 7.91 (d,  $J = 2.4$  Hz, 1 H), 11.49 (s, 1 H), 13.60 (br. s, 1 H).

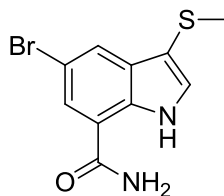
### 6.3.2. 5-Bromo-3-chloro-1H-indole-7-carboxamide, **25**



A mixture of 5-bromo-3-chloro-1H-indole-7-carboxylic acid (405 mg, 1.48 mmol), HATU (561 mg, 1.48 mmol) and DIPEA (0.26 mL, 1.48 mmol) in DMF (14 mL) was stirred at room temperature. After 10 min,  $\text{NH}_3$  (0.84 mL of a 7 M solution in methanol, 5.90 mmol) was added and stirring was continued for 2 h. The solvent was removed under reduced pressure and the residue was taken up in water (30 mL). The suspension was sonicated and the solid was collected by suction filtration. The filtered solid was taken up in MeCN (30 mL) and heated to 50 °C with stirring until the solid dissolved. The solvent was removed under reduced pressure. The solid was taken up in MeCN (5 mL), heated to 50 °C then cooled to 0 °C and collected by suction filtration to afford **25** (90 mg, 22%) as a cream solid. LCMS (Method A, UV, ESI)  $R_t = 1.00$  min,  $[M-H]^- = 273$ , 98% purity;  $^1\text{H NMR}$  (400 MHz,  $d_6$ -DMSO)  $\delta$  7.49 (d,  $J = 2.8$  Hz, 1 H), 7.59 (br. s, 1 H), 7.80 (d,  $J = 1.6$  Hz, 1 H), 7.94 (d,  $J = 1.6$  Hz, 1 H), 8.23 (br. s, 1 H), 11.48 (br. s, 1 H).

**6.3.3. 3-Chloro-5-(4-fluorophenyl)-1H-indole-7-carboxamide, 26**

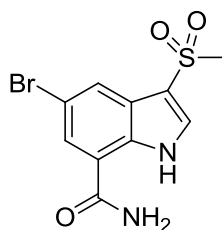
A mixture of 5-bromo-3-chloro-1H-indole-7-carboxamide (50 mg, 0.18 mmol), 4-(fluorophenyl)boronic acid (28 mg, 0.20 mmol), PdCl<sub>2</sub>(dppf)-CH<sub>2</sub>Cl<sub>2</sub> adduct (12 mg, 0.02 mmol) and Na<sub>2</sub>CO<sub>3</sub> (97 mg, 0.91 mmol) in 1,4-dioxane (1.2 mL) and water (0.48 mL) was heated in a microwave at 130 °C for 45 min. The mixture was diluted with water (25 mL) and extracted with DCM (25 mL). A solid was observed between the organic and aqueous phases so this was removed by suction filtration. The organic phase was concentrated under reduced pressure. The crude material was purified by MDAP Method A3 and the product-containing fractions were concentrated under reduced pressure to afford **26** (15 mg, 28%) as a cream solid. Mp 225 °C (decomposed). LCMS (Method A, UV, ESI) *R*<sub>t</sub> = 1.13 min, [M-H]<sup>-</sup> = 287, 100% purity; <sup>1</sup>H NMR (400 MHz, *d*<sub>6</sub>-DMSO) δ 7.28 – 7.36 (m, 2 H), 7.47 (d, *J* = 2.4 Hz, 1 H), 7.52 (br. s, 1 H), 7.82-7.89 (m, 3 H), 8.08 (d, *J* = 1.5 Hz, 1 H), 8.30 (br. s, 1 H), 11.33 (br. s, 1 H); <sup>13</sup>C NMR (101 MHz, *d*<sub>6</sub>-DMSO) δ 103.7, 115.4, 115.6, 117.8, 118.3, 121.1, 124.4, 126.5, 128.8, 128.9, 130.8, 132.8, 136.8, 136.9, 168.4; IR (*v*<sub>max</sub> /cm<sup>-1</sup>): 1675, 3171 (br.), 3436, 3475; HR-ESIMS (*m/z*) calcd for C<sub>15</sub>H<sub>10</sub>ClFN<sub>2</sub>O [M-H<sup>+</sup>] 289.0544, found 289.0541.

**6.4. Preparation of 3-Methylsulfonyl Indole Carboxamides****6.4.1. 5-Bromo-3-(methylthio)-1H-indole-7-carboxamide, 33**

Sulfonyl chloride (0.10 mL, 1.26 mmol) was added to a solution of methyl disulfide (0.11 mL, 1.26 mmol) in DCM (2 mL) at room temperature under an

atmosphere of nitrogen. The mixture was stirred for 10 min then added to a solution of 5-bromo-1*H*-indole-7-carboxamide (200 mg, 0.84 mmol) in DMF (2 mL). Stirring was continued for 1 h then the mixture was quenched with water (2 mL). The aqueous phase was extracted with DCM (2 x 5 mL) and the combined organic extracts were concentrated under reduced pressure. The crude residue was taken up in MeOH (2 mL) and a solid precipitated and was removed by suction filtration. Silica was added to the filtrate and the solvent was removed under reduced pressure. The crude material was purified by chromatography on FlashMaster II silica (10 g) eluting with 0-25% MeOH/DCM over 30 min then reverse phase chromatography on a C18 column (30 g), eluting with 15-80% MeCN/water with a formic acid modifier. The product-containing fractions were concentrated under reduced pressure to afford **33** (27 mg, 11%) as a white solid. LCMS (Method A, UV, ESI)  $R_t = 1.04$  min,  $[M-H]^+ = 285/287$ , 100% purity;  $^1H$  NMR (400 MHz,  $d_6$ -DMSO)  $\delta$  2.31 (s, 3 H), 7.48 (d,  $J = 1.8$  Hz, 1 H), 7.54 (br. s, 1 H), 7.87 (d,  $J = 1.5$  Hz, 1 H), 7.91 (d,  $J = 1.8$  Hz, 1 H), 8.20 (br. s, 1 H), 11.44 (br. s, 1 H).

#### 6.4.2. 5-Bromo-3-(methylsulfonyl)-1*H*-indole-7-carboxamide, **34**

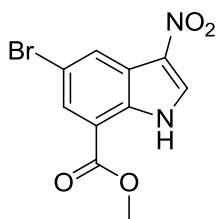


*m*CPBA (33 mg of  $\leq 77\%$  grade material, 0.19 mmol) was added to a solution of 5-bromo-3-(methylthio)-1*H*-indole-7-carboxamide (27 mg, 0.10 mmol) in  $CHCl_3$  (1 mL) at room temperature under an atmosphere of nitrogen. The mixture was stirred at room temperature for 1 h then saturated sodium sulfite solution (5 mL) was added. The aqueous phase was extracted with DCM (2 x 5 mL) and the combined organic extracts were concentrated under reduced pressure. The aqueous phase remained a suspension so the solid was collected by suction filtration and combined with the residue from the concentrated organic extracts. The crude material was purified by MDAP Method A2 and the product-containing fractions

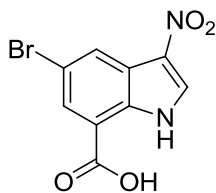
were concentrated under reduced pressure to afford **34** (11 mg, 38%) as a white solid. LCMS (Method A, UV, ESI)  $R_t = 0.73$  min,  $[M-H]^- = 315/317$ , 100% purity;  $^1H$  NMR (400 MHz,  $d_4$ -MeOH)  $\delta$  3.19 (s, 3 H), 7.97 (s, 1 H), 7.99 (d,  $J = 1.6$  Hz, 1 H), 8.21 (d,  $J = 1.6$  Hz, 1 H), three protons not observed.

## 6.5. Preparation of 3-Nitroindole-7-carboxamides

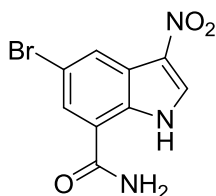
### 6.5.1. Methyl 5-bromo-3-nitro-1H-indole-7-carboxylate, **35**



A mixture of copper(II) nitrate (1.82 g, 8.8 mmol) and acetic anhydride (10 mL, 106 mmol) was cooled to 0 °C under an atmosphere of nitrogen. After stirring for 20 min, a solution of methyl 5-bromo-1H-indole-7-carboxylate (2.04 g, 8.0 mmol) in acetic anhydride (20 mL, 212 mmol) was added dropwise. The mixture was stirred at 0 °C for 30 min then allowed to warm to room temperature and stirring was continued for 30 min. A solid precipitated and was collected by suction filtration and washed with acetic anhydride (10 mL). The filtrate was poured into ice-water (100 mL) and the mixture was stirred for 3 h. A solid precipitated and was collected by suction filtration and washed with water (2 x 5 mL). The solid was transferred to a flask, washing with MeOH (~10 mL), and the solvent was evaporated under reduced pressure. The solid was dried on a high vacuum line (0.01 mmHg) for 18 h to afford **35** (1.27 g, 44%) as a red solid. LCMS (Method A, UV, ESI)  $R_t = 1.14$  min,  $[M-H]^- = 297/299$ , 83% purity;  $^1H$  NMR (400 MHz,  $CDCl_3$ )  $\delta$  4.04 (s, 3 H), 8.14 (d,  $J = 1.8$  Hz, 1 H), 8.28 (d,  $J = 3.3$  Hz, 1 H), 8.70 (d,  $J = 1.8$  Hz, 1 H), 10.48 (br. s, 1 H).

**6.5.2. 5-Bromo-3-nitro-1H-indole-7-carboxylic acid, 36**

A mixture of methyl 5-bromo-3-nitro-1H-indole-7-carboxylate (529 mg, 1.77 mmol) and NaOH (as a 2 M aqueous solution, 5 mL) in MeOH (10 mL) was stirred at room temperature for 18 h. More NaOH (as a 2 M aqueous solution, 2 mL) was added and stirring was continued for 2 h. The mixture was diluted with water (100 mL) and washed with DCM (50 mL). The aqueous phase was acidified to pH 1 with HCl (as a 2 M aqueous solution) and the solid was collected by suction filtration, washed with water (5 mL), then dried in a vacuum oven (0.01 mmHg) at 48 °C for 18 h to afford **36** (442 mg, 75%) as a red solid. LCMS (Method A, UV, ESI)  $R_t = 0.95$  min,  $[M-H]^- = 283/285$ , 85% purity;  $^1H$  NMR (400 MHz,  $d_6$ -DMSO)  $\delta$  7.97 (br. s, 1 H), 8.44 (br. s, 1 H), 8.48 (br. s, 1 H), 12.52 (br. s, 1 H), 13.97 (br. s, 1 H).

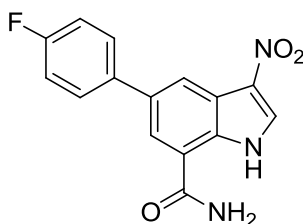
**6.5.3. 5-Bromo-3-nitro-1H-indole-7-carboxamide, 37**

A mixture of 5-bromo-3-nitro-1H-indole-7-carboxylic acid (380 mg, 1.33 mmol), HATU (560 mg, 1.47 mmol) and DIPEA (0.26 mL, 1.47 mmol) in DMF (5 mL) was stirred at room temperature. After 30 min,  $NH_3$  (0.76 mL of a 7 M solution in MeOH, 5.33 mmol) was added and stirring was continued for 45 min. The reaction mixture was concentrated under reduced pressure. The residue was taken up in water (50 mL) and the solid was collected by suction filtration then dried in the vacuum oven (0.01 mmHg) at 45 °C for 18 h to afford **37** (130 mg, 32%) as a pale brown solid. Mp 249 °C (decomposed). LCMS (Method A, UV, ESI)  $R_t = 0.84$  min,  $[M-H]^- = 284/286$ , 92% purity;  $^1H$  NMR (400 MHz,  $d_6$ -DMSO)  $\delta$  7.76 (br. s, 1 H), 8.03 (s, 1



H), 8.32 (s, 1 H), 8.39 (s, 1 H), 8.72 (br. s, 1 H), 12.58 (br. s, 1 H);  $^{13}\text{C}$  NMR (101 MHz,  $d_6$ -DMSO)  $\delta$  115.6, 120.4, 122.5, 124.8, 125.8, 127.6, 131.9, 132.1, 166.5; IR ( $\nu_{\text{max}}$  / $\text{cm}^{-1}$ ): 1373, 1666, 3266 (br.), 3314, 3341; HR-ESIMS ( $m/z$ ) calcd for  $\text{C}_9\text{H}_6\text{BrN}_3\text{O}_3$  [ $\text{M}^+$ ] 283.9671, found 283.9668.

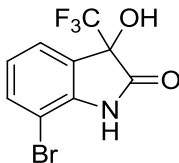
#### 6.5.4. 5-(4-Fluorophenyl)-3-nitro-1H-indole-7-carboxamide, **38**



A mixture of 5-bromo-3-nitro-1H-indole-7-carboxamide (50 mg, 0.18 mmol), (4-fluorophenyl)boronic acid (28 mg, 0.20 mmol),  $\text{K}_2\text{CO}_3$  (73 mg, 0.53 mmol) and  $\text{PdCl}_2(\text{dppf})$  (13 mg, 0.02 mmol) in 1,4-dioxane (1 mL) and water (0.5 mL) was heated in the microwave at 100 °C for 30 min, then at 120 °C for 30 min and finally at 150 °C for 1 h. More  $\text{PdCl}_2(\text{dppf})$  (13 mg, 0.02 mmol) was added and the mixture was heated in a microwave at 150 °C for 1 h. More 4-(fluorophenyl)boronic acid (28 mg, 0.20 mmol) was added and the mixture was heated in the microwave at 150 °C for 1 h. The mixture was diluted with DCM (10 mL) and filtered, washing the solid with further DCM (2 x 5 mL). The filtrate was washed with water (10 mL) then brine (10 mL) and the organic phase was concentrated under a stream of nitrogen. The crude material was purified by MDAP Method A3 and the product-containing fractions were concentrated under reduced pressure to afford **38** (3 mg, 4%) as a brown solid. LCMS (Method A, UV, ESI)  $R_t$  = 0.99 min,  $[\text{M}-\text{H}]^-$  = 298, 100% purity;  $^1\text{H}$  NMR (400 MHz,  $d_6$ -DMSO)  $\delta$  7.33 – 7.40 (m, 2 H), 7.70 (br. s, 1 H), 7.83 (dd,  $J$  = 8.7 Hz,  $J_{\text{H-F}}$  = 5.4 Hz, 2 H), 8.17 (d,  $J$  = 1.3 Hz, 1 H), 8.40 (s, 1 H), 8.43 (d,  $J$  = 1.3 Hz, 1 H), 8.65 (br. s, 1 H), 12.47 (br. s, 1 H).

## 6.6. Preparation of 3-Trifluoromethylindole-7-carboxamides

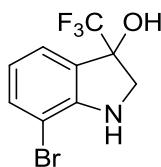
### 6.6.1. 7-Bromo-3-hydroxy-3-(trifluoromethyl)indolin-2-one, **40**



KOt-Bu (45 g, 0.40 mol) was added portionwise over 30 min to a mixture of 7-bromoindoline-2,3-dione (45 g, 0.20 mol), KF (4.5 g, 0.08 mmol) and (trifluoromethyl)trimethylsilane (56 g, 0.40 mol) in DMF (500 mL) at 0 °C. The mixture was warmed to room temperature and stirring was continued for 18 h. Water (1 L) was added and the mixture was acidified with concentrated HCl and extracted with EtOAc. The organic phase was washed with water and the solvent was removed under reduced pressure. The crude material was recrystallised from toluene to afford **40** (37.6 g, 64%). <sup>1</sup>H NMR (400 MHz, *d*<sub>6</sub>-DMSO) δ 7.01 (t, *J* = 7.6 Hz, 1 H), 7.39 (d, *J* = 7.4 Hz, 1 H), 7.55 (d, *J* = 7.4 Hz, 1 H), 7.79 (s, 1 H), 11.15 (br. s, 1 H); <sup>19</sup>F NMR (377 MHz, *d*<sub>6</sub>-DMSO) δ -29.5.

Peakdale Molecular, unpublished results.

### 6.6.2. 7-Bromo-3-(trifluoromethyl)indolin-3-ol, **41**

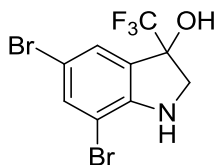


Borane-THF (635 mL of a 1.0 M solution in THF, 0.64 mol) was added slowly to a solution of 7-bromo-3-hydroxy-3-(trifluoromethyl)indolin-2-one (37.6 g, 0.13 mol) in THF (500 mL) at room temperature and the mixture was stirred for 1 h then heated to reflux for 3 h. The mixture was cooled and poured onto ice-water (100 mL). The aqueous phase was extracted with EtOAc and the organic phase was washed with water then the solvent was removed under reduced pressure to afford **41** (28.8 g, 80%). <sup>1</sup>H NMR (400 MHz, *d*<sub>6</sub>-DMSO) δ 3.47 (d, <sup>2</sup>*J* = 10.8 Hz, 1 H), 3.71 (d, <sup>2</sup>*J* = 10.8 Hz, 1 H), 6.00 (s, 1 H), 6.60 (t, *J* = 7.5 Hz, 1 H), 7.20 (d, *J* = 7.4 Hz, 1 H),

7.35 (d,  $J = 7.4$  Hz, 1 H), one proton not observed;  $^{19}\text{F}$  NMR (377 MHz,  $d_6$ -DMSO)  $\delta$  -22.5.

Peakdale Molecular, unpublished results.

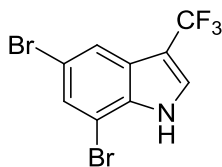
#### 6.6.3. 5,7-Dibromo-3-(trifluoromethyl)indolin-3-ol, **42**



A mixture of 7-bromo-3-(trifluoromethyl)indolin-3-ol (20 g, 71 mmol) and NBS (12.7 g, 71 mmol) in DCM (400 mL) was stirred at room temperature for 1 h. The organic phase was washed with water and the solvent was removed under reduced pressure to afford **42** (26.7 g, used crude in next stage).  $^1\text{H}$  NMR (400 MHz,  $\text{CDCl}_3$ )  $\delta$  3.70 (d,  $^2J = 10.8$  Hz, 1 H), 3.95 (d,  $^2J = 10.8$  Hz, 1 H), 7.40 (s, 1 H), 7.50 (s, 1 H), two protons not observed;  $^{19}\text{F}$  NMR (377 MHz,  $\text{CDCl}_3$ )  $\delta$  -30.0.

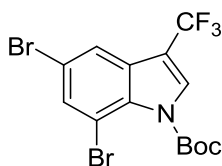
Peakdale Molecular, unpublished results.

#### 6.6.4. 5,7-Dibromo-3-(trifluoromethyl)-1H-indole, **43**



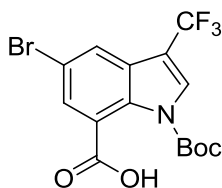
A mixture of 5,7-dibromo-3-(trifluoromethyl)indolin-3-ol (26.7 g, 74 mmol) and TsOH (1.35 g, 7.1 mmol) in toluene (500 mL) was heated to reflux with a Dean-Stark trap attached. The mixture was stirred for 3 h then allowed to cool to room temperature and the solvent was removed under reduced pressure. The crude material was passed through a pad of silica to afford **43** (20 g, 82% over two steps).  $^1\text{H}$  NMR (400 MHz,  $\text{CDCl}_3$ )  $\delta$  7.55 (s, 1 H), 7.60 (s, 1 H), 7.80 (s, 1 H), 8.60 (br. s, 1 H);  $^{19}\text{F}$  NMR (377 MHz,  $\text{CDCl}_3$ )  $\delta$  -16.2.

Peakdale Molecular, unpublished results.

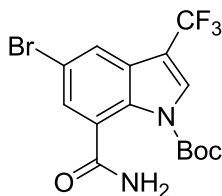
**6.6.5. *tert*-Butyl 5,7-dibromo-3-(trifluoromethyl)-1*H*-indole-1-carboxylate, **44****

A mixture of 5,7-dibromo-3-(trifluoromethyl)-1*H*-indole (20 g, 58 mmol), Boc<sub>2</sub>O (12.7 g, 58 mmol), NEt<sub>3</sub> (2 mL, 14 mmol) and DMAP (0.71 g, 5.8 mmol) in DCM (400 mL) was stirred at room temperature for 30 min. The solvent was removed under reduced pressure and the crude material was recrystallised from IPA to afford **44** (19 g, 74%). <sup>1</sup>H NMR (400 MHz, CDCl<sub>3</sub>) δ 1.65 (s, 9 H), 7.78 (s, 1 H), 7.75 (s, 1 H), 7.85 (s, 1 H); <sup>19</sup>F NMR (377 MHz, CDCl<sub>3</sub>) δ -16.3.

Peakdale Molecular, unpublished results.

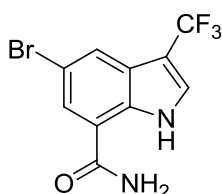
**6.6.6. 5-Bromo-1-(*tert*-butoxycarbonyl)-3-methyl-1*H*-indole-7-carboxylic acid, **45****

*n*-BuLi (7.8 mL of a 1.6 M solution in hexanes, 12.5 mmol) was added to a solution of *tert*-butyl 5,7-dibromo-3-(trifluoromethyl)-1*H*-indole-1-carboxylate (6 g, 13.6 mmol) in THF (120 mL) at -70 °C under an atmosphere of nitrogen. The reaction mixture was stirred for 5 min at -70 °C then quenched with CO<sub>2</sub> (dry ice). The mixture was allowed to warm to room temperature and saturated aqueous NH<sub>4</sub>Cl was added. The aqueous phase was extracted with EtOAc then the organic phase was washed with water and brine and the solvent was removed under reduced pressure. The crude material was purified by chromatography on silica, eluting with heptane/EtOAc (85:15) then the residue was recrystallised from heptane to afford **45** (3.3 g, 66%). <sup>1</sup>H NMR (400 MHz, *d*<sub>6</sub>-DMSO) δ 1.55 (s, 9 H), 7.75 (s, 1 H), 7.90 (s, 1 H), 8.40 (s, 1 H), one proton was not observed; <sup>19</sup>F NMR (377 MHz, *d*<sub>6</sub>-DMSO) δ -16.2. Peakdale Molecular, unpublished results.

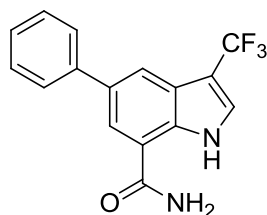
**6.6.7. *tert*-Butyl 5-bromo-7-carbamoyl-3-(trifluoromethyl)-1*H*-indole-1-carboxylate, **46****

A mixture of 5-bromo-1-(*tert*-butoxycarbonyl)-3-methyl-1*H*-indole-7-carboxylic acid (2.9 g, 7.1 mmol), HATU (2.7 g, 7.1 mmol) and NEt<sub>3</sub> (10 mL, 71 mmol) in DMF (30 mL) was stirred at room temperature for 30 min. NH<sub>3</sub> (as a 14% solution in MeOH, 10 mL) was added and stirring was continued for 30 min. The mixture was concentrated under reduced pressure and the residue was poured into water. The resulting solid was isolated by suction filtration and the crude material was recrystallised from IPA to afford **46** (1.75 g, 58%). <sup>1</sup>H NMR (400 MHz, *d*<sub>6</sub>-DMSO) δ 1.45 (s, 9 H), 7.90 (s, 2 H), 8.08 (s, 1 H), 10.91 (br. s, 1 H), 12.18 (br. s, 1 H); <sup>19</sup>F NMR (377 MHz, *d*<sub>6</sub>-DMSO) δ -15.7.

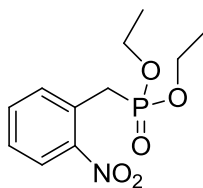
Peakdale Molecular, unpublished results.

**6.6.8. 5-Bromo-3-(trifluoromethyl)-1*H*-indole-7-carboxamide, **47****

A mixture of *tert*-butyl 5-bromo-7-carbamoyl-3-(trifluoromethyl)-1*H*-indole-1-carboxylate (1.75 g, 4.3 mmol) and HCl (as a 4 M solution in 1,4-dioxane, 20 mL, 80 mmol) was heated to 40 °C and stirred for 2 h. The mixture was concentrated under reduced pressure and the crude material was recrystallised from IPA to afford **47** (1.1 g, 83%). LCMS (Method A, UV, ESI) *R*<sub>t</sub> = 0.83 min, [M-H]<sup>-</sup> = 305, 100% purity; <sup>1</sup>H NMR (400 MHz, *d*<sub>6</sub>-DMSO) δ 7.70 (br. s, 1 H), 7.85 (s, 2 H), 8.00 (s, 1 H), 8.30 (br. s, 1 H), 11.95 (br. s, 1 H); <sup>19</sup>F NMR (377 MHz, *d*<sub>6</sub>-DMSO) δ -15.6. Peakdale Molecular, unpublished results.

**6.6.9. 5-Phenyl-3-(trifluoromethyl)-1H-indole-7-carboxamide, 48**

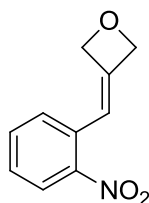
A mixture of 5-bromo-3-(trifluoromethyl)-1H-indole-7-carboxamide (20 mg, 0.07 mmol), tetraphenyltin (32 mg, 0.08 mmol) and Pd(PPh<sub>3</sub>)<sub>4</sub> (7 mg, 0.01 mmol) in DMF (1 mL) was heated in a microwave at 80 °C for 30 min, then at 110 °C for 30 min and finally at 150 °C for 30 min. Saturated KF (5 mL) was added and the mixture was extracted with EtOAc (10 mL). The organic phase was concentrated under a stream of nitrogen. The crude material was purified by MDAP Method A3 and the product-containing fractions were concentrated under reduced pressure to afford **48** (3 mg, 15%) as a brown solid. LCMS (Method A, UV, ESI)  $R_t = 1.13$  min,  $[M-H]^+ = 305$ , 100% purity; <sup>1</sup>H NMR (400 MHz, *d*<sub>4</sub>-MeOH)  $\delta$  7.42 – 7.47 (m, 1 H), 7.56 (t,  $J = 7.3$  Hz, 2 H), 7.80 (d,  $J = 7.6$  Hz, 2 H), 7.87 (s, 1 H), 8.10 (s, 1 H), 8.16 (s, 1 H), three protons were not observed.

**6.7. Preparation of 3-(Oxetan-3-yl)indazole-7-carboxamides****6.7.1. Diethyl 2-nitrobenzylphosphonate, 66**

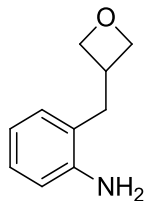
Triethyl phosphite (9.2 mL, 52.6 mmol) was added dropwise to a solution of 1-(bromomethyl)-2-nitrobenzene (10.3 g, 47.8 mmol) in toluene (200 mL) under an atmosphere of nitrogen. The reaction mixture was heated to 110 °C for 18 h. The mixture was cooled to room temperature and the solvent was removed under reduced pressure. The residue was partitioned between EtOAc (50 mL) and water (50 mL). The organic phase was separated and the aqueous phase was extracted with more EtOAc (2 x 50 mL). The combined organic extracts were washed with brine, dried

by passing through a hydrophobic frit and concentrated under reduced pressure. The crude material was purified by chromatography on Companion silica (330 g), eluting with 0-100% EtOAc/cyclohexane over 1 h. The product-containing fractions were concentrated under reduced pressure to afford **66** (10.2 g, 77%) as a yellow oil. LCMS (Method A, UV, ESI)  $R_t = 0.86$  min,  $[M-H]^+ = 274$ , 98% purity;  $^1\text{H NMR}$  (400 MHz,  $\text{CDCl}_3$ )  $\delta$  1.23 (t,  $J = 7.1$  Hz, 6 H), 3.70 (d,  $J_{H-P} = 24$  Hz, 2 H), 3.99-4.06 (m, 4 H), 7.40 – 7.46 (m, 1 H), 7.47 – 7.51 (m, 1 H), 7.54 – 7.59 (m, 1 H), 7.95 (d,  $J = 8.3$  Hz, 1 H).

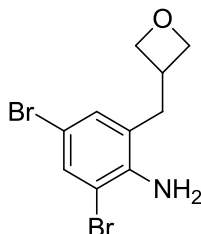
### 6.7.2. 3-(2-Nitrobenzylidene)oxetane, **67**



NaH (2.3 g of a 60% dispersion in mineral oil, 56.5 mmol) was added portionwise to a solution of diethyl 2-nitrobenzylphosphonate (10.2 g, 37.5 mmol) in DMF (40 mL) at 0 °C under an atmosphere of nitrogen. The mixture was stirred at 0 °C for 10 min then 3-oxetanone (4.1 g, 56.3 mmol) in DMF (40 mL) was added. The mixture was allowed to warm to room temperature and stirring was continued for 18 h. The solvent was removed under reduced pressure at 50 °C and the residue was partitioned between EtOAc (50 mL) and water (50 mL). The aqueous phase was extracted further with EtOAc (2 x 50 mL). The combined organic extracts and the original organic phase were washed with brine (50 mL), dried by passing through a hydrophobic frit and concentrated under reduced pressure. The crude material was purified by chromatography on Companion silica (330 g), eluting with 0-50% EtOAc/cyclohexane. The product-containing fractions were concentrated under reduced pressure to afford **67** (5.0 g, 70%) as a yellow solid. LCMS (Method A, UV, ESI)  $R_t = 0.87$  min,  $[M-H]^+ = 192$ , 100% purity;  $^1\text{H NMR}$  (400 MHz,  $d_6$ -DMSO)  $\delta$  5.27 – 5.33 (m, 2 H), 5.45 – 5.51 (m, 2 H), 6.48 – 6.53 (m, 1 H), 7.26 (d,  $J = 7.6$  Hz, 1 H), 7.49 (td,  $J = 7.2$  Hz, 1.1 Hz, 1 H), 7.67 (td,  $J = 7.2$  Hz, 1.1 Hz, 1 H), 7.96 (dd,  $J = 8.2$  Hz, 1.1 Hz, 1 H).

**6.7.3. 2-(Oxetan-3-ylmethyl)aniline, 68**

3-(2-Nitrobenzylidene)oxetane (1.8 g, 9.4 mmol) was taken up in MeOH (180 mL) and hydrogenated using an H-Cube<sup>®</sup> with a 10% palladium on carbon CatCart<sup>®</sup>. The starting material solution was passed through the flow reactor at 45 °C and 8 bar H<sub>2</sub> with a flow rate of 1 mL/min. The solution was left standing overnight. The CatCart<sup>®</sup> was replaced and the solution was passed through the flow reactor again at 45 °C and 10 bar H<sub>2</sub>, with a flow rate of 2 mL/min. The solvent was removed under reduced pressure to afford **68** (1.5 g, 97%) as a pale yellow oil. LCMS (Method A, UV, ESI)  $R_t = 0.46$  min,  $[M-H]^+ = 164$ , 99% purity; <sup>1</sup>H NMR (400 MHz, CDCl<sub>3</sub>)  $\delta$  2.90 (d,  $J = 7.8$  Hz, 2 H), 3.39-3.46 (m, 1 H), 3.61 (br. s, 2 H), 4.49 (dd,  $^2J = 7.5$  Hz,  $J = 6.0$  Hz, 2 H), 4.87 (dd,  $^2J = 7.5$  Hz,  $J = 6.0$  Hz, 2 H), 6.69 – 6.79 (m, 2 H), 6.88 – 6.93 (m, 1 H), 7.05 – 7.12 (m, 1 H).

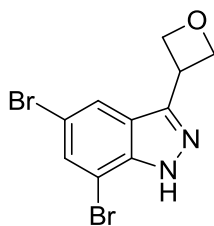
**6.7.4. 2,4-Dibromo-6-(oxetan-3-ylmethyl)aniline, 69**

NBS (2.7 g, 15.2 mmol) was added to a solution of 2-(oxetan-3-ylmethyl)aniline (1.2 g, 7.6 mmol) in DCM (40 mL) at 0 °C under an atmosphere of nitrogen. The mixture was stirred for 30 min then saturated aqueous NaHCO<sub>3</sub> solution (40 mL) was added and stirring was continued for 15 min. The mixture was diluted with DCM (40 mL) and warmed to room temperature. The organic phase was separated and the solvent was removed under reduced pressure. The crude material was purified by chromatography on FlashMaster II silica (2 x 100 g), eluting with 0-100% EtOAc/cyclohexane over 40 min. The required fractions were combined and



the solvent removed under reduced pressure. The residue was dried on a high vacuum line (0.01 mmHg) for 1 h to afford **69** (1.5 g, 64%) as an orange solid. LCMS (Method A, UV, ESI)  $R_t = 1.09$  min,  $[M-H]^+ = 320/322/324$ , 90% purity;  $^1H$  NMR (400 MHz,  $CDCl_3$ )  $\delta$  2.89 (d,  $J = 7.8$  Hz, 2 H), 3.34-3.44 (m, 1 H), 4.12 (br. s, 2 H), 4.44 (dd,  $^2J = 7.6$  Hz,  $J = 6.3$  Hz, 2 H), 4.87 (dd,  $^2J = 7.6$  Hz,  $J = 6.3$  Hz, 2 H), 6.93 (d,  $J = 2.0$  Hz, 1 H), 7.47 (d,  $J = 2.3$  Hz, 1 H).

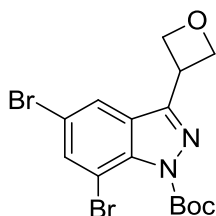
#### 6.7.5. 5,7-Dibromo-3-(oxetan-3-yl)-1H-indazole, **70**



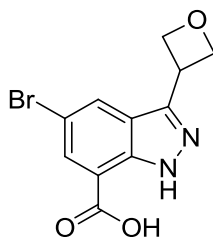
2,4-Dibromo-6-(oxetan-3-ylmethyl)aniline (899 mg, 2.8 mmol) was dissolved in  $CHCl_3$  (25 mL) at room temperature under an atmosphere of nitrogen. KOAc (275 mg, 2.8 mmol), acetic anhydride (0.26 mL, 2.8 mmol) and 18-crown-6 (148 mg, 0.56 mmol) were added sequentially to the solution and stirring was continued for 15 min. Acetic anhydride (0.26 mL, 2.8 mmol), acetic acid (0.16 mL, 2.8 mmol) and *tert*-butyl nitrite (0.64 mL, 5.6 mmol) were then added sequentially to the reaction mixture at room temperature and the mixture was heated at reflux for 30 min. The mixture was cooled to room temperature and quenched with saturated aqueous  $NaHCO_3$  solution (25 mL). More  $CHCl_3$  was added (50 mL) and the phases were separated. Some solid remained in the aqueous layer so this was collected by suction filtration and dried in a vacuum oven (0.01 mmHg) at 40 °C for 2 h to afford **70** as a pale orange solid. The organic portion was concentrated under reduced pressure and the residue was triturated with  $Et_2O$  (~ 10 mL). The solid was collected by suction filtration and dried in a vacuum oven (0.01 mmHg) at 40 °C for 1 h to afford **70** as a brown solid. The filtrate was concentrated under reduced pressure to give an oily brown solid that was taken up in MeOH and preadsorbed onto Florisil®. This was purified by FlashMaster II silica (50 g), eluting with 0-50% EtOAc/cyclohexane over 40 min and the product-containing fractions were

concentrated under reduced pressure to afford **70** as an orange solid. The three product batches were combined to afford **70** (607 mg, 65%) as an orange solid. Mp 220-221 °C. LCMS (Method A, UV, ESI)  $R_t = 0.98$  min,  $[M-H]^+ = 331/333/335$ , 100% purity;  $^1H$  NMR (400 MHz,  $CDCl_3$ )  $\delta$  4.60-4.69 (m, 1 H), 4.84 (dd,  $^2J = 8.4$  Hz,  $J = 5.7$  Hz, 2 H), 5.01 (dd,  $^2J = 8.4$  Hz,  $J = 5.7$  Hz, 2 H), 7.79 (d,  $J = 1.5$  Hz, 1 H), 8.08 (d,  $J = 1.5$  Hz, 1 H), 13.55 (br. s, 1 H);  $^{13}C$  NMR (101 MHz,  $d_6$ -DMSO)  $\delta$  32.4, 75.7 (2C), 103.8, 112.0, 121.8, 123.2, 130.6, 139.3, 145.7; IR ( $\nu_{max}/cm^{-1}$ ): 3163 (br.); HR-ESIMS ( $m/z$ ) calcd for  $C_{10}H_8Br_2N_2O$   $[M^+]$  330.9082, found 330.9071.

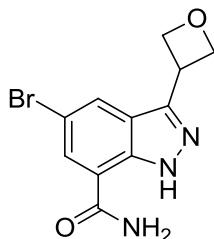
#### 6.7.6. *tert*-Butyl 5,7-dibromo-3-(oxetan-3-yl)-1*H*-indazole-1-carboxylate, **71**



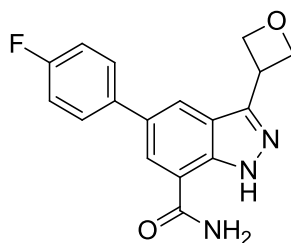
A mixture of 5,7-dibromo-3-(oxetan-3-yl)-1*H*-indazole (534 mg, 1.02 mmol), DMAP (20 mg, 0.16 mmol), triethylamine (0.23 mL, 1.61 mmol) and  $Boc_2O$  (702 mg, 3.22 mmol) in DCM (15 mL) was stirred at room temperature for 72 h. More  $Boc_2O$  (702 mg, 3.22 mmol), DMAP (20 mg, 0.16 mmol) and triethylamine (0.23 mL, 1.61 mmol) were added to the mixture and stirring was continued for 18 h. The mixture was heated to 35 °C for 23 h. The mixture was cooled to room temperature and diluted with DCM (10 mL). The organic phase was washed with citric acid (3 x 20 mL of a 5% w/v aqueous solution), saturated aqueous  $NaHCO_3$  solution (20 mL) then water (20 mL) and brine (20 mL). The organic phase was dried by passing through a hydrophobic frit and concentrated under reduced pressure. The residue was taken up in  $Et_2O$  (~5 mL) and the mixture was sonicated until a solid formed. The material was dried on a high vacuum line (0.01 mmHg) for 1 h to afford **71** (623 mg, 90%) as an orange solid. LCMS (Method A, UV, ESI)  $R_t = 1.34$  min,  $[M-H]^+ = 431/433/435$ , 97% purity;  $^1H$  NMR (400 MHz,  $d_6$ -DMSO)  $\delta$  1.63 (s, 9 H), 4.62-4.72 (m, 1 H), 4.83 (dd,  $^2J = 8.8$  Hz,  $J = 6.0$  Hz, 2 H), 5.02 (dd,  $^2J = 8.8$  Hz,  $J = 6.0$  Hz, 2 H), 8.06 (d,  $J = 1.8$  Hz, 1 H), 8.19 (d,  $J = 1.8$  Hz, 1 H).

**6.7.7. 5-Bromo-3-(oxetan-3-yl)-1H-indazole-7-carboxylic acid, 72**

*t*-BuLi (0.81 mL of a 1.7 M solution pentane, 1.38 mmol) was added dropwise to a solution of *tert*-butyl 5,7-dibromo-3-(oxetan-3-yl)-1*H*-indazole-1-carboxylate (298 mg, 0.69 mmol) in THF (5 mL) at -78 °C under an atmosphere of nitrogen. The reaction mixture was stirred for 10 min at -78 °C then quenched with CO<sub>2</sub> (dry ice) (1.1 g, 25.0 mmol), which had been crushed to a powder in a pestle and mortar under an atmosphere of nitrogen and was added quickly to the reaction mixture. The reaction mixture was stirred at -78 °C for 20 min then warmed slowly to room temperature over 40 min and stirring was continued for 1 h. Water (10 mL) was added to the mixture and the pH was adjusted to 12 by the addition of NaOH (as a 1 M aqueous solution). The aqueous phase was heated to 50 °C for 4 h. The mixture was cooled then acidified to pH 1 with HCl (as a 2 M aqueous solution) and extracted with EtOAc (3 x 20 mL). The combined organic extracts were dried by passing through a hydrophobic frit and concentrated under reduced pressure to afford **72** (193 mg, 76%) as a cream solid. LCMS (Method A, UV, ESI) *R*<sub>t</sub> = 0.75 min, [M-H]<sup>+</sup> = 297/299, 81% purity; <sup>1</sup>H NMR (400 MHz, *d*<sub>6</sub>-DMSO) δ 4.64-4.74 (m, 1 H), 4.83 (dd, <sup>2</sup>*J* = 8.4 Hz, *J* = 5.9 Hz, 2 H), 5.02 (dd, <sup>2</sup>*J* = 8.4 Hz, *J* = 5.9 Hz, 2 H), 7.98 (d, *J* = 1.8 Hz, 1 H), 8.32 (d, *J* = 1.8 Hz, 1 H), 13.17 (s, 1 H), 13.65 (br. s, 1 H).

**6.7.8. 5-Bromo-3-(oxetan-3-yl)-1H-indazole-7-carboxamide, 73**

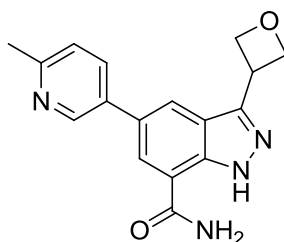
A mixture of 5-bromo-3-(oxetan-3-yl)-1H-indazole-7-carboxylic acid (193 mg, 0.65 mmol), HATU (272 mg, 0.72 mmol) and DIPEA (0.13 mL, 0.72 mmol) in DMF (4 mL) was stirred at room temperature. After 30 min, NH<sub>3</sub> (0.37 mL of a 7 M solution in methanol, 2.60 mmol) was added and stirring was continued for 2 h. The mixture was concentrated under reduced pressure and the residue was dissolved in EtOAc (30 mL) then washed with water (30 mL). The aqueous phase was extracted with further EtOAc (2 x 30 mL). The combined organic extracts were washed with water (5 x 30 mL) and brine (30 mL), dried by passing through a hydrophobic frit and concentrated under a stream of nitrogen to afford **73** (104 mg, 45%) as a cream solid. Mp 228 °C (decomposed). LCMS (Method A, UV, ESI)  $R_t = 0.65$  min,  $[M-H]^+ = 296/298$ , 83% purity; <sup>1</sup>H NMR (400 MHz, *d*<sub>6</sub>-DMSO)  $\delta$  4.62-4.72 (m, 1 H), 4.84 (dd, <sup>2</sup>*J* = 8.8 Hz, *J* = 6.0 Hz, 2 H), 5.02 (dd, <sup>2</sup>*J* = 8.8 Hz, *J* = 6.0 Hz, 2 H), 7.61 (br. s, 1 H), 8.08 (d, *J* = 1.8 Hz, 1 H), 8.20 (d, *J* = 1.8 Hz, 1 H), 8.24 (br. s, 1 H), 13.06 (br. s, 1 H); <sup>13</sup>C NMR (101 MHz, *d*<sub>6</sub>-DMSO)  $\delta$  32.3, 75.6 (2C), 111.3, 118.6, 123.7, 125.6, 127.9, 137.9, 144.4, 166.5; IR ( $\nu_{\max}$ /cm<sup>-1</sup>): 1656, 3190 (br.), 3371 (br.), 3446; HR-ESIMS (*m/z*) calcd for C<sub>11</sub>H<sub>9</sub>BrN<sub>2</sub>O<sub>3</sub> [M<sup>+</sup>] 296.0035, found 296.0025.

**6.7.9. 5-(4-Fluorophenyl)-3-(oxetan-3-yl)-1H-indazole-7-carboxamide, 74a**

A mixture of 5-bromo-3-(oxetan-3-yl)-1H-indazole-7-carboxamide (30 mg, 0.10 mmol), (4-fluorophenyl)boronic acid (46 mg, 0.33 mmol), Pd(PPh<sub>3</sub>)<sub>4</sub> (13 mg,

0.01 mmol) and  $K_2CO_3$  (84 mg, 0.61 mmol) in IPA (0.7 mL) was heated in the microwave at 100 °C for 30 min. Water (0.1 mL) was added to the reaction mixture and it was heated in the microwave at 110 °C for a further 30 min. The reaction mixture was partitioned between EtOAc (10 mL) and water (10 mL). The aqueous phase was extracted further with EtOAc (2 x 10 mL). The combined organic extracts were dried by passing through a hydrophobic frit and concentrated under a stream of nitrogen. The crude material was purified by MDAP Method B2 and the product-containing fractions were concentrated under reduced pressure to afford **74a** (8 mg, 25%) as a white solid. LCMS (Method A, UV, ESI)  $R_t = 0.82$  min,  $[M-H]^+ = 312$ , 99% purity;  $^1H$  NMR (400 MHz,  $d_6$ -DMSO)  $\delta$  4.68-4.79 (m, 1 H), 4.92 (dd,  $^2J = 8.6$  Hz,  $J = 5.6$  Hz, 2 H), 5.05 (dd,  $^2J = 8.6$  Hz,  $J = 5.6$  Hz, 2 H), 7.32 (t,  $J = 8.8$  Hz, 2 H), 7.53 (br. s, 1 H), 7.85 (dd,  $J = 8.6$  Hz, 5.5 Hz, 2 H), 8.21 (s, 1 H), 8.23 (s, 1 H), 8.35 (br. s, 1 H), 12.90 (br. s, 1 H).

**6.7.10. 5-(6-Methylpyridin-3-yl)-3-(oxetan-3-yl)-1H-indazole-7-carboxamide, 74b**

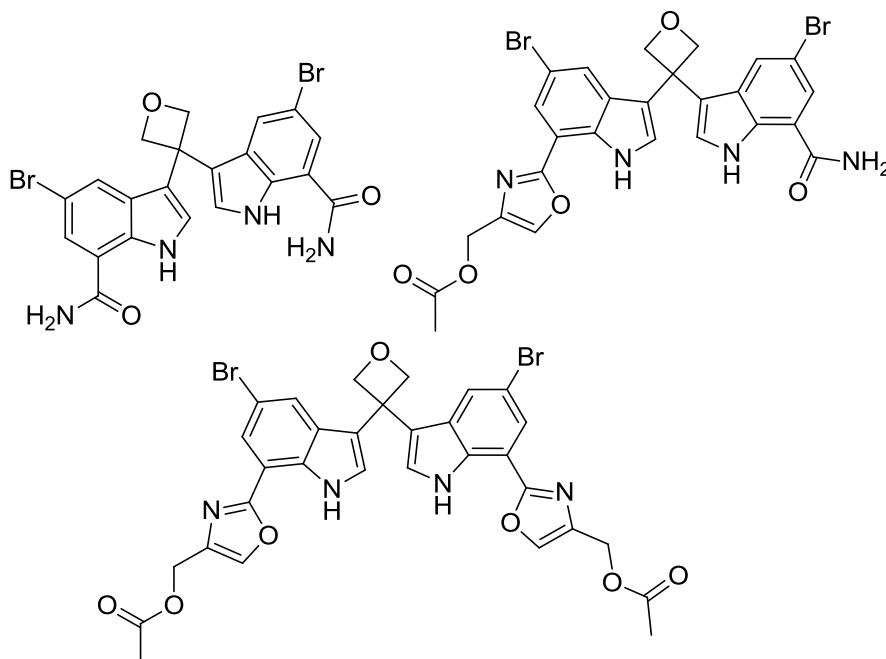


A mixture of 5-bromo-3-(oxetan-3-yl)-1H-indazole-7-carboxamide (30 mg, 0.10 mmol), (6-methylpyridin-3-yl)boronic acid (42 mg, 0.30 mmol),  $Pd(PPh_3)_4$  (12 mg, 0.01 mmol) and  $K_2CO_3$  (84 mg, 0.61 mmol) in IPA (0.7 mL) and water (0.1 mL) was heated in the microwave at 100 °C for 50 min then at 120 °C for 1 h. The reaction mixture was filtered, washing with MeOH (~5 mL). The filtrate was loaded onto a 2 g SCX-2 cartridge that had been preconditioned with MeOH. The cartridge was eluted with MeOH (2 CV) then  $NH_3$  (as a 2 M solution in MeOH, 2 CV). The basic fraction was concentrated under a stream of nitrogen. The crude material was purified by MDAP Method B2 and the product-containing fractions were concentrated under reduced pressure to afford **74b** (6 mg, 19%) as a yellow solid.

LCMS (Method A, UV, ESI)  $R_t = 0.42$  min,  $[M-H]^+ = 309$ , 100% purity;  $^1H$  NMR (400 MHz,  $d_6$ -DMSO)  $\delta$  2.50 (s, 3 H), 4.67-4.77 (m, 1 H), 4.90 (dd,  $^2J = 8.6$  Hz,  $J = 5.6$  Hz, 2 H), 5.02 (dd,  $^2J = 8.6$  Hz,  $J = 5.6$  Hz, 2 H), 7.35 (d,  $J = 8.1$  Hz, 1 H), 7.35 (br. s, 1 H), 8.08 (dd,  $J = 9.2$  Hz,  $J = 3.2$  Hz, 1 H), 8.25 (s, 2 H), 8.30 (br. s., 1H), 8.89 (d,  $J = 2.3$  Hz, 1 H), 12.90 (br. s, 1 H).

## 6.8. Preparation of 3-(Oxetan-3-yl)indole-7-carboxamides

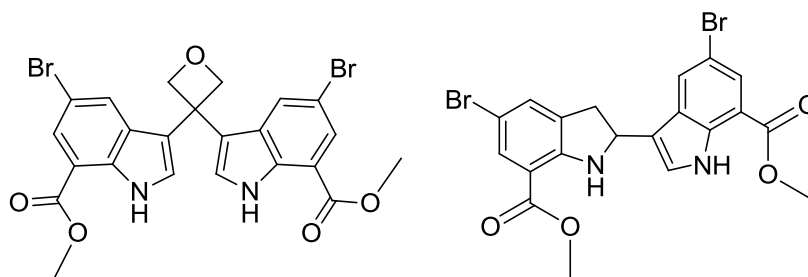
6.8.1. 3,3'-(Oxetane-3,3-diyl)bis(5-bromo-1H-indole-7-carboxamide, 89, (2-(5-Bromo-3-(3-(5-bromo-7-carbamoyl-1H-indol-3-yl)oxetan-3-yl)-1H-indol-7-yl)oxazol-4-yl)methyl acetate, 90, and (2,2'-(3,3'-(Oxetane-3,3-diyl)bis(5-bromo-1H-indole-7,3-diyl))bis(oxazole-4,2-diyl))bis(methylene) diacetate, 91



A mixture of 5-bromo-1H-indole-7-carboxamide (100 mg, 0.42 mmol), 3-oxetanone (90 mg, 1.26 mmol) and sulfamic acid (61 mg, 0.63 mmol) in acetic acid (2 mL) was heated at 80 °C under an atmosphere of nitrogen for 18 h. The reaction mixture was allowed to cool to room temperature and the solid was collected by suction filtration and washed with acetic acid (5 mL). The solid was taken up in

water (5 mL) and basified to pH > 12 with NaOH (as a 2 M aqueous solution). The solid was collected by suction filtration and washed with water (10 mL) then dried in air. The filtrate was concentrated under reduced pressure then cyclohexane (10 mL) was added and the solvent was again removed under reduced pressure. The crude material was purified by reverse phase chromatography on a C18 column (60 g), eluting with 15-95% MeCN/water with a formic acid modifier to afford **89** as an oil after concentration under reduced pressure. LCMS (Method A, UV, ESI)  $R_t = 0.86$  min,  $[M-H]^- = 529/531/533$ , 75% purity;  $^1H$  NMR (400 MHz,  $d_6$ -DMSO)  $\delta$  5.22 (s, 4 H), 7.27 (d,  $J = 2.4$  Hz, 2 H), 7.48 (br. s, 2 H), 7.70 (d,  $J = 1.8$  Hz, 2 H), 7.83 (d,  $J = 1.8$  Hz, 2 H), 8.16 (br. s, 2 H), 11.19 (d,  $J = 2.2$  Hz, 2 H);  $^{13}C$  NMR (151 MHz,  $d_6$ -DMSO)  $\delta$  40.5, 82.5 (2C), 110.4 (2C), 118.3 (2C), 118.6 (2C), 123.1 (2C), 124.7 (2C), 125.7 (2C), 128.5 (2C), 134.2 (2C), 167.8 (2C); followed by **90** as an oil after concentration under reduced pressure. LCMS (Method A, UV, ESI)  $R_t = 1.17$  min,  $[M-H]^+ = 627/629$ , 76% purity;  $^1H$  NMR (400 MHz,  $d_6$ -DMSO)  $\delta$  2.04 (s, 3 H), 5.06 (s, 2 H), 5.17-5.25 (m, 4 H), 7.28 (d,  $J = 2.6$  Hz, 1 H), 7.41 (d,  $J = 2.6$  Hz, 1 H), 7.45 (br. s, 1 H), 7.68 (d,  $J = 1.8$  Hz, 1 H), 7.70 (d,  $J = 1.8$  Hz, 1 H), 7.75 (d,  $J = 1.8$  Hz, 1 H), 7.80 (d,  $J = 1.8$  Hz, 1 H), 8.13 (d,  $J = 2.0$  Hz, 1 H), 8.27 (br. s, 1 H), 11.15 (d,  $J = 2.2$  Hz, 1 H), 11.18 (d,  $J = 2.4$  Hz, 1 H);  $^{13}C$  NMR (151 MHz,  $d_6$ -DMSO)  $\delta$  20.7, 40.5, 57.7, 82.5 (2C), 110.4, 111.0, 111.8, 118.1, 118.7, 119.3, 121.5, 123.1, 124.1, 124.7, 125.7, 126.2, 128.5, 128.6, 131.5, 134.2, 137.1, 138.4, 158.9, 167.8, 170.3; and then **91** as an oil after concentration under reduced pressure. LCMS (Method A, UV, ESI)  $R_t = 1.44$  min,  $[M-H]^+ = 723/725$ , 78% purity;  $^1H$  NMR (400 MHz,  $d_6$ -DMSO)  $\delta$  2.08 (s, 6 H), 5.10 (s, 4 H), 5.29 (s, 4 H), 7.49 (d,  $J = 2.6$  Hz, 2 H), 7.75 (d,  $J = 1.8$  Hz, 2 H), 7.79 (d,  $J = 1.8$  Hz, 2 H), 8.31 (s, 2 H), 11.21 (d,  $J = 2.2$  Hz, 2 H);  $^{13}C$  NMR (151 MHz,  $d_6$ -DMSO)  $\delta$  20.7 (2C), 40.6, 57.6 (2C), 82.4 (2C), 111.0 (2C), 111.8 (2C), 119.1 (2C), 121.5 (2C), 124.1 (2C), 126.3 (2C), 128.6 (2C), 131.5 (2C), 127.1 (2C), 138.5 (2C), 158.9 (2C), 170.3 (2C).

**6.8.2. Dimethyl 3,3-(oxetane-3,3-diyl)bis(5-bromo-1H-indole-7-carboxylate), **102** and Methyl 5-bromo-3-(5-bromo-7-(methoxycarbonyl)indolin-2-yl)-1H-indole-7-carboxylate, **103****



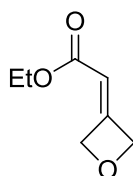
**METHOD A:** Trimethylsilyl trifluoromethanesulfonate (0.15 mL, 0.8 mmol) was added dropwise to a solution of 3-oxetanone (0.35 mL, 4.8 mmol) in DCM (16 mL) at -5 °C under an atmosphere of nitrogen. A solution of methyl 5-bromo-1H-indole-7-carboxylate (1.02 g, 4.0 mmol) in DCM (8 mL) was added and the mixture was allowed to warm to room temperature and stirring was continued for 18 h. Triethylsilane (0.96 mL, 6.0 mmol) was added and stirring was continued for 5 h. Saturated aqueous NaHCO<sub>3</sub> solution (10 mL) was added and the mixture was extracted with DCM (2 x 10 mL). The combined organic extracts were washed with HCl (as a 2 M aqueous solution, 10 mL) then dried by passing through a hydrophobic frit and concentrated under reduced pressure. The residue was taken up firstly in DCM (~5 mL), then in Et<sub>2</sub>O (~5 mL), collecting the solid by suction filtration each time. The filtered solid was purified by chromatography on FlashMaster II silica (70 g) eluting with 0-50% EtOAc/cyclohexane over 1 h. The DCM and Et<sub>2</sub>O filtrates were concentrated under reduced pressure. The residues were combined and purified by chromatography on FlashMaster II silica (50 g) eluting with 0-50% EtOAc/cyclohexane over 1 h to afford **102** as an oil after concentration under reduced pressure. LCMS (Method A, UV, ESI)  $R_t = 1.37$  min,  $[M-H]^- = 559/561/563$ , 78% purity; <sup>1</sup>H NMR (400 MHz, *d*<sub>6</sub>-DMSO)  $\delta$  3.94 (s, 6H), 5.26 (s, 4H), 5.29 (s, 4H), 7.48 (d,  $J = 2.7$  Hz, 2H), 7.78 (d,  $J = 1.2$  Hz, 2H), 7.85 (d,  $J = 1.2$  Hz, 2H), 11.30 (d,  $J = 2.7$  Hz, 2H); and then **103** as an oil after concentration under reduced pressure. LCMS (Method A, UV, ESI)  $R_t = 1.51$  min,  $[M-H]^+ = 507/509/511$ , 97% purity; <sup>1</sup>H NMR (400 MHz, *d*<sub>6</sub>-DMSO)  $\delta$  3.03 (dd, <sup>2</sup> $J =$



18 Hz,  $J = 7.6$  Hz, 1 H), 3.55 (dd,  $^2J = 18$  Hz,  $J = 9.2$  Hz, 1 H), 3.80 (s, 3 H), 3.94 (s, 3 H), 5.39 (t,  $J = 8.5$  Hz, 1 H), 7.02 (s, 1 H), 7.36 (s, 1 H), 7.37 (d,  $J = 1.2$  Hz, 1 H), 7.56 (d,  $J = 1.2$  Hz, 1 H), 7.81 (d,  $J = 1.2$  Hz, 1 H), 7.98 (d,  $J = 1.2$  Hz, 1 H), 11.24 (s, 1 H).

**METHOD B:** A solution of triethylsilane (0.19 mL, 1.18 mmol) and trichloroacetic acid (96 mg, 0.59 mmol) in toluene (2 mL) was heated to 70 °C under an atmosphere of nitrogen. A solution of methyl 5-bromo-1*H*-indole-7-carboxylate (100 mg, 0.39 mmol) and 3-oxetanone (0.03 mL, 0.43 mmol) in toluene (2 mL) was added dropwise over 5 min. The reaction mixture was heated at 70 °C for 18 h. More 3-oxetanone (0.03 mL, 0.433 mmol) was added and stirring was continued at 70 °C for 3 h. A further portion of 3-oxetanone (0.12 mL, 1.97 mmol) was added and stirring was continued at 70 °C for 1 h. Finally, more 3-oxetanone (0.12 mL, 1.97 mmol), triethylsilane (0.19 mL, 1.18 mmol) and trichloroacetic acid (96 mg, 0.59 mmol) were added to the mixture and stirring was continued for 18 h. The mixture was cooled to room temperature and quenched with saturated aqueous NaHCO<sub>3</sub> solution (10 mL). The aqueous phase was extracted with DCM (3 x 10 mL) and the combined organic extracts were dried by passing through a hydrophobic frit then concentrated under reduced pressure to afford **102** (212 mg, 74%) as an oil. LCMS (Method A, UV, ESI)  $R_t = 1.38$  min,  $[M-H]^- = 559/561/563$ , 77% purity.

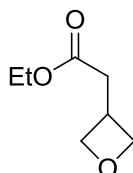
### 6.8.3. Ethyl 2-(oxetan-3-ylidene)acetate, **107**



(Carbethoxymethylene)triphenylphosphorane (1.28 g, 3.66 mmol) was added to a solution of 3-oxetanone (0.24 g, 3.33 mmol) in DCM (5 mL) at 0 °C under an atmosphere of nitrogen. The solution was allowed to warm to room temperature and stirring was continued for 30 min. The solution was added to the top of a 20 g silica cartridge and eluted with cyclohexane/EtOAc (2 CV of a 2:1v/v mixture). The product-containing fractions were concentrated under reduced pressure

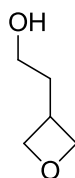
to afford **107** (0.39 g, 81%) as a colourless oil. LCMS (Method A, UV, ESI)  $R_t = 0.64$  min,  $[M-H]^+ = 143$ , 98% purity;  $^1\text{H NMR}$  (400 MHz,  $\text{CDCl}_3$ )  $\delta$  1.28 (t,  $J = 7.2$  Hz, 3 H), 4.17 (q,  $J = 7.1$  Hz, 2 H), 5.30 – 5.35 (m, 2 H), 5.50 – 5.55 (m, 2 H), 5.63 – 5.67 (m, 1 H). This is consistent with literature data.<sup>4</sup>

#### 6.8.4. Ethyl 2-(oxetan-3-yl)acetate, **108**



A solution of ethyl 3-oxetanylideneacetate (323 mg, 2.27 mmol) in EtOH (40 mL) was hydrogenated at room temperature and 8 bar  $\text{H}_2$  on the H-Cube using a 10% Pd/C CatCart<sup>®</sup>. The solution was concentrated to dryness under a stream of nitrogen to afford **108** (262 mg, 76%) as a colourless oil.  $^1\text{H NMR}$  (400 MHz,  $\text{CDCl}_3$ )  $\delta$  1.25 (t,  $J = 7.1$  Hz, 3 H), 2.72 (d,  $J = 8.1$  Hz, 2 H), 3.31-3.42 (m, 1 H), 4.13 (q,  $J = 7.1$  Hz, 2 H), 4.43 (dd,  $^2J = 7.8$  Hz,  $J = 6.3$  Hz, 2 H), 5.52 (dd,  $^2J = 7.8$  Hz,  $J = 6.3$  Hz, 2 H). LCMS data was not recorded due to the inability to detect (no chromophore present).

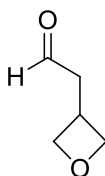
#### 6.8.5. 2-(Oxetan-3-yl)ethanol, **109**



Lithium aluminium hydride (3.3 mL of a 1 M solution in THF, 3.3 mmol) was added dropwise to a solution of ethyl 3-oxetanylacetate (470 mg, 3.3 mmol) in THF (5 mL) at 1 °C. The mixture was stirred at 1-2 °C for 2 h then allowed to warm to room temperature; stirring was continued for 1 h. The mixture was cooled to 1-2 °C, quenched by slow addition of water (5 mL) and stirring was continued for 30 min. The resulting solid was removed by suction filtration and washed with THF (~10 mL). The filtrate was concentrated under reduced pressure and the residue was taken up in  $\text{CHCl}_3$  (10 mL). The resulting solid was removed by suction filtration

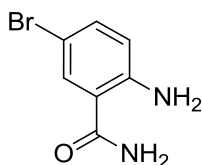
and the filtrate was concentrated under reduced pressure to afford **109** (281 mg, 68%) as a yellow oil.  $^1\text{H NMR}$  (400 MHz,  $\text{CDCl}_3$ )  $\delta$  1.98 (q,  $J = 6.5$  Hz, 2 H), 3.10-3.21 (m, 1 H), 3.62 (t,  $J = 6.4$  Hz, 2 H), 4.47 (t,  $J = 6.2$  Hz, 2 H), 5.52 (dd,  $^2J = 7.9$  Hz,  $J = 5.9$  Hz, 2 H), one proton was not observed. LCMS data was not recorded due to the inability to detect (no chromophore present). This is consistent with literature data.<sup>5</sup>

#### 6.8.6. 2-(Oxetan-3-yl)acetaldehyde, **110**



A solution of 2-(oxetan-3-yl)ethanol (0.34 g, 3.32 mmol) in DCM (10 mL) was added to a mixture of DMP (1.71 g, 4.03 mmol) in DCM (15 mL) at room temperature under an atmosphere of nitrogen. The reaction mixture was stirred for 4 h then poured into a solution of sodium thiosulfate (5.25 g, 33.2 mmol) in saturated aqueous  $\text{Na}_2\text{CO}_3$  solution (50 mL). The mixture was stirred vigorously for 30 min then the organic phase was separated and washed with saturated aqueous  $\text{NaHCO}_3$  solution (50 mL) and water (50 mL). The organic phase was dried by passing through a hydrophobic frit and concentrated under reduced pressure to afford **110** (90 mg, 16%) as a yellow oil.  $^1\text{H NMR}$  (400 MHz,  $\text{CDCl}_3$ )  $\delta$  1.96 (d,  $J = 7.3$  Hz, 2 H), 3.37-3.50 (m, 1 H), 4.39 (dd,  $^2J = 7.8$  Hz,  $J = 6.3$  Hz, 2 H), 4.91 (dd,  $^2J = 7.8$  Hz,  $J = 6.3$  Hz, 2 H), 9.79 (s, 1 H). LCMS data was not recorded due to the inability to detect (no chromophore present).

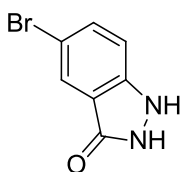
#### 6.8.7. 2-Amino-5-bromobenzamide, **114**



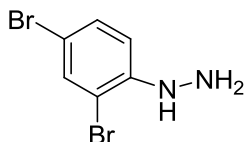
A mixture of 2-amino-5-bromobenzoic acid (1.05 g, 4.86 mmol), HATU (2.03 g, 5.35 mmol) and DIPEA (0.93 mL, 5.35 mmol) in DMF (10 mL) was stirred

at room temperature. After 30 min,  $\text{NH}_3$  (2.78 mL of a 7 M solution in MeOH, 19.44 mmol) was added and stirring was continued for 30 min. A solid precipitated and was removed by suction filtration. The filtrate was concentrated under reduced pressure and the residue was partitioned between EtOAc (100 mL) and water (100 mL). The aqueous phase was extracted with further EtOAc (2 x 50 mL). The combined organic extracts were washed with water (5 x 50 mL) and brine (50 mL), dried by passing through a hydrophobic frit and concentrated under reduced pressure to afford **114** (0.87 g, 81%) as a cream solid. LCMS (Method A, UV, ESI)  $R_t = 0.67$  min,  $[\text{M-H}]^+ = 215/217$ , 97% purity;  $^1\text{H NMR}$  (400 MHz,  $d_6$ -DMSO)  $\delta$  6.70 (d,  $J = 8.8$  Hz, 1 H), 6.72 (br. s, 2 H), 7.16 (br. s, 1 H), 7.24 (dd,  $J = 8.8$  Hz,  $J = 2.3$  Hz, 1 H), 7.70 (d,  $J = 2.3$  Hz, 1 H), 7.83 (br. s, 1 H).

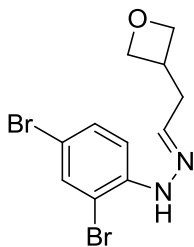
#### 6.8.8. 5-Bromo-1,2-dihydro-3H-indazol-3-one, **115**



Concentrated HCl (0.5 mL, 16.5 mmol) was added to a suspension of 2-amino-5-bromobenzamide (106 mg, 0.49 mmol) in water (1 mL) at 0 °C. A cooled solution of sodium nitrite (51 mg, 0.74 mmol) in water (1 mL) was then added and stirring was continued for 1 h. The mixture was added to an ice-cooled solution of sodium metabisulfite (281 mg, 1.48 mmol) in water (1 mL) and Et<sub>2</sub>O (1 mL). Stirring was continued for 30 min at 0 °C then at room temperature for 1 h. The pH was adjusted to 14 by addition of NaOH (as a 2 M aqueous solution) and the aqueous phase was extracted with EtOAc (3 x 10 mL). The combined organic extracts were concentrated under reduced pressure. The crude material was purified by MDAP Method A2 and the product-containing fractions were concentrated under reduced pressure to afford **115** (10 mg, 9%) as a white solid. LCMS (Method A, UV, ESI)  $R_t = 0.64$  min,  $[\text{M-H}]^+ = 213/215$ , 100% purity;  $^1\text{H NMR}$  (400 MHz,  $d_6$ -DMSO)  $\delta$  7.28 (d,  $J = 8.8$  Hz, 1 H), 7.38 (dd,  $J = 8.8$  Hz,  $J = 1.6$  Hz, 1 H), 7.80 (d,  $J = 1.6$  Hz, 1 H), 11.04 (br. s, 2 H).

**6.8.9. 2,4-(Dibromophenyl)hydrazine, 117**

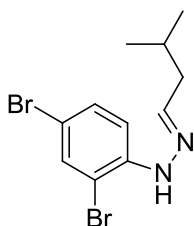
A cooled solution of sodium nitrite (0.24 g, 3.46 mmol) in water (5 mL) was added dropwise to 2,4-dibromoaniline (0.50 g, 1.99 mmol) in concentrated HCl (5 mL, 165 mmol) at 1-2 °C. The mixture was stirred for 1 h then a solution of tin(II) chloride dihydrate (1.35 g, 5.98 mmol) in concentrated HCl (5 mL, 165 mmol) was added dropwise. The reaction mixture was allowed to warm to room temperature and stirring was continued for 18 h. The mixture was cooled to 0 °C and the pH was adjusted to 14 by addition of NaOH (as a 50% w/v aqueous solution) and the aqueous phase was extracted with EtOAc (3 x 20 mL). The combined organic extracts were washed with water (10 mL) and brine (10 mL), dried by passing through a hydrophobic frit and concentrated under reduced pressure. The crude material was purified by chromatography on FlashMaster II silica (20 g), eluting with 0-100% EtOAc/cyclohexane over 20 min. The product-containing fractions were concentrated under reduced pressure to afford **117** (0.35 g, 63%) as a white solid. LCMS (Method A, UV, ESI)  $R_t = 0.72$  min,  $[M-H]^+ = 186/188$ , 100% purity;  $^1H$  NMR (400 MHz,  $d_6$ -DMSO)  $\delta$  4.20 (s, 2 H), 6.48 (br. s, 1 H), 7.12 (d,  $J = 8.8$  Hz, 1 H), 7.35 (dd,  $J = 8.8$  Hz,  $J = 2.3$  Hz, 1 H), 7.51 (d,  $J = 2.0$  Hz, 1 H).

**6.8.10. 1-(2,4-Dibromophenyl)-2-(2-(oxetan-3-yl)ethylidene)hydrazine, 118**

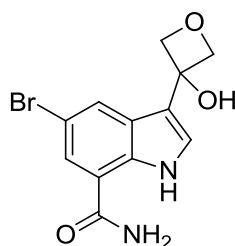
A solution of 2-(oxetan-3-yl)acetaldehyde (57 mg, 0.57 mmol) in toluene (1 mL) was added to (2,4-dibromophenyl)hydrazine (150 mg, 0.56 mmol) in toluene

(1.5 mL) and the mixture was stirred at room temperature for 5 h then at 60 °C for 1 h. The mixture was cooled to room temperature and stirring was continued for 18 h. The mixture was concentrated under reduced pressure and Et<sub>2</sub>O (2 mL) was added to the residue. The solvent was removed under reduced pressure and the crude material was purified by chromatography on FlashMaster II silica (10 g), eluting with 0-100% DCM/cyclohexane over 30 min. The product-containing fractions were concentrated under reduced pressure to afford **118** (45 mg, 20%) as an orange oil. LCMS (Method A, UV, ESI)  $R_t = 1.19$  min,  $[M-H]^+ = 347/349/351$ , 88% purity; <sup>1</sup>H NMR (400 MHz, CDCl<sub>3</sub>)  $\delta$  2.74 (dd,  $J = 7.3$  Hz, 4.3 Hz, 2 H), 3.30-3.47 (m, 1 H), 4.49 (t,  $J = 6.2$  Hz, 2 H), 4.85-4.98 (m, 2 H), 7.24 (t,  $J = 4.5$  Hz, 1 H), 7.26 (d,  $J = 8.8$  Hz, 1 H), 7.35 (dd,  $J = 8.8$  Hz,  $J = 2.3$  Hz, 1 H), 7.56 (d,  $J = 2.3$  Hz, 1 H), 7.71 (br. s, 1 H); <sup>13</sup>C NMR (151 MHz, CHCl<sub>3</sub>)  $\delta$  32.6, 35.9, 77.1 (2C), 106.5, 110.9, 115.2, 131.4, 134.1, 140.3, 141.1.

#### 6.8.11. 1-(2,4-Dibromophenyl)-2-(3-methylbutylidene)hydrazine, **120**



A solution of isovaleraldehyde (0.06 mL, 0.51 mmol) was added to (2,4-dibromophenyl)hydrazine (136 mg, 0.51 mmol) in toluene (2 mL) and the mixture was stirred at room temperature for 4 h. The solvent was removed under reduced pressure to afford **120** (140 mg, 66%) as an orange oil. LCMS (Method A, UV, ESI)  $R_t = 1.57$  min,  $[M-H]^+ = 333/335/337$ , 80% purity; <sup>1</sup>H NMR (400 MHz, CDCl<sub>3</sub>)  $\delta$  1.00 (d,  $J = 6.6$  Hz, 6 H), 1.85-1.95 (m, 1 H), 2.22 (t,  $J = 6.3$  Hz, 2 H), 7.18 (t,  $J = 4.3$  Hz, 1 H), 7.23 (d,  $J = 8.8$  Hz, 1 H), 7.26 (dd,  $J = 8.8$  Hz,  $J = 2.3$  Hz, 1 H), 7.27 (d,  $J = 2.3$  Hz, 1 H), 7.54 (br. s, 1 H).

**6.8.12. 5-Bromo-3-(3-hydroxyoxetan-3-yl)-1H-indole-7-carboxamide, 86**

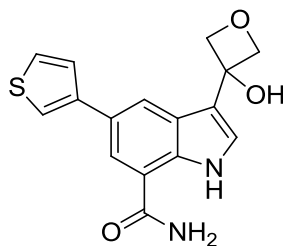
**METHOD A:** Methylmagnesium bromide (3.1 mL of a 3 M solution in Et<sub>2</sub>O, 9.3 mmol) was added dropwise to a suspension of 5-bromo-1H-indole-7-carboxamide (2.0 g, 8.4 mmol) in DCM (50 mL) at 0 °C under an atmosphere of nitrogen. The mixture was allowed to warm to room temperature and stirred for 1 h. A solution of 3-oxetanone (0.7 g, 9.2 mmol) in DCM (5 mL) was added dropwise and stirring was continued for 2 h. The mixture was quenched with saturated aqueous NH<sub>4</sub>Cl solution (50 mL) and stirring was continued for 30 min. The aqueous phase was extracted with DCM (3 x 20 mL) and the combined organic extracts were concentrated under reduced pressure to afford **86** (98 mg, 3%) as an orange oil. LCMS (Method A, UV, ESI)  $R_t = 0.60$  min,  $[M-H]^- = 308/310$ , 77% purity.

**METHOD B:** A mixture of 5-bromo-3-(3-hydroxyoxetan-3-yl)-1H-indole-7-carboxylic acid (1.11 g, 3.6 mmol), HATU (1.49 g, 3.9 mmol) and DIPEA (0.683 mL, 3.9 mmol) in DMF (20 mL) was stirred at room temperature under an atmosphere of nitrogen. After 30 min, NH<sub>3</sub> (as a 0.5 M solution in 1,4-dioxane, 7.82 mL, 3.9 mmol) was added and stirring was continued for 40 min. The mixture was concentrated under reduced pressure and the residue was taken up in EtOAc (50 mL). The organic phase was washed with water (3 x 50 mL) and brine (50 mL). The solvent was removed under a stream of nitrogen and the crude material was purified by chromatography on a C18 column (130 g), eluting with 5-95% MeCN/water with an ammonium bicarbonate modifier over 10 CV. The product-containing fractions were concentrated under reduced pressure to afford **86** (378 mg, 34%) as a pale brown solid. Mp 116-118 °C. LCMS (Method A, UV, ESI)  $R_t = 0.59$  min,  $[M-H]^+ = 309/311$ , 99% purity; <sup>1</sup>H NMR (400 MHz, *d*<sub>6</sub>-DMSO)  $\delta$  4.75 – 4.88 (m, 4 H), 6.16 (s, 1 H), 7.42 (d,  $J = 2.5$  Hz, 1 H), 7.49 (br. s, 1 H), 7.88 (d,  $J = 1.5$  Hz, 1 H), 8.00 (d,  $J$

= 1.5 Hz, 1 H), 8.15 (br. s, 1 H), 11.18 (s, 1 H);  $^{13}\text{C}$  NMR (101 MHz,  $d_6$ -DMSO)  $\delta$  71.3, 84.4 (2C), 110.4, 117.6, 118.1, 122.9, 125.0, 125.1, 128.2, 134.1, 167.7; IR ( $\nu_{\text{max}}/\text{cm}^{-1}$ ): 1660, 3358 (br.); HR-ESIMS ( $m/z$ ) calcd for  $\text{C}_{12}\text{H}_{12}\text{N}_2\text{O}_3\text{Br}$  [ $\text{M}^+$ ] 311.0031, found 311.0022.

**METHOD C:** A solution of 4-*tert*-butyl-2,6-dimethylphenylsulfur trifluoride (30 mg, 0.12 mmol) in DCM (0.5 mL) was added dropwise to a solution of 5-bromo-3-(3-hydroxyoxetan-3-yl)-1*H*-indole-7-carboxylic acid (25 mg, 0.08 mmol) in DCM (0.5 mL) at 0 °C under an atmosphere of nitrogen. The mixture was stirred at 0 °C for 30 min then  $\text{NH}_3$  (as a 28% aqueous solution, 2 mL) was added slowly to the reaction mixture and stirring was continued for 15 min to afford **86** (not isolated). LCMS (Method A, UV, ESI)  $R_t = 0.59$  min,  $[\text{M}-\text{H}]^+ = 309/311$ .

**6.8.13. 3-(3-Hydroxyoxetan-3-yl)-5-(thiophen-3-yl)-1*H*-indole-7-carboxamide, **122a****

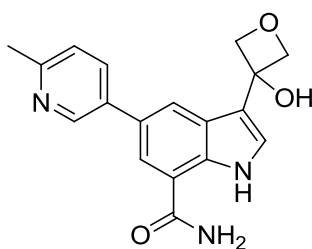


A mixture of 5-bromo-3-(3-hydroxyoxetan-3-yl)-1*H*-indole-7-carboxamide (57 mg, 0.14 mmol), 4,4,5,5-tetramethyl-2-(thiophen-3-yl)-1,3,2-dioxaborolane (89 mg, 0.42 mmol),  $\text{Pd}(\text{PPh}_3)_4$  (17 mg, 0.02 mmol) and  $\text{K}_2\text{CO}_3$  (122 mg, 0.88 mmol) in IPA (1 mL) and water (0.1 mL) was degassed with nitrogen before being heated in the microwave at 100 °C for 1 h. The reaction mixture was partitioned between EtOAc (10 mL) and water (10 mL). The aqueous phase was extracted further with EtOAc (2 x 10 mL). The combined organic extracts were dried by passing through a hydrophobic frit and concentrated under a stream of nitrogen. The crude material was purified by MDAP Method B2 and the product-containing fractions were concentrated under reduced pressure to afford **122a** (14 mg, 30%) as a cream solid. Mp 204 °C (decomposed). LCMS (Method A, UV, ESI)  $R_t = 0.71$  min,  $[\text{M}-\text{H}]^+ = 313$ , 100% purity;  $^1\text{H}$  NMR (400 MHz,  $d_4$ -MeOH)  $\delta$  4.99 (d,  $^2J = 6.6$  Hz, 2 H), 5.07

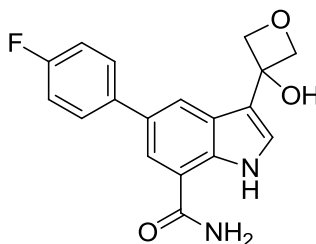


(d,  $^2J = 6.6$  Hz, 2 H), 7.45 (s, 1 H), 7.46 (dd,  $J = 5.4$  Hz, 3.0 Hz, 1 H), 7.54 (dd,  $J = 5.4$  Hz, 1.3 Hz, 1 H), 7.62 (dd,  $J = 2.7$  Hz, 1.3 Hz, 1 H), 8.04 (d,  $J = 1.3$  Hz, 1 H), 8.22 (d,  $J = 1.3$  Hz, 1 H), four protons not observed;  $^{13}\text{C}$  NMR (101 MHz,  $d_6$ -DMSO)  $\delta$  72.4, 84.8 (2C), 116.0, 117.6, 118.8, 119.9, 120.8, 123.5, 125.6, 126.0, 127.1, 127.2, 135.3, 142.6, 171.1; IR ( $\nu_{\text{max}}/\text{cm}^{-1}$ ): 1650, 3142 (br.), 3335 (br.); HR-ESIMS ( $m/z$ ) calcd for  $\text{C}_{16}\text{H}_{15}\text{N}_2\text{O}_3\text{S}$  [ $\text{M}^+$ ] 315.0803, found 315.0806.

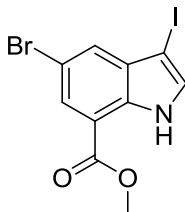
**6.8.14. 3-(3-Hydroxyoxetan-3-yl)-5-(6-methylpyridin-3-yl)-1H-indole-7-carboxamide, 122b**



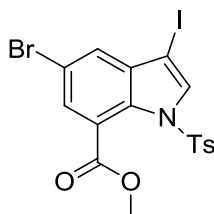
A mixture of 5-bromo-3-(3-hydroxyoxetan-3-yl)-1H-indole-7-carboxamide (50 mg, 0.12 mmol), (6-methylpyridin-3-yl)boronic acid (50 mg, 0.37 mmol),  $\text{Pd}(\text{PPh}_3)_4$  (15 mg, 0.01 mmol) and  $\text{K}_2\text{CO}_3$  (103 mg, 0.74 mmol) in IPA (1 mL) and water (0.1 mL) was degassed with nitrogen before being heated in the microwave at 100 °C for 1 h. The mixture was partitioned between EtOAc (10 mL) and water (10 mL). The aqueous phase was extracted further with EtOAc (2 x 10 mL). The combined organic extracts were concentrated under a stream of nitrogen. The crude material was purified by MDAP Method A1 and the product-containing fractions were concentrated under reduced pressure to afford **122b** (8 mg, 17%) as a cream solid. LCMS (Method A, UV, ESI)  $R_t = 0.39$  min,  $[\text{M}-\text{H}]^+ = 324$ , 100% purity;  $^1\text{H}$  NMR (400 MHz,  $d_4$ -MeOH)  $\delta$  2.61 (s, 3 H), 5.03 (d,  $^2J = 6.8$  Hz, 2 H), 5.09 (d,  $^2J = 6.8$  Hz, 2 H), 7.43 (d,  $J = 8.1$  Hz, 1 H), 7.53 (s, 1 H), 8.03 (d,  $J = 1.5$  Hz, 1 H), 8.12 (dd,  $J = 8.1$  Hz,  $J = 1.5$  Hz, 1 H), 8.23 (d,  $J = 1.5$  Hz, 1 H), 8.78 (d,  $J = 2.3$  Hz, 1 H), four protons not observed;  $^{13}\text{C}$  NMR (151 MHz,  $d_6$ -DMSO)  $\delta$  23.7, 71.5, 84.5 (2C), 117.3, 118.3, 119.9, 121.0, 123.0, 124.5, 127.3, 127.6, 133.7, 134.4, 135.1, 147.1, 155.9, 168.9; IR ( $\nu_{\text{max}}/\text{cm}^{-1}$ ): 1671, 3159 (br.), 3350 (br.); HR-ESIMS ( $m/z$ ) calcd for  $\text{C}_{18}\text{H}_{18}\text{N}_3\text{O}_3$  [ $\text{M}^+$ ] 324.1348, found 324.1346.

**6.8.15. 5-(4-Fluorophenyl)-3-(3-hydroxyoxetan-3-yl)-1H-indole-7-carboxamide, 122c**

5-bromo-3-(3-hydroxyoxetan-3-yl)-1H-indole-7-carboxamide (148 mg, 0.41 mmol), (4-fluorophenyl)boronic acid (174 mg, 1.24 mmol), Pd(PPh<sub>3</sub>)<sub>4</sub> (48 mg, 0.04 mmol) and K<sub>2</sub>CO<sub>3</sub> (343 mg, 2.483 mmol) in IPA (2 mL) and water (0.2 mL) was degassed with nitrogen before being heated in the microwave at 100 °C for 3 h. The reaction mixture was partitioned between EtOAc (10 mL) and water (10 mL). The aqueous phase was extracted further with EtOAc (2 x 10 mL). The combined organic extracts were dried by passing through a hydrophobic frit and concentrated under reduced pressure. The crude material was purified by chromatography on FlashMaster II silica (10 g), eluting with 0-100% EtOAc/DCM over 30 min. The product-containing fractions were concentrated under reduced pressure and the residue was purified further by MDAP Method B2. The product-containing fractions were concentrated under reduced pressure to afford **122c** (12 mg, 9%) as a white solid. LCMS (Method A, UV, ESI)  $R_t = 0.76$  min,  $[M-H]^- = 325$ , 100% purity; <sup>1</sup>H NMR (400 MHz, *d*<sub>6</sub>-DMSO)  $\delta$  4.84 (d, <sup>2</sup>*J* = 6.6 Hz, 2 H), 4.89 (d, <sup>2</sup>*J* = 6.6 Hz, 2 H), 6.11 (s, 1 H), 7.28 – 7.36 (m, 2 H), 7.40 (d, *J* = 2.5 Hz, 1 H), 7.41 (br. s, 1 H), 7.74 – 7.80 (m, 2 H), 8.01 (d, *J* = 1.3 Hz, 1 H), 8.09 (d, *J* = 1.3 Hz, 1 H), 8.23 (br. s, 1 H), 11.03 (s, 1 H).

**6.8.16. Methyl 5-bromo-3-iodo-1*H*-indole-7-carboxylate, 126**

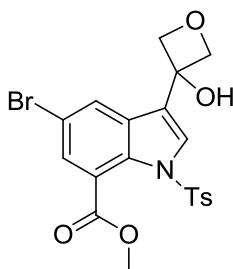
A mixture of methyl 5-bromo-1*H*-indole-7-carboxylate (5.0 g, 19.7 mmol) and NIS (4.4 g, 19.7 mmol) in DCM (100 mL) was stirred at room temperature under an atmosphere of nitrogen for 1 h. More DCM (50 mL) was added and the organic phase was washed with water (50 mL) and brine (50 mL) then dried by passing through a hydrophobic frit. The solvent was removed under reduced pressure and the crude material was purified by chromatography on FlashMaster II silica (2 x 100 g), eluting with 0-50% EtOAc/cyclohexane over 40 min. The product-containing fractions were concentrated under reduced pressure to afford **126** (6.07 g, 76%) as a brown solid. LCMS (Method A, UV, ESI)  $R_t = 1.31$  min,  $[M-H]^- = 378/380$ , 94% purity;  $^1\text{H NMR}$  (400 MHz,  $d_6$ -DMSO)  $\delta$  3.95 (s, 3 H), 7.65 (d,  $J = 2.8$  Hz, 1 H), 7.70 (d,  $J = 1.8$  Hz, 1 H), 7.87 (d,  $J = 1.8$  Hz, 1 H), 11.73 (s, 1 H).

**6.8.17. Methyl 5-bromo-3-iodo-1-tosyl-1*H*-indole-7-carboxylate, 127**

NaH (0.79 g of a 60% dispersion in mineral oil, 19.8 mmol) was added portionwise to a solution of methyl 5-bromo-3-iodo-1*H*-indole-7-carboxylate (6.85 g, 18.1 mmol) in DMF (60 mL) at 0 °C under an atmosphere of nitrogen. The mixture was stirred at 0 °C for 10 min then at room temperature for 30 min. TsCl (3.78 g, 19.8 mmol) was added and stirring was continued for 3 h. The solvent was removed under reduced pressure, the residue was taken up in DCM (100 mL) and the organic phase was washed with water (100 mL). The aqueous phase was extracted with DCM (50 mL) and the combined organic extracts were washed with brine (50 mL)

and dried by passing through a hydrophobic frit. Florisil<sup>®</sup> (~2 g) was added and the solvent was removed under reduced pressure. The crude material was purified by chromatography on FlashMaster II silica (2 x 100 g), eluting with 0-25% EtOAc/cyclohexane over 1 h to afford an oil. The oil was taken up in Et<sub>2</sub>O (10 mL) to force solidification and the solvent was removed under reduced pressure. The residue was dried on a high vacuum line (0.01 mmHg) for 30 min to afford **127** (6.18 g, 69%) as a white solid. LCMS (Method A, UV, ESI)  $R_t = 1.44$  min,  $[M-H]^+ = 534/536$ , 100% purity; <sup>1</sup>H NMR (400 MHz, *d*<sub>6</sub>-DMSO)  $\delta$  2.36 (s, 3 H), 3.84 (s, 3 H), 7.40 (d,  $J = 8.2$  Hz, 2 H), 7.65 (d,  $J = 2.0$  Hz, 1 H), 7.71 (d,  $J = 8.2$  Hz, 2 H), 7.73 (d,  $J = 2.0$  Hz, 1 H), 8.19 (s, 1 H).

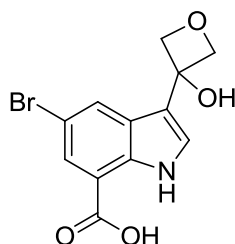
**6.8.18. Methyl 5-bromo-3-(3-hydroxyoxetan-3-yl)-1-tosyl-1H-indole-7-carboxylate, 129**



*i*-PrMgCl.LiCl (7.90 mL, 10.28 mmol) was added dropwise to a solution of methyl 5-bromo-3-iodo-1-tosyl-1H-indole-7-carboxylate (4.99 g, 9.34 mmol) in THF (40 mL) at -15 °C under an atmosphere of nitrogen. The mixture was stirred at -15 °C for 20 min. A solution of 3-oxetanone (0.77 g, 10.67 mmol) in THF (5 mL) was added dropwise and stirring was continued at 0 °C for 15 min. The mixture was allowed to warm to 10 °C and saturated aqueous NH<sub>4</sub>Cl (50 mL) was added. The aqueous mixture was extracted with EtOAc (2 x 50 mL) and the combined organic extracts were dried by passing through a hydrophobic frit and concentrated under reduced pressure. The crude material was purified by chromatography on FlashMaster II silica (2 x 100 g), eluting with 0-50% EtOAc/cyclohexane over 40 min to give a foam that was dried on a high vacuum line (0.01 mmHg) for 24 h to afford **129** (4.37 g, 97%) as a pale yellow solid. Mp 73-75 °C. LCMS (Method A, UV, ESI)  $R_t = 1.06$  min, 100% purity; <sup>1</sup>H NMR (400 MHz, *d*<sub>6</sub>-DMSO)  $\delta$  2.35 (s, 3

H), 3.83 (s, 3 H), 4.73 – 4.77 (m, 4 H), 6.51 (s, 1 H), 7.39 (d,  $J = 8.5$  Hz, 2 H), 7.64 (d,  $J = 2.0$  Hz, 1 H), 7.70 (d,  $J = 8.5$  Hz, 2 H), 7.91 (s, 1 H), 7.99 (d,  $J = 2.0$  Hz, 1 H);  $^{13}\text{C}$  NMR (151 MHz,  $d_6$ -DMSO)  $\delta$  21.0, 52.6, 70.6, 83.1 (2 C), 116.2, 123.7, 125.8, 126.6, 126.7 (2C), 127.3, 127.7, 129.9 (2C), 130.8, 132.3, 133.9, 145.5, 166.3; IR ( $\nu_{\text{max}}$  / $\text{cm}^{-1}$ ): 1172, 1266, 1730, 3395 (br.); HR-ESIMS ( $m/z$ ) calcd for  $\text{C}_{20}\text{H}_{19}\text{BrNO}_6\text{S}$  [ $\text{M}^+$ ] 480.0111, found 480.0106.

#### 6.8.19. 5-Bromo-3-(3-hydroxyoxetan-3-yl)-1H-indole-7-carboxylic acid, **131**

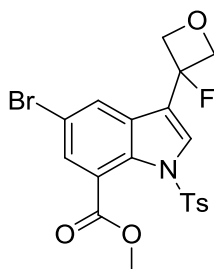


**METHOD A:** NaOH (as a 2 M aqueous solution, 10 mL) was added to a solution of methyl 5-bromo-3-(3-hydroxyoxetan-3-yl)-1-tosyl-1H-indole-7-carboxylate (1.75 g, 3.6 mmol) in 1,4-dioxane (10 mL). The mixture was stirred at room temperature for 72 h. More NaOH (as a 2 M aqueous solution, 2 mL) was added and stirring was continued for 2 h. The mixture was diluted with water (50 mL) and washed with DCM (50 mL). The aqueous phase was then acidified to pH 1 with HCl (as a 2 M aqueous solution) and extracted with EtOAc (3 x 100 mL). The combined organic extracts were dried by passing through a hydrophobic frit and concentrated under reduced pressure. The resulting foam was dried further on a high vacuum line (0.01 mmHg) overnight to afford **131** (1.23 g, 84%) as a yellow solid. LCMS (Method A, UV, ESI)  $R_t = 0.70$  min,  $[\text{M}-\text{H}]^- = 310/312$ , 78% purity;  $^1\text{H}$  NMR (400 MHz,  $d_6$ -DMSO)  $\delta$  4.80 – 4.85 (m, 4 H), 6.20 (s, 1 H), 7.46 (d,  $J = 2.5$  Hz, 1 H), 7.81 (d,  $J = 1.8$  Hz, 1 H), 8.10 (d,  $J = 1.8$  Hz, 1 H), 11.17 (s, 1 H), 13.28-13.48 (br. s, 1 H).

**METHOD B:** NaOH (as a 2 M aqueous solution, 0.3 mL) was added to a solution of methyl 5-bromo-3-(3-fluorooxetan-3-yl)-1-tosyl-1H-indole-7-carboxylate (16 mg, 0.28 mmol) in 1,4-dioxane (0.6 mL) at room temperature. The mixture was concentrated under reduced pressure to give a white solid. The residue was taken up

in 1,4-dioxane (2 mL) and NaOH (as a 2M aqueous solution, 1 mL) was added. The mixture was stirred at room temperature for 18 h then water (5 mL) was added. The aqueous phase was extracted with DCM (5 mL) then acidified to pH 1 with HCl (as a 2 M aqueous solution) and the resulting solid was collected by suction filtration. The crude material was purified by MDAP Method A2 and the product-containing fractions were concentrated under reduced pressure to afford **131** (3 mg, 28%) as a white solid. LCMS (Method A, UV, ESI)  $R_t = 0.70$  min,  $[M-H]^- = 310/312$ , 97% purity;  $^1H$  NMR (400 MHz,  $d_6$ -DMSO)  $\delta$  4.80-4.83 (m, 4 H), 6.19 (br. s, 1 H), 7.44 (d,  $J = 2.3$  Hz, 1 H), 7.79 (d,  $J = 1.8$  Hz, 1 H), 8.09 (d,  $J = 1.8$  Hz, 1 H), 11.16 (s, 1 H), one proton not observed.

**6.8.20. Methyl 5-bromo-3-(3-fluorooxetan-3-yl)-1-tosyl-1H-indole-7-carboxylate, 132**



**METHOD A:** DAST (0.14 mL, 1.08 mmol) was added dropwise to a solution of methyl 5-bromo-3-(3-hydroxyoxetan-3-yl)-1-tosyl-1H-indole-7-carboxylate (493 mg, 1.03 mmol) in DCM (5 mL) at  $-78$  °C under an atmosphere of nitrogen. The reaction mixture was poured onto ice and neutralised with saturated aqueous  $NaHCO_3$  solution. The aqueous phase was extracted with DCM (2 x 20 mL) and the combined organic extracts were dried by passing through a hydrophobic frit and concentrated under a stream of nitrogen. The crude material was purified by chromatography on FlashMaster II silica (20 g), eluting with 0-50% EtOAc/cyclohexane over 40 min to give an oil that was dried on a high vacuum line (0.01 mmHg) for 30 min to afford **132** (145 mg, 28%) as a white solid. LCMS (Method A, UV, ESI)  $R_t = 1.24$  min,  $[M-H]^+ = 482/484$ , 99% purity;  $^1H$  NMR (400 MHz,  $d_6$ -DMSO)  $\delta$  2.36 (s, 3 H), 3.83 (s, 3 H), 4.98-5.09 (m, 4 H), 7.43 (d,  $J = 8.3$

Hz, 2 H), 7.71 (d,  $J = 1.8$  Hz, 1 H), 7.43 (d,  $J = 8.3$  Hz, 2 H), 7.85 (t,  $J = 1.3$  Hz, 1 H), 8.33 (d,  $J = 3.0$  Hz, 1 H).  $^{19}\text{F}$  NMR (377 MHz,  $d_6$ -DMSO)  $\delta$  -139.57;  $^{13}\text{C}$  NMR (101 MHz,  $d_6$ -DMSO)  $\delta$  52.7, 79.7, 79.9, 90.7, 92.7, 116.6, 119.9, 120.2, 123.6, 125.1, 126.8 (2C), 127.9, 129.9 (2C), 130.4, 131.0, 133.9, 145.7, 166.1; HR-ESIMS ( $m/z$ ) calcd for  $\text{C}_{20}\text{H}_{18}\text{BrFNO}_5\text{S}$  [ $\text{M}^+$ ] 482.0068, found 482.0069.

**METHOD B:** A solution of methyl 5-bromo-3-(3-hydroxyoxetan-3-yl)-1-tosyl-1*H*-indole-7-carboxylate (500 mg, 1.04 mmol) in DCM (4 mL) was added dropwise over 10 min to a solution of 4-*tert*-butyl-2,6-dimethylphenylsulfur trifluoride (391 mg, 1.56 mmol) in DCM (4 mL) at 0 °C under an atmosphere of nitrogen. The mixture was stirred at 0 °C for 30 min then poured into cold NaOH (as a 5% w/v aqueous solution, 10 mL) and stirred for 30 min. The aqueous phase was extracted with DCM (2 x 10 mL) and the combined organic extracts were dried over  $\text{MgSO}_4$  then concentrated under a stream of nitrogen. The crude material was purified by chromatography on FlashMaster II silica (20 g), eluting with 0-50% EtOAc/cyclohexane over 30 min. The product-containing fractions were concentrated under reduced pressure to afford **132** (385 mg, 73%) as a white solid. LCMS (Method A, UV, ESI)  $R_t = 1.19$  min,  $[\text{M-H}]^+ = 482/484$ , 98% purity;  $^1\text{H}$  NMR (400 MHz,  $d_6$ -DMSO)  $\delta$  2.36 (s, 3 H), 3.83 (s, 3 H), 4.98-5.09 (m, 4 H), 7.43 (d,  $J = 8.3$  Hz, 2 H), 7.71 (d,  $J = 1.8$  Hz, 1 H), 7.43 (d,  $J = 8.3$  Hz, 2 H), 7.85 (t,  $J = 1.3$  Hz, 1 H), 8.33 (d,  $J = 3.0$  Hz, 1 H).  $^{19}\text{F}$  NMR (377 MHz,  $d_6$ -DMSO)  $\delta$  -140.05.

**6.8.21. Conditions Attempted for the Deoxofluorination of 5-Bromo-3-(3-hydroxyoxetan-3-yl)-1H-indole-7-carboxamide 86**

Reaction	Reagents	Solvent	Atmosphere	Conc (mol/L)	Temp (°C)	Time (h)
1	<b>86</b> (76 mg, 0.244 mmol) Fluolead (92 mg, 0.366 mmol)	DCM (4.5 mL)	N <sub>2</sub>	0.054	1. 0 2. rt	0.5 3
2	<b>86</b> (76 mg, 0.244 mmol) DAST (9 μL, 0.366 mmol)	DCM (1.0 mL)	N <sub>2</sub>	0.064	1. -78 2. 0	0.5 1
3	<b>86</b> (20 mg, 0.064 mmol) DAST (9 μL, 0.366 mmol)	THF (0.5 mL)	N <sub>2</sub>	0.129	1. -78 2. 0 3. rt	0.5 1 1

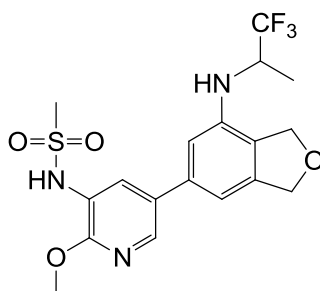


**6.8.22. Conditions Attempted for the Deoxygenation of 5-Bromo-3-(3-hydroxyoxetan-3-yl)-1H-indole-7-carboxamide 86**

Reaction	Reagents	Solvent	Atmosphere	Conc (mol/L)	Temp (°C)	Time (h)
1	<b>86</b> (20 mg, 0.06 mmol) NaBH <sub>4</sub> (3 mg, 0.08 mmol)	THF (1.0 mL)	N <sub>2</sub>	0.064	1. 0	0.5
					2. rt	0.5
2	<b>86</b> (20 mg, 0.06 mmol) LiAlH <sub>4</sub> (0.5 mL of a 1.0 M solution in THF, 0.50 mmol)	THF (0.5 mL)	N <sub>2</sub>	0.129	1. 0	0.5
					2. rt	2
3	(i) <b>86</b> (26 mg, 0.08 mmol) NaH (7 mg of a 60% dispersion in mineral oil, 0.18 mmol) TsCl (34 mg, 0.18 mmol)	THF (0.5 mL)	N <sub>2</sub>	0.167	1. 0	0.5
					2. rt	18
	(ii) LiAlH <sub>4</sub> (0.5 mL of a 1.0 M solution in THF, 0.50 mmol)	1. -78	0.5			
		2. 0	0.5			
	(iii) NaOH (as a 2 M aqueous solution, 1 mL)	1. 0	0.5			
		2. rt	1			

## 6.9. Preparation of Truncated Dihydroisobenzofuran Compounds 175, 176, 178-180.

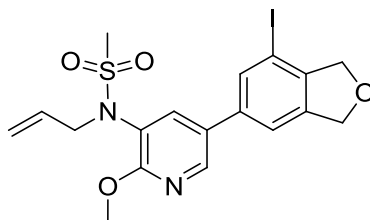
### 6.9.1. *N*-(2-Methoxy-5-(7-((1,1,1-trifluoropropan-2-yl)amino)-1,3-dihydroisobenzofuran-5-yl)pyridin-3-yl)methanesulfonamide, **175**



Sodium cyanoborohydride (13 mg, 0.22 mmol) was added portionwise to *N*-(5-(7-amino-1,3-dihydroisobenzofuran-5-yl)-2-methoxypyridin-3-yl)methanesulfonamide (36 mg, 0.11 mmol) in TFA (1 mL) at 0 °C under an atmosphere of nitrogen. The mixture was stirred for 15 min then 1,1,1-trifluoropropan-2-one (0.012 mL, 0.13 mmol) was added. The mixture was allowed to warm to room temperature and stirring was continued overnight. The mixture was quenched by the addition of saturated aqueous NaHCO<sub>3</sub> solution (2 mL) and the aqueous phase was extracted with DCM (2 x 5 mL). The combined organic extracts were dried by passing through a hydrophobic frit and concentrated under reduced pressure. The crude material was purified by MDAP Method B3 and the product-containing fractions were concentrated under reduced pressure to afford **175** (11 mg, 23%) as a white solid. Mp 94-97 °C; LCMS (Method A, UV, ESI) *R*<sub>t</sub> = 0.98 min, [M-H]<sup>+</sup> = 432, 100% purity; <sup>1</sup>H NMR (600 MHz, *d*<sub>6</sub>-DMSO) δ 1.35 (d, *J* = 7.0 Hz, 3 H), 3.06 (s, 3 H), 3.96 (s, 3 H), 4.59 – 4.67 (m, 1 H), 4.88 - 4.98 (m, 2 H), 4.99 (s, 2 H), 5.55 (d, *J* = 8.8 Hz, 1 H), 6.81 (s, 1 H), 6.92 (s, 1 H), 7.82 (d, *J* = 2.2 Hz, 1 H), 8.28 (d, *J* = 2.2 Hz, 1 H), 9.27 (br. s, 1 H); <sup>13</sup>C NMR (151 MHz, *d*<sub>6</sub>-DMSO) δ 14.3, 40.1, 40.7, 53.6, 71.7, 73.1, 107.9, 108.1, 120.9, 123.1, 130.5, 131.4, 137.4, 140.7, 140.9, 141.4, 156.2, CF<sub>3</sub> and *J*<sub>C-F</sub> couplings too weak to be observed; <sup>19</sup>F NMR (376

MHz,  $d_4$ -MeOH)  $\delta$  -78.4; IR ( $\nu_{\max}$  / $\text{cm}^{-1}$ ): 1134, 1327; HR-ESIMS ( $m/z$ ) calcd for  $\text{C}_{18}\text{H}_{21}\text{F}_3\text{N}_3\text{O}_4\text{S}$   $[\text{M}+\text{H}]^+$  432.1199, found 432.1190.

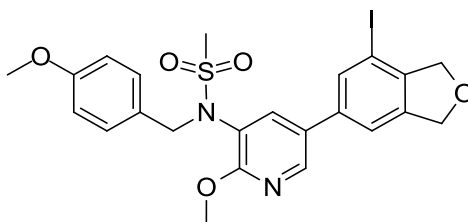
**6.9.2. *N*-Allyl-*N*-(5-(7-iodo-1,3-dihydroisobenzofuran-5-yl)-2-methoxypyridin-3-yl)methanesulfonamide, **188a****



Allyl bromide (0.21 mL, 2.39 mmol) was added to a suspension of *N*-(5-(7-iodo-1,3-dihydroisobenzofuran-5-yl)-2-methoxypyridin-3-yl)methanesulfonamide (710 mg, 1.59 mmol) and KF on alumina (40% w/w, 658 mg, 4.53 mmol, synthesised by I. Campbell, GlaxoSmithKline, unpublished results) in MeCN (8 mL). The mixture was stirred at 60 °C for 1.5 h. More allyl bromide (0.07 mL, 0.80 mmol) was added and stirring was continued overnight. The cooled suspension was diluted with EtOAc (20 mL), filtered through Celite<sup>®</sup> and the filtrate was concentrated under reduced pressure. The residue was taken up in EtOAc (10 mL), washed with water (10 mL) and brine (10 mL), dried by passing through a hydrophobic frit and concentrated under reduced pressure to afford **188a** (770 mg, 100%) as a beige foam. LCMS (Method A, UV, ESI)  $R_t$  = 1.23 min,  $[\text{M}-\text{H}]^+$  = 487, 100% purity;  $^1\text{H}$  NMR (400 MHz,  $d_6$ -DMSO)  $\delta$  3.12 (s, 3 H), 3.98 (s, 3 H), 4.23 (d,  $J$  = 6.0 Hz, 2 H), 4.92 (s, 2 H), 5.06 (d,  $J$  = 10.3 Hz, 1 H), 5.16 (d,  $J$  = 17.0 Hz, 1 H), 5.21 (s, 2 H), 5.81 (ddt,  $J$  = 17.0 Hz, 10.3 Hz, 6.2 Hz, 1 H), 7.64 (s, 1 H), 7.95 (s, 1 H), 8.00 (d,  $J$  = 1.5 Hz, 1 H), 8.47 (d,  $J$  = 1.5 Hz, 1 H).

Deprotection: A mixture of *N*-allyl-*N*-(5-(7-iodo-1,3-dihydroisobenzofuran-5-yl)-2-methoxypyridin-3-yl)methanesulfonamide (30 mg, 62  $\mu\text{mol}$ ) and rhodium(III) chloride (1.5 mg, 7  $\mu\text{mol}$ ) in 1-propanol (0.25 mL) was heated to 98 °C for 1 h to afford *N*-(5-(7-iodo-1,3-dihydroisobenzofuran-5-yl)-2-methoxypyridin-3-yl)methanesulfonamide, which was not isolated. LCMS (Method A, UV, ESI)  $R_t$  = 1.05 min,  $[\text{M}-\text{H}]^+$  = 447, 95% purity.

**6.9.3. *N*-(5-(7-Iodo-1,3-dihydroisobenzofuran-5-yl)-2-methoxypyridin-3-yl)-*N*-(4-methoxybenzyl)methanesulfonamide, **188b****

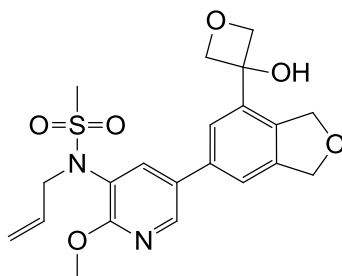


A mixture of *N*-(5-(7-iodo-1,3-dihydroisobenzofuran-5-yl)-2-methoxypyridin-3-yl)methanesulfonamide (209 mg, 0.47 mmol) and NaH (23 mg of a 60% dispersion in mineral oil, 0.56 mmol) in DMF (2 mL) was stirred at 0 °C for 10 min. 1-(Bromomethyl)-4-methoxybenzene (0.08 mL, 0.56 mmol) was added, the mixture was allowed to warm to room temperature and stirring was continued overnight. The mixture was quenched by the addition of saturated aqueous NH<sub>4</sub>Cl solution (5 mL) and extracted with EtOAc (2 x 10 mL). The combined organic extracts were washed with water (2 x 10 mL) then brine (10 mL), dried by passing through a hydrophobic frit and concentrated under reduced pressure. The crude material was purified by chromatography on FlashMaster II silica (10 g), eluting with 0-100% EtOAc/cyclohexane over 30 min. The product-containing fractions were concentrated under reduced pressure and the residue was dried on a high vacuum line (0.01 mmHg) overnight to afford **188b** (226 mg, 85%) as a white solid. Mp 147-149 °C; LCMS (Method A, UV, ESI)  $R_t = 1.27$  min,  $[M-H]^+ = 567$ , 96% purity; <sup>1</sup>H NMR (400 MHz, *d*<sub>6</sub>-DMSO)  $\delta$  3.17 (s, 3 H), 3.69 (s, 3 H), 3.96 (s, 3 H), 4.73 (br. s, 2 H), 4.90 (s, 2 H), 5.19 (s, 2 H), 6.82 (d,  $J = 8.6$  Hz, 2 H), 7.19 (d,  $J = 8.6$  Hz, 2 H), 7.49 (s, 1 H), 7.71 (d,  $J = 2.3$  Hz, 1 H), 7.77 (s, 1 H), 8.39 (d,  $J = 2.3$  Hz, 1 H); <sup>13</sup>C NMR (101 MHz, *d*<sub>6</sub>-DMSO)  $\delta$  51.9, 53.8, 55.0, 74.1, 76.3, 88.5, 113.6 (2 C), 119.1, 122.0, 128.0, 128.1, 129.8 (2 C), 133.7, 137.5, 139.3, 140.9, 142.8, 144.1, 158.7, 160.0, 1 carbon peak was not observed. IR ( $\nu_{\max}$ /cm<sup>-1</sup>): 1156, 1344; HR-ESIMS ( $m/z$ ) calcd for C<sub>23</sub>H<sub>24</sub>IN<sub>2</sub>O<sub>5</sub>S  $[M+H]^+ 567.0445$ , found 567.0445.

Deprotection: *N*-(5-(7-iodo-1,3-dihydroisobenzofuran-5-yl)-2-methoxypyridin-3-yl)-*N*-(4-methoxybenzyl)methanesulfonamide (33 mg, 0.06 mmol) and TFA (0.25 mL) in DCM (0.25 mL) were heated in a microwave at 80 °C

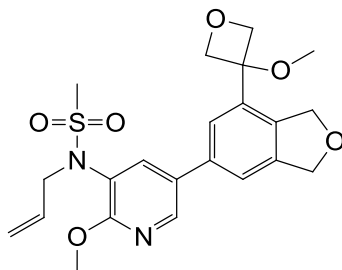
for 15 min to afford *N*-(5-(7-iodo-1,3-dihydroisobenzofuran-5-yl)-2-methoxypyridin-3-yl)methanesulfonamide, which was not isolated. LCMS (Method A, UV, ESI)  $R_t = 1.05$  min,  $[M-H]^+ = 447$ , 97% purity.

**6.9.4. *N*-Allyl-*N*-(2-methoxy-5-(7-(3-methoxyoxetan-3-yl)-1,3-dihydroisobenzofuran-5-yl)pyridin-3-yl)methanesulfonamide, **196****

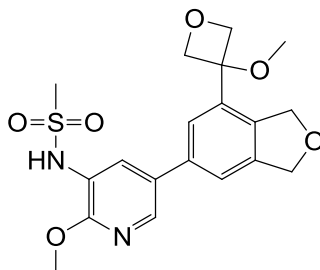


Isopropylmagnesiumchloride-lithium chloride complex (0.48 mL of a 1.3 M solution in THF, 0.62 mmol) was added dropwise to a stirring solution of *N*-allyl-*N*-(5-(7-iodo-1,3-dihydroisobenzofuran-5-yl)-2-methoxypyridin-3-yl)methanesulfonamide (200 mg, 0.41 mmol) in THF (2 mL) at  $-72$  °C under nitrogen. The mixture was stirred for 30 min. 3-Oxetanone (0.04 mL, 0.62 mmol) was added and stirring was continued for 40 min. More 3-oxetanone (0.04 mL, 0.62 mmol) was added and stirring was continued for 1 h. The mixture was quenched with saturated aqueous  $\text{NH}_4\text{Cl}$  solution (5 mL) and extracted with DCM (2 x 10 mL). The combined organic extracts were dried by passing through a hydrophobic frit and concentrated under reduced pressure. The crude material was purified by chromatography on FlashMaster II silica (10 g), eluting with 0-100% EtOAc/cyclohexane over 20 min. The product-containing fractions were concentrated under reduced pressure to afford **196** (90 mg, 51%) as a white solid. LCMS (Method B, UV, ESI)  $R_t = 0.89$  min,  $[M-H]^+ = 433$ , 100% purity;  $^1\text{H}$  NMR (400 MHz,  $d_6$ -DMSO)  $\delta$  3.12 (s, 3 H), 3.99 (s, 3 H), 4.24 (d,  $J = 6.3$  Hz, 2 H), 4.73 (d,  $^2J = 6.9$  Hz, 2 H), 4.92 (d,  $^2J = 6.9$  Hz, 2 H), 5.03 (s, 2 H), 5.05 (d,  $J = 1.4$  Hz, 1 H), 5.08 (s, 2 H), 5.17 (dd,  $J = 17.0$  Hz, 1.4 Hz, 1 H), 5.82 (ddt,  $J = 17.0$  Hz, 10.3 Hz, 6.3 Hz, 1 H), 6.34 (s, 1 H), 7.55 (s, 1 H), 7.63 (s, 1 H), 7.99 (d,  $J = 2.4$  Hz, 1 H), 8.51 (d,  $J = 2.4$  Hz, 1 H).

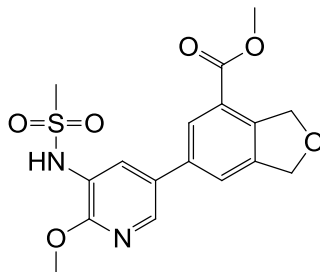
6.9.5. *N*-Allyl-*N*-(2-methoxy-5-(7-(3-methoxyoxetan-3-yl)-1,3-dihydroisobenzofuran-5-yl)pyridin-3-yl)methanesulfonamide, **198**



KO*t*-Bu (27 mg, 0.24 mmol) was added to a solution of *N*-allyl-*N*-(5-(7-(3-hydroxyoxetan-3-yl)-1,3-dihydroisobenzofuran-5-yl)-2-methoxypyridin-3-yl)methanesulfonamide (86 mg, 0.20 mmol) in THF (1 mL). The mixture was stirred for 10 min then MsCl (0.02 mL, 0.24 mmol) was added and stirring was continued for 30 min. More KO*t*-Bu (27 mg, 0.24 mmol) was added followed by MsCl (0.02 mL, 0.24 mmol) after 10 min. After 1 h more KO*t*-Bu (27 mg, 0.24 mmol) was added and stirring was continued for 1 h. More KO*t*-Bu (27 mg, 0.24 mmol) was then added and stirring was continued for 1 h. Methanol (2 mL) was added to the reaction mixture and stirring was continued for 48 h. The mixture was concentrated under reduced pressure, taken up in DCM (5 mL) and washed with water (5 mL). The aqueous phase was extracted with further DCM (5 mL) and the combined organic extracts were dried by passing through a hydrophobic frit and concentrated under reduced pressure to afford **198** (122 mg, 95%) as a yellow oil. LCMS (Method B, UV, ESI)  $R_t = 0.94$  min,  $[M-H]^+ = 447$ , 69% purity. The material was taken forward directly without further purification or characterisation.

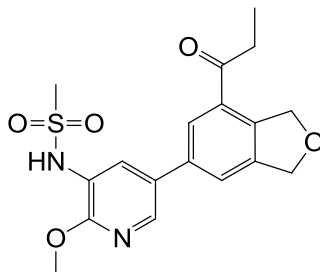
**6.9.6. N-(2-Methoxy-5-(7-(3-methoxyoxetan-3-yl)-1,3-dihydroisobenzofuran-5-yl)pyridin-3-yl)methanesulfonamide, 180**

A mixture of *N*-allyl-*N*-(2-methoxy-5-(7-(3-methoxyoxetan-3-yl)-1,3-dihydroisobenzofuran-5-yl)pyridin-3-yl)methanesulfonamide (6 mg, 0.18 mmol) and rhodium(III) chloride (4 mg, 19  $\mu$ mol) in 1-propanol (2 mL) was heated at 98 °C for 2.5 h. More rhodium(III) chloride (2 mg, 9.5  $\mu$ mol) was added and stirring was continued for 20 min. The mixture was cooled to room temperature and diluted with DCM (10 mL). The organic phase was washed with water (5 mL), dried by passing through a hydrophobic frit and concentrated under a stream of nitrogen. The crude material was purified by MDAP Method B1 and the product-containing fractions were concentrated under reduced pressure to afford **180** (11 mg, 13%) as a cream solid. Mp 166-168°C; LCMS (Method B, UV, ESI)  $R_t$  = 0.62 min,  $[M-H]^+$  = 407, 97% purity;  $^1\text{H}$  NMR (600 MHz,  $d_6$ -DMSO)  $\delta$  2.98 (s, 3 H), 3.07 (s, 3 H), 3.97 (s, 3 H), 4.73 (d,  $^2J$  = 7.1 Hz, 2 H), 4.91 (s, 2 H), 4.94 (d,  $^2J$  = 7.1 Hz, 2 H), 5.06 (s, 2 H), 7.58 (s, 2 H), 7.91 (d,  $J$  = 2.2 Hz, 1 H), 8.36 (d,  $J$  = 2.2 Hz, 1 H), 9.31 (br. s, 1 H);  $^{13}\text{C}$  NMR (151 MHz,  $d_6$ -DMSO)  $\delta$  40.1, 40.7, 51.0, 53.7, 71.7, 72.1, 78.3 (2 C), 80.7, 119.2, 124.0, 129.5, 131.1, 133.4, 136.3, 136.4, 140.8, 141.5, 156.4; IR ( $\nu_{\text{max}}$  / $\text{cm}^{-1}$ ): 1148, 1320, 3292 (br.); HR-ESIMS ( $m/z$ ) calcd for  $\text{C}_{19}\text{H}_{23}\text{N}_2\text{O}_6\text{S}$   $[M+H]^+$  407.1271, found 407.1269.

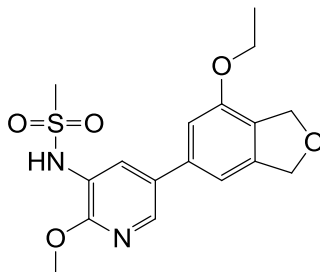
**6.9.7. Methyl 6-(6-methoxy-5-(methylsulfonamido)pyridin-3-yl)-1,3-dihydroisobenzofuran-4-carboxylate, 179**

1-Chloro-*N,N*-2-trimethyl-1-propenylamine (0.02 mL, 0.15 mmol) was added to a solution of 6-(6-methoxy-5-(methylsulfonamido)pyridin-3-yl)-1,3-dihydroisobenzofuran-4-carboxylic acid (50 mg, 0.14 mmol) in THF (1 mL) at room temperature. After stirring for 20 min more 1-chloro-*N,N*-2-trimethyl-1-propenylamine (0.02 mL, 0.15 mmol) was added and stirring was continued for 45 min. More 1-chloro-*N,N*-2-trimethyl-1-propenylamine (0.09 mL, 0.69 mmol) was added and stirring was continued for 30 min. MeOH (5 mL) was added to the reaction mixture and the mixture was left to stand overnight. The solvent was removed under reduced pressure and the crude material was purified by MDAP Method B2. The product-containing fractions were concentrated under reduced pressure to afford **179** (21 mg, 40%) as a white solid. Mp 205-207 °C; LCMS (Method A, UV, ESI)  $R_t = 0.88$  min,  $[M-H]^+ = 379$ , 100% purity;  $^1H$  NMR (600 MHz,  $d_6$ -DMSO)  $\delta$  3.09 (s, 3 H), 3.88 (s, 3 H), 3.98 (s, 3 H), 5.11 (s, 2 H), 5.27 (s, 2 H), 7.88 (s, 1 H), 7.90 (d,  $J = 2.2$  Hz, 1 H), 8.01 (s, 1 H), 8.32 (d,  $J = 2.2$  Hz, 1 H), 9.34 (s, 1 H);  $^{13}C$  NMR (151 MHz,  $d_6$ -DMSO)  $\delta$  40.7, 52.3, 53.8, 72.1, 73.6, 121.5, 124.0, 124.5, 126.3, 128.7, 130.5, 136.7, 140.3, 140.5, 142.0, 156.3, 165.5; IR ( $\nu_{max}$  / $cm^{-1}$ ); 1131, 1338, 1718, 3236 (br.); HR-ESIMS ( $m/z$ ) calcd for  $C_{17}H_{19}N_2O_6S$   $[M+H]^+$  379.0958, found 379.0959.



**6.9.8. *N*-(2-Methoxy-5-(7-propionyl-1,3-dihydroisobenzofuran-5-yl)pyridin-3-yl)methanesulfonamide, **178****

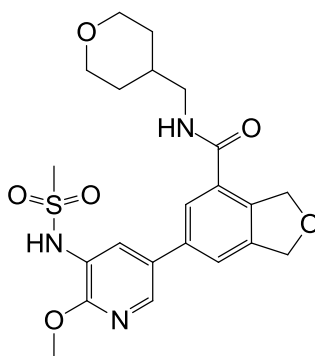
EtMgBr (0.09 mL of a 3.4 M solution in 2-MeTHF, 0.29 mmol) was added to a solution of *N*-(5-(7-formyl-1,3-dihydroisobenzofuran-5-yl)-2-methoxypyridin-3-yl)methanesulfonamide (51 mg, 0.15 mmol) in THF (0.5 mL) at -78 °C under an atmosphere of nitrogen. The mixture was stirred at room temperature for 1 h. More EtMgBr (0.04 mL of a 3.4 M solution in 2-MeTHF, 0.15 mmol) was added and stirring was continued for 20 min. A solution of *N*-tert-butylphenylsulfinimidoyl chloride (63 mg, 0.292 mmol) in THF (0.5 mL) was added and stirring was continued for 20 min. The mixture was allowed to warm to room temperature over 20 min then quenched by addition of HCl (as a 2 M aqueous solution, 2 mL). The aqueous phase was extracted with DCM (2 x 5 mL). The combined organic extracts were washed with water (5 mL) then brine (5 mL), dried by passing through a hydrophobic frit and concentrated under a stream of nitrogen. The crude material was purified by MDAP Method B2 and the product-containing fractions were concentrated under reduced pressure to afford **178** (5 mg, 10%) as a white solid. LCMS (Method B, UV, ESI)  $R_t = 0.75$  min,  $[M-H]^+ = 377$ , 95% purity;  $^1\text{H}$  NMR (400 MHz,  $d_6$ -DMSO)  $\delta$  1.10 (t,  $J = 7.2$  Hz, 3 H), 3.08 (s, 3 H), 3.17 (q,  $J = 7.2$  Hz, 2 H), 3.98 (s, 3 H), 5.07 (s, 2 H), 5.26 (s, 2 H), 7.83 (s, 1 H), 7.95 (d,  $J = 2.3$  Hz, 1 H), 8.15 (s, 1 H), 8.39 (d,  $J = 2.3$  Hz, 1 H), 9.38 (br. s, 1 H); HR-ESIMS ( $m/z$ ) calcd for  $\text{C}_{18}\text{H}_{21}\text{N}_2\text{O}_5\text{S}$   $[M+H]^+ 377.1166$ , found 377.1173.

**6.9.9. N-(5-(7-Ethoxy-1,3-dihydroisobenzofuran-5-yl)-2-methoxy-3-yl)pyridin-3-yl)methanesulfonamide, 176**

Copper(I) iodide (3 mg, 0.02 mmol) was added to *N*-(5-(7-iodo-1,3-dihydroisobenzofuran-5-yl)-2-methoxy-3-yl)pyridin-3-yl)methanesulfonamide (47 mg, 0.11 mmol) and 1,10-phenanthroline (38 mg, 0.21 mmol) in EtOH (1 mL). The mixture was degassed under nitrogen for 5 min. KO*t*-Bu (0.35 mL of a 1 M solution in THF, 0.35 mmol) was added and the resulting solution was heated in the microwave at 150 °C for 1 h. The reaction mixture was partitioned between DCM (10 mL) and water (10 mL). The phases were separated using a hydrophobic frit and the aqueous phase extracted with DCM (5 mL). The combined organic extracts were dried by passing through a hydrophobic frit and concentrated under a stream of nitrogen. The crude material was purified by MDAP Method A1 and the product-containing fractions were concentrated under reduced pressure to afford **176** (19 mg, 50%) as a white solid. Mp 122-124 °C; LCMS (Method A, UV, ESI)  $R_t = 0.97$  min,  $[M-H]^+ = 365$ , 100% purity;  $^1\text{H NMR}$  (400 MHz,  $d_6$ -DMSO)  $\delta$  1.34 (t,  $J = 7.0$  Hz, 3 H), 3.07 (s, 3 H), 3.96 (s, 3 H), 4.18 (q,  $J = 7.0$  Hz, 2 H), 4.99 (s, 2 H), 5.05 (s, 2 H), 7.11 (s, 1 H), 7.07 (s, 1 H), 7.85 (d,  $J = 2.3$  Hz, 1 H), 8.30 (d,  $J = 2.3$  Hz, 1 H), 9.35 (br. s, 1 H);  $^{13}\text{C NMR}$  (101 MHz,  $d_6$ -DMSO)  $\delta$  14.6, 40.7, 53.7, 63.4, 70.9, 73.1, 109.0, 111.5, 121.3, 125.8, 130.0, 131.0, 138.3, 140.6, 141.8, 153.4, 156.2; IR ( $\nu_{\text{max}}$  / $\text{cm}^{-1}$ ); 1142, 3235 (br.); HR-ESIMS ( $m/z$ ) calcd for  $\text{C}_{17}\text{H}_{21}\text{N}_2\text{O}_5\text{S}$   $[M+H]^+$  365.1166, found 365.1168.

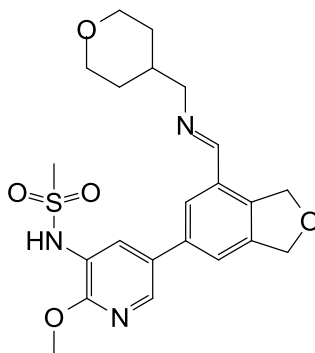
## 6.10. Preparation of Fully Elaborated Dihydroisobenzofuran Compounds 181-184.

### 6.10.1. 6-(6-Methoxy-5-(methylsulfonamido)pyridin-3-yl)-*N*-((tetrahydro-2*H*-pyran-4-yl)methyl)-1,3-dihydroisobenzofuran-4-carboxamide, **182**



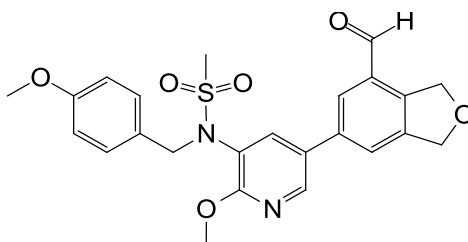
A mixture of 6-(6-methoxy-5-(methylsulfonamido)pyridin-3-yl)-1,3-dihydroisobenzofuran-4-carboxylic acid (75 mg, 0.21 mmol), PyBop (118 mg, 0.23 mmol) and DIPEA (0.07 mL, 0.41 mmol) in DMF (1 mL) was stirred at room temperature for 10 min. 4-(Aminomethyl)tetrahydropyran (26 mg, 0.23 mmol) was added and stirring was continued for 30 min. The mixture was diluted with DCM (5 mL) and washed with water (5 mL) then brine (5 mL). The organic phase was dried by passing through a hydrophobic frit and concentrated under a stream of nitrogen. The crude material was purified MDAP Method B1 and the product-containing fractions were concentrated under reduced pressure. The residue was further purified by MDAP Method E and the product-containing fractions were concentrated under reduced pressure to afford **182** (20 mg, 20%) as a white solid. LCMS (Method A, UV, ESI)  $R_t = 0.76$  min,  $[M-H]^+ = 462$ , 95% purity;  $^1\text{H NMR}$  (400 MHz,  $d_4$ -MeOH)  $\delta$  1.30 – 1.46 (m, 2 H), 1.72 (d,  $^2J = 11.9$  Hz, 2 H), 1.84 - 2.02 (m, 1 H), 3.03 (s, 3 H), 3.37 (s, 2 H), 3.44 (t,  $J = 11.6$  Hz, 2 H), 3.98 (d,  $^2J = 11.4$  Hz, 2 H), 4.07 (s, 3 H), 5.15 (s, 2 H), 5.35 (s, 2 H), 7.69 (s, 1 H), 7.87 (s, 1 H), 8.04 (s, 1 H), 8.27 (s, 1 H), two proton peaks were not observed.

**6.10.2. N-(2-Methoxy-5-(7-(((tetrahydro-2H-pyran-4-yl)methyl)imino)methyl)-1,3-dihydroisobenzofuran-5-yl)pyridin-3-yl)methanesulfonamide, **206****



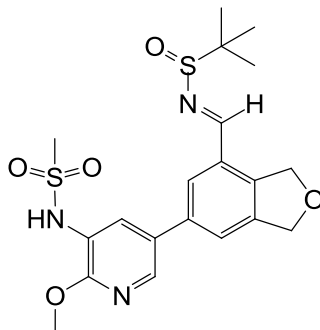
A mixture of 4-(aminomethyl)tetrahydropyran (40 mg, 0.35 mmol),  $\text{NEt}_3$  (0.05 mL, 0.34 mmol) and  $\text{MgSO}_4$  (73 mg, 0.61 mmol) in DCM (2 mL) was stirred at room temperature for 30 min under an atmosphere of nitrogen. *N*-(5-(7-formyl-1,3-dihydroisobenzofuran-5-yl)-2-methoxypyridin-3-yl)methanesulfonamide (100 mg, 0.29 mmol) was added and stirring was continued overnight. The  $\text{MgSO}_4$  was removed by suction filtration, washing with DCM (10 mL). The organic phase and washings were combined and washed with water (5 mL) and brine (5 mL), dried by passing through a hydrophobic frit and concentrated under reduced pressure to afford **206** (121 mg, 85%) as a brown oil. LCMS (Method B, UV, ESI)  $R_t = 0.88$  min,  $[\text{M}-\text{H}]^+ = 446$ , 95% purity;  $^1\text{H}$  NMR (400 MHz,  $d_6$ -DMSO)  $\delta$  1.22 – 1.36 (m, 2 H), 1.60 (d,  $J = 11.5$  Hz, 2 H), 1.76 - 1.92 (m, 1 H), 3.05 (s, 3 H), 3.30 - 3.37 (m, 2 H), 3.51 (d,  $J = 6.0$  Hz, 2 H), 3.86 (dd,  $^2J = 11.5$  Hz,  $J = 3.4$  Hz, 2 H), 3.96 (s, 3 H), 5.06 (s, 2 H), 5.20 (s, 2 H), 7.66 (s, 1 H), 7.80 (s, 1 H), 7.88 (d,  $J = 2.3$  Hz, 1 H), 8.28 (d,  $J = 2.3$  Hz, 1 H), 8.48 (s, 1 H), 8.75 (br. s, 1 H).

**6.10.3. *N*-(5-(7-Formyl-1,3-dihydroisobenzofuran-5-yl)-2-methoxypyridin-3-yl)-*N*-(4-methoxybenzyl)methanesulfonamide, **215****



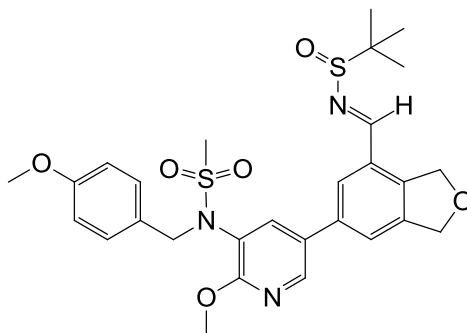
A mixture of *N*-(5-(7-formyl-1,3-dihydroisobenzofuran-5-yl)-2-methoxypyridin-3-yl)methanesulfonamide (508 mg, 1.46 mmol),  $K_2CO_3$  (403 mg, 2.92 mmol) and *para*-methoxybenzyl bromide (0.43 mL, 2.92 mmol) in DMF (5 mL) was stirred at room temperature for 72 h. EtOAc (30 mL), water (30 mL) and LiCl (7.5% w/v aqueous solution, 10 mL) were added to the mixture. The resulting solid was removed by suction filtration. The organic phase was separated and washed with water (2 x 20 mL) and brine (20 mL) then dried by passing through a hydrophobic frit and concentrated under reduced pressure. The crude material was purified by chromatography on FlashMaster II silica (10 g), eluting with 0-100% EtOAc/cyclohexane over 20 min. The product-containing fractions were concentrated under reduced pressure then dried further in a vacuum oven (0.01 mmHg) at 45 °C overnight to afford **215** (219 mg, 32%) as a pale yellow solid. LCMS (Method A, UV, ESI)  $R_t = 1.08$  min,  $[M-H]^+ = 469$ , 96% purity;  $^1H$  NMR (400 MHz,  $d_6$ -DMSO)  $\delta$  3.18 (s, 3 H), 3.67 (s, 3 H), 3.99 (s, 3 H), 4.75 (s, 2 H), 5.06 (s, 2 H), 5.26 (s, 2 H), 6.82 (d,  $J = 8.6$  Hz, 2 H), 7.20 (d,  $J = 8.6$  Hz, 2 H), 7.82 (d,  $J = 2.3$  Hz, 1 H), 7.85 (s, 1 H), 8.09 (s, 1 H), 8.50 (d,  $J = 2.3$  Hz, 1 H), 10.1 (s, 1 H).

**6.10.4. *N*-(5-(7-(((*tert*-Butylsulfinyl)imino)methyl)-1,3-dihydroisobenzofuran-5-yl)-2-methoxy-pyridin-3-yl)methanesulfonamide, 216a**



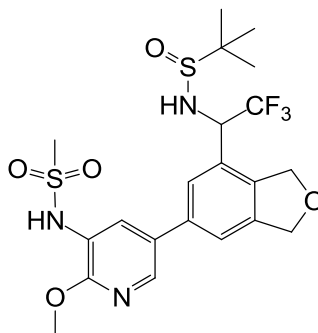
A mixture of *N*-(5-(7-formyl-1,3-dihydroisobenzofuran-5-yl)-2-methoxy-pyridin-3-yl)methanesulfonamide (500 mg, 1.44 mmol), 2-methyl-2-propanesulfinamide (209 mg, 1.72 mmol) and titanium(IV) ethoxide (1.20 mL, 5.74 mmol) in THF (8 mL) was stirred at room temperature under an atmosphere of nitrogen overnight. The mixture was heated to 50 °C for 4 h. The mixture was cooled to room temperature and stirring was continued for 48 h. Water (20 mL) was added and the resulting suspension was stirred vigorously for 5 min then filtered through Celite<sup>®</sup>, washing with more water (10 mL) then EtOAc (2 x 20 mL). The filtrate was separated and the aqueous phase was extracted with further EtOAc (20 mL). The combined organic extracts were washed with brine (10 mL), dried by passing through a hydrophobic frit and concentrated under reduced pressure to give a residue that was dried further on a high vacuum line (0.01 mmHg) for 1 h to afford **216a** (106 mg, 16%) as a brown gum. LCMS (Method A, UV, ESI)  $R_t = 1.00$  min,  $[M-H]^+ = 452$ , 67% purity. The material was taken forward directly without further purification or characterisation.

**6.10.5. *N*-(5-(7-(((*tert*-Butylsulfinyl)imino)methyl)-1,3-dihydroisobenzofuran-5-yl)-2-methoxypyridin-3-yl)-*N*-(4-methoxybenzyl)methanesulfonamide, **216b****



A mixture of *N*-(5-(7-formyl-1,3-dihydroisobenzofuran-5-yl)-2-methoxypyridin-3-yl)-*N*-(4-methoxybenzyl)methanesulfonamide (162 mg, 0.35 mmol), 2-methyl-2-propanesulfinamide (49 mg, 0.40 mmol) and titanium(IV) ethoxide (0.29 mL, 1.38 mmol) in THF (2 mL) was stirred at room temperature under an atmosphere of nitrogen for 3 h. More titanium(IV) ethoxide (0.07 mL, 0.35 mmol) was added and stirring was continued overnight. Water (10 mL) was added and the resulting suspension was stirred vigorously for 5 min then filtered through Celite<sup>®</sup>, washing with more water (10 mL) then EtOAc (2 x 10 mL). The filtrate was separated and the combined organic extracts were dried by passing through a hydrophobic frit and concentrated under reduced pressure to give gum that was dried further on a high vacuum line (0.01 mmHg) for 30 min to afford **216b** (170 mg, 86%) as a yellow gum. LCMS (Method A, UV, ESI)  $R_t = 1.22$  min,  $[M-H]^+ = 572$ , 97% purity; <sup>1</sup>H NMR (400 MHz, *d*<sub>6</sub>-DMSO)  $\delta$  1.20 (s, 9 H), 3.18 (s, 3 H), 3.67 (s, 3 H), 3.98 (s, 3 H), 4.75 (s, 2 H), 5.09 (s, 2 H), 5.21 (d, <sup>2</sup>*J* = 14.7 Hz, 1 H), 5.29 (d, <sup>2</sup>*J* = 14.7 Hz, 1 H), 6.81 (d, *J* = 8.8 Hz, 2 H), 7.21 (d, *J* = 8.8 Hz, 2 H), 7.75 (s, 1 H), 7.89 (d, *J* = 2.3 Hz, 1 H), 8.11 (s, 1 H), 8.50 (d, *J* = 2.3 Hz, 1 H), 8.69 (s, 1 H).

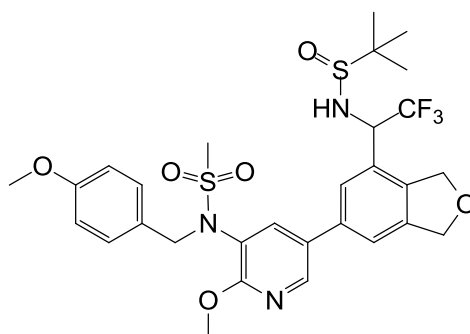
**6.10.6. *N*-(5-(7-(1-(1,1-Dimethylethylsulfinamido)-2,2,2-trifluoroethyl)-1,3-dihydroisobenzofuran-5-yl)-2-methoxypyridin-3-yl)methanesulfonamide, **217a****



Trimethyl(trifluoromethyl)silane (0.042 mL, 0.28 mmol) was added to a mixture of *N*-(5-(7-(((tert-butylsulfinyl)imino)methyl)-1,3-dihydroisobenzofuran-5-yl)-2-methoxypyridin-3-yl)methanesulfonamide (106 mg, 0.24 mmol) and TBAT (139 mg, 0.26 mmol) at -55 °C. The mixture was stirred for 20 min. More trimethyl(trifluoromethyl)silane (0.042 mL, 0.28 mmol) was added and stirring was continued for 1 h. The mixture was allowed to warm to room temperature and stirring was continued for 30 min. More trimethyl(trifluoromethyl)silane (0.042 mL, 0.28 mmol) was added and stirring was continued overnight. More TBAT (63 mg, 0.12 mmol) and trimethyl(trifluoromethyl)silane (0.042 mL, 0.282 mmol) were added and stirring was continued for 1 h. Saturated aqueous NH<sub>4</sub>Cl solution (5 mL) was added to the mixture and the aqueous phase was extracted with EtOAc (2 x 10 mL). The combined organic extracts were dried by passing through a hydrophobic frit and concentrated under a stream of nitrogen. The crude material was purified by MDAP Method C3 and the product-containing fractions were concentrated under reduced pressure to afford **217a** (19 mg, 16%) as a brown oil. LCMS (Method A, UV, ESI)  $R_t = 1.00$  min,  $[M-H]^+ = 522$ , 87% purity. The material was taken forward directly without further purification or characterisation.

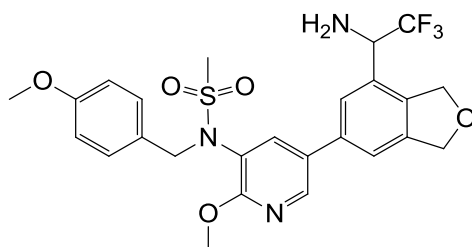


**6.10.7. *N*-(5-(7-(1-(1,1-Dimethylethylsulfinamido)-2,2,2-trifluoroethyl)-1,3-dihydroisobenzofuran-5-yl)-2-methoxypyridin-3-yl)-*N*-(4-methoxybenzyl)methanesulfonamide, **217b****



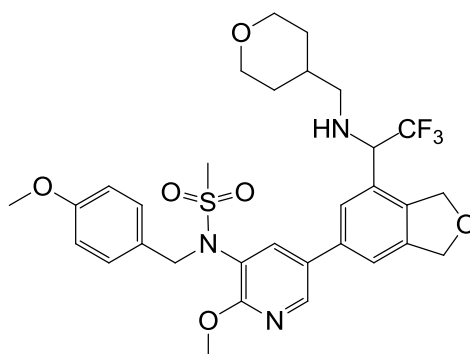
Trimethyl(trifluoromethyl)silane (0.05 mL, 0.35 mmol) in THF (1 mL) was added to a mixture of *N*-(5-(7-(((tert-butylsulfinyl)imino)methyl)-1,3-dihydroisobenzofuran-5-yl)-2-methoxypyridin-3-yl)-*N*-(4-methoxybenzyl)methanesulfonamide (168 mg, 0.29 mmol) and TBAT (175 mg, 0.32 mmol) in THF (1 mL) at 0 °C. The mixture was stirred for 20 min then more trimethyl(trifluoromethyl)silane (0.05 mL, 0.35 mmol) was added and stirring was continued for 30 min. Saturated aqueous NH<sub>4</sub>Cl solution (5 mL) was added to the mixture and the aqueous phase was extracted with EtOAc (2 x 10 mL). The combined organic extracts were dried by passing through a hydrophobic frit and concentrated under reduced pressure. The crude material was purified by chromatography on FlashMaster II silica (20 g), eluting with 0-100% EtOAc/DCM over 40 min. The product-containing fractions were concentrated under reduced pressure to afford **217b** (107 mg, 57%) as a pale yellow solid. LCMS (Method A, UV, ESI)  $R_t = 1.19$  min,  $[M-H]^+ = 642$ , 90% purity; <sup>1</sup>H NMR (400 MHz, *d*<sub>4</sub>-MeOH)  $\delta$  1.22 (s, 9 H), 3.11 (s, 3 H), 3.70 (s, 3 H), 4.08 (s, 3 H), 4.77 (br. s, 2 H), 4.97 (q,  $J_H-F = 7.8$  Hz, 1 H), 5.11 (s, 2 H), 5.18 (d,  $^2J = 12.8$  Hz, 1 H), 5.28 (d,  $^2J = 12.8$  Hz, 1 H), 6.79 (d,  $J = 8.6$  Hz, 2 H), 7.15 (d,  $J = 8.6$  Hz, 2 H), 7.35 (s, 1 H), 7.52 (d,  $J = 2.3$  Hz, 1 H), 7.59 (s, 1 H), 8.33 (d,  $J = 2.3$  Hz, 1 H), one proton signal was not observed; <sup>19</sup>F NMR (376 MHz, *d*<sub>4</sub>-MeOH)  $\delta$  -75.0.

**6.10.8. *N*-(5-(7-(1-Amino-2,2,2-trifluoroethyl)-1,3-dihydroisobenzofuran-5-yl)-2-methoxy-pyridin-3-yl)-*N*-(4-methoxybenzyl)methanesulfonamide, **218****



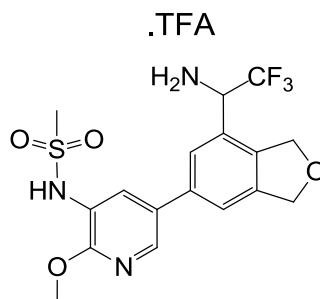
*N*-(5-(7-(1-(1,1-dimethylethylsulfonamido)-2,2,2-trifluoroethyl)-1,3-dihydroisobenzofuran-5-yl)-2-methoxy-pyridin-3-yl)-*N*-(4-methoxybenzyl)methanesulfonamide (57 mg, 0.09 mmol) and HCl (as a 4 M solution in 1,4-dioxane, 0.11 mL, 0.44 mmol) in MeOH (1 mL) was stirred at room temperature for 2 h. The mixture was neutralised with NaOH (as a 2 M aqueous solution) and extracted with DCM (4 x 5 mL). The combined organic extracts were concentrated under a stream of nitrogen to afford **218** (53 mg, 99%) as a colourless oil. LCMS (Method A, UV, ESI)  $R_t = 0.99$  min,  $[M-H]^+ = 538$ , 89% purity;  $^1\text{H}$  NMR (400 MHz,  $d_4$ -MeOH)  $\delta$  3.14 (s, 3 H), 3.67 (s, 3 H), 4.10 (s, 3 H), 4.48 (q,  $J_{H-F} = 7.6$  Hz, 1 H), 4.77 (br. s, 2 H), 5.12 (s, 2 H), 5.16 (d,  $^2J = 12.6$  Hz, 1 H), 5.23 (d,  $^2J = 12.6$  Hz, 1 H), 6.82 (d,  $J = 8.8$  Hz, 2 H), 7.18 (d,  $J = 8.8$  Hz, 2 H), 7.34 (s, 1 H), 7.50 (s, 1 H), 7.51 (d,  $J = 2.3$  Hz, 1 H), 8.35 (d,  $J = 2.3$  Hz, 1 H), two proton signals were not observed.  $^{19}\text{F}$  NMR (376 MHz,  $d_4$ -MeOH)  $\delta$  -77.4.

**6.10.9. *N*-(2-Methoxy-5-(7-(2,2,2-trifluoro-1-(((tetrahydro-2H-pyran-4-yl)methyl)amino)ethyl)-1,3-dihydroisobenzofuran-5-yl)pyridin-3-yl)-*N*-(4-methoxybenzyl)methanesulfonamide, **219****



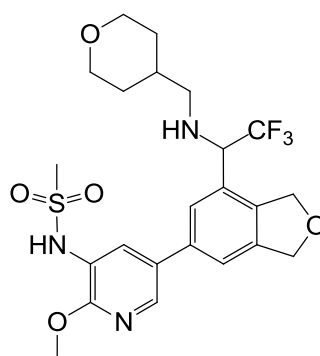
A mixture of *N*-(5-(7-(1-amino-2,2,2-trifluoroethyl)-1,3-dihydroisobenzofuran-5-yl)-2-methoxypyridin-3-yl)-*N*-(4-methoxybenzyl)methanesulfonamide (20 mg, 0.04 mmol) and  $\text{NEt}_3$  (6  $\mu\text{L}$ , 0.04 mmol) in MeCN (0.5 mL) was stirred for 5 min. Tetrahydro-2H-pyran-4-carbaldehyde (6  $\mu\text{L}$ , 0.05 mmol) was added, followed by STAB (11 mg, 0.05 mmol). Stirring was continued at room temperature for 1 h then more STAB (11 mg, 0.05 mmol) was added and stirring was continued for 4 h. More STAB (11. mg, 0.05 mmol) was added and stirring was continued overnight. More  $\text{NEt}_3$  (6  $\mu\text{L}$ , 0.04 mmol) and STAB (11 mg, 0.05 mmol) were added and stirring was continued for 1 h. The solvent was removed under reduced pressure and the residue was taken up in saturated aqueous  $\text{NaHCO}_3$  solution (5 mL). The aqueous phase was extracted with DCM (2 x 5 mL) and the combined organic extracts were concentrated under a stream of nitrogen afford **219** (20 mg, 90%) as a pale orange oil. LCMS (Method B, UV, ESI)  $R_t$  = 1.26 min,  $[\text{M}-\text{H}]^+$  = 636, 59% purity. The material was taken forward directly without further purification or characterisation.

**6.10.10. *N*-(5-(7-(1-Amino-2,2,2-trifluoroethyl)-1,3-dihydroisobenzofuran-5-yl)-2-methoxypyridin-3-yl)methanesulfonamide, trifluoroacetic acid salt, 220**



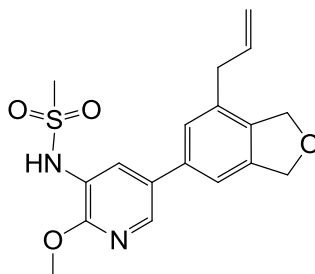
A mixture of *N*-(5-(7-(1-amino-2,2,2-trifluoroethyl)-1,3-dihydroisobenzofuran-5-yl)-2-methoxypyridin-3-yl)-*N*-(4-methoxybenzyl)methanesulfonamide (20 mg, 0.04 mmol), DCM (0.2 mL) and TFA (0.2 mL) was stirred at room temperature for 30 min. The mixture was transferred to a microwave vial and was heated at 40 °C in the microwave for 10 min, then 50 °C for 30 min, 80 °C for 10 min and finally 50 °C for 5 h. The mixture was concentrated under a stream of nitrogen to afford **220** (26 mg, 131%) as a brown oil. LCMS (Method A, UV, ESI)  $R_t = 0.69$  min,  $[M-H]^+ = 418$ , 48% purity. The material was taken forward directly without further purification or characterisation.

**6.10.11. *N*-(2-Methoxy-5-(7-(2,2,2-trifluoro-1-((tetrahydro-2*H*-pyran-4-yl)methyl)amino)ethyl)-1,3-dihydroisobenzofuran-5-yl)pyridin-3-yl)methanesulfonamide, 183**

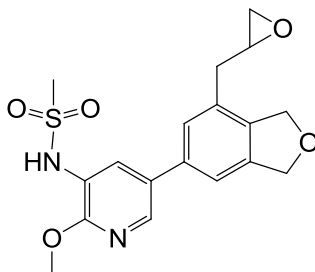


A mixture of *N*-(5-(7-(1-amino-2,2,2-trifluoroethyl)-1,3-dihydroisobenzofuran-5-yl)-2-methoxypyridin-3-yl)methanesulfonamide,

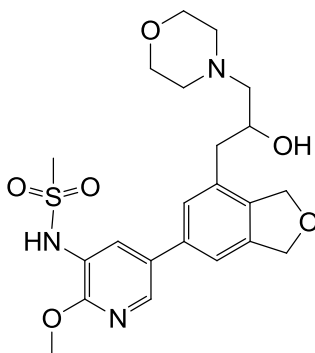
trifluoroacetic acid salt (26 mg, 0.05 mmol) and  $\text{NEt}_3$  (11  $\mu\text{L}$ , 0.08 mmol) in MeCN (0.5 mL) was stirred for 5 min. Tetrahydro-2*H*-pyran-4-carbaldehyde (9  $\mu\text{L}$ , 0.08 mmol) was added, followed by STAB (16 mg, 0.08 mmol), and stirring was continued at room temperature for 2 h. More  $\text{NEt}_3$  (11  $\mu\text{L}$ , 0.08 mmol) and STAB (16 mg, 0.08 mmol) were added and stirring was continued for 1 h. More tetrahydro-2*H*-pyran-4-carbaldehyde (9  $\mu\text{L}$ , 0.08 mmol) was added and stirring was continued overnight. DCM (0.2 mL) was added followed by DMSO (1 drop) to aid solubility and stirring was continued for 2 h. More STAB (16 mg, 0.08 mmol) and tetrahydro-2*H*-pyran-4-carbaldehyde (9  $\mu\text{L}$ , 0.08 mmol) were added and stirring was continued over the weekend. Activated molecular sieves (3Å) were added and stirring was continued for 1.5 h. More tetrahydro-2*H*-pyran-4-carbaldehyde (9  $\mu\text{L}$ , 0.08 mmol) was added and stirring was continued for 1 h. STAB (3 mg, 0.08 mmol) was added and stirring was continued for 30 min. The mixture was concentrated under reduced pressure and the residue was taken up in saturated aqueous  $\text{NaHCO}_3$  solution (5 mL). The aqueous phase was extracted with DCM (2 x 5 mL) and the combined organic extracts were concentrated under a stream of nitrogen. The crude material was purified by MDAP Method F and the product-containing fractions were concentrated under reduced pressure to afford **183** (5 mg, 19%) as a white solid. LCMS (Method B, UV, ESI)  $R_t = 0.91$  min,  $[\text{M-H}]^+ = 516$ , 100% purity;  $^1\text{H}$  NMR (400 MHz,  $d_4$ -MeOH)  $\delta$  1.18 – 1.34 (m, 2 H), 1.62 – 1.84 (m, 3 H), 2.36 – 2.58 (m, 2 H), 3.05 (s, 3 H), 3.38 – 3.49 (m, 2 H), 3.90 – 4.01 (m, 2 H), 4.09 (s, 3 H), 4.32 – 4.40 (m, 1 H), 5.19 (s, 2 H), 5.24 (d,  $^2J = 6.0$  Hz, 2 H), 7.57 (s, 1 H), 7.70 (s, 1 H), 8.01 (d,  $J = 2.3$  Hz, 1 H), 8.24 (d,  $J = 2.3$  Hz, 1 H), two proton signals were not observed;  $^{19}\text{F}$  NMR (376 MHz,  $d_4$ -MeOH)  $\delta$  -75.0.

**6.10.12. N-(5-(7-Allyl-1,3-dihydroisobenzofuran-5-yl)-2-methoxypyridin-3-yl)methanesulfonamide, 221**

A mixture of *N*-(5-(7-iodo-1,3-dihydroisobenzofuran-5-yl)-2-methoxypyridin-3-yl)methanesulfonamide (448 mg, 1.00 mmol), 2-allyl-4,4,5,5-tetramethyl-1,3,2-dioxaborolane (0.28 mL, 1.51 mmol), Pd(PPh<sub>3</sub>)<sub>4</sub> (118 mg, 0.10 mmol) and K<sub>2</sub>CO<sub>3</sub> (428 mg, 3.10 mmol) in 1,4-dioxane (3 mL) and water (1 mL) was heated in a microwave at 100 °C for 1 h then at 120 °C for 30 min. More 2-allyl-4,4,5,5-tetramethyl-1,3,2-dioxaborolane (0.28 mL, 1.51 mmol) and Pd(PPh<sub>3</sub>)<sub>4</sub> (118 mg, 0.10 mmol) were added and the mixture was heated again in the microwave at 100 °C for 30 min. The mixture was diluted with EtOAc (30 mL) and filtered through Celite, washing with further EtOAc (10 mL). The original organic phase and washings were combined, washed with water (40 mL), brine (40 mL) and dried by passing through a hydrophobic frit. The solvent was removed under reduced pressure and the crude material was purified by chromatography on FlashMaster II silica (100 g), eluting with 0-100% EtOAc/cyclohexane over 40 min. The product-containing fractions were concentrated under reduced pressure to afford **221** (324 mg, 90%) as a yellow solid. LCMS (Method A, UV, ESI) *R*<sub>t</sub> = 1.01 min, [M-H]<sup>+</sup> = 361, 100% purity; <sup>1</sup>H NMR (400 MHz, *d*<sub>6</sub>-DMSO) δ 3.07 (s, 3 H), 3.37 (d, *J* = 6.6 Hz, 2 H), 3.96 (s, 3 H), 5.02 (s, 2 H), 5.07 (s, 2 H), 5.06 – 5.14 (m, 2 H), 5.95 (ddt, *J* = 16.9 Hz, 10.1 Hz, 6.6 Hz, 1 H), 7.34 (s, 1 H), 7.42 (s, 1 H), 7.84 (d, *J* = 2.3 Hz, 1 H), 8.27 (d, *J* = 2.3 Hz, 1 H), 9.30 (s, 1 H).

**6.10.13. *N*-(2-Methoxy-5-(7-(oxiran-2-ylmethyl)-1,3-dihydroisobenzofuran-5-yl)pyridin-3-yl)methanesulfonamide, 222**

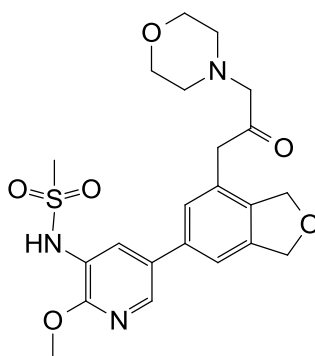
*m*CPBA (350 mg of  $\leq 77\%$  grade material, 1.56 mmol) was added portionwise to a solution of *N*-(5-(7-allyl-1,3-dihydroisobenzofuran-5-yl)-2-methoxypyridin-3-yl)methanesulfonamide (225 mg, 0.62 mmol) in  $\text{CHCl}_3$  (5 mL) at room temperature and the mixture was stirred for 64 h. The reaction mixture was added to the top of a 5 g aminopropyl cartridge that had been preconditioned with  $\text{CHCl}_3$ . The cartridge was eluted with  $\text{CHCl}_3$  (2 CV) and the fraction obtained was concentrated under reduced pressure to afford **222** (122 mg, 52%) as a yellow oil. LCMS (Method B, UV, ESI)  $R_t = 0.66$  min,  $[\text{M}-\text{H}]^+ = 377$ , 47% purity. The material was taken forward directly without further purification or characterisation.

**6.10.14. *N*-(5-(7-(2-Hydroxy-3-morpholinopropyl)-1,3-dihydroisobenzofuran-5-yl)-2-methoxypyridin-3-yl)methanesulfonamide, 223**

A mixture of *N*-(2-methoxy-5-(7-(oxiran-2-ylmethyl)-1,3-dihydroisobenzofuran-5-yl)pyridin-3-yl)methanesulfonamide (122 mg, 0.19 mmol) and morpholine (0.02 mL, 0.19 mmol) in MeOH (0.3 mL) was heated in a microwave at 100 °C for 1 h. The reaction mixture was added to the top of a 2 g

SCX-2 cartridge that had been pre-conditioned with MeOH. The cartridge was eluted with MeOH (2 CV) then NH<sub>3</sub> (as a 10% w/v solution in MeOH, 2 CV). The basic fraction was concentrated under a stream of nitrogen to afford **223** (44 mg, 49%) as a yellow oil. LCMS (Method B, UV, ESI)  $R_t = 0.62$  min,  $[M-H]^+ = 464$ , 69% purity. The material was taken forward directly without further purification or characterisation.

**6.10.15. *N*-(2-Methoxy-5-(7-(3-morpholino-2-oxopropyl)-1,3-dihydroisobenzofuran-5-yl)pyridin-3-yl)methanesulfonamide, 181**



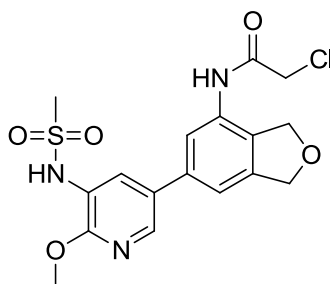
Pyridine sulfur trioxide complex (278mg, 0.18 mmol) in DMSO (0.1 mL) was added to mixture of *N*-(5-(7-(2-hydroxy-3-morpholinopropyl)-1,3-dihydroisobenzofuran-5-yl)-2-methoxypyridin-3-yl)methanesulfonamide (27 mg, 0.06 mmol) and NEt<sub>3</sub> (0.04 mL, 0.29 mmol) in DMSO (0.1 mL) at room temperature under a stream of nitrogen. The mixture was stirred for 48 h. More pyridine sulfur trioxide (28 mg, 0.18 mmol) was added and stirring was continued for 1 h. Then, more pyridine sulfur trioxide (28 mg, 0.18 mmol) was added and stirring was continued for 1 h. The mixture was diluted with water (5 mL) and extracted with DCM (2 x 5 mL). The combined organic extracts were dried by passing through a hydrophobic frit. Product remaining in the aqueous phase was isolated by loading onto an Oasis HLB cartridge (500 mg) that had been preconditioned with MeOH (1 CV) then water (1 CV). The cartridge was eluted with water (1 CV) then MeOH (2 CV). The methanolic fraction was combined with the organic phase from the initial work-up and the solvent was removed under reduced pressure. The crude material was purified by MDAP Method G and the product-containing fractions were



concentrated under reduced pressure to afford **181** (5 mg, 18%) as a white solid. LCMS (Method B, UV, ESI)  $R_t = 0.61$  min,  $[M-H]^+ = 462$ , 100% purity;  $^1H$  NMR (400 MHz,  $d_4$ -MeOH)  $\delta$  2.40 - 2.53 (m, 4 H), 2.97 (s, 3 H), 3.34 (s, 2 H), 3.37 (s, 2 H), 3.61 - 3.73 (m, 4 H), 4.02 (s, 3 H), 5.07 (s, 2 H), 5.13 (s, 2 H), 7.34 (s, 1 H), 7.39 (s, 1 H), 7.92 (d,  $J = 2.3$  Hz, 1 H), 8.09 (d,  $J = 2.3$  Hz, 1 H), one proton signal was not observed.

## 6.11. Preparation of Intermediate for Dihydroisobenzofuran Array.

### 6.11.1. 2-Chloro-*N*-(6-(6-methoxy-5-(methylsulfonamido)pyridin-3-yl)-1,3-dihydroisobenzofuran-4-yl)acetamide, **224**

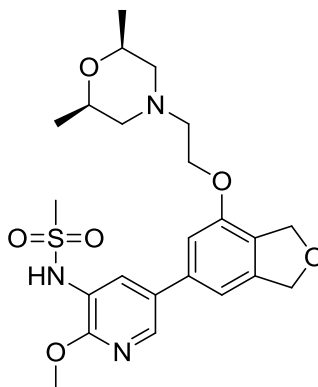


2-Chloroacetyl chloride (0.03 mL, 0.30 mmol) in 2-MeTHF (50 mL) was added to a solution of *N*-(5-(7-amino-1,3-dihydroisobenzofuran-5-yl)-2-methoxypyridin-3-yl)methanesulfonamide (1.22 g, 3.64 mmol) and  $NEt_3$  (0.02 mL, 0.22 mmol) in 2-MeTHF (1 mL) at 0 °C. The reaction mixture was stirred and slowly warmed to room temperature over 1 h. Stirring was continued for 5 h.  $NEt_3$  (0.51 mL, 3.64 mmol) and 2-chloroacetyl chloride (0.37 mL, 3.64 mmol) was added to the reaction mixture and stirring was continued for 72 h. Silica was added and the solvent was removed under reduced pressure. The crude material was purified by chromatography on FlashMaster II silica (2 x 100 g), eluting with 25-100% EtOAc/cyclohexane over 1 h. The product-containing fractions were concentrated under reduced pressure to afford **224** (1.09 g, 73%) as a white solid. Mp 205-208 °C ; LCMS (Method A, UV, ESI)  $R_t = 0.76$  min,  $[M-H]^+ = 412$ , 100% purity;  $^1H$  NMR (400 MHz,  $d_6$ -DMSO)  $\delta$  3.08 (s, 3 H), 3.97 (s, 3 H), 4.31 (s, 2 H), 4.97 (s, 2

H), 5.07 (s, 2 H), 7.40 (s, 1 H), 7.65 (s, 1 H), 7.83 (d,  $J = 2.3$  Hz, 1 H), 8.25 (d,  $J = 2.3$  Hz, 1 H), 9.31 (s, 1 H), 10.08 (s, 1 H);  $^{13}\text{C}$  NMR (101 MHz,  $d_6$ -DMSO)  $\delta$  40.9, 43.3, 54.0, 72.1, 73.0, 116.0, 119.4, 121.6, 129.6, 130.6, 131.3, 132.2, 137.1, 140.5, 142.1, 156.3, 165.0; IR ( $\nu_{\text{max}}$  / $\text{cm}^{-1}$ ); 769, 1320, 1671, 3204 (br.), 3259 (br.); HR-ESIMS ( $m/z$ ) calcd for  $\text{C}_{17}\text{H}_{19}\text{ClN}_3\text{O}_5\text{S}$   $[\text{M}+\text{H}]^+$  412.0729, found 412.0724.

## 6.12. Preparation of 4-Ether Substituted Dihydroisobenzofurans.

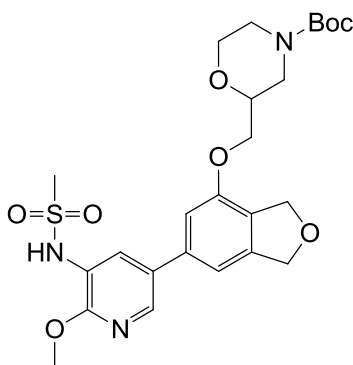
### 6.12.1. *N*-(5-(7-(*cis*-2,6-Dimethylmorpholino)ethoxy)-1,3-dihydroisobenzofuran-5-yl)-2-methoxypyridin-3-yl)methanesulfonamide, **226**



Lithium *tert*-butoxide (135 mg, 1.68 mmol) and *cis*-2,6-dimethylmorpholino)ethanol (803 mg, 5.04 mmol) were added to a mixture of *N*-(5-(7-iodo-1,3-dihydroisobenzofuran-5-yl)-2-methoxypyridin-3-yl)methanesulfonamide (150 mg, 0.34 mmol) and copper(I) iodide (32.0 mg, 0.17 mmol) in DMSO (1.5 mL). The mixture was heated in a microwave at 150 °C for 1 h then 160 °C for 1.5 h. The mixture was diluted with MeOH (2 mL) and loaded on a 2 g SCX-2 cartridge that had been pre-conditioned with MeOH (1 CV). The cartridge was washed with MeOH (2 CV) then eluted with  $\text{NH}_3$  (as a 2 M solution in MeOH, 2 CV). The basic fraction was concentrated under reduced pressure and the crude material was purified by MDAP Method B2. The product-containing fractions were concentrated under reduced pressure to afford **226** (47 mg, 29%) as a white solid. Mp 153-156 °C. LCMS (Method A, UV, ESI)  $R_t = 0.63$  min,  $[\text{M}-\text{H}]^+ = 478$ , 100% purity;  $^1\text{H}$  NMR (400 MHz,  $d_6$ -DMSO)  $\delta$  1.04 (d,  $J = 6.3$  Hz, 6 H), 1.75 (t,  $J = 10.5$  Hz, 2 H), 2.69 (t,

$J = 5.8$  Hz, 2 H), 2.82 (d,  $^2J = 10.5$  Hz, 2 H), 3.06 (s, 3 H), 3.49 – 3.59 (m, 2 H), 3.96 (s, 3 H), 4.25 (t,  $J = 5.8$  Hz, 2 H), 4.98 (s, 2 H), 5.05 (s, 2 H), 7.12 (s, 2 H), 7.86 (d,  $J = 2.3$  Hz, 1 H), 8.31 (d,  $J = 2.3$  Hz, 1 H), 9.29 (br. s, 1 H);  $^{13}\text{C}$  NMR (101 MHz,  $d_6$ -DMSO)  $\delta$  18.9 (2 C), 40.7, 53.7, 56.4, 59.3 (2 C), 65.9, 70.9 (2 C), 73.1, 109.3, 111.6, 121.1, 125.9, 129.9, 131.3, 138.3, 140.8, 141.8, 153.3, 156.3, one carbon peak was not observed; IR ( $\nu_{\text{max}}$  / $\text{cm}^{-1}$ ); 1139, 1330; HR-ESIMS ( $m/z$ ) calcd for  $\text{C}_{23}\text{H}_{32}\text{N}_3\text{O}_6\text{S}$   $[\text{M}+\text{H}]^+$  478.2006, found 478.2004.

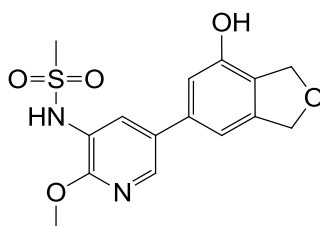
**6.12.2. *tert*-Butyl-2-(((6-(6-methoxy-5-(methylsulfonamido)pyridin-3-yl)-1,3-dihydroisobenzofuran-4-yl)oxy)methyl)morpholine-4-carboxylate, 232**



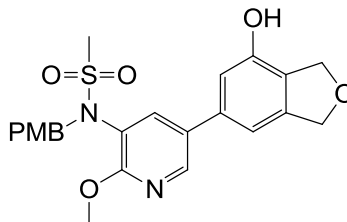
A mixture of *N*-(5-(7-iodo-1,3-dihydroisobenzofuran-5-yl)-2-methoxypyridin-3-yl)methanesulfonamide (207 mg, 0.46 mmol), copper(I) iodide (53 mg, 0.28 mmol), *tert*-butyl-2-(hydroxymethyl)morpholine-4-carboxylate (418 mg, 1.92 mmol) and lithium *tert*-butoxide (183 mg, 2.29 mmol) in DMSO (1 mL) was degassed in a microwave vial with nitrogen for 5 min. The mixture was heated in a microwave at 150 °C for 1 h then concentrated under reduced pressure. The residue was taken up in DCM (15 mL) and washed with water (15 mL). The aqueous phase was extracted with DCM (15 mL). The combined organic extracts were dried by passing through a hydrophobic frit and concentrated under reduced pressure. The crude material was purified by Normal Phase Chromatography on FlashMaster II silica (50 g), eluting with 0-100% EtOAc/cylohexane over 40 min. The product-containing fractions were concentrated under reduced pressure to afford **232** (138 mg, 21%) as a yellow oil. LCMS (Method A, UV, ESI)  $R_t = 1.08$  min,  $[\text{M}-\text{H}]^- = 534$ ,

100% purity;  $^1\text{H}$  NMR (400 MHz,  $d_6$ -DMSO)  $\delta$  1.41 (s, 9 H), 2.71 - 2.86 (m, 1 H), 2.86 - 2.99 (m, 1 H), 3.08 (s, 3 H), 3.37 - 3.53 (m, 1 H), 3.63 - 3.78 (m, 2 H), 3.81 - 3.96 (m, 2 H), 3.97 (s, 3 H), 4.09 - 4.27 (m, 2 H), 5.01 (s, 2 H), 5.06 (s, 2 H), 7.16 (s, 2 H), 7.88 (d,  $J = 2.3$  Hz, 1 H), 8.33 (d,  $J = 2.3$  Hz, 1 H), 9.29 (br. s, 1 H).

**6.12.3. *N*-(5-(7-Hydroxy-1,3-dihydroisobenzofuran-5-yl)-2-methoxy-3-yl)methanesulfonamide, **233****



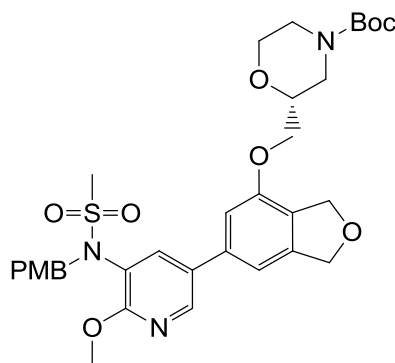
A mixture of *N*-(5-(7-iodo-1,3-dihydroisobenzofuran-5-yl)-2-methoxy-3-yl)methanesulfonamide (7.0 g, 15.7 mmol), copper(I) iodide (0.6 g, 3.1 mmol), 2-methylquinolin-8-ol (1.1 g, 7.1 mmol) in DMSO (50 mL) was split equally between five 20 mL microwave vials under an atmosphere of nitrogen. *n*-Bu<sub>4</sub>NOH (6.16 mL of a 40% w/w aqueous solution, 9.4 mmol) was added slowly to each vial. The vials were heated in a microwave at 120 °C for 2.5 h. The mixtures were combined and partitioned between EtOAc (130 mL) and water (150 mL). The organic phase was separated and the aqueous layer was acidified to pH 1 with HCl (as a 2 M aqueous solution). The aqueous phase was extracted with EtOAc (2 x 150 mL) and the combined organic extracts were washed with brine (100 mL), dried (MgSO<sub>4</sub>) and concentrated under reduced pressure. The crude material was purified by Normal Phase Chromatography on Companion silica (330 g), eluting with 0-100% EtOAc/cyclohexane over 1 h. The product-containing fractions were concentrated under reduced pressure to afford **233** (3.3 g, 61%) as an orange solid. LCMS (Method A, UV, ESI)  $R_t = 0.72$  min,  $[\text{M-H}]^+ = 337$ , 100% purity;  $^1\text{H}$  NMR (400 MHz,  $d_6$ -DMSO)  $\delta$  3.07 (s, 3 H), 3.96 (s, 3 H), 4.96 (s, 2 H), 5.02 (s, 2 H), 6.89 (s, 1 H), 7.00 (s, 1 H), 7.79 (d,  $J = 2.3$  Hz, 1 H), 8.20 (d,  $J = 2.3$  Hz, 1 H), 9.30 (s, 1 H), 9.82 (s, 1 H).

**6.12.4. N-(5-(7-Hydroxy-1,3-dihydroisobenzofuran-5-yl)-2-methoxypyridin-3-yl)-N-(4-methoxybenzyl)methanesulfonamide, 235**

A mixture of *N*-(5-(7-hydroxy-1,3-dihydroisobenzofuran-5-yl)-2-methoxypyridin-3-yl)methanesulfonamide (218 mg, 0.65 mmol), *para*-methoxybenzyl chloride (0.08 mL, 0.71 mmol) and  $K_2CO_3$  (134 mg, 0.97 mmol) in DMF (3 mL) was stirred at room temperature under nitrogen over the weekend. Further *para*-methoxybenzyl chloride (0.04 mL, 0.26 mmol) was added and the mixture stirred for 2.5 h. The reaction mixture was filtered and the filtrate concentrated under reduced pressure. The residue was taken up in DCM (5 mL) and TFA (3 mL, 38.9 mmol) was added. Stirring was continued for 30 min then the mixture was diluted with DCM (5 mL) and quenched by cautious addition of saturated aqueous  $NaHCO_3$  solution (10 mL). The phases were separated and the aqueous phase was extracted with DCM (2 x 10 mL). The combined organic extracts were dried by passing through a hydrophobic frit then concentrated under reduced pressure. The crude material was purified by Normal Phase Chromatography on Companion silica (40 g), eluting with 30-70% EtOAc/cyclohexane over 9 CV. The product-containing fractions were concentrated under reduced pressure to afford **235** (182 mg, 62%) as a white solid. Mp 212-215 °C. LCMS (Method A, UV, ESI)  $R_t = 0.98$  min,  $[M-H]^+ = 457$ , 96% purity;  $^1H$  NMR (400 MHz,  $d_6$ -DMSO)  $\delta$  3.15 (s, 3 H), 3.68 (s, 3 H), 3.98 (s, 3 H), 4.72 (br. s, 2 H), 4.94 (s, 2 H), 4.99 (s, 2 H), 6.78 (s, 1 H), 6.82 (d,  $J = 8.7$  Hz, 2 H), 6.87 (s, 1 H), 7.17 (d,  $J = 8.7$  Hz, 2 H), 7.55 (d,  $J = 2.3$  Hz, 1 H), 8.30 (d,  $J = 2.3$  Hz, 1 H), 9.77 (s, 1 H).  $^{13}C$  NMR (101 MHz,  $d_6$ -DMSO)  $\delta$  51.7, 53.8, 55.0, 70.9, 73.0, 109.9, 112.0, 113.7 (2 C), 121.7, 124.6, 128.1, 129.7 (2 C), 137.0, 139.5, 142.1, 143.7, 152.0, 158.6, 159.5, two carbon peaks were not

observed; IR ( $\nu_{\max}$  / $\text{cm}^{-1}$ ); 1149, 1330, 3364 (br.); HR-ESIMS ( $m/z$ ) calcd for  $\text{C}_{23}\text{H}_{25}\text{N}_2\text{O}_6\text{S}$   $[\text{M}+\text{H}]^+$  457.1428, found 457.1420.

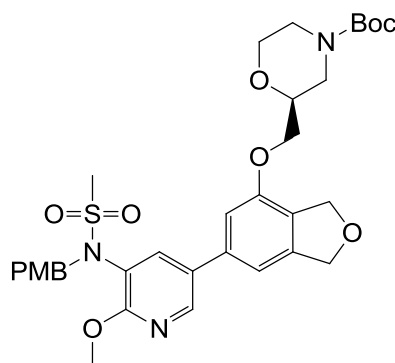
**6.12.5. (R)-tert-Butyl-2-(((6-(6-methoxy-5-(N-(4-methoxybenzyl)methylsulfonamido)pyridin-3-yl)-1,3-dihydroisobenzofuran-4-yl)oxy)methyl)morpholine-4-carboxylate, 239a**



A mixture of *N*-(5-(7-hydroxy-1,3-dihydroisobenzofuran-5-yl)-2-methoxypyridin-3-yl)-*N*-(4-methoxybenzyl)methanesulfonamide (205 mg, 0.45 mmol), (*R*)-*tert*-butyl 2-(hydroxymethyl)morpholine-4-carboxylate (357 mg, 1.64 mmol) and 2-(tributylphosphoranylidene)acetonitrile (0.25 mL, 0.90 mmol) in toluene (3 mL) was degassed in a microwave vial with nitrogen for 5 min then heated in a microwave at 120 °C for 1 h. The mixture was concentrated under reduced pressure and taken up in EtOAc (10 mL). The organic phase was washed with water (10 mL) then brine (10 mL), then dried by passing through a hydrophobic frit and concentrated under reduced pressure. The crude material was purified by Reverse Phase Chromatography on Companion C18 (120 g), eluting with 30-95% MeCN (containing 0.1% ammonium bicarbonate)/water (as a 0.1% w/v solution of ammonium bicarbonate) over 8 CV. The product-containing fractions were combined and concentrated under reduced pressure to remove MeCN. The aqueous phase was extracted with EtOAc (2 x 20 mL). The combined organic extracts were dried by passing through a hydrophobic frit and concentrated under reduced pressure to afford **239a** (218 mg, 74%) as a white solid. LCMS (Method A, UV, ESI)  $R_t$  = 1.27 min,  $[\text{M}-\text{H}]^+ = 656$ , 99% purity;  $^1\text{H}$  NMR (400 MHz,  $d_6$ -DMSO)  $\delta$  1.40 (s, 9

H), 2.71 – 3.00 (m, 2 H), 3.17 (s, 3 H), 3.39 - 3.51 (m, 1 H), 3.68 (s, 3 H), 3.68 - 3.76 (m, 2 H), 3.80 - 3.95 (m, 2 H), 3.97 (s, 3 H), 4.07 - 4.22 (m, 2 H), 4.71 (br. s, 2 H), 4.98 (s, 2 H), 5.02 (s, 2 H), 6.82 (d,  $J = 8.7$  Hz, 2 H), 6.99 (s, 1 H), 7.04 (s, 1 H), 7.20 (d,  $J = 8.7$  Hz, 2 H), 7.69 (d,  $J = 2.5$  Hz, 1 H), 8.42 (d,  $J = 2.5$  Hz, 1 H).

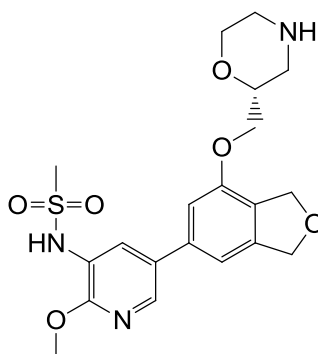
**6.12.6. (*S*)-*tert*-Butyl-2-(((6-(6-methoxy-5-(*N*-(4-methoxybenzyl)methylsulfonamido)pyridin-3-yl)-1,3-dihydroisobenzofuran-4-yl)oxy)methyl)morpholine-4-carboxylate, 239b**



A mixture of *N*-(5-(7-hydroxy-1,3-dihydroisobenzofuran-5-yl)-2-methoxypyridin-3-yl)-*N*-(4-methoxybenzyl)methanesulfonamide (199 mg, 0.44 mmol), (*S*)-*tert*-butyl 2-(hydroxymethyl)morpholine-4-carboxylate (345 mg, 1.59 mmol) and 2-(tributylphosphoranylidene)acetonitrile (0.24 mL, 0.87 mmol) in toluene (3 mL) was degassed in a microwave vial with nitrogen for 5 min then heated in a microwave at 120 °C for 1 h. The mixture was concentrated under reduced pressure and taken up in EtOAc (10 mL). The organic phase was washed with water (10 mL) then brine (10 mL), then dried by passing through a hydrophobic frit and concentrated under reduced pressure. The crude material was purified by Normal Phase Chromatography on FlashMaster II silica (50 g), eluting with 0-50% EtOAc/DCM over 40 min. The product-containing fractions were concentrated under reduced pressure to afford **265b** (289 mg, 100%) as a colourless glass. LCMS (Method A, UV, ESI)  $R_t = 1.27$  min,  $[M-H]^+ = 656$ , 70% purity;  $^1H$  NMR (400 MHz,  $d_6$ -DMSO)  $\delta$  1.41 (s, 9 H), 2.72 – 2.95 (m, 2 H), 3.17 (s, 3 H), 3.38 - 3.52 (m, 1 H), 3.68 (s, 3 H), 3.69 - 3.76 (m, 2 H), 3.82 - 3.95 (m, 2 H), 3.97 (s, 3 H), 4.09 - 4.22 (m, 2 H), 4.71 (br. s, 2 H), 4.98 (s, 2 H), 5.02 (s, 2 H), 6.82 (d,  $J = 8.6$  Hz, 2 H),

6.99 (s, 1 H), 7.04 (s, 1 H), 7.19 (d,  $J = 8.6$  Hz, 2 H), 7.68 (d,  $J = 2.3$  Hz, 1 H), 8.42 (d,  $J = 2.3$  Hz, 1 H), contains ~30% w/w (*S*)-*tert*-butyl 2-(hydroxymethyl)morpholine-4-carboxylate. The material was taken forward directly without further purification or characterisation.

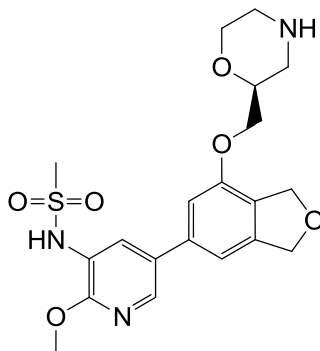
**6.12.7. (*R*)-*N*-(2-Methoxy-5-(7-(morpholin-2-ylmethoxy)-1,3-dihydroisobenzofuran-5-yl)pyridin-3-yl)methanesulfonamide, 240a**



A mixture of (*R*)-*tert*-butyl 2-(((6-(6-methoxy-5-(*N*-(4-methoxybenzyl)methylsulfonamido)pyridin-3-yl)-1,3-dihydroisobenzofuran-4-yl)oxy)methyl)morpholine-4-carboxylate (218 mg, 0.33 mmol) and TFA (1 mL) in DCM (2 mL) was heated in a microwave at 50 °C for 1 h, then at 80 °C for 20 min. The reaction mixture was loaded onto a 5 g SCX-2 cartridge that had been preconditioned with MeOH. The cartridge was eluted with MeOH (2 CV) then NH<sub>3</sub> (as a 7 M solution in MeOH, 2 CV). The basic fraction was concentrated under a stream of nitrogen to afford **240a** (134 mg, 93%) as a pale orange glass. Mp 109-114 °C; LCMS (Method B, UV, ESI)  $R_t = 0.58$  min,  $[M-H]^+ = 436$ , 98% purity; <sup>1</sup>H NMR (400 MHz, *d*<sub>6</sub>-DMSO)  $\delta$  2.52 - 2.62 (m, 1 H), 2.65 - 2.78 (m, 2 H), 2.85 - 2.99 (m, 1 H), 3.07 (s, 3 H), 3.43 - 3.56 (m, 1 H), 3.69 - 3.82 (m, 2 H), 3.96 (s, 3 H), 4.02 - 4.15 (m, 2 H), 5.00 (s, 2 H), 5.05 (s, 2 H), 7.11 (s, 1 H), 7.14 (s, 1 H), 7.86 (d,  $J = 2.3$  Hz, 1 H), 8.31 (d,  $J = 2.3$  Hz, 1 H), two proton signals were not observed; <sup>13</sup>C NMR (101 MHz, *d*<sub>6</sub>-DMSO)  $\delta$  40.7, 45.0, 47.2, 53.7, 66.6, 69.2, 70.9, 73.0, 74.1, 109.3, 111.7, 121.3, 125.9, 129.9, 131.0, 138.3, 140.6, 141.9, 153.3, 156.3; IR ( $\nu_{\max}$ /cm<sup>-1</sup>); 1144, 1326, 3307 (br.); HR-ESIMS ( $m/z$ ) calcd for C<sub>20</sub>H<sub>26</sub>N<sub>3</sub>O<sub>6</sub>S  $[M+H]^+$  436.1537, found 436.1530.

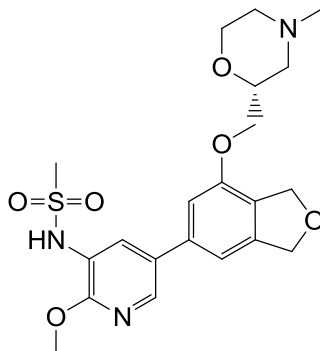


6.12.8. (*S*)-*N*-(2-Methoxy-5-(7-(morpholin-2-ylmethoxy)-1,3-dihydroisobenzofuran-5-yl)pyridin-3-yl)methanesulfonamide, **240b**



A mixture of (*S*)-*tert*-butyl-2-(((6-(6-methoxy-5-(*N*-(4-methoxybenzyl)methylsulfonamido)pyridin-3-yl)-1,3-dihydroisobenzofuran-4-yl)oxy)methyl)morpholine-4-carboxylate (289 mg, 0.44 mmol) and TFA (1 mL) in DCM (2 mL) was heated in a microwave at 50 °C for 1 h, then at 80 °C for 20 min. The reaction mixture was loaded onto a 5 g SCX-2 cartridge that had been preconditioned with MeOH. The cartridge was eluted with MeOH (2 CV) then NH<sub>3</sub> (as a 7 M solution in MeOH, 2 CV). The basic fraction was concentrated under a stream of nitrogen to afford **240b** (160 mg, 83%) as a pale orange glass. LCMS (Method B, UV, ESI)  $R_t = 0.58$  min,  $[M-H]^+ = 436$ , 80% purity; <sup>1</sup>H NMR (400 MHz, *d*<sub>6</sub>-DMSO)  $\delta$  2.52 - 2.62 (m, 1 H), 2.65 - 2.78 (m, 2 H), 2.85 - 2.99 (m, 1 H), 3.07 (s, 3 H), 3.43 - 3.56 (m, 1 H), 3.69 - 3.82 (m, 2 H), 3.96 (s, 3 H), 4.02 - 4.15 (m, 2 H), 5.00 (s, 2 H), 5.05 (s, 2 H), 7.11 (s, 1 H), 7.14 (s, 1 H), 7.86 (d,  $J = 2.3$  Hz, 1 H), 8.31 (d,  $J = 2.3$  Hz, 1 H), two proton signals were not observed, contains ~20% w/w (*S*)-*tert*-butyl 2-(hydroxymethyl)morpholine-4-carboxylate. The material was taken forward directly without further purification or characterisation.

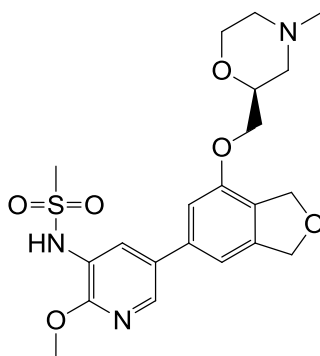
6.12.9. (*R*)-*N*-(2-Methoxy-5-(7-((4-methylmorpholin-2-yl)methoxy)-1,3-dihydroisobenzofuran-5-yl)pyridin-3-yl)methanesulfonamide, **228a**



Formaldehyde (as a 37% aqueous solution, 0.05 mL, 0.67 mmol) was added to (*R*)-*N*-(2-methoxy-5-(7-(morpholin-2-ylmethoxy)-1,3-dihydroisobenzofuran-5-yl)pyridin-3-yl)methanesulfonamide (100 mg, 0.23 mmol) in formic acid (as an 88% aqueous solution, 1.0 mL, 22.9 mmol). The mixture was stirred at 80 °C for 5 h. HCl (as a 2 M aqueous solution, 1 mL) was added and the aqueous phase was washed with DCM (2 x 1 mL). The aqueous phase was basified with NaOH (as a 2 M aqueous solution) and extracted with DCM (2 x 2 mL). All the combined organic extracts were dried by passing through a hydrophobic frit and concentrated under reduced pressure. The aqueous phase still contained product so it was concentrated under reduced pressure. The residue was taken up in MeOH and added to the top of a 2 g SCX-2 cartridge that had been preconditioned with MeOH. The cartridge was eluted with MeOH (2 CV) then NH<sub>3</sub> (as a 2 M solution in MeOH, 2 CV). Both fractions contained product and starting material so were combined and concentrated under reduced pressure. The residue was taken up in DMSO and combined with the residue from the organic extracts. The sample was filtered then purified by MDAP Method B2 and the product-containing fractions were concentrated under reduced pressure to afford **228a** (33 mg, 32%) as a white solid. Mp 136-139 °C; LCMS (Method B, UV, ESI)  $R_t = 0.66$  min,  $[M-H]^+ = 450$ , 100% purity; chiral HPLC (Method A)  $R_t = 16.51$  min; <sup>1</sup>H NMR (400 MHz, *d*<sub>6</sub>-DMSO)  $\delta$  1.87 (t,  $J = 10.6$  Hz, 1 H), 1.95 – 2.06 (m, 1 H), 2.19 (s, 3 H), 2.59 (d,  $^2J = 11.3$  Hz, 1 H), 2.78 (d,  $^2J = 11.3$  Hz, 1 H), 3.07 (s, 3 H), 3.48 – 3.60 (m, 1 H), 3.67 - 3.85 (m, 2 H), 3.96 (s, 3 H), 4.06

- 4.23 (m, 2 H), 5.00 (s, 2 H), 5.05 (s, 2 H), 7.11 (s, 1 H), 7.13 (s, 1 H), 7.86 (d,  $J = 2.3$  Hz, 1 H), 8.30 (d,  $J = 2.3$  Hz, 1 H), 9.26 (br. s, 1 H);  $^{13}\text{C}$  NMR (101 MHz,  $d_6$ -DMSO)  $\delta$  40.7, 45.9, 53.7, 54.4, 56.6, 65.7, 69.2, 70.9, 73.1, 73.5, 109.3, 111.8, 121.3, 125.9, 129.9, 131.0, 138.3, 140.6, 141.9, 153.3, 156.3; IR ( $\nu_{\text{max}}$ /cm $^{-1}$ ): 1145, 1334; HR-ESIMS ( $m/z$ ) calcd for  $\text{C}_{21}\text{H}_{28}\text{N}_3\text{O}_6\text{S}$   $[\text{M}+\text{H}]^+$  450.1693, found 450.1682.

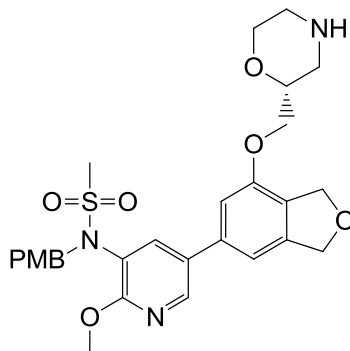
**6.12.10. (S)-N-(2-Methoxy-5-(7-((4-methylmorpholin-2-yl)methoxy)-1,3-dihydroisobenzofuran-5-yl)pyridin-3-yl)methanesulfonamide, 228b**



Formaldehyde (0.06 mL of a 37% aqueous solution, 0.81 mmol) was added to (S)-N-(2-methoxy-5-(7-(morpholin-2-ylmethoxy)-1,3-dihydroisobenzofuran-5-yl)pyridin-3-yl)methanesulfonamide (130 mg, 0.30 mmol) in formic acid (1.3 mL of an 88% aqueous solution, 29.8 mmol). The mixture was stirred at 80 °C for 5 h. HCl (as a 2 M aqueous solution, 1 mL) was added and the aqueous phase was washed with DCM (2 x 1 mL). The aqueous phase was basified with NaOH (as a 2 M aqueous solution) and extracted with DCM (2 x 2 mL). All the combined organic extracts were dried by passing through a hydrophobic frit and concentrated under reduced pressure. The aqueous phase still contained product so was concentrated under reduced pressure. The residue was taken up in DMSO (1 mL) and combined with the residue from the organic extracts. The sample was filtered then purified by MDAP Method B2 and the product-containing fractions were concentrated under reduced pressure to afford **228b** (19 mg, 14%) as a white solid. LCMS (Method B, UV, ESI)  $R_t = 0.66$  min,  $[\text{M}-\text{H}]^+ = 450$ , 97% purity; chiral HPLC (Method A)  $R_t = 18.64$  min;  $^1\text{H}$  NMR (400 MHz,  $d_6$ -DMSO)  $\delta$  1.87 (t,  $J = 10.6$  Hz, 1 H), 1.95 – 2.06

(m, 1 H), 2.19 (s, 3 H), 2.59 (d,  $J = 11.3$  Hz, 1 H), 2.78 (d,  $J = 11.3$  Hz, 1 H), 3.07 (s, 3 H), 3.48 – 3.60 (m, 1 H), 3.67 - 3.85 (m, 2 H), 3.96 (s, 3 H), 4.06 - 4.23 (m, 2 H), 5.00 (s, 2 H), 5.05 (s, 2 H), 7.11 (s, 1 H), 7.13 (s, 1 H), 7.86 (d,  $J = 2.3$  Hz, 1 H), 8.30 (d,  $J = 2.3$  Hz, 1 H), 9.26 (br. s, 1 H).

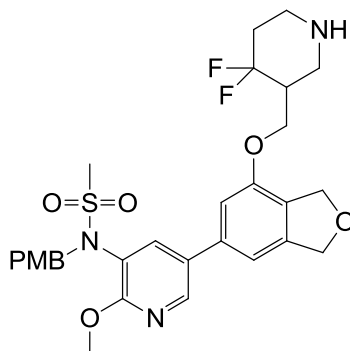
**6.12.11. (R)-N-(2-Methoxy-5-(7-(morpholin-2-ylmethoxy)-1,3-dihydroisobenzofuran-5-yl)pyridin-3-yl)-N-(4-methoxybenzyl)methanesulfonamide, 250**



TFA (2 mL, 26.0 mmol) was added to a mixture of (*R*)-*tert*-butyl-2-(((6-(6-methoxy-5-(*N*-(4-methoxybenzyl)methylsulfonamido)pyridin-3-yl)-1,3-dihydroisobenzofuran-4-yl)oxy)methyl)morpholine-4-carboxylate (500 mg, 0.46 mmol) in DCM (5 mL). The mixture was stirred at room temperature for 1 h. The reaction mixture was diluted with DCM (5 mL) and quenched with saturated aqueous NaHCO<sub>3</sub> solution (5 mL). The phases were separated and the aqueous phase was extracted with DCM (3 x 10 mL). The combined organic extracts were dried by passing through a hydrophobic frit and concentrated under reduced pressure. The residue was taken up in MeOH (1 mL) and added to the top of a 5 g SCX-2 cartridge that had been preconditioned with MeOH (1 CV). The cartridge was eluted with MeOH (3 CV) then NH<sub>3</sub> (as a 7 M solution in MeOH, 3 CV). The basic fraction was concentrated under reduced pressure to afford **250** (132 mg, 52%) as a white solid. LCMS (Method A, UV, ESI)  $R_t = 0.82$  min,  $[M-H]^+ = 556$ , 100% purity; <sup>1</sup>H NMR (400 MHz, *d*<sub>6</sub>-DMSO)  $\delta$  2.53 – 2.59 (m, 1 H), 2.62 - 2.76 (m, 2 H), 2.876 – 2.94 (m, 1 H), 3.17 (s, 3 H), 3.42 – 3.53 (m, 1 H), 3.68 (s, 3 H), 3.69 - 3.80 (m, 2 H), 3.97 (s, 3 H), 4.01 - 4.12 (m, 2 H), 4.72 (br. s, 2 H), 4.97 (s, 2 H), 5.02 (s, 2 H), 6.82 (d,  $J = 8.6$

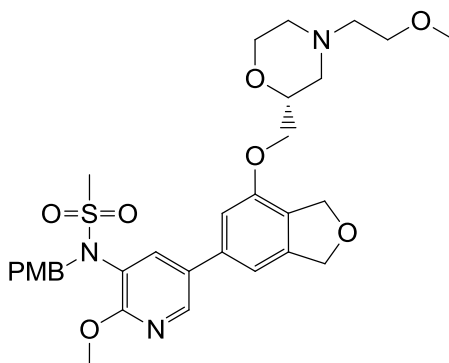
Hz, 2 H), 6.96 (s, 1 H), 7.02 (s, 1 H), 7.19 (d,  $J = 8.6$  Hz, 2 H), 7.68 (d,  $J = 2.3$  Hz, 1 H), 8.41 (d,  $J = 2.3$  Hz, 1 H), one proton signal was not observed.

**6.12.12. *N*-(5-(7-((4,4-Difluoropiperidin-3-yl)methoxy)-1,3-dihydroisobenzofuran-5-yl)-2-methoxypyridin-3-yl)-*N*-(4-methoxybenzyl)methanesulfonamide, **251****



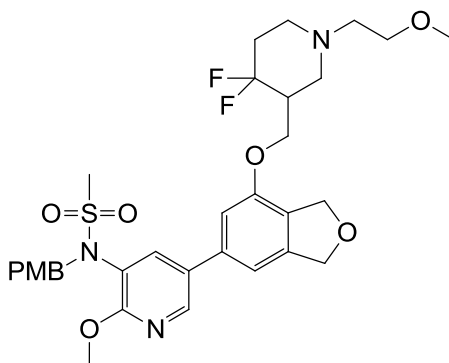
TFA (0.6 mL, 7.79 mmol) was added to a solution of *tert*-butyl-4,4-difluoro-3-(((6-(6-methoxy-5-(*N*-(4-methoxybenzyl)methylsulfonamido)pyridin-3-yl)-1,3-dihydroisobenzofuran-4-yl)oxy)methyl)piperidine-1-carboxylate (230 mg, 0.33 mmol) in DCM (1.8 mL). The mixture stirred at room temperature for 2 h then concentrated under reduced pressure. The residue was taken up in MeOH (1 mL) and added to the top of a 5 g SCX-2 cartridge that had been pre-conditioned with MeOH (1 CV). The cartridge was eluted with MeOH (2 CV) then  $\text{NH}_3$  (as a 2 M solution in MeOH, 3 CV). The basic fraction was concentrated under reduced pressure to afford **251** (150 mg, 76%) as a brown gum. LCMS (Method A, UV, ESI)  $R_t = 0.85$  min,  $[\text{M}-\text{H}]^+ = 590$ , 91% purity. The material was taken forward directly without further purification or characterisation.

**6.12.13. (*R*)-*N*-(2-Methoxy-5-(7-((4-(2-methoxyethyl)morpholin-2-yl)methoxy)-1,3-dihydroisobenzofuran-5-yl)pyridin-3-yl)-*N*-(4-methoxybenzyl)methanesulfonamide, **253****

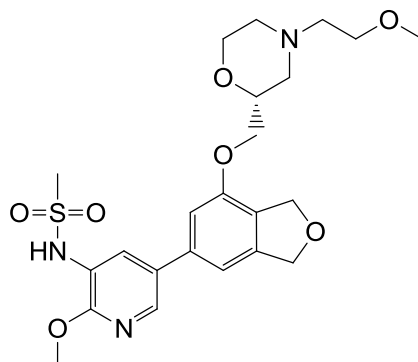


$\text{K}_2\text{CO}_3$  (33 mg, 0.24 mmol) and NaI (2 mg, 0.01 mmol) were added to a solution of (*R*)-*N*-(2-methoxy-5-(7-(morpholin-2-ylmethoxy)-1,3-dihydroisobenzofuran-5-yl)pyridin-3-yl)-*N*-(4-methoxybenzyl)methanesulfonamide (65 mg, 0.12 mmol) in MeCN (2 mL). 1-Bromo-2-methoxyethane (0.02 mL, 0.13 mmol) was added and the mixture was heated at 80 °C for 1 h. Stirring was continued overnight, then the mixture was cooled to room temperature and left to stand for 24 h. The mixture was added to the top of a 2 g SCX-2 cartridge that had been pre-conditioned with MeOH (1 CV). The cartridge was eluted with MeOH (2 CV) then  $\text{NH}_3$  (as a 2 M solution in MeOH, 3 CV). The basic fraction was concentrated under reduced pressure to afford **253** (55 mg, 77%) as an orange oil. LCMS (Method A, UV, ESI)  $R_t = 1.14$  min,  $[\text{M}-\text{H}]^+ = 614$ , 92% purity. The material was taken forward directly without further purification or characterisation.

**6.12.14. *N*-(5-(7-((4,4-Difluoro-1-(2-methoxyethyl)piperidin-3-yl)methoxy)-1,3-dihydroisobenzofuran-5-yl)-2-methoxypyridin-3-yl)-*N*-(4-methoxybenzyl)methanesulfonamide, 254**



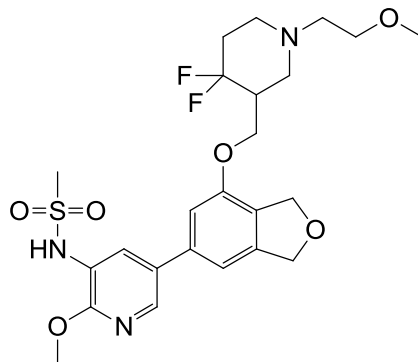
A mixture of *N*-(5-(7-((4,4-difluoropiperidin-3-yl)methoxy)-1,3-dihydroisobenzofuran-5-yl)-2-methoxypyridin-3-yl)-*N*-(4-methoxybenzyl)methanesulfonamide (152 mg, 0.26 mmol), 1-bromo-2-methoxyethane (0.05 mL, 0.53 mmol),  $K_2CO_3$  (91 mg, 0.66 mmol) and NaI (11 mg, 0.07 mmol) in MeCN (3 mL) was heated in a microwave at 70 °C for 2.5 h, then 90 °C for 20 min and finally 110 °C for 1.5 h. The inorganic solids were removed by filtration, washing with EtOAc (5 mL). The filtrate was concentrated under reduced pressure to afford **254** (115 mg, 69%) as a brown gum. LCMS (Method A, UV, ESI)  $R_t = 0.95$  min,  $[M-H]^+ = 648$ , 83% purity. The material was taken forward directly without further purification or characterisation.

**6.12.15. (R)-N-(2-Methoxy-5-(7-((4-(2-methoxyethyl)morpholin-2-yl)methoxy)-1,3-dihydroisobenzofuran-5-yl)pyridin-3-yl)methanesulfonamide, 242**

A mixture of (*R*)-*N*-(2-methoxy-5-(7-((4-(2-methoxyethyl)morpholin-2-yl)methoxy)-1,3-dihydroisobenzofuran-5-yl)pyridin-3-yl)-*N*-(4-methoxybenzyl)methanesulfonamide (50 mg, 0.08 mmol) and TFA (0.5 mL, 6.49 mmol) in DCM (0.5 mL) was heated in a microwave at 70 °C for 1 h. More DCM (5 mL) was added and the mixture was quenched with saturated aqueous NaHCO<sub>3</sub> solution (5 mL). The organic phase was separated, dried by passing through a hydrophobic frit and concentrated under reduced pressure. The crude material was purified by MDAP Method B2 and the product-containing fractions were concentrated under reduced pressure to afford **242** (22 mg, 52%) as a colourless gum; LCMS (Method B, UV, ESI) *R*<sub>t</sub> = 0.75 min, [M-H]<sup>+</sup> = 494, 99% purity; <sup>1</sup>H NMR (400 MHz, *d*<sub>6</sub>-DMSO) δ 1.93 – 2.17 (m, 2 H), 2.71 (m, 1 H), 2.89 (m, 1 H), 3.07 (s, 3 H), 3.24 (s, 3 H), 3.39 – 3.49 (m, 2 H), 3.49 - 3.59 (m, 1 H), 3.68 - 3.85 (m, 2 H), 3.97 (s, 3 H), 4.04 - 4.21 (m, 2 H), 5.00 (s, 2 H), 5.05 (s, 2 H), 7.12 (s, 1 H), 7.14 (s, 1 H), 7.86 (d, *J* = 2.0 Hz, 1 H), 8.31 (d, *J* = 2.0 Hz, 1 H), 9.29 (br. s, 1 H), two proton signals were obscured by the residual solvent peak.

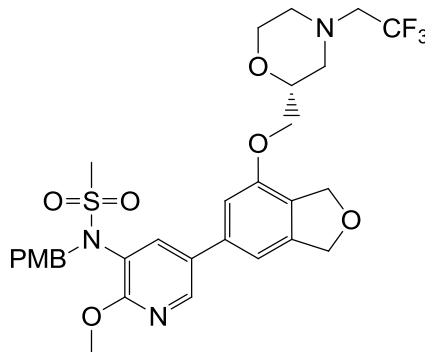


**6.12.16. *N*-(5-(7-((4,4-Difluoro-1-(2-methoxyethyl)piperidin-3-yl)methoxy)-1,3-dihydroisobenzofuran-5-yl)-2-methoxypyridin-3-yl)methanesulfonamide, 243**



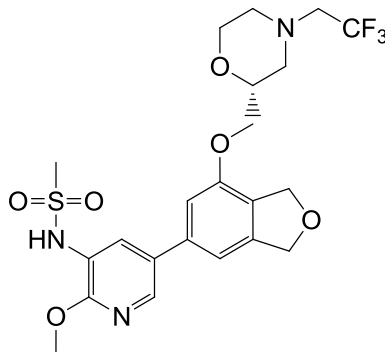
A mixture of *N*-(5-(7-((4,4-difluoro-1-(2-methoxyethyl)piperidin-3-yl)methoxy)-1,3-dihydroisobenzofuran-5-yl)-2-methoxypyridin-3-yl)-*N*-(4-methoxybenzyl)methanesulfonamide (115 mg, 0.18 mmol) and TFA (0.6 mL, 7.79 mmol) in DCM (2 mL) was heated in a microwave 70 °C for 1.5 h. The mixture was concentrated under reduced pressure and purified by MDAP Method B3. The product-containing fractions were concentrated under reduced pressure to afford **243** (37 mg, 40%) as a white solid. Mp 107-109 °C; LCMS (Method B, UV, ESI)  $R_t = 0.94$  min,  $[M-H]^+ = 528$ , 98% purity;  $^1H$  NMR (400 MHz,  $CDCl_3$ )  $\delta$  2.00 - 2.18 (m, 2 H), 2.28 - 2.47 (m, 2 H), 2.56 - 2.75 (m, 3 H), 2.86 - 2.98 (m, 1 H), 3.04 (s, 3 H), 3.10 - 3.21 (m, 1 H), 3.36 (s, 3 H), 3.49 - 3.56 (m, 2 H), 4.02 - 4.07 (m, 1H), 4.08 (s, 3 H), 4.44 (dd,  $J = 9.7, 3.7$  Hz, 1 H), 5.13 (s, 2 H), 5.16 (s, 2 H), 6.74 (s, 1 H), 6.89 (s, 1 H), 6.99 (s, 1 H), 7.97 (d,  $J = 2.3$  Hz, 1 H), 8.15 (d,  $J = 2.3$  Hz, 1 H);  $^{13}C$  NMR (101 MHz,  $d_6$ -DMSO)  $\delta$  33.5 (t,  $^2J_{C-F} = 20$  Hz), 41.2, 42.9 (t,  $^2J_{C-F} = 20$  Hz), 50.3, 53.3, 54.2, 56.4, 58.5, 64.7, 70.7, 71.3, 73.6, 109.7, 112.5, 121.6, 126.5, 130.4, 131.8, 138.9, 141.4, 142.5, 153.6, 156.8, one carbon peak was not observed;  $^{19}F$  NMR (376 MHz,  $CDCl_3$ )  $\delta$  -99.9, -99.3; IR ( $\nu_{max}/cm^{-1}$ ): 1139, 1331; HR-ESIMS ( $m/z$ ) calcd for  $C_{24}H_{32}F_2N_3O_6S$   $[M+H]^+ 528.1974$ , found 528.1960.

**6.12.17. (*R*)-*N*-(2-Methoxy-5-(7-((4-(2,2,2-trifluoroethyl)morpholin-2-yl)methoxy)-1,3-dihydroisobenzofuran-5-yl)pyridin-3-yl)-*N*-(4-methoxybenzyl)methanesulfonamide, **252****



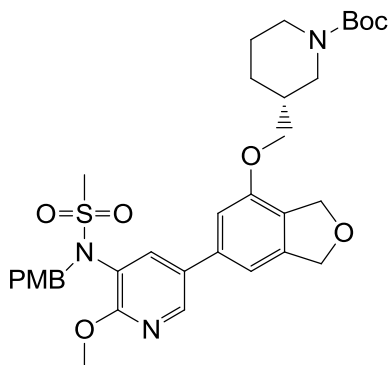
A mixture of (*R*)-*N*-(2-methoxy-5-(7-(morpholin-2-ylmethoxy)-1,3-dihydroisobenzofuran-5-yl)pyridin-3-yl)-*N*-(4-methoxybenzyl)methanesulfonamide (80 mg, 0.14 mmol), 2,2,2-trifluoroethyl trifluoromethylsulfonate (23  $\mu$ L, 0.16 mmol) and  $\text{Na}_2\text{CO}_3$  (24 mg, 0.29 mmol) in EtOH (2 mL) was heated to 78  $^\circ\text{C}$  overnight. More 2,2,2-trifluoroethyl trifluoromethylsulfonate (5  $\mu$ L, 0.04 mmol) was added and heating was continued for 2 h. The mixture was cooled to room temperature and the solvent was removed under reduced pressure. Water (5 mL) was added and the aqueous phase was extracted with DCM (2 x 5 mL). The combined organic extracts were dried by passing through a hydrophobic frit and concentrated under a stream of nitrogen to give afford **252** (60 mg, 65%) as a colourless oil. LCMS (Method B, UV, ESI)  $R_t = 1.26$  min,  $[\text{M}-\text{H}]^+ = 638$ , 74% purity. The material was taken forward directly without further purification or characterisation.

**6.12.18. (R)-N-(2-Methoxy-5-(7-((4-(2,2,2-trifluoroethyl)morpholin-2-yl)methoxy)-1,3-dihydroisobenzofuran-5-yl)pyridin-3-yl)methanesulfonamide, 241**



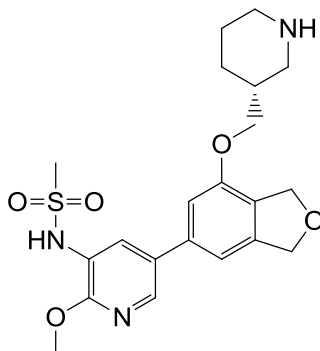
A solution of (R)-N-(2-methoxy-5-(7-((4-(2,2,2-trifluoroethyl)morpholin-2-yl)methoxy)-1,3-dihydroisobenzofuran-5-yl)pyridin-3-yl)-N-(4-methoxybenzyl)methanesulfonamide (59 mg, 0.09 mmol) and TFA (0.5 mL, 6.49 mmol) in DCM (0.5 mL) was heated in a microwave at 70 °C for 1 h. The mixture was concentrated under reduced pressure and the residue was purified by MDAP Method B3. The product-containing fractions were concentrated under reduced pressure to afford **241** (27 mg, 56%) as a white solid. Mp 184-187 °C; LCMS (Method B, UV, ESI)  $R_t = 0.94$  min,  $[M-H]^+ = 518$ , 100% purity;  $^1H$  NMR (400 MHz,  $d_6$ -DMSO)  $\delta$  2.31 – 2.36 (m, 1 H), 2.41 - 2.48 (m, 1 H), 2.74 – 2.79 (m, 1 H), 2.92 – 2.97 (m, 1 H), 3.07 (s, 3 H), 3.23 (q,  $J_{H-F} = 10.2$  Hz, 2 H), 3.50 - 3.62 (m, 1 H), 3.76 – 3.81 (m, 1 H), 3.80 - 3.86 (m, 1 H), 3.96 (s, 3 H), 4.08 – 4.13 (m, 1 H), 4.14 – 4.19 (m, 1 H), 5.00 (s, 2 H), 5.04 (s, 2 H), 7.11 (s, 1 H), 7.14 (s, 1 H), 7.86 (d,  $J = 2.3$  Hz, 1 H), 8.31 (d,  $J = 2.3$  Hz, 1 H), 9.26 (br. s, 1 H).  $^{19}F$  NMR (376 MHz,  $d_6$ -DMSO)  $\delta$  -68.0;  $^{13}C$  NMR (101 MHz,  $d_6$ -DMSO)  $\delta$  40.7, 52.7, 53.7, 54.9, 57.0 (q,  $^2J_{C-F} = 29.6$  Hz), 65.9, 69.0, 70.9, 73.1, 73.6, 109.4, 111.9, 121.3, 125.9, 129.9, 131.1, 138.3, 140.7, 141.9, 153.3, 156.3, the signal from the  $CF_3$  group was too weak to be observed; IR ( $\nu_{max}/cm^{-1}$ ): 1098, 1146, 1271, 1330, 3139 (br.); HR-ESIMS ( $m/z$ ) calcd for  $C_{22}H_{27}F_3N_3O_6S$   $[M+H]^+ 518.1567$ , found 518.1551.

**6.12.19. (*R*)-*tert*-Butyl-3-(((6-(6-methoxy-5-(*N*-(4-methoxybenzyl)methylsulfonamido)pyridin-3-yl)-1,3-dihydroisobenzofuran-4-yl)oxy)methyl)piperidine-1-carboxylate, **257****

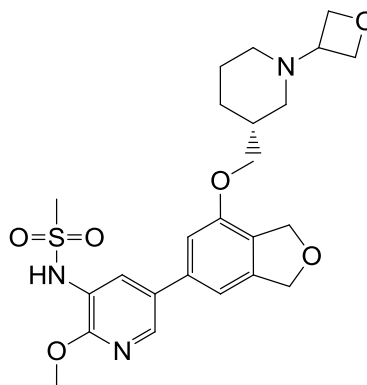


A mixture of (*R*)-*tert*-butyl 3-(hydroxymethyl)piperidine-1-carboxylate (52 mg, 0.24 mmol), *N*-(5-(7-hydroxy-1,3-dihydroisobenzofuran-5-yl)-2-methoxypyridin-3-yl)-*N*-(4-methoxybenzyl)methanesulfonamide (100 mg, 0.22 mmol) and 2-(tributylphosphoranylidene)acetonitrile (0.12 mL, 0.44 mmol) in toluene (1 mL) was heated in the microwave at 120 °C for 1 h. The mixture was concentrated under reduced pressure and purified by Normal Phase Chromatography on FlashMaster II silica (10 g), eluting with 0-100% EtOAc/cyclohexane over 30 min. The product-containing fractions were concentrated under reduced pressure to afford **257** (139 mg, 89%) as an orange oil. LCMS (Method B, UV, ESI)  $R_t = 1.39$  min,  $[M-H]^+ = 654$ , 92% purity. The material was taken forward directly without further purification or characterisation.

6.12.20. (*R*)-*N*-(2-Methoxy-5-(7-(piperidin-3-ylmethoxy)-1,3-dihydroisobenzofuran-5-yl)pyridin-3-yl)methanesulfonamide, **258**



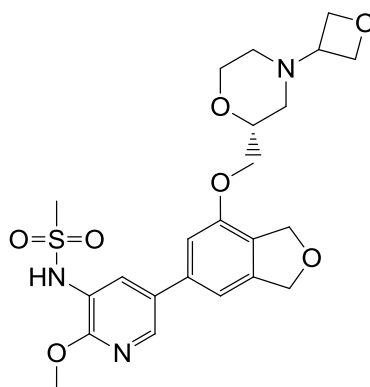
A mixture of (*R*)-*tert*-butyl-3-(((6-(6-methoxy-5-(*N*-(4-methoxybenzyl)methylsulfonamido)pyridin-3-yl)-1,3-dihydroisobenzofuran-4-yl)oxy)methyl)piperidine-1-carboxylate (139 mg, 0.21 mmol) and TFA (1.5 mL, 19.47 mmol) in DCM (1 mL) was heated in a microwave at 70 °C for 45 min. DCM (5 mL) was added and saturated aqueous NaHCO<sub>3</sub> solution (5 mL) was added until the pH reached 8. The aqueous phase was extracted with DCM (3 x 10 mL). The combined organic extracts were dried by passing through a hydrophobic frit and concentrated under reduced pressure. The crude material was taken up in MeOH/DCM (1 mL of a 1:1 mixture) and added to the top of a 2 g SCX-2 cartridge that had been preconditioned with MeOH (1 CV). The cartridge was eluted with MeOH (2 CV) then NH<sub>3</sub> (as a 2 M solution in MeOH, 3 CV). The basic fraction was concentrated under reduced pressure to afford **258** (83 mg, 79%) as a brown oil. LCMS (Method B, UV, ESI)  $R_t = 0.63$  min,  $[M-H]^+ = 434$ , 88% purity. The material was taken forward directly without further purification or characterisation.

**6.12.21. (R)-N-(2-Methoxy-5-(7-((1-(oxetan-3-yl)piperidin-3-yl)methoxy)-1,3-dihydroisobenzofuran-5-yl)pyridin-3-yl)methanesulfonamide, 244**

A mixture of (*R*)-*N*-(2-methoxy-5-(7-(piperidin-3-ylmethoxy)-1,3-dihydroisobenzofuran-5-yl)pyridin-3-yl)methanesulfonamide (83 mg, 0.19 mmol), STAB (122 mg, 0.57 mmol) and 3-oxetanone (41 mg, 0.57 mmol) in THF (1.5 mL) was stirred at room temperature under an atmosphere of nitrogen for 48 h. More 3-oxetanone (82 mg, 1.14 mmol) and STAB (122 mg, 0.57 mmol) was added and stirring was continued for 1 h. More 3-oxetanone (41 mg, 0.57 mmol) and STAB (122 mg, 0.57 mmol) were added and stirring was continued for 1 h. The mixture was partitioned between water (7 mL) and EtOAc (10 mL). The organic phase was separated and the aqueous phase was neutralised with NaOH (as a 2 M aqueous solution). The aqueous phase was then extracted with EtOAc (3 x 10 mL). The combined organic extracts were dried by passing through a hydrophobic frit and concentrated under reduced pressure. The crude material was purified by MDAP Method B2 and the product-containing fractions were concentrated under reduced pressure to afford **244** (15 mg, 15%) as a colourless oil. Mp 111-114 °C. LCMS (Method B, UV, ESI)  $R_t = 0.83$  min,  $[M-H]^+ = 490$ , 92% purity;  $^1H$  NMR (400 MHz,  $CDCl_3$ )  $\delta$  1.06 - 1.32 (m, 1 H), 1.41 - 1.58 (m, 1 H), 1.72 - 2.01 (m, 4 H), 1.94 - 2.02 (m, 1 H), 2.52 - 2.60 (m, 1 H), 2.64 - 2.73 (m, 1 H), 3.07 (s, 3 H), 3.33 - 3.42 (m, 1 H), 3.97 (s, 3 H), 4.02 (d,  $J = 6.6$  Hz, 2 H), 4.39 - 4.45 (m, 2 H), 4.50 - 4.56 (m, 2 H), 4.99 (s, 2 H), 5.05 (s, 2 H), 7.09 (s, 1 H), 7.12 (s, 1 H), 7.85 (d,  $J = 2.3$  Hz, 1 H), 8.30 (d,  $J = 2.3$  Hz, 1 H), one proton signal was not observed;  $^{13}C$  NMR (101 MHz,

$d_6$ -DMSO)  $\delta$  23.7, 26.5, 35.2, 40.7, 49.9, 52.5, 53.7, 58.8, 70.5, 70.8, 73.1, 74.5, 74.6, 109.2, 111.6, 121.1, 125.9, 129.9, 131.2, 138.3, 140.8, 141.9, 153.5, 156.3; IR ( $\nu_{\max}/\text{cm}^{-1}$ ): 1139, 1330; HR-ESIMS ( $m/z$ ) calcd for  $\text{C}_{24}\text{H}_{32}\text{N}_3\text{O}_6\text{S}$   $[\text{M}+\text{H}]^+$  490.2006, found 490.1998.

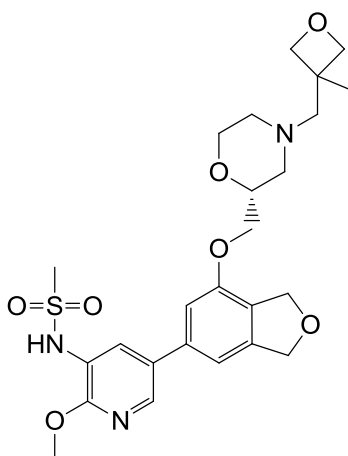
**6.12.22. (R)-N-(2-Methoxy-5-(7-((4-(oxetan-3-yl)morpholin-2-yl)methoxy)-1,3-dihydroisobenzofuran-5-yl)pyridin-3-yl)methanesulfonamide, 245**



A mixture of (R)-N-(2-methoxy-5-(7-(morpholin-2-yl)methoxy)-1,3-dihydroisobenzofuran-5-yl)pyridin-3-yl)methanesulfonamide (50 mg, 0.12 mmol), STAB (73 mg, 0.34 mmol) and 3-oxetanone (20  $\mu\text{L}$ , 0.34 mmol) in THF (1 mL) under nitrogen. The reaction was stirred at room temperature under an atmosphere of nitrogen for 5 h. More 3-oxetanone (10  $\mu\text{L}$ , 0.17 mmol), STAB (37 mg, 0.18 mmol) were added and stirring was continued overnight. The reaction was quenched by the addition of water (5 mL) and the aqueous phase was extracted with EtOAc (2 x 5 mL). The combined organic extracts were dried by passing through a hydrophobic frit and concentrated under reduced pressure. The crude material was purified by MDAP Method B2 and the product-containing fractions were concentrated under reduced pressure to afford **245** (16 mg, 28%) as a white solid. Mp 200-202  $^{\circ}\text{C}$ ; LCMS (Method B, UV, ESI)  $R_t = 0.66$  min,  $[\text{M}-\text{H}]^+ = 492$ , 97% purity;  $^1\text{H}$  NMR (400 MHz,  $d_6$ -DMSO)  $\delta$  1.86 (t,  $J = 10.6$  Hz, 1 H), 1.97 (td,  $J = 11.3, 3.2$  Hz, 1 H), 2.58 (d,  $^2J = 11.1$  Hz, 1 H), 2.75 (d,  $^2J = 11.1$  Hz, 1 H), 3.07 (s, 3 H), 3.44 (m, 1 H), 3.57 (td,  $J = 11.3$  Hz, 3.2 Hz, 1 H), 3.77 – 3.89 (m, 2 H), 3.96 (s, 3 H), 4.14 (d,  $J = 5.5$  Hz, 2 H), 4.43 – 4.50 (m, 2 H), 4.51 – 4.58 (m, 2 H), 4.99 (s, 2 H), 5.05 (s, 2 H),

7.12 (s, 1 H), 7.14 (s, 1 H), 7.86 (d,  $J = 2.3$  Hz, 1 H), 8.30 (d,  $J = 2.3$  Hz, 1 H), one proton signal was not observed;  $^{13}\text{C}$  NMR (101 MHz,  $d_6$ -DMSO)  $\delta$  40.7, 48.9, 50.9, 53.7, 58.6, 65.6, 69.3, 70.9, 73.1, 73.5, 74.0, 74.0, 109.4, 111.8, 121.3, 126.0, 129.9, 131.1, 138.3, 140.7, 142.0, 153.4, 156.3; IR ( $\nu_{\text{max}}$ /cm $^{-1}$ ): 1147, 1329, 3148 (br.); HR-ESIMS ( $m/z$ ) calcd for  $\text{C}_{23}\text{H}_{30}\text{N}_3\text{O}_7\text{S}$   $[\text{M}+\text{H}]^+$  492.1799, found 492.1792.

**6.12.23. (*R*)-*N*-(2-Methoxy-5-(7-((4-((3-methyloxetan-3-yl)methyl)morpholin-2-yl)methoxy)-1,3-dihydroisobenzofuran-5-yl)pyridin-3-yl)methanesulfonamide, **247****

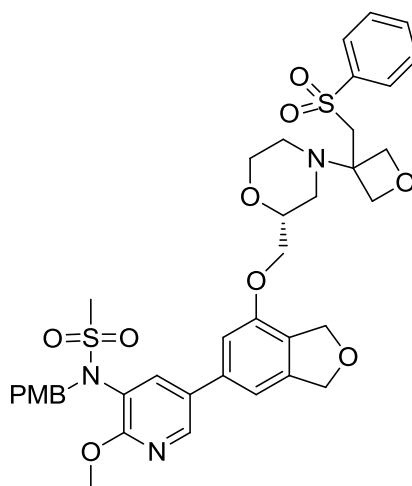


A mixture of (*R*)-*N*-(2-methoxy-5-(7-(morpholin-2-ylmethoxy)-1,3-dihydroisobenzofuran-5-yl)pyridin-3-yl)methanesulfonamide (50 mg, 0.12 mmol), STAB (73 mg, 0.34 mmol) and 3-methyloxetane-3-carbaldehyde (35 mg, 0.34 mmol) in THF (1 mL) was stirred at room temperature under an atmosphere of nitrogen for 48 h. The mixture was partitioned between water (5 mL) and EtOAc (10 mL). The organic phase was separated and the aqueous phase was neutralised with NaOH (as a 2 M aqueous solution). The aqueous phase was then extracted with EtOAc (3 x 10 mL). The combined organic extracts were dried by passing through a hydrophobic frit and concentrated under reduced pressure. The crude material was purified by MDAP Method B2 and the product-containing fractions were concentrated under reduced pressure to afford **247** (23 mg, 39%) as a white solid. Mp 100-104 °C; LCMS (Method B, UV, ESI)  $R_t = 0.79$  min,  $[\text{M}-\text{H}]^+ = 520$ , 100% purity;  $^1\text{H}$  NMR (400 MHz,  $d_6$ -DMSO)  $\delta$  1.32 (s, 3 H), 1.96 (t,  $J = 10.6$  Hz, 1 H),



2.12 (td,  $J = 11.1$  Hz, 2.8 Hz, 1 H), 2.41 (d,  $J = 11.3$  Hz, 1 H), 2.60 (d,  $J = 11.1$  Hz, 1 H), 3.06 (s, 3 H), 3.53 (td,  $J = 11.1$  Hz, 2.4 Hz, 1 H), 3.71 - 3.85 (m, 2 H), 3.96 (s, 3 H), 4.07 - 4.17 (m, 2 H), 4.17 - 4.21 (m, 2 H), 4.33 - 4.39 (m, 2 H), 4.99 (s, 2 H), 5.05 (s, 2 H), 7.11 (s, 1 H), 7.13 (s, 1 H), 7.86 (d,  $J = 2.3$  Hz, 1 H), 8.30 (d,  $J = 2.3$  Hz, 1 H), 9.32 (br. s, 1 H), two protons were not observed;  $^{13}\text{C}$  NMR (101 MHz,  $d_6$ -DMSO)  $\delta$  22.2, 38.6, 40.7, 52.8, 53.7, 55.0, 65.1, 65.7, 69.1, 70.8, 73.1, 73.5, 81.0, 81.1, 109.4, 111.8, 125.9, 129.8, 131.0, 138.3, 140.6, 141.9, 153.3, 156.3, one carbon was not observed; IR ( $\nu_{\text{max}}$  / $\text{cm}^{-1}$ ): 1145, 1331; HR-ESIMS ( $m/z$ ) calcd for  $\text{C}_{25}\text{H}_{34}\text{N}_3\text{O}_7\text{S}$   $[\text{M}+\text{H}]^+$  520.2112, found 520.2103.

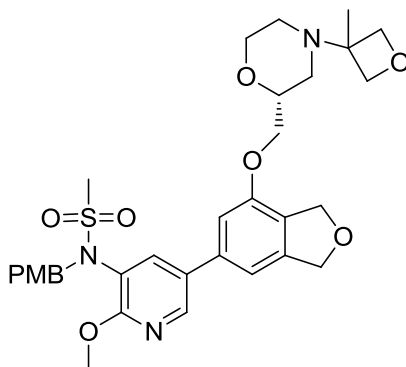
**6.12.24. (*R*)-*N*-(2-Methoxy-5-(7-((4-(3-((phenylsulfonyl)methyl)oxetan-3-yl)morpholin-2-yl)methoxy)-1,3-dihydroisobenzofuran-5-yl)pyridin-3-yl)-*N*-(4-methoxybenzyl)methanesulfonamide, 261**



A mixture of (*R*)-*N*-(2-methoxy-5-(7-(morpholin-2-ylmethoxy)-1,3-dihydroisobenzofuran-5-yl)pyridin-3-yl)-*N*-(4-methoxybenzyl)methanesulfonamide (87 mg, 0.16 mmol) and 3-((phenylsulfonyl)methylene)oxetane (33 mg, 0.16 mmol) in THF (1 mL) was heated to 65 °C for 48 h. The mixture was concentrated under reduced pressure and purified by Normal Phase Chromatography on FlashMaster II silica (10 g), eluting with 0-100% EtOAc/cyclohexane over 40 min. The product-containing fractions were concentrated under reduced pressure to afford **261** (52 mg, 43%) as a brown solid. LCMS (Method B, UV, ESI)  $R_t = 1.15$  min,  $[\text{M}-\text{H}]^+ = 766$ ,

89% purity. The material was taken forward directly without further purification or characterisation.

**6.12.25. (*R*)-*N*-(2-Methoxy-5-(7-((4-(3-methyloxetan-3-yl)morpholin-2-yl)methoxy)-1,3-dihydroisobenzofuran-5-yl)pyridin-3-yl)-*N*-(4-methoxybenzyl)methanesulfonamide, 262**



**Desulfonylation Reaction A:** Magnesium turnings (8 mg, 0.34 mmol) were ground to a powder in a pestle and mortar under a stream of nitrogen and added to a solution of (*R*)-*N*-(2-methoxy-5-(7-((4-(3-((phenylsulfonyl)methyl)oxetan-3-yl)morpholin-2-yl)methoxy)-1,3-dihydroisobenzofuran-5-yl)pyridin-3-yl)-*N*-(4-methoxybenzyl)methanesulfonamide (52 mg, 0.07 mmol) in MeOH (2 mL) at room temperature under an atmosphere of nitrogen. The mixture was placed in an ultrasound bath for 30 s then stirring was continued for 24 h. Iodine (3 crystals) was added and stirring was continued for 18 h. Rieke<sup>®</sup> magnesium (0.07 mL of a 2.5 g suspension in 100 mL THF, 2.7 mmol) was added and stirring was continued for 18 h. The mixture was heated to 50 °C for 1 h. Et<sub>2</sub>O (10 mL) was added followed by a saturated aqueous solution of Na<sub>2</sub>SO<sub>4</sub> (10 mL). The insoluble material was removed by filtration through Celite<sup>®</sup> and the organic phase was separated. The aqueous phase was extracted with more Et<sub>2</sub>O (2 x 10 mL). The combined organic extracts were dried by passing through a hydrophobic frit and concentrated under reduced pressure to afford recovered starting material (50 mg, 96%) as brown oil. LCMS (Method B, UV, ESI)  $R_t = 1.13$  min,  $[M-H]^+ = 766$ , 93% purity.

**Desulfonylation Reaction B:** SmI<sub>2</sub> (0.65 mL of a 0.1 M solution in THF, 0.07 mmol) and NiI<sub>2</sub> (0.20 mg, 0.65 μmol) were added to a solution of (*R*)-*N*-(2-

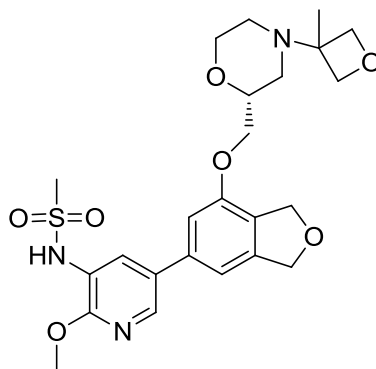
methoxy-5-(7-((4-(3-((phenylsulfonyl)methyl)oxetan-3-yl)morpholin-2-yl)methoxy)-1,3-dihydroisobenzofuran-5-yl)pyridin-3-yl)-*N*-(4-methoxybenzyl)methanesulfonamide (50 mg, 0.07 mmol) in THF (1 mL) under an atmosphere of nitrogen. The mixture was heated at 65 °C for 18 h. LCMS analysis showed no desired product and only starting material remained. The reaction mixture was quenched by addition to mixture of saturated aqueous K<sub>2</sub>CO<sub>3</sub> (3 mL) and saturated aqueous potassium sodium tartrate (3 mL) and disposed of.

**Bruylants Reaction A:** A mixture of (*R*)-*N*-(2-methoxy-5-(7-(morpholin-2-ylmethoxy)-1,3-dihydroisobenzofuran-5-yl)pyridin-3-yl)-*N*-(4-methoxybenzyl)methanesulfonamide (50 mg, 0.12 mmol), 3-oxetanone (8 mg, 0.11 mmol), 1,2,3-triazole (7.2 μL, 0.13 mmol) in toluene (1 mL) was heated to 110 °C while collecting water *via* a Dean Stark trap. The reaction mixture was cooled to room temperature and MeMgBr (0.13 mL of a 3.2 M solution in Et<sub>2</sub>O, 0.42 mmol) was added over 30 min. Stirring was continued for 1 h then the mixture was quenched with NH<sub>4</sub>Cl (as a 20% aqueous solution, 5 mL). The organic phase was separated and the aqueous layer was neutralised with NaOH (as a 2 M aqueous solution) then extracted with EtOAc (3 x 15mL). The combined organic extracts were passed through a hydrophobic frit and concentrated under reduced pressure. The crude material was purified by MDAP Method B3 and the product-containing fractions were concentrated under reduced pressure to afford **262** (1 mg, 2%). LCMS (Method B, UV, ESI) *R*<sub>t</sub> = 1.10 min, [M-H]<sup>+</sup> = 626, 97% purity.

**Bruylants Reaction B:** A mixture of (*R*)-*N*-(2-methoxy-5-(7-(morpholin-2-ylmethoxy)-1,3-dihydroisobenzofuran-5-yl)pyridin-3-yl)-*N*-(4-methoxybenzyl)methanesulfonamide (40 mg, 0.07 mmol), 3-oxetanone (6 mg, 0.7 mmol), 1,2,3-triazole (4.6 μL, 0.08 mmol) in THF (1 mL) was degassed with nitrogen and heated in the microwave at 120 °C for 30 min. The mixture was cooled to 0 °C and MeMgBr (0.03 mL of a 3.2 M solution in Et<sub>2</sub>O, 0.8 mmol) was added over a period of 30 min. The reaction mixture was allowed to warm to room temperature and stirring was continued for 1 h. More MeMgBr (0.03 mL of a 3.2 M solution in Et<sub>2</sub>O, 0.8 mmol) was added and stirring continued for 72 h. More

MeMgBr (0.03 mL of a 3.2 M solution in Et<sub>2</sub>O, 0.8 mmol) was added and stirring continued for 2 h. The mixture was quenched with NH<sub>4</sub>Cl (as a 20% aqueous solution, 5 mL). The organic phase was separated and the aqueous layer was neutralised with NaOH (as a 2 M aqueous solution) then extracted with EtOAc (3 x 15mL). The combined organic extracts were passed through a hydrophobic frit and concentrated under reduced pressure. The crude material was purified by MDAP Method B3 and the product-containing fractions were concentrated under reduced pressure to afford **262** (10 mg, 22%). LCMS (Method B, UV, ESI)  $R_t = 1.10$  min,  $[M-H]^+ = 626$ , 98% purity; <sup>1</sup>H NMR (400 MHz, CDCl<sub>3</sub>)  $\delta$  1.44 (br. s, 3 H), 2.15 - 2.31 (m, 1 H), 2.32 - 2.48 (m, 2 H), 2.50 - 2.64 (m, 1 H), 3.06 (s, 3 H), 3.75 (s, 4 H), 3.88 - 4.09 (m, 4 H), 4.10 (s, 3 H), 4.26 (d,  $J = 5.0$  Hz, 2 H), 4.55 - 4.69 (m, 2 H), 4.76 (br. s, 2 H), 5.11 (s, 4 H), 6.68 (s, 1 H), 6.78 (d,  $J = 8.8$  Hz, 2 H), 6.81 (s, 1 H), 7.17 (d,  $J = 8.8$  Hz, 2 H), 7.43 (d,  $J = 2.3$  Hz, 1 H), 8.25 (d,  $J = 2.3$  Hz, 1 H).

**6.12.26. (R)-N-(2-Methoxy-5-(7-((4-(3-methyloxetan-3-yl)morpholin-2-yl)methoxy)-1,3-dihydroisobenzofuran-5-yl)pyridin-3-yl)methanesulfonamide, 248**



A mixture of (R)-N-(2-methoxy-5-(7-((4-(3-methyloxetan-3-yl)morpholin-2-yl)methoxy)-1,3-dihydroisobenzofuran-5-yl)pyridin-3-yl)-N-(4-methoxybenzyl)methanesulfonamide (10 mg, 0.02 mmol) and TFA (0.1 mL, 1.30 mmol) in DCM (0.3 mL) was heated in a microwave for 1 h 15 min. The mixture was concentrated under reduced pressure and the crude material purified by MDAP Method B2. The product-containing fractions were concentrated under reduced pressure to afford **248** (2 mg, 24%) as a white solid. LCMS (Method B, UV, ESI)  $R_t$

= 0.77 min,  $[M-H]^+ = 506$ , 98% purity;  $^1H$  NMR (400 MHz,  $CDCl_3$ )  $\delta$  1.40 (s, 3 H), 2.19 – 2.28 (m, 1 H), 2.31 - 2.45 (m, 2 H), 2.58 – 2.65 (m, 1 H), 3.04 (s, 3 H), 3.73 – 3.82 (m, 1 H), 3.91 - 4.01 (m, 2 H), 4.06 (m, 1 H), 4.07 (s, 3 H), 4.10 - 4.19 (m, 1 H), 4.26 (d,  $J = 5.8$  Hz, 2 H), 4.59 – 4.65 (m, 2 H), 5.15 (s, 4 H), 6.74 (br. s, 1 H), 6.89 (s, 1 H), 7.00 (s, 1 H), 7.97 (d,  $J = 2.3$  Hz, 1 H), 8.14 (d,  $J = 2.3$  Hz, 1 H).

### 6.13. References

- (1) Jin, Q., "Preparation of dihydroisoindolylmethoxyethylsulfonylpiperidinylindolecarboxamide derivatives for use as IKK2 inhibitors", WO 2010102968, 2010.
- (2) Smith, S., GlaxoSmithKline: 2013, unpublished results.
- (3) Lewis, T., GlaxoSmithKline: 2013, unpublished results.
- (4) Wuitschik, G.; Rogers-Evans, M.; Mueller, K.; Fischer, H.; Wagner, B.; Schuler, F.; Polonnchuk, L.; Carreira, E. M. *Angew. Chem., Int. Ed.* **2006**, *45*, 7736.
- (5) Fuji, K.; Watanabe, Y.; Ohtsubo, T.; Nuruzzaman, M.; Hamajima, Y.; Kohno, M. *Chem. Pharm. Bull.* **1999**, *47*, 1334.

# **Appendix**

## Single-Step Microwave-Mediated Synthesis of Oxazoles and Thiazoles from 3-Oxetanone: A Synthetic and Computational Study

David Orr,<sup>[a]</sup> Alexandra Tolfrey,<sup>[a]</sup> Jonathan M. Percy,<sup>\*,[a]</sup> Joanna Frieman,<sup>[a]</sup> Zoë A. Harrison,<sup>\*,[b]</sup> Matthew Campbell-Crawford,<sup>[c]</sup> and Vipulkumar K. Patel<sup>[b]</sup>

**Abstract:** The direct microwave-mediated condensation between 3-oxetanone and primary amides and thioamides has delivered moderate to good yields of (hydroxymethyl)oxazoles and (hydroxymethyl)thiazoles. The reactions use a sustainable solvent and only require short reaction times. These are highly competitive methods for the construction of two classes of valuable heteroarenes, which bear a useful locus for further elaboration. Electronic

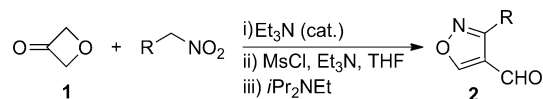
structure calculations have shown that the order of events involves chalcogen atom attack at sp<sup>3</sup> carbon and alkyl-oxygen cleavage. The critical role of acid catalysis was shown clearly, and the importance of acid strength was

demonstrated. The calculated barriers were also fully consistent with the observed order of thioamide and amide reactivity. Spontaneous ring opening involves a modest degree of C–O cleavage, moderating the extent of strain relief. On the acid-catalysed pathway, C–O cleavage is less extensive still, but proton transfer to the nucleofuge is well advanced with the carboxylic acid catalysts, and essentially complete with methanesulfonic acid.

**Keywords:** annulation • density functional calculations • microwave chemistry • nitrogen heterocycles • sulfur heterocycles

## Introduction

Oxetanes are rapidly becoming an important part of the repertoire of the medicinal chemist, because of the ability of these heterocycles to mimic ketonic carbonyl groups and *gem*-dimethylated sp<sup>3</sup> centres.<sup>[1]</sup> Methods for the introduction of the oxetanyl motif are becoming more developed<sup>[2]</sup> and there is a growing array of procedures that allow the complete oxetane unit to be introduced.<sup>[3]</sup> However, oxetane derivatives may also be interesting synthetic building blocks for the construction of other heterocycles. There are relatively few examples of oxetane ring-opening reactions in the literature, but recently, Carreira and co-workers<sup>[4]</sup> showed how isoxazoles **2** could be formed in a sequence begun by the reaction of the conjugate base of a nitroalkane with 3-



Scheme 1. Carreira and co-workers' isoxazole synthesis from 3-oxetanone begins with a Henry reaction and features a pivotal ring opening through an oxete intermediate.

oxetanone (**1**; Scheme 1). The heterocyclic ketone **1** is now commercially available and, while it is relatively expensive, its latent reactivity in strain-relieving ring opening makes it a very interesting species for further exploration.

During the course of the synthesis of a drug lead, we discovered trace amounts of an oxazole product when a benzamide was condensed with **1** under acidic conditions (acetic acid/sulfamic acid). Oxazoles and the related thiazoles occur widely in natural products, including species in which they are linked, and in some drug leads. Figure 1 shows a number of natural products that contain these heteroarenes. Virginiamycin M1 (**3**) is used to treat resistant bacterial infections,<sup>[5]</sup> (–)-Mycothiazole (**4**) is a marine natural product with cytotoxicity against lung cancer cells,<sup>[6]</sup> while Bistratamide C (**5**) is one of the *Lissoclinum* cyclopeptides, a class of cytotoxic agents from marine Ascidians.<sup>[7]</sup> There has been considerable recent interest in the synthesis of these heteroarenes<sup>[8]</sup> reflecting their frequent occurrence, prompting us to explore our serendipitous finding to see if a useful synthetic method could be discovered. It has also provided an opportunity to explore some of the mechanisms available for oxetanone ring opening, a process that has not been explored to our knowledge, apart from in a preliminary manner by Carreira and co-workers.

[a] D. Orr, A. Tolfrey, Prof. Dr. J. M. Percy, J. Frieman  
WestCHEM Department of Pure and Applied Chemistry  
University of Strathclyde, Thomas Graham Building  
295 Cathedral Street, Glasgow G1 1XL (UK)  
Fax: (+44)0141-548-4822  
E-mail: jonathan.percy@strath.ac.uk

[b] Z. A. Harrison, Dr. V. K. Patel  
Refractory Respiratory Inflammation DPU  
GlaxoSmithKline Medicines Research Centre  
Gunnels Wood Road, Stevenage SG1 2NY (UK)  
Fax: (+44)01438 768302  
E-mail: zoe.x.harrison@gsk.com

[c] M. Campbell-Crawford  
Fibrosis DPU, GlaxoSmithKline Medicines Research Centre  
Gunnels Wood Road, Stevenage SG1 2NY (UK)

Supporting information for this article is available on the WWW under <http://dx.doi.org/10.1002/chem.201301011>.

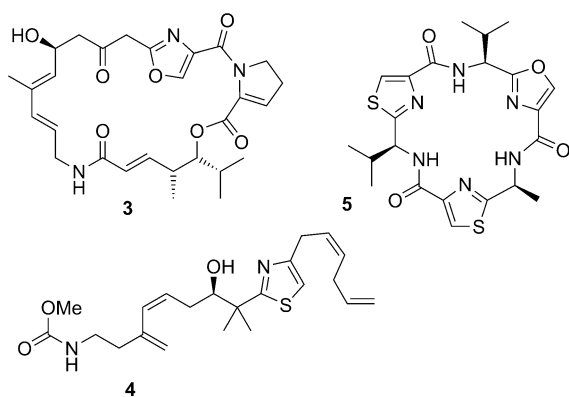
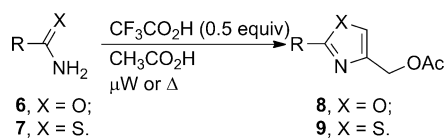


Figure 1. Oxazole- and thiazole-containing natural products.

## Results and Discussion

To optimise our use of costly 3-oxetanone, we fixed the initial stoichiometry for the reaction with benzamide at 1:1 and retained acetic acid as the solvent, because it is inexpensive, polar and sustainable.<sup>[9]</sup> A reaction screen was carried out on a 0.5 mmol scale in the microwave; the parameters varied were temperature (80–140 °C), time (20–300 min), stronger acid catalyst (none, sulfamic acid, trifluoroacetic acid, and HCl, generated in situ from tetramethylsilyl chloride), equivalents of stronger acid (0.1–0.5 equivalents) and reaction concentration (0.4–2.1 M). Reactions that achieved the highest conversions of benzamide with the lowest levels of side-product formation (assayed by GC-MS) were selected for further investigation. The following generalities emerged; a stronger acid catalyst was essential (or the reaction was very slow) and trifluoroacetic acid was the most effective of the three used in the initial screen (Scheme 2).



Scheme 2. First-generation microwave-mediated azole syntheses in trifluoroacetic acid/acetic acid mixtures.

A high loading of catalyst (0.5 equivalents) was required and the combination of a reaction temperature of 120 °C and concentration of 0.4 M gave high (>95%) conversion of the amide and consistent results. Acetates **8a–c** were prepared in good (47–60%) yields under these conditions (Table 1); cyclohexyl congener **8d** reacted less successfully (21% isolated yield at full conversion). Thiazolyl analogue **9a** (52%) was also prepared from commercial thiobenzamide. The mass balance in these reactions is unfortunately accounted for by tar formation; in some cases, traces of the corresponding trifluoroacetate esters were detected in the crude products by GC-MS, but we were unable to isolate them. We tried dividing the total microwave irradiation time

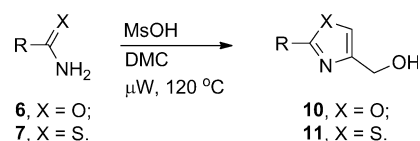
Table 1. First-generation microwave-mediated azole syntheses in trifluoroacetic acid/acetic acid mixtures.

Amide or thioamide	X	Product	Method <sup>[a,b]</sup>	T [°C]	Time [h]	Yield [%] <sup>[c]</sup>
<b>6a</b> , R = Ph	O	<b>8a</b>	A	120	3.5	47 <sup>[d]</sup>
			B	80	28	48
<b>6b</b> , E-PhHC=CH	O	<b>8b</b>	A	120	2.5	60
			B	80	51	52
<b>6c</b> , 2-thiophenyl	O	<b>8c</b>	A	120	2.5	50
			B	80	52	68 <sup>[e]</sup>
<b>6d</b> , cyclohexyl	O	<b>8d</b>	A	120	3.0	21
			B	80	192	31 <sup>[f]</sup>
<b>7a</b> , Ph	S	<b>9a</b>	A	85	3.5	52

[a] Method A: microwave heating. [b] Method B: conventional heating. [c] All reactions were carried out on 1–2 mmol scale at 120 °C. [d] 10 mmol scale, 120 °C. [e] Crude GC/MS yield. [f] Crude yield.

into a series of short pulses as described by Ley and co-workers,<sup>[10]</sup> but there was no improvement in isolated yield (20 min periods of heating at 120 °C, followed by 10 min rest periods).

Conventional heating at 80 °C could also be used to prepare **8a–d**; yields were comparable though a very long reaction time was required for **8d**. These results were pleasing, but the products would have more value if the free hydroxyl group was available for oxidation to the aldehyde or other manipulation without the need for an ester cleavage. Another reaction solvent that could not act as an acetyl donor was clearly required and we selected dimethyl carbonate, which has a lower dielectric constant ( $\epsilon_s = 3.1$ )<sup>[11]</sup> than acetic acid ( $\epsilon_s = 6.2$ ). Solvents with such low dielectric constants do not usually respond strongly to microwave heating,<sup>[12]</sup> but dimethyl carbonate has good solvent characteristics for scale-up and sustainable synthesis,<sup>[13]</sup> and some promise as a sustainable methylating agent.<sup>[14]</sup> A range of acids were deployed including trifluoroacetic, oxalic, sulfamic, methanesulfonic and *p*-toluenesulfonic acids; the effective combination emerging from the screen was methanesulfonic acid in DMC. There was no correlation between acid strength and performance; the relevant  $pK_a$  values are TsOH ( $pK_a -2.8$ ),<sup>[15a]</sup> MsOH ( $pK_a -1.9$ ),<sup>[15a]</sup> TFA ( $pK_a 0.23$ ),<sup>[15b]</sup>  $\text{H}_2\text{NSO}_3\text{H}$  ( $pK_a 1.0$ ),<sup>[15c]</sup> oxalic acid ( $pK_a 1.23$ ),<sup>[15d]</sup> and acetic acid ( $pK_a 4.76$ )<sup>[15d]</sup> so the most effective acid was neither the strongest nor the weakest.<sup>[15]</sup> Scheme 3 shows the best conditions discovered from a screen; the yields of free (oxazolyl)-methyl alcohols were lower than those of the acetates, but are still acceptable given the directness and simplicity of the synthetic procedures. Crystals of sufficiently high quality to allow analysis by X-ray diffraction were grown for alcohol **10a**, confirming its structure. However, the method is much



Scheme 3. Second-generation microwave-mediated oxazole and thiazole syntheses in methanesulfonic acid/dimethyl carbonate mixtures.



more effective for thiazole synthesis. A higher (54%) yield of thiazole **11a** was obtained under these conditions, and a change in reaction stoichiometry to use a 50% molar excess of thioamide increased the yield further to 64% (with thioamide recovery possible). Unfortunately, this tactic was not effective for oxazole synthesis because the amides and oxazole products often had very similar  $R_F$  values, making chromatographic purification very difficult.

A range of primary thioamides<sup>[16]</sup> was prepared (see the Supporting Information for details) using the extremely convenient microwave method of Perlmutter and co-workers,<sup>[17]</sup> which exposes the primary amides (we held a stock of these compounds) to diphosphorus pentasulfide supported on alumina; Table 2 summarises the results obtained to date and makes clear the efficacy of this approach for thiazole synthesis.

Table 2. Second-generation microwave-mediated azole syntheses in methanesulfonic acid/dimethyl carbonate mixtures.

R	Amide	X=O	Yield [%]	Thioamide	X=S	Yield [%] <sup>[a]</sup>
Ph	<b>6a</b>	<b>10a</b>	36	<b>7a</b>	<b>11a</b>	64
<i>E</i> -PhHC=CH	<b>6b</b>	<b>10b</b>	24	<b>7b</b>	<b>11b</b>	44
2-thiophenyl	<b>6c</b>	<b>10c</b>	22	<b>7c</b>	<b>11c</b>	50 <sup>[b]</sup>
cyclohexyl	<b>6d</b>	<b>10d</b>	17	<b>7d</b>	<b>11d</b>	63
(3-MeO)Ph	<b>6e</b>	n.d.	n.d.	<b>7e</b>	<b>11e</b>	47 <sup>[b]</sup>
(4-MeO)Ph	<b>6f</b>	<b>10f</b>	15	<b>7f</b>	<b>11f</b>	50
(4-Br)Ph	<b>6g</b>	<b>10g</b>	13	<b>7g</b>	<b>11g</b>	37
(3-F <sub>3</sub> C)Ph	<b>6h</b>	<b>10h</b>	24	<b>7h</b>	<b>11h</b>	36
<i>t</i> Bu	<b>6i</b>	<b>10i</b>	14	<b>7i</b>	<b>11i</b>	40 <sup>[b]</sup>
(2-Cl)Ph	<b>6j</b>	–	– <sup>[c]</sup>	<b>7j</b>	<b>11j</b>	41
(2-Me)Ph	<b>6k</b>	–	–	<b>7k</b>	<b>11k</b>	48

[a] All yields were obtained with 1.5 equivalents of thioamide unless stated otherwise. [b] In this case, a better yield was obtained with 1.0 equivalent of thioamide; the use of an excess resulted in yield loss in mixed fractions in the chromatography. [c] Reaction attempted for 4 h with incomplete conversion.

A range of aromatic substituents were tolerated as were secondary and tertiary alkyl groups; the *E*-cinnamyl group also survived the reaction conditions. There were no trends between substituent character and reaction yield; the main factor determining the yield was the ease of separation of heteroarene product from unreacted amide or thioamide. Literature routes that build thiazoles with this 2,4-disubstitution pattern include Hantzsch syntheses<sup>[18]</sup> (thioamide condensations with pyruvate-type electrophiles), and thiazoline oxidation<sup>[19]</sup> or bromination/dehydrobromination<sup>[20]</sup> procedures. Our procedure is extremely competitive because of its directness and high atom-efficiency.

There is very little mechanistic work on oxetane or oxetanone ring-opening in the literature. Oxetane, the parent heterocycle for the synthetic building block used in this study, is a strained cyclic ether; opening of this ring<sup>[21]</sup> releases a significant strain energy of 25.5 kcal mol<sup>-1</sup> according to experiment<sup>[22]</sup> and theory.<sup>[23]</sup> However, ring-opening reactions must overcome a high kinetic barrier; Banks evaluated  $\Delta G^\ddagger$  (gas phase) at 58.4 kcal mol<sup>-1</sup> for the ring-opening reaction

with ammonia (MP2(Full)/6-311++G(d,p)/MP2(Full)/6-31+G\*). We have used electronic structure calculations to examine a range of possible ring-opening modes and attempt to gain insight into the reaction mechanism. Because of the high kinetic cost of opening the ring, we assume that locating the lowest energy transition structure which involves C–O scission will reveal the most favoured mode of ring opening and that mapping the entire energy surface will provide no additional insights.

Initial structures were obtained at the RI-MP2/6-31G\* level of theory, then reoptimised (MP2/6-31+G\*) with full frequency calculations, implemented in Spartan'08.<sup>[24]</sup> Transition structure **12a** (Figure 2) reported by Banks was repro-

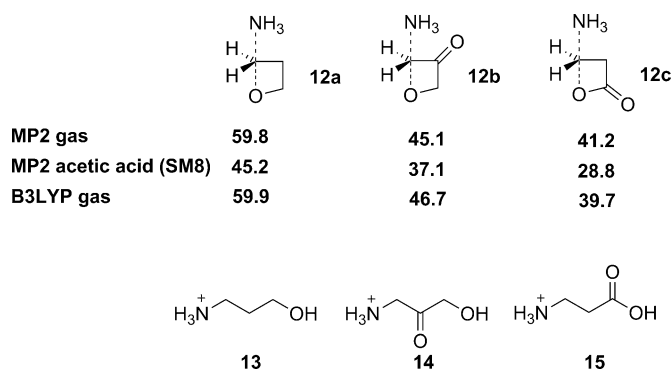
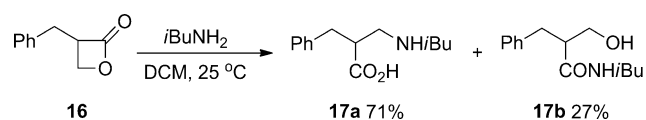


Figure 2. Calculated  $\Delta G^\ddagger$  (kcal mol<sup>-1</sup>, 298 K) for nucleophilic ring opening of oxetane, 3-oxetanone and 2-oxetanone with ammonia, (MP2/6-31+G\* and B3LYP/6-311+G\*\*) and the products of ring opening used to evaluate leaving group  $pK_a$ .

duced by an MP2/6-31+G\* geometry optimisation;  $\Delta G^\ddagger$  (gas phase) calculated by this method was 59.8 kcal mol<sup>-1</sup>, which is in excellent agreement with the published value and instils confidence that the use of the much smaller basis will deliver useful results. Carriera and co-workers used a different level of theory (B3LYP/6-311G(d,p), or 6-311G\*\*) to interrogate aspects of the isoxazole-forming reaction of Scheme 1. Because the implementation of this method is more economical with Spartan'08, we also examined all the key reactions using this additional level of theory. The use of the B3LYP functional has been subject to criticism in recent years, but Goodman<sup>[25]</sup> has provided evidence of its effectiveness for dealing with transition states of reactions of small organic molecules, and of its relatively low degree of vulnerability to the integration grid errors attributed<sup>[26]</sup> to the Q-CHEM grid used by the Spartan programmes.

We did not expect that the presence of the carbonyl group in 3-oxetanone would lower the barrier to C–O scission significantly; while nucleophilic substitution next to a carbonyl group is usually accelerated,<sup>[27]</sup> the scissile  $\sigma$ -bond and the relevant carbonyl group orbital would be expected to be orthogonal<sup>[28]</sup> if the oxetanone ring was planar. However, the barrier to oxetane ring opening is considerably lower at 45.1 kcal mol<sup>-1</sup>, predicting that the ring-opening reaction of 3-oxetanone with ammonia would be 10<sup>11</sup> times

faster than the reaction of oxetane itself. The products of ring opening are **13** and **14** and their hydroxyl group  $pK_a$  values (in water at 298 K, calculated using ACD/Labs software within CAS SciFinder) are 14.95 and 12.94, so it is clear that lower nucleofuge basicity alone cannot be responsible for the higher reactivity of 3-oxetanone. A decrease in leaving group basicity of 2  $pK_a$  units and a Brønsted  $\beta_L$  of  $-1.0$  predicts only a 100-fold increase in reactivity. In the transition structures **12a** and **b**, the ring is twisted, resembling the puckered conformation of cyclobutane; in the 3-oxetanone structure **12b**, the C=O bond sits at approximately  $45^\circ$  to the forming C–N bond. This twisting distorts the O–C–N angle to  $164^\circ$  (from  $175.5^\circ$  in **12a**) and **12b** is slightly earlier with respect to C–N bond formation (C–N is 1.83 compared to 1.76 Å in **12a**). The location of the carbonyl group suggests strongly that some degree of transition state stabilisation is being achieved by the C=O group. The C2–C3 bond length changes from 1.53 to 1.48 Å between **1** and transition structure **12b**, consistent with the development of some partial double bond character between the two carbons at the transition state. The  $\Delta G^\ddagger$  (gas phase) value calculated for **12c** is lower still at  $41.2 \text{ kcal mol}^{-1}$ , and the atoms of the opening ring are coplanar, with C–O and C–N distances similar to those for **12a**; in this case, the calculated carboxylate  $pK_a$  is 3.65. Scheme 4 shows the ring opening of



Scheme 4. Competitive acyl and alkyl C–O cleavage modes for 2-oxetanone derivative **16**.

**16** by benzylamine in dichloromethane; this reaction involves competitive acyl and alkyl C–O cleavage to afford **17a** and **b** respectively under mild conditions,<sup>[29]</sup> and suggests very strongly that a calculated barrier of  $40 \text{ kcal mol}^{-1}$  in the gas phase corresponds to a cleavage reaction, which can occur readily in solution under relatively mild conditions.

Amides are significantly less nucleophilic than ammonia so we examined a wider set of reactions related to the ring opening of **1**; however, simple intermolecular reactions lead to the lowest energy barriers (Table 3) via transition structures of types **18** or **19** (Figure 3; a wider set of ring-opening reactions is described fully in the Supporting Information).

The barrier  $\Delta G^\ddagger$  calculated for the ring opening of **1** with model amide formamide (O-attack) rose to  $49.3 \text{ kcal mol}^{-1}$  from the lower value ( $45.1 \text{ kcal mol}^{-1}$ ) for the more nucleophilic ammonia. A higher barrier ( $59.1 \text{ kcal mol}^{-1}$ ) was calculated for formamide N-attack while S-attack for thioformamide ( $41.4 \text{ kcal mol}^{-1}$ ) via **18b** was the most favourable pathway. All the modes of intermolecular attack involved N–H $\cdots$ O=C hydrogen-bond formation; these interactions formed during the optimisation even when the two functional groups were initially remote. The intermolecular O-attack

Table 3. Free-energy barriers ( $\Delta G^\ddagger$ ,  $\text{kcal mol}^{-1}$ , 298 K) calculated for opening of 3-oxetanone **1** for nucleophilic O- and S-attack by amides and thioamides transition structures **19a–h** and **20**.

Structure	R <sup>1</sup>	X	R <sup>2</sup>	MP2/gas <sup>[a]</sup>	MP2/acetic acid <sup>[a]</sup>	B3LYP/gas <sup>[b]</sup>
<b>18a</b>	–	O	–	49.3	47.1	51.7
<b>18b</b>	–	S	–	41.4	40.4	43.2
<b>19a</b>	H	O	CH <sub>3</sub>	35.8	38.7	38.0
<b>19b</b>	H	S	CH <sub>3</sub>	31.4	34.2	35.5
<b>19c</b>	H	O	CF <sub>3</sub>	26.7	29.0	31.2
<b>19d</b>	H	S	CF <sub>3</sub>	24.0	27.5	27.1
<b>19e</b>	Ph	O	CH <sub>3</sub>	33.7	–	37.7
<b>19f</b>	Ph	S	CH <sub>3</sub>	30.2	–	34.3
<b>19g</b>	Ph	O	CF <sub>3</sub>	23.2	–	30.7
<b>19h</b>	Ph	S	CF <sub>3</sub>	22.5	–	29.0
<b>20</b>	–	–	–	21.2	–	–

[a] (MP2/6-31+G\*) gas phase and [SM8]. [b] (B3LYP/6-311+G\*\*).

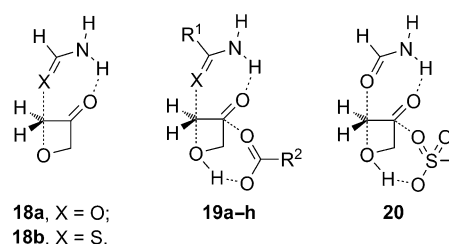


Figure 3. Spontaneous and acid-catalysed transition structure types for opening of 3-oxetanone **1** through nucleophilic O- and S-attack by amides and thioamides.

mode of ring-opening was therefore examined further. A molecule of acetic acid or trifluoroacetic acid was placed so that the acid O–H proton was within approximately hydrogen bonding distance of the oxetanyl oxygen, and optimisation was carried out without constraint. Allowing the optimisation to find the best position for the proton should accommodate both general and specific acid catalysis. Various changes occurred during the optimisation, including flattening of the oxetanyl ring, turning of the attacking amide to hydrogen bond to the acetic acid molecule and partial proton transfer to the oxetanyl oxygen (see the Supporting Information for graphical representations of the transition structures and an overlay).

With the acetic acid molecule present in **19a** (Figure 4b),  $\Delta G^\ddagger$  fell to  $35.8 \text{ kcal mol}^{-1}$  (gas phase). The lower  $\Delta G^\ddagger$  value for this reaction is remarkable given the high entropic cost of termolecular reactions compared to their bimolecular counterparts.<sup>[30]</sup>

The C2–C3 distance is longer when the acetic acid is present and the natural charge on the carbonyl oxygen is lower ( $-0.479$ ) compared to the structure in the absence of the acetic acid ( $-0.689$ ); these differences are consistent with an interaction between the substitution centre and the carbonyl group in **18a**; once the acetic acid is present in **19a**, strong stabilisation of the developing charge on the leaving group can occur and the need for ring twisting is relieved. With trifluoroacetic acid posed near the oxetanyl oxygen, the energy for opening by formamide fell still further to

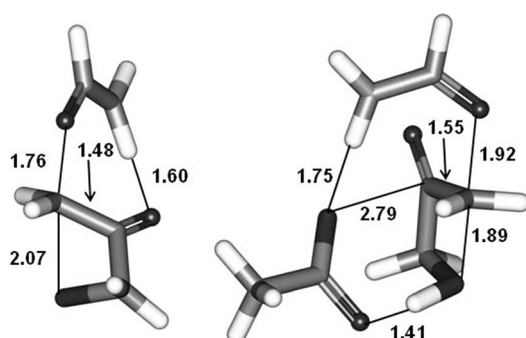


Figure 4. Optimised (gas phase, MP2/6-31+G\*) transition structures for a) 3-oxetanone opening with formamide **18a**; b) 3-oxetanone opening with formamide in the presence of acetic acid **19a**. Distances are shown in Å.

26.7 kcal mol<sup>-1</sup> (gas phase), consistent with the significantly higher acidity of trifluoroacetic acid (the pK<sub>a</sub> values of trifluoroacetic acid and acetic acid are 0.23 and 4.76 respectively, *vide infra*). With thioformamide and trifluoroacetic acid as the nucleophile and catalyst, the barrier fell to 24 kcal mol<sup>-1</sup> (gas phase), while for formamide in the presence of methanesulfonic acid (pK<sub>a</sub> -1.9), ΔG<sup>‡</sup> fell further still to 21.2 kcal mol<sup>-1</sup> (gas phase). Transition structures were reoptimised (MP2/6-31+G\*) using Cramer and Truhlar's SM8 method<sup>[31]</sup> specifying acetic acid as the reaction solvent; unfortunately, a full range of parameters are not available for dimethyl carbonate or related species, so while we can treat the initial reaction conditions (acetic acid/trifluoroacetic acid), the second generation method cannot be dealt with using this solvation treatment. As expected, lower values of ΔG<sup>‡</sup> were obtained using the SM8 method (by 14.6, 8.0 and 12.4 kcal mol<sup>-1</sup> for **12a**, **b** and **c** respectively), but structural differences between gas phase and solution structures were minimal. Intermolecular transition structures **18a** and **b** were slightly lower in (free) energy in acetic acid, but the barriers calculated for **19a–d** were all slightly higher in acetic acid. To gain some insight into this behaviour, we compared the dipole moments of complex **21** (*D* = 4.14 debye), obtained by relaxing transition structure **19a**, with transition structure **19a** itself (*D* = 4.18 debye) (Figure 5). There was no significant change in dipole moment on progression to the transition structure, consistent with the absence of a strong transition state stabilising

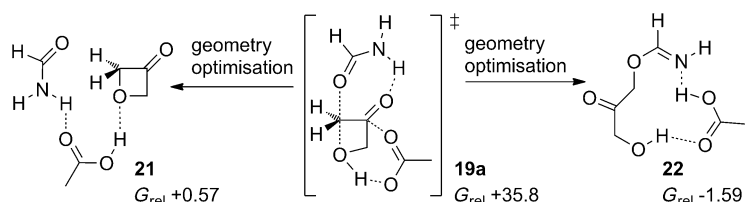
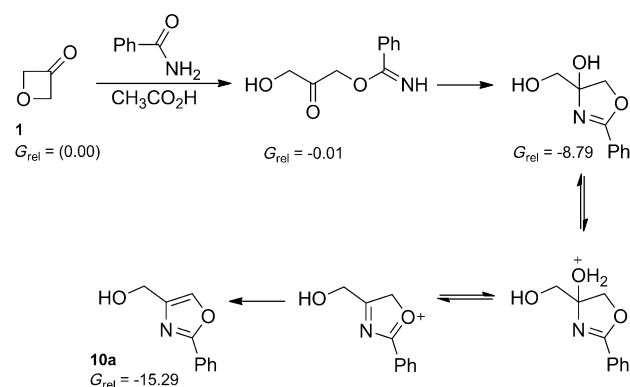


Figure 5. Structures used to calculate dipole moment changes during ring opening of **1** by formamide (gas phase). Free energies (*G*<sub>rel</sub>/kcal mol<sup>-1</sup>) are calculated relative to **1**, formamide and acetic acid as separate molecules.

effect in acetic acid. Finally, selected calculations were carried out with the full benzamide or thiobenzamide nucleophiles (**19e–h**) reproducing the trends observed for the formamide and thioformamide models.

The optimised structures from the gas phase calculations were used to quantify approximately the extent of C–O cleavage in the spontaneous and catalysed reactions. The sum of the carbon and oxygen van der Waals radii was used as an estimate of full C–O cleavage and the extension of the C–O bond relative to the oxetanone C–O bond length was used to calculate the percentage extension. A similar approach was used to quantify the extent of O–H formation. In the spontaneous ring opening with ammonia and formamide, C–O cleavage approaches 30%, indicating that the release of ring strain will be modest at the transition state. On the acid catalysed pathway, C–O cleavage is less well advanced at approximately 20%, whereas proton transfer to the oxetanyl oxygen is well advanced (approximately 90%) at the transition state with proton movement involved in the imaginary frequency, whereas proton transfer was complete with the stronger methanesulfonic acid. The two pathways are represented in the More–O'Ferrall–Jencks<sup>[32]</sup> diagram of Figure 6. After ring opening, a sequence of conventional steps is proposed for oxazole or thiazole formation, summarised in Scheme 5 for **10a** with acetic acid catalysis.



Scheme 5. Intermediates on the pathway to oxazole product **10a** and their free energies (kcal mol<sup>-1</sup>, 298 K, MP2/6-31+G\*).

Overall, the sequence is strongly exergonic, consistent with strain relief and the formation of an aromatic product.

## Conclusion

The direct microwave-mediated condensation between 3-oxetanone and primary amides and thioamides has delivered moderate to good yields of (hydroxymethyl)oxazoles and (hydroxymethyl)thiazoles. The reactions use a sustainable solvent and require only short reaction times. These are highly competitive methods for the construction of two classes of valuable heteroarenes, which bear a useful locus for further elaboration.

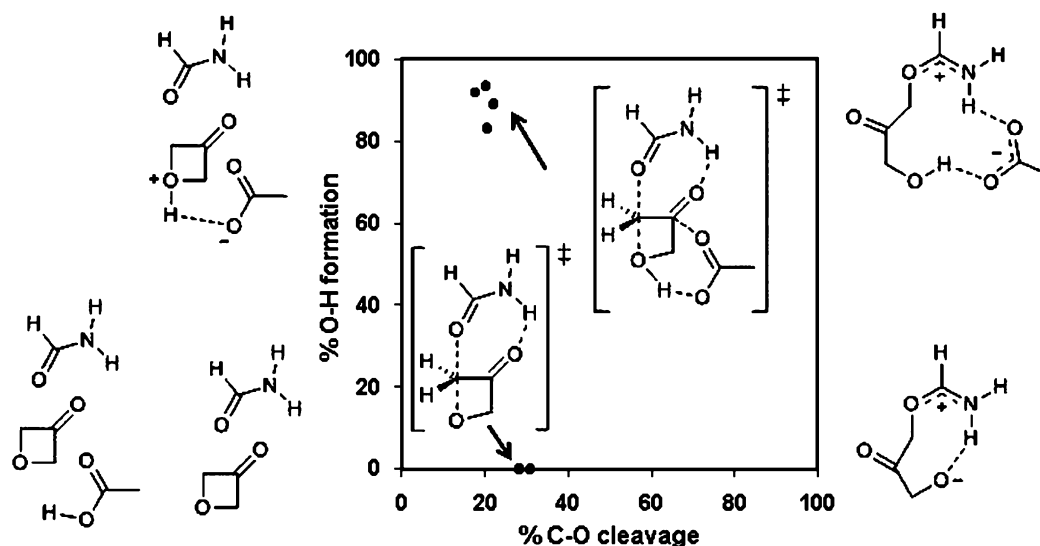


Figure 6. More-O'Ferrall-Jencks diagram showing spontaneous and acid-catalysed oxetanone ring-opening reactions. The bottom right-hand structure is unstable with respect to proton transfer from cationic N to anionic O.

Electronic structure calculations have shown that the order of events involves chalcogen atom attack at  $sp^3$  carbon and alkyl-oxygen cleavage; the favoured termolecular mode of ring opening revealed by the computational study was unexpected. The critical role of acid catalysis was shown clearly, and the importance of acid strength was demonstrated. The calculated barriers were also fully consistent with the observed order of thioamide and amide reactivities. Spontaneous ring opening involves a modest degree of C-O cleavage, moderating the extent of strain relief. On the acid-catalysed pathway, C-O cleavage is less extensive still, but proton transfer to the nucleofuge is well advanced with the carboxylic acid catalysts, and essentially complete with methanesulfonic acid.

## Experimental Section

**General:** NMR spectra were recorded on Bruker DPX-400 or Avance DRX-500 spectrometers.  $^1\text{H}$ ,  $^{19}\text{F}$  and  $^{13}\text{C}$  NMR spectra were recorded using the deuterated solvent as the lock and the residual solvent as the internal reference. The multiplicities of the spectroscopic data are presented in the following manner: s=singlet, bs=broad singlet, d=doublet, dd=doublet, ddd=doublet of doublets, dt=doublet of triplets, qd=quartet of doublets, t=triplet, tt=triplet of triplets and m=multiplet. Homocouplings (H-H, H-F, C-F) are given in Hertz and specified by  $J$ ; the nuclei involved in heteronuclear couplings are defined with the observed nucleus given first. Unless stated otherwise, all refer to  $^3J$  couplings. HRMS measurements were obtained from Thermofisher LTQ Orbitrap XL at the Engineering and Physical Sciences Research Council National Mass Spectrometry Service Centre, Swansea. Elemental analysis was performed on a PerkinElmer 2400 CHN analyser. GC-MS spectra were obtained on an instrument fitted with a DB5-type column ( $30\text{ m} \times 0.25\ \mu\text{m}$ ) running a 40–320 °C (70–320 °C for acetates) temperature program, ramp rate  $20\text{ }^\circ\text{C min}^{-1}$  with helium carrier gas flow at  $1\text{ cm}^3\text{ min}^{-1}$ . Electrospray mass spectra were obtained on a Thermo Finnigan LCQ Duo mass spectrometer (spray voltage 4.5 kV, mobile phase methanol). Melting points were recorded on a Griffin apparatus using open capillaries. IR spectra were recorded as films on a Shimadzu spec-

trometer with a Pike MIRacle horizontal single reflection ATR attachment. Thin layer chromatography was performed on pre-coated aluminium-backed silica gel plates (silica gel 60 F<sub>254</sub>, thickness 0.2 mm, Merck KGaA, Darmstadt). Visualisation was achieved using vanillin or anisaldehyde staining and UV detection at 254 and 356 nm. Semi-automated column chromatography was performed on silica gel (Zeoprep 60 HYD, 40–63  $\mu\text{m}$ , Zeochem) using a Büchi Sepacore system. Hexane was distilled before chromatography. Tetrahydrofuran and diethyl ether (for thioamide synthesis) were dried using a PureSolv system from Innovative Technology, Inc. Dimethyl carbonate was used as obtained from a chemical supplier. Microwave reactions were carried out in sealed vials in a Biotage Initiator 2.5.

**Typical procedure: Preparation of 8a:** Oxetan-3-one (0.68 mL, 10.6 mmol) followed by trifluoroacetic acid (0.40 mL, 5 mmol) were added to a solution of benzamide (1.21 g, 10 mmol) in acetic acid (20 mL). The colourless solution was heated to 120 °C for 3.5 h in a microwave reactor, then allowed to cool to room temperature. After venting and opening the vial, the black reaction mixture was concentrated under reduced pressure to remove any residual acid. The residue was treated with toluene (10 mL) then evaporated to afford crude product as a black tar (2.29 g). The crude product was taken up in a minimum volume of ethyl acetate (20 mL) and evaporated onto silica gel (1.5 g). The silica gel was made into a pad in a sinter funnel and washed with diethyl ether (250 mL). The washings were concentrated under reduced pressure to afford crude product as an orange/brown oil (2.1 g). Purification by column chromatography over silica gel (gradient 1:2 to 1:1 diethyl ether/hexane) afforded 2-phenyl 4-(acetoxymethyl)-oxazole (**8a**) as a colourless solid (932 mg, 47%);  $R_f=0.36$  (2:5 diethyl ether/hexane); m.p. 39–40 °C (lit. m.p. 39.5–40 °C);  $^{13}\text{C}$  NMR (400 MHz,  $\text{CDCl}_3$ ):  $\delta=8.08$ – $8.05$  (m, 2H; ArH), 7.74 (s, 1H;  $H_5$ ), 7.49–7.46 (m, 3H; ArH), 5.12 (d,  $^4J=0.7$  Hz, 2H;  $\text{CH}_2\text{OAc}$ ), 2.13 ppm (s, 3H;  $\text{CH}_3$ );  $^{13}\text{C}$  NMR (100 MHz,  $\text{CDCl}_3$ ):  $\delta=170.3$ , 161.7, 136.7, 136.6, 130.1, 128.3, 126.7, 126.0, 57.6, 20.4 ppm; IR (film):  $\tilde{\nu}=1735$ , 1554, 1383, 1449, 1382, 1362, 1343, 1229  $\text{cm}^{-1}$ ; MS (CI):  $m/z$  (%): 258 (6) [ $M+\text{C}_2\text{H}_5$ ] $^+$ , 246 (10), [ $M+\text{C}_2\text{H}_5$ ] $^+$ , 218 (22) [ $M+\text{H}$ ] $^+$ , 174 (11) [ $M-\text{Ac}$ ], 158 (100) [ $M-\text{OAc}$ ], 104 (12); HRMS (ES-TOF):  $m/z$  calcd for  $\text{C}_{12}\text{H}_{12}\text{NO}_3$ : 218.0812 [ $M+\text{H}$ ] $^+$ ; found: 218.0806;  $t_R$  (GC) = 12.20 min.

**Typical procedure: Preparation of 10a:** Oxetan-3-one (0.13 mL, 2 mmol) followed by methanesulfonic acid (65  $\mu\text{L}$ , 1 mmol) were added to a suspension of benzamide (245 mg, 2.0 mmol) in dimethyl carbonate (4 mL). The reaction mixture was heated in a microwave reactor at 120 °C for 80 min; TLC confirmed full conversion. The reaction mixture was loaded onto a dry pad of celite (7.6 g), which was washed with dichloromethane

(125 mL). The filtrate was concentrated under reduced pressure and purified by column chromatography on silica gel (2:3 to 1:1 gradient of ethyl acetate in hexane) to afford 2-phenyl-4-(hydroxymethyl)-oxazole (**10a**) as a light brown solid (125 mg, 36%);  $R_f=0.25$  (1:1 ethyl acetate/hexane); m.p. 80–81 °C (lit. m.p. 82–83 °C);  $^{13}\text{C}$  NMR (400 MHz,  $\text{CDCl}_3$ ):  $\delta=8.08\text{--}8.05$  (m, 2H; ArH), 7.68 (s, 1H;  $\text{H}_5$ ), 7.49–7.47 (m, 3H; ArH), 4.71 (d,  $J=4.6$  Hz, 2H; ArCH<sub>2</sub>OH); 2.26 ppm (brs, 1H; CH<sub>2</sub>OH);  $^{13}\text{C}$  NMR (100 MHz,  $\text{CDCl}_3$ ):  $\delta=161.7$ , 141.1, 134.5, 130.0, 128.3, 126.8, 126.0, 58.4 ppm; IR (film):  $\tilde{\nu}=3221$ , 3116, 1740, 1552, 1351, 1231, 1023  $\text{cm}^{-1}$ ; MS (CI):  $m/z$  (%): 216 (7) [ $M+\text{C}_3\text{H}_5$ ]<sup>+</sup>, 204 (13) [ $M+\text{C}_2\text{H}_5$ ]<sup>+</sup>, 176 (40) [ $M+\text{H}$ ]<sup>+</sup>, 158 (100) [ $M-\text{OH}$ ]<sup>+</sup>, 130 (5); HRMS (ESI):  $m/z$  calcd for  $\text{C}_{10}\text{H}_{10}\text{NO}_2$ : 176.0706 [ $M+\text{H}$ ]<sup>+</sup>; found: 176.0705;  $t_R$  (GC)=12.71 min. Crystal data for  $\text{C}_{10}\text{H}_{10}\text{NO}_2$ : Formula weight: 175.18; Temperature: 123(2) K;  $\lambda=0.71073$  Å; Monoclinic system; Crystal size:  $0.24\times 0.18\times 0.10$  mm<sup>3</sup>; Unit cell dimensions:  $a=8.5610(5)$ ,  $b=14.5900(8)$ ,  $c=7.0504(4)$  Å,  $a=90$ ,  $b=104.625(6)$ ,  $\gamma=90^\circ$ ;  $Z=4$ ; Reflection collected: 3925;  $R$  indices (all data):  $R1=0.0647$ ,  $wR2=0.1033$ .

**Typical procedure: Preparation of 7f:** 4-Methoxybenzamide (376 mg, 2.5 mmol) was added to a suspension of  $\text{P}_2\text{S}_5$ /alumina reagent (773 mg, 3.5 mmol) in anhydrous THF (5 mL) and the reaction mixture was heated in a microwave reactor at 60 °C for 20 min until TLC showed complete conversion. The reaction mixture was evaporated onto a pad of silica gel (8.6 g), eluted with diethyl ether (50 mL), and the eluent was concentrated under reduced pressure to afford crude thioamide **7f** as a yellow solid (660 mg). The crude product was taken up in anhydrous THF (4 mL) and evaporated onto silica gel (2.6 g). The solid was transferred onto a pad of silica (10.6 g) in a sinter funnel that had been conditioned with 1:1 diethyl ether/hexane. Non-polar impurities were removed using 1:1 diethyl ether/hexane and product was eluted with 4:1 diethyl ether/hexane to afford 4-(methoxy)thiobenzamide **7f** as a yellow solid (280 mg, 67%);  $R_f=0.23$  (4:1 diethyl ether/hexane); m.p. 141–143 °C;  $^1\text{H}$  NMR (400 MHz,  $\text{CDCl}_3$ ):  $\delta=7.92\text{--}7.88$  (m, 2H; one half of an AA'BB' system, ArH), 7.48 (brs, 1H; C(S)NH<sub>2</sub>H<sub>b</sub>), 7.09 (brs, 1H; C(S)NH<sub>2</sub>H<sub>b</sub>), 6.92–6.88 (m, 2H; one half of an AA'BB' system ArH), 3.86 ppm (s, 3H; ArOCH<sub>3</sub>);  $^{13}\text{C}$  NMR (100 MHz,  $\text{CDCl}_3$ ):  $\delta=201.4$ , 163.0, 131.3, 129.1, 113.6, 55.6 ppm; IR (film):  $\tilde{\nu}=3367$ , 3278, 3157, 2363, 1626, 1597, 1510, 1427, 1389, 1330, 1285, 1258, 1184, 1138, 1020  $\text{cm}^{-1}$ ; MS (ESI):  $m/z$  (%): 168 (100) [ $M+\text{H}$ ]<sup>+</sup>, 151 (30) [ $M-\text{NH}_2$ ], 135 (15). The spectroscopic data were in agreement with those reported in the literature.<sup>[16a]</sup>

**Computational methods:** Electronic structure calculations were carried out on a Dell Precision T1500 (Intel 4 Core i7 CPU 870@ 2.93 GHz Processor, 8 GB RAM) running Spartan'08 V1.2.0, 64 Bit. Transition structures were located via initial guesses that were optimised using the PM3 semi-empirical method, then re-optimised initially at the RI-MP2/6-31G\* or B3LYP/6-31G\* levels of theory. These structures were then used as the starting points for MP2/6-31+G\* or B3LYP/6-311+G\*\* optimisations with full frequency calculation at 298 K. Free energies were evaluated (in au) using Spartan's internal algorithm and transferred to Excel for further manipulation. Optimised structures had no imaginary frequencies; unique imaginary frequencies were found for transition structures and these are listed fully with the Cartesian coordinates in the Supporting Information.

## Acknowledgements

We thank EPSRC and GSK (Industrial CASE studentship to A.T.), GSK and the University of Strathclyde (studentship to D. O.), GSK Refractory Respiratory Inflammation DPU for consumables, the EPSRC National Mass Spectrometry Service Centre, Swansea for accurate mass measurements, Dr Alan Kennedy (Pure and Applied Chemistry, University of Strathclyde) for the X-ray structural determination of **10a**, Dr. Rob Young (GSK Stevenage) for helpful discussions about work-up methods, and David Black (University of Strathclyde) for preliminary syntheses of oxazoles **10**.

- [1] G. Wuitschik, E. M. Carreira, B. Wagner, H. Fischer, I. Parrilla, F. Schuler, M. Rogers-Evans, K. Muller, *J. Med. Chem.* **2010**, *53*, 3227–3246.
- [2] a) L. W. Ye, W. M. He, L. M. Zhang, *J. Am. Chem. Soc.* **2010**, *132*, 8550–8551; b) B. O. Beasley, G. J. Clarkson, M. Shipman, *Tetrahedron Lett.* **2012**, *53*, 2951–2953.
- [3] a) M. A. J. Duncton, M. A. Estiarte, D. Tan, C. Kaub, D. J. R. O'Mahony, R. J. Johnson, M. Cox, W. T. Edwards, M. Wan, J. Kincaid, M. G. Kelly, *Org. Lett.* **2008**, *10*, 3259–3262; b) M. A. J. Duncton, M. A. Estiarte, R. J. Johnson, M. Cox, D. J. R. O'Mahony, W. T. Edwards, M. G. Kelly, *J. Org. Chem.* **2009**, *74*, 6354–6357.
- [4] J. A. Burkhard, B. H. Tchitchanov, E. M. Carreira, *Angew. Chem.* **2011**, *123*, 5491–5494; *Angew. Chem. Int. Ed.* **2011**, *50*, 5379–5382.
- [5] T. A. Mukhtar, G. D. Wright, *Chem. Rev.* **2005**, *105*, 529–542.
- [6] F. Batt, F. Fache, *Eur. J. Org. Chem.* **2011**, 6039–6055.
- [7] P. Wipf, *Chem. Rev.* **1995**, *95*, 2115–2134.
- [8] a) R. Martín, A. Cuenca, S. L. Buchwald, *Org. Lett.* **2007**, *9*, 5521–5524; b) E. F. Flegau, M. E. Popkin, M. F. Greaney, *Org. Lett.* **2008**, *10*, 2717–2720; c) S. A. Ohnmacht, P. Mamone, A. J. Culshaw, M. F. Greaney, *Chem. Commun.* **2008**, 1241–1243; d) C. K. Skepper, T. Quach, T. F. Molinski, *J. Am. Chem. Soc.* **2010**, *132*, 10286–10292; e) C. M. Counciller, C. C. Eichman, N. Proust, J. P. Stambuli, *Adv. Synth. Catal.* **2011**, *353*, 79–83; f) I. Cano, E. Alvares, M. C. Nicasio, P. J. Perez, *J. Am. Chem. Soc.* **2011**, *133*, 191–193; g) C. L. Paradise, P. R. Sarkar, M. Razzak, J. K. De Brabander, *Org. Biomol. Chem.* **2011**, *9*, 4017–4020; h) G. Bartoli, C. Cimarelli, R. Cipolletti, S. Diomed, R. Giovannini, M. Mari, L. Marsili, E. Marcantoni, *Eur. J. Org. Chem.* **2012**, 630–636; i) A. E. Wendlandt, S. S. Stahl, *Org. Biomol. Chem.* **2012**, *10*, 3866–3870.
- [9] R. K. Henderson, C. Jimenez-Gonzalez, D. J. C. Constable, S. R. Alston, G. G. A. Inglis, G. Fisher, J. Sherwood, S. P. Binks, A. D. Curzons, *Green Chem.* **2011**, *13*, 854–862.
- [10] T. Durand-Reville, L. B. Gobbi, B. L. Gray, S. V. Ley, J. S. Scott, *Org. Lett.* **2002**, *4*, 3847–3850.
- [11] M. L. P. Le, L. Cointeaux, P. Strobel, J. C. Lepretre, P. Judeinstein, F. Alloin, *J. Phys. Chem. C* **2012**, *116*, 7712–7718.
- [12] a) C. Gabriel, S. Gabriel, E. H. Grant, B. S. J. Halstead, D. M. P. Mingos, *Chem. Soc. Rev.* **1998**, *27*, 213–223; b) P. Lidström, J. Tierney, B. Wathey, J. Westman, *Tetrahedron* **2001**, *57*, 9225–9283.
- [13] a) H. Bilel, N. Hamdi, F. Zagrouba, C. Fischmeister, C. Bruneau, *Green Chem.* **2011**, *13*, 1448–1452; b) X. W. Miao, C. Fischmeister, C. Bruneau, P. H. Dixneuf, *ChemSusChem* **2008**, *1*, 813–816.
- [14] a) C. M. Hou, Y. F. Chen, W. Li, *Carbohydr. Res.* **2012**, *355*, 87–91; b) U. Tilstam, *Org. Process Res. Dev.* **2012**, *16*, 1150–1153.
- [15] a) J. P. Guthrie, *Can. J. Chem.* **1978**, *56*, 2342–2354; b) J. F. J. Dippy, S. R. C. Hughes, A. Rozanski, *J. Chem. Soc.* **1959**, 2492–2498; c) J. P. Candlin, R. G. Wilkins, *J. Chem. Soc.* **1960**, 4236–4241; d) W. P. Jencks, J. Regenstein in *Handbook of Biochemistry and Molecular Biology* (Ed.: G. D. Fasman), CRC, Boca Raton, **1976**, pp. 305–351.
- [16] For syntheses of thioamides from nitriles, see: a) P. Y. Lin, W. S. Ku, M. J. Shiao, *Synthesis* **1992**, 1219–1220; b) M. C. Bagley, K. Chapanneri, C. Glover, E. A. Merritt, *Synlett* **2004**, 2615–2617; c) M. Nagl, C. Panuschka, A. Barta, W. Schmid, *Synthesis* **2008**, 4012–4018.
- [17] H. R. Lagiakos, A. Walker, M. I. Aguilar, P. Perlmutter, *Tetrahedron Lett.* **2011**, *52*, 5131–5132.
- [18] a) P. Ratcliffe, J. M. Adam, J. Baker, R. Bursi, R. Campbell, J. K. Clark, J. E. Cottney, M. Deehan, A. M. Easson, D. Ecker, D. Edwards, O. Epemolu, L. Evans, R. Fields, S. Francis, P. Harradine, F. Jeremiah, T. Kiyoi, D. McArthur, A. Morrison, P. Passier, J. Pick, P. G. Schnabel, J. Schulz, H. Steinbrede, G. Walker, P. Westwood, G. Wishart, J. U. de Haes, *Bioorg. Med. Chem. Lett.* **2011**, *21*, 2541–2546; b) M. Rega, P. Candal, C. Jimenez, J. Rodriguez, *Eur. J. Org. Chem.* **2007**, 934–942; c) R. Uy, L. Q. Yang, H. X. Zhou, S. C. Price, W. You, *Macromolecules* **2011**, *44*, 9146–9154.
- [19] a) Z. Y. Li, L. Ma, J. Y. Xu, L. Y. Kong, X. M. Wu, H. Q. Yao, *Chem. Commun.* **2012**, 48, 3763–3765; b) B. Di Credico, G. Regina-to, L. Gonsalvi, M. Peruzzini, A. Rossin, *Tetrahedron* **2011**, *67*, 267–

- 274; c) H. Sugiyama, F. Yokokawa, T. Shioiri, *Org. Lett.* **2000**, *2*, 2149–2152.
- [20] D. Sellanes, F. Campot, I. Nunez, G. Lin, P. Esposito, S. Dematteis, J. Saldana, L. Dominguez, E. Manta, G. Serra, *Tetrahedron* **2010**, *66*, 5384–5395.
- [21] M. Yamaguchi, Y. Nobayashi, I. Hirao, *Tetrahedron Lett.* **1983**, *24*, 5121–5122.
- [22] C. J. M. Stirling, *Tetrahedron* **1985**, *41*, 1613–1666.
- [23] H. D. Banks, *Org. Biomol. Chem.* **2009**, *7*, 4496–4501.
- [24] Spartan '08, Wavefunction, Irvine, CA, **2008**.
- [25] L. Simón, J. M. Goodman, *Org. Biomol. Chem.* **2011**, *9*, 689–700.
- [26] S. E. Wheeler, K. N. Houk, *J. Chem. Theory Comput.* **2010**, *6*, 395–404.
- [27] a) J. B. Conant, W. R. Kirner, R. E. Hussey, *J. Am. Chem. Soc.* **1925**, *47*, 488–501; for examples in which adjacent unsaturation has little or no effect on the rate of nucleophilic substitution at sp<sup>3</sup> carbon, see b) D. N. Kevill, C. B. Kim, *J. Org. Chem.* **2005**, *70*, 1490–1493.
- [28] For detailed MO treatments of the effect of adjacent unsaturation on nucleophilic substitution at sp<sup>3</sup> carbon, see a) D. Kost, K. Aviram, *J. Am. Chem. Soc.* **1986**, *108*, 2006–2013; b) R. E. Rawlings, A. K. McKerlie, D. J. Bates, Y. R. Mo, J. M. Karty, *Eur. J. Org. Chem.* **2012**, 5991–6004.
- [29] A. Noel, B. Delpéch, D. Crich, *Org. Biomol. Chem.* **2012**, *10*, 6480–6483.
- [30] A reviewer pointed out that the usual ideal gas equation penalises bimolecular reactions entropically at the expense of unimolecular reactions, and that termolecular reactions may suffer a still more severe penalty; for QM calculations on termolecular reaction steps, see a) S. K. Ignatov, P. G. Sennikov, A. G. Razuvaev, O. Schrems, *J. Phys. Chem. A* **2004**, *108*, 3642–3649; b) M. Ismael, R. Sahnoun, A. Suzuki, M. Koyama, H. Tsuboi, N. Hatakeyama, A. Endou, H. Takaba, M. Kubo, S. Shimizu, C. A. Del Carpio, A. Miyamoto, *Int. J. Greenhouse Gas Control* **2009**, *3*, 612–616; c) H. Yamada, Y. Matsuzaki, T. Higashii, S. Kazama, *J. Phys. Chem. A* **2011**, *115*, 3079–3086; d) M. Torrent-Sucarrat, J. S. Francisco, J. M. Anglada, *J. Am. Chem. Soc.* **2012**, *134*, 20632–20644; for an approach to the evaluation of Gibbs energy barriers for reactions of higher molecularity, see D. Ardura, R. Lopez, T. L. Sordo, *J. Phys. Chem. B* **2005**, *109*, 23618–23623.
- [31] a) A. C. Chamberlin, C. J. Cramer, D. G. Truhlar, *J. Phys. Chem. B* **2008**, *112*, 8651–8655; b) C. J. Cramer, D. G. Truhlar, *Acc. Chem. Res.* **2008**, *41*, 760–768.
- [32] a) W. P. Jencks, *Chem. Rev.* **1972**, *72*, 705–718; b) R. A. O'Ferrall, *J. Chem. Soc. B* **1970**, 274–277.
- [33] A. B. A. Jansen, M. Szelke, *J. Chem. Soc.* **1961**, 405–411.

Received: March 16, 2013  
Published online: June 13, 2013